NASA/CR-20250002267

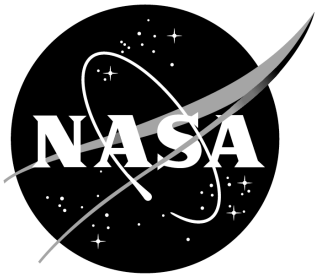

Evaluation, Analysis, and Application of Internal Strain-Gage Balance Data

Third Edition of NASA/CR-20210026455

Norbert Ulbrich
Amentum Services, Inc., Moffett Field, California

Contract 80ARC022DA011

February 2025

NASA STI Program ... in Profile

Since its founding, NASA has been dedicated to the advancement of aeronautics and space science. The NASA scientific and technical information (STI) program plays a key part in helping NASA maintain this important role.

The NASA STI program operates under the auspices of the Agency Chief Information Officer. It collects, organizes, provides for archiving, and disseminates NASA's STI. The NASA STI program provides access to the NASA Aeronautics and Space Database and its public interface, the NASA Technical Reports Server, thus providing one of the largest collections of aeronautical and space science STI in the world. Results are published in both non-NASA channels and by NASA in the NASA STI Report Series, which includes the following report types:

- TECHNICAL PUBLICATION. Reports of completed research or a major significant phase of research that present the results of NASA Programs and include extensive data or theoretical analysis. Includes compilations of significant scientific and technical data and information deemed to be of continuing reference value. NASA counterpart of peer-reviewed formal professional papers but has less stringent limitations on manuscript length and extent of graphic presentations.

- TECHNICAL MEMORANDUM. Scientific and technical findings that are preliminary or of specialized interest, e.g., quick release reports, working papers, and bibliographies that contain minimal annotation. Does not contain extensive analysis.

- CONTRACTOR REPORT. Scientific and technical findings by NASA-sponsored contractors and grantees.

- CONFERENCE PUBLICATION. Collected papers from scientific and technical conferences, symposia, seminars, or other meetings sponsored or co-sponsored by NASA.

- SPECIAL PUBLICATION. Scientific, technical, or historical information from NASA programs, projects, and missions, often concerned with subjects having substantial public interest.

- TECHNICAL TRANSLATION. English-language translations of foreign scientific and technical material pertinent to NASA's mission.

Specialized services also include organizing and publishing research results, distributing specialized research announcements and feeds, providing information desk and personal search support, and enabling data exchange services.

For more information about the NASA STI program, see the following:

- Access the NASA STI program home page at http://www.sti.nasa.gov

- E-mail your question to help@sti.nasa.gov

- Fax your question to the NASA STI Information Desk at 443-757-5803

- Phone the NASA STI Information Desk at 443-757-5802

- Write to:
  STI Information Desk
  NASA Center for AeroSpace Information
  7115 Standard Drive
  Hanover, MD 21076-1320

NASA/CR-20250002267

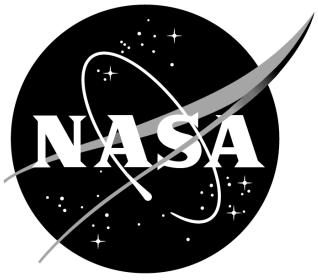

Evaluation, Analysis, and Application of Internal Strain-Gage Balance Data

Third Edition of NASA/CR-20210026455

Norbert Ulbrich
Amentum Services, Inc.
P.O. Box 366, M/S 227-4
Moffett Field, CA 94035-1000

National Aeronautics and
Space Administration

Ames Research Center
Moffett Field, California 94035-1000

Prepared for Ames Research Center
under Contract 80ARC022DA011

February 2025

Acknowledgments

The author would like to express his sincere appreciation and gratitude to *Bob Gisler* of NASA and *Tom Volden* of Jacobs Technology for the many suggestions and comments that they made over the years. The contractor report would have never come together without the countless discussions that the author had with them during the past sixteen years. They were also members of the team of experts who reviewed the report's final manuscript. In addition, *Tom Volden* is co–developer of NASA's BALFIT software that was used to implement, verify, and refine most processes and algorithms that are presented in the contractor report.

The author would like to acknowledge *Jon Bader, Tom Hegland, Maureen Delgado, James Bell,* and *Frank Kmak* of the Wind Tunnel Division at NASA Ames Research Center for enthusiastically supporting his work in the area of strain–gage balance data analysis. Thanks also go to *Max Amaya*, *Alan L'Esperance*, *Nick Capdevila*, and *Mike Treece* of NASA who helped with the review of the manuscript. In addition, contributions made by *Michael Wright*, *Jordan Hu*, and *Kevin James* of NASA, *Hiep Khuc* of Aerodyne Industries, and *James Prunty* and *Tim Steiger* of Jacobs Technology are appreciated.

The author is grateful for suggestions and recommendations that were made by *Richard DeLoach* and *Mike Acheson* of NASA Langley Research Center during the development of key algorithms that are discussed in the contractor report. Comments made by *Devin Burns* of NASA Langley Research Center and *Mark Kammeyer* of The Boeing Company during the final review of the manuscript are greatly appreciated. Thanks also go to *Ray Rhew*, *Peter Parker*, *Sean Commo*, and *Ken Toro* of NASA Langley Research Center, *Johannes van Aken* of National Aerospace Solutions, *Ryan Kew* and *Dennis Booth* of Calspan Systems Corporation, *Claus Zimmermann* of RUAG AG, and *Chris Lynn* of Lynn Engineering for the many suggestions that they made during past collaborations.

Last but not least, benefits of personal contacts with colleagues from all over the world must not be underestimated. Therefore, the author is thankful for countless comments and constructive criticism that he received at conferences and other events from balance designers, analysts, and test engineers associated with three NASA Centers, NASA's industry partners, universities, and other aerospace testing organizations.

Level of Review: This material has been reviewed by NASA technical management.
(all photos used in the document are courtesy of NASA Ames Research Center)

Available from

NASA Center for Aerospace Information
7115 Standard Drive
Hanover, MD 21076–1320

National Technical Information Service
5301 Shawnee Road
Alexandria, VA 22312

Available electronically at http://www.sti.nasa.gov

Preface

Evaluation, analysis, application, and reporting of internal strain–gage balance data were greatly improved at NASA Ames Research Center during the past sixteen years. Consequently, the aerodynamic load prediction process has become more transparent to both wind tunnel operator and customer. In addition, a more complete list of balance load prediction approaches is now supported. These approaches are either used by NASA and its industry partners or were developed to address specific data analysis challenges.

A good understanding of the improved analysis processes and reporting procedures for strain–gage balance data is important in order to gain confidence in specific analysis results and to improve communication between balance designers, calibration laboratory staff, test engineers, and wind tunnel customers. Detailed descriptions of these processes and procedures were originally scattered across more than forty conference papers that were published between 2005 and 2021. Therefore, it became necessary to summarize the most important descriptions and conclusions in a single document so that the information can more easily be reviewed, understood, and referenced.

The contractor report is intended to provide an overview of a variety of methods and algorithms that the author successfully applied during both evaluation and analysis of wind tunnel strain–gage balance data. Therefore, the report's contents will always remain incomplete as many analysts use analysis approaches that are either tailored to site–specific needs or that are the result of their own experiences and research. Nevertheless, the author hopes that the contractor report will help document some of his observations and conclusions in a format that will make them accessible to a wider audience.

Moffett Field, California *Norbert Ulbrich*
December 2021

Changes in the Second Edition

Only minor differences between this report and NASA/CR–20210026455 exist. Spelling mistakes were corrected. Stylistic changes were made to parts of the text. The word *gage* was replaced with the word *bridge* whenever possible to make the report's terminology more precise. Historical notes were updated or added. The formatting of a few tables, figures, and equations was improved. Section 7.3 of App. 7 and section 15.4 of App. 15 were revised. Appendices 24, 25, and 26 were newly added. Appendix 24 discusses balance interactions. Appendix 25 defines a universal load iteration equation. Appendix 26 derives an estimate of the axial force error that results from a misaligned normal or side force. The subject index was updated. – The author wants to thank *Bob Gisler* of NASA who reviewed the three new appendices. Thanks also go to *Heather Clark* of the Aerodynamics Laboratory, National Research Council Canada. She supplied an extensive list of comments and suggestions after reading the first edition of the report from cover to cover. Finally, *Robin Galway* (retired IAR/NRC) provided valuable background information and other explanations that helped improve the report.

Moffett Field, California *Norbert Ulbrich*
September 2023

Changes in the Third Edition

Minor revisions, updates, and additions were made. A less complex weighting factor definition was included in App. 22. A method for the assessment of balance interaction differences of two balance data sets was added to App. 24. Three new appendices were also prepared. Appendix 27 discusses the analysis of calibration data of a one–component load cell. Appendix 28 provides an alternate description of *Cook's* sequential analysis method. Appendix 29 reviews the historical evolution of balance load prediction methods. Finally, table of contents, list of references, and subject index were updated. – The author wants to thank *Lindsey Drone* of NASA and *Tom Volden* of Amentum Services for reviewing the manuscript of the third edition. *Tom Volden* also made suggestions that helped improve the description of the less complex weighting factor definition.

Moffett Field, California *Norbert Ulbrich*
February 2025

Abstract

Experimental processes, analytical methods, and numerical algorithms are described that may be used to predict the forces and moments of an internal strain–gage balance during a wind tunnel test. First, the control volume model of a strain–gage balance and the concepts of load state, load space, and output space are introduced. These important abstractions provide a better understanding of fundamental characteristics of different balance load prediction approaches. Then, the description of strain–gage balance data and the definition of the primary bridge sensitivity are discussed. Afterwards, basic elements of the calibration of a typical six–component balance are reviewed. Two fundamentally different balance load prediction methods, the processing of check loads, and related topics are also discussed. Three real–world balance data examples are reviewed in great detail to illustrate typical analysis results for a variety of strain–gage balance designs. Finally, important observations are summarized and recommendations are provided. – Additional information and detailed mathematical derivations can be found in the appendices of the document. They include the following topics: balance terminology, definitions of important statistical metrics, balance axis system conventions, balance load transformations, the combined load diagram, electrical output format options, bi–directional output characteristics, determination of the natural zeros, derivation of two balance load prediction methods, description of two tare load iteration algorithms, modeling of balance temperature effects, basics of three–component moment balances, definition of the percent contribution, detection of linear and near–linear dependencies in balance calibration data, a regression model search algorithm, balance interactions, and other related information.

Table of Contents

List of Symbols

Regular Letters

$\mathbf{A}$	matrix with regression model term values
$\mathbf{A}_k$	column vector with values of a regression model term
$A_{k,\nu}$	value of a regression model term
$\mathbf{A}'$	matrix needed for the calculation of tare loads
$\mathbf{A}^\star$	transformed matrix related to the regression analysis problem
AF	axial force
AF_{max}	capacity of the axial force
a	distance between normal force bridges; bending moment arm
a_0	intercept term of the regression model of a fitted load
$a_0,\ a_1,\ \ldots$	coefficients of the regression model of a fitted load
a_{max}	maximum of the bending moment arm
a_{min}	minimum of the bending moment arm
a_η	coefficient of the output difference term
a_μ	coefficient of the primary output difference term
a_ξ	coefficient of a term of the regression model of a fitted load
a_ψ	coefficient of the absolute value term of the output difference
$a_{i,0}$	intercept term of the regression model of a fitted load
$a_{i,0},\ a_{i,1},\ \ldots$	coefficients of the regression model of a fitted load
$a_{i,\omega}$	term of the regression model of a fitted load
a'	corrected bending moment arm
$\mathbf{B}$	matrix/vector used for the regression analysis or load prediction
$\mathbf{B_1}$	matrix needed for the alternate load iteration equation
B_1	coefficient of matrix $\mathbf{B_1}$
$\mathbf{B_2}$	matrix needed for the alternate load iteration equation
B_2	coefficient of matrix $\mathbf{B_2}$
$\mathbf{B}'$	matrix needed to compute intermediate estimates of tare loads
$\mathbf{B}''$	matrix needed to compute a load associated with intercepts
BM	bending moment at the balance moment center
BM'	corrected bending moment at the balance moment center

$BM1$	bending moment at the first bending moment bridge
$BM2$	bending moment at the second bending moment bridge
$\mathbf{b}$	vector with intercepts of regression models of the fitted outputs
b	intercept; side force bridge distance; torsion moment arm
b_0	intercept term of the regression model of a fitted output
$b_0,\ b_1,\ \ldots$	regression coefficients of a fitted output or fitted interactions
b_η	coefficient of a primary load term
b_μ	coefficient of a primary load term
b_ξ	coefficient of a term of the regression model of a fitted output
b_ψ	coefficient of the absolute value term of a primary load
$b_{i,0}$	intercept term of the regression model of a fitted output
$b_{i,0},\ b_{i,1},\ \ldots$	coefficients of the regression model of a fitted output
$b_{i,\omega}$	term of the regression model of a fitted output
$\mathbf{C}$	regression coefficient matrix
C	coefficient of matrix $\mathbf{C}$
$\mathbf{C_1}$	part of matrix $\mathbf{C}$ that has the coefficients of all linear terms
C_1	coefficient of matrix $\mathbf{C_1}$
$\mathbf{C_2}$	part of matrix $\mathbf{C}$ that has the coefficients of all non–linear terms
C_2	coefficient of matrix $\mathbf{C_2}$
$\mathbf{C}'$	extended regression coefficient matrix
C'	coefficient of matrix $\mathbf{C}'$
c	distance between second bending moment bridge and moment center
$c_0,\ c_1,\ \ldots$	coefficients of a regression model of calibration data
c_1	x–coordinate of the forward force/moment bridge
c_2	x–coordinate of the aft force/moment bridge
$\mathbf{D}$	vector with differences between raw output and natural zero
$\mathbf{D}'$	uncorrected electrical output differences of a data point
$\mathbf{D}''$	corrected electrical output differences of a data point
$\mathbf{D_0}$, $\mathbf{D_1}$, $\mathbf{D_2}$	matrices used to define the universal load iteration equation
D_1	output difference of the first bending moment bridge
D_2	output difference of the second bending moment bridge

D_3	output difference of the torsion moment bridge
D_i	raw output minus natural zero
D_μ	primary output difference
D_ψ	difference between raw output and natural zero of a bridge
$D_i{}'$	raw output minus raw output of the zero load point of a load series
$D_i{}''$	output difference $D_i{}'$ after removal of outputs of residual loads
$D_\mu{}^\star$	capacity of a primary output difference
d	distance between the forward and aft bridges of a balance
$d_1,\ d_2$	coordinate differences
$\mathbf{E}$	inverse of the correlation matrix
$E_{i,j}$	coefficient of the inverse of the correlation matrix
$\mathbf{F}$	load vector
F	force; load component
F_1	force at the forward bridge of a force balance
F_2	force at the aft bridge of a force balance
$F_1,\ F_2,\ \ldots$	load components of a strain–gage balance
F_i	balance load component or variable with index i
F_j	balance load component or variable with index j
F_k	balance load component or variable with index k
$F_x,\ F_y,\ F_z$	forces in a right–handed balance axis system
$\mathbf{F}_{bal}$	vector with the predicted balance loads of a data point
$\mathbf{F}_{cor}$	rectangular matrix with tare corrected balance loads
F_{max}	capacity of a balance load component
$\mathbf{F}_{res}$	residual machine load vector of a data point
$\mathbf{F}_{unc}$	rectangular matrix with applied/uncorrected balance loads
$\mathbf{F}_\eta,\ \mathbf{F}_\nu$	balance load vectors
F_μ	primary load component
$\mathbf{F}_\xi$	vector with balance loads at iteration step ξ
F_ξ	balance load at iteration step ξ
F_φ	load component
$\mathbf{F}_\psi$	upper bound of the load vector

F_{ψ_i}	component of vector $\mathbf{F}_{\psi}$
$\mathbf{F}_{\infty}$	load vector obtained after an infinite number of iterations
$\mathbf{F}'$	vector with load capacities
$\mathbf{F}''$	vector with loads of data point with greatest dimensionless length
$\mathbf{F}'''$	vector with largest tare corrected loads
$F_{\mu}{}^{\star}$	capacity of a primary load component
$\mathbf{f}$	vector function in n–dimensional space
f_i	function in n–dimensional space; force or moment function
$\mathbf{G}$	matrix that is a function of balance loads
G	coefficient of matrix $\mathbf{G}$
$\mathbf{G}^{'}$	extended matrix that is a function of balance loads
G'	coefficient of matrix $\mathbf{G}^{'}$
$\mathbf{g}$	auxiliary vector
g	distance between pitching moment bridges
g_i	component of auxiliary vector $\mathbf{g}$ with index i
$\mathbf{H}$	part of matrix $\mathbf{G}$ with absolute value and non–linear terms
H	coefficient of matrix $\mathbf{H}$
h	distance between yawing moment bridges
$\mathbf{I}$	identity matrix
i	index of a load component; index of a bridge output
$\mathbf{J}$	first auxiliary matrix for *Variance Inflation Factor* calculation
$\mathcal{J}$	*Jacobian Matrix*
$\mathbf{J}_k$	vector with regression model term values
$\mathbf{J}'_k$	vector with centered regression model term values
$J'_{k,\nu}$	component of column vector $\mathbf{J}'_k$
$\mathbf{J}''$	second auxiliary matrix for *Variance Inflation Factor* calculation
$\mathbf{J}''_k$	vector with scaled & centered regression model term values
$J''_{k,\nu}$	component of column vector $\mathbf{J}''_k$
j	index of a load component, bridge output, or regression coefficient
$\mathbf{K}$	auxiliary square matrix that is populated with zeros
k	index of a load series, regression model term, or variable

$\mathbf{L}$	linear part of the regression coefficient matrix
L	left–hand side of an equation
L_{max}	upper bound of the *Lipschitz Constant*
M	moment; moment at the balance moment center
M_1	moment at the forward bridge of a moment balance
M_2	moment at the aft bridge of a moment balance
$M_x,\ M_y,\ M_z$	moments in a right–handed balance axis system
M'	computed moment, i.e., true moment plus moment error
m	maximum number of regression model terms (excluding intercept)
$\mathbf{N}$	vector with natural zeros
N	natural zero
N_i	natural zero
N_μ	natural zero associated with a primary bridge output
n	number of loads; number of outputs; number of variables
n_φ	number of intentionally loaded bridges of a data point
n'	number of variables of the extended variable set
$N1$	normal force at the forward normal force bridge
$N2$	normal force at the aft normal force bridge
NF	normal force
NF'	corrected normal force at the balance moment center
$\mathbf{P}$	inverse of square matrix $\mathbf{L}$ or square matrix $\mathbf{C_1}$
P	percent contribution of the regression model term of a fitted load
p	total number of data points
PM	pitching moment
$PM1$	pitching moment at the forward pitching moment bridge
$PM2$	pitching moment at the aft pitching moment bridge
$\mathbf{Q}_\xi$	matrix that is used for the description of residual machine loads
Q	percent contribution of the regression model term of a fitted output
q	total number of load series of a balance calibration data set
$q_{i,j}$	coefficient of matrix $\mathbf{Q}_\xi$
$\mathbf{R}$	dependent variable vector of a global regression analysis problem

RM	rolling moment
r	radius of a circular arc
rAF	electrical output of the axial force bridge
$rAF_\circ$	natural zero of the axial force bridge
rC_i	output capacity
$\mathbf{rF}$	output vector
rF	output of a balance bridge
$rF_1,\ rF_2,\ \ldots$	electrical outputs of a strain–gage balance
rF_i	raw output of a balance bridge
$\mathbf{rF}_{diff}$	matrix with output differences of balance calibration data
$\mathbf{rF}_{raw}$	matrix with raw outputs of balance calibration data
rF_μ	raw output of a balance bridge
$rN1$	electrical output of the forward normal force bridge
$rN1_\circ$	natural zero of the forward normal force bridge
$rN2$	electrical output of the aft normal force bridge
$rN2_\circ$	natural zero of the aft normal force bridge
rNF	electrical output of the normal force bridge
$rNF_\circ$	natural zero of the normal force bridge
rPM	electrical output of the pitching moment bridge
$rPM_\circ$	natural zero of the pitching moment bridge
$rPM1$	electrical output of the forward pitching moment bridge
$rPM2$	electrical output of the aft pitching moment bridge
rRM	electrical output of the rolling moment bridge
$rRM_\circ$	natural zero of the rolling moment bridge
$rS1$	electrical output of the forward side force bridge
$rS1_\circ$	natural zero of the forward side force bridge
$rS2$	electrical output of the aft side force bridge
$rS2_\circ$	natural zero of the aft side force bridge
rSF	electrical output of the side force bridge
$rSF_\circ$	natural zero of the side force bridge
rYM	electrical output of the yawing moment bridge

$rYM_{\circ}$	natural zero of the yawing moment bridge
$rYM1$	electrical output of the forward yawing moment bridge
$rYM2$	electrical output of the aft yawing moment bridge
$\mathbf{S}$	matrix with inverted load capacities on its principal diagonal
S_{BM}	sensitivity of a bending moment bridge
$\mathcal{S}_{\xi}$	regression model term of a fitted load
S_{ψ}	term group of the regression model of a fitted load
$S1$	side force at the forward side force bridge
$S2$	side force at the aft side force bridge
SF	side force
s	moment arm
$s_1,\ s_2,\ \ldots$	singular values $\equiv$ result of *Singular Value Decomposition*
T	uniform balance temperature; bridge output threshold
$T_{\circ}$	reference temperature
T_{ξ}	uniform balance temperature
$\mathcal{T}_{\xi}$	regression model term of a fitted bridge output
T_{ψ}	term group of the regression model of a fitted bridge output
TM	torsion moment at the balance moment center
TOL	tolerance used for the balance load iteration process
$\mathbf{U}$	auxiliary matrix
$\mathbf{V}$	auxiliary vector
V	metric used for the tare load iteration convergence test
VIF	*Variance Inflation Factor*
VIF_{max}	maximum of *Variance Inflation Factor* set
$\mathbf{W}$	matrix with weighting factors of data points
W	physical weight of the metric part of a balance
$\mathcal{W}$	matrix with square root of weighting factors of data points
w_{φ}	weighting factor of a data point
$\mathbf{X}$	auxiliary vector
$X_1,\ X_2,\ \ldots$	generic variables; independent variables of a regression model
X_i	vector component; independent variable of a regression model

X_j	generalized force or moment that defines the *Lipschitz Constant*
$X_i^\star$	transformed independent variable value
$\mathbf{x}$	vector with regression coefficients
x	coordinate of the balance axis system; coordinate of an applied force
$x_1,\ x_2$	coordinates used to defined the bi–directional part of an output
Y	dependent variable of a regression model
$\mathbf{y}$	vector with regression coefficients
y	coordinate of the balance axis system
YM	yawing moment
$YM1$	yawing moment at the forward yawing moment bridge
$YM2$	yawing moment at the aft yawing moment bridge
$\mathbf{z}$	regression coefficient matrix
z	coordinate of the balance axis system
Z_i	output of the zero load point of a load series
$\mathbf{Z}_k$	vector of zero load outputs of a load series
$Z_{i,k}$	zero load output of a bridge for a specific load series

Greek Letters

$\alpha_{j,k}$	regression coefficient
$\beta_{j,k}$	regression coefficient
Γ	capacity of a load, output, or temperature difference
$\Gamma_i,\ \Gamma_j$	capacity of a variable with index i or index j
Γ_φ	capacity of a variable with index φ
$\gamma_{j,k}$	regression coefficient
δ	total number of supported regression model terms; deflection angle
δ_{jk}	*Kronecker delta*
ΔAF	axial force residual; tare correction of the axial force
δAF	axial force error resulting from a misaligned normal or side force
ΔBM	error of the bending moment
$\Delta BM1$	error of the bending moment at the first bending moment bridge
$\Delta BM2$	error of the bending moment at the second bending moment bridge

ΔD_1	error of the output difference of the first bending moment bridge
ΔD_2	error of the output difference of the second bending moment bridge
$\mathbf{\Delta F}$	vector or matrix with tare loads of all calibration points
ΔF	force error
ΔF_i	load correction derived from bridge sensitivity shift
ΔF_j	step size of load component F_j
$\mathbf{\Delta F}_k$	vector with the tare loads of a load series
ΔF_k	tare load
$\mathbf{\Delta F'}$	rectangular matrix with tare loads of all load series
ΔM	moment error
ΔN_i	temperature–dependent shift of the natural zero
$\Delta N1$	tare correction of the forward normal force
$\Delta N2$	tare correction of the aft normal force
ΔNF	normal force residual; error of the predicted normal force
$\mathbf{\Delta rF}$	output difference vector $\equiv$ delta bridge output vector
$\mathbf{\Delta rF_1}$	auxiliary output difference vector
$\mathbf{\Delta rF_2}$	auxiliary output difference vector
ΔRM	rolling moment residual; tare correction of the rolling moment
Δs	moment arm error $\equiv$ error of a distance/length measurement
$\Delta S1$	forward side force residual; tare correction of the forward side force
$\Delta S2$	tare correction of the aft side force
ΔT	difference between balance temperature and reference temperature
$\mathbf{\Delta Z}_0$	vector with electrical description of zero absolute load
$\mathbf{\Delta Z}_k$	difference between vector $\mathbf{Z}_k$ and vector $\mathbf{N}$
$\Delta Z_{i,0}$	zero output $\equiv$ electrical description of zero absolute load
$\Delta Z_{i,k}$	difference between zero load output of load series and natural zero
$\delta\mathbf{F}$	vector with the load change; vector with the tare load change
$\delta\mathbf{F'}$	matrix with tare load changes
δF_k	tare load change of a load series
ε	relative machine precision
η	data point index; number of terms (excluding intercept)

$\eta_0,\ \eta_1,\ \ldots$	regression coefficients
Θ	output threshold; load iteration tolerance
ϑ	term index; x–coordinate of the balance moment center
Λ	bi–directional part of output; machine–precision–dependent threshold
λ	maximum number of regression model terms (including intercept)
$\lambda_0,\ \lambda_1,\ \ldots$	regression coefficients
λ_j	characteristic length scale of load with index j
λ_φ	auxiliary variable
μ	load index; output index; load series index; tare load iteration step
$\mu_0,\ \mu_1,\ \ldots$	regression coefficients
μ_φ	multivariate regression model of a balance load component
ν	data point index
$\nu_0,\ \nu_1,\ \ldots$	regression coefficients
ξ	index; multiplier; threshold; small angle describing a misalignment
$\xi_0,\ \xi_1,\ \ldots$	regression coefficients
ξ_ψ	multivariate regression model of a bridge output difference
σ_ψ	total number of terms of a regression model term group
$\sigma(\nu)$	transformation between load series index k and point index ν
Υ_i	capacity–dependent threshold $\equiv$ *Math Model Selection Threshold*
Φ	test metric for linear or near–linear dependency test
φ	load component index; data point index
$\varphi(j,k)$	term of a double summation
Ψ	correlation matrix of regression model terms
ψ	output index; term group index; upper bound; exponent
Ω	bi–directional part of a bridge output at load capacity
Ω'	bi–directional part of a bridge output
ω	index of a regression model term; index of a regression coefficient

I. Introduction

In principle, an internal strain–gage balance is designed to measure the loads, i.e., the forces and moments that act on a test article during a wind tunnel test. The loads are predicted by combining the electrical outputs of the balance bridges with a mathematical relationship that defines the connection between the loads and outputs of the balance. This mathematical relationship can be a multivariate regression model that is obtained after applying *global regression*[†] to calibration data of the balance. Ultimately, the predicted balance loads need to be described in the body axis system of the model so that they can easily be interpreted by aerodynamicists and other wind tunnel users (see, e.g., Ref. [1], pp. 12–15, or App. 3 for a discussion of the coordinate systems of a wind tunnel model). Figure 1 below shows, for example, a six–component force balance that is used for wind tunnel tests at the NASA Ames Unitary Plan Wind Tunnel.

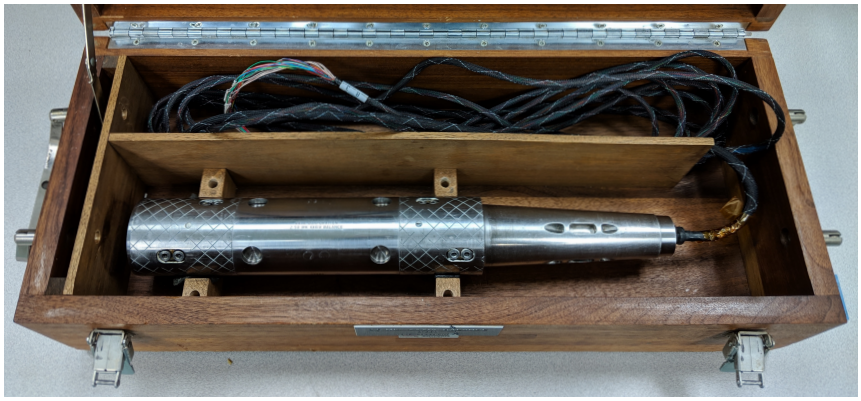

Fig. 1 The NASA 2.5 inch diameter MK34A force balance.

A variety of publications exist that describe different aspects of design, calibration, and use of internal strain–gage balances (see, e.g., Refs. [2] to [7]). The author developed a novel description of a strain–gage balance during the past few years that can be used to explain certain fundamental aspects of the balance load prediction process (for more details see Refs. [8] & [9]). His description uses the concepts of load state, load space, and output space in order to address questions related to (i) the selection of variables that best describe the load state of a balance and (ii) the uniqueness of the balance load prediction process. The description also applies some fundamental ideas from mechanics in order to better define the balance load measurement problem. A primary wind tunnel balance typically measures six load components as any solid object in three–dimensional space can experience a maximum of three forces and three moments at its moment reference center. Any combination of the six loads puts the balance into a unique load state that needs to be predicted during a wind tunnel test by using the bridge output measurements.

Different descriptions of the load state of a balance can be envisioned. For example, it is possible to describe the load state in an n–dimensional load space if the chosen balance

[†] The term *global regression* indicates that a single least squares fit is used to calculate the coefficients of a multivariate regression model of balance calibration data.

is an n–component balance. The variables defining the load space are, for example, the normal force, side force, axial force, pitching moment, yawing moment, and rolling moment if loads of a six–component single–piece balance are described in direct–read format (see App. 4 for a description of different balance load format choices). Similarly, the variables defining the load space are the forward & aft normal force, the forward & aft side force, the axial force, and the rolling moment if the loads of a six–component force balance are described in force balance format.

It is also possible to describe the load state of the balance in an n–dimensional output space. In that case, the bridge output measurements of the balance replace the load measurements. However, this electrical description of the load state is only unique if the temperature of the balance remains constant. The temperature is a state variable as far as the description of the physical behavior of the balance is concerned. Therefore, it must be introduced as an additional variable in both the load space and the output space descriptions if the temperature of the balance does not remain constant during use.

In theory, the description of the load state of a balance in the load space must be equivalent to the description of the same load state in the output space. It is like describing something in two different languages. Therefore, an analyst needs to find a mathematical relationship between the two descriptions so that the balance loads on a wind tunnel model can be predicted from the measured electrical outputs of the balance bridges. This relationship is typically obtained after applying *global regression* analysis to a balance calibration data set that describes different load states of the balance. Figure 2 below

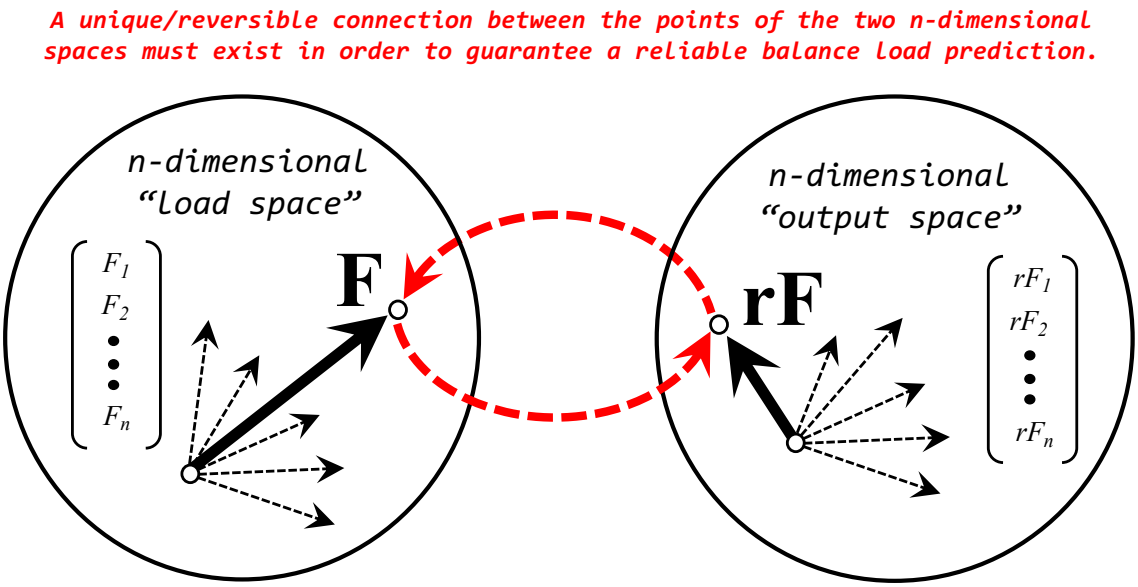

Fig. 2 Load & output space definitions for an n–component balance assuming that the balance temperature is constant.

shows the connection between load space and output space for an n–component balance assuming that the balance temperature is constant. The symbols F_1, F_2, ..., F_n are

the individual components of the load vector **F** of the balance. Similarly, the symbols $rF_1,\ rF_2,\ \ldots,\ rF_n$ represent the individual components of the bridge output vector **rF** of the balance. It is important to point out that the balance must be designed such that a unique, i.e., reversible connection between the points of the two spaces exists. A reliable load prediction process can only be constructed from balance calibration data if the balance satisfies this fundamental requirement.

An analyst can expect that the standard deviation of the differences between applied and predicted calibration loads, i.e., the standard deviation of the load residuals of a six–component balance should be on the order of 0.10 % of the capacity of a load component. This empirical threshold for the evaluation of either the regression model of a load component or the load prediction process is widely used in the aerospace testing community. The threshold of 0.10 % for the standard deviation also means that approximately 98.8 % of all load residuals should be within ±0.25 % of the capacity of the load component if the residuals follow a normal distribution (percentages are taken from a table of two–tailed Gaussian probabilities). Therefore, analysts often use the threshold of 0.25 % of capacity for the assessment of the absolute value of the load residual of an individual calibration data point. These two important thresholds are summarized for reference below.

Expected Load Prediction Accuracy

standard deviation of all calibration load residuals	$\leq$	0.10 % *of load capacity*
absolute value of the load residual of an individual calibration data point	$\leq$	0.25 % *of load capacity*

The accuracy expectations described in the previous paragraph can only be achieved if the calibration experiment is properly designed and limitations of the chosen data analysis method are understood. In addition, data formats of both the calibration loads and the electrical outputs of the balance bridges are important choices that also influence the overall accuracy of the regression model of the calibration data (load format choices are discussed in App. 4; output format choices are discussed in App. 6 and Ref. [10]). Finally, it may be necessary to apply tare corrections to the calibration loads so that all loads are described relative to the common datum of zero absolute load (algorithms for the calculation of the tare corrections can be found in App. 12, App. 13, Ref. [7], and Ref. [11]).

Characteristics of the load prediction equations also influence the accuracy of the predicted loads. Two fundamentally different methods, i.e., the *Non–Iterative Method* and the *Iterative Method* are used in the aerospace testing community for the development of the load prediction equations. They are the result of a historical evolution that started in the 1950s (see also App. 29). The *Non–Iterative Method* directly fits tare corrected

calibration loads of the balance as a function of the bridge outputs and other variables (see App. 9 and Ref. [12]). The *Iterative Method*, on the other hand, first fits the outputs of each balance bridge as a function of the tare corrected calibration loads (see App. 10 and Refs. [7], [12]). Afterwards, a load iteration equation is constructed from the regression models of the bridge outputs so that loads can be predicted from outputs during a wind tunnel test. Experience showed that both load prediction methods are equally accurate as long as (i) the regression models of the data use similar combinations of regression model terms and (ii) the chosen regression models do not have hidden linear or near–linear dependencies. Typical regression model term choices for the description of balance calibration data characteristics are given in Table 9–1 (App. 9) and Table 10–1 (App. 10). In addition, the detection of unwanted linear or near–linear dependencies in regression models of multivariate balance data is discussed in App. 17 and App. 18. Connections between the load prediction equations of the *Non–Iterative* and *Iterative Method* exist. They are illustrated in App. 27 with calibration data from a one–component load cell.

Some data analysis characteristics are specifically related to the *Iterative Method*. They need to be considered when the regression analysis of balance calibration data is performed. For example, the use of the temperature or the temperature difference in connection with the *Iterative Method* may require the use of the temperature as both an independent and dependent variable if the temperature is directly used in the regression model of the balance calibration data (see Ref. [13]). Similarly, the existence of the primary sensitivities of the balance bridges depends on the load format choice. Unfortunately, undefined primary sensitivities can negatively influence the convergence behavior of one of the two possible load iteration equations that the *Iterative Method* uses (see Ref. [14]).

It is recommended to assess the convergence of a load iteration equation within the use envelope that a balance will experience during a wind tunnel test. An improved convergence test was developed for this purpose. It is described in App. 11. The improved test was derived in order to correct an analytical error that is contained in the original version of the test (Ref. [63]). The error first surfaced during the application of the original test to the iteration equation of a semi–span balance. This balance had load capacities that differed by several orders of magnitude (for more details see Ref. [15], pp. 9–10).

Highly asymmetric calibration load schedule designs can also have a negative impact on the numerical estimate of the primary sensitivity of a balance bridge if *global regression* is used to analyze balance calibration data. Better estimates are often obtained if a weighted least squares fit is applied to the calibration data (see Refs. [16], [17]).

Balance load prediction methods for five–component semi–span balances and three–component auxiliary balances are very similar to methods used for six–component balances. Nevertheless, some differences exist between these balance types that need to be understood (see also App. 15 and Refs. [18] & [19]).

The author studied a wide variety of methods that apply *global regression* during the analysis of strain–gage balance calibration data (see Refs. [20] to [32]). Some of these

investigations lead to the development of two regression model term search algorithms (see Refs. [20] to [27]). These algorithms simplify the regression analysis task as individual terms of a multivariate regression model of the balance data no longer have to be selected by using an analyst's subject matter knowledge. The regression model term selection for balances with bi–directional bridge output characteristics was also investigated (see Refs. [33] to [35]). Temperature effects during the balance load prediction and required additional calibration experiments were also studied (see Refs. [36] to [39]). In addition, problems resulting from the use of flow–through balances were also reviewed (see Ref. [40]).

Four important ideas were originally suggested and/or developed by *R. Galway* of NRC Canada that greatly improved description and analysis of balance calibration data. First, *Galway* recognized the many benefits of applying the *matrix solution*[†] of the least squares problem to balance calibration data (Ref. [6], p. 13, Eq. (36)). He also understood the advantage of the use of the absolute value function in regression models of data from balances with bi–directional outputs and extended the idea to higher order terms (Ref. [6], pp. 21–23; Ref. [79], p. 5). Furthermore, he recommended the use of the natural zero as the global datum for the electrical output of a balance bridge (Ref. [6], p. 27; *Galway* uses the synonym *buoyant component offset* in that context). Finally, *Galway* developed the tare load iteration process. His algorithm was first published in 1999 (Ref. [80]). Afterwards, AIAA's Internal Balance Technology Working Group adopted the algorithm for use with the *Iterative Method* (see 1st edition of Ref. [7]). *Galway's* four ideas must be implemented in a balance data analysis tool if an analyst wants to systematically apply *global regression* to data from all known balance types and calibration load schedule designs.

The design of the calibration experiment has a significant influence on the load prediction accuracy that can be achieved with a strain–gage balance. In theory, a calibration data set should be collected that best describes the expected physical behavior of the balance. The calibration experiment is sometimes structured such that a specific regression model of the data is supported. Important research was done in that area by *Parker et al.* at NASA Langley Research Center (Refs. [41] to [46]). In addition, load schedules for balance calibration machines and related topics were investigated at the NASA Ames Balance Calibration Laboratory (Refs. [47] to [50]).

Either *Guarino's Method* or *sequential regression* may be used instead of *global regression* for the determination of the coefficients of the regression models of the outputs that the *Iterative Method* needs. Detailed discussions of these two alternate analysis techniques can be found in the literature (see Refs. [51], [52]). Both techniques are variations of *Cook's Method* (see Ref. [5] or App. 28). Therefore, they can only be applied to balance calibration data sets that satisfy very specific load schedule design requirements.

Other topics related to both calibration and use of strain–gage balances were also studied at the NASA Ames Balance Calibration Laboratory (Refs. [53] to [62]). For example,

[†] The *matrix solution* is an application of the *Moore-Penrose* pseudo inverse that British physicist and Nobel Prize laureate *R. Penrose* first proposed in 1956 (Refs. [77], [78]).

new thresholds for the evaluation of load and output residuals of balance calibration data were developed that take built–in design limitations of the balance into account (Refs. [53], [54]). An algorithm was also defined that uses *global regression* analysis for the prediction of wind tunnel model weight corrections (Ref. [55]). In addition, a conservative pre–test estimate of the precision error of the drag coefficient of a wind tunnel model was developed that uses balance characteristics as input (Refs. [56], [57]). Finally, tools were prepared to more easily compare the use envelope of a balance during a wind tunnel test with the load schedule that was applied during its calibration (Ref. [58]).

The current document provides an overview of the most important algorithms and processes that were either developed or refined during the past sixteen years at the NASA Ames Balance Calibration Laboratory. Most of these algorithms and processes were implemented and verified using NASA's BALFIT software tool that may be used for the regression analysis of multivariate balance data (see Refs. [74] to [76]).

It is always a challenge to describe complex processes within the body of the text of a document without overwhelming the reader with technical details. Therefore, the author decided to separate the presentation of technical details from the body of the text. Consequently, the document is structured such that ideas and concepts are primarily presented in the body of the text. These chapters are followed by detailed discussions of calibration data analysis results that were obtained for three different balance designs. Finally, balance terminology, statistical metrics, and more advanced technical details are described in the appendices of the document. Each appendix is more or less written as a stand–alone section so that the reader can more easily follow the descriptions. The contents of about half of the appendices is presented using basic concepts from mathematics. The contents of App. 9 to 14 and App. 17 to 25 requires a more advanced background in linear algebra and multivariate regression analysis in order to be understood.

The body of the text consists of eleven chapters. The second chapter discusses fundamental concepts and assumptions that are needed for a better understanding of the balance load prediction process. Afterwards, the balance data description itself is reviewed. This chapter includes discussions of the absolute load datum, the balance axis system, balance load format options, and the primary sensitivities of the balance bridges. The next chapter describes elements of the manual calibration of a six–component balance. Then, the use of the *Non–Iterative Method* and the *Iterative Method* during balance calibration data analysis and load prediction is discussed. The next chapter describes miscellaneous topics related to the use of strain–gage balances. First, the processing of balance check load data is reviewed. Afterwards, a weight assessment of individual balance parts is presented, balance temperature effects and the application of air balances are reviewed, and the use of three–component moment balances is discussed. The subsequent three chapters discuss calibration data analysis results for three typical balance designs. Finally, the most important observations, conclusions, and recommendations are summarized.

II. Fundamental Concepts

Balance Component Parts

A strain–gage balance is used during a wind tunnel test to measure loads, i.e., forces and moments, that act in the body axis system of a test article. The design of a strain–gage balance itself is a compromise. It is influenced by (i) the chosen number of load components, (ii) the expected load magnitudes on the model, (iii) load prediction accuracy requirements, and (iv) fabrication & model installation constraints. The total number of independently measured load components can vary from one to six. A set of six load components is the theoretical maximum as the resultant force and moment vectors at the balance moment center of a test article can only have a maximum of three independent components each in three–dimensional space.

A six–component balance is typically used in wind tunnel testing to measure the six primary load components on a model. Three basic design variations of this balance type exist: direct–read balance, force balance, and moment balance (see, e.g., Ref. [7] or App. 4 for a description of different balance types). In theory, each balance type is designed such that the internal strain caused by six independently applied load components, i.e., either three forces and three moments, or, five forces and one moment, or, five moments and one force, can be related to six independently measured bridge outputs. It must be possible to uniquely map balance loads that are described as a point in a six–dimensional load space to a set of measured bridge outputs that are described as a point in a six–dimensional output space.

Figure 3 below shows a simplified description of an unloaded six–component single–piece balance. Three basic parts of the balance can be identified: (i) metric part, (ii) non–

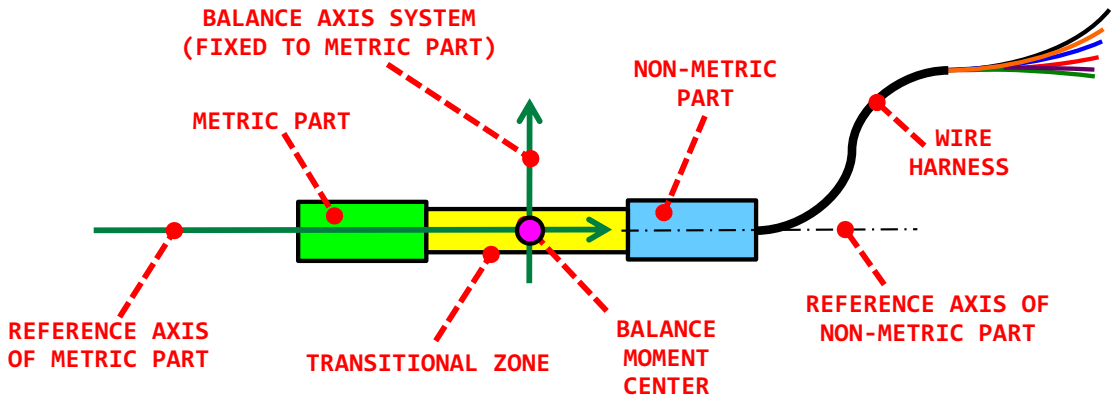

Fig. 3 Simplified description of an unloaded six–component single–piece balance.

metric part, and (iii) transitional zone. The metric and non–metric parts are assumed to be rigid. The metric part establishes the connection between the balance and either the wind tunnel model or the calibration body. It defines the balance axis system as it is the rigid part of the balance that interfaces with the model. The metric part should

also be used as a reference for the description of the balance moment center. This choice guarantees that the moment center's location relative to the body axis system of the model is fixed as the metric part is assumed to be rigid. The non–metric part, on the other hand, attaches the balance to the model support system. It is the location where bridge wire sets are assembled in a wire harness so that the electrical outputs of the bridges can be sent to a data acquisition system. It is also indicated in Fig. 3 above that the reference axes of the metric and non–metric parts coincide if the balance is unloaded.

The transitional zone is the physical interface between metric and non–metric part where flexures, gages, and Wheatstone bridges are located. The transitional zone elastically deforms under load. Figure 4 below shows the description of a loaded six–component

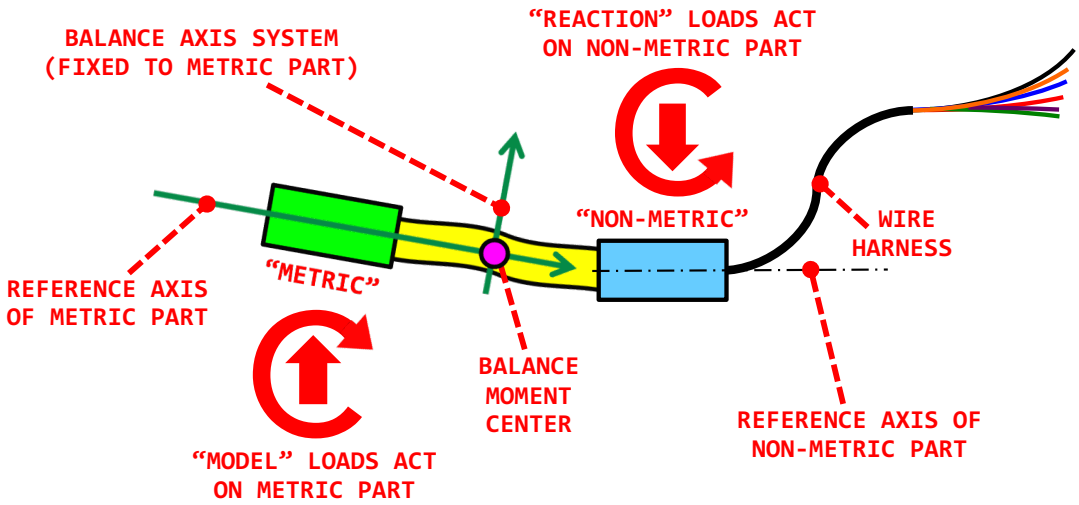

Fig. 4 Simplified description of a loaded six–component single–piece balance.

single–piece balance. Model loads act on the metric part of the balance. Reaction loads, on the other hand, act on the non–metric part. The reaction loads are equal in magnitude but opposite in sign to the model loads. It can also be seen in Fig. 4 that the reference axes of the metric and non–metric parts of the balance no longer coincide if the balance is in a loaded state.

The simplified descriptions of a strain–gage balance shown in Fig. 3 and Fig. 4 above are very general in nature. They can be applied to all balance types that use strain gages to measure the elastic deformation of component parts of a loaded balance. Figure 5 below shows, for example, how the descriptions of Fig. 3 can be applied to a six–component multi–piece balance that has a metric outer sleeve instead of a metric end and a non–metric inner rod instead of a non–metric end. Two widely used multi–piece balance designs have a metric outer sleeve. One design is called a Task/Able balance. It is manufactured by Aerophysics Research Instruments, Corona, California. This balance design has the unique characteristic that four of its six bridge outputs are bi–directional when plotted versus the related primary bridge loads (see the discussion of this characteristic in App. 7).

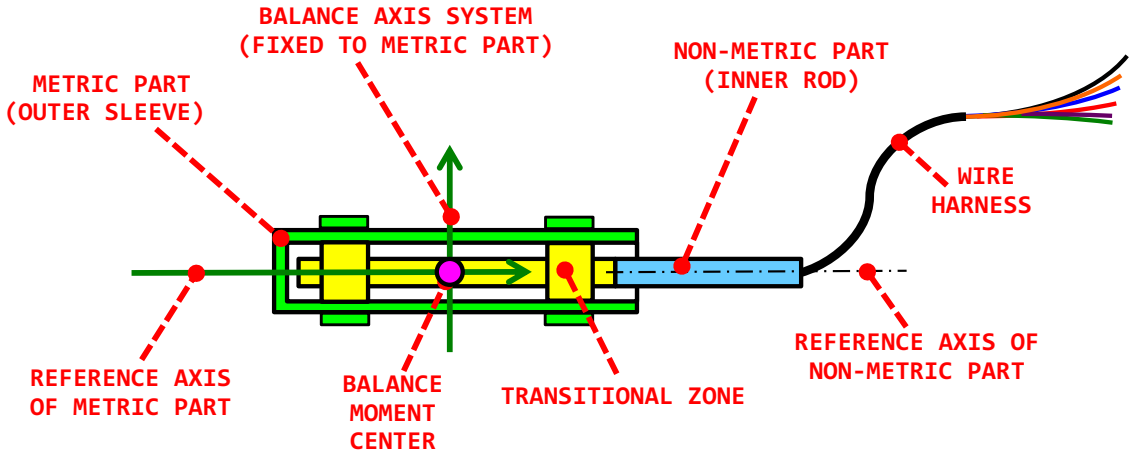

Fig. 5 Simplified description of an unloaded six–component multi–piece balance.

A HiCap balance is another balance design with a metric outer sleeve. It is manufactured by Calspan Force Measurement Systems, San Diego, California. Its bridge outputs do not have bi–directional characteristics. Figure 6 below shows the description of a loaded six–component multi–piece balance. Again, as it was the case for a single–piece

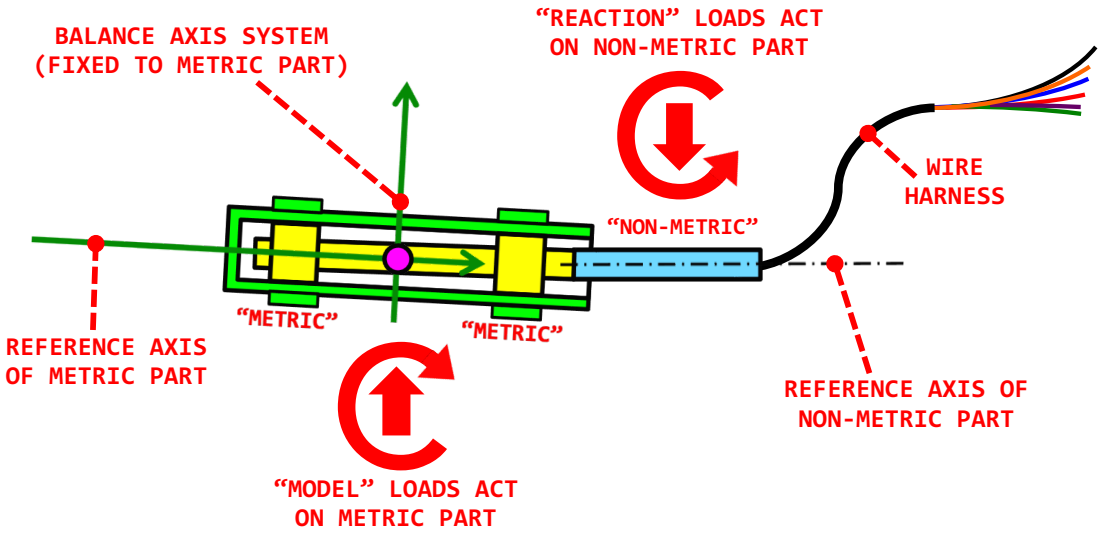

Fig. 6 Simplified description of a loaded six–component multi–piece balance.

balance, model loads act on the metric part and reaction loads act on the non–metric part. The reaction loads are equal in magnitude but opposite in sign to the model loads.

A universally applicable control volume analysis of the inputs and outputs of a strain–gage balance is introduced in the next section to better support the hypothesis that the maximum number of applied load components and the number of independently measured bridge outputs of a strain–gage balance must always match if the balance temperature

is assumed to be constant. This hypothesis is the fundamental assumption that makes it possible to use a unique set of electrical output measurements for the prediction of a unique set of balance loads (see also Refs. [8], [9] for additional explanations).

Control Volume Analysis of a Strain–Gage Balance

The uniqueness of balance load predictions can be linked to the hypothesis that the maximum number of independently applied load components of a balance must always match the number of bridge outputs that are independently being measured. It is not immediately obvious that this statement is valid for all balance types because, for example, temperature effects or bellows pressures of an air balance also influence the electrical outputs of a balance. A control volume analysis may be applied to a balance to better illustrate the connection between the number of load components and bridge outputs.

By definition, a control volume is a physical space that has precisely defined boundaries. A strain–gage balance may be placed inside of a control volume. Figure 7 below shows results of an analysis of the control volume of a balance. The chosen generic description of the balance is applicable to most balance types that are used for the measurement of loads during a wind tunnel test. The analysis of the inputs and outputs of the control

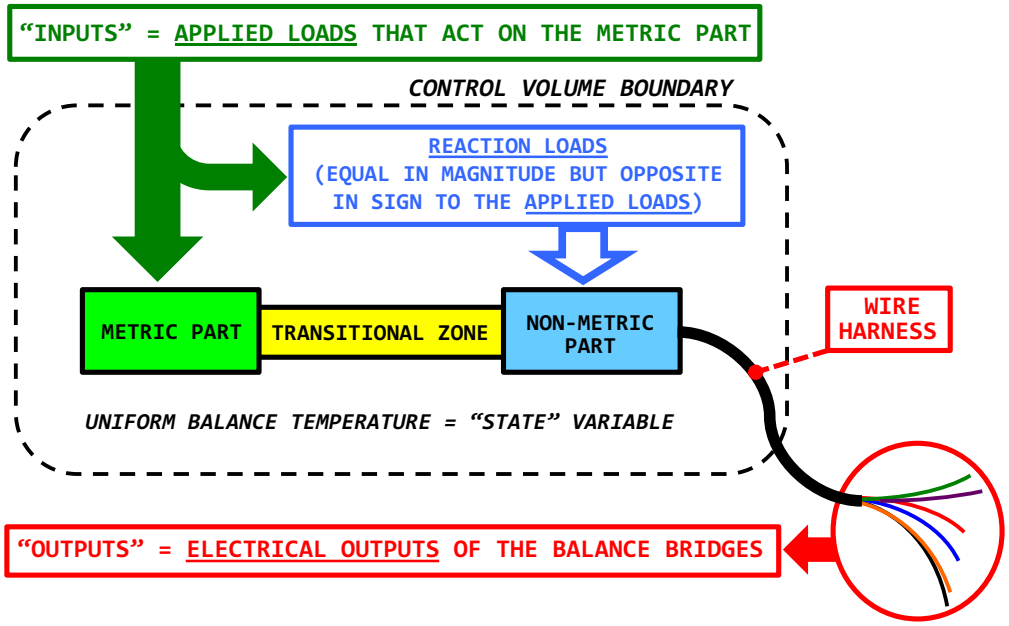

Fig. 7 Results of a control volume analysis of a strain–gage balance.

volume makes it possible to systematically identify and separate all variables that either influence or characterize the load state of a strain–gage balance. These variables represent information that flows across the boundaries or exists inside of the control volume. Three types of variables can be identified: (i) input variables, (ii) output variables, and (iii) state variables. Information crosses the control volume boundaries if it is described by either input or output variables. On the other hand, information represented by state variables describes conditions inside of the control volume.

It is helpful to discuss some results of the control volume analysis in more detail. The input variables of the control volume are the loads, i.e., the forces and moments that act on the metric support. The metric support is either the calibration body or the part of the wind tunnel model that is rigidly attached to the metric part of the balance. The output variables of the control volume are the electrical signals of the Wheatstone bridges that are bundled together in a wire harness. The uniform balance temperature is an example of a state variable that influences the bridge output measurements.

Now, let us assume that a specific load combination is applied to the balance while keeping all state variables constant. Then, it is reasonable to expect that the information leaving the control volume cannot be greater than the information entering the control volume. The total amount of information entering the control volume is connected to the number of independently applied load components that act on the balance. Similarly, the total amount of information leaving the control volume is connected to the number of independently measured bridge outputs that exit through the wire harness. Furthermore, it is logical to assume that a unique and reversible load prediction can only be guaranteed if the dimensions of the input and output variable sets of the control volume match. It is concluded from these assumptions and observations that nothing can be gained if the number of bridge output measurements exceeds the maximum number of applied load components. The maximum number of applied load components simply limits the number of independent bridge output measurements that a balance can have. This statement can be expressed as a universal balance design requirement if linear combinations of bridge outputs, i.e., sums and differences of bridge outputs are included in the description:

Balance Design Requirement

The maximum number of applied load components of a balance must equal the total number of bridge outputs (or linear combinations of bridge outputs) that are independently measured.

Conclusions drawn in the previous paragraph can easily be put into a practical context. For example, let us assume that a balance measures four bridge outputs (rF_1, rF_2, rF_3, rF_4). Let us also assume that only the normal force (NF), the axial force (AF), and the pitching moment (PM) were independently applied during its calibration. Consequently, the four bridge outputs can only be a function of the three applied load components. In addition, according to the *General Theorem on the Inversion of Transformations* (for more detail see Ref. [73], pp. 261–277), the three load components may be inverted implicitly to give $NF = \mathcal{F}(rF_1, rF_2, rF_3)$, $AF = \mathcal{G}(rF_1, rF_2, rF_3)$, and $PM = \mathcal{H}(rF_1, rF_2, rF_3)$. Therefore, the fourth bridge output rF_4 must be a function of rF_1, rF_2, and rF_3 because (i) the output rF_4 can only be a function of the three load components that were independently applied during the balance calibration and (ii) the applied load components themselves can be expressed as functions of rF_1, rF_2, and rF_3.

Load State, Load Space, Output Space

The correct selection of the physical location of flexures and bridges on the balance relative to the expected test article loads is critical as far as the existence of a unique mapping between loads and bridge outputs is concerned. In this context, the term unique mapping means that one point located in the load space of the balance only maps to one point in the output space of the balance (and vice versa). It also means that two equivalent unique descriptions of any load state of the balance must exist. One description is located in the load space. A second alternate description is located in the output space. Then, assuming it is possible to define a unique, i.e., reversible mathematical relationship between points located in the load space and points located in the output space, measurements recorded in the output space may be used for the prediction of the corresponding load set in the load space. Figure 8 below shows the connection between the load space and the output space for a six–component balance assuming that all state variables are constant. The mathematical relationship between the two spaces, i.e., between the load set $F_1,\ F_2,\ \ldots,\ F_6$

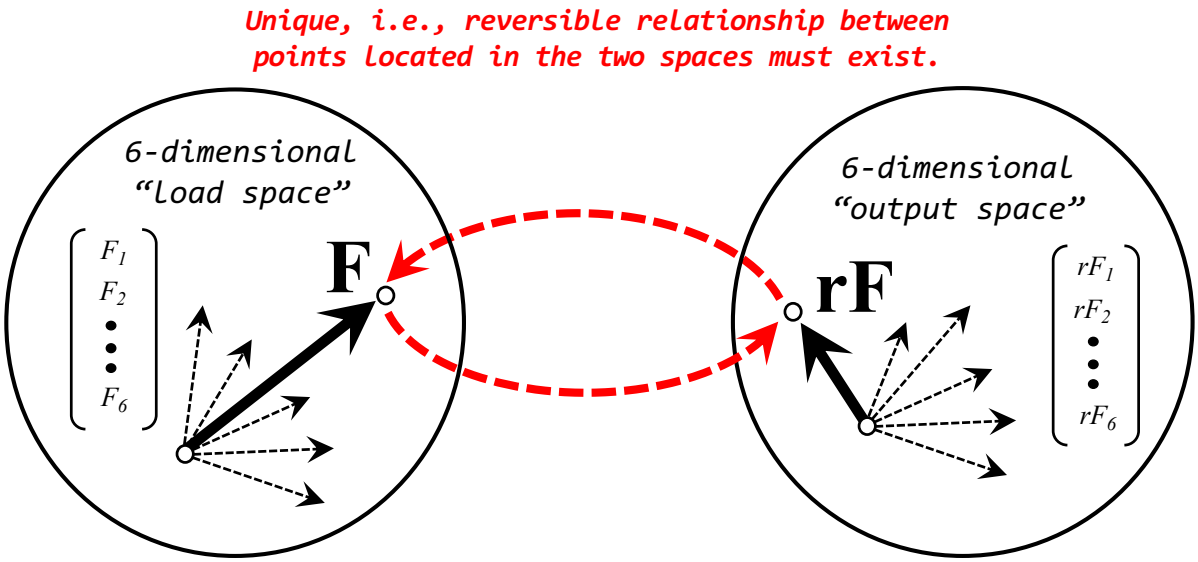

Fig. 8 Load & output space definitions for a six–component balance.

and the output set $rF_1,\ rF_2,\ \ldots,\ rF_6$, is traditionally obtained from a balance calibration data set. This data set is processed by using multivariate regression analysis in combination with either the *Non–Iterative Method* or the *Iterative Method* (see App. 9 and App. 10 for more details). The final balance load prediction accuracy highly depends on (i) the calibration load schedule design characteristics and (ii) the requirement that the chosen multivariate regression models of the balance calibration data must not have any unwanted linear or near–linear dependencies (see App. 17 and App. 18 for a detailed discussion of the detection of linear and near–linear dependencies).

So far, it was assumed that all state variables influencing the balance bridge outputs are constant. The impact of varying state variables on the balance load prediction is investigated in more detail in the next section.

State Variables

Strain–gage balance applications exist when varying state variables have a significant impact on the bridge output measurements. These variables need to be included in the development of a balance load prediction process. One example for the influence of a state variable on the load prediction is the use of a semi–span balance in a pressurized wind tunnel. In that case, assuming that the semi–span balance is not placed inside a temperature–controlled enclosure, any change of the uniform balance temperature influences both the bridge outputs and the balance load prediction. Consequently, the balance temperature change must be described and introduced as a state variable.

Similarly, an air balance is often used with a propulsion simulator that is attached to a wind tunnel model. Then, high pressure air flows across the control volume boundary. By design, the air supply line of an air balance bridges the metric and non–metric parts. The load path from metric to non–metric part may change whenever supply line pressure changes occur. Consequently, the bellows pressure change of the air balance may be used as a state variable because (i) it describes internal pressure effects on both balance geometry and bridge outputs and (ii) it can easily be measured. On the other hand, the mass flow rate through an air balance is directly linked to additional external loads that act on a wind tunnel model. These additional external loads, similar to the loads associated with the model's weight, are always a part of the resultant loads that act on the model during a wind tunnel test. Therefore, the mass flow rate can be ignored during the calibration of an air balance as long as it doesn't cause internal elastic deformations of the balance.

State variables have another important characteristic: they are neither inputs nor outputs of the control volume. Instead, they describe the physical state of the balance while (i) loads are being applied on the metric support and (ii) bridge outputs are being measured at the flexures. This conclusion can be summarized as follows:

State Variable Characteristics

State variables of the balance, e.g., temperature or pressure differences, need to accompany the description of <u>both</u> input and output variable sets because inputs (loads) were applied and outputs (bridge outputs) were measured while the given state variables had specific values.

It is mentioned above that a state variable must accompany the description of both input and output variable sets if its value does not remain constant during the use of the

balance. Consequently, the state variable has to be introduced as an additional dimension in both the load space and the output space of the balance. Figure 9 below shows the connection between the expanded load and output spaces for a six–component balance if a single state variable, e.g., the temperature difference ΔT, is included as the seventh

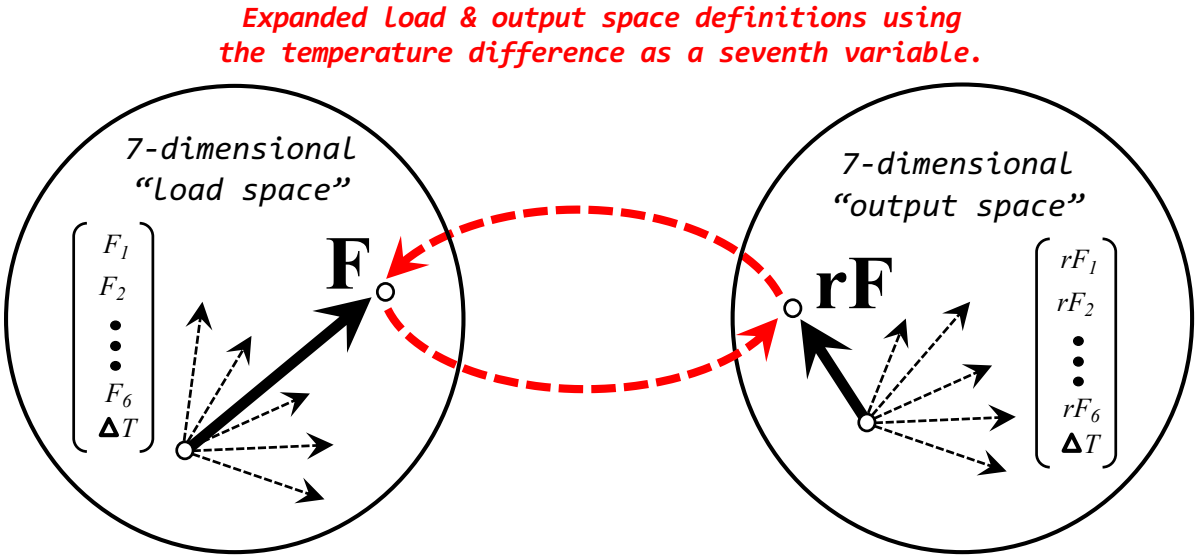

Fig. 9 Expanded load & output space definitions for a six–component balance.

independent variable in the definitions of the two spaces. Both the load space and the output space are extended to seven–dimensional spaces so that a unique temperature–dependent load prediction becomes possible.

Uniqueness Test

It is possible to objectively test if the load component set of the load space and the bridge output set of the output space have the same number of independent variables (see also Refs. [8], [9]). The test assesses the linear independence of the load space and the output space separately by computing the maximum *Variance Inflation Factor* (VIF) of simple linear math models of the balance calibration data (see App. 18 for a discussion of the *Variance Inflation Factor*).

First, the load component set of the balance calibration data is tested for linear independence by computing the maximum VIF of a math model of the calibration data that is constructed from the linear terms defined by each load component. Afterwards, the bridge output set of the balance calibration data is tested for linear independence by computing the maximum VIF of a math model that is constructed from the linear terms defined by each bridge output. Now, the maximum VIF of each set is compared with recommended thresholds from the literature in order to decide if the set is linearly independent or dependent. The test considers a load or bridge output set to be linearly independent if its VIF maximum is less than the conservative threshold of 5 (threshold is

taken from Ref. [69], p. 658). Similarly, the test considers a load or bridge output set to be linearly dependent if its VIF maximum exceeds the threshold of 50. The uniqueness test uses the threshold values of 5 and 50 instead of the often recommended single threshold value of 10. This choice was made because the use of 5 instead of 10 makes the test for linear independence more reliable. Likewise, the use of 50 instead of 10 makes the test for linear dependence more reliable.

Table 1 below lists four cases that are of special interest as far as the interpretation of the uniqueness test results are concerned. Case 1 describes the situation when the maximum VIF of both the load component and bridge output set is less than the literature recommended threshold of 5. This result means that a highly unique mapping between the load component set and the bridge output set can be constructed from the calibration

Table 1: List of four typical results of the uniqueness test.

Case	Load Component Set	Bridge Output Set	Comments
1	$VIF_{max} < 5$	$VIF_{max} < 5$	linearly independent loads & outputs
2	$VIF_{max} > 50$	$VIF_{max} > 50$	experimental design issue
3	$VIF_{max} > 50$	$VIF_{max} < 5$	theoretically impossible result
4	$VIF_{max} < 5$	$VIF_{max} > 50$	linearly dependent bridge outputs

data. On the other hand, it is observed for Case 2 that the maximum VIF of both sets is greater than 50. This observation may indicate a potential experimental design issue that should be addressed because linear dependencies of the load component set are directly reflected in linear dependencies of the bridge output set. Case 3 describes a situation when the maximum VIF of the load component set exceeds 50 while, at the same time, the maximum VIF of the bridge output set is smaller than 5. This situation is theoretically impossible because, based on the control volume analysis of the inputs and outputs of a strain–gage balance, the measurements recorded by the bridge output set cannot have more independent information than the applied load component set. Finally, Case 4 describes a situation when the maximum VIF of the load component set is smaller than 5 while, at the same time, the maximum VIF of the bridge output set is greater than 50. This observation is an indication that the bridge output set may be linearly dependent. Therefore, the balance load predictions may not be very reliable because a reversible mapping between load space and output space may not exist.

It is important to point out that the suggested uniqueness test does not require a least squares fit of the balance calibration data. Only VIFs are computed by using either loads or bridge outputs for the definition of the regressors of a simple linear math model of the data. This simple model does not have any absolute value, quadratic, cubic, or cross–product terms. The VIF was selected as a metric for the uniqueness test because it has the ability to identify both linear and near–linear dependencies between regressors.

Tare Loads

It was mentioned earlier that each point of a multi–dimensional load space represents a specific load state of a balance. Points in the load space are described by using a *Cartesian* coordinate system. The origin of this coordinate system is the load datum of zero absolute load. Consequently, it is important to describe all load states of a balance relative to this common load datum whenever (i) a calibration data set is used to populate the load space and (ii) global regression is applied during the analysis.

The description of the load states is often complicated by the fact that the calibration experiment needs to be broken up into individual load series. Then, characteristic load states can be established that describe the expected physical behavior of the balance. The load states result from either the application of a single load component or from the application of load combinations. Different sets of hardware are used for the application of the loads during a calibration. They may consist of a calibration body, rods, weight pans, moment arms, knife edges, and flexures if gravity weights are used for the load application. The combined weight of the calibration hardware and the metric part of the balance is responsible for hidden loads that may change from load series to load series. They need to be included in any precise description of the load state of the balance. Only in this case, all loads are described relative to the common load datum of zero absolute load.

The determination of tare loads, i.e., of loads resulting from the combined weight of the calibration hardware and the metric part of the balance can become very complex. In theory, it requires (i) the weighing of each calibration hardware part and (ii) the determination of the distance between a part's center of gravity and the balance moment center. In addition, loads resulting from the weight of the metric part must be included. They have to be estimated using the metric part's volume and material density. All these difficulties can be avoided if a tare load iteration algorithm is applied during the balance calibration data analysis. *Galway* of NRC Canada developed key elements of this iterative process in the 1970s. His algorithm first appeared in the open literature in 1999 (Ref. [80]). It is also described in AIAA's Recommended Practice document on strain–gage balances (Ref. [7]). The algorithm uses the electrical outputs resulting from the combined weight of the calibration hardware and the metric part of the balance and preliminary estimates of the load prediction equations for the determination of the tare loads (see App. 12 and App. 13 for more details). Afterwards, tare load estimates are added to the applied loads before the final analysis of the calibration data is performed and the load prediction equations are generated. This final step guarantees that the loads of all individual load states of the balance are systematically described relative to the common load datum of zero absolute load.

Load Prediction Process

So far, fundamental concepts were described and reviewed that benefit a better understanding of the inputs and outputs of a strain–gage balance. It remains to list the most important steps that need to be taken in order to successfully develop the balance load

prediction equations. The steps can be described as follows:

Step 1 – Balance Selection
Step 2 – Calibration Load Schedule Definition
Step 3 – Calibration Experiment Execution
Step 4 – Calibration Data Analysis
Step 5 – Load Prediction Equation Implementation

Choices made during the execution of each step may have an influence on the final load prediction accuracy that can be achieved. Therefore, the five steps need to be discussed in more detail.

Step 1 – Balance Selection: First, a balance needs to be selected for the chosen wind tunnel model. The selection influences the overall accuracy of the load prediction during a wind tunnel test as the capacities of the balance load components need to be closely matched to load magnitudes that the wind tunnel model will experience. Load prediction accuracy and load resolution are directly related to the primary sensitivities of the balance bridges as long as temperature and hysteresis effects are kept under control. In fact, the primary sensitivities are built–in physical constants of the balance.

In theory, the primary sensitivity is defined as the first derivative of a primary bridge output with respect to the related primary load. Numerical estimates of the primary bridge sensitivities are typically obtained from the regression coefficients of balance calibration data. The following rule of thumb can often be applied:

Primary Bridge Sensitivity (Rule of Thumb)

The higher the primary bridge sensitivity of a balance bridge is the better the resolution of the predicted primary load will be as long as temperature and hysteresis effects are controlled.

It was mentioned above that the primary bridge sensitivity is directly connected to the load resolution that a balance can achieve. Therefore, load prediction accuracy during a wind tunnel test can be maximized if a balance experiences loads across the entire load range and not just, say, within the first 20 % to 30 % of its range.

Step 2 – Calibration Load Schedule Definition: In the next step, the calibration load schedule needs to be defined. In principle, loads should to be applied during the calibration that best capture the physical behavior of the balance. Some analysts prefer to choose a load schedule that supports a specific regression model of the data. These load schedule design goals cannot always be achieved as the ability to apply certain loads or load combinations is often dictated by (i) the calibration hardware that a calibration laboratory owns

and (ii) the load application method that is used. Consequently, the final calibration load schedule is a compromise between desired and achievable loads or load combinations.

It must not be forgotten that tare loads, i.e., load caused by the weight of the calibration equipment and the metric part of the balance, may have an influence on the calibration load schedule definition if heavy calibration hardware is needed to apply certain load combinations. Any omission of important loads or load combinations will negatively influence the accuracy of the load prediction equations as they can only predict the physical behavior of the balance that the chosen calibration load schedule describes.

Balance calibration machines are also in use in the aerospace testing community. A calibration machine has two important advantages when compared with a traditional manual calibration: (i) complex load combinations can more easily be applied; (ii) an entire calibration load schedule can be completed within a few hours. Calibration machines, however, are complex. Therefore, additional check loads may have to be recorded in a manual calibration rig to independently verify the machine calibration data.

Step 3 – Calibration Experiment Execution: The calibration experiment itself needs to be conducted after the calibration load schedule is defined. First, the natural zeros of the balance bridges need to be determined. They are the electrical representation of zero absolute load (see also App. 8). Afterwards, the load schedule has to be applied by using gravity weights, hydraulic actuators, or other techniques in combination with the available calibration hardware. The resulting loads and outputs of each calibration data point need to be recorded and stored during the load application process on a point–by–point basis. It is critical to measure the raw outputs during the calibration with the same instrumentation that was used to determine the natural zeros of the balance bridges so that instrumentation dependent bias errors can be removed during the data analysis. In addition, zero load points should be taken for each load series so that tare corrections can be computed by using a tare load iteration process. These tare loads need to be added to the applied loads so that all loads are referenced to the datum of zero absolute load. An analyst needs to pay close attention to the alignment of the applied loads during the calibration. Any hidden misalignment or other calibration data quality issue will have an immediate negative influence on the accuracy of the load prediction process.

Step 4 – Calibration Data Analysis: The balance calibration data set needs to be analyzed after completion of the calibration experiment. The goal of this analysis is the generation of load prediction equations that will be used during the wind tunnel test to predict balance loads from bridge outputs. It is important that both loads and outputs are described relative to the absolute load datum of the balance before the final analysis of the calibration data is performed and load prediction equations are generated. Therefore, a tare load iteration needs to be performed so that loads caused by the weight of the metric part of the balance and the calibration hardware are included. In addition, the author recommends to use the difference between the raw bridge outputs and the corresponding natural zeros for the final description of the electrical outputs. This choice has two advantages. First,

instrumentation dependent output shifts are removed from the data. In addition, the electrical representation of zero absolute load is zero output for all bridges.

In principle, the balance experiences a finite number of load states during its calibration that the chosen load schedule defines. Each load state can be described by using either the tare corrected loads or the electrical output differences relative to the natural zeros. Both descriptions are equivalent. It is like describing something in two different languages. Consequently, an analyst has the freedom to use the tare corrected loads as either the independent or dependent variable set during the calibration data analysis.

The load prediction equations themselves are obtained by using either the *Non–Iterative Method* or the *Iterative Method* for the analysis of the calibration data. The *Non–Iterative Method* directly fits the tare corrected calibration loads as a function of the output differences of the bridges (see App. 9 for more details). The *Iterative Method*, on the other hand, is more complicated. It first fits the output differences of the bridges as a function of the tare corrected calibration loads. Afterwards, a load iteration equation is constructed from the regression models of the outputs so that loads can be predicted from outputs during a wind tunnel test (see App. 10 for more details).

An analyst must ensure that only regression model terms supported by the balance calibration data are used in the regression model. In addition, the chosen regression models must not have any linear or near–linear dependencies (see App. 17 and App. 18 for more details). Sometimes it may be an advantage to remove insignificant terms from the regression models to suppress over–fitting of the data. These terms can be identified by either using the percent contribution of a regression model term or suitable statistical metrics (see, e.g., App. 16 for a discussion of the percent contribution). The term removal itself could be done by visual inspection or by using a regression model search algorithm (see, e.g., App. 19 or Ref. [69], pp. 640–655, for additional details).

Step 5 – Load Prediction Equation Implementation: The development of the load prediction process for a strain–gage balance is completed after the load prediction equations are implemented in the wind tunnel's data system. It is an advantage if a tunnel's data system uses a fixed format for the transfer of the load prediction equations. Then, load prediction equations from different balance types can easily be applied. It is also recommended to measure the natural zeros of the balance bridges using the tunnel's instrumentation so that (i) instrumentation dependent bias errors are removed from the output measurements and (ii) the raw outputs can be referenced to the outputs at zero absolute load. Finally, check loads may have to be applied to verify both the installation of the balance and the implementation of the load prediction equations in the tunnel's data system. At this point, the load prediction equations are ready to be used during the wind tunnel test.

III. Balance Data Description

Introduction

Loads and electrical outputs of a strain–gage balance can be described in different ways. The chosen description has an influence on both the calibration data analysis results and the load prediction characteristics during a wind tunnel test. Therefore, they need to be understood so that the best possible accuracy of the balance load prediction during a wind tunnel test can be achieved.

The description of the balance axis system, the definition of the absolute load datum of the balance, the load format, the output format, and electrical units are discussed in the following sections. Afterwards, the relationship between balance design, load format choice, and the primary sensitivities of the balance bridges is reviewed.

Axis System Definition

In general, a Cartesian coordinate system in 3–dimensional space is needed to describe the loads that act at the balance moment center. Then, balance loads can easily be transformed to loads that act at the moment center of the wind tunnel model. Loads of a six–component primary balance are typically expressed as the resolved loads, i.e., as the three forces and three moments that act at its moment center. Possible balance axis system choices and related load sign conventions are discussed in detail in App. 3. Therefore, only a few general comments are made in this section.

In theory, the balance axis system should be defined such that balance loads can easily be transformed to loads that act in the body axis system of the wind tunnel model. Consequently, it is an advantage to attach the balance axis system to the rigid part of the balance that is connected to the model. Then, simple transformations can be used to connect loads at the balance moment center to loads at the model's moment center.

Two cases must be distinguished as far as the attachment of the balance to a wind tunnel model is concerned. First, a primary six–component balance is considered. In that case, the metric part is assumed to be the rigid interface between balance and wind tunnel model. Therefore, it is reasonable to attach the balance axis system to the metric part of the balance. Sometimes, a small three–component auxiliary balance is attached to a wind tunnel model that measures loads on a subassembly (e.g., a lifting surface, a control surface, a canard, etc.). In that case, the rigid section of the non–metric part of the balance is attached to the wind tunnel model. Therefore, the balance axis system of an auxiliary balance should be attached to the rigid section of the non–metric part of the balance in order to simplify the description of balance loads in the body axis system of the wind tunnel model (see also related discussions in App. 15).

Absolute Load Datum

The purpose of a strain–gage balance is to measure loads, i.e., forces and moments, that act on a wind tunnel model. These load sets represent one possible description of the

load state of the balance in the load space (see also the discussion of the terms load state, load space, and output space in Chapter II). Each load state is represented by a point in the load space. This interpretation is possible if a Cartesian coordinate system is defined in the load space that describes each load component value on a separate coordinate system axis. Consequently, the required coordinate system has six dimensions if, for example, all loads of a six–component balance are described while keeping state variable values fixed.

The description of any coordinate system in the load space requires a coordinate system origin. By definition, all load components are zero at the origin. In other words, the origin defines the absolute load datum of the balance in the load space assuming that all state variables are constant. The absolute load datum can also be described as a hypothetical situation when the balance is in a weightless condition. This alternate description of the absolute load datum of the balance is shown in Fig. 10 below.

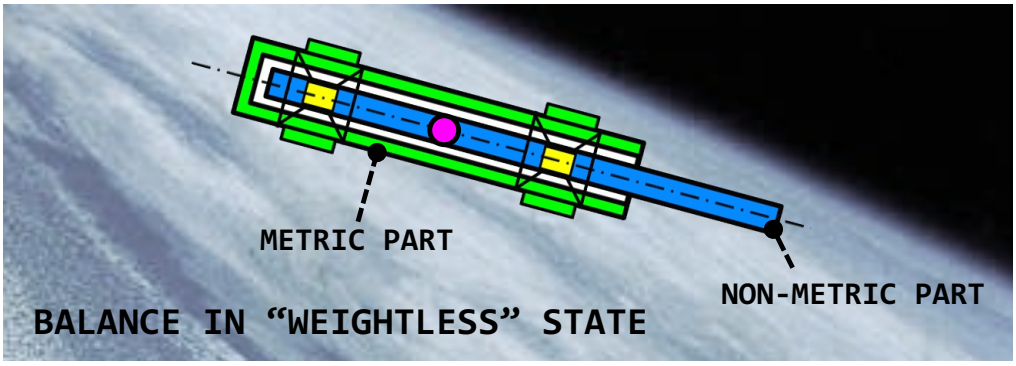

Fig. 10 Absolute load datum of a strain–gage balance.

So far, only the interpretation of the origin of the coordinate system of the load space was discussed. A similar interpretation exists for the origin of the coordinate system of the output space. In principle, the raw electrical outputs of the balance bridges at zero absolute load may be used to define the origin of the coordinate system of the output space. These raw outputs are also called the natural zeros of the balance bridges (see App. 8 for a detailed description of the natural zeros for different balance types). Two options exist that an analyst may use for the definition of the origin of the output space. They depend on the chosen format that describes the measured outputs (see App. 6 for a discussion of different bridge output format choices).

First, let us assume that the bridge output format *Raw Output* is directly used to describe the electrical outputs of a six–component balance. Then, the origin of the load space is not mapped to the origin of the output space. Instead, the point described by the vector with the natural zeros of the bridges as its components is the electrical description of zero absolute load in the output space. In other words, the origin of the output space does not describe the absolute load datum of the balance if outputs are described by using the format *Raw Output*. Figure 11 below shows the mapping of the absolute load datum of the load space to the output space if output format *Raw Output* is used. The symbols

$F_1, \ldots, F_6$ represent the six load components. The symbols $rF_1, \ldots, rF_6$ represent the raw outputs of the six balance bridges.

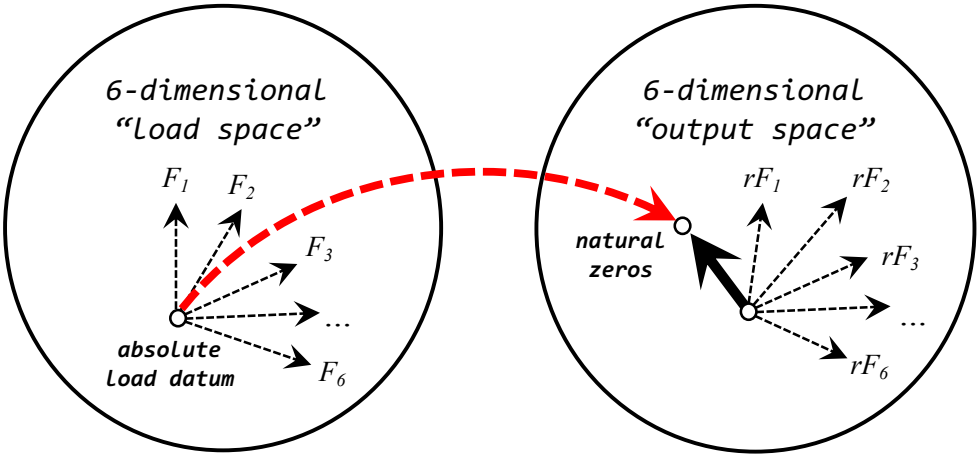

Fig. 11 Mapping of the absolute load datum if output format *Raw Output* is used.

Alternatively, let us assume that the bridge output format *Difference Type 1* is used to describe the outputs of a six–component balance. This format is defined as the difference between a raw output of a bridge and its natural zero. Consequently, the origin of the load space is mapped to the origin of the output space as the output differences of the natural zeros relative to themselves are zeros. In other words, the origin of the output space also describes the absolute load datum of the balance if bridge output format *Difference Type 1* is used. Figure 12 shows the mapping of the absolute load datum of the load space to the output space if output format *Difference Type 1* is used. The symbols $N_1, \ldots, N_6$ represent the natural zeros of the six balance bridges.

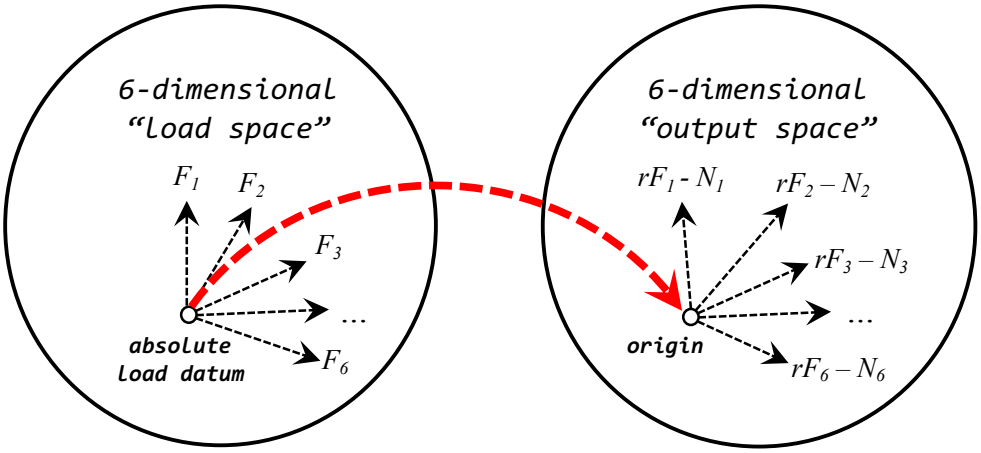

Fig. 12 Mapping of the absolute load datum if output format *Difference Type 1* is used.

Table 2 below summarizes the relationship between the origins of the load and output spaces for two bridge output format choices that an analyst can make.

Table 2: Interpretation of the origins of the load & output spaces.

Output Format (see App. 6)	Interpretation of Coordinate System Origins
Raw Output	The origin of the load space is mapped to a point in the output space that is defined by the natural zeros of the bridges. $\underbrace{[\,0,\,0,\,\ldots\,,\,0\,]}_{load\ space} \iff \underbrace{[\,N_1,\,N_2,\,\ldots\,,\,N_6\,]}_{output\ space}$
Difference Type 1	The origin of the load space is mapped to the origin of the output space. $\underbrace{[\,0,\,0,\,\ldots\,,\,0\,]}_{load\ space} \iff \underbrace{[\,0,\,0,\,\ldots\,,\,0\,]}_{output\ space}$

Now, let us assume that the state variables are no longer constant during both calibration and use of the balance. In addition, it is assumed that the state variable values are expressed as differences relative to suitable reference values (see also related comments in Chapter II). Then, the coordinate system definition of the expanded load space and the related description of the absolute load datum can easily be modified as the state variable value differences relative to a reference value are zero at the origin.

Load Format Options

Three different load formats exist that may be used to describe the load state of a six–component primary balance in the load space. They are called direct–read format, force balance format, and moment balance format (see also App. 4 for additional details). The direct–read format describes the load state of the balance in the universal vector format that Classical Mechanics uses for the description of forces and moments in three–dimensional space. In that case, three forces and three moments are used. They are the components of the resultant force and moment vectors at the balance moment center. The forces are called (i) normal force, (ii) side force, and (iii) axial force. The moments are called (i) pitching moment, (ii) yawing moment, and (iii) rolling moment. Single–piece balances are typically wired such that their loads and outputs have direct–read format characteristics. It must be mentioned that the direct–read format is not balance design specific. In other words, it can be defined for any six–component balance.

Two alternate load format choices are balance design specific. They make it possible to separate load components and bridge outputs such that a single bridge output primarily responds to a single load component. This load component often explains 80 % to 90 % of the electrical output of the related bridge. Therefore, design specific load formats have

the advantage that (i) all bridge sensitivities can easily be quantified by applying single–component loadings and (ii) troubleshooting during use of the balance is simplified.

The first balance design specific load format is called force balance format. It is used for force balances. The corresponding six load components are called (i) forward normal force, (ii) aft normal force, (iii) forward side force, (iv) aft side force, (v) axial force, and (vi) rolling moment. This load set can be converted to the universally applicable direct–read format by using transformation equations that are derived in App. 4.

The second balance design specific load format is called moment balance format. It is used for moment balances. The corresponding six load components are called (i) forward pitching moment, (ii) aft pitching moment, (iii) forward yawing moment, (iv) aft yawing moment, (v) rolling moment, and (vi) axial force. Again, this balance design specific load set can be converted to the universally applicable direct–read format by using transformation equations that are derived in App. 4.

Output Format Options

Advantages and disadvantages of different output format choices are discussed in App. 6. Therefore, only a few comments related to output format *Raw Output* and output format *Difference Type 1* are made in this section. It is concluded from the discussion of the absolute load datum above that the use of output format *Difference Type 1* has an important advantage over the use of the output format *Raw Output*: the origin of the output space is the electrical description of zero absolute load if *Difference Type 1* is chosen. This characteristic simplifies the development of a mathematical relationship that may be used for the balance load prediction during a wind tunnel test. In addition, output format *Difference Type 1* is defined as the difference between a raw output and the natural zero of a balance bridge (see App. 6). Therefore, the use of *Difference Type 1* makes the output description independent of the instrumentation hardware as long as the same instrumentation set is used for the measurement of the raw outputs and natural zeros.

The author recommends output format *Difference Type 1* for the description of the electrical outputs of balance bridges. This output format can be applied to data from all known balance designs. In addition, it supports the tare load iteration process and makes outputs independent of instrumentation hardware characteristics. Finally, it allows for the use of either the *Non–Iterative Method* or the *Iterative Method* for the load prediction.

Electrical Units

Different unit choices exist to describe the electrical outputs, i.e., the voltages of a strain–gage balance. In theory, voltages could be expressed as $milliV$ or $microV$. They could also be made dimensionless after dividing the outputs by the excitation voltage of the bridge. Then, voltages may be expressed in units of $milliV/V$ or $microV/V$.

Experience showed that it is an advantage to divide the measured outputs of a strain–gage balance by the excitation voltage. Then, reporting and use of the outputs are sim-

plified as the excitation voltage is no longer needed for the description of the outputs. In addition, the author observed that the unit choice is directly related to an analyst's ability to visually inspect the magnitude of the electrical outputs in a data file. Therefore, he recommends the use of the electrical unit $microV/V$ for most balance applications. In that case, the magnitude of the output values of a typical balance will be a number between 0.1 and 1.0 $microV/V$ at the lower end and a number between 1000 and 3000 $microV/V$ at the upper end. These number ranges are easily understood and inspected because people often deal with them in their daily lives.

The benefit of using $microV/V$ instead of $milliV/V$ becomes immediately obvious if the above output ranges are expressed in units of $milliV/V$. Then, the following number ranges are obtained: between 0.0001 and 0.001 $milliV/V$ at the lower end and between 1 and 3 $milliV/V$ at the upper end. These number ranges are more difficult to inspect because the majority of output values will be between 0.001 and 1 $milliV/V$.

Primary Bridge Sensitivity

The primary sensitivity of a balance bridge is an important metric of a balance. It is defined as the first derivative of a primary bridge output with respect to the related primary bridge load. It allows an analyst to estimate the magnitude of an output change as a function of an applied load change by computing the product of the sensitivity and the load change.

The balance data description has an influence on the ability to compute a primary bridge sensitivity. Table 3 below lists different cases that illustrate the connection between balance design, load format, and the sensitivities for a six–component balance.

Table 3: Existence of the primary bridge sensitivities of a six–component balance.

Design	Load Format	Primary Bridge Sensitivities
direct–read balance	direct–read format (NF, SF, AF, PM, YM, RM)	all six primary sensitivities exist $(\partial rNF/\partial NF,\ \ldots,\ \partial rRM/\partial RM)$
force balance	force balance format $(N1, N2, S1, S2, AF, RM)$	all six primary sensitivities exist $(\partial rN1/\partial N1,\ \ldots,\ \partial rRM/\partial RM)$
force balance	direct–read format (NF, SF, AF, PM, YM, RM)	only two of six primary sensitivities exist $(\partial rAF/\partial AF$ and $\partial rRM/\partial RM)$
moment balance	moment balance format $(PM1, PM2, YM1, YM2, AF, RM)$	all six primary sensitivities exist $(\partial rPM1/\partial PM1,\ \ldots,\ \partial rRM/\partial RM)$
moment balance	direct–read format (NF, SF, AF, PM, YM, RM)	only two of six primary sensitivities exist $(\partial rAF/\partial AF$ and $\partial rRM/\partial RM)$

In general, it is recommended to both describe and analyze balance loads in the design format of a balance. In other words, loads of a direct–read balance should be formatted

in direct–read format, or, loads of a force balance should be formatted in force balance format, or, loads of a moment balance should be formatted in moment balance format. Then, all primary sensitivities of the balance can be computed as each bridge primarily responds to a single load component.

An example may be used to illustrate that not all primary bridge sensitivities exist if a balance data set is not described in the design format. Let us assume that an analyst chooses to describe loads of a force balance in direct–read format before the balance calibration data analysis is performed and load prediction equations are generated. Then, according to the third row in Table 3 above, four of the six primary bridge sensitivities do not exist. They are the sensitivities of the forward & aft normal force bridges and the sensitivities of the forward & aft side force bridges. In that case, for example, the forward normal force bridge ($rN1$) has two load components, i.e., NF and PM, that significantly influence its output. Therefore, the primary sensitivity cannot uniquely be defined during the regression analysis of the calibration data because more than one load component significantly influences the output of the bridge.

IV. Calibration of a Six–Component Balance

Introduction

The load schedule for the manual calibration of a six–component balance is primarily influenced by (i) the capacities of its loads and (ii) capabilities of the calibration hardware that a calibration laboratory owns. In addition, experience has shown that both single–component and two–component loads must be applied at a minimum during the calibration to define regression models that correctly capture the physical behavior of the balance. A calibration laboratory typically owns hardware that supports the application of single–component loads to a six–component balance. The application of two–component loads is often more challenging. It may be limited by the laboratory's capabilities. Consequently, it is frequently observed that only a subset of the fifteen possible combinations of two load components is applied during the manual calibration of a six–component balance.

Three load components, i.e., the normal force, the axial force, and the pitching moment, are often simultaneously applied during a calibration if a balance is used for the performance test of an aircraft. However, traditionally used regression models of balance calibration data do not support cross–product terms that are the product of three independent variables. Therefore, information contained in those load combinations is distributed across related two–component cross–product terms of the independent variables. In other words, the information is captured by $\{rNF \cdot rAF\}$, $\{rNF \cdot rPM\}$, and $\{rAF \cdot rPM\}$ if the *Non–Iterative Method* is used for the analysis. Similarly, the information is captured by $\{NF \cdot AF\}$, $\{NF \cdot PM\}$, and $\{AF \cdot PM\}$ if the *Iterative Method* is used for the analysis.

It is possible to define a reference load schedule for a six–component balance that takes basic capabilities of a calibration laboratory into account. This load schedule is, to some degree, applicable to all six–component balance designs, i.e., to a direct–read balance, to a force balance, or to a moment balance, as long as (i) the individual load states of the balance during its calibration are described relative to the balance moment center, and (ii) gravity weights are used to apply loads to the balance. The reference load schedule can be constructed by varying one variable at a time for each load series. For convenience, it was decided to describe the reference load schedule in direct–read format. Corresponding load components in force balance or moment balance format can be obtained by simply applying load transformations that are listed in App. 4. Balance load sign conventions of North American wind tunnels are used for the definition of the reference load schedule (App. 3, Fig. 3–2). Details of the suggested reference load schedule for a six–component balance are described in the next section.

Reference Load Schedule

The suggested reference load schedule consists of (i) single component loads for each load component and (ii) a reasonable subset of the fifteen possible two–component loads that can be defined for a six–component balance. This subset of two–component load combinations is assumed to cover all important two–component load combinations that

the wind tunnel model is expected to experience during the wind tunnel test.

The reference load schedule is defined assuming that gravity weights are used for the load application. The applied loads themselves are described by specifying (i) the orientation of the calibration body (or metric part) relative to the direction of the gravitational acceleration and (ii) the location of a load point on the calibration body relative to the balance moment center. Table 4 below relates the generic term load point to a specific balance design. Forward and aft load points are distinguished. Loads may directly be applied over primary balance bridges as long as the design of the balance and the attached calibration hardware support this choice.

Table 4: Definition of forward and aft load points for different balance designs.

Balance Design	Forward Load Point	Aft Load Point
direct–read balance	load point located between the balance face and the balance moment center	load point located between the balance moment center and the balance support
force balance	forward normal or side force bridge location	aft normal or side force bridge location
moment balance	forward pitching or yawing moment bridge location	aft pitching or yawing moment bridge location

The description of the reference load schedule is split into several parts. First, the application of the normal force and the pitching moment is discussed. Figure 13 below shows different parts of the calibration hardware that could be used to apply them to a

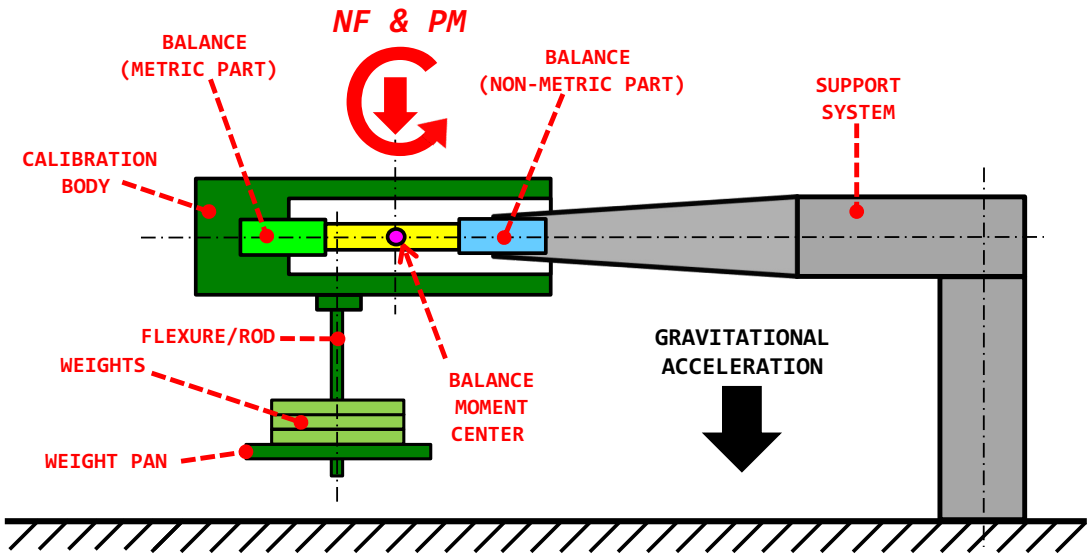

Fig. 13 Application of the normal force and the pitching moment.

strain–gage balance. For simplicity, it was decided to depict the balance as a single–piece balance. The load schedule, however, is also applicable to a force or moment balance as long as the load transformations described in App. 4 are applied. Table 5 below summarizes

the description of a set of normal force and pitching moment loads that may be applied to a six–component balance.

Table 5: Normal force and pitching moment loads for a six–component balance.

Series	Description of Load Application	Applied Load[†]
1	• positive normal force marker on the balance face points down • the gravity weight is applied at the forward load point	$\{+NF, +PM\}$
2	• positive normal force marker on the balance face points down • the gravity weight is applied at the balance moment center	$\{+NF\}$
3	• positive normal force marker on the balance face points down • the gravity weight is applied at the aft load point	$\{+NF, -PM\}$
4	• positive normal force marker on the balance face points up • the gravity weight is applied at the forward load point	$\{-NF, -PM\}$
5	• positive normal force marker on the balance face points up • the gravity weight is applied at the balance moment center	$\{-NF\}$
6	• positive normal force marker on the balance face points up • the gravity weight is applied at the aft load point	$\{-NF, +PM\}$

[†]Applied load(s) are listed in direct–read format using nomenclature that is defined in App. 4.

The six load series above are obtained by using (i) three load points on the calibration body (forward load point, balance moment center, aft load point) and (ii) two orientations of the normal force relative to the direction of the gravitational acceleration. The location of a load point relative to the balance moment center influences the pitching moment sign. In addition, the two orientations down and up result in sign changes of the normal force and the pitching moment.

It is an advantage if the distance between the forward load point and the balance moment center equals the distance between the aft load point and the balance moment center. Then, equations needed for the description of the applied loads at the bridge locations are less complex. In addition, the forward or aft load point should directly be located over the forward or aft bridge if the chosen balance is either a force balance or a moment balance. These two assumptions make it easier to describe the normal force and pitching moment in the corresponding design format of the balance.

The third column of Table 5 lists the applied load of each load series in direct–read format. Load descriptions in other formats can be obtained by applying load transformations that are discussed in App. 4. The load application process for each load series is identical for all load formats.

The application of the side force and yawing moment is analogous to the application of the normal force and the pitching moment that is described in Table 5 above. It is only required to align the side force instead of the normal force with the direction of the gravitational acceleration. Table 6 below summarizes characteristics of the six load series

that describe the application of the side force and the yawing moment. Again, as it was the case for the normal force and the pitching moment, the six load series are obtained by

Table 6: Side force and yawing moment loads for a six–component balance.

Series	Description of Load Application	Applied Load[†]
7	• positive side force marker on the balance face points down • the gravity weight is applied at the forward load point	$\{+SF, +YM\}$
8	• positive side force marker on the balance face points down • the gravity weight is applied at the balance moment center	$\{+SF\}$
9	• positive side force marker on the balance face points down • the gravity weight is applied at the aft load point	$\{+SF, -YM\}$
10	• positive side force marker on the balance face points up • the gravity weight is applied at the forward load point	$\{-SF, -YM\}$
11	• positive side force marker on the balance face points up • the gravity weight is applied at the balance moment center	$\{-SF\}$
12	• positive side force marker on the balance face points up • the gravity weight is applied at the aft load point	$\{-SF, +YM\}$

[†]Applied load(s) are listed in direct–read format using nomenclature that is defined in App. 4.

using (i) three different load points on the calibration body (forward load point, balance moment center, aft load point) and (ii) two orientations of the side force relative to the direction of the gravitational acceleration. Descriptions of the load state of the balance in the load space are simplified if (i) the distance between the forward load point and the balance moment center equals the distance between the aft load point and the balance moment center and (ii) the forward or aft load point is directly located over the forward or aft bridge if the chosen balance is either a force balance or a moment balance.

The application of the rolling moment with gravity weights requires the attachment of a rolling moment arm pair to the calibration body. First, the calibration body should be oriented such that the direction of the normal force is parallel to the direction of the gravitational acceleration. The normal force instead of the side force is typically chosen to be in the direction of the gravitational acceleration because the sensitivity of a normal force bridge is typically lower than the sensitivity of a side force bridge. The moment arm pair should be attached to the calibration body such that its longitudinal axis intersects the roll axis of the balance at the balance moment center. This selection helps minimize interactions that act in the normal force direction. Finally, weight pans are attached to the two ends of the rolling moment arms.

The application of the rolling moment starts by first placing an equal number of weights on each weight pan. Afterwards, weights are shifted from one pan to another to generate a rolling moment. This strategy has the advantage that the simultaneously acting normal force remains constant during the entire application of the rolling moment. Figure 14 below shows a front view of parts of the calibration hardware that

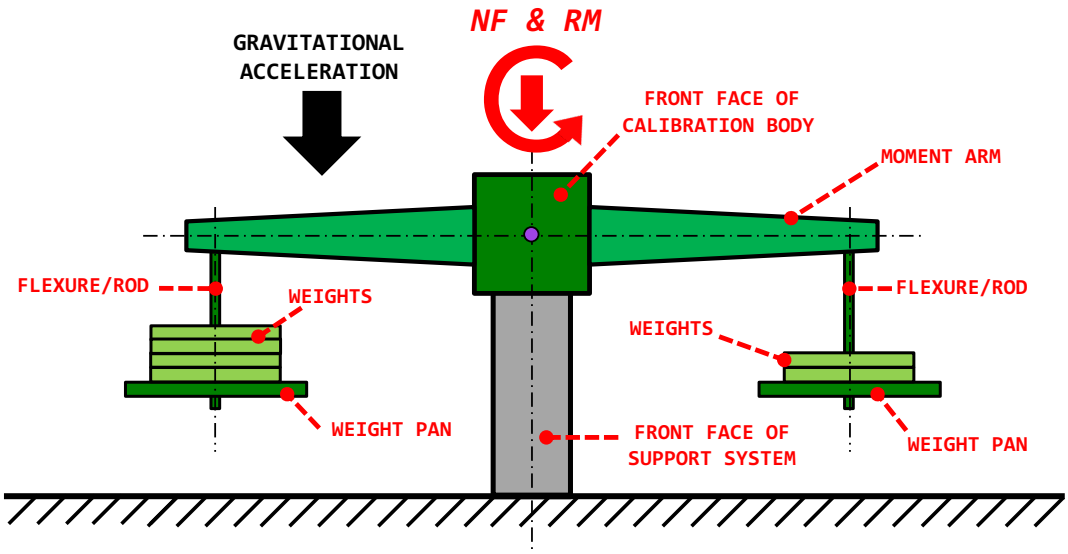

Fig. 14 Application of the rolling moment.

could be used to apply a rolling moment to a balance. The unwanted normal force interaction can be minimized by maximizing the length of the moment arm pair. Then, the maximum rolling moment can be achieved by using a smaller normal force. In other words, the longer the moment arm pair is the more the applied rolling moment approximates the behavior of a true single–component load. Table 7 below lists characteristics of load series 13 and 14 that describe the application of the rolling moment.

Table 7: Rolling moment loads for a six–component balance.

Series	Description of Load Application	Applied Load†
13	• positive normal force marker on the balance face points down • rolling moment arm pair is attached at balance moment center • equal number of weights is placed on each weight pan • weights are shifted between weight pans (non-zero moment)	$\{\pm RM, +NF\}$
14	• positive normal force marker on the balance face points up • rolling moment arm pair is attached at balance moment center • equal number of weights is placed on each weight pan • weights are shifted between weight pans (non-zero moment)	$\{\pm RM, -NF\}$

†Applied load(s) are listed in direct–read format using nomenclature that is defined in App. 4.

A detailed comparison of series 13 with series 14 reveals that series 14 is a close repeat of series 13. Only the orientation of the normal force relative to the direction of the gravitational acceleration is the opposite. This strategy has the advantage that unwanted load schedule asymmetries are suppressed during the application of the rolling moment that could negatively influence regression analysis results of the calibration data.

It remains to describe the behavior of the balance when either an axial force or a combination of the axial force, normal force, and pitching moment is applied. The accurate

application of an axial force is often challenging as (i) the alignment of the calibration body relative to the applied axial force can be complex and (ii) the sensitivity of an axial force bridge is typically one order of magnitude greater than the sensitivity of a normal force bridge. Therefore, different methods were developed in the aerospace testing community to address challenges resulting from the required precise application of the axial force. One approach, for example, orients the balance such that its roll axis is parallel to the direction of the gravitational acceleration. Figure 15 below shows parts of the calibration hardware

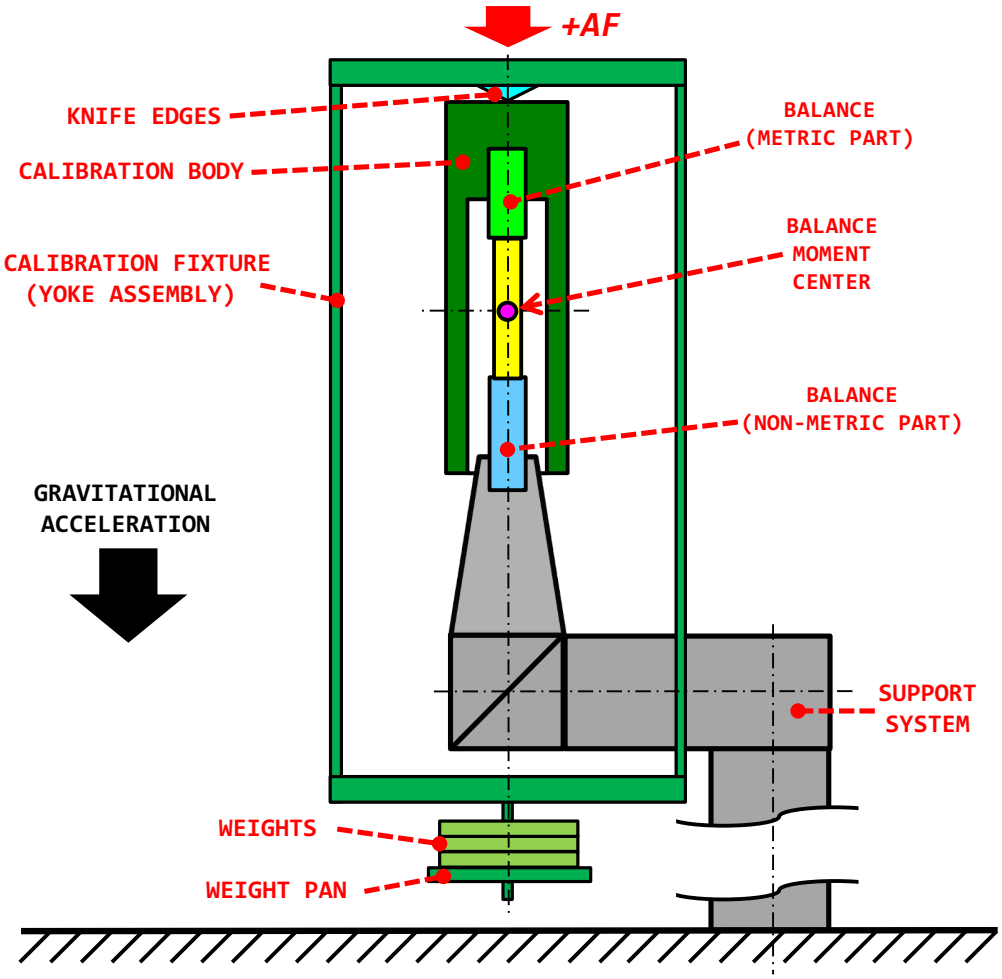

Fig. 15 Application of a pure positive axial force.

that uses this approach. Gravity weights are attached to the calibration body by using a yoke with knife edges and a weight pan. The metric part of the balance is pointing up. Therefore, the applied axial force has a positive sign.

Similarly, after rotating the balance assembly by 180 degrees such that the metric part of the balance is pointing down, a flexure/rod fixture with a weight pan can be attached to the face of the calibration body in order to apply a negative axial force. Figure 16 below shows a detailed description of this approach.

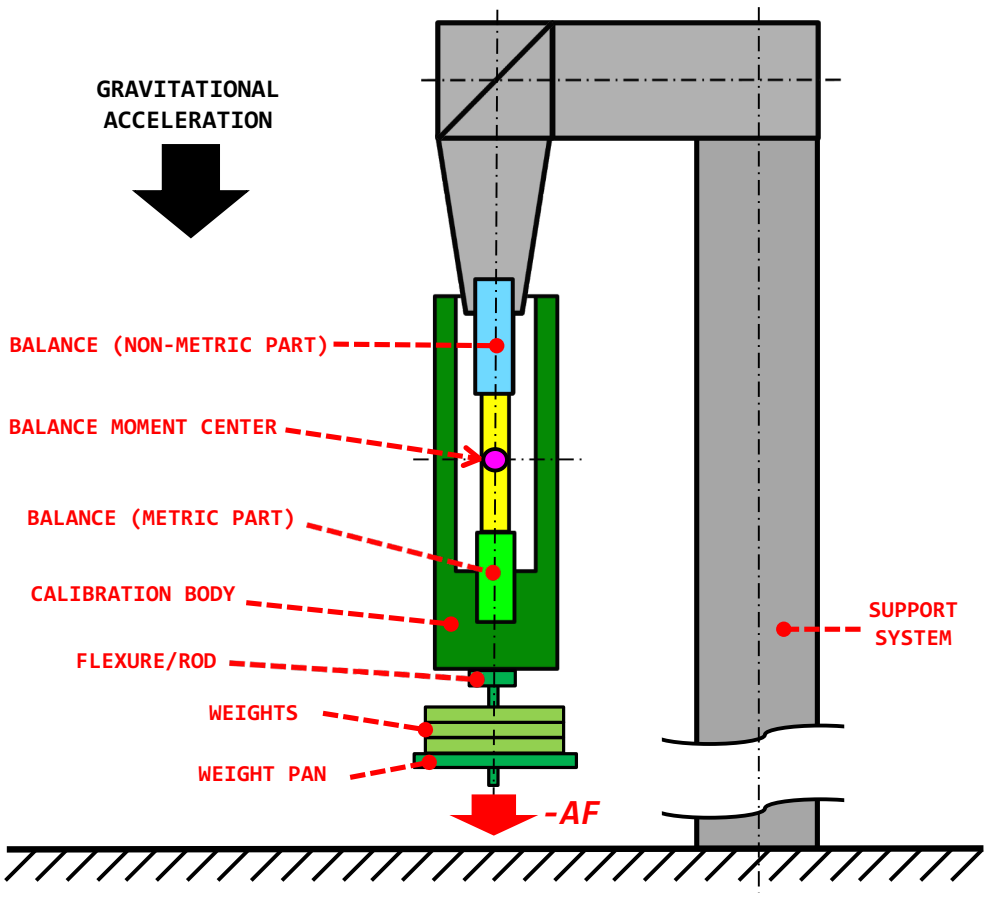

Fig. 16 Application of a pure negative axial force.

The two methods shown in Fig. 15 and Fig. 16 are often used at the Ames Balance Calibration Laboratory to apply pure positive & negative axial forces. Characteristics of the methods are summarized in Table 8. The two methods have the advantage that

Table 8: Application of a pure axial force to a six–component balance.

Series	Description of Load Application	Applied Load
15	• roll axis is parallel to direction of gravitational acceleration • balance face and calibration body are pointing upward • weights are placed on weight pan supported by a yoke	$\{+AF\}$
16	• roll axis is parallel to direction of gravitational acceleration • balance face and calibration body are pointing downward • weights are placed on weight pan supported by a flexure	$\{-AF\}$

only the axial force bridge is loaded. Consequently, the outputs of the remaining five bridges will be close to the natural zeros of the balance. This conclusion also means that a tare correction only needs to be applied to the axial force as the weight of the calibration hardware can only act on that load component during load series 15 and 16. This statement

is valid as long as (i) the calibration body is precisely aligned with the direction of the gravitational acceleration and (ii) the common center of gravity of calibration body and calibration hardware is located on the roll axis of the balance.

An axial force may also be applied after aligning the balance such that the normal force is parallel to the direction of the gravitational acceleration. This situation is shown in Fig. 17 below. In this case, a positive or negative axial force is applied by using a leveled

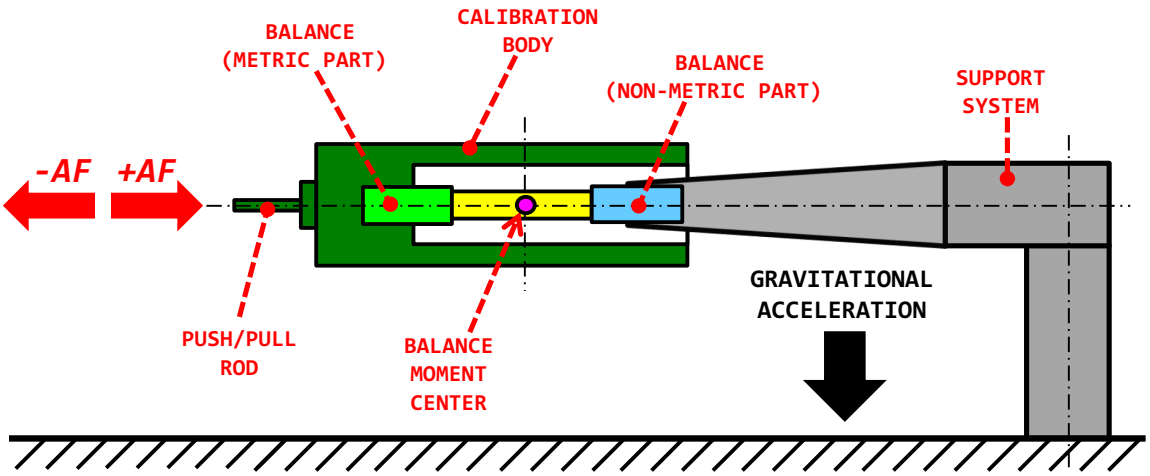

Fig. 17 Alternate method for the application of the axial force.

push/pull rod that is attached to the calibration body at the intersection of the roll axis and the face of the calibration body. The axial force could be generated by using either a leveled hydraulic cylinder or calibration hardware that allows for the frictionless redirection of a gravity force. Figure 18 below shows a schematic of the type of load hardware that is

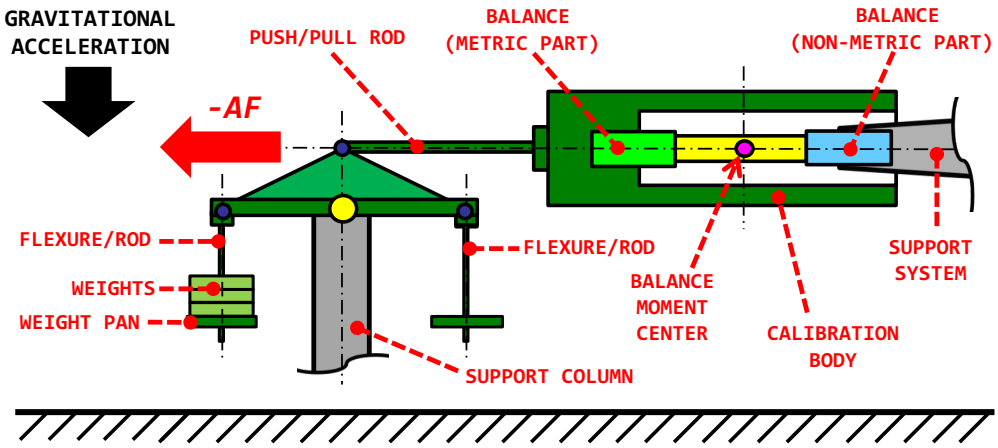

Fig. 18 Application of the axial force using a push/pull rod and gravity weights.

used in the model preparation room of the Ames 11ft Transonic Wind Tunnel for the application of both positive and negative axial forces. In that case, a triangular load fixture is attached to a support column. The top corner of the triangular fixture connects

to the push/pull rod. The other two corners allow for the attachment of weight pans. A negative axial force is obtained if weights are placed on the left weight pan. Similarly, a positive axial force is obtained if weights are placed on the right weight pan. The support column of the fixture must be movable in both the horizontal and vertical direction so that the push/pull rod can be leveled. In addition, the connection between triangular fixture and support column must be made frictionless by using, for example, roller bearings (a yellow circle in Fig. 18 marks the frictionless connection).

It must not be overlooked that the alignment of the push/pull rod can be time consuming. The rod must be located (i) in the plane that the axial & normal force define and (ii) in the plane that the axial & side force define. A precision spirit level may be used, for example, to place the rod into the plane that is defined by the axial & side force. In addition, an observation of output changes of the side force bridge may be needed to also place the rod into the plane that is defined by the axial & normal force. The application of the alternate method results in tare loads on the balance that act in the normal force direction. They are caused by the combined weight of (i) the metric part of the balance, (ii) the calibration body, and (iii) the push/pull rod.

A simultaneous application of the axial force, normal force, and pitching moment adds additional complexity to the manual calibration of a six–component balance. These load combinations are often needed to improve the accuracy of the balance load prediction during performance tests of a wind tunnel model. Figure 19 below shows a calibration

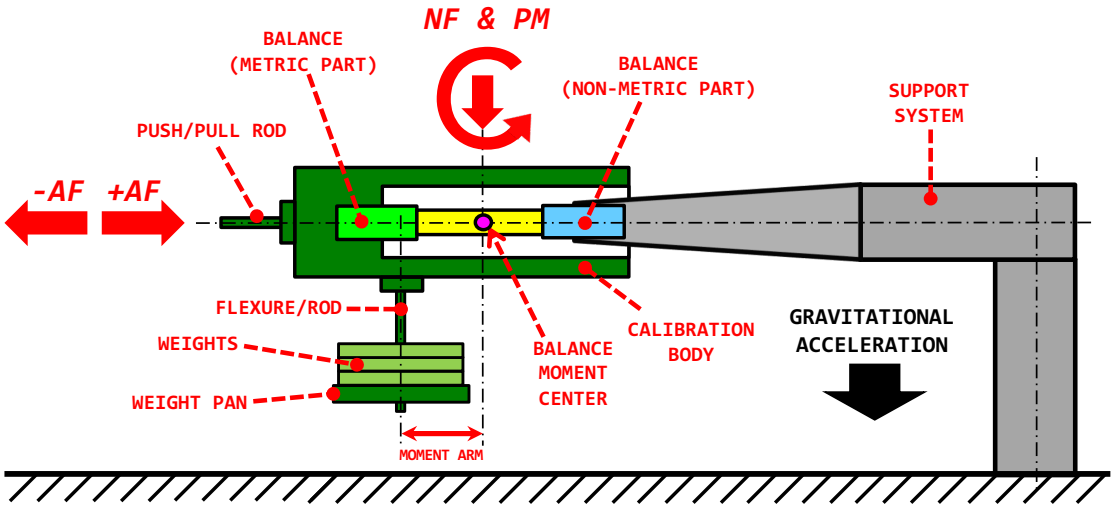

Fig. 19 Application of the axial force, the normal force, and the pitching moment.

hardware setup that could be used for the simultaneous application of the three load components. It is best to only vary the axial force during a load series while keeping (i) the normal force and (ii) the pitching moment arm constant. Table 9 below summarizes characteristics of corresponding load series assuming that (i) the normal force and the

pitching moment arm are kept constant during each load series and that (ii) gravity weights are attached to the calibration body somewhere between the balance moment center and

Table 9: Combined application of axial force, normal force, and pitching moment.

Series	Description of Load Application	Applied Load†
17	• balance roll axis is perpendicular to gravitational acceleration • positive normal force marker on the balance face points down • aligned load rod pushes at the center of the balance face • the gravity weight is applied at the balance moment center	$\{+AF\}$ and ... $\{+NF, +PM\}$
18	• balance roll axis is perpendicular to gravitational acceleration • positive normal force marker on the balance face points down • aligned load rod pulls at the center of the balance face • the gravity weight is applied at the balance moment center	$\{-AF\}$ and ... $\{+NF, +PM\}$
19	• balance roll axis is perpendicular to gravitational acceleration • positive normal force marker on the balance face points up • aligned load rod pushes at the center of the balance face • the gravity weight is applied at the balance moment center	$\{+AF\}$ and ... $\{-NF, -PM\}$
20	• balance roll axis is perpendicular to gravitational acceleration • positive normal force marker on the balance face points up • aligned load rod pulls at the center of the balance face • the gravity weight is applied at the balance moment center	$\{-AF\}$ and ... $\{-NF, -PM\}$

†Applied load(s) are listed in direct–read format using nomenclature that is defined in App. 4.

the front face of the calibration body. Series 17 to 20 summarize different steps that are needed for a simultaneous application of axial force, normal force, and pitching moment. The sign of the normal force and pitching moment is changed by rotating the balance 180 degrees about its roll axis (normal force marker is pointing up or down). It must be emphasized that the normal force and the pitching moment arm should be kept constant within each load series. Only the axial force should be varied. This strategy is the preferred approach as the applied normal force is often one order of magnitude larger than the applied axial force. Consequently, unwanted balance dynamics are avoided that could result from a normal force change during the application of a load series.

Load Spacing

The selection of the spacing of the individual calibration loads also has an influence on the overall load prediction accuracy that can be achieved. It influences the results of the regression analysis of the calibration data. The spacing primarily depends on characteristics of the gravity weight set that a calibration laboratory owns. The author recommends to apply a sufficient number of both positive and negative loads to the balance. The chosen load magnitudes should be between zero and the capacity of a load component. Then,

good estimates of the regression coefficients of the primary linear term, absolute value terms (if needed), and quadratic terms of each dependent variable can be obtained during the regression analysis. This requirement can often already be met if at least three load steps are applied between zero and the capacity of the load component.

Load Series Repeats

A balance calibration data set describes experimental data that is typically processed by applying regression analysis. Therefore, a reasonable number of repeats should be included in the calibration load schedule. These repeats will capture small bridge output variations that are caused by the calibration process and hardware imperfections. In particular, it is an advantage to repeat load series with single–component loads at regular intervals during the calibration (e.g., at the beginning, in the middle, and at the end of the calibration). Then, time–dependent variations of the bridge outputs are captured that will lead to better estimates of the primary bridge sensitivities. In addition, the implicit weighting of the single–component loads increases during the regression analysis of the data if the load schedule has a greater number of single–component loads (see Ref. [16] for a discussion of the influence of implicit weighting on calibration data analysis results).

Accuracy of Applied Forces and Moments

Either a force or a moment is applied during the balance calibration. The magnitude of an applied force, for example, is specified during a calibration by using either a known gravity weight or a load cell measurement. The magnitude of the force needs to have a relative error of 0.01 % or less in order to fulfill the basic requirement that the accuracy of an applied load during a calibration should be at least one order of magnitude below the empirical threshold of 0.10 % of load capacity. This threshold is often used in the aerospace testing community to assess the standard deviation of load residuals that are predicted from regression models of balance calibration data. The accuracy requirement is summarized in Eq. (1) below where $\Delta F/F$ describes the relative error of the applied

Accuracy Requirement for the Applied Force

$$\frac{\Delta F}{F} \times 100\,\% \quad \leq \quad 0.01\,\% \qquad (1)$$

force. A similar requirement must be fulfilled for a moment that is applied to the balance during the calibration. This second requirement is given in Eq. (2) below where $\Delta M/M$ is the relative error of the applied moment. Unfortunately, the specification of the relative error of the applied moment is complicated by the fact that two independent physical

Accuracy Requirement for the Applied Moment (Version 1)

$$\frac{\Delta M}{M} \times 100\,\% \quad \leq \quad 0.01\,\% \qquad (2)$$

quantities are needed for its description. The first quantity is the force that is applied at a certain distance from the balance moment center. It is specified by using either a known gravity weight or a load cell measurement. The second quantity is the moment arm, i.e., the physical distance of the applied force from the balance moment center. It is specified by using geometric information from drawings of the calibration hardware. Both the applied force and the moment arm have relative errors associated with them. They need to be connected to the relative error of the applied moment so that the accuracy requirement for the moment can precisely be defined.

The analytic connection between the relative errors of moment, force, and moment arm can be understood if the moment is constructed from the true values and the absolute errors of the force and moment arm. The resulting relationship is given in Eq. (3) below

$$M' \;=\; (F+\Delta F)\cdot(s+\Delta s) \;=\; \underbrace{\{\; F\cdot s \;\}}_{true\ value} + \underbrace{\{\; F\cdot\Delta s \;+\; \Delta F\cdot s \;+\; \Delta F\cdot\Delta s \;\}}_{error\ of\ applied\ moment} \qquad (3)$$

where symbol F represents the true value of the applied force, symbol s represents the true value of the moment arm, and symbols ΔF and Δs are the assumed absolute errors of the two quantities. It can be seen that the contents of the first bracket on the right–hand side of Eq. (3) above represents the true value of the applied moment. The contents of the second bracket, on the other hand, describes the error of the applied moment. These conclusions can be summarized by the two relationships below where the symbol M

$$true\ value\ of\ applied\ moment \implies M \;=\; F\;\cdot\;s \qquad (4a)$$

$$error\ of\ applied\ moment \implies \Delta M \;=\; F\cdot\Delta s \;+\; \Delta F\cdot s \;+\; \Delta F\cdot\Delta s \qquad (4b)$$

represents the true value of the applied moment and the symbol ΔM represents the error of the applied moment. Now, the relative error of the applied moment can be obtained if the left– and right–hand sides of Eq. (4b) are divided by the left– and right–hand sides of Eq. (4a). Then, after simplifying the result, we get the following relationship:

$$relative\ error\ of\ moment \implies \frac{\Delta M}{M} \;=\; \left\{\frac{\Delta s}{s}\right\} \;+\; \left\{\frac{\Delta F}{F}\right\} \;+\; \left\{\frac{\Delta F}{F}\cdot\frac{\Delta s}{s}\right\} \qquad (5)$$

Two first order error terms and one second order error term can be identified on the right–hand side of Eq. (5) above. In general, it is known that the magnitude of a first

order error term is significantly larger than the magnitude of a second order error term. This conclusion is summarized in Eq. (6) below. Therefore, it is possible to simplify the

$$\underbrace{\left|\frac{\Delta s}{s}\right|}_{1st\ order} \gg \underbrace{\left|\frac{\Delta F}{F}\cdot\frac{\Delta s}{s}\right|}_{2nd\ order} \quad and \quad \underbrace{\left|\frac{\Delta F}{F}\right|}_{1st\ order} \gg \underbrace{\left|\frac{\Delta F}{F}\cdot\frac{\Delta s}{s}\right|}_{2nd\ order} \tag{6}$$

right–hand side of Eq. (5) above by dropping the second order error term. Then, we get the following relationship between the relative errors of force, moment, and moment arm:

Relative Error of Applied Moment

$$\frac{\Delta M}{M} \approx \frac{\Delta s}{s} + \frac{\Delta F}{F} \tag{7}$$

Finally, after replacing the relative error of the applied moment in Eq. (2) above by the right–hand side of Eq. (7), we get the following requirement for the applied moment:

Accuracy Requirement for the Applied Moment (Version 2)

$$\left\{ \frac{\Delta s}{s} + \frac{\Delta F}{F} \right\} \times 100\,\% \leq 0.01\,\% \tag{8}$$

It is concluded from Eq. (8) above that the influence of the relative error of the moment arm on the accuracy of the applied moment must not be underestimated. In fact, the use of a large moment arm is an advantage because the relative error of the moment arm decreases with increasing moment arm length. In addition, the absolute error of the moment arm is more or less constant for all practical purposes. This assumption is reasonable as the absolute error of a moment arm is a combination of (1) machining errors of the calibration hardware and (2) load placement errors of the applied gravity weights.

The benefit of using a large instead of a small moment arm for the application of a moment to a balance can be illustrated with a numerical example. The example assumes that a gravity weight is used to apply a pitching moment to a balance. The weight is attached to the end of a beam that is attached to the calibration body. Furthermore, it is assumed that the relative error of the force associated with a gravity weight is 0.01 %. This estimate is a typical value that is used to describe the accuracy of a gravity weight

during a strain–gage balance calibration. The relative error of the gravity weight can be summarized by the following relationship:

$$\textit{gravity weights} \implies \Delta F / F \times 100\,\% \approx 0.0100\,\% \tag{9}$$

It is also known from hardware drawings that the nominal moment arm, i.e., the distance between balance moment center and attachment point of the gravity weight, is large, i.e., 40.0 *in*. In addition, the absolute error of the moment arm is estimated to be 0.005 *in*. Then, the relative error of the given large moment arm is obtained:

$$\textit{large moment arm} \implies \Delta s / s \times 100\,\% \approx \frac{0.005\ in}{40.0\ in} \times 100\,\% \approx 0.0125\,\% \tag{10}$$

It is concluded after comparing the right–hand sides of Eqs. (9) and (10) that the relative errors of the applied force and the large moment arm are similar in magnitude. This result can be summarized by the following relationship:

$$\textit{large moment arm} \implies \Delta s / s \approx \Delta F / F \tag{11}$$

Alternatively, a load point on the calibration body itself in combination with a large gravity weight may be used for the application of the pitching moment. The resulting moment arm is small. It is assumed to be 4.0 *in*, i.e., one tenth of the magnitude of the large moment arm. Furthermore, it is assumed that the absolute error of the moment arm has not changed. Then, the relative error of the small moment arm is obtained:

$$\textit{small moment arm} \implies \Delta s / s \times 100\,\% \approx \frac{0.005\ in}{4.0\ in} \times 100\,\% \approx 0.125\,\% \tag{12}$$

It is concluded after comparing the right–hand sides of Eqs. (9) and (12) that the relative error of the small moment arm is one order of magnitude greater than the relative error of the applied force. This result can be summarized by the following relationship:

$$\textit{small moment arm} \implies \Delta s / s \gg \Delta F / F \tag{13}$$

The two numerical examples clearly illustrate that it is better to use a large moment arm in combination with a small gravity weight instead of a small moment arm in combination with a large gravity weight for the application of a moment to a balance. Then, errors associated with the specification of the moment arm, i.e., the distance between applied force and balance moment center, can better be controlled.

V. Non–Iterative Method

Introduction

Two fundamentally different methods are used in the aerospace testing community for the prediction of strain–gage balance loads from a set of measured electrical outputs. In both cases, load prediction equations may be obtained after applying a multivariate regression analysis to balance calibration data.

One of the two methods is called the *Non–Iterative Method*. This approach directly fits tare corrected balance loads as a function of the difference between (i) the raw outputs and (ii) the natural zeros of the balance bridges. A detailed derivation of the method, a discussion of bridge output formats, and the description of the related tare load iteration process can be found in App. 6, App. 9, and App. 12. Therefore, only basic characteristics of the method are summarized in this chapter.

First, the development of the regression model of a load component from the output differences of a balance calibration data set is reviewed. Afterwards, the load prediction and the use of the regression models of the loads during a wind tunnel test are discussed. Finally, comments related to the reporting of calibration analysis results are made.

Regression Model Selection and Evaluation

The *Non–Iterative Method* directly fits calibration loads as a function of the differences between the raw outputs and the natural zeros of the balance bridges. In other words, each load component is connected to output differences that were recorded during the balance calibration. It is assumed that the given balance has a total number of n independent load components and n independent bridge output measurements. Then, the regression model of a single load component can be expressed by the following generic relationship

Generic Regression Model of a Balance Load Component

$$F_\varphi = \mu_\varphi(D_1, \ldots, D_\psi, \ldots, D_n) \qquad (14)$$

where

$1 \leq \varphi \leq n \iff$ *load component index range*

$1 \leq \psi \leq n \iff$ *bridge output index range*

where F_φ is the chosen load component, $D_1, \ldots, D_n$ are differences between the raw outputs and natural zeros of the balance bridges, index φ represents a load component, index ψ represents a bridge output, and μ_φ describes the chosen regression model. Now, a regression model μ_φ of the load component needs to be defined that satisfies the following

requirements: (i) the chosen regression model contains only terms that represent the true physical behavior of the balance; (ii) all terms in the chosen regression model are supported by the balance calibration data; (iii) the chosen regression model is free of linear or massive near-linear dependencies. These requirements need to be discussed in more detail.

First, it is important that an analyst chooses a set of regression model terms that can represent the physical behavior of the balance. Different term choices exist that are discussed in App. 9. The term selection highly depends on specific design characteristics of the balance. Consequently, the selection is often made based on an analyst's subject–matter knowledge. For example, the regression model for a single–piece balance may have to be constructed by using linear terms D_i, quadratic terms D_i^2, and cross–product terms $D_i \cdot D_j$ where i and j are bridge output indices. On the other hand, balances of *Task/Able* design may need additional terms to correctly model the bi–directional characteristics of some of its bridges. In that case, absolute value terms $|D_i|$ and the terms $D_i \cdot |D_i|$ may have to be added to the set of terms that is traditionally used for a single–piece balance.

In the next step, after all suitable terms have been selected, individual terms of the regression model need to be identified that the given balance calibration data set supports. This task is accomplished in two steps. First, terms resulting in linear dependencies between regression model terms are detected and removed. An algorithm is applied for that purpose that is described in App. 17. This algorithm applies *Singular Value Decomposition* (SVD) to a modified set of variables that are used to construct the regression model term values. It is still possible that unwanted, i.e., large near–linear dependencies exist in the remaining regression model term combination even after SVD was applied. These dependencies could also result in unreliable load predictions if the regression model is not reduced in size. Therefore, it is important to screen the remaining regression model term combination for near–linear dependencies by using the *Variance Inflation Factor* (VIF) as a test metric (see App. 18 for more details).

At this point, the regression model term selection itself is finished. Tare corrections still need to be applied to the calibration loads themselves before the final regression analysis of the balance calibration data can be performed. These tare corrections describe balance loads that are associated with the weight of the metric part of the balance and all attached calibration hardware pieces. The determination of the tare loads is done iteratively by using an algorithm that was improved over the years (see App. 12 for more details). The final regression model of a load component is obtained after the tare corrected calibration loads are fitted using the output differences of the bridges and the chosen regression model term combination as input. The entire balance data analysis process has to be repeated for each load component of the balance as each component is fitted independent of all other components.

Now, the load prediction equation for the given balance load component is ready to be used during the wind tunnel test. This process is discussed in detail in the next section.

Load Prediction Process

The application of the regression model of the load component, i.e., Eq. (14) during a wind tunnel test is simple. First, it is required to measure the natural zeros of the balance bridges using the tunnel's instrumentation. These values are needed so that the differences between the raw outputs and the natural zeros of the balance bridges can be computed from the tunnel's instrumentation. Afterwards, the output differences of a wind tunnel data point are used to compute the terms of the regression model of the load component. Then, the terms are multiplied with corresponding regression coefficients. Finally, the total sum of the products of all terms with the related coefficients is computed. This value is the predicted absolute load value of the load component.

By design, the predicted load value is computed relative to the datum of zero absolute load as the raw outputs of the data point were referenced to the natural zeros of the bridges when the output differences were defined. This absolute load is caused by aerodynamic effects and the physical weight of the wind tunnel model whenever outputs of a data point are recorded in wind–on condition during a wind tunnel test. Therefore, a wind–off estimate of the balance load also has to be computed for the given orientation of the model in the wind tunnel by using corresponding output differences as input for the regression model. Then, the load caused by the physical weight of the wind tunnel model can be predicted and subtracted from the total load that is measured for a wind–on data point so that the aerodynamic load on the model is obtained. Finally, the process is repeated for the regression models of all remaining load components so that the complete set of aerodynamic loads for the wind tunnel test point is obtained.

A detailed description of the use of the *Non–Iterative Method* for the calculation of balance loads is given in App. 9. In general, it is observed that the load predictions of the *Non–Iterative Method* are as accurate and reliable as the load predictions of the *Iterative Method* as long as four conditions are met: (i) the regression models are obtained from a good calibration load schedule design, (ii) the calibration data quality meets accepted standards, (iii) the regression models are constructed from similar function classes, and (iv) the regression models do not have linear or massive near–linear dependencies. It also needs to be mentioned that the load prediction equations of the *Non–Iterative Method* are more easily understood and implemented. No load iteration needs to be performed in order to obtain load estimates from the measured electrical outputs of the bridges during a wind tunnel test. In addition, the application of the *Non–Iterative Method* is not limited by the requirement that higher–order terms can only make small contributions during the load prediction. The method will work with more influential higher–order terms as long as a reversible mapping between loads and bridge outputs exists.

Reporting of Analysis Results

All important results need to be reported after a regression analysis of a balance calibration data set was successfully completed. The author recommends to provide the

following results:

- Natural zeros of the balance bridges;
- Measured bridge output differences;
- Applied calibration loads;
- Tare loads for each load series (if applicable);
- Tare corrected calibration loads;
- Regression models of the load components;
- *Variance Inflation Factors* of all chosen regression model terms;
- *Percent Contributions* of all chosen regression model terms;
- Load residuals ≡ difference between fitted and tare corrected loads;
- Standard deviation of load residuals (engineering units & percent of capacity).

These results will provide an analyst with a better understanding of the expected accuracy and reliability of the load predictions. It needs to be mentioned for completeness that the tare load iteration process is described in App. 12, the calculation of the *Percent Contribution* is explained in App. 16, and the calculation of the *Variance Inflation Factor* is summarized in App. 18. It may also be helpful to provide *Analysis of Variance* (ANOVA) results to an analyst who has a strong background in statistics. Metrics reported in an ANOVA table including the calculation of the p–value of the t–statistics of the coefficient of a regression model term are explained in the literature (see, e.g., Refs. [68] to [70]).

VI. Iterative Method

Introduction

The *Iterative Method* is another approach that is used in the aerospace testing community for the prediction of strain–gage balance loads. This method is described in great detail in Refs. [6] & [7] and App. 10. The *Iterative Method*, similar to the alternate *Non–Iterative Method*, uses a mathematical algorithm for the prediction of balance loads from a set of electrical outputs of the balance bridges. The loads are obtained by applying a load iteration equation that is typically derived from the result of a multivariate regression analysis of balance calibration data.

The *Iterative Method* is substantially more complex than the alternate *Non–Iterative Method* that was discussed in the previous chapter. It first fits electrical outputs of the balance bridges as a function of the tare corrected calibration loads that are obtained after applying a tare load iteration algorithm to the original balance calibration data set (for more details see App. 13). Afterwards, a load iteration equation is constructed from the regression models of the outputs so that balance loads can be predicted from electrical outputs that are measured during a wind tunnel test.

In theory, an analyst can construct the least squares fit of the electrical outputs from either the raw outputs or the differences between the raw outputs and the natural zeros of the bridges as long as an intercept term, i.e., a constant term is included in the regression model of each output (see App. 10 for more details). Consequently, the intercept becomes a least squares approximation of the natural zero of the bridge if raw outputs are fitted. Alternatively, the intercept becomes a least squares approximation of zero output if output differences of the bridge are fitted. Corresponding fitted regression coefficient sets for the two output format options will be identical with the exception of the intercept term as long as the same regression model term combination is used for the analysis (see App. 6 for a detailed discussion of different bridge output formats).

Finally, a load iteration equation is derived from the regression models of the fitted outputs. This iteration equation may use, for example, the difference between a raw output and the natural zero of the balance bridge as input for the balance load prediction.

The development of the regression model of an electrical output of a balance bridge is presented in the next section. Afterwards, the load prediction process and the use of the iteration equation during a wind tunnel test are discussed. Finally, recommendations related to the reporting of balance calibration analysis results and the load iteration equation are summarized.

Regression Model Selection and Evaluation

The definition of the regression model of the balance calibration data starts with the selection of the bridge output format that is used for the analysis. It is assumed that the electrical outputs of the balance calibration data are formatted as the difference between

the raw outputs and the natural zeros of the balance bridges (see also the description of *Difference Type 1* in App. 6). Then, the use of the intercept term in the regression model of the outputs becomes optional. In addition, the generic description of the regression model of an output may use the same nomenclature that the description of the regression model of a balance load component used in the previous chapter.

In theory, each output difference is a function of the tare corrected loads that the balance experienced during its calibration. Consequently, regression model terms of an output difference have to be constructed from the load components of the balance. Let us assume, for example, that the balance has a total of n load components and n bridge outputs. Then, the regression model of the output difference of a single bridge can be expressed by the relationship given in Eq. (15) below where D_ψ is the output difference, $F_1, \ \ldots, \ F_n$ are the balance load components, index ψ represents a bridge output, index φ represents a load component, and ξ_ψ is the chosen regression model of the output difference.

Generic Regression Model of a Bridge Output Difference

$$D_\psi \ = \ \xi_\psi(F_1, \ \ldots \ , F_\varphi, \ \ldots \ , F_n) \qquad (15)$$

where

$1 \ \leq \ \varphi \ \leq \ n \quad \Longleftrightarrow \quad$ *load component index range*

$1 \ \leq \ \psi \ \leq \ n \quad \Longleftrightarrow \quad$ *bridge output index range*

Now, the regression model ξ_ψ needs to be defined such that the following three requirements are satisfied: (i) a set of regression model terms is selected that can represent the physical behavior of the balance; (ii) all chosen regression model terms are supported by the balance calibration data; (iii) the regression model must be free of unwanted linear or massive near–linear dependencies. These requirements need to be discussed in detail.

First, an analyst must select a set of regression model terms that can model the anticipated physical behavior of the balance. Different choices for the regression model of an output difference exist that are discussed in App. 10. The term selection highly depends on specific design characteristics of the balance. Consequently, the selection is often made based on an analyst's subject–matter knowledge. For example, the regression model of the output difference of the bridge of a single–piece balance may have to be constructed by using linear terms F_i, quadratic terms F_i^2, and cross–product terms $F_i \cdot F_j$ where i and j are load component indices. On the other hand, balances of *Task/Able* design may need

additional terms to correctly model bi–directional characteristics of some of its bridges. In that case, absolute value terms $|F_i|$ of a primary load and terms $F_i \cdot |F_i|$ may have to be added to the terms that are traditionally used for a single–piece balance.

In the next step, after suitable terms have been selected, individual terms of the regression model need to be identified that the given balance calibration data set supports. This goal is usually achieved in two stages. First, terms resulting in linear dependencies between regression model terms are identified and removed. This task can be accomplished by using an algorithm that is described in App. 17. This algorithm applies *Singular Value Decomposition* (SVD) to a modified set of the independent variables that are used to construct the regression model term values. It is still possible that unwanted near–linear dependencies are contained in the remaining regression model term combination that may result in inaccurate or unreliable load predictions. Therefore, it is important to screen the remaining term combination for near–linear dependencies by using the *Variance Inflation Factor* (VIF) as a test metric (see App. 18 for more details).

At this point, the regression model term selection itself is completed. Tare corrections still need to be applied to the calibration loads themselves before the final regression analysis of the balance calibration data can be performed. The tare corrections describe balance loads that are associated with the physical weight of the metric part of the balance and all attached calibration hardware pieces. The determination of the tare loads is done iteratively by using a tare load iteration algorithm (see App. 13). The final regression model of an output difference is obtained after the output difference is fitted as a function of (i) the tare corrected calibration loads and (ii) the chosen regression model term combination. The entire balance data analysis process has to be repeated for the output difference of each balance bridge as the output of each bridge is fitted independent of the outputs of all other bridges. Finally, after completion of the least squares fits of all bridge outputs, the load iteration equation is constructed from the regression coefficients so that loads can be predicted during a wind tunnel test by using output differences as input.

Two load iteration equation options exist that may be used with the *Iterative Method* for the load prediction. The first option is recommended in Ref. [7]. It is identified as *Primary Load Iteration Equation* in App. 10 (see Eq. 10.27a). The second option is identified as *Alternate Load Iteration Equation* in App. 10 (see Eq. 10.31a). Both iteration equations are derived from the same set of regression coefficients of the outputs. Therefore, they will lead to identical balance load estimates as long as the load iterations themselves converge. The second iteration equation option is more limited. It can only be applied if the primary sensitivities of all bridges exist. Therefore, it will only work if a balance data set is described in the design format of the balance. The first iteration equation, on the other hand, is more universally applicable. It will work even if not all primary sensitivities of the balance bridges are defined.

Convergence characteristics of the load iteration equation should also be investigated. The author developed an improved iteration convergence test for that purpose that is

described in great detail in App. 11. The test is very conservative in nature. It evaluates the convergence characteristics of the iteration equation in a very large hypothetical region that includes the actual use envelope of the balance as a small subset. Load iterations are guaranteed to converge within the region if the upper bound of the *Lipschitz Constant* is less than one.

At this point, the load iteration equation for the chosen balance is ready to be used during the wind tunnel test. This process is discussed in detail in the next section.

Load Prediction Process

The application of load iteration equation during a wind tunnel test is straight forward. First, the iteration equation is implemented in the wind tunnel's data system. The iteration equation coefficients themselves are stored in a so–called data reduction matrix that the data system reads. Then, natural zeros of the balance bridges must be measured using the wind tunnel's instrumentation. They are needed as an output datum so that the difference between raw outputs and natural zeros of the balance bridges can be computed. Afterwards, output differences of a wind tunnel data point may be used as input for the load iteration equation. The convergence of the load iterations is rapid in most applications. A total of 5 to 10 iteration steps is typically needed to meet the convergence criterion. The criterion assumes convergence of the load iterations if the largest difference of all load components for two consecutive load estimates is less than a threshold. The empirical threshold value of 0.0001 % of load capacity is typically used in the aerospace testing community for the load iteration convergence test.

By design, the predicted loads of a data point are quantified relative to the datum of zero absolute load. They equal the sum of loads caused by aerodynamic effects and the physical weight of the wind tunnel model whenever loads are computed in wind–on condition during a wind tunnel test. Therefore, a wind–off estimate of the balance load set for the same model orientation in the tunnel also has to be computed by using corresponding output differences as input for the load iteration. Then, the aerodynamic load set of the data point can be obtained after subtracting the predicted load set in wind–off condition from the total load set that is computed in wind–on condition.

It is the author's experience that the load predictions of the *Iterative Method* are as accurate and reliable as the load predictions of the *Non–Iterative Method* as long as the regression models of the output differences were obtained from a good calibration load schedule design, the calibration data quality meets accepted standards in the aerospace testing community, and the applied regression models do not have any linear or massive near–linear dependencies.

Reporting of Analysis Results

All important results need to be reported after a successful analysis of balance calibration data in order to justify the load iteration equation that the *Iterative Method* uses

for the balance load prediction. The author recommends to list the following results:

- Natural zeros of the balance bridges;
- Measured bridge output differences;
- Applied calibration loads;
- Tare loads for each load series (if applicable);
- Tare corrected calibration loads;
- Regression models of the output differences;
- *Variance Inflation Factors* of all chosen regression model terms;
- *Percent Contributions* of all chosen regression model terms;
- Load iteration equation ≡ data reduction matrix;
- Convergence test results (*Lipschitz Condition* & *Constant*, App. 11);
- Load residuals ≡ difference between fitted and tare corrected loads;
- Standard deviation of load residuals (engineering units & percent of capacity).

These results will provide an analyst with a better understanding of the expected accuracy and reliability of the load predictions. It needs to be mentioned for completeness that the tare load iteration process is described in App. 13, the calculation of the *Percent Contribution* is explained in App. 16, and the calculation of the *Variance Inflation Factor* is summarized in App. 18. It may also be helpful to provide *Analysis of Variance* (ANOVA) results to an analyst who has a strong background in statistics. Metrics reported in an ANOVA table including the calculation of the p–value of the t–statistics of the coefficient of a regression model term are explained in the literature (see, e.g., Refs. [68] to [70]).

Reliability of Balance Load Predictions

The following statement is found in the literature regarding the reliability of strain–gage balance load predictions (taken from Ref. [7], p. 16):

> ... An added reason for the recommendation that the iterative model be used lies in the fact that the presence of invalid coefficients ... will likely cause the iterative solution to fail, thus drawing attention to the problem. However, with the non–iterative math model such invalid coefficients often will pass undetected in a back–calculation of the parent data set, but can lead to incorrect results in later use of the balance with different data which may be difficult to detect. ...

It is also known that the iterative solution may converge under certain circumstances despite the fact that the related regression models of the bridge outputs contain an invalid or unsupported term. Therefore, it is concluded that the use of both the *Iterative* and the *Non–Iterative Method* for the balance load prediction is only reliable if invalid terms in the regression models of the balance data are identified and removed before the final load prediction equations are generated. Further investigations showed that a failure of the load iterations of the *Iterative Method* is often associated with the presence of massive near–linear dependencies in the regression models of the bridge outputs. This connection is described in the literature as follows (taken from Ref. [27], p. 4):

> ... In addition, Ulbrich observed a direct connection between the divergence of an iter–ation equation used for the regression analysis of wind tunnel strain–gage balance calibra–tion data and the presence of massive near–linear dependencies in a regression model. ...

Consequently, terms of a multivariate regression model of balance calibration data need to be identified that could cause massive near–linear dependencies. The following metric is recommended for this purpose in the literature (taken from Ref. [27], p. 4):

> ... Different techniques are recommended in the literature that help to diagnose and avoid near–linear dependencies in a regression model ... . Many researchers regard the variance inflation factor (VIF) as one of the most reliable metrics that may be used for this purpose. ...

The above statement means that the complete set of *Variance Inflation Factors* of the selected regression model terms of the balance calibration data needs to be determined in order to systematically investigate the reliability of the load predictions. The chosen regression model term combination should only be used for the final data analysis if the maximum of the set of *Variance Inflation Factors* is below a recommended threshold (for more details see App. 18). The regression models used during the application of the *Iterative Method* must fulfill this requirement. Similarly, the regression models used during the application of the *Non–Iterative Method* must fulfill this requirement. Then, an analyst can be sure that the load prediction equations of the *Non–Iterative Method* are as reliable as the load prediction equations of the *Iterative Method*. This statement is valid as long as (i) the regression models of the balance calibration data do not have linear or massive near–linear dependencies, (ii) the calibration loads are tare corrected, and (iii) similar function classes are used for the definition of the regression models of the data.

VII. Miscellaneous Topics

Processing of Check Loads

The physical and electrical condition of the balance, the wire harness connections to the wind tunnel's data system, and the accuracy of the regression models of the balance load components need to be examined and verified before a balance can successfully be used during a wind tunnel test. Therefore, a limited number of check loads must be applied to the balance in the model preparation room of the wind tunnel facility in order to guarantee that the balance will perform as expected. It is assumed that the balance has no physical or electrical defects. Then, the check load process consists of three major parts: (i) the determination of the natural zeros of the balance bridges; (ii) the application of single–component loads; (iii) the application of combined loads. The three parts are discussed in more detail below.

Natural Zeros $\Longrightarrow$ The natural zeros, i.e., the electrical outputs of the balance bridges at zero absolute load, need to be determined by using one of the approaches that are discussed in App. 8. Ideally, the differences between the natural zeros measured during the original calibration of the balance and corresponding values determined during the check loading process should not exceed the empirical threshold of ≈ 5.0 $microV/V$.

Single–component Loads $\Longrightarrow$ Single–component loads of all load components in both positive and negative direction should be applied over the entire load range. They are needed to independently verify the primary bridge sensitivities that were determined during the regression analysis of the original calibration data. Single–component loads are often applied by using gravity weights. Tare loads also need to be accounted for so that loads caused by the applied gravity weights can be isolated from the total loads that the balance experiences. It is best to first determine the tare loads associated with the weight of the calibration equipment by using outputs of the balance bridges as input for a load calculation before any weight is placed on a weight pan. Then, a second load calculation is performed after weights are placed on the weight pan. Finally, the difference between the second load and the predicted tare load is compared with the theoretical load estimate that is obtained from the known gravity weights and the moment arm (if applicable). In general, the absolute value of the difference between predicted and applied load should be less than the empirical threshold of 0.25 % of the load capacity. This accuracy goal can sometimes not be achieved if significant interactions between balance bridges exist. In that case, larger load residuals near zero applied load may be observed that are primarily caused by built–in balance design characteristics.

Combined Loads $\Longrightarrow$ Two or three load components should be applied simultaneously that are within the physical limitations of the given calibration hardware. Again, as it was the case with single–component loads, it is necessary to first determine the tare loads of the calibration equipment by using corresponding outputs of the balance bridges as input for a separate load calculation before any weight is placed on a weight pan. Then,

a second load calculation is performed after weights are placed on the weight pan and the loads of the chosen load combination are applied. Finally, differences between the second load set and the predicted tare loads are compared with the theoretical load estimates that are obtained from the known gravity weights and the moment arm. Again, the absolute value of differences between predicted and applied balance loads should be less than the empirical threshold of 0.25 % of the load capacity assuming that only small or moderate bridge interactions exist.

The check loads themselves can be either forces or moments. A force is obtained from a known set of gravity weights or from a load cell measurement. A moment, on the other hand, is quantified by multiplying a known force with a known moment arm. The moment arm is the distance between the load application point and the balance moment center. More accurate descriptions of an applied moment can be achieved if a large moment arm is used in combination with a small force instead of a small moment arm in combination with a large force (see Chapter 4 for a detailed discussion of this topic).

It is recommended to use differences between raw outputs and natural zeros of the balance bridges as input for both calibration data analysis and load prediction. The natural zeros should be obtained by using the model preparation room's instrumentation so that instrumentation dependent bias errors are not introduced during the check load prediction.

The check load process is typically organized as a set of load series. Only one load component is varied during each load series while keeping all other load components constant. This approach also works with combined loads as one load component, i.e., the auxiliary load, is fixed at a certain percentage of its capacity while the other load component is varied. Each check load series should have a zero load point at the beginning and end of the series. Its outputs should only be caused by the weight of the calibration equipment. This approach has two benefits. First, a comparison of the outputs of the first and last points of the series allows an analyst to understand how well the data set repeats and if hysteresis effects are an issue. In addition, the difference of the outputs of either the first or the last point of the series relative to the natural zeros may be used as input for the prediction of the tare loads of the load series. These tare loads have to be subtracted from the predicted loads of all remaining data points of the load series assuming that also the differences between the raw outputs of those check load points and the natural zeros are used for the load prediction. Ultimately, the difference between the predicted loads of a check load point and the predicted tare loads of the related load series have to be compared with the applied check loads in order to assess the accuracy of the load prediction.

Interactions between load components and bridge outputs also need to be assessed during the check load process. They are observed as predicted loads that are physically not applied. Often, small interactions cannot be avoided because they may be the result of built–in balance design characteristics. However, interactions may also exist that could be caused by hidden load alignment problems. They could negatively influence the overall quality of the check load data unless they are detected and avoided.

Natural zeros, applied check loads, check load residuals, and interactions between load components should be plotted and listed in a check load analysis report so that both strengths and weaknesses of a specific balance design are understood and documented.

Balance Component Weight Assessment

It is possible to estimate the individual weight of the metric part of the balance, the non–metric part of the balance, or any other calibration hardware piece by using related electrical outputs as input for the load prediction process. In particular, the weight of the metric part is of interest. It is the only part of the tare loads that cannot physically be measured. Consequently, balance component weight estimates may provide information that could lead to a better understanding of the accuracy of the tare load estimates after a calibration data analysis was done (see App. 12 and App. 13). In addition, it may give an analyst an idea of the absolute accuracy of the load prediction for a single load state of the balance as it is often possible to directly weigh component parts of the calibration equipment using a precision scale or load cell.

In principle, the weight of a part of either the balance or the calibration equipment is predicted by using electrical output changes relative to the natural zeros of the bridges as input for a load calculation. These output differences are an input for the load prediction processes that both the *Non–Iterative Method* and the *Iterative Method* use. The component weight is predicted as the normal force, side force, or axial force of the balance depending on its orientation relative to the direction of the gravitational acceleration. The weight prediction approach can be applied to balances of all types as long as the computed balance loads are transformed from the design load format of the balance to direct–read format (see App. 4 for a description of different balance load formats).

The natural zeros of the balance bridges play an important role during the assessment of balance component weights. They are the electrical outputs of the bridges when the balance is in an assumed weightless state (see also Fig. 20 below). In other words, they

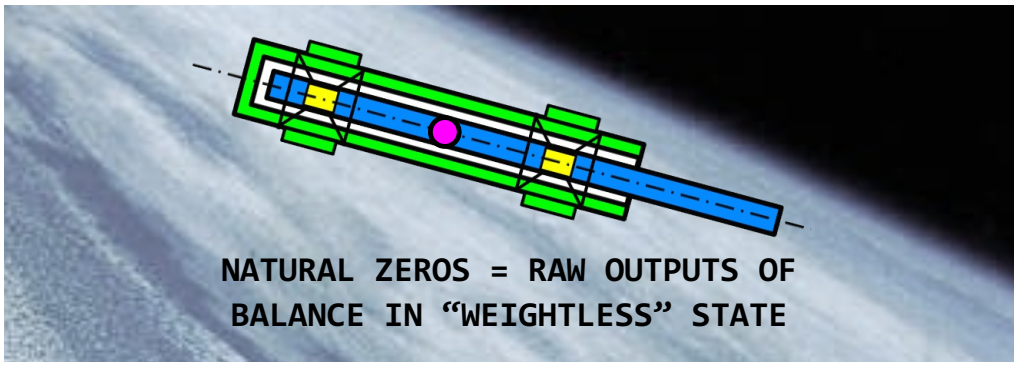

Fig. 20 Electrical output datum ≡ natural zeros of the balance bridges.

are the electrical representation of zero absolute load.

Three examples may be used to illustrate (i) the calculation of the weight of the metric and non–metric parts of a six–component balance and (ii) the calculation of the weight of

the calibration hardware. All examples assume that the given balance has a metric outer sleeve and a non–metric inner rod. The first example satisfies the following conditions: (i) nothing is attached to the metric part of the balance, (ii) the non–metric part is attached to a balance support stand, (iii) the positive normal force marker on the face of the balance points down (i.e., in the direction of the gravitational acceleration), and (vi) the metric part is leveled. Figure 21 below shows a balance that meets these conditions. In that case,

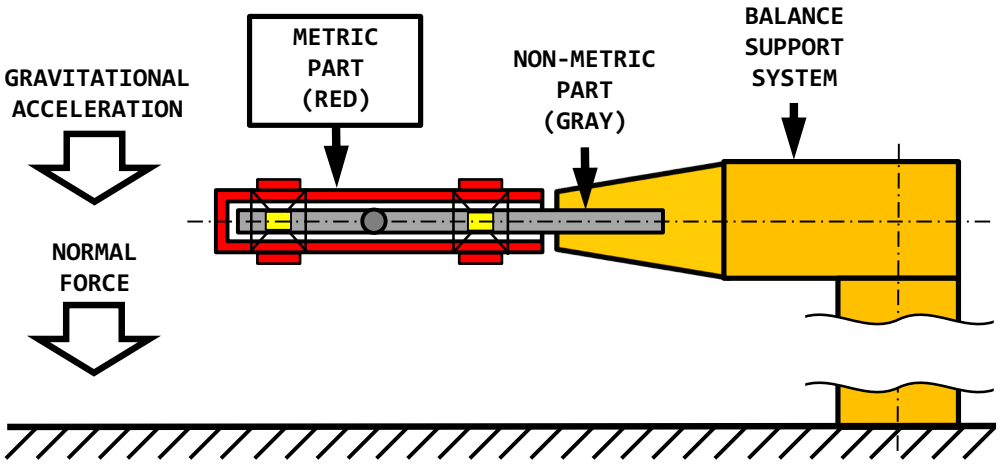

Fig. 21 Prediction of the weight of the metric part of a balance.

the observed electrical output changes of the bridges relative to the natural zeros are exclusively caused by the weight of the metric part of the balance. Consequently, the predicted normal force must be an estimate of the weight of the metric part.

The second example assumes that (i) nothing is attached to the non–metric part of the balance with the exception of the wire harness, (ii) the wire harness is unsupported and hung from the non–metric part, (iii) the metric part is attached to the calibration body that is placed on a leveling table, and (iv) the positive normal force marker on the face of the balance points down (i.e., in the direction of the gravitational acceleration). Figure 22 below shows a balance that meets these requirements. Now, the observed output changes

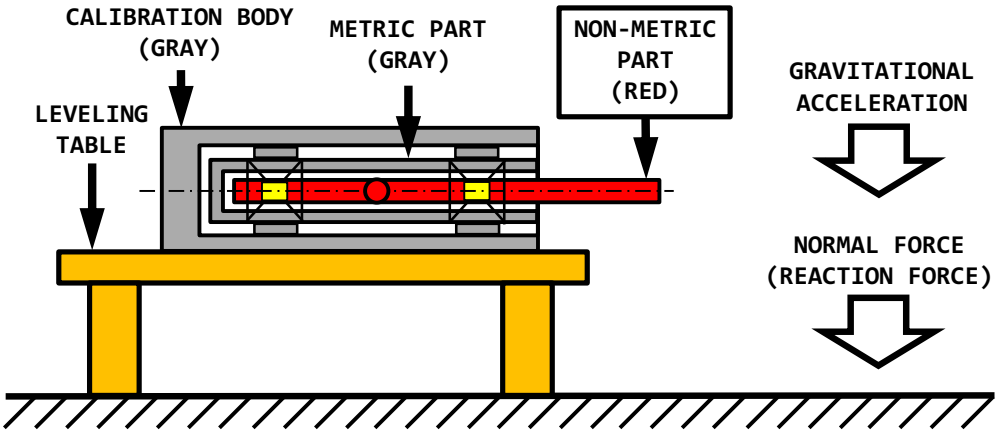

Fig. 22 Prediction of the weight of the non–metric part of a balance.

of the balance bridges relative to the natural zeros are caused by the combined weight of (i) the non–metric part of the balance and (ii) the wire harness. This time, the negative of the predicted normal force is the estimate of the combined weight of the non–metric part and the wire harness. The result is expected because the weight of the non–metric part is causing a reaction load that acts on the non–metric side of the balance. Therefore, the predicted normal force has a negative sign even though the positive normal force marker on the metric part of the balance points down. The estimated combined weight of the non–metric part and the wire harness of the balance can be added to the estimated weight of the metric part from the first example. The result is the estimated total weight of the balance. This value could be compared with an alternate weight estimate that is obtained after placing balance and wire harness on a precision scale.

The final example assumes that (i) the calibration body is attached to the metric part of the balance, (ii) the non–metric part is attached to a balance support stand, (iii) the positive normal force marker on the face of the balance points down (i.e., in the direction of the gravitational acceleration), and (vi) the calibration body is leveled. Figure 23 below shows a balance that meets these conditions. In this situation, the observed electrical

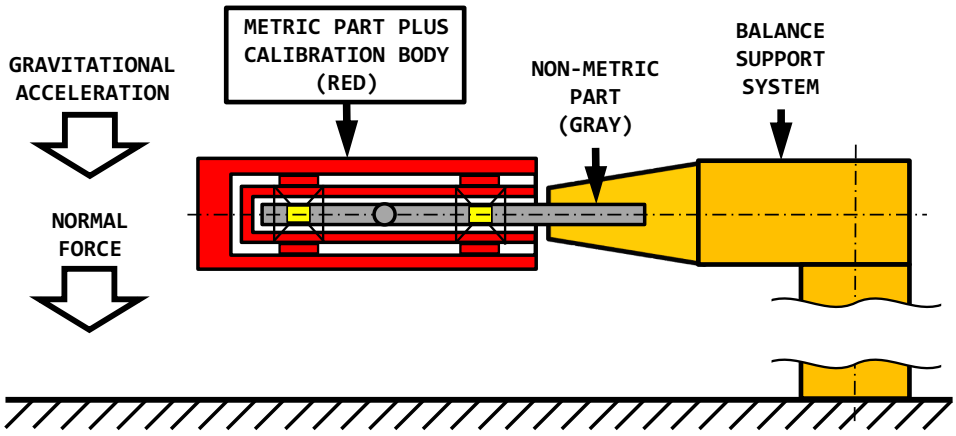

Fig. 23 Prediction of the combined weight of metric part and calibration body.

output changes of the bridges relative to the natural zeros must be caused by the combined weight of (i) the metric part of the balance and (ii) the calibration body. Consequently, the predicted normal force must be an estimate of the combined weight of the metric part of the balance and the calibration body. The weight of the metric part of the balance can be separated from the predicted combined weight if the estimated weight of the metric part from the first example is subtracted from the predicted combined weight. The result of the subtraction is the estimated weight of the calibration body. It may be compared with an alternate weight estimate that is obtained after placing the calibration body itself on a precision scale.

It must be mentioned for completeness that the approaches used in the three examples can also be applied to other balance designs as long as (i) a metric and non–metric part

of the balance can be identified, (ii) the natural zeros of the balance bridges are known, and (iii) the forces on the balance can be obtained in direct–read format by applying corresponding load transformations (see App. 4). The component weight prediction for a semi–span balance, for example, is described in great detail in Ref. [31].

Temperature Effects

The most accurate load predictions within the limitations of a given calibration load schedule design can be achieved if (i) the balance is calibrated at a constant uniform temperature and (ii) the temperature of the balance during its calibration matches the temperature of the balance during its use in the wind tunnel. These two conditions cannot always be fulfilled. They are influenced by the combined thermal characteristics of the wind tunnel, the model, and the model support system. These effects need to be quantified by collecting calibration data at different temperatures if an analyst wants to include the temperature as an independent variable in the load prediction process.

Differences between the balance temperatures during calibration and use in the tunnel may result in changes of two measurements that are related to the prediction of the loads. First, the outputs of the bridges may shift even if no loads are acting on the balance. This bias shift has to be represented by an additional term in the regression model of the calibration data that is defined as the temperature difference of the balance relative to a chosen reference temperature (see App. 14). The contribution of the term may be negligible if the temperature compensation of the balance bridges is very good.

Balance bridges may also experience a temperature–dependent sensitivity shift (see discussions in Ref. [38] and App. 14). In principle, two options exist to address the influence of a sensitivity shift on the predicted loads. The first option simply applies an explicit correction to each load that is a function of (i) the sensitivity change with respect to temperature, (ii) the observed temperature change, and (iii) the bridge output difference relative to the natural zero (see App. 14, Eq. (14.12c)). The second option includes an additional cross–product term in the regression model of the calibration data in order to capture the sensitivity shift. This cross–product term equals the product of the temperature difference and the primary output if the *Non–Iterative Method* is used for the balance load prediction (see App. 14, Eq. (14.14)). Similarly, the cross–product term equals the product of the temperature difference and the primary load if the *Iterative Method* is used for the balance load prediction (see App. 14, Eq. (14.22)). Table 10 below summarizes the two options

Table 10: Correction options for temperature–dependent bridge sensitivity shift.

Option	Correction Approach
Option 1 ... App. 14, Eq. (14.12c)	$\Delta F_i \;=\; \{\; d\; a_{i,i}\;/\;d\; T\;\} \cdot \Delta T \cdot D_i$
Option 2† ... App. 14, Eq. (14.14)	$F_i \;=\; \ldots \;+\; a_{\xi} \cdot \{D_i \cdot \Delta T\} \;+\; \ldots$
Option 2‡ ... App. 14, Eq. (14.22)	$D_i \;=\; \ldots \;+\; b_{\xi} \cdot \{F_i \cdot \Delta T\} \;+\; \ldots$

†extends regression model of Non–Iterative Method ; ‡extends regression model of Iterative Method

that may be used to address a temperature–dependent bridge sensitivity shift. The symbol ΔF_i describes an explicit load correction, $a_{i,i}$ is the bridge sensitivity, T is the temperature, ΔT is the temperature change, D_i is the output difference, F_i is the tare corrected load, and a_ξ and b_ξ are regression coefficients of temperature–dependent cross–product terms. Option 1 works with both the *Non–Iterative Method* and the *Iterative Method*. On the other hand, the description of Option 2 depends on the chosen load prediction method. The sensitivity shift itself can be quantified if single–component loads of each load component are applied at different temperatures during the calibration.

Temperature gradients inside the balance itself can also negatively influence the balance load prediction accuracy. They must be avoided at all cost as the experimental characterization of a temperature gradient and its subsequent use during the load prediction may be too complex for practical applications.

Flow–Through Balances

Flow–through balances are sometimes needed during wind tunnel tests when a propulsion simulator is attached to a wind tunnel model in order to simulate the interaction between a propeller slip stream or an exhaust jet and the model geometry (see, e.g., Ref. [40]). This balance type has the characteristic that the non–metric and metric parts of the balance are bridged by a high–pressure air supply that serves as the power source for the operation of the propulsion simulator. The routing of the high–pressure air through the balance introduces internal loads that act on the balance. These internal loads are responsible for changes of the bridge outputs that cannot be ignored. Therefore, the air pressure is introduced as an additional independent variable for the balance load prediction in order to better characterize the physical behavior of the flow–through balance.

The calibration of a flow–through balance can become very complex. No air has to flow through the balance during its calibration as the effect of internal static pressures on the bridge outputs needs to be quantified. Consequently, only the openings of the air supply lines on the balance need to be sealed such that a family of constant static pressures can be applied while the calibration loads themselves are acting on the balance. It is best to describe each applied pressure as a difference relative to a reference pressure. This pressure difference may be used as a new independent variable in a regression model of the balance calibration data if an analyst wants to directly include pressure effects in the load prediction process.

It is recommended to apply the same set of loadings for each pressure difference. In that case, it is possible, for example, to use the calibration data such that (i) the two nearest pressure differences to the wind tunnel test condition are found, (ii) loads are separately computed for each pressure difference, and (iii) linear interpolation is used to get the loads at the nominal test condition.

In general, the use of the pressure difference as an additional calibration variable and the pressurization of the balance during load application greatly increase complexity and

duration of the balance calibration. Therefore, it may be an advantage to use a balance calibration machine for the calibration of a flow–through balance. This approach was used during the calibration of the MC–130 balance that is described in Ref. [40].

Three–Component Moment Balances

A large model for production wind tunnel tests often has (i) a primary six–component balance to measure loads that act at the model's moment center and (ii) multiple auxiliary balances to measure loads on other model parts. An example of an auxiliary balance is a three–component moment balance. It is frequently used to measure aerodynamic loads on a control surface, a fin, or a canard that is attached to the fuselage or wing of a model.

The user of a three–component moment balance is primarily interested in knowing (i) the normal force, (ii) the bending moment, and (iii) the torsion moment so that the material stress acting on the model part can be monitored. These three load components are predicted by using the electrical outputs of two bending moment bridges and a torsion moment bridge that are attached to the balance surface.

Fundamental differences between a three–component moment balance and a six–component primary balance exist. They must be understood and taken into consideration during design, calibration, and use of the balance. The differences are discussed in great detail in App. 15. Therefore, only the most important observations and results are reviewed in this section.

By design, the metric part of a three–component moment balance is flexible. It goes from the outer edge of the balance to the closest bridge, i.e., the first bending moment bridge. This definition of the metric part of the balance results from the fact that the output of the first bending moment bridge remains constant and becomes unusable if a hypothetical load is applied between its location and the balance moment center. This conclusion assumes that no temporary load fixture is attached to the balance that allows for the application of loads over the bending moment bridges or between the first bending moment bridge and the balance moment center.

The non–metric part of a three–component moment balance, on the other hand, consists of two sections. A flexible section where the bridges are located and a rigid section that attaches the balance to the wind tunnel model. It is best to use the rigid section of the non–metric part for the definition of the balance axis system of the three–component moment balance. Then, its loads can easily be described in the body axis system of the wind tunnel model.

Several recommendations can be made that are related to design and calibration of three–component moment balances (see App. 15 for rigorous derivations of the recommendations). First, the product between (i) bending moment bridge distance and (ii) bending moment bridge sensitivity should be maximized in order to minimize the load prediction error for the normal force. It is also suggested to apply a significant number of calibration loads in the vicinity of the first bending moment bridge in order to avoid a situation when

the two bending moment bridge outputs of the balance appear to be linearly related. A correction formula for the bending moment arm is also developed in App. 15 that takes the elastic deformation of the metric part of the balance under load into account.

VIII. Single–piece Balance Example

Introduction

A manual calibration data set of a NASA single–piece balance was processed to illustrate typical analysis results for a six–component balance. First, basic characteristics of the balance are reviewed. Then, the natural zeros and bi–directional bridge output characteristics are discussed. Afterwards, regression models of the calibration data are presented that the *Non–Iterative Method* and the *Iterative Method* often use for calibration data analysis and load prediction of single–piece balances. Tare load corrections were also applied to the balance calibration data before the data analysis was performed. Finally, selected results for each analysis method are discussed and compared. Table 11 below summarizes characteristics of the given calibration data of the NASA single–piece balance.

Table 11: Characteristics of the NASA single–piece balance data example.

Balance Name	Balance Design (load format)	Calibration Method	Comments
NASA single–piece balance	single–piece design $(NF, SF, AF; PM, YM, RM)$	manual calibration	bridge outputs are <u>not</u> bi–directional

The chosen single–piece balance belongs to a family of balances that has successfully been used for many years at NASA wind tunnels. The balance was calibrated using LaRC's 5–Point Design (Ref. [41], Table 2, Fig. 15). This load schedule was specifically developed for the application of NASA's improved version of *Guarino's Method*. This balance data analysis approach is a variation of the *Iterative Method* that is based on ideas first published in Ref. [51] (additional details related to *Guarino's Method* and *Sequential Regression* can be found in Ref. [52]). *Guarino's Method* replaces global regression analysis with twenty–one sequential analysis tasks in order to determine the regression model coefficients of the output differences that are needed for the definition of the load iteration equation. Consequently, the structure of LaRC's 5–Point Design is not necessarily the best choice if global regression analysis is applied to balance calibration data. Nevertheless, it is the author's experience that data from LaRC's 5–Point Design can successfully be processed using global regression analysis as long as (i) a tare load iteration is performed and (ii) the explicit data point weighting scheme described in App. 22 is applied. This weighting scheme assigns greater weight to single–component loads so that global regression analysis results are less sensitive to the large number of auxiliary loads that LaRC's 5–Point Design uses. Basic characteristics of LaRC's 5–Point Design are reviewed in the next section.

Calibration Description

The calibration of the NASA balance was done using LaRC's 5–Point Design. Characteristics of this load schedule design are described in the literature in great detail (see, e.g., Ref. [41]). Therefore, only basic features of the load schedule are reviewed.

The calibration load schedule consisted of 410 data points that were distributed across 82 load series. Only one load component was varied during the application of each load series while keeping all other load components either near zero or at a constant value. Each load series had a zero load point at the beginning and end of the series. Therefore, it was possible to do a tare load iteration and also assess potential hysteresis effects using the electrical output measurements. Positive and negative loads of each load component were applied over the entire load range. A single load component was applied during 22 load series, two load components were applied during 54 load series, and three load components were applied during 6 load series. Four repeat data points of the original calibration data set were omitted during the data analysis because of suspected data quality issues. Therefore, loads and outputs of 406 data points were used for the development of the balance load prediction equations.

Figure 24 below lists basic characteristics of the first ten load series of LaRC's 5–Point Design. Load values are reported as a percentage of the load capacities after tare load cor–

SERIES	POINTS	NF	SF	AF	PM	YM	RM
1	5	< ±2%	< ±2%	+AF +12.0% to +112.0%	< ±2%	< ±2%	< ±2%
2	5	< ±2%	< ±2%	−AF −111.6% to −11.6%	< ±2%	< ±2%	< ±2%
3	5	+NF +2.0% to +102.3%	< ±2%	< ±2%	< ±2%	< ±2%	< ±2%
4	5	−NF −102.2% to −1.9%	< ±2%	< ±2%	< ±2%	< ±2%	< ±2%
5	5	+8.4% to +8.4%	< ±2%	< ±2%	+PM +1.5% to +99.9%	< ±2%	< ±2%
6	5	−8.5% to −8.5%	< ±2%	< ±2%	+PM −1.6% to +96.9%	< ±2%	< ±2%
7	5	+8.4% to +8.4%	< ±2%	< ±2%	−PM −97.0% to +1.5%	< ±2%	< ±2%
8	5	−8.5% to −8.5%	< ±2%	< ±2%	−PM −100.0% to −1.6%	< ±2%	< ±2%
9	5	+5.5% to +5.5%	< ±2%	< ±2%	< ±2%	< ±2%	+RM +0.0% to +90.5%
10	5	−5.6% to −5.6%	< ±2%	< ±2%	< ±2%	< ±2%	+RM +0.0% to +90.6%

Fig. 24 Characteristics of the first ten load series of the calibration data of the NASA balance (load series ≡ 82; used data points ≡ 406; omitted data points ≡ 4).

rections were applied. Each load series consisted of five data points, i.e., three unique loadings and two repeats. Pure axial force loads were applied during series 1 and 2 as the magnitude of all remaining load components was below 2 % of load capacity. Similarly, pure normal force loadings were applied during series 3 and 4. Pitching moments were applied in series 5, 6, 7, and 8. In those cases, the weight of the calibration equipment caused a constant normal force tare load of approximately ±8.5 % of capacity. Rolling moments were applied in series 9 and 10. This time, the weight of the calibration equipment caused

a constant normal force tare load of approximately ±5.5 % of capacity. The natural zeros are important balance specific constants. Therefore, the determination of the natural zeros of the NASA balance is briefly discussed in the next section.

Natural Zero Determination

The natural zeros are the raw electrical outputs that the balance bridges would have in an assumed weightless condition. They make it possible to describe the raw outputs as instrumentation independent output differences. In addition, they are needed as the global output datum during both calibration data analysis and tare load iteration.

Different methods may be used to determine the natural zeros of a strain–gage balance. The most common approach first orients the balance such that either the normal force or the side force direction is parallel to the direction of the gravitational acceleration. Then, raw outputs of the bridges are recorded. Afterwards, the balance is rolled by 90 deg, 180 deg, and 270 deg. Again, raw outputs are recorded for each roll angle. Finally, arithmetic mean values of the raw outputs of the four orientations are computed. They are the natural zeros of the balance bridges. Table 12 below lists the computed natural zeros of the NASA balance.

Table 12: Natural zeros of the six bridges of the NASA single–piece balance.

$rNF_\circ$ microV/V	$rSF_\circ$ microV/V	$rAF_\circ$ microV/V	$rPM_\circ$ microV/V	$rYM_\circ$ microV/V	$rRM_\circ$ microV/V
+10.5	−647.7	+315.0	−106.3	+4.7	+158.4

Bi–directional characteristics of the six bridge outputs of the NASA balance are discussed in the next section. Afterwards, selected data analysis results are presented.

Bi–directional Output Characteristics

A semi–empirical test was developed that determines if an output of a balance bridge is bi–directional (for more details see App. 7). Results of this test may be used to justify the use of absolute value terms in the regression models of balance data as this type of regression model term should only be used with bi–directional outputs. The test works with both the *Non–Iterative Method* and the *Iterative Method*. Two conditions need to be fulfilled for an output to be considered bi–directional. First, the bi–directional part of the output at load capacity needs to exceed 0.5 % of the to–capacity–scaled maximum of the difference between the raw bridge output and its natural zero. Table 13 below lists estimates of the bi–directional part at load capacity and the corresponding threshold for the NASA balance. The estimates were computed during the application *Non–Iterative Method* and the *Iterative Method* using the approach that is described in App. 7. It is observed that

Table 13: Bi–directional part at load capacity of the bridges of the NASA balance.†

	$\Lambda(D_1,NF)$ microV/V	$\Lambda(D_2,SF)$ microV/V	$\Lambda(D_3,AF)$ microV/V	$\Lambda(D_4,PM)$ microV/V	$\Lambda(D_5,YM)$ microV/V	$\Lambda(D_6,RM)$ microV/V
Non–Iterative	+0.33	+0.34	+0.24	+0.32	+0.09	+0.04
Iterative	+0.31	+0.17	+0.31	+0.40	+0.06	+0.06
Threshold	±9.72	±9.30	±6.59	±6.78	±5.46	±4.28

† $D_1{=}rNF{-}rNF_\circ, D_2{=}rSF{-}rSF_\circ, D_3{=}rAF{-}rAF_\circ, D_4{=}rPM{-}rPM_\circ, D_5{=}rYM{-}rYM_\circ, D_6{=}rRM{-}rRM_\circ$.

the agreement between the estimates from the two analysis methods is excellent as the estimate differences are well below the threshold of 1 $microV/V$. In addition, the bi–directional part of none of the six bridges exceeds the threshold that is listed in the last row of Table 13. Therefore, it is concluded that the bridge outputs of the NASA balance are not bi–directional. This result is expected as the NASA balance is a single–piece design. The test result can also be confirmed after examining the second condition of the test. Therefore, p–values of the principal absolute value terms of the regression model of either the fitted balance load (*Non–Iterative Method*) or the fitted output difference (*Iterative Method*) were computed. This metric must be less than the threshold of 0.0010 if a bridge output has bi–directional characteristics. Table 14 below lists computed p–values of each principal absolute value term of the bridge output differences that were obtained during the application of the *Non–Iterative Method*. It is observed that the

Table 14: Non–Iterative Method $\Longrightarrow$ p–value of the absolute value term of the primary bridge output difference of each fitted load component.†

$p\{\lvert D_1\rvert\}$	$p\{\lvert D_2\rvert\}$	$p\{\lvert D_3\rvert\}$	$p\{\lvert D_4\rvert\}$	$p\{\lvert D_5\rvert\}$	$p\{\lvert D_6\rvert\}$
0.4759 not significant	0.6383 not significant	0.7630 not significant	0.3794 not significant	0.8509 not significant	0.8717 not significant

† $D_1{=}rNF{-}rNF_\circ, D_2{=}rSF{-}rSF_\circ, D_3{=}rAF{-}rAF_\circ, D_4{=}rPM{-}rPM_\circ, D_5{=}rYM{-}rYM_\circ, D_6{=}rRM{-}rRM_\circ$.

p–values of all terms are well above 0.0010. Therefore, the terms are <u>not</u> statistically significant. In other words, no justification for the use of absolute value terms exists.

Similarly, Table 15 below lists the computed p–values of each principal absolute value term of the primary load components that were obtained during the application of the *Iterative Method* to the calibration data. Again, the p–values of all six terms are well

Table 15: Iterative Method $\Longrightarrow$ p–value of the absolute value term of the primary load component of each fitted bridge output difference.

$p\{\lvert NF\rvert\}$	$p\{\lvert SF\rvert\}$	$p\{\lvert AF\rvert\}$	$p\{\lvert PM\rvert\}$	$p\{\lvert YM\rvert\}$	$p\{\lvert RM\rvert\}$
0.5074 not significant	0.8188 not significant	0.7666 not significant	0.2650 not significant	0.9065 not significant	0.8166 not significant

above the threshold of 0.0010. Therefore, the bridge outputs are <u>not</u> bi–directional. In

other words, no justification for the use of absolute value terms exists. Table 16 below summarizes the final test results.

Table 16: Assessment of the bridge output characteristics of the NASA balance.†

	rNF	rSF	rAF	rPM	rYM	rRM
Is bridge output bi–directional ?	no	no	no	no	no	no

†A bridge output is bi–directional if two conditions are met: (i) the bi–directional part at capacity exceeds the threshold (Tbl. 13) and (ii) the p–value of the principal absolute value term is less than 0.001 (Tbls. 14/15).

Bi–directional parts of two of the six bridge outputs are shown in the two figures below. Outputs of the normal force and rolling moment bridges were chosen as an example. Figure 25a below shows the bi–directional part of the normal force bridge output. It can

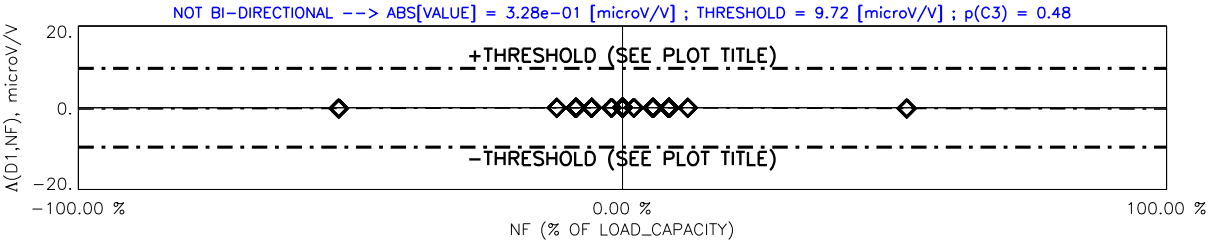

Fig. 25a Bi–directional part of the electrical output of the normal force bridge plotted versus the tare corrected normal force.

clearly be seen in Fig. 25a above that the bi–directional part is well below the empirical threshold at load capacity. This observation confirms that the normal force bridge output of the NASA balance is not bi–directional. Figure 25b below shows the bi–directional part of the output of the rolling moment bridge. Again, the bi–directional part at capacity is well

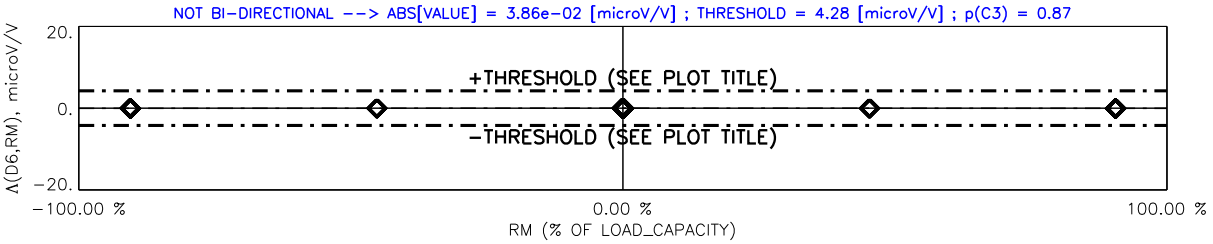

Fig. 25b Bi–directional part of the electrical output of the rolling moment bridge plotted versus the tare corrected rolling moment.

below the threshold that is listed in Table 13 for the rolling moment bridge output. This observation confirms the test result that the rolling moment bridge output of the NASA balance is also not bi–directional. – Selected calibration data analysis results for both the *Non–Iterative Method* and the *Iterative Method* are discussed in the following two sections.

Analysis Results for the Non–Iterative Method

First, the *Non–Iterative Method* was used for the development of the load prediction equation set for the NASA balance from the given balance calibration data (see App. 9 for a detailed description of the method). This approach directly fits the balance load com-

ponents NF, SF, AF, PM, YM, and RM as a function of the bridge output differences D_1, D_2, D_3, D_4, D_5, and D_6 assuming that all balance loads are described relative to the absolute load datum of zero load. Table 17 below shows the selected regression model term combination for each one of the six load components of the balance. Absolute value terms were omitted in the regression models of the load components because the bridge outputs

Table 17: Regression model terms of the six load components of the NASA balance.

Intercept Term
Principal Linear Terms $\{D_1,\ D_2,\ D_3,\ D_4,\ D_5,\ D_6\}^{\dagger}$
Quadratic Terms $D_1^2,\ D_2^2,\ D_3^2,\ D_4^2,\ D_5^2,\ D_6^2$
Cross–product Terms $(D_1 \cdot D_2), (D_1 \cdot D_3), (D_1 \cdot D_4), (D_1 \cdot D_5), (D_1 \cdot D_6), (D_2 \cdot D_3),\ (D_2 \cdot D_4), (D_2 \cdot D_5)$ $(D_2 \cdot D_6), (D_3 \cdot D_4), (D_3 \cdot D_5),\ (D_3 \cdot D_6), (D_4 \cdot D_5), (D_4 \cdot D_6), (D_5 \cdot D_6)$

† $D_1{=}rNF{-}rNF_{\circ}, D_2{=}rSF{-}rSF_{\circ}, D_3{=}rAF{-}rAF_{\circ}, D_4{=}rPM{-}rPM_{\circ}, D_5{=}rYM{-}rYM_{\circ}, D_6{=}rRM{-}rRM_{\circ}$.

are not bi–directional. A total of 28 terms, i.e., the intercept, six linear terms, six quadratic terms, and fifteen cross–product terms were chosen for each load component as (i) LaRC's 5–Point Design supports all these terms and (ii) no near–linear dependencies were detected between the column vectors that the chosen regression model terms and the output differences of the bridges define. In addition, *Weighting Method A* of App. 22 was applied so that single component loads have more influence on the final regression analysis results.

Percent contributions of the regression model terms are also frequently used in the aerospace testing community to assess the importance of regression model terms (see App. 16 for more details). Figure 26 below shows the percent contributions of the thirty–

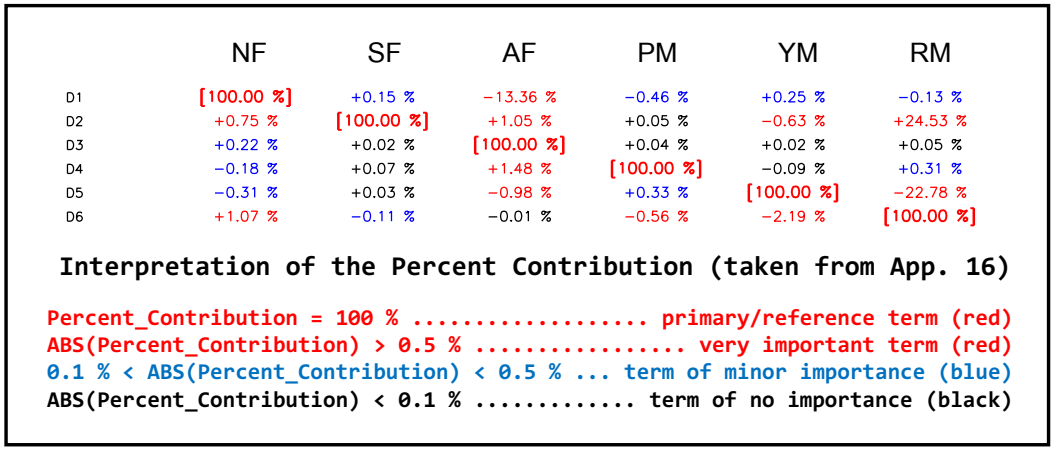

Fig. 26 Percent contributions of the thirty–six principal linear regression model terms of the six fitted balance load components.

six principal linear terms of the regression models of the load components (for simplicity,

percent contributions of higher order terms are not discussed). Red color marks percent contributions of very important terms. Blue color is used to identify terms that are of minor importance. Finally, black color is used to mark terms of no importance. It is concluded after an assessment of the percent contributions that eleven of the thirty off–diagonal terms, i.e., interaction terms can be characterized as very important. They must be included in the regression models so that interactions between the bridges are taken into account during the analysis of the balance data. For example, the bridge output differences D_2 and D_5 make an important contribution in the regression model of the rolling moment RM as their percent contributions are $+24.53\,\%$ and $-22.78\,\%$.

The influence of interactions between loads and bridge outputs can directly be visualized if the primary output of a bridge is plotted versus the corresponding primary load. For example, Fig. 27a below shows the output difference of the normal force bridge plotted versus the tare corrected normal force. It is known from Fig. 26 and other information

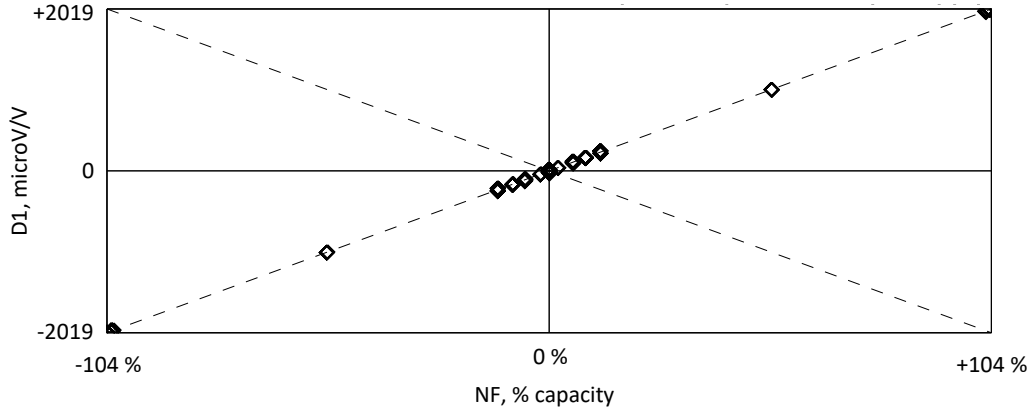

Fig. 27a *Non–Iterative Method* $\Longrightarrow$ Output difference of the normal force bridge (D_1) of the NASA balance plotted versus the tare corrected normal force (NF).

that the normal force bridge output has very small interactions. Consequently, the data points shown in Fig. 27a closely follow a straight line. The situation is completely different for the rolling moment bridge. Figure 27b shows the output difference of the rolling moment

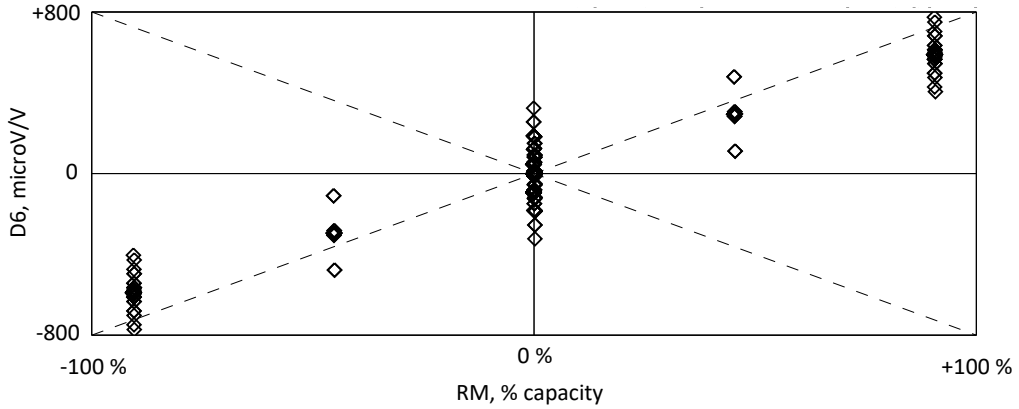

Fig. 27b *Non–Iterative Method* $\Longrightarrow$ Output difference of the rolling moment bridge (D_6) of the NASA balance plotted versus the tare corrected rolling moment (RM).

bridge plotted versus the tare corrected rolling moment. It is known from Fig. 26 that the rolling moment (RM) has very large interactions with the side force bridge output (D_2) and the yawing moment bridge output (D_5). Consequently, data points no longer only appear on a straight line when the rolling moment bridge output difference, i.e., D_6, is plotted versus the tare corrected rolling moment. The observed vertical scatter of the rolling moment bridge output difference is simply caused by the fact that any non–zero side force or yawing moment applied during the balance calibration causes an unwanted but unavoidable change of the electrical output of the rolling moment bridge.

A tare load iteration was performed during the data analysis. Consequently, loads resulting from the weight of the calibration equipment and the metric part of the balance were included in the load set that was used for the regression analysis of the data. Table 18 below lists the computed tare loads for the first ten load series.

Table 18: *Non–Iterative Method* $\Longrightarrow$ Predicted tare loads of the first ten load series of the calibration data of the NASA balance; loads are listed as a percentage of the load capacity.

Series	NF, %	SF, %	AF, %	PM, %	YM, %	RM, %
1	–0.03	+0.01	+12.03	–0.05	≈ 0	+0.11
2	+0.04	+0.03	–11.56	–0.01	+0.03	≈ 0
3	+2.00	+0.06	+0.17	+1.60	+0.03	–0.18
4	–1.91	+0.05	+0.17	–1.57	+0.02	–0.16
5	+8.43	+0.03	+0.03	+1.48	+0.03	–0.15
6	–8.48	–0.02	+0.01	–1.57	≈ 0	+0.06
7	+8.42	+0.02	+0.02	+1.50	+0.02	–0.15
8	–8.49	–0.01	+0.01	–1.55	≈ 0	+0.06
9	+5.54	+0.02	+0.04	+1.51	+0.03	–0.09
10	–5.61	–0.01	–0.03	–1.59	≈ 0	+0.06

The regression analysis of the data was successfully completed using (i) the tare corrected loads and (ii) output differences relative to the natural zeros as input. Table 19 below lists the standard deviation of the load residuals of the calibration data for each load component of the NASA balance. The standard deviations are very small. They are well below the threshold of 0.10 % of capacity that is traditionally used for the assessment of the standard deviation of balance calibration load residuals.

Table 19: *Non–Iterative Method* $\Longrightarrow$ Standard deviation of the load residuals.[†]

NF	SF	AF	PM	YM	RM
0.023 %	0.056 %	0.039 %	0.040 %	0.056 %	0.049 %

[†]Standard deviations are expressed as a percentage of the load capacity.

Normal force residuals of the balance are plotted versus the tare corrected normal force in Fig. 28 below to illustrate typical results. The residuals are within the threshold

of $\pm 0.25\,\%$ of capacity that is often used to evaluate residuals of individual data points.

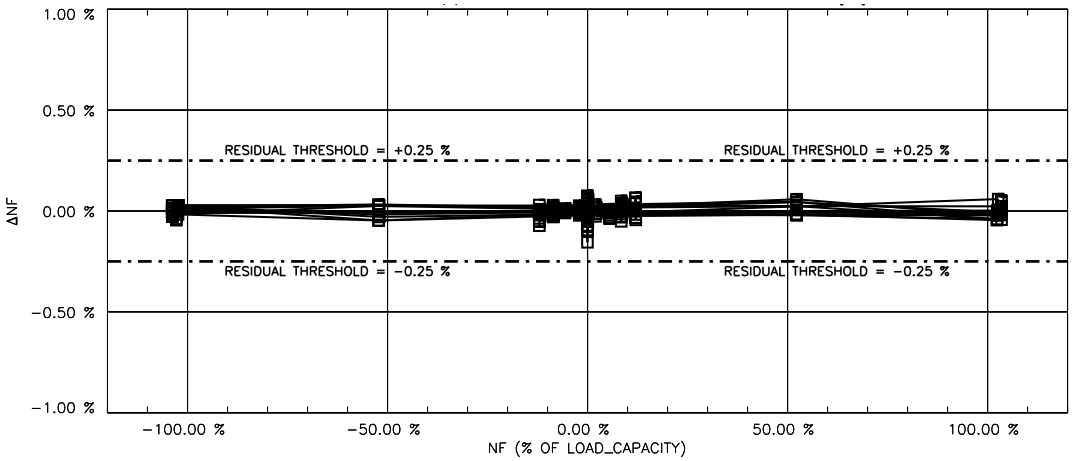

Fig. 28 *Non–Iterative Method* $\Longrightarrow$ Normal force residuals (ΔNF) of the NASA balance plotted versus the tare corrected normal force (NF).

Similarly, rolling moment residuals of the balance are plotted versus the tare corrected rolling moment in Fig. 29 below. Again, individual residuals are within the threshold of $\pm 0.25\,\%$ of load capacity. However, larger residuals can be spotted near zero and near the absolute minimum & maximum of the rolling moment. This behavior can be explained by the fact that the rolling moment bridge output has significant interactions that cannot completely be described by the regression models of the calibration data. Nevertheless, the influence of interactions on rolling moment residuals is still acceptable because they do not cause individual values that exceed the $\pm 0.25\,\%$ threshold.

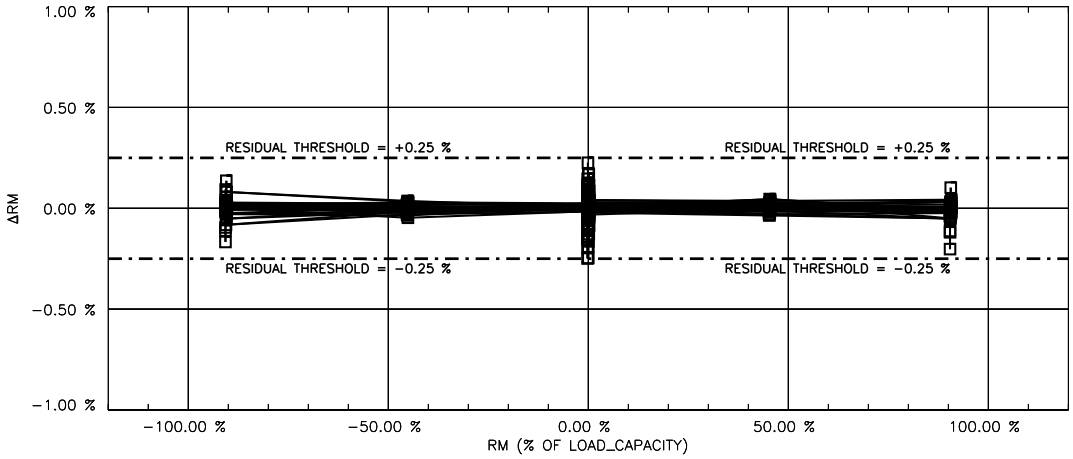

Fig. 29 *Non–Iterative Method* $\Longrightarrow$ Rolling moment residuals (ΔRM) of the NASA balance plotted versus the tare corrected rolling moment (RM).

Primary sensitivities of the six balance bridges were also computed so that the maximum output at capacity could be estimated. The primary sensitivity of a balance bridge is defined as the first derivative of a bridge output with respect to the corresponding primary load. It equals the inverse of the coefficient of the primary output difference that is used

in the regression model of a load component if the *Non–Iterative Method* is used for the load prediction. This statement can be illustrated by using the regression model of the normal force as an example. This model can be defined by the following relationship:

$$NF \;=\; a_0 \;+\; a_1 \cdot D_1 \;+\; a_2 \cdot D_2 \;+\; a_3 \cdot D_3 \;+\; a_4 \cdot D_4 \;+\; \ldots \tag{16}$$

Then, the inverse of the primary sensitivity of the normal force bridge output is obtained:

$$a_1 \;=\; \frac{\partial\, NF}{\partial\, D_1} \;\approx\; \left\{ \frac{\partial\, D_1}{\partial\, NF} \right\}^{-1} = \left\{ \frac{\partial\, [\, rNF - \overbrace{rNF_\circ}^{const.}\,]}{\partial\, NF} \right\}^{-1} = \left\{ \frac{\partial\, rNF}{\partial\, NF} \right\}^{-1} \tag{17}$$

Finally, the primary sensitivity of the normal force bridge is obtained:

$$\textit{primary sensitivity (normal force bridge)} \;\Longrightarrow\; \partial\, rNF \;/\; \partial\, NF \;\approx\; 1 \;/\; a_1 \tag{18}$$

Now, the maximum output at capacity of the six bridges can be determined. This metric is often used to scale instrumentation inputs so that the best accuracy of the electrical output measurement can be achieved. The metric is defined as the product of (i) the primary sensitivity of a bridge with (ii) the capacity of the related load component. Table 20 below lists values that were obtained for the bridges of the NASA balance. It is observed that the maximum output of the rolling moment bridge is only 647.3 $microV/V$. This value is much lower than corresponding values for the other five bridges. Therefore, the resolution of the rolling moment bridge output measurements across the rolling moment range is not as good as the resolution of the output measurements of the other bridges.

Table 20: *Non–Iterative Method* $\Longrightarrow$ Maximum outputs† of the NASA balance.

rNF $microV/V$	rSF $microV/V$	rAF $microV/V$	rPM $microV/V$	rYM $microV/V$	rRM $microV/V$
1943.4	1861.6	1177.7	1347.4	1063.5	647.3

†Maximum output ≡ product of primary bridge sensitivity and capacity of the related load component.

Analysis Results for the Iterative Method

The *Iterative Method* may also be used for the data analysis and load prediction of the NASA balance (see App. 10 for a description of the method). This alternate load prediction method fits the six output differences D_1, D_2, D_3, D_4, D_5, and D_6 as a function of the six tare corrected loads NF, SF, AF, PM, YM, and RM. Afterwards, a load iteration scheme is constructed from the regression models of the outputs so that loads can be predicted from the outputs during a wind tunnel test. Table 21 below shows the regression model term combination for each one of the output differences of the balance. Again, absolute value terms were omitted in the regression models of the output differences because the outputs are not bi–directional. A total of 28 terms,

Table 21: Regression model terms of the six output differences of the NASA balance.

Intercept Term
Principal Linear Terms $NF,\ SF,\ AF,\ PM,\ YM,\ RM$
Quadratic Terms $NF^2,\ SF^2,\ AF^2,\ PM^2,\ YM^2,\ RM^2$
Cross–product Terms $(NF \cdot SF),\ (NF \cdot AF),\ (NF \cdot PM),\ (NF \cdot YM),\ (NF \cdot RM)$ $(SF \cdot AF),\ (SF \cdot PM),\ (SF \cdot YM),\ (SF \cdot RM),\ (AF \cdot PM)$ $(AF \cdot YM),\ (AF \cdot RM),\ (PM \cdot YM),\ (PM \cdot RM),\ (YM \cdot RM)$

† $D_1 = rNF - rNF_\circ, D_2 = rSF - rSF_\circ, D_3 = rAF - rAF_\circ, D_4 = rPM - rPM_\circ, D_5 = rYM - rYM_\circ, D_6 = rRM - rRM_\circ$.

i.e., the intercept, six linear terms, six quadratic terms, and fifteen cross–product terms were chosen for each output difference as (i) LaRC's 5–Point Design supports all these terms and (ii) no near–linear dependencies were detected between the column vectors that the chosen terms and the tare corrected loads define. In addition, *Weighting Method A* of App. 22 was applied during the analysis so that single component loads have more influence on the regression analysis results.

Percent contributions of the regression model terms were also computed in order to assess the importance of regression model terms (see App. 16 for more details). Figure 30 below shows the percent contributions of the thirty–six principal linear terms of the re–

	D_1	D_2	D_3	D_4	D_5	D_6
NF	[100.00 %]	−0.16 %	+15.37 %	+0.45 %	−0.32 %	+0.11 %
SF	−0.46 %	[100.00 %]	−1.24 %	−0.19 %	+0.10 %	−28.05 %
AF	−0.19 %	−0.02 %	[100.00 %]	−0.03 %	−0.02 %	−0.05 %
PM	+0.18 %	−0.08 %	−1.66 %	[100.00 %]	+0.10 %	−0.32 %
YM	+0.05 %	−5.4e−03 %	+0.91 %	−0.16 %	[100.00 %]	+21.40 %
RM	−0.89 %	+0.10 %	−0.11 %	+0.46 %	+2.34 %	[100.00 %]

Interpretation of the Percent Contribution (taken from App. 16)

```
Percent_Contribution = 100 % ..................... primary/reference term (red)
ABS(Percent_Contribution) > 0.5 % ................. very important term (red)
0.1 % < ABS(Percent_Contribution) < 0.5 % ... term of minor importance (blue)
ABS(Percent_Contribution) < 0.1 % ............. term of no importance (black)
```

Fig. 30 Percent contributions of the thirty–six principal linear regression model terms of the six fitted bridge output differences.

gression models of the output differences after global regression was used for the analysis. Again, as it was the case for the regression models of the load components, interactions are observed that cannot be neglected. For example, the side force SF and the yawing moment YM make an important contribution in the regression model of the rolling moment bridge output difference D_6 as their percent contributions are $-28.05\,\%$ and $+21.40\,\%$. As

expected, these two values are similar in magnitude but opposite in sign to corresponding percent contribution estimates of +24.53 % and −22.78 % for D_2 and D_5 that were obtained for the regression model of the rolling moment RM (see Fig. 26; a rigorous proof of this relationship between percent contribution sets is given in App. 16).

A tare load iteration was performed before global regression analysis was used to determine the coefficients of the regression models of the six output differences. Therefore, balance loads resulting from the weight of the calibration equipment and the metric part of the balance were included in the load set that was used as input for the global regression analysis of the calibration data. Table 22 below lists the computed tare loads for the first ten load series. The tare loads listed in Table 22 above can be compared with values that are listed in Table 18 for the *Non–Iterative Method*. The largest observed differences are on the order of 0.01 % of capacity. These differences are more than one order of magnitude below the threshold of 0.25 % that is typically used for the assessment of individual balance load residuals. Therefore, it is concluded that the agreement between the tare load estimates obtained from the *Non–Iterative Method* and *Iterative Method* is excellent.

Table 22: *Iterative Method* $\Longrightarrow$ Predicted tare loads of the first ten load series of the NASA balance calibration data; loads are listed as a percentage of the load capacity.[†]

Series	NF, %	SF, %	AF, %	PM, %	YM, %	RM, %
1	–0.03	+0.01	+12.03	–0.05	≈ 0	+0.11
2	+0.04	+0.03	–11.56	–0.01	+0.03	≈ 0
3	+2.00	+0.06	**+0.18**	+1.60	+0.03	–0.18
4	–1.91	+0.05	+0.17	–1.57	+0.02	–0.16
5	+8.43	+0.03	+0.03	+1.48	+0.03	–0.15
6	**−8.49**	–0.02	+0.01	–1.57	≈ 0	+0.06
7	+8.42	+0.02	+0.02	+1.50	+0.02	–0.15
8	–8.49	–0.01	+0.01	**−1.56**	≈ 0	+0.06
9	+5.54	+0.02	+0.04	+1.51	+0.03	–0.09
10	–5.61	–0.01	–0.03	–1.59	≈ 0	+0.06

[†]Boldface marks tare load estimates that slightly differ from values reported in Table 18.

The regression analysis of the data was successfully completed using (i) the tare corrected loads and (ii) output differences relative to the natural zeros as input. Afterwards, the load iteration equation was generated and calibration load residuals were computed. Table 23 below lists the standard deviation of the load residuals of the calibration data for each load component of the NASA balance. Overall, the agreement between these standard deviations and corresponding values reported in Table 19 for the *Non–Iterative Method* is excellent. Only the difference between the standard deviation values for the axial force is 0.005 %. However, this difference is negligible because it is well below the threshold of 0.10 % that is traditionally used to assess the standard deviation of load residuals.

Table 23: *Iterative Method* $\Longrightarrow$ Standard deviation of the load residuals.[†]

NF	SF	AF	PM	YM	RM
0.023 %	0.057 %	0.044 %	0.040 %	0.056 %	0.048 %

[†]Standard deviations are expressed as a percentage of the load capacity.

Normal force residuals are plotted versus the tare corrected normal force in Fig. 31 below. As expected, the residuals show good qualitative and quantitative agreement with corresponding values for the *Non–Iterative Method* (see Fig. 28).

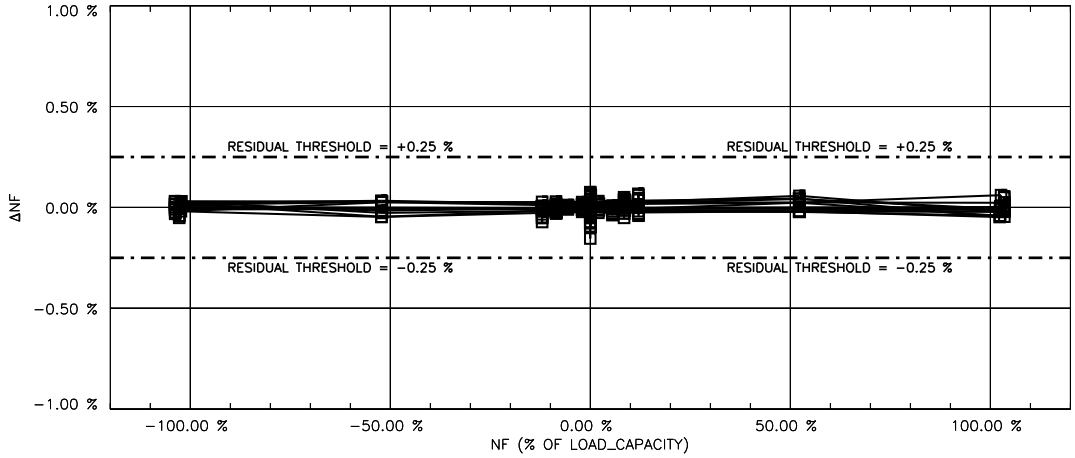

Fig. 31 *Iterative Method* $\Longrightarrow$ Normal force residuals (ΔNF) of the NASA balance plotted versus the tare corrected normal force (NF).

Figure 32 below shows rolling moment residuals plotted versus the tare corrected rolling moment. Again, the residuals show good qualitative and quantitative agreement with corresponding values for the *Non–Iterative Method* (see Fig. 29).

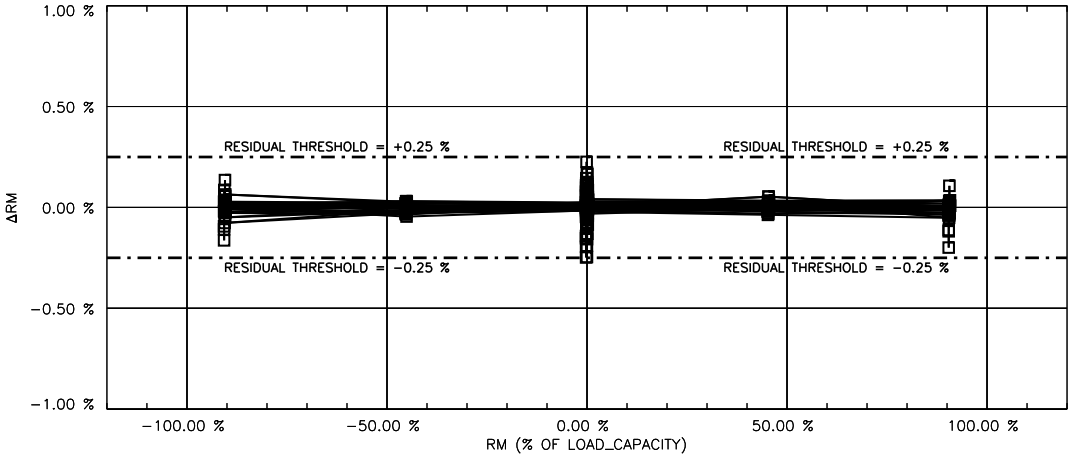

Fig. 32 *Iterative Method* $\Longrightarrow$ Rolling moment residuals (ΔRM) of the NASA balance plotted versus the tare corrected rolling moment (RM).

The maximum output at capacity of each balance bridge was also determined using primary sensitivity estimates that were derived from the regression models of the output differences. The primary sensitivity of a bridge is defined in this context as the coefficient

of the primary load component that is used in the regression model of a bridge output difference. This statement can be illustrated by using the regression model of the output difference D_1 of the normal force bridge as an example. This regression model is given by the following relationship where $rNF_\circ$ is the natural zero of the normal force bridge:

$$D_1 \;=\; rNF - rNF_\circ \;=\; b_0 \;+\; b_1 \cdot NF \;+\; b_2 \cdot SF \;+\; b_3 \cdot AF \;+\; b_4 \cdot PM \;+\; \ldots \quad (19)$$

By definition, coefficient b_1 is the primary sensitivity of D_1. Then, because D_1 and rNF differ by a constant, the primary sensitivity of the normal force bridge is obtained:

$$\begin{matrix} \textit{Primary Sensitivity} \\ (\textit{normal force bridge}) \end{matrix} \quad \Longrightarrow \quad b_1 \;=\; \frac{\partial\, D_1}{\partial\, NF} \;=\; \frac{\partial\, [\, rNF - \overbrace{rNF_\circ}^{const.}\,]}{\partial\, NF} \;=\; \frac{\partial\, rNF}{\partial\, NF} \quad (20)$$

Now, the maximum output at load capacity of the balance bridges can be computed. Table 24 below lists values that were obtained for the six bridges of the NASA balance.

Table 24: *Iterative Method* $\Longrightarrow$ Maximum outputs† of the NASA balance.

rNF $microV/V$	rSF $microV/V$	rAF $microV/V$	rPM $microV/V$	rYM $microV/V$	rRM $microV/V$
1942.8	1860.9	1177.5	1347.4	1068.8	650.4

†Maximum output $\equiv$ product of primary bridge sensitivity and capacity of the related load component.

The numerical estimates listed in Table 24 above can be compared with alternate estimates that were obtained during the application of the *Non–Iterative Method* to the calibration data (see Table 20). The absolute value of the differences between related estimates is given in Table 25 below. The differences for four of the six bridges are very

Table 25: Difference between estimated maximum outputs (Table 20 versus Table 24).

rNF $microV/V$	rSF $microV/V$	rAF $microV/V$	rPM $microV/V$	rYM $microV/V$	rRM $microV/V$
0.6	0.7	0.2	0.0	5.3	3.1

small, i.e., they are less than the empirical threshold of 1.0 $microV/V$ that may be used to identify negligible output changes. The yawing moment and rolling moment bridge outputs are the exception. In those cases, the differences are 5.3 $microV/V$ and 3.1 $microV/V$. They still indicate an acceptable agreement between the independent estimates of the maximum outputs at load capacity.

In conclusion, it was shown for a single–piece balance data example that the agreement between load residuals, percent contributions, tare load estimates, and maximum outputs at capacity of the *Non–Iterative Method* and the *Iterative Method* is excellent. These results illustrate using real–world balance data that the accuracy of the two methods is the same for all practical purposes.

IX. Force Balance Example

Introduction

A manual calibration data set of NASA's MK40A six–component force balance is used to illustrate the analysis of data from a balance with known bi–directional bridge output characteristics. First, physical characteristics of the balance and the calibration load schedule are reviewed. Then, the determination of the natural zeros and the assessment of bridge output characteristics are discussed. Afterwards, the selection of suitable regression models is presented that support both the use of the *Non–Iterative Method* and the *Iterative Method* for the balance load prediction. Tare load corrections are also applied to the calibration loads before the regression analysis is performed. Consequently, the calibration loads can be described relative to the absolute load datum of zero load. Finally, regression analysis results and the load prediction accuracy of the balance are examined. Table 26 below summarizes the most important characteristics of the chosen balance calibration data set of the MK40A six–component force balance.

Table 26: Overview of balance calibration data analysis example characteristics.

Balance Name (diameter)	Balance Design (load format)	Calibration Method	Comments
MK40A (2.50 inches)	force balance design $(N1, N2, S1, S2, AF, RM)$	manual calibration	normal & side force bridge outputs are bi–directional

The MK40A balance belongs to a family of six–component force balances that was designed and manufactured by the Task/Able Corporation. The balance is frequently used for tests in the NASA Ames 11–ft Transonic Wind Tunnel (TWT). Its load capacities are close to the expected load range of typical aircraft models that are tested in this tunnel. Figure 33 below shows the overall layout of the MK40A balance.

Fig. 33 Basic layout of NASA's 2.5 inch MK40A force balance.

By design, the MK40A balance is a multi–piece force balance. It measures five forces (forward & aft normal force, forward & aft side force, axial force) and one moment (rolling moment). These loads can easily be converted to direct–read format by applying load

transformations that are listed in App. 4. The balance has a cylindrical metric outer sleeve and a non–metric inner rod (diameter of the outer sleeve = 2.50 in; total length of the balance $\approx$ 11.0 in). Table 27 below lists capacities of the six load components of the MK40A balance in engineering units.

Table 27: Load capacities of the MK40A balance ($lbs \equiv$ pounds of force).

$N1$, lbs	$N2$, lbs	$S1$, lbs	$S2$, lbs	AF, lbs	RM, $in-lbs$
3500	3500	2500	2500	400	8000

The non–metric part of the balance is typically mounted on a sting that is attached to the rear model support strut of the Ames 11–ft TWT. A basic calibration of the MK40A balance was performed in 2006 that only applied a limited number of combined loadings to the balance. A data set from this calibration was selected for the discussion of force balance characteristics. The data set is well suited for the demonstration of some basic ideas and processes that are associated with calibration data analysis and the load prediction of force balances. Details of the calibration are described in the next section.

Calibration Description

The manual calibration of the MK40A balance took place in 2006 at the Ames Balance Calibration Laboratory. First, physical and electrical checks of the balance were performed. Then, the natural zeros of the balance bridges were determined by using Method I that is described in App. 8. Afterwards, the non–metric part of the balance was attached to the load stand that is used for manual calibrations at the Ames Balance Calibration Laboratory. Finally, the calibration body was attached to the metric part of the balance so that calibration loads could be applied on its surfaces.

The selected load stand allows for the leveling of the calibration body by using manually operated roll and pitch controls. The spatial orientation of the calibration body, i.e., the inputs for its alignment relative to the direction of the gravitational acceleration, are provided by using an Angle Measurement System unit that is rigidly connected to the calibration body.

Manual loads were applied to the balance using gravity weights that were connected to the calibration body by using a variety of hardware pieces (knife edges, yokes, moment arms, threaded rods, flexures, and weight pans). The calibration body was leveled each time an individual gravity weight was added or removed from a weight pan by using the roll and pitch controls of the load stand. It is important to mention that the process of leveling establishes a known orientation of the balance axis system relative to the direction of the gravitational acceleration so that loads caused by gravity weights can easily be described in the design load format of the balance.

Figure 34 below shows the chosen calibration load schedule for the MK40A balance. The North American load sign conventions were used to describe the loads that acted on

the balance (see Ref. [7] and App. 3 for more details). It can be seen that single–component loads and a limited number of combined loads were applied. Single–component loads of

SERIES	POINTS	N1	N2	S1	S2	AF	RM
1	9	+N1 +1.3% to +64.1%	< ±2%	< ±2%	< ±2%	< ±2%	< ±2%
2	9	−N1 −64.0% to −1.2%	< ±2%	< ±2%	< ±2%	< ±2%	< ±2%
3	9	< ±2%	+N2 +1.1% to +64.0%	< ±2%	< ±2%	< ±2%	< ±2%
4	9	< ±2%	−N2 −63.8% to −1.0%	< ±2%	< ±2%	< ±2%	< ±2%
5	9	+N1 +0.9% to +32.3%	+N2 +0.8% to +32.2%	< ±2%	< ±2%	< ±2%	< ±2%
6	9	−N1 −32.3% to −0.9%	−N2 −32.1% to −0.7%	< ±2%	< ±2%	< ±2%	< ±2%
7	9	< ±2%	< ±2%	+S1 +1.6% to +89.6%	< ±2%	< ±2%	< ±2%
8	9	< ±2%	< ±2%	−S1 −89.7% to −1.7%	< ±2%	< ±2%	< ±2%
9	9	< ±2%	< ±2%	< ±2%	+S2 +1.5% to +89.5%	< ±2%	< ±2%
10	9	< ±2%	< ±2%	< ±2%	−S2 −81.4% to −1.4%	< ±2%	< ±2%
11	9	< ±2%	< ±2%	+S1 +1.2% to +45.2%	+S2 +0.8% to +44.8%	< ±2%	< ±2%
12	9	< ±2%	< ±2%	−S1 −45.4% to −1.4%	−S2 −44.9% to −0.9%	< ±2%	< ±2%
13	9	< ±2%	< ±2%	< ±2%	< ±2%	+AF +16.0% to +116.0%	< ±2%
14	9	< ±2%	< ±2%	< ±2%	< ±2%	−AF −111.3% to −11.3%	< ±2%
15	18	+6.6% to +6.6%	+6.4% to +6.4%	< ±2%	< ±2%	< ±2%	±RM −100.0% to +100.0%
16	18	−6.6% to −6.6%	−6.4% to −6.4%	< ±2%	< ±2%	< ±2%	±RM −100.0% to +100.0%

Fig. 34 Manual calibration load schedule of the MK40A force balance (total number of load series ≡ 16; total number of data points ≡ 162).

the normal and side forces were applied by loading directly over corresponding forward and aft bridges while keeping the roll axis of the balance perpendicular to the direction of the gravitational acceleration. A sign change of an applied load at a forward or aft bridge was achieved after rolling the calibration body by 180 degrees.

It was mentioned in the previous paragraph that only a limited number of combined loadings were applied. For example, gravity weights were applied directly over the balance moment center in load series 5 and 6 while the roll axis of the balance was perpendicular to the direction of the gravitational acceleration. This approach results in combined loadings of the forward and aft normal force, i.e., $N1$ and $N2$, whenever the normal force marker on the balance face is parallel to the direction of the gravitational acceleration. Similarly, combined loadings of the forward and aft side force, i.e., $S1$ and $S2$, are achieved in series 11 and 12 after aligning the side force marker on the balance face with the direction of the gravitational acceleration. Table 28 below summarizes the forward and aft normal force loads and load combinations that were applied during the calibration of the balance.

Table 28: Applied forward & aft normal forces of the calibration load schedule.

Series	Load	Comments
1	$+N1$	• Positive normal force marker on balance face points towards the floor. • Gravity weights are applied over the forward normal force bridge.
2	$-N1$	• Negative normal force marker on balance face points towards the floor. • Gravity weights are applied over the forward normal force bridge.
3	$+N2$	• Positive normal force marker on balance face points towards the floor. • Gravity weights are applied over the aft normal force bridge.
4	$-N2$	• Negative normal force marker on balance face points towards the floor. • Gravity weights are applied over the aft normal force bridge.
5	$+N1, +N2$	• Positive normal force marker on balance face points towards the floor. • Gravity weights are applied over the balance moment center.
6	$-N1, -N2$	• Negative normal force marker on balance face points towards the floor. • Gravity weights are applied over the balance moment center.

Similarly, Table 29 below summarizes the side force loads and load combinations that were applied during the calibration of the MK40A balance.

Table 29: Applied forward & aft side forces of the calibration load schedule.

Series	Load	Comments
7	$+S1$	• Positive side force marker on balance face points towards the floor. • Gravity weights are applied over the forward side force bridge.
8	$-S1$	• Negative side force marker on balance face points towards the floor. • Gravity weights are applied over the forward side force bridge.
9	$+S2$	• Positive side force marker on balance face points towards the floor. • Gravity weights are applied over the aft side force bridge.
10	$-S2$	• Negative side force marker on balance face points towards the floor. • Gravity weights are applied over the aft side force bridge.
11	$+S1, +S2$	• Positive side force marker on balance face points towards the floor. • Gravity weights are applied over the balance moment center.
12	$-S1, -S2$	• Negative side force marker on balance face points towards the floor. • Gravity weights are applied over the balance moment center.

A different strategy was used for the application of the axial force. In that case, the roll axis of the balance was oriented parallel to the direction of the gravitational acceleration. Then, knife edges, a yoke, and a weight pan were used to apply the positive axial force on the front face of the calibration body assuming that the balance is pointing up. Afterwards, the orientation was changed such that the balance was pointing down. In that case, the weight pan was directly attached with a flexure to the front face of the calibration body so that a negative axial force could be applied. Table 30 below summarizes all axial force

loads that were applied during the calibration of the MK40A balance.

Table 30: Applied axial forces of the calibration load schedule.

Series	Load	Comments
13	$+AF$	• Roll axis is parallel to the direction of the gravitational acceleration. • Positive axial force points towards the floor. • Gravity weights are applied at intersection of calibration body & roll axis.
14	$-AF$	• Roll axis is parallel to the direction of the gravitational acceleration. • Negative axial force points towards the floor. • Gravity weights are applied at intersection of calibration body & roll axis.

The MK40A is a force balance that is primarily used for wind tunnel tests of aircraft. Therefore, the normal force capacities are about one order of magnitude greater than the axial force capacities (see Table 27). This characteristic also means that the sensitivity of the axial force bridge is substantially larger than the sensitivities of the normal force bridges. Consequently, it is important during the application of the normal forces to minimize possible alignment errors of the calibration body so that interactions between the applied normal forces and the axial force bridge outputs are kept to a minimum.

In theory, it is useful during the calibration of a balance to apply normal and axial forces simultaneously so that built–in interactions resulting from physical characteristics of the balance can clearly be separated from interactions that are caused by small misalignments of the applied loads. Unfortunately, no hardware was available during the 2006 calibration of the MK40A balance to simultaneously apply the normal forces and the axial force. Therefore, these load combination are not included in the load schedule that is discussed in this section.

Finally, single–component loads of the rolling moment were applied after orienting the calibration body such that (i) its roll axis is perpendicular to the direction of the gravitational acceleration and (ii) the positive normal force direction marker on the balance face is pointing towards the floor. Then, two rolling moment arms with a pair of weight pans were attached to the calibration body at the location of the balance moment center. Afterwards, an equal number of weights was placed on each weight pan and shifted from one weight pan to the other so that both positive and negative rolling moments could be applied. It always benefits the overall calibration data quality if the calibration load schedule of a balance is symmetric. Therefore, the author recommends to repeat the rolling moment loadings after rolling the calibration body by 180 degrees so that the negative normal force marker on the balance face points towards the floor.

Gravity weights result in a small but constant normal force load on the balance if the rolling moment is applied by using the approach that is described in the previous paragraph. This unwanted normal force can be minimized by making the rolling moment arms as long as possible. It should also be mentioned that the normal force instead of the side

force was aligned with the direction of the gravitational acceleration during the application of the rolling moments. This choice was made because the normal force capacities of the balance are substantially larger than the side force capacities. Consequently, interactions between the rolling moment and the balance bridges are kept to a minimum during the application of the rolling moments. Table 31 below summarizes the rolling moments that were applied during the calibration of the MK40A balance.

Table 31: Applied rolling moments of the basic calibration load schedule.

Series	Load	Comments
15	$\pm RM$	• Roll axis is perpendicular to the direction of the gravitational acceleration. • Positive normal force points towards the floor. • Moment arms are attached to calibration body at balance moment center. • Weight pans are attached to the ends of the moment arms. • Equal number of gravity weights is placed on each weight pan. • Gravity weights are shifted between pair of weight pans.
16	$\pm RM$	• Roll axis is perpendicular to the direction of the gravitational acceleration. • Negative normal force points towards the floor. • Moment arms are attached to calibration body at balance moment center. • Weight pans are attached to the ends of the moment arms. • Equal number of gravity weights is placed on each weight pan. • Gravity weights are shifted between pair of weight pans.

Again, as mentioned before, the total normal force is kept constant during the application of the rolling moment because weights are simply shifted between the pair of weight pans. Therefore, it is possible to make the total normal force a part of the tare loads of those load series that are associated with the application of the rolling moments. This approach has the advantage that individual loads on the forward & aft normal force bridges are the result of the tare load iteration process. In other words, an analyst does not have to explicitly compute and specify the normal forces for series 15 and 16 in the calibration data input file as they are treated as tare loads.

A tare load iteration has to be applied during the calibration data analysis. Therefore, it is critical that each one of the 16 load series of the calibration load schedule has zero load points at the beginning and end of each series. These zero load points should have outputs that are exclusively caused by (i) the combined weight of the metric part of the balance, the calibration body, and the calibration hardware and, if applicable, by (ii) constant auxiliary loads that are intentionally treated as part of the tare loads. Then, it is possible to format the calibration data input file such that a tare load iteration can be performed (see App. 12 and App. 13 for more details). In addition, a comparison of the outputs at the beginning and end of a load series helps an analyst to understand and quantify possible hysteresis effects that may be a physical characteristic of the given balance design.

The load spacing within each load series is dictated by the size of the weights and the dimensions of the rolling moment arms that a balance calibration laboratory owns. Ideally, at least two loads should be applied between 0 % and 100 % capacity. Then, information is collected that could potentially be used to support a quadratic term in the regression model of the calibration data. – The natural zeros of the balance bridges are the electrical outputs that the balance would have in a weightless condition. Their determination is briefly discussed in the next section.

Natural Zero Determination

It was decided to use Method I of App. 8 for the determination of the natural zeros of the balance. Therefore, the balance was simply placed on a leveling table using V–blocks and oriented such that the negative forward/aft normal force was pointing in the direction of the gravitational acceleration. Then, raw outputs were recorded. Afterwards, the balance was rotated by 90 deg, 180 deg, and 270 deg in order to obtain three more sets of raw output readings. Finally, the electrical outputs of the four orientations were averaged in order to get the natural zeros of the six bridges. Measured raw outputs and results of the application of Method I are shown in Table 32 below.

Table 32: Natural zeros of the MK40A balance.

Roll Angle (Orientation)	$rN1_\circ$ microV/V	$rN2_\circ$ microV/V	$rS1_\circ$ microV/V	$rS2_\circ$ microV/V	$rAF_\circ$ microV/V	$rRM_\circ$ microV/V
0°	−20.17	−2.71	−1.38	−56.87	−138.59	−19.77
90°	−19.23	−1.98	+0.10	−55.77	−138.79	−19.88
180°	−18.29	−1.26	−1.25	−56.81	−138.79	−19.64
270°	−19.24	−2.01	−2.68	−57.94	−138.76	−19.56
Natural Zeros†	−19.23	−1.99	−1.30	−56.85	−138.73	−19.71

†The natural zeros are the arithmetic mean of the column values.

In theory, the natural zeros are repeatable physical constants as long as (i) no changes to both wiring and gaging of the balance are made and (ii) the balance does not experience plastic deformation during use. Therefore, the estimates of the natural zeros of 2006 (Table 32) were compared with corresponding estimates that were obtained in 2004. Table 33 below shows the estimated natural zeros of 2004 and 2006. The maximum

Table 33: Repeatability of the estimated natural zeros of the MK40A balance.

Calibration Date	$rN1_\circ$ microV/V	$rN2_\circ$ microV/V	$rS1_\circ$ microV/V	$rS2_\circ$ microV/V	$rAF_\circ$ microV/V	$rRM_\circ$ microV/V
2004	−20.21	−3.91	−2.98	−57.65	−139.98	−19.83
2006	−19.23	−1.99	−1.30	−56.85	−138.73	−19.71

difference between the estimates of 2004 and 2006 is on the order of 2.0 $microV/V$. These variations are typical values that may be observed in a balance calibration laboratory. They may be the result of small instrumentation set–up and/or measurement process changes that influenced the measurement of the electrical outputs of the bridges. It is the author's experience that (i) better instrumentation, (ii) improved process control, and (iii) rigorous laboratory staff training may reduce the observed natural zero variations to values that can be between 0.5 $microV/V$ and 1.0 $microV/V$.

Bi–directional characteristics of the bridge outputs of the MK40A balance are investigated in detail in the next section.

Bi–directional Output Characteristics

A semi–empirical test was developed that determines if an output of a balance bridge has bi–directional characteristics if it is plotted versus the related primary bridge load (see App. 7, section 7.3.2). Test results may be used to justify the inclusion of absolute value terms in regression models of balance calibration data. Those types of terms should only be chosen if the outputs of a balance bridge have known bi–directional characteristics.

The test works with both the *Non–Iterative Method* and the *Iterative Method*. Two conditions need to be fulfilled for an output to be considered bi–directional if it is plotted versus the related primary load component. First, the bi–directional part of the output at load capacity needs to exceed 0.5 % of the to–capacity–scaled maximum of the difference between the bridge output and its natural zero. In addition, the p–value of the principal absolute value term must be less than 0.001. First, the bi–directional parts are examined. Table 34 below lists the bi–directional part at load capacity for each bridge output of the MK40A balance. The estimates were computed during the application of the *Non–Iterative Method* and the *Iterative Method* to data from the MK40A balance.

Table 34: Bi–directional part at load capacity of the bridges of the MK40A balance.†

	$\Lambda(D_1,N1)$ microV/V	$\Lambda(D_2,N2)$ microV/V	$\Lambda(D_3,S1)$ microV/V	$\Lambda(D_4,S2)$ microV/V	$\Lambda(D_5,AF)$ microV/V	$\Lambda(D_6,RM)$ microV/V
Non–Iterative	+6.46	+12.81	+23.64	+26.09	+1.21	−0.31
Iterative	+7.52	+11.79	+22.42	+25.05	+0.74	−0.27
Threshold	±6.12	±6.65	±6.29	±6.48	±7.14	±6.54

† D_1=$rN1-rN1_\circ$, D_2=$rN2-rN2_\circ$, D_3=$rS1-rS1_\circ$, D_4=$rS2-rS2_\circ$, D_5=$rAF-rAF_\circ$, D_6=$rRM-rRM_\circ$.

It is observed that the bi–directional parts of three bridges, i.e., $rN2$, $rS1$, and $rS2$, are well above the threshold that is listed in the last row of Table 34. The bi–directional part of one bridge output, i.e., $rN1$, is at the threshold and the bi–directional parts of two bridge outputs, i.e., rAF and rRM, are well below the threshold.

Next, the p–value of the t–statistic of the principal absolute value term was computed. First, results for the *Non–Iterative Method* are reviewed. Table 35 below lists the computed p–values of each absolute value term that were obtained after the *Non–Iterative Method* was applied. It is observed that the absolute value terms related to output differences

Table 35: *Non–Iterative Method* $\Longrightarrow$ p–value of the absolute value term of the primary bridge output difference of each fitted load component.[†]

$p\{\lvert D_1\rvert\}$	$p\{\lvert D_2\rvert\}$	$p\{\lvert D_3\rvert\}$	$p\{\lvert D_4\rvert\}$	$p\{\lvert D_5\rvert\}$	$p\{\lvert D_6\rvert\}$
0.0463 not significant	< 0.001 **significant**	< 0.001 **significant**	< 0.001 **significant**	0.5102 not significant	0.5926 not significant

[†] D_1=$rN1-rN1_\circ$, D_2=$rN2-rN2_\circ$, D_3=$rS1-rS1_\circ$, D_4=$rS2-rS2_\circ$, D_5=$rAF-rAF_\circ$, D_6=$rRM-rRM_\circ$.

D_2, D_3, and D_4 are statistically significant. Similarly, results for the *Iterative Method* are examined. Table 36 below lists the computed p–values of each absolute value term that were obtained after the *Iterative Method* was applied. Again, it is observed that the three absolute value terms related to the load components $N2$, $S1$, and $S2$ are statistically

Table 36: *Iterative Method* $\Longrightarrow$ p–value of the absolute value term of the primary load component of each fitted bridge output difference.

$p\{\lvert N1\rvert\}$	$p\{\lvert N2\rvert\}$	$p\{\lvert S1\rvert\}$	$p\{\lvert S2\rvert\}$	$p\{\lvert AF\rvert\}$	$p\{\lvert RM\rvert\}$
0.0223 not significant	< 0.001 **significant**	< 0.001 **significant**	< 0.001 **significant**	0.6853 not significant	0.6352 not significant

significant. It is concluded, after reviewing the test results listed in Tables 34, 35, and 36 that three of the six bridge outputs are bi–directional. They are the aft normal force bridge output and the forward & aft side force bridge outputs. Final test results are summarized in Table 37 below.

Table 37: Assessment of the bridge output characteristics of the MK40A balance.[†]

	$rN1$	$rN2$	$rS1$	$rS2$	rAF	rRM
Is output bi–directional ?	no	**yes**	**yes**	**yes**	no	no

[†] A bridge output is bi–directional if two conditions are met: (i) the bi–directional part at capacity exceeds its threshold (Tbl. 34) and (ii) the p–value of the principal absolute value term is less than 0.001 (Tbls. 35/36).

It is useful to illustrate the bi–directional part of two of the six outputs as an example. The forward side force and the rolling moment bridge outputs were chosen for that purpose. Figure 35 below shows the bi–directional part of the output of the forward side force bridge.

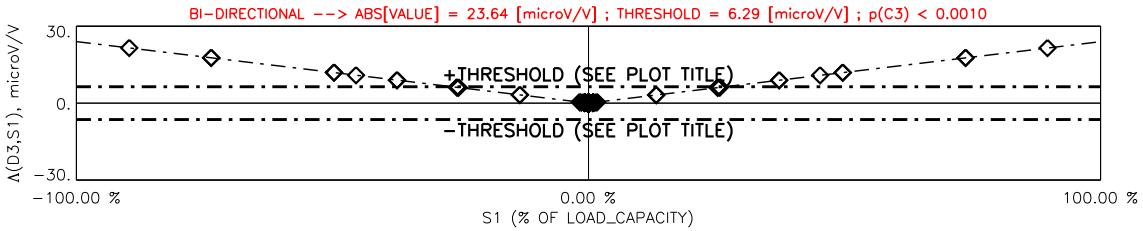

Fig. 35 Bi–directional part of the electrical output of the forward side force bridge plotted versus the tare corrected forward side force.

It can clearly be seen that the bi–directional part is above the empirical threshold at load capacity. This observation visually confirms that the forward side force bridge output of the MK40A balance has bi–directional characteristics when plotted versus the forward side force. Figure 36 below shows the bi–directional part of the electrical output of the

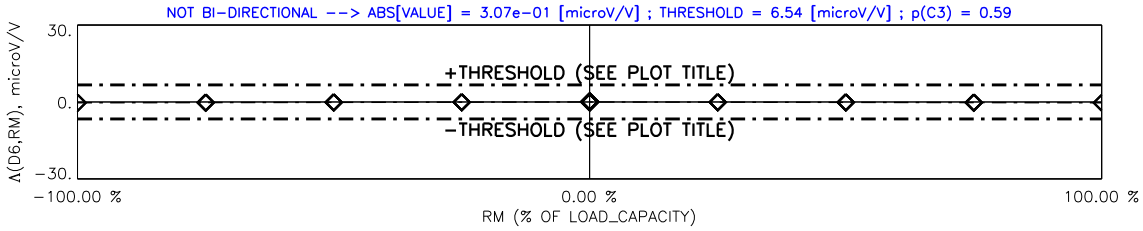

Fig. 36 Bi–directional part of the electrical output of the rolling moment bridge plotted versus the tare corrected rolling moment.

rolling moment bridge. In this case, the bi–directional part at capacity is well below the threshold that is listed for the rolling moment bridge output in Table 34. This observation visually confirms the test result that the rolling moment bridge output of the MK40A balance is not bi–directional when plotted versus the rolling moment.

It must be mentioned at this point that results of the semi–empirical test only allow an analyst to assess bi–directional characteristics between a bridge output and the related primary load of the bridge. The test cannot investigate more complex bi–directional characteristics that may exist between a bridge output and other balance loads components. In that case, it is recommended (i) to temporarily include absolute value terms in the regression models of the balance data, (ii) to perform a preliminary analysis, and (iii) to use the percent contributions of the absolute value terms as a test metric in order to determine if the chosen absolute value terms can model more complex connections between bridge outputs and balance loads (see also the discussion in App. 7, section 7.5). The importance of modeling more complex bi–directional connections between bridge outputs and balance loads in the load prediction equations must not be underestimated. An omission of an important bi–directional connection typically results in an unwanted increase of the calibration load residuals.

Complex bi–directional connections between the rolling moment and the outputs of the rolling moment bridge and the forward side force bridge of the MK40A balance exist. They can be used to illustrate their influence on the observed outputs of the balance

bridges. Table 38 below shows the applied rolling moment, the rolling moment bridge output difference, the forward side force, and the forward side force bridge output differ–

Table 38: Rolling moment, rolling moment bridge output difference, forward side force, and forward side force bridge output difference of series 15.

RM $in-lbs$	$D_6 = rRM - rRM_\circ$ $microV/V$	$S1$ lbs	$D_3 = rS1 - rS1_\circ$ $microV/V$
−8000	−1305.45	0.0	−13.50
−6000	−979.84	0.0	−9.25
−4000	−653.94	0.0	−2.29
−2000	−327.39	0.0	+4.10
0	−0.26	0.0	+3.81
+2000	+326.80	0.0	+21.26
+4000	+653.94	0.0	+30.90
+6000	+980.60	0.0	+39.14
+8000	+1307.11	0.0	+46.85

ence of a subset of nine data points of load series 15. As expected, the rolling moment bridge output difference (D_6) shows a highly linear relationship with the applied rolling moment (RM). This result is expected as (i) the rolling moment is its primary bridge load and (ii) it is known that the rolling moment bridge output does not have bi–directional characteristics when plotted versus the rolling moment (see also Table 37 and Fig. 36).

It is also observed in Table 38 that the forward side force bridge output difference (D_3) responds to the rolling moment (RM). The output range of the forward side force bridge output is 60.35 $microV/V$ for a rolling moment range of 16000 $in–lbs$. This output range is well above the empirical threshold of 1 $microV/V$ that is often used to identify negligible output changes. Therefore, the observed output range indicates an interaction between the rolling moment (RM) and forward side force bridge output difference (D_3) that cannot be ignored when the regression analysis of the calibration data is performed. The rolling moment is considered an independent variable if the *Iterative Method* is used to analyze balance calibration data. Consequently, the rolling moment is needed in the regression model of the forward side force bridge output difference, i.e., D_3, if the *Iterative Method* is used to analyze the calibration data of the MK40A balance.

The connection shown in Table 38 must be interpreted differently if the *Non–Iterative Method* is used for the balance calibration data analysis. In that case, independent and dependent variables are switched. Then, the rolling moment (RM) becomes the rolling moment bridge output difference (D_6) and the forward side force bridge output difference (D_3) becomes the forward side force ($S1$). Consequently, the rolling moment bridge output

difference (D_6) is needed in the regression model of the forward side force ($S1$) if the *Non–Iterative Method* is used to analyze the calibration data. Otherwise, the source of the output range on the forward side force bridge output difference (D_3) would not correctly be interpreted in the regression model of the forward side force ($S1$) as the applied values of the forward side force were all zero during series 15.

It is also observed in Table 38 that the forward side force bridge output difference (D_3) shows a bi–directional connection with the rolling moment (RM) as the output is -13.50 $microV/V$ for -8000 *in–lbs* and $+46.85$ $microV/V$ for $+8000$ *in–lbs*. The connection would not be bi–directional if the output differences at ± 8000 *in–lbs* would be similar in magnitude (e.g., ± 30.18 $microV/V$). Therefore, the absolute value term of the rolling moment is needed in the regression model of the forward side force bridge output difference if the *Iterative Method* is used to analyze the calibration data. Similarly, the absolute value term of the rolling moment bridge output difference is needed in the regression model of the forward side force if the *Non–Iterative Method* is applied.

The percent contributions of the regression model terms are also used in the next two sections to illustrate conclusions resulting from the bi–directional connection between rolling moment and forward side force bridge output difference.

Analysis Results for the Non–Iterative Method

The *Non–Iterative Method* is used in this section for the development of the load prediction equations for the MK40A balance from the given calibration data (see App. 9 for a description of the method). This approach directly fits the six balance load components, i.e., $N1$, $N2$, $S1$, $S2$, AF, and RM as a function of the bridge output differences D_1, D_2, ..., D_6 assuming that all loads are described relative to the absolute load datum of zero load. Table 39 below shows the selected regression model term combination for each one of the six load components of the balance. Absolute value terms were included in the

Table 39: Regression model terms of the six load components of the MK40A balance.

Intercept Term
Principal Linear Terms[†] $D_1,\ D_2,\ D_3,\ D_4,\ D_5,\ D_6$
Principal Absolute Value Terms $\lvert D_1\rvert,\ \lvert D_2\rvert,\ \lvert D_3\rvert,\ \lvert D_4\rvert,\ \lvert D_5\rvert,\ \lvert D_6\rvert$
Quadratic Terms $D_1^2,\ D_2^2,\ D_3^2,\ D_4^2,\ D_5^2,\ D_6^2$
Principal Linear $\times$ Principal Absolute Value Terms $D_1 \cdot \lvert D_1\rvert,\ D_2 \cdot \lvert D_2\rvert,\ D_3 \cdot \lvert D_3\rvert,\ D_4 \cdot \lvert D_4\rvert,\ D_5 \cdot \lvert D_5\rvert,\ D_6 \cdot \lvert D_6\rvert$
Cross–product Terms $(D_1 \cdot D_2),\ (D_3 \cdot D_4)$

[†] D_1=$rN1-rN1_\circ$, D_2=$rN2-rN2_\circ$, D_3=$rS1-rS1_\circ$, D_4=$rS2-rS2_\circ$, D_5=$rAF-rAF_\circ$, D_6=$rRM-rRM_\circ$

regression models of the load components because (i) three of the six bridge outputs have bi–directional characteristics when plotted versus the related primary load component and (ii) it is unknown if more complex bi–directional characteristics exist. No term reduction was done during the regression analysis of the data, i.e., 27 terms were used to separately fit each load component.

Figure 37a below shows the fitted coefficient value, standard error, t–statistic, p–value, and *Variance Inflation Factor* for each term of the regression model of the forward normal force as an example. These metrics may be used to assess the reliability of the regression model of the load component. As expected, the t–statistic of the output difference D_1 of the forward normal force bridge output $rN1$ has the greatest magnitude, i.e., ≈ 873, as it is, by design, the primary output of the forward normal force. Its p–value of less than 0.0001 indicates that the regression model term is highly significant. It is also observed that moderate near–linear dependencies exists between many of the chosen regression model terms. Related *Variance Inflation Factors* are between 14 and 21. They are highlighted in blue color in Fig. 37a. *Variance Inflation Factors* at these levels are no surprise as they are frequently observed with data from balances with bi–directional bridge outputs (see also App. 18 for details related to the calculation of the *Variance Inflation Factor*).

TERM NAME	COEFFICIENT VALUE	STANDARD ERROR	T–STATISTIC OF COEFFICIENT	P–VALUE OF COEFFICIENT	VARIANCE INFLATION FACTOR
INTERCEPT	−0.0213	+0.4196	−0.0508	–	–
D1	+2.9213	+0.0033	+872.6156	< 0.0001	+12.6069
D2	+0.0819	+0.0031	+26.1836	< 0.0001	+12.3453
D3	−0.0013	+0.0026	−0.4953	+0.6212	+14.3465
D4	−0.0047	+0.0026	−1.7997	+0.0741	+14.8176
D5	+0.0012	+0.0020	+0.6003	+0.5493	+14.5497
D6	−0.0099	+0.0018	−5.4057	< 0.0001	+14.3690
|D1|	−0.0174	+0.0046	−3.8132	+0.0002	+18.3752
|D2|	−0.0152	+0.0044	−3.4858	+0.0007	+18.6683
|D3|	+0.0144	+0.0032	+4.4582	< 0.0001	+19.3063
|D4|	+0.0061	+0.0033	+1.8201	+0.0710	+20.7829
|D5|	−0.0005	+0.0022	−0.2274	+0.8204	+16.7036
|D6|	+0.0242	+0.0020	+12.1261	< 0.0001	+14.6488
D1*D1	−7.8603e−06	+7.3361e−06	−1.0714	+0.2859	+18.3721
D2*D2	+2.4865e−07	+5.9898e−06	+0.0415	+0.9669	+16.3903
D3*D3	−7.1659e−06	+3.4960e−06	−2.0497	+0.0423	+16.9983
D4*D4	−4.1908e−06	+3.5560e−06	−1.1785	+0.2407	+17.9797
D5*D5	+1.2637e−07	+1.6126e−06	+0.0784	+0.9377	+15.2918
D6*D6	−7.5512e−06	+1.8076e−06	−4.1775	< 0.0001	+13.8255
D1*|D1|	−4.1275e−05	+5.7175e−06	−7.2189	< 0.0001	+12.2725
D2*|D2|	−3.5553e−05	+4.7403e−06	−7.5002	< 0.0001	+11.2300
D3*|D3|	+5.0798e−06	+2.9922e−06	+1.6977	+0.0919	+13.5945
D4*|D4|	+6.5680e−06	+3.0237e−06	+2.1722	+0.0316	+14.1836
D5*|D5|	−6.4172e−08	+1.5293e−06	−0.0420	+0.9666	+14.6346
D6*|D6|	+3.3000e−06	+1.7394e−06	+1.8973	+0.0599	+14.3176
D1*D2	+6.5766e−06	+1.0204e−05	+0.6445	+0.5203	+2.4459
D3*D4	−1.0673e−05	+5.5015e−06	−1.9400	+0.0545	+2.5532

Fig. 37a Coefficient values, standard error, t–statistic, p–value, and *Variance Inflation Factors* of the regression model terms of the forward normal force ($N1$).

Percent contributions of the regression model terms were also determined after completion of the regression analysis of the calibration data. Figure 37b below shows the

percent contributions of the thirty–six principal linear terms and the thirty–six principal absolute value terms of the regression models of the six load components (for simplicity, percent contributions of higher order terms are not discussed). Red color marks percent contributions of very important terms. Blue color is used to identify terms that are of minor importance. Finally, black color is used to mark terms of no importance. In general, it can be seen that the interactions between the bridges cannot be neglected. A total of 26 of the 72 terms are highlighted in red color (not counting the percent contribution of 100 %). These 26 terms are considered to be very important terms as the magnitude of

	N1	N2	S1	S2	AF	RM
D1	[100.00 %]	+12.61 %	−2.57 %	−0.44 %	−2.08 %	−0.07 %
D2	+2.80 %	[100.00 %]	−0.67 %	−1.19 %	+1.28 %	−0.02 %
D3	−0.04 %	−0.73 %	[100.00 %]	+4.43 %	+0.44 %	−0.09 %
D4	−0.16 %	−0.47 %	+1.44 %	[100.00 %]	−1.22 %	+0.10 %
D5	+0.04 %	+0.10 %	+7.8e−04 %	+0.04 %	[100.00 %]	−0.36 %
D6	−0.34 %	+0.43 %	−3.01 %	−3.16 %	−1.34 %	[100.00 %]
|D1|	−0.60 %	−0.29 %	+0.54 %	+0.34 %	−1.10 %	−0.05 %
|D2|	−0.52 %	−1.05 %	+0.25 %	+0.80 %	+0.06 %	−5.5e−03 %
|D3|	+0.49 %	+0.33 %	−1.87 %	−0.35 %	−0.19 %	+0.06 %
|D4|	+0.21 %	+0.34 %	−0.39 %	−2.09 %	−0.43 %	+0.04 %
|D5|	−0.02 %	−0.04 %	+0.07 %	+0.08 %	−0.07 %	+1.3e−03 %
|D6|	+0.83 %	+0.86 %	−2.41 %	−1.26 %	−0.25 %	+0.02 %

Interpretation of the Percent Contribution (taken from App. 16)

```
Percent_Contribution = 100 % ..................... primary/reference term (red)
ABS(Percent_Contribution) > 0.5 % ................. very important term (red)
0.1 % < ABS(Percent_Contribution) < 0.5 % ... term of minor importance (blue)
ABS(Percent_Contribution) < 0.1 % ............. term of no importance (black)
```

Fig. 37b Percent contributions of the principal linear and absolute value terms of the six fitted balance load components.

their percent contributions exceeds the empirical threshold of 0.5 %. It is also interesting to examine the relationship between the forward side force ($S1$) and the rolling moment bridge output difference (D_6) that was discussed in an earlier section. As expected, the rolling moment bridge output difference (D_6) is needed in the regression model of the forward side force ($S1$) as a connection between the rolling moment bridge output (D_6) and the forward side force ($S1$) exists. The percent contribution of the term D_6 of the regression model of $S1$ has the relatively large value of -3.01 %. In addition, it is known that the connection between the rolling moment bridge output (D_6) and the forward side force ($S1$) is bi–directional. This relationship is reflected in Fig. 37b above by the fact that the percent contribution of the term $|D_6|$ also has the relatively large value of -2.41 %.

A tare load iteration was performed during the calibration data analysis so that balance loads resulting from the weight of the calibration equipment and the metric part of the balance would be included in the load set that was ultimately used as input for the re-

gression analysis (App. 12 describes the tare load iteration process that the *Non–Iterative Method* uses). Table 40 below lists the computed tare loads for the sixteen load series.

Table 40: *Non–Iterative Method* $\Longrightarrow$ Predicted tare loads of the calibration data of the MK40A balance; tare loads are listed as a percentage of the load capacity.

Series	$N1$, %	$N2$, %	$S1$, %	$S2$, %	AF, %	RM, %
1	+1.28	+0.38	+0.01	–0.01	+0.16	+0.01
2	–1.19	–0.37	–0.02	–0.01	+0.17	≈ 0
3	+0.62	+1.10	–0.07	≈ 0	+0.10	≈ 0
4	–0.53	–0.99	–0.08	–0.05	+0.10	–0.01
5	+0.90	+0.79	–0.02	+0.01	+0.12	–0.01
6	–0.85	–0.71	–0.05	–0.03	+0.18	–0.02
7	+0.03	+0.06	+1.64	+0.47	+0.20	–0.03
8	–0.01	≈ 0	–1.69	–0.44	+0.16	≈ 0
9	+0.03	+0.05	+0.86	+1.47	+0.14	–0.03
10	+0.01	+0.02	–0.76	–1.36	+0.15	≈ 0
11	+0.04	+0.04	+1.23	+0.85	+0.18	–0.03
12	≈ 0	+0.01	–1.40	–0.94	+0.17	≈ 0
13	+0.02	+0.04	≈ 0	+0.02	+15.97	≈ 0
14	+0.04	≈ 0	+0.04	–0.03	–11.30	≈ 0
15	+6.64	+6.41	+0.16	+0.15	+0.01	+0.02
16	–6.59	–6.42	+0.10	+0.05	+0.08	+0.04

The regression analysis of the data was successfully completed using (i) the tare corrected loads and (ii) output differences relative to the natural zeros of the balance as input. Table 41 below lists the standard deviation of the load residuals, i.e., of the difference between measured and fitted load, for each load component of the MK40A balance. The standard deviations of all load components are well below the threshold of 0.10 % of load capacity that is traditionally used in the aerospace testing community for the assessment of the standard deviation of balance load residuals.

Table 41: *Non–Iterative Method* $\Longrightarrow$ Standard deviation of the load residuals.[†]

$N1$ lbs	$N2$ lbs	$S1$ lbs	$S2$ lbs	AF lbs	RM $in-lbs$
1.91 (0.055 %)	1.84 (0.053 %)	2.21 (0.089 %)	1.80 (0.072 %)	0.28 (0.070 %)	2.05 (0.026 %)

[†]Standard deviations expressed as a percentage of the load capacity are listed in brackets.

As an example, forward side force residuals of the MK40A balance are plotted versus the tare corrected forward side force in Fig. 38a below. Most residuals are well within the threshold of $\pm 0.25\,\%$ of capacity that is traditionally used for the assessment of individual load residuals. A few outliers are detected that appear near zero load. They are caused

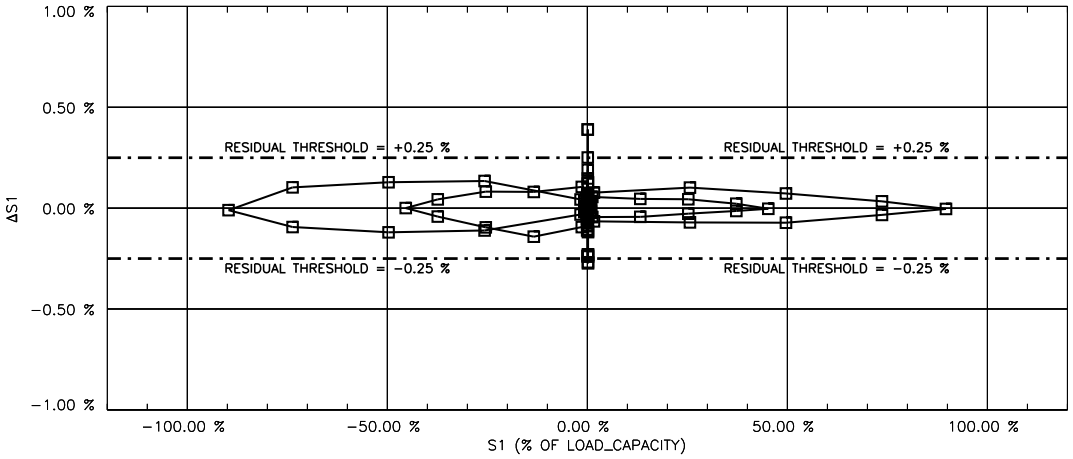

Fig. 38a *Non–Iterative Method* $\Longrightarrow$ Forward side force residuals ($\Delta S1$) of the MK40A balance plotted versus the tare corrected forward side force ($S1$).

by interactions. Therefore, it was decided to also plot the load residuals versus data point index and load series number in Fig. 38b below in order to identify the source of the residual outliers. It can clearly be seen in Fig. 38b that the residual outliers are located in

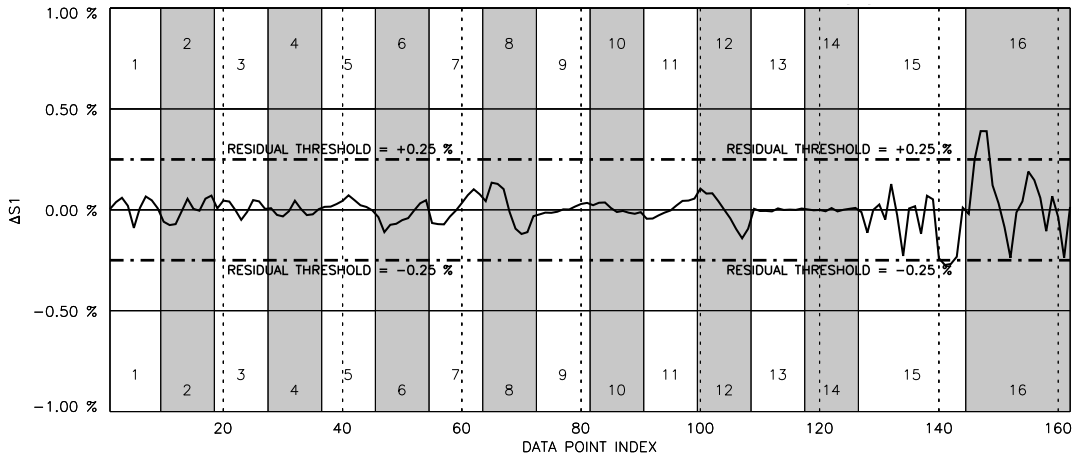

Fig. 38b *Non–Iterative Method* $\Longrightarrow$ Forward side force residuals ($\Delta S1$) of the MK40A balance plotted versus data point index and load series number.

load series 15 and 16 (the alternating gray scale used in Fig. 38b above identifies individual load series). The rolling moment was applied during both load series (see also Fig. 34). Therefore, the threshold outliers are caused by interactions between the rolling moment and the forward side force bridge output.

Similarly, the rolling moment residuals of the MK40A balance are plotted versus the tare corrected rolling moment in Fig. 39 below. This time, all residuals are within the threshold of $\pm 0.25\,\%$ of capacity. This result is no surprise because the regression model of the fitted rolling moment showed highly linear characteristics and interactions were very small (see also percent contributions listed in the last column of Fig. 37b).

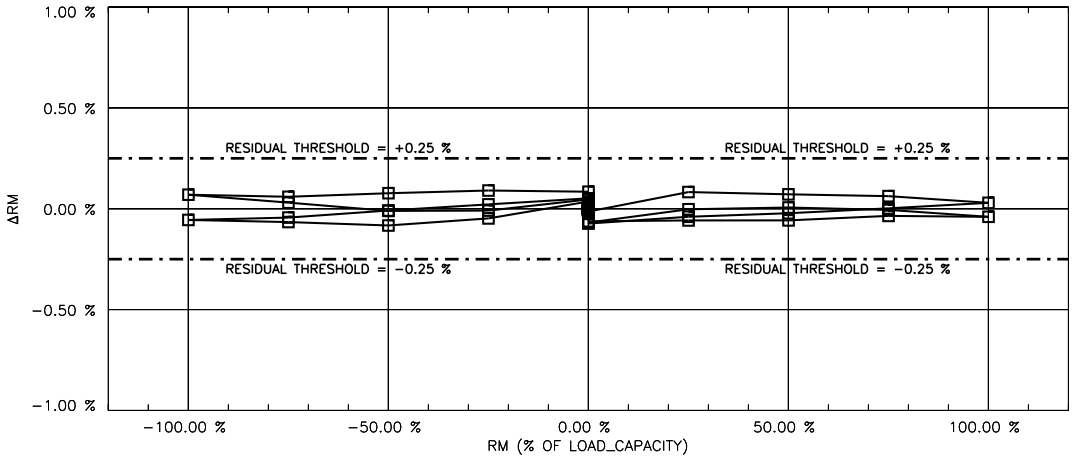

Fig. 39 *Non–Iterative Method* $\Longrightarrow$ Rolling moment residuals (ΔRM) of the MK40A balance plotted versus the tare corrected rolling moment (RM).

The primary sensitivities of the balance bridges were also computed during the regression analysis of the calibration data. The primary sensitivity of a balance bridge is defined as the first derivative of a bridge output with respect to the corresponding primary bridge load. Therefore, it equals the inverse of the coefficient of the primary output difference that is used in the regression model of a balance load component if the *Non–Iterative Method* is used for the balance load prediction. This statement can be illustrated by using the regression model of the forward normal force as an example. It is defined by the equation

$$N1 \;=\; a_0 \;+\; a_1 \cdot D_1 \;+\; a_2 \cdot D_2 \;+\; a_3 \cdot D_3 \;+\; a_4 \cdot D_4 \;+\; \ldots \tag{21}$$

where the inverse of the primary sensitivity of the forward normal force bridge equals

$$a_1 \;=\; \frac{\partial\, N1}{\partial\, D_1} \;\approx\; \left\{ \frac{\partial\, D_1}{\partial\, N1} \right\}^{-1} = \left\{ \frac{\partial\, [\, rN1 - \overbrace{rN1_\circ}^{const.}\,]}{\partial\, N1} \right\}^{-1} = \left\{ \frac{\partial\, rN1}{\partial\, N1} \right\}^{-1} \tag{22}$$

Consequently, the primary sensitivity of the forward normal force bridge output becomes:

$$\begin{matrix} Primary\ Sensitivity \\ (forward\ normal\ force\ bridge) \end{matrix} \quad \Longrightarrow \quad \frac{\partial\, rN1}{\partial\, N1} \;\approx\; \frac{1}{a_1} \tag{23}$$

Table 42 below lists the primary sensitivities of the MK40A balance. As expected, the axial force bridge has the highest sensitivity of all balance bridges because the axial force capacity is about one order of magnitude below the normal and side force capacities.

Table 42: *Non–Iterative Method* $\Longrightarrow$ Primary sensitivities of the MK40A balance.

$\frac{\partial\, rN1}{\partial\, N1}$	$\frac{\partial\, rN2}{\partial\, N2}$	$\frac{\partial\, rS1}{\partial\, S1}$	$\frac{\partial\, rS2}{\partial\, S2}$	$\frac{\partial\, rAF}{\partial\, AF}$	$\frac{\partial\, rRM}{\partial\, RM}$
$0.3423^{\dagger}$	$0.3708^{\dagger}$	$0.4897^{\dagger}$	$0.5025^{\dagger}$	$3.5684^{\dagger}$	$0.1639^{\ddagger}$

$^{\dagger}[microV/V]\,/\,[lbs]$; $^{\ddagger}[microV/V]\,/\,[in\text{–}lbs]$.

It is also useful to compare the maximum output at load capacity of the six bridges of the MK40A balance. This metric is frequently used to scale instrumentation inputs so that the best accuracy of the electrical output measurement of the balance bridges can be achieved. The metric is defined as the product of (i) the prime sensitivity of a bridge with (ii) the capacity of the related load component. Table 43 below lists corresponding values that were obtained for the six bridges of the MK40A balance.

Table 43: *Non–Iterative Method* $\Longrightarrow$ Maximum output† of the MK40A balance.

$rN1$ $microV/V$	$rN2$ $microV/V$	$rS1$ $microV/V$	$rS2$ $microV/V$	rAF $microV/V$	rRM $microV/V$
1198.1	1297.9	1224.3	1256.2	1427.3	1311.0

†Maximum output $\equiv$ product of the primary bridge sensitivity and the capacity of the related load component.

It is observed that the maximum output has values between 1198 $microV/V$ and 1427 $microV/V$. This result indicates that bridge outputs and load capacities are matched very well as (i) the maximum outputs of all bridges are above 1000 $microV/V$ and (ii) the smallest and largest value only differ by 229 $microV/V$.

Table 44 below shows the subset of the thirty–six principal linear coefficients of the regression models of the six load components of the MK40A balance that were ob–

Table 44: *Non–Iterative Method* $\Longrightarrow$ Principal linear coefficients of the fitted regression model of each balance load component.

	D1	D2	D3	D4	D5	D6
N1	2.921295E+00	8.185590E-02	-1.270812E-03	-4.671090E-03	1.182397E-03	-9.864305E-03
N2	3.400873E-01	2.696682E+00	-1.970753E-02	-1.263236E-02	2.601478E-03	1.165878E-02
S1	-5.246381E-02	-1.360457E-02	2.041915E+00	2.945034E-02	1.593378E-05	-6.155622E-02
S2	-8.699317E-03	-2.376486E-02	8.825065E-02	1.990140E+00	6.996121E-04	-6.283255E-02
AF	-5.825329E-03	3.576150E-03	1.246866E-03	-3.406365E-03	2.802414E-01	-3.766000E-03
RM	-4.065943E-03	-1.185076E-03	-5.785828E-03	5.982193E-03	-2.190301E-02	6.102319E+00

tained. These coefficient values will be compared in the next section with corresponding values that were obtained after the application of the *Iterative Method*.

Analysis Results for the Iterative Method

The *Iterative Method* is used in this section for calibration data analysis and the load prediction of the MK40A balance (see Ref. [7] and App. 10 for a description of the method). This approach first fits the electrical outputs of the balance bridges as a function of the balance loads. Afterwards, a load iteration equation is constructed from the regression coefficients of the fitted outputs so that loads can be predicted from measured outputs during a wind tunnel test. Finally, iteration equation coefficients are stored in a standardized data reduction matrix so that the iteration equation can easily be shared and/or implemented in the data system of a wind tunnel.

Table 45 below shows the selected regression model term combination for each one of the six bridge output differences D_1, D_2, ..., D_6 assuming that all balance loads are described relative to the absolute load datum of zero load. The final regression model of each output difference consisted of 27 terms (no term reduction was performed). Absolute

Table 45: Regression model terms of the six output differences[†] of the MK40A balance.

Intercept Term
Principal Linear Terms $N1,\ N2,\ S1,\ S2,\ AF,\ RM$
Principal Absolute Value Terms $\|N1\|,\ \|N2\|,\ \|S1\|,\ \|S2\|,\ \|AF\|,\ \|RM\|$
Quadratic Terms $N1^2,\ N2^2,\ S1^2,\ S2^2,\ AF^2,\ RM^2$
Principal Linear $\times$ Principal Absolute Value Terms $N1 \cdot \|N1\|,\ N2 \cdot \|N2\|,\ S1 \cdot \|S1\|,\ S2 \cdot \|S2\|,\ AF \cdot \|AF\|,\ RM \cdot \|RM\|$
Cross–product Terms $(N1 \cdot N2),\ (S1 \cdot S2)$

[†] $D_1 = rN1 - rN1_\circ$, $D_2 = rN2 - rN2_\circ$, $D_3 = rS1 - rS1_\circ$, $D_4 = rS2 - rS2_\circ$, $D_5 = rAF - rAF_\circ$, $D_6 = rRM - rRM_\circ$

value terms were included in the regression models of the bridge output differences because (i) three of the six bridge outputs have bi–directional characteristics when plotted versus the related primary load component and (ii) it is unknown if more complex bi–directional characteristics exist. No term reduction was done during the regression analysis of the data, i.e., 27 terms were used to separately fit each output difference.

Figure 40a below shows the fitted coefficient value, standard error, t–statistic, p–value, and *Variance Inflation Factor* of each term of the regression model of the forward normal

force bridge output difference as an example. These metrics may be used to assess the reliability of the regression model of the output difference. As expected, the t–statistic of the forward normal force ($N1$) has the greatest magnitude, i.e., ≈ 792, as it is, by design, the primary load component of the forward normal force bridge output difference. Its p–value of less than 0.0001 indicates that the regression model term is highly significant. It is also observed that moderate near–linear dependencies exists between many of the chosen regression model terms. Related *Variance Inflation Factors* are between 14 and 21. They are highlighted in blue color in Fig. 40a. *Variance Inflation Factors* at these levels are no surprise as they are frequently observed with data from balances with bi–directional bridge outputs (see also App. 18 for details related to the *Variance Inflation Factor*).

TERM NAME	COEFFICIENT VALUE	STANDARD ERROR	T–STATISTIC OF COEFFICIENT	P–VALUE OF COEFFICIENT	VARIANCE INFLATION FACTOR
INTERCEPT	−0.0014	+0.1502	−0.0095	–	–
N1	+0.3432	+0.0004	+792.1407	< 0.0001	+14.3555
N2	−0.0106	+0.0004	−24.2175	< 0.0001	+14.4598
S1	+0.0001	+0.0005	+0.2608	+0.7947	+14.9813
S2	+0.0007	+0.0005	+1.4861	+0.1396	+15.8624
AF	−0.0013	+0.0025	−0.5118	+0.6096	+14.5430
RM	+0.0006	+0.0001	+5.2763	< 0.0001	+14.2873
|N1|	+0.0021	+0.0006	+3.8311	+0.0002	+18.8177
|N2|	+0.0016	+0.0006	+2.8048	+0.0058	+18.8003
|S1|	−0.0022	+0.0006	−3.9464	+0.0001	+19.9021
|S2|	−0.0008	+0.0006	−1.4275	+0.1557	+21.2204
|AF|	+0.0006	+0.0028	+0.2017	+0.8405	+16.9299
|RM|	−0.0013	+0.0001	−11.6172	< 0.0001	+14.9330
N1*N1	+4.0884e−07	+2.8381e−07	+1.4405	+0.1520	+15.3622
N2*N2	+1.6386e−07	+2.8504e−07	+0.5749	+0.5663	+15.2876
S1*S1	+4.4147e−07	+2.8790e−07	+1.5334	+0.1275	+15.8999
S2*S2	+2.5138e−07	+3.1188e−07	+0.8060	+0.4216	+17.0633
AF*AF	−6.3129e−07	+7.2514e−06	−0.0871	+0.9308	+15.3292
RM*RM	+6.7971e−08	+1.7045e−08	+3.9877	+0.0001	+13.8521
N1*|N1|	+1.8088e−06	+2.4189e−07	+7.4776	< 0.0001	+12.3056
N2*|N2|	+1.7357e−06	+2.4432e−07	+7.1042	< 0.0001	+12.3749
S1*|S1|	−4.2032e−07	+2.5365e−07	−1.6570	+0.0998	+13.4868
S2*|S2|	−5.2057e−07	+2.7401e−07	−1.8998	+0.0596	+14.4190
AF*|AF|	+1.1782e−07	+6.8685e−06	+0.0172	+0.9863	+14.6348
RM*|RM|	−2.8508e−08	+1.6370e−08	−1.7415	+0.0839	+14.2874
N1*N2	−6.2347e−07	+4.7615e−07	−1.3094	+0.1926	+2.6404
S1*S2	+7.9647e−07	+4.8395e−07	+1.6458	+0.1021	+2.7716

Fig. 40a Coefficient values, standard error, t–statistic, p–value, and *Variance Inflation Factors* of the regression model of the forward normal force bridge output difference (D_1).

Percent contributions of the regression model terms were also determined after completion of the regression analysis of the calibration data. Figure 40b below shows the percent contributions of the thirty–six principal linear terms and the thirty–six principal absolute value terms of the regression models of the six bridge output differences (for simplicity, percent contributions of higher order terms are not discussed). Red color marks percent contributions of very important terms. Blue color is used to identify terms that are of minor importance. Finally, black color is used to mark terms of no importance. In general, it can be seen that the interactions between the bridges cannot be neglected. A total of 24 of the 72 terms are highlighted in red color (not counting the percent contribution of 100 %). These 24 terms are considered to be very important terms as the magnitude of

	D_1	D_2	D_3	D_4	D_5	D_6
N1	[100.00 %]	−11.72 %	+2.47 %	+0.22 %	+1.87 %	+0.08 %
N2	−3.09 %	[100.00 %]	+0.70 %	+1.26 %	−1.24 %	+0.01 %
S1	+0.02 %	+0.68 %	[100.00 %]	−4.32 %	−0.43 %	+0.09 %
S2	+0.15 %	+0.42 %	−1.46 %	[100.00 %]	+1.10 %	−0.09 %
AF	−0.04 %	−0.10 %	+0.02 %	−0.02 %	[100.00 %]	+0.40 %
RM	+0.37 %	−0.46 %	+3.24 %	+3.19 %	+1.28 %	[100.00 %]
|N1|	+0.63 %	+0.24 %	−0.47 %	−0.31 %	+0.94 %	+0.06 %
|N2|	+0.46 %	+0.91 %	−0.13 %	−0.75 %	−0.13 %	−6.3e−03 %
|S1|	−0.46 %	−0.21 %	+1.83 %	+0.25 %	+0.16 %	−0.05 %
|S2|	−0.18 %	−0.27 %	+0.32 %	+2.04 %	+0.40 %	−0.03 %
|AF|	+0.02 %	+0.04 %	−0.05 %	−0.07 %	+0.05 %	+3.6e−03 %
|RM|	−0.90 %	−0.75 %	+2.60 %	+1.26 %	+0.25 %	−0.02 %

Interpretation of the Percent Contribution (taken from App. 16)

```
Percent_Contribution = 100 % ..................... primary/reference term (red)
ABS(Percent_Contribution) > 0.5 % ................. very important term (red)
0.1 % < ABS(Percent_Contribution) < 0.5 % ... term of minor importance (blue)
ABS(Percent_Contribution) < 0.1 % ............. term of no importance (black)
```

Fig. 40b Percent contributions of the principal linear and absolute value terms of the six fitted bridge output differences.

their percent contributions exceeds the empirical threshold of 0.5 %. More complex bi–directional connections between load components and bridge output differences were detected. It is interesting to examine the relationship between the forward side force bridge output difference (D_3) and the rolling moment (RM) that was discussed in an earlier section. As expected, the rolling moment (RM) is needed in the regression model of the forward side force bridge output difference (D_3) as a connection between the rolling moment and the forward side force bridge output difference exists (see also Table 38). Therefore, the percent contribution of the rolling moment (RM) to the regression model of the forward side force bridge output difference (D_3) has the relatively large value of +3.24 %. In addition, it is known that the connection between the rolling moment (RM) and the forward side force bridge output difference (D_3) is bi–directional. This relationship is reflected in Fig. 40b above by the fact that the percent contribution of the absolute value of the rolling moment ($|RM|$) has the relatively large value of +2.60 %.

It is rigorously proven in App. 16 that a direct connection between the percent contributions of the regression models of the loads and the output differences of a balance exists: percent contributions of pairs of related terms have to be similar in magnitude but opposite in sign. This connection can be illustrated by using the percent contributions that were discussed in the previous paragraph. First, it known from the regression model of the forward side force bridge output difference (D_3) that (i) the percent contribution of the rolling moment (RM) equals +3.24 % and (ii) the percent contribution of the absolute value of the rolling moment ($|RM|$) equals +2.60 % (taken from Fig. 40b). Now, the *Non–Iterative Method* is used instead of the *Iterative Method* for the calibration data analysis. Consequently, the forward side force ($S1$) is the related term to the forward side force

bridge output difference (D_3). Similarly, the rolling moment bridge output difference (D_6) is the related term to the rolling moment (RM). Then, it known from the regression model of the forward side force (S_1) that (i) the percent contribution of the rolling moment bridge output difference (D_6) equals $-3.01\,\%$ and (ii) the percent contribution of the absolute value of the rolling moment bridge output difference ($|D_6|$) equals $-2.41\,\%$ (values were copied from Fig. 37b). As predicted, the percent contribution of D_6 ($-3.01\,\%$) is similar in magnitude but opposite in sign to the percent contribution of RM ($+3.24\,\%$). Likewise, the percent contribution of $|D_6|$ ($-2.41\,\%$) is similar in magnitude but opposite in sign to the percent contribution of $|RM|$ ($+2.60\,\%$).

A tare load iteration was performed during the calibration data analysis so that balance loads resulting from the weight of the calibration equipment and the metric part of the balance would be included in the load set that was ultimately used for the regression analysis (App. 13 describes the tare load iteration process that the *Iterative Method* uses). Table 46 below lists the computed tare loads for the sixteen load series. These values can directly be compared with values that are listed in Table 40 for the *Non–Iterative Method*. The maximum observed differences are very small ($\approx 0.01\,\%$ of load capacity). Therefore, it is concluded that tare load estimates obtained after application

Table 46: *Iterative Method* $\Longrightarrow$ Predicted tare loads of the calibration data of the MK40A balance; tare loads are listed as a percentage of the load capacity.[†]

Series	$N1$, %	$N2$, %	$S1$, %	$S2$, %	AF, %	RM, %
1	+1.28	+0.38	+0.01	$\approx$ **0**	+0.16	+0.01
2	–1.19	–0.37	–0.02	–0.01	+0.17	≈ 0
3	+0.62	+1.10	–0.07	≈ 0	+0.10	≈ 0
4	–0.53	–0.99	–0.08	–0.05	+0.10	–0.01
5	+0.90	+0.79	–0.02	+0.01	**+0.13**	–0.01
6	**–0.86**	–0.71	–0.05	–0.03	+0.18	–0.02
7	+0.03	+0.06	+1.64	+0.47	+0.20	–0.03
8	–0.01	≈ 0	–1.69	–0.44	+0.16	≈ 0
9	+0.03	+0.05	+0.86	+1.47	**+0.13**	–0.03
10	+0.01	+0.02	–0.76	–1.36	+0.15	≈ 0
11	+0.04	+0.04	+1.23	**+0.84**	+0.18	–0.03
12	≈ 0	+0.01	–1.40	–0.94	+0.17	≈ 0
13	+0.02	+0.04	≈ 0	**+0.01**	+15.97	≈ 0
14	+0.04	≈ 0	+0.04	–0.03	–11.30	≈ 0
15	**+6.65**	**+6.42**	**+0.15**	+0.15	**+0.02**	+0.02
16	**–6.60**	**–6.44**	+0.10	**+0.06**	+0.08	+0.04

[†]Boldface marks tare load estimates that differ $\approx 0.01\,\%$ from values reported in Table 40.

of the *Iterative Method* are in excellent agreement with tare load estimates obtained after application of the *Non–Iterative Method*.

The regression analysis of the data was successfully completed using (i) the tare corrected loads and (ii) output differences relative to the natural zeros of the balance as input. Afterwards, a data reduction matrix for the load prediction was generated. Table 47 below lists the standard deviation of the load residuals of the calibration data, i.e., of the difference between measured and fitted load, for each load component of the MK40A balance in engineering units (corresponding values expressed as a percentage of the capacity are listed in brackets). The standard deviations of the predicted loads are well below the threshold of 0.10 % that is traditionally used in the aerospace testing community for

Table 47: *Iterative Method* $\Longrightarrow$ Standard deviation of the load residuals.[†]

$N1$ lbs	$N2$ lbs	$S1$ lbs	$S2$ lbs	AF lbs	RM $in-lbs$
2.01 (0.058 %)	1.96 (0.056 %)	2.26 (0.090 %)	1.81 (0.073 %)	0.28 (0.070 %)	2.06 (0.026 %)

[†]Standard deviations expressed as a percentage of the load capacity are listed in brackets.

the assessment of the standard deviation of balance load residuals. The standard deviations shown in Table 47 can be compared with corresponding values that are listed in Table 41 for the *Non–Iterative Method*. The maximum difference between the standard deviations is very small ($\approx$ 0.003 %). Therefore, it is concluded that the standard deviation of the load residuals show excellent agreement with corresponding values that were obtained after the application of the *Non–Iterative Method*.

As an example, forward side force residuals of the MK40A balance are plotted versus the tare corrected forward side force in Fig. 41a below. Most load residuals are well within

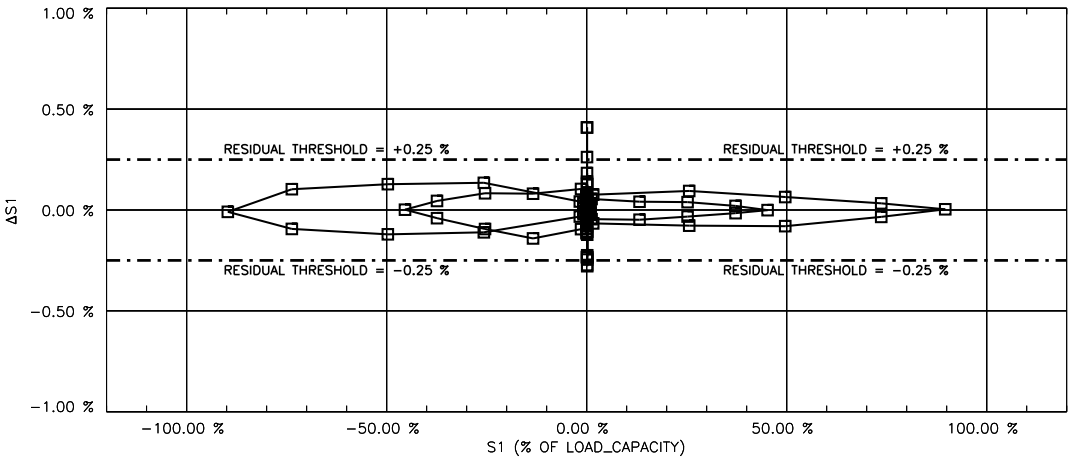

Fig. 41a *Iterative Method* $\Longrightarrow$ Forward side force residuals ($\Delta S1$) of the MK40A balance plotted versus the tare corrected forward side force ($S1$).

the threshold of $\pm 0.25\,\%$ of capacity that is traditionally used to assess individual load residual values. The residuals show excellent qualitative and quantitative agreement with corresponding values that are shown in Fig. 38a for the *Non–Iterative Method*.

Similarly, Fig. 41b below shows the same load residuals plotted versus data point index and load series number. Again, the residuals show excellent qualitative and quantitative agreement with the residuals that are seen in Fig. 38b for the *Non–Iterative Method*.

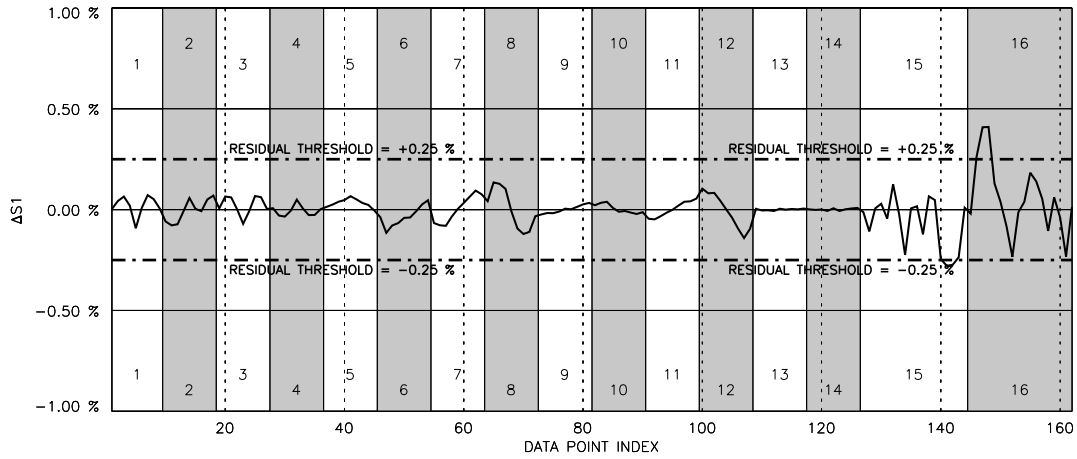

Fig. 41b *Iterative Method* $\Longrightarrow$ Forward side force residuals ($\Delta S1$) of the MK40A balance plotted versus data point index and load series number.

Finally, rolling moment residuals of the MK40A balance are plotted versus the tare corrected rolling moment in Fig. 42 below. Again, all residuals are within the threshold of $\pm 0.25\,\%$ of capacity that is used to assess individual load residuals. In addition, the residuals show excellent qualitative and quantitative agreement with the residuals that are seen in Fig. 39 for the *Non–Iterative Method*.

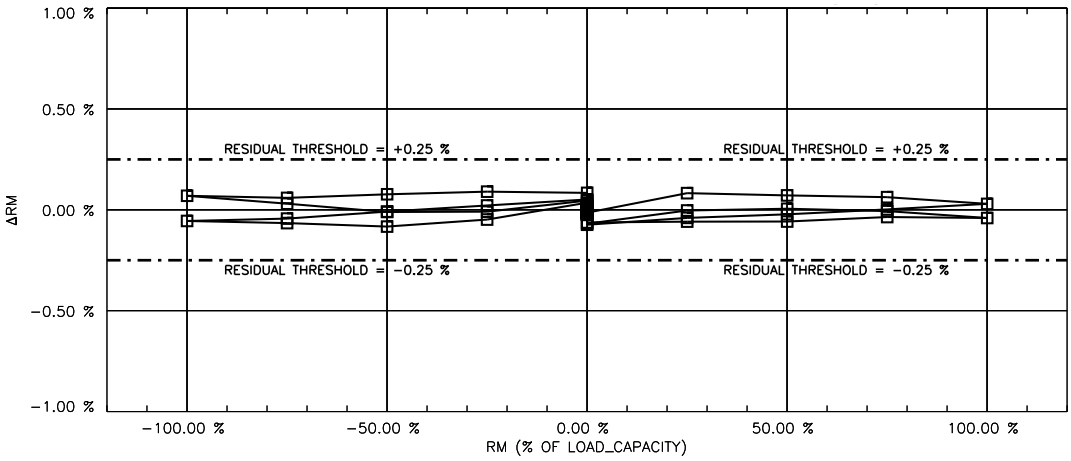

Fig. 42 *Iterative Method* $\Longrightarrow$ Rolling moment residuals (ΔRM) of the MK40A balance plotted versus the tare corrected rolling moment (RM).

The primary sensitivities of the balance bridges were also computed during the regression analysis of the calibration data. The primary sensitivity of a bridge is defined in this context as the coefficient of the primary load component that is used in the regression model of a bridge output difference. This general statement can be illustrated by using the regression model of the bridge output difference D_1 of the forward normal force bridge as an example. This regression model is defined in Eq. (24) below. The primary sensitivity of

$$D_1 \;=\; rN1 \;-\; rN1_{\circ} \;=\; b_0 \;+\; b_1 \cdot N1 \;+\; b_2 \cdot N2 \;+\; b_3 \cdot S1 \;+\; b_4 \cdot S2 \;+\; \ldots \qquad (24)$$

output difference D_1 equals the coefficient of the forward normal force. Then, we get:

$$\underset{\substack{Primary\ Sensitivity \\ (forward\ normal\ force\ bridge)}}{\Longrightarrow} \; b_1 \;=\; \frac{\partial\, D_1}{\partial\, N1} \;=\; \frac{\partial\, [\, rN1 - \overbrace{rN1_{\circ}}^{const.}\,]}{\partial\, N1} \;=\; \frac{\partial\, rN1}{\partial\, N1} \qquad (25)$$

Table 48 below lists the primary sensitivities for the MK40A balance. Again, the axial force bridge has the highest sensitivity of all balance bridges because the axial force capacity is about one order of magnitude below the capacities of the normal and side forces.

Table 48: *Iterative Method* $\Longrightarrow$ Primary sensitivities of the MK40A balance.

$\frac{\partial\, rN1}{\partial\, N1}$	$\frac{\partial\, rN2}{\partial\, N2}$	$\frac{\partial\, rS1}{\partial\, S1}$	$\frac{\partial\, rS2}{\partial\, S2}$	$\frac{\partial\, rAF}{\partial\, AF}$	$\frac{\partial\, rRM}{\partial\, RM}$
$0.3432^{\dagger}$	$0.3719^{\dagger}$	$0.4901^{\dagger}$	$0.5030^{\dagger}$	$3.5677^{\dagger}$	$0.1639^{\ddagger}$

$^{\dagger}[microV/V]/[lbs]$; $^{\ddagger}[microV/V]/[in\text{–}lbs]$.

The maximum output at capacity of the six balance bridges was also computed. This metric is defined as the product of (i) the primary sensitivity of a bridge with (ii) the capacity of the related load component. Table 49 below lists corresponding values that were obtained for the six bridges of the MK40A balance.

Table 49: *Iterative Method* $\Longrightarrow$ Maximum output† of the MK40A balance.

$rN1$ $microV/V$	$rN2$ $microV/V$	$rS1$ $microV/V$	$rS2$ $microV/V$	rAF $microV/V$	rRM $microV/V$
1201.2	1301.8	1225.3	1257.4	1427.1	1311.0

†Maximum output $\equiv$ product of the primary bridge sensitivity and the capacity of the related load component.

The numerical estimates listed in Table 49 above can be compared with alternate estimates that were obtained during the application of the *Non–Iterative Method* to the calibration data (see Table 43). The absolute value of the differences between related estimates is given in Table 50 below. The differences for four of the six bridges are very

Table 50: Difference between estimated maximum outputs (Table 43 versus Table 49).

$rN1$ $microV/V$	$rN2$ $microV/V$	$rS1$ $microV/V$	$rS2$ $microV/V$	rAF $microV/V$	rRM $microV/V$
3.1	3.9	1.0	1.2	0.2	< 0.1

small. They are near or below the threshold of 1.0 $microV/V$ that is used to identify negligible output differences. The normal force bridge outputs are the exception. In those cases, the differences are 3.1 $microV/V$ and 3.9 $microV/V$. They are still relatively small and indicate a good agreement between the independent estimates of the maximum output.

Finally, it is interesting to examine the non–iterative part of the load iteration equation that is obtained after the application of the *Iterative Method*. The non–iterative part equals square matrix $\mathbf{C_1}^{-1}$ that is traditionally used to define the primary load iteration equation (see Ref. [7] or App. 10 for more details). Table 51 below lists the values of matrix $\mathbf{C_1}^{-1}$ that were obtained from the calibration data set of the MK40A balance. In theory, these

Table 51: *Iterative Method* $\Longrightarrow$ Coefficients of square matrix $\mathbf{C_1}^{-1}$. This matrix is the constant, i.e., non–iterative part of the load iteration equation.

	D1	D2	D3	D4	D5	D6
N1	2.924367E+00	8.334239E-02	-1.488930E-03	-4.505349E-03	1.149637E-03	-9.333192E-03
N2	3.433268E-01	2.698702E+00	-2.001978E-02	-1.247416E-02	2.542825E-03	1.210165E-02
S1	-5.331877E-02	-1.529739E-02	2.041838E+00	2.912285E-02	-8.532762E-05	-6.260388E-02
S2	-9.910861E-03	-2.508709E-02	8.839700E-02	1.989473E+00	5.174015E-04	-6.356952E-02
AF	-5.779212E-03	3.685231E-03	1.215347E-03	-3.480901E-03	2.803107E-01	-3.785567E-03
RM	-4.916728E-03	-1.305874E-03	-5.733329E-03	6.241274E-03	-2.224617E-02	6.102504E+00

values should show good agreement with the thirty–six principal linear terms that were obtained after the application of the *Non–Iterative Method* to the calibration data (Table 44). The values of Table 51 can be compared with the values of Table 44 by simply examining the ratio between two corresponding values. This ratio would equal one if a value pair shows perfect agreement. The ratios of the thirty–six coefficients were computed. Then, the arithmetic mean of the ratios was determined. A mean value of 0.9567 was obtained. This value is very close to the value of one that describes perfect agreement between the coefficient sets. This result confirms again that the load prediction accuracy differences between *Non–Iterative Method* and *Iterative Method* can be neglected for all practical purposes as long as regression models with similar function classes are used for the regression analysis of the calibration data and a tare load iteration is performed.

In conclusion, it was shown that the agreement between the load residuals, percent contributions, tare load estimates, and maximum outputs at capacity of the *Non–Iterative Method* and the *Iterative Method* is excellent if the given calibration data of the MK40A force balance is analyzed. These results quantitatively confirm that the accuracy of the two methods is the same for all practical purposes.

X. Semi–span Balance Example

Introduction

A calibration data set of NASA's MC60 five–component semi–span balance is discussed in this chapter. First, basic characteristics of the balance and the chosen calibration load schedule are reviewed. Then, the determination of the natural zeros and a test of bi–directional bridge output characteristics is discussed. Afterwards, regression models of the calibration data for both the *Non–Iterative Method* and *Iterative Method* are presented that may be used for the balance load prediction. Tare load corrections are also applied to the data before the analysis is performed. Finally, regression analysis results are reviewed. Table 52 below summarizes key characteristics of the calibration data of the MC60 balance.

Table 52: Overview of balance calibration data analysis example characteristics.

Balance Name (diameter)	Balance Design (load format)	Calibration Method	Comments
MC60 (27.5 in)	semi–span balance design (NF, AF, PM, YM, RM)	manual calibration	outputs are not bi–directional (absolute value terms not needed)

The MC60 semi–span balance belongs to a family of three five–component semi–span balances that are used as floor balances for tests in the NASA Ames 11–ft Transonic Wind Tunnel (TWT). Figure 43 below shows, for example, the overall layout and the principal dimensions of one of NASA's five–component semi–span balances.

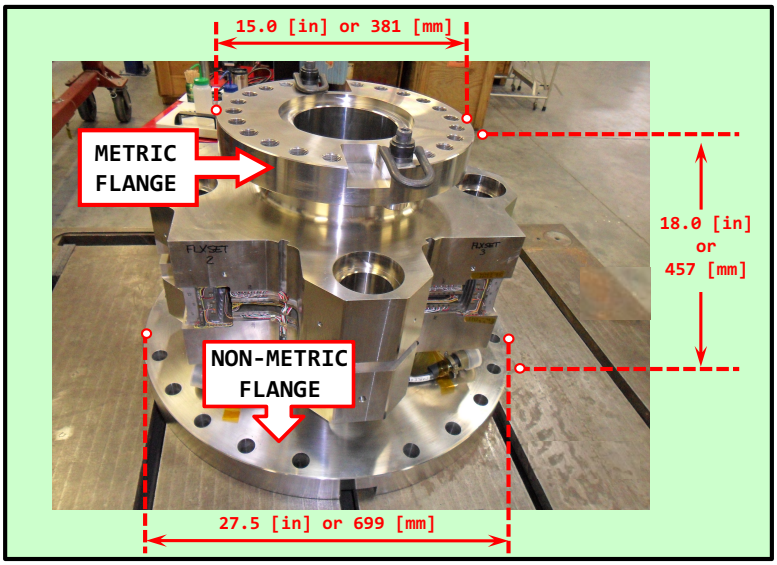

Fig. 43 Principal dimensions of NASA's semi–span balances.

The MC60 is a semi–span balance of single–piece design. It measures the normal force, axial force, pitching moment, yawing moment, and the rolling moment on the model. The balance is large. The diameter of the metric flange, for example, is 15.0 in (381 mm). Figure 44 below shows details of the metric flange of the balance.

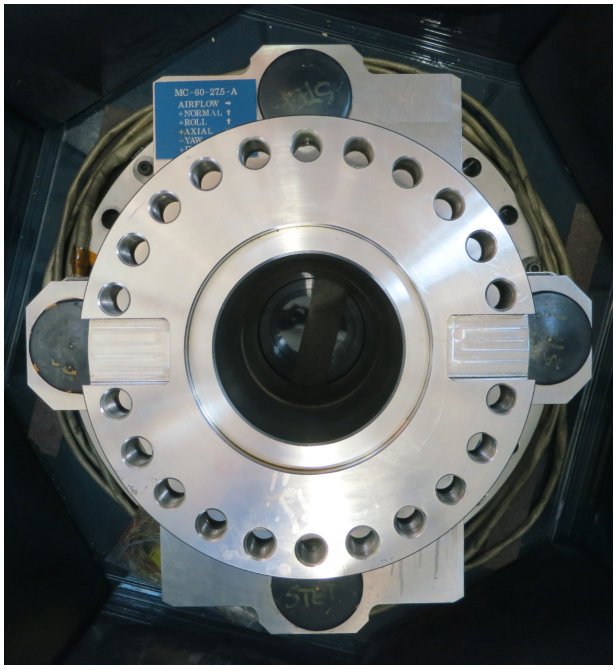

Fig. 44 Details of the metric flange of NASA's MC60 balance.

NASA's five–component semi–span balances have similar geometry and balance–to–model interfaces. They only differ in the capacities of the individual load components. Table 53 below lists capacities of the five load components of the MC60 balance.

Table 53: Load capacities of the MC60 semi–span balance ($lbs \equiv$ pounds of force).

NF, lbs	AF, lbs	SF, lbs	PM, $in{-}lbs$	YM, $in{-}lbs$	RM, $in{-}lbs$
6000	1200	*not measured*	36000	72000	360000

The balance is mounted on a turntable that is located below the floor of the test section. Consequently, the combined weight of the model and the metric part of the balance is forced to act in the direction of the side force. This constraint results in two advantages. First, the natural zeros can directly be measured in the tunnel before the model is attached to the balance. In addition, the influence of the model weight on the measurement of the aerodynamic loads is minimized as the outputs in the wind–off condition are independent of the pitch angle of the model. These outputs are needed so that loads resulting from the combined weight of the model and the metric part can be computed and subtracted from the wind–on loads that the model experiences during a wind tunnel test.

In general, the calibration of a high–capacity semi–span balance is challenging because very large loads have to be precisely applied (see, e.g., discussions in Refs. [31] and [32]). In addition, the MC60 balance has a net weight of approximately 1300 *lbs* and must be handled with great care. The single–piece design used on NASA's five–component semi–span balances has proven itself to be extremely repeatable. Therefore, existing calibration data can often successfully be used for a long period of time. The MC60 semi–span balance was last calibrated in 2019. Details of this calibration are described in the next section.

Calibration Description

The MC60 balance has the lowest capacities of NASA's family of five–component semi–span balances. Therefore, a different approach had to be used for the application of the axial force during the calibration as the axial force capacity of 1200 *lbs* was on the order of the combined weight of the calibration hardware and the metric part of the balance. The calibration of the balance took place in Calspan Force Measurement Systems' Large Load Rig (LLR). The LLR is one of a few existing load rigs that can be used for the calibration of NASA's five–component semi–span balances. The normal force and the rolling moment were applied by attaching a load chain with a leveling plate, flexure, load cell, and hydraulic actuator to a load boom that was rigidly connected to the metric part of the balance. The axial force and the yawing moment were applied by attaching a horizontal load arm to the load boom at the same lateral positions that were used for the application of normal force and rolling moment. Again, the axial force load chain consisted of a flexure, a load cell, and a hydraulic actuator. The pitching moment, on the other hand, was applied by using a separate moment arm pair in combination with gravity weights.

The North American balance load sign conventions were used during the calibration of the MC60 balance assuming that the left–hand wing of an aircraft is attached to the metric part of the balance. Corresponding load signs are specified in App. 3.

The chosen calibration load schedule consisted of 1839 data points that were distributed across 127 load series. A maximum of four load components, i.e., NF, AF, RM, and YM, were simultaneously applied during the calibration. No single–component loads could be applied because the calibration hardware did not support those types of loadings.

Electrical outputs of all data points were measured for both bridge sets. In addition, electrical outputs of zero load points were recorded at the beginning and end of each load series. They are needed as input for the tare load iteration process. This process determines hidden balance loads that are caused by the weight of the metric part and the calibration hardware (see also App. 12 & 13). In addition, differences between the first and last zero load point of a load series were used to monitor bridge output hysteresis effects.

The natural zeros of the balance bridges are the electrical outputs that the balance would have in a weightless condition. They are an electrical description of the absolute load datum of the balance. Three different methods may be used to determine the natural zeros of a semi–span balance (see also App. 8). They are summarized in the next section.

Natural Zero Determination

In principle, three independent methods may be used to determine the natural zeros of a five–component semi–span balance. The methods differ in (i) the orientation of the pitch axis of the balance in space relative to the direction of the gravitational acceleration, (ii) the hardware that is attached to the metric part of the balance, and (iii) the process that is used to calculate the natural zeros. Figure 45 below shows typical orientations of the pitch axis of a semi–span balance relative to the direction of the gravitational acceleration.

The signs of the forces are assigned assuming that the left wing of an aircraft is attached to the semi–span balance (see also the discussions in App. 3).

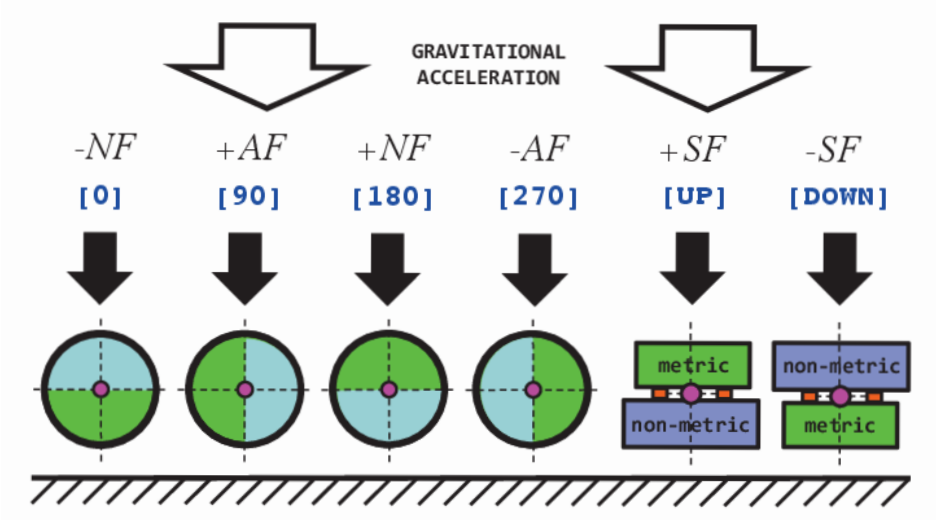

Fig. 45 Description of semi–span balance orientations relative to the direction of the gravitational acceleration.

The first four orientations in Fig. 45 above, i.e., [0], [90], [180], [270], show the front face of the metric part of the balance assuming that the pitch axis is perpendicular to the direction of the gravitational acceleration. The arithmetic mean of the raw output measurements of each bridge from the four orientations is an estimate of the natural zeros.

The remaining two orientations, i.e., [UP] and [DOWN], assume that the pitch axis of the balance is parallel to the direction of the gravitational acceleration. In both cases, all balance bridges are unloaded. Therefore, the measured raw outputs of either orientation [UP] or orientation [DOWN] directly describe the natural zeros of the balance.

Figure 46a below shows the first method that may be used to determine the natural zeros of the balance (Method I). The metric part of the balance is simply placed on a leveled surface. In that case, as indicated in the previous paragraph, all balance bridges are unloaded as the weight of the metric part acts in the direction of the side force. Consequently, the measured raw outputs of the bridges are the natural zeros of the balance.

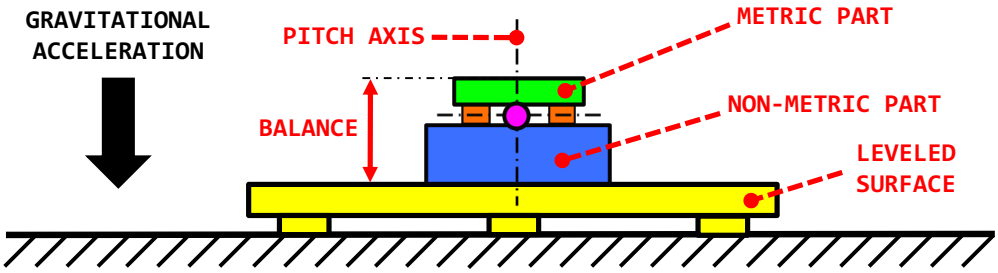

Fig. 46a Method I: Determination of the natural zeros by using a leveled surface.

Figure 46b below shows the second method that may be used to determine the natural zeros (Method II). In this case, the balance is mounted on a support system such that its

pitch axis is perpendicular to the direction of the gravitational acceleration. Now, the electrical outputs of the five bridges are caused by the weight of the metric part of the balance. The electrical outputs of all bridges are recorded for the four balance orientations [0], [90], [180], and [270] that are defined in Fig. 45. The arithmetic mean values of those output measurements are the natural zeros of the five balance bridges.

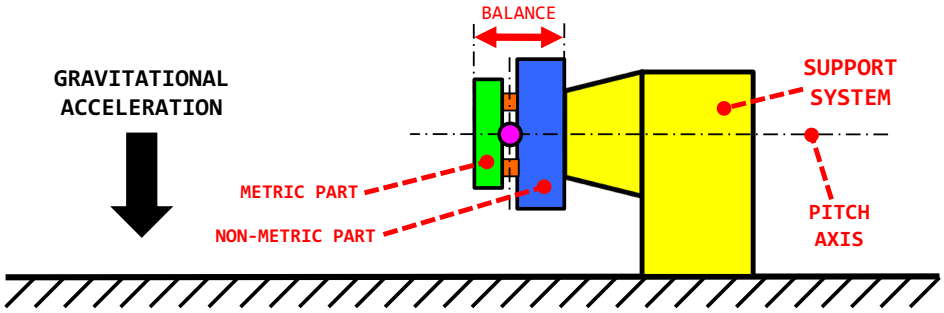

Fig. 46b Method II: Determination of the natural zeros by rotating the balance about the pitch axis.

Finally, Fig. 46c below shows the third method that may be used to obtain the natural zeros (Method III). This time, the balance plus the attached calibration hardware, i.e., the balance assembly, is mounted on a support system such that the pitch axis is perpendicular to the direction of the gravitational acceleration. Now, the electrical outputs of the bridges are caused by the weight of the metric assembly that consists of (i) the metric part of the balance and (ii) the attached calibration hardware. Again, electrical outputs of all bridges are recorded for the first four orientations that are defined in Fig. 45, i.e., [0], [90], [180], and [270]. Then, the arithmetic mean values of those measurements are computed for each bridge. They are the estimates of the natural zeros of the balance bridges.

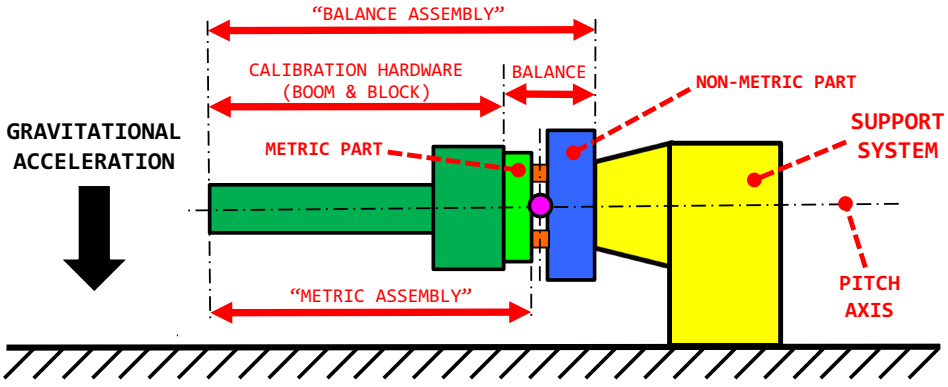

Fig. 46c Method III: Determination of natural zeros by rotating the balance assembly, i.e., the balance plus attached calibration hardware, about the pitch axis.

It must be mentioned for completeness that the natural zeros of the five bridges are instrumentation dependent physical constants of the balance. In other words, small output differences will be observed if bridge output voltages are measured using different sets of instrumentation. Therefore, it is critical to use the same instrumentation for the output

measurements if results of Methods I, II, and III are to be compared. Then, an analyst can expect that the maximum difference between the independent natural zero estimates from the three methods is on the order 1.0 $microV/V$. Table 54 below shows, for example, the directly measured natural zeros of the MC60 balance after Method I was applied.

Table 54: Estimated natural zeros of the balance bridges after application of Method I.

ORIENTATION	rNF $microV/V$	rAF $microV/V$	rPM $microV/V$	rYM $microV/V$	rRM $microV/V$
UP†	+162.68	+24.34	+80.40	+97.24	+42.22

†The pitch axis is parallel to the direction of the gravitational acceleration.

Similarly, Table 55 below shows the natural zeros after Method II was applied. In that case, no hardware was attached to the metric part when the four sets of outputs for the determination of the natural zeros were recorded.

Table 55: Estimated natural zeros of the balance bridges after application of Method II.

ORIENTATION	rNF $microV/V$	rAF $microV/V$	rPM $microV/V$	rYM $microV/V$	rRM $microV/V$
0	+87.10	+24.41	+84.90	+97.06	+38.42
90	+171.03	+301.59	+85.33	+86.19	+41.45
180	+238.94	+22.95	+81.16	+97.50	+46.36
270	+155.01	−254.37	+80.27	+108.35	+43.47
natural zero†	+163.02	+23.65	+82.92	+97.28	+42.43

†The natural zeros are the arithmetic mean of the column values.

Finally, Table 56 below shows the natural zeros after Method III was applied. This time, calibration hardware was attached to the metric part when the outputs for the determination of the natural zeros were recorded. As expected, a larger output range for each bridge is observed if the electrical outputs for different orientations are compared.

Table 56: Estimated natural zeros of the balance bridges after application of Method III.

ORIENTATION	rNF $microV/V$	rAF $microV/V$	rPM $microV/V$	rYM $microV/V$	rRM $microV/V$
0	−77.32	+26.58	+87.58	+96.79	−19.90
90	+188.51	+907.49	+91.18	−52.93	+39.97
180	+402.49	+20.72	+78.53	+97.51	+107.12
270	+136.28	−861.18	+74.38	+247.54	+46.93
natural zero†	+162.49	+23.40	+82.92	+97.23	+43.53

†The natural zeros are the arithmetic mean of the column values.

It was decided to use the arithmetic mean of the natural zero values of the three methods for the final analysis of the balance calibration data of the MC60 semi–span balance. The resulting reference values are listed in Table 57 below.

Table 57: Arithmetic mean of estimated natural zeros of Tables 54, 55, and 56.

rNF $microV/V$	rAF $microV/V$	rPM $microV/V$	rYM $microV/V$	rRM $microV/V$
+162.73	+23.80	+82.08	+97.25	+42.73

A comparison of the natural zero values listed in Tables 54, 55, and 56 confirms that the values obtained after application of the three methods do not differ by more than 2.0 $microV/V$ from the reference values that are reported in Table 57 above. – The bi–directional output characteristics of the balance bridges are investigated in the next section. They need to be understood so that suitable regression model terms can be selected for calibration data analysis and balance load prediction.

Bi–directional Output Characteristics

The author developed a semi–empirical test in order to determine if the electrical output of a balance bridge is bi–directional (for more details see App. 7). Test results may be used to justify the inclusion of absolute value terms in the regression models of the balance data. Those types of terms should only be used in a regression model if the outputs of a balance bridge have known bi–directional characteristics.

The author's test performs a preliminary linear fit of the calibration data using three terms: intercept, primary linear term, and primary absolute value term (see App. 7). Results of this fit provide the required numerical inputs for the application of the test. The test can be summarized as follows: the output of a balance bridge is bi–directional if (i) the estimated bi–directional part of the output at load capacity exceeds 0.5 % of the to–capacity–scaled maximum of the difference between the bridge output and its natural zero, and (ii) the p–value of the absolute value term is less than 0.001.

The test works best if it is applied to the subset of the balance calibration data that exclusively consists of single–component loads. However, the test can also be applied to an entire balance calibration data set as long as (i) no significant asymmetries exist in the balance calibration load schedule design, (ii) the overall quality of the calibration data is excellent, and (iii) the calibration data set is not over–fitted.

First, bi–directional parts of the balance bridge outputs are examined. Table 58 below summarizes the estimated bi–directional parts of the five bridges of the balance that were computed by using both the regression coefficients of the *Non–Iterative Method* and the regression coefficients of the *Iterative Method*. In general, the agreement between the estimates of the bi–directional parts is excellent. It is seen that the bi–directional parts of the bridges are well below the threshold that is listed in the last row of Table 58. This observations indicates that the bridge outputs are most likely not bi–directional.

Table 58: Bi–directional part at load capacity and threshold of the MC60 balance.†

	$\Lambda(D_1,NF)$ microV/V	$\Lambda(D_2,AF)$ microV/V	$\Lambda(D_3,PM)$ microV/V	$\Lambda(D_4,YM)$ microV/V	$\Lambda(D_5,RM)$ microV/V
Non–Iterative	+0.13	+0.83	+0.87	+0.87	−0.25
Iterative	+0.18	+0.67	+0.82	+0.72	−0.22
Threshold	±5.59	±4.18	±4.38	±2.81	±6.11

† D_1=$rNF-rNF_\circ$, D_2=$rAF-rAF_\circ$, D_3=$rPM-rPM_\circ$, D_4=$rYM-rYM_\circ$, D_5=$rRM-rRM_\circ$

The application of the test also requires the calculation of the p–value of the t–statistic of the temporarily included absolute value term. This metric tests the statistical significance of the absolute value term assuming it would be used to fit the balance data. In general, a term is statistically significant if its p–value is less than the threshold of 0.0010. Table 59 below lists the computed p–values of each absolute value term if the *Non–Iterative Method* is used for the balance calibration data analysis. Only the absolute value term of

Table 59: Non–Iterative Method $\Longrightarrow$ p–value of the absolute value term of the primary bridge output difference of each fitted load component.†

$p\{\lvert D_1\rvert\}$	$p\{\lvert D_2\rvert\}$	$p\{\lvert D_3\rvert\}$	$p\{\lvert D_4\rvert\}$	$p\{\lvert D_5\rvert\}$
0.1870 insignificant	0.1110 insignificant	< 0.001 **significant**	0.0073 insignificant	0.2830 insignificant

† D_1=$rNF-rNF_\circ$, D_2=$rAF-rAF_\circ$, D_3=$rPM-rPM_\circ$, D_4=$rYM-rYM_\circ$, D_5=$rRM-rRM_\circ$

the output difference of the pitching moment bridge, i.e., $|D_3|$, appears to be statistically significant. Table 60 below lists the computed p–values of each absolute value term if the *Iterative Method* is used for the balance calibration data analysis. Now, the absolute value term of the pitching moment, i.e., $|PM|$, appears to be statistically significant. At this

Table 60: Iterative Method $\Longrightarrow$ p–value of the absolute value term of the primary load component of each fitted bridge output difference.

$p\{\lvert NF\rvert\}$	$p\{\lvert AF\rvert\}$	$p\{\lvert PM\rvert\}$	$p\{\lvert YM\rvert\}$	$p\{\lvert RM\rvert\}$
0.1163 insignificant	0.2210 insignificant	< 0.001 **significant**	0.0291 insignificant	0.0969 insignificant

point, all information is available to apply the semi–empirical test. It is concluded from Table 58 above that the bi–directional parts of all outputs are well below corresponding thresholds. In addition, only the absolute value term related to the pitching moment appears to be statistically significant (see Tables 59/60). Consequently, the test of bi–directional output characteristics failed for all bridges as both test conditions must simultaneously be fulfilled. None of the bridges of the MC60 balance has bi–directional output

characteristics. Therefore, the use of absolute value terms in the regression models of the balance cannot be justified. Final test results are summarized again in Table 61 below.

Table 61: Assessment of the bridge output characteristics of the MC60 balance.†

	rNF	rAF	rPM	rYM	rRM
Is output bi–directional ?	no	no	no	no	no

†A bridge output is bi–directional if two conditions are met: (i) the bi–directional part at capacity exceeds the threshold (Tbl. 58) and (ii) the p–value of the principal absolute value term is less than 0.001 (Tbls. 59/60).

It is interesting to show the bi–directional part of two of the five balance bridges as an example. The normal force and the axial force bridge outputs were chosen for this purpose. Figure 47 below shows the bi–directional part of the output of the normal force bridge. It

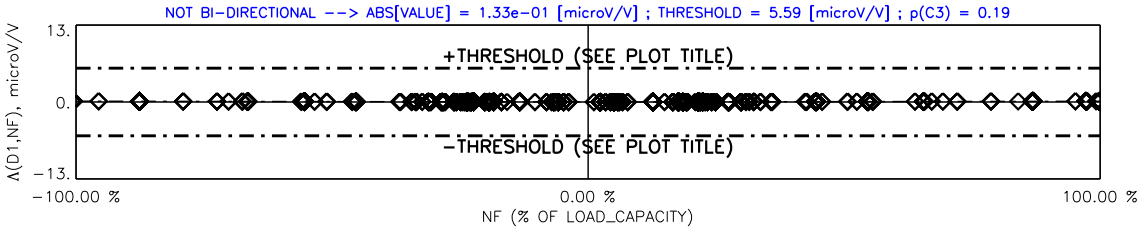

Fig. 47 Bi–directional part of the electrical output of the normal force bridge plotted versus the tare corrected normal force.

can clearly be seen in Fig. 47 that the bi–directional part is well below the empirical threshold at load capacity. This observation confirms that the normal force bridge output of the MC60 balance does not have bi–directional characteristics. Figure 48 below shows the bi–directional part of the output of the axial force bridge. Again, the bi–directional part

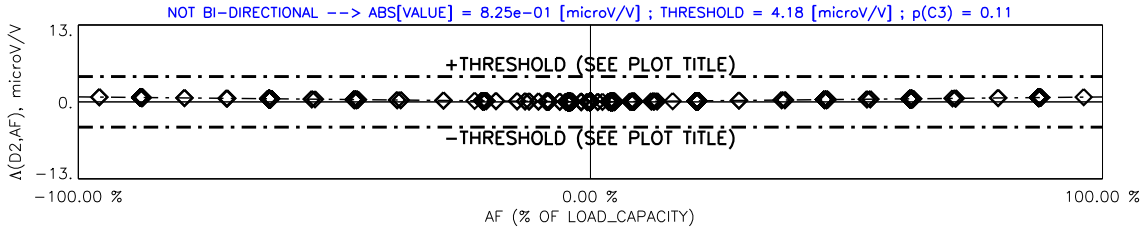

Fig. 48 Bi–directional part of the electrical output of the axial force bridge plotted versus the tare corrected axial force.

at capacity is well below the threshold that is listed for the axial force bridge output in Table 58. This observation confirms that the axial force bridge output of the MC60 balance is not bi–directional.

Analysis Results for the Non–Iterative Method

First, the *Non–Iterative Method* is used for the development of the load prediction equations for the MC60 semi–span balance from the given balance calibration data (see

App. 9 for a description of the method). This approach directly fits the five balance load components NF, AF, PM, YM, RM as a function of the bridge output differences D_1, D_2, ..., D_5 assuming that all balance loads are described relative to the absolute load datum of zero load. Table 62 below shows the selected regression model term combination for each one of the five load components of the balance. Absolute value terms were omitted

Table 62: Regression model terms of the five load components of the MC60 balance.

Intercept Term $\Longrightarrow$ used in the regression model of each load component
Principal Linear Terms $\{D_1,\ D_2,\ D_3,\ D_4,\ D_5\}^{\dagger} \Longrightarrow$ used in the regression model of each load component
Quadratic Terms $D_5^2 \Longrightarrow$ used in the regression models of NF, AF, PM, and YM
Cross–product Terms $(D_2 \cdot D_3) \Longrightarrow$ used in the regression model of NF $(D_3 \cdot D_5) \Longrightarrow$ used in the regression model of AF $(D_2 \cdot D_5),\ (D_4 \cdot D_5) \Longrightarrow$ used in the regression model of PM $(D_1 \cdot D_3),\ (D_1 \cdot D_4) \Longrightarrow$ used in the regression model of YM $(D_2 \cdot D_3) \Longrightarrow$ used in the regression model of RM

$^{\dagger} D_1 = rNF - rNF_{\circ}\ ,\ D_2 = rAF - rAF_{\circ}\ ,\ D_3 = rPM - rPM_{\circ}\ ,\ D_4 = rYM - rYM_{\circ}\ ,\ D_5 = rRM - rRM_{\circ}$

because the balance bridge outputs do not have bi–directional characteristics. Term reduction was performed during the data analysis to prevent over–fitting of the calibration data. The term reduction itself was executed by using a simplified term reduction algorithm that is described in App. 19 of the current document. Figure 49a below shows the fitted coefficient values, standard error, t–statistic, p–value, and *Variance Inflation Factor* of the regression model of the normal force as an example. These metrics may be used to assess

TERM NAME	COEFFICIENT VALUE	STANDARD ERROR	T–STATISTIC OF COEFFICIENT	P–VALUE OF COEFFICIENT	VARIANCE INFLATION FACTOR
INTERCEPT	+0.1791	+0.0454	+3.9434	–	–
D1	+5.3670	+0.0002	+27090.3175	< 0.0001	+5.1158
D2	−0.1536	+0.0005	−304.0072	< 0.0001	+23.9660
D3	+0.1683	+0.0002	+746.7712	< 0.0001	+1.0216
D4	+0.0245	+0.0008	+28.9925	< 0.0001	+23.9406
D5	+0.1730	+0.0002	+944.5075	< 0.0001	+5.1157
D5*D5	+5.1495e−06	+9.3845e−08	+54.8721	< 0.0001	+1.0030
D2*D3	+2.1031e−05	+5.0629e−07	+41.5388	< 0.0001	+1.0007

Fig. 49a Coefficient values, standard error, t–statistic, p–value, and *Variance Inflation Factors* of the regression model terms of the normal force (NF).

the reliability of the regression model of the load component. The t–statistic of the output difference D_1 of the normal force bridge output rNF has the greatest magnitude. It is

approximately 27090. This results is expected as it is the primary output of the normal force. A p–value of less than 0.0001 indicates that the regression model term is highly significant. It is also observed that a moderate near–linear dependency exists between the axial force bridge output (D_2) and the yawing moment bridge output (D_4). Related *Variance Inflation Factors* of 23.97 and 23.94 are highlighted in blue color in Fig. 49a. This dependency is caused by the fact that no single–component loads of the load components could be applied during the calibration of the balance (see also App. 18 for details related to the calculation of the *Variance Inflation Factor*).

Percent contributions of the regression model terms are also frequently used in the aerospace testing community to assess the importance of regression model terms (see App. 16 for more details). Figure 49b below shows the percent contributions of the twenty–

	NF	AF	PM	YM	RM
D1	[100.00 %]	+1.85 %	+3.36 %	−0.86 %	+1.38 %
D2	−1.91 %	[100.00 %]	−0.86 %	−0.17 %	+0.24 %
D3	+2.35 %	−1.55 %	[100.00 %]	−3.87 %	+0.11 %
D4	+0.23 %	+1.20 %	+0.15 %	[100.00 %]	−0.05 %
D5	+3.22 %	+0.18 %	−3.20 %	+1.40 %	[100.00 %]

Interpretation of the Percent Contribution (taken from App. 16)

```
Percent_Contribution = 100 % ..................... primary/reference term (red)
ABS(Percent_Contribution) > 0.5 % ................. very important term (red)
0.1 % < ABS(Percent_Contribution) < 0.5 % ... term of minor importance (blue)
ABS(Percent_Contribution) < 0.1 % ............. term of no importance (black)
```

Fig. 49b Percent contributions of the twenty–five principal linear regression model terms of the five fitted balance load components.

five principal linear terms of the regression models of the load components (for simplicity, percent contributions of higher order terms are not discussed). Red color marks percent contributions of very important terms. Blue color is used to identify terms that are of minor importance. Finally, black color is used to mark terms of no importance. In general, it can be seen that the interactions between the bridges cannot be neglected. This observation is no surprise as the MC60 balance is a single–piece balance. Therefore, for example, the bridge output differences D_1 and D_5 make an important contribution in the regression model of the pitching moment (PM) as their percent contributions are $+3.36\,\%$ and $-3.20\,\%$.

A tare load iteration was also performed so that balance loads resulting from the weight of the calibration equipment and the metric part of the balance would be included in the load set that is ultimately used as input for the regression analysis (see App. 12 for details about the tare load iteration process if the *Non–Iterative Method* is used for the data analysis). Table 63 below lists the computed tare loads for the first six load series.

Table 63: *Non–Iterative Method* $\Longrightarrow$ Predicted tare loads of the first six load series of the calibration data of the MC60 balance (listed as a percentage of the load capacity).

Series	NF, %	AF, %	PM, %	YM, %	RM, %	Comment
1	+21.52	+4.30	–0.25	–2.49	+5.10	—
2	+21.51	+4.33	–0.27	–2.50	+5.11	repeat of series 1
3	+21.51	–4.04	–0.27	+3.06	+5.11	—
4	+21.52	–4.09	–0.27	+3.09	+5.11	repeat of series 3
5	+21.52	–4.07	–0.28	+3.76	+5.15	—
6	+21.52	–4.09	–0.29	+3.78	+5.15	repeat of series 5

The regression analysis of the data was completed using (i) the tare corrected loads and (ii) output differences relative to the natural zeros as input. Table 64 below lists the standard deviation of the load residuals of the calibration data, i.e., of the difference between measured and fitted load, for each load component of the MC60 balance in both engineering units and as a percentage of capacity. It is observed that the standard deviations of the fitted load components are well below the empirical threshold of 0.10 % that is often used for the assessment the standard deviation of balance load residuals.

Table 64: *Non–Iterative Method* $\Longrightarrow$ Standard deviation of the load residuals.†

NF, *lbs*	AF, *lbs*	PM, *in–lbs*	YM, *in–lbs*	RM, *in–lbs*
1.68 (0.028 %)	0.93 (0.077 %)	22.55 (0.063 %)	44.42 (0.062 %)	125.20 (0.035 %)

†Standard deviations expressed as a percentage of the load capacity are listed in brackets.

Normal force residuals of the MC60 balance are plotted versus the tare corrected normal force in Fig. 50 below. The residuals are well within the threshold of ±0.25 % of capacity that is traditionally used to assess load residuals of individual data points.

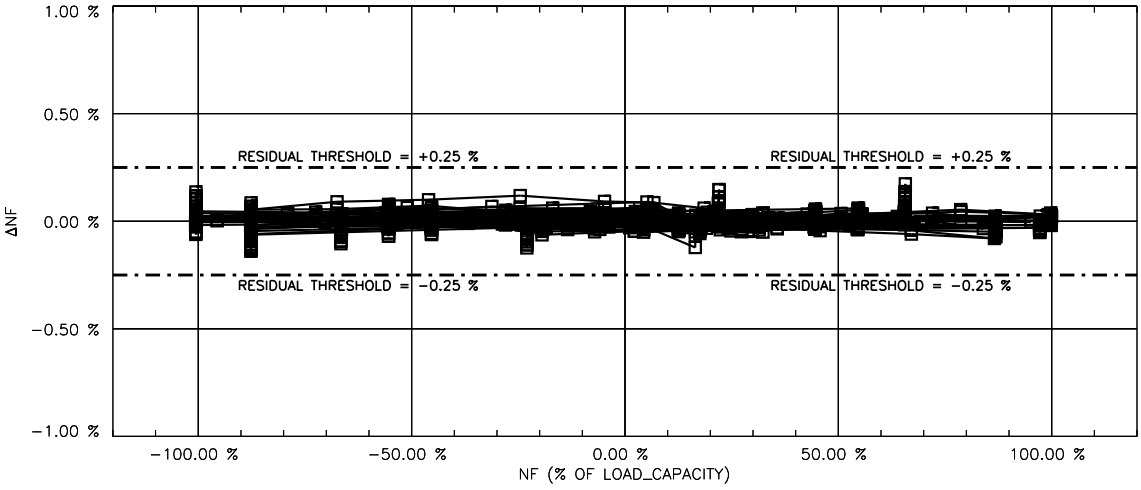

Fig. 50 *Non–Iterative Method* $\Longrightarrow$ Normal force residuals (ΔNF) of the MC60 balance plotted versus the tare corrected normal force (NF).

Similarly, axial force residuals of the MC60 balance are plotted versus the tare corrected axial force in Fig. 51 below. Again, most residuals are within the threshold of $\pm 0.25\,\%$ of capacity that is used to assess residuals of individual data points. It is ob–

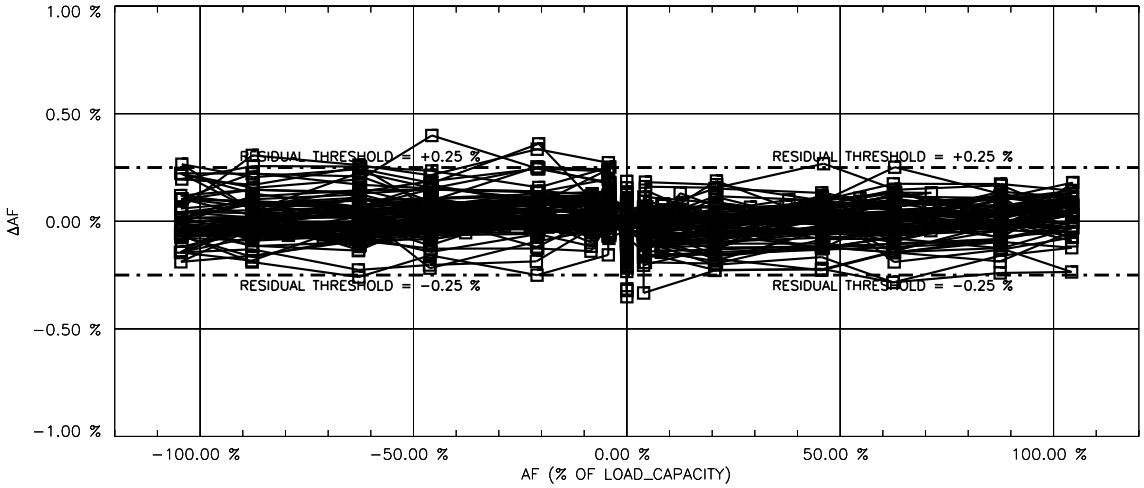

Fig. 51 *Non–Iterative Method* $\Longrightarrow$ Axial force residuals (ΔAF) of the MC60 balance plotted versus the tare corrected axial force (AF).

served that the axial force residuals have more scatter than the normal force residuals if Fig. 50 is compared with Fig. 51. These differences between the residuals of the normal and axial force can better be understood if the primary sensitivities of the five balance bridges and related maximum outputs at capacity are determined and compared.

In general, the primary sensitivity of a balance bridge is defined as the first derivative of a bridge output with respect to the corresponding primary bridge load. Therefore, it equals the inverse of the coefficient of the primary output difference that is used in the regression model of a balance load component if the *Non–Iterative Method* is used for the balance load prediction. This statement can be illustrated by using the regression model of the normal force as an example. The regression model is defined in Eq. (26) below where the inverse

$$NF \;=\; a_0 \;+\; a_1 \cdot D_1 \;+\; a_2 \cdot D_2 \;+\; a_3 \cdot D_3 \;+\; a_4 \cdot D_4 \;+\; \ldots \qquad (26)$$

of the primary sensitivity of the normal force bridge output equals the regression coefficient of the output difference D_1. This conclusion is summarized in Eq. (27) below after taking into account that the natural zero, i.e., $rNF_\circ$, is a constant.

$$a_1 \;=\; \frac{\partial\, NF}{\partial\, D_1} \;\approx\; \left\{\frac{\partial\, D_1}{\partial\, NF}\right\}^{-1} = \left\{\frac{\partial\,[\,rNF - rNF_\circ\,]}{\partial\, NF}\right\}^{-1} = \left\{\frac{\partial\, rNF}{\partial\, NF}\right\}^{-1} \qquad (27)$$

Then, we get the following equation for the primary sensitivity of the normal force bridge:

$$\textit{primary sensitivity (normal force bridge)} \;\Longrightarrow\; \partial\, rNF \,/\, \partial\, NF \;\approx\; 1 \,/\, a_1 \qquad (28)$$

Table 65 below lists estimated primary sensitivities for the MC60 balance that were obtained after completion of the regression analysis of the five load components of the balance. As expected, the axial force bridge has the highest sensitivity of all balance bridges because the axial force capacity is only one–fifth of the normal force capacity.

Table 65: *Non–Iterative Method* $\Longrightarrow$ Primary sensitivities of the MC60 balance.

$\frac{\partial\, rNF}{\partial\, NF}$	$\frac{\partial\, rAF}{\partial\, AF}$	$\frac{\partial\, rPM}{\partial\, PM}$	$\frac{\partial\, rYM}{\partial\, YM}$	$\frac{\partial\, rRM}{\partial\, RM}$
$0.186325^{\dagger}$	$0.677216^{\dagger}$	$0.024099^{\ddagger}$	$0.007761^{\ddagger}$	$0.003419^{\ddagger}$

$^{\dagger}[microV/V]\,/\,[lbs]$; $^{\ddagger}[microV/V]\,/\,[in\text{–}lbs]$.

Now, the maximum output at capacity of the five bridges can be determined. This metric is often used to scale instrumentation inputs so that the best accuracy of the electrical output measurement can be achieved. The metric is defined as the product of (i) the primary sensitivity of a bridge with (ii) the capacity of the related load component. Table 66 below lists values were obtained for the five bridges of the MC60 balance.

Table 66: *Non–Iterative Method* $\Longrightarrow$ Maximum output† of the MC60 balance.

rNF $microV/V$	rAF $microV/V$	rPM $microV/V$	rYM $microV/V$	rRM $microV/V$
1118.0	812.7	867.6	558.8	1230.8

†Maximum output $\equiv$ product of the primary bridge sensitivity and the capacity of the related load component.

It can be seen that the maximum output at capacity of the normal force bridge is almost 300 $microV/V$ greater than the maximum output of the axial force bridge. This difference is partially responsible for the fact that the normal force residuals shown in Fig. 50 are significantly smaller than the axial force residuals shown in Fig. 51.

Table 67 below shows the subset of twenty–five principal linear coefficients of the regression models of the five load components of the MC60 semi–span balance that were

Table 67: *Non–Iterative Method* $\Longrightarrow$ Principal linear coefficients of the fitted regression model of each balance load component.

	D1	D2	D3	D4	D5
NF	5.366962E+00	-1.535608E-01	1.683199E-01	2.452200E-02	1.730398E-01
AF	1.820616E-02	1.476634E+00	-2.034223E-02	2.365195E-02	1.757165E-03
PM	1.045022E+00	-4.001659E-01	4.149635E+01	9.458456E-02	-9.950402E-01
YM	-5.557137E-01	-1.602064E-01	-3.326270E+00	1.288493E+02	9.050402E-01
RM	4.039898E+00	1.059515E+00	4.228806E-01	-3.145863E-01	2.924989E+02

obtained. These coefficient values will be compared later with corresponding results that were obtained for the *Iterative Method*.

Analysis Results for the Iterative Method

The *Iterative Method* can also be used for calibration data analysis and load prediction of the MC60 semi–span balance. This approach first fits the outputs of the balance bridges as a function of the balance loads. Afterwards, a load iteration equation is constructed from the regression coefficients of the outputs so that loads can be predicted from outputs during a wind tunnel test (see Ref. [7] and App. 10 for a description of the method).

It was decided to use output differences relative to the natural zeros of the balance bridges instead of raw outputs during the application of the *Iterative Method* to the calibration data. In addition, term reduction was applied to prevent over–fitting (the algorithm described in App. 19 was used for this purpose). Table 68 below shows the resulting regression model terms for each one of the five output differences of the balance. Absolute

Table 68: Regression model terms of the five output differences† of the MC60 balance.

Intercept Term $\Longrightarrow$ used in the regression model of each output difference
Principal Linear Terms
$NF,\ AF,\ PM,\ YM,\ RM \Longrightarrow$ used in the regression model of each output difference
Quadratic Terms
$PM^2,\ RM^2 \Longrightarrow$ used in the regression model of D_1
$NF^2,\ RM^2 \Longrightarrow$ used in the regression model of D_2
$RM^2 \Longrightarrow$ used in the regression model of D_3
$RM^2 \Longrightarrow$ used in the regression model of D_4
Cross–product Terms
$(AF \cdot RM),\ (PM \cdot YM),\ (PM \cdot RM) \Longrightarrow$ used in the regression model of D_1
$(NF \cdot YM),\ (PM \cdot RM) \Longrightarrow$ used in the regression model of D_2
$(AF \cdot RM),\ (YM \cdot RM) \Longrightarrow$ used in the regression model of D_3
$(NF \cdot PM),\ (NF \cdot YM) \Longrightarrow$ used in the regression model of D_4
$(PM \cdot YM) \Longrightarrow$ used in the regression model of D_5

† $D_1 = rNF - rNF_\circ$, $D_2 = rAF - rAF_\circ$, $D_3 = rPM - rPM_\circ$, $D_4 = rYM - rYM_\circ$, $D_5 = rRM - rRM_\circ$

value terms were intentionally excluded in the regression models of the five output differences because the outputs of the balance are not bi–directional.

Figure 52a below shows the coefficient value, standard error, t–statistic, p–value, and *Variance Inflation Factor* for each term of the regression model of the normal force bridge output difference as an example. These metrics may be used to assess the reliability of the regression model of the output. As expected, the t–statistic of the coefficient of the normal force has the greatest magnitude, i.e., 31687, because it is the primary load component of the normal force bridge. A p–value of less than 0.0001 indicates that the regression model

term is highly significant. In addition, *Variance Inflation Factors* on the order of 10 or less indicate that no near–linear dependencies exist in a regression model (see also App. 18 for details related to the calculation of this metric). In our case, a moderate near–linear dependency appears to exist between the axial force (AF) and the yawing moment (YM) as the related pair of *Variance Inflation Factors* is approximately 24.

TERM NAME	COEFFICIENT VALUE	STANDARD ERROR	T–STATISTIC OF COEFFICIENT	P–VALUE OF COEFFICIENT	VARIANCE INFLATION FACTOR
INTERCEPT	−0.0332	+0.0074	−4.4753	–	–
NF	+0.1865	+5.8852e−06	+31687.3914	< 0.0001	+5.5613
AF	+0.0193	+0.0001	+356.7454	< 0.0001	+23.6657
PM	−0.0007	+8.4947e−07	−882.0853	< 0.0001	+1.0007
YM	−3.8038e−05	+1.0267e−06	−37.0475	< 0.0001	+23.6675
RM	−0.0001	+1.0176e−07	−1108.9889	< 0.0001	+5.5541
PM*PM	−1.3020e−10	+3.3703e−11	−3.8631	+0.0001	+1.0027
RM*RM	−1.0331e−11	+1.6931e−13	−61.0177	< 0.0001	+1.0043
AF*RM	−2.1125e−09	+7.0645e−11	−29.9032	< 0.0001	+1.0006
PM*YM	+1.0607e−09	+2.2013e−11	+48.1836	< 0.0001	+1.0009
PM*RM	+1.1206e−10	+6.6796e−12	+16.7772	< 0.0001	+1.0007

Fig. 52a Coefficient values, standard error, t–statistic, p–value, and *Variance Inflation Factors* of the regression model terms of the normal force bridge output difference (D_1).

A tare load iteration was performed and regression coefficients of the five output differences of the balance bridges were successfully computed. The percent contributions of the regression model terms were also determined (see App. 16 for a definition of the metric). Figure 52b below shows the computed percent contributions of the twenty–five principal linear terms of the fitted bridge output differences. As expected, the percent contributions

	D_1	D_2	D_3	D_4	D_5
NF	[100.00 %]	−1.75 %	−3.30 %	+0.75 %	−1.25 %
AF	+2.07 %	[100.00 %]	+0.83 %	+0.24 %	−0.27 %
PM	−2.41 %	+1.47 %	[100.00 %]	+3.99 %	−0.07 %
YM	−0.24 %	−1.10 %	−0.15 %	[100.00 %]	+0.05 %
RM	−3.63 %	−0.06 %	+3.52 %	−1.44 %	[100.00 %]

Interpretation of the Percent Contribution (taken from App. 16)

Percent_Contribution = 100 % ..... primary/reference term (red)
ABS(Percent_Contribution) > 0.5 % ..... very important term (red)
0.1 % < ABS(Percent_Contribution) < 0.5 % ... term of minor importance (blue)
ABS(Percent_Contribution) < 0.1 % ..... term of no importance (black)

Fig. 52b Percent contributions of the twenty–five principal linear regression model terms of the five fitted bridge output differences.

show good agreement with related percent contributions that are listed in Fig. 49b for the corresponding regression models of the five load components. For example, the percent contributions of the terms NF and RM of the regression model of the pitching moment

bridge output difference D_3 are $-3.30\,\%$ and $+3.52\,\%$ (taken from Fig. 52b above). Similarly, the percent contributions of the terms D_1 and D_5 of the regression model of the pitching moment PM are $+3.36\,\%$ and $-3.20\,\%$ (taken from Fig. 49b). This result numerically illustrates the fact that the percent contribution of related terms of the regression models of a load and an output difference must be similar in magnitude but opposite in sign (a rigorous derivation of this connection in given in App. 16).

It was mentioned earlier that a tare load iteration was performed. Therefore, balance loads resulting from the weight of the calibration equipment and the metric part of the balance were included in the load set that was ultimately used as input for the regression analysis. Table 69 below lists computed tare loads for the first six load series of the

Table 69: *Iterative Method* $\Longrightarrow$ Predicted tare loads of the first six load series of the calibration data of the MC60 balance (listed as a percentage of the load capacity).

Series	NF, %	AF, %	PM, %	YM, %	RM, %	Comment
1	+21.52	+4.30	–0.25	–2.49	+5.10	—
2	+21.51	+4.33	–0.27	–2.50	+5.11	repeat of series 1
3	+21.51	–4.04	–0.27	+3.06	+5.11	—
4	+21.52	–4.09	–0.27	+3.09	+5.11	repeat of series 3
5	+21.52	–4.07	–0.28	+3.76	+5.15	—
6	+21.52	–4.09	–0.29	+3.78	+5.15	repeat of series 5

calibration data. These values show excellent agreement with corresponding values that are listed in Table 63 for the *Non–Iterative Method*.

The regression analysis of the calibration data was successfully completed using (i) the tare corrected loads and (ii) output differences relative to the natural zeros of the balance as input. Table 70 below lists the standard deviations of the load residuals, i.e., of the difference between measured and fitted load, for each load component of the MC60 balance in engineering units (corresponding values expressed as a percentage of the capacity are listed in brackets). All five standard deviations are below the empirical threshold of $0.10\,\%$ of load capacity that is often used for the assessment of the standard deviation of balance load residuals. The computed standard deviations also show excellent agreement with corresponding values that are listed in Table 64 for the *Non–Iterative Method*.

Table 70: *Iterative Method* $\Longrightarrow$ Standard deviation of the load residuals.[†]

NF, *lbs*	AF, *lbs*	PM, *in–lbs*	YM, *in–lbs*	RM, *in–lbs*
1.50 (0.025 %)	0.94 (0.078 %)	22.62 (0.063 %)	44.50 (0.062 %)	125.26 (0.035 %)

[†]Standard deviations expressed as a percentage of the load capacity are listed in brackets.

Normal force residuals of the calibration data are depicted as an example in Fig. 53 below. The residuals show excellent qualitative and quantitative agreement with corresponding residuals that were obtained after applying the *Non–Iterative Method* (see Fig. 50).

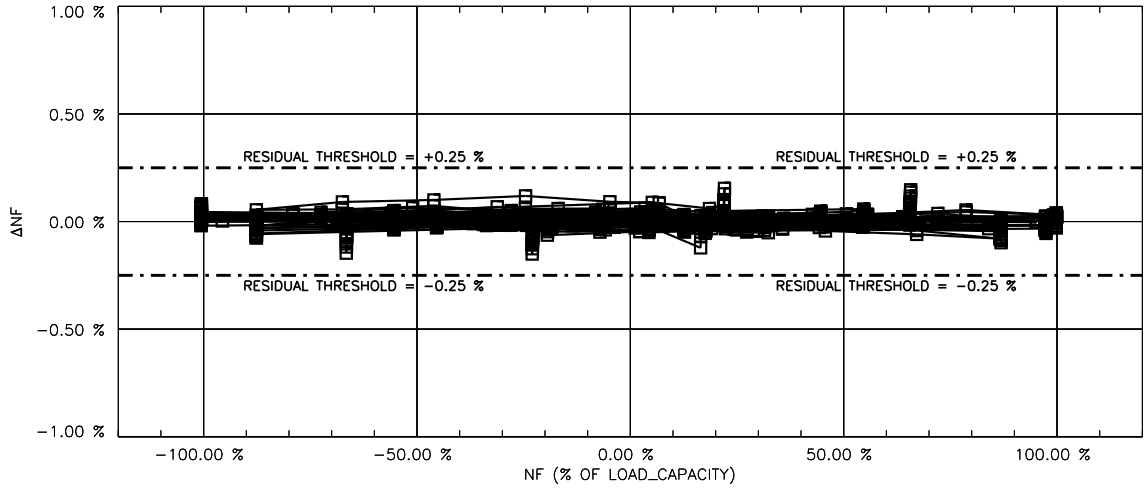

Fig. 53 *Iterative Method* $\Longrightarrow$ Normal force residuals (ΔNF) of the MC60 balance plotted versus the tare corrected normal force (NF).

Similarly, axial force residuals of the calibration data are depicted in Fig. 54 below. Again, the residuals show excellent agreement with corresponding residuals that were computed after applying the *Non–Iterative Method* (see Fig. 51).

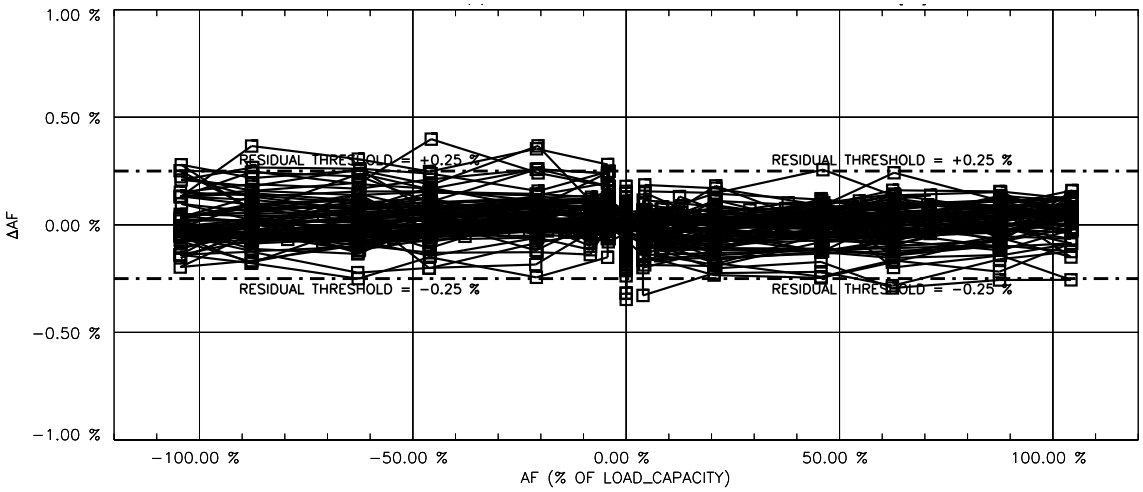

Fig. 54 *Iterative Method* $\Longrightarrow$ Axial force residuals (ΔAF) of the MC60 balance plotted versus the tare corrected axial force (AF).

The excellent agreement between the standard deviations of the load residuals confirms that the load prediction accuracy of the *Non–Iterative Method* and the *Iterative Method* is more or less the same for the given semi–span balance calibration data set.

The primary sensitivities of the five balance bridges were also computed during the regression analysis of the calibration data and compared with corresponding values that were obtained after the application of the *Non–Iterative Method*. The primary sensitivity of a bridge output is defined as the coefficient of the primary load component that is used in the regression model of the related output difference. This general statement can be illustrated by using the regression model of the output difference of the normal force bridge (D_1) as an example. This regression model is defined in Eq. (29) below where

$$D_1 \;=\; rNF \;-\; rNF_{\circ} \;=\; b_0 \;+\; b_1 \cdot NF \;+\; b_2 \cdot AF \;+\; b_3 \cdot PM \;+\; b_4 \cdot YM \;+\; \ldots \quad (29)$$

the primary sensitivity of the normal force bridge output is the first derivative of the output difference with respect to the normal force. The derivative equals the regression coefficient of the normal force. This conclusion is summarized in Eq. (30) below.

$$\underset{(normal\ force\ bridge)}{Primary\ Sensitivity} \quad \Longrightarrow \quad b_1 \;=\; \frac{\partial\ D_1}{\partial\ NF} \;=\; \frac{\partial\ [\ rNF - \overbrace{rNF_{\circ}}^{const.}\ ]}{\partial\ NF} \;=\; \frac{\partial\ rNF}{\partial\ NF} \qquad (30)$$

Table 71 below lists primary sensitivities that were obtained from the regression models of the output differences. As expected, the estimates show excellent agreement with corresponding values that are reported in Table 65 for the *Non–Iterative Method*.

Table 71: *Iterative Method* $\Longrightarrow$ Primary sensitivities of the MC60 balance.

$\frac{\partial\ rNF}{\partial\ NF}$	$\frac{\partial\ rAF}{\partial\ AF}$	$\frac{\partial\ rPM}{\partial\ PM}$	$\frac{\partial\ rYM}{\partial\ YM}$	$\frac{\partial\ rRM}{\partial\ RM}$
$0.186485^{\dagger}$	$0.677075^{\dagger}$	$0.024119^{\ddagger}$	$0.007760^{\ddagger}$	$0.003420^{\ddagger}$

$^{\dagger}[microV/V]/[lbs]$; $^{\ddagger}[microV/V]/[in\text{–}lbs]$.

Now, the maximum output at capacity of the five balance bridges can be computed. The metric is defined as the product of (i) the primary sensitivity of a bridge with (ii) the capacity of the related load component. Table 72 below lists corresponding values were obtained for the five bridges of the MC60 balance.

Table 72: *Iterative Method* $\Longrightarrow$ Maximum output† of the MC60 balance.

rNF $microV/V$	rAF $microV/V$	rPM $microV/V$	rYM $microV/V$	rRM $microV/V$
1118.9	812.5	868.3	558.7	1231.3

†Maximum output $\equiv$ product of the primary bridge sensitivity and the capacity of the related load component.

The values listed in Table 72 above can easily be compared with corresponding estimates that were obtained after the application of the *Non–Iterative Method*. The absolute values of the differences between the independent estimates are listed in Table 73 below. The differences are very small. They are below the empirical threshold of 1 microV/V that is often used to identify negligible bridge output differences.

Table 73: Difference between estimated maximum outputs (Table 66 versus Table 72).

rNF $microV/V$	rAF $microV/V$	rPM $microV/V$	rYM $microV/V$	rRM $microV/V$
0.9	0.2	0.7	0.1	0.5

Finally, it is interesting to examine the non–iterative part of the load iteration equation that is obtained after the application of the *Iterative Method*. The non–iterative part equals square matrix $\mathbf{C_1}^{-1}$ that is traditionally used to define the primary load iteration equation (see Ref. [7] or App. 10 for more details). Table 74 below lists coefficients of matrix $\mathbf{C_1}^{-1}$ that were obtained from the calibration data set of the MC60 balance. In theory, these

Table 74: *Iterative Method* $\Longrightarrow$ Coefficients of square matrix $\mathbf{C_1}^{-1}$. This matrix is the constant, i.e., non–iterative part of the load iteration equation.

	D1	D2	D3	D4	D5
NF	5.367001E+00	-1.538779E-01	1.684140E-01	2.402574E-02	1.730078E-01
AF	1.819106E-02	1.476571E+00	-2.034743E-02	2.361110E-02	1.819016E-03
PM	1.045062E+00	-4.002401E-01	4.149508E+01	9.449750E-02	-9.951182E-01
YM	-5.559243E-01	-1.611894E-01	-3.326093E+00	1.288478E+02	9.050901E-01
RM	4.040177E+00	1.058770E+00	4.230080E-01	-3.152626E-01	2.924990E+02

values should show good agreement with the twenty–five principal linear terms that were obtained after the application of the *Non–Iterative Method* to the calibration data (see Table 67). The values of Table 74 can be compared with the values of Table 67 by simply examining the ratio between two corresponding values. The ratio equals one if a value pair shows perfect agreement. The ratios of the twenty–five coefficients were computed. Then, the arithmetic mean of the ratios was calculated. A mean value of 0.9992 was obtained. This value is very close to the value of one that describes a perfect agreement between the independently computed coefficient sets. The result confirms again that load prediction accuracy differences between the *Non–Iterative Method* and the *Iterative Method* are very small. They can be neglected for all practical purposes as long as (i) regression models with similar function classes are used for the regression analysis of the calibration data and (ii) a tare load iteration is performed.

Moment Arm Range Requirements

It is important to review connections between (i) the locations of the resultant normal and axial forces on a semi–span model and (ii) the rolling and yawing moment arm range of the calibration rig that is used for the balance calibration. They need to be understood so that a calibration data set is not used outside its calibration range.

The discussion of the moment arm range requirements assumes that the semi–span model of a commercial transport type aircraft is installed on the floor of the test section of a wind tunnel. Figure 55 below shows, for example, the installation of the UHB semi–span model in the test section of the NASA Ames 11–ft Transonic Wind Tunnel. First, the

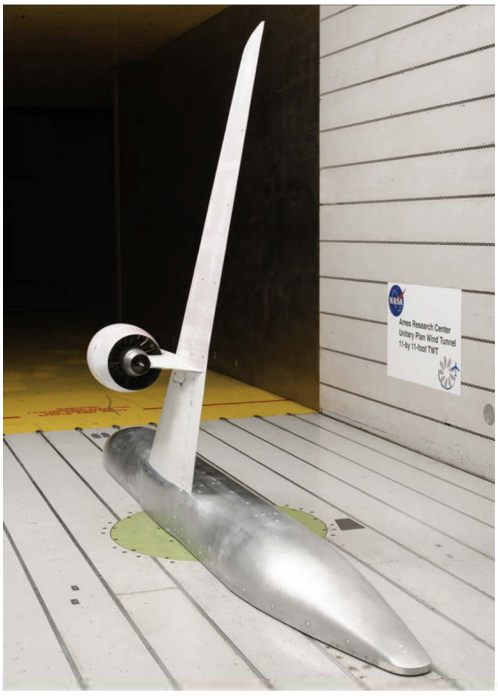

Fig. 55 Installation of the UHB semi–span model in the Ames 11–ft TWT.

connection between normal force and rolling moment arm range is investigated. It is known from theoretical considerations that the resultant wind–on normal force on a semi–span model of a commercial transport type aircraft is located somewhere between a point that is close to the metric flange of the balance and a point that is located near 50 % of the semi–span of the model. These two points are shown in Fig. 56a below as a pair of blue points that are located on the pitch axis of the balance. In addition, a typical calibration rig can often only apply the normal force at a small number of selected load points, i.e., rolling moment arms, relative to the balance moment center. The resulting minimum and maximum of the rolling moment arm and the associated built–in range of the load points are identified in Fig. 56a below as a pair of green points that are located on the pitch axis of the balance. Consequently, the range of the resultant normal force

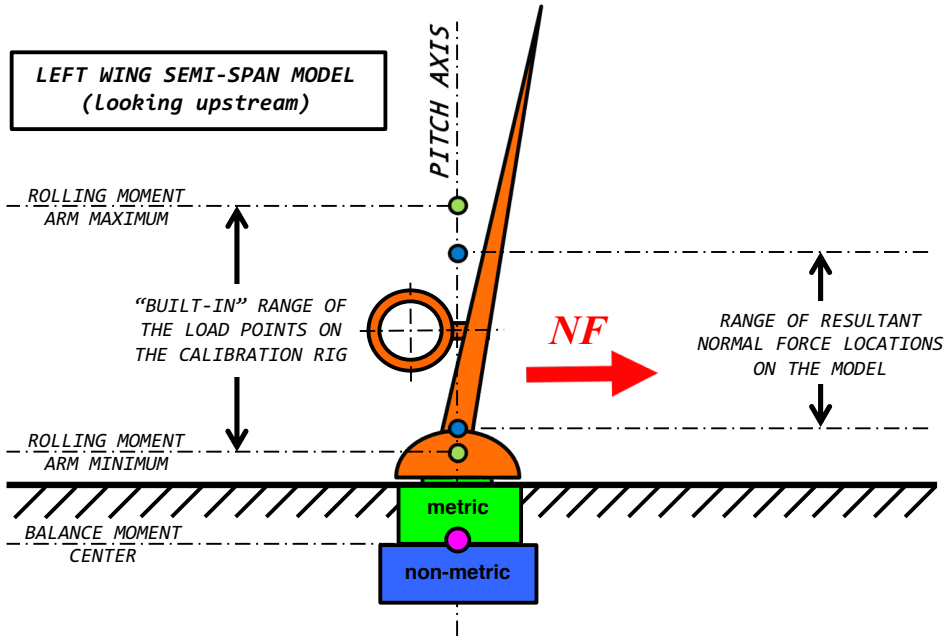

Fig. 56a Rolling moment arm range requirement of the calibration rig.

locations on the model, i.e., the pair of blue points in Fig. 56a, must be located inside the built–in range of the load points on the calibration rig in order to achieve the most accurate normal force predictions. In all other cases, the predicted normal force on the model will be extrapolated with an associated reduction of the load prediction accuracy.

Similar relationships between between axial force and yawing moment arm range exist. Figure 56b below shows the corresponding relationships. Again, it is known from theo–

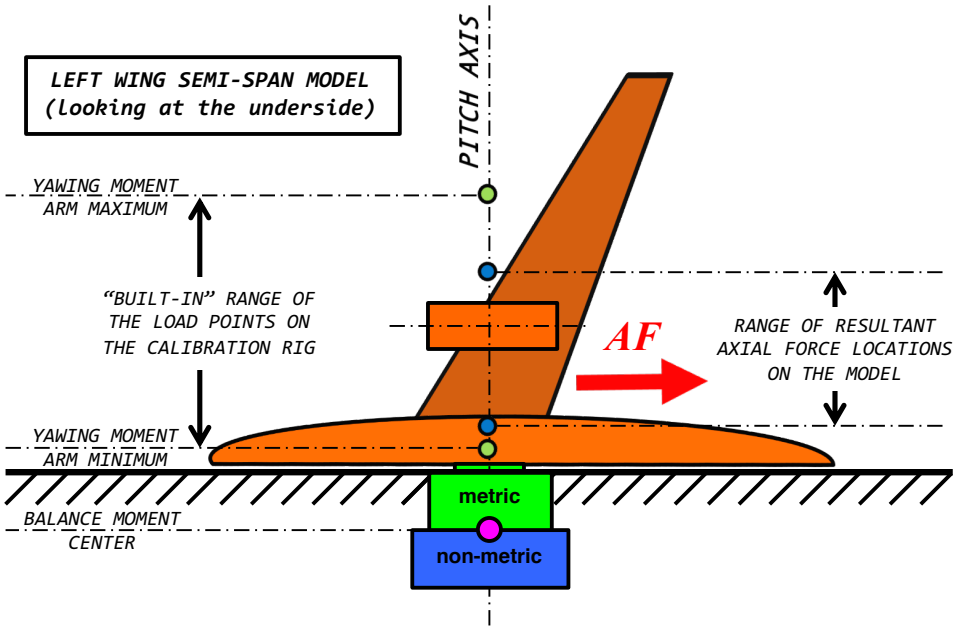

Fig. 56b Yawing moment arm range requirement of the calibration rig.

retical considerations that the resultant wind–on axial force is located somewhere between a point that is close to the metric flange of the balance and a point that is located near 50 % of the semi–span of the model. These two points are identified in Fig. 56b above as a pair of blue points that are located on the pitch axis of the balance. In addition, a calibration rig can often only apply the axial force at a small number of selected load points, i.e., yawing moment arms, relative to the balance moment center. The resulting minimum and maximum of the yawing moment arm and the associated range of the load points are identified in Fig. 56b above as a pair of green points that are located on the pitch axis of the balance. Again, as it was the case for the normal force, the range of the resultant axial force locations on the model, i.e., the pair of blue points in Fig. 56b, must be located inside the built–in range of the load points on the calibration rig in order to achieve the most accurate axial force predictions. In all other cases, the axial force will be extrapolated with an associated decrease of the load prediction accuracy.

The discussion of the moment arm range requirements indicates that it is an advantage if the calibration rig used for the characterization of a semi–span balance allows for the direct application of the normal and axial forces at the balance moment center. Then, the built–in range of the load points on the calibration rig would extend all the way to the balance moment center. In addition, more reliable estimates of the primary sensitivities of the normal and axial force bridges would be obtained as both load components could also be applied as single–component loads during the balance calibration.

XI. Observations, Conclusions, and Recommendations

General Remarks

Different ways to format, analyze, evaluate, and use strain–gage balance data are discussed in the report. This approach was chosen so that a variety of data analysis and load prediction approaches could be compared side–by–side. The author's most important observations, conclusions, and recommendations are summarized in this part of the document. This summary must remain incomplete because it is primarily based on the author's personal experiences. Nevertheless, the summary may provide information that could be helpful for a novice balance engineer. In addition, it could become a starting point for discussions among more experienced analysts, balance engineers, and balance users who either made similar observations or came to alternate conclusions.

Fundamental Concepts

Load State $\Longrightarrow$ In general, a strain–gage balance experiences different load states during calibration and use in the wind tunnel that may be observed as elastic deformations of the balance geometry. Then, assuming that the balance is at a constant temperature, each load state can be described by using either a set of tare corrected loads or a set of measured electrical outputs of the balance bridges. Both descriptions of the load state are equivalent. It is like describing something in two different languages. Therefore, the following two conclusions can be drawn. First, the mathematical connection between the tare corrected loads and the measured electrical outputs of the balance bridges must be unique. In other words, a balance must be designed such that one specific load combination only relates to one specific electrical output combination and vice versa. In addition, according to the *General Theorem of the Inversion of Transformations* (see Ref. [73], pp. 261–277), the total number of independent load components of a balance must always match the total number of independent bridge output measurements.

Interpretation and Use of Balance Calibration Data $\Longrightarrow$ Calibration data of a balance can be interpreted as a set of load states that an analyst selects to best describe the physical relationship between tare corrected loads and measured electrical outputs of the balance. The data set is analyzed by using either the *Non–Iterative Method* or the *Iterative Method*. Each method establishes a mathematical relationship between loads and electrical outputs of the balance that can be used for the load prediction during a wind tunnel test.

Absolute Load and Output Datum $\Longrightarrow$ It is critical to reference all loads and outputs to an absolute datum if global regression analysis is applied to balance calibration data. Therefore, it is recommended to perform a tare load iteration during the analysis of the calibration data so that all loads are referenced to the datum of zero absolute load. Similarly, it is recommended to measure the natural zeros of the balance bridges. They need to be subtracted from the raw outputs of the bridges so that all outputs are referenced to the datum of zero output. Then, the regression models obtained from the calibration data will map the datum of zero absolute load to the datum of zero output (and vice versa).

Electrical Outputs

Electrical Units $\Longrightarrow$ Electrical outputs of the balance bridges are best described as a dimensionless quantity. It is defined as the raw output measurement in units of *micro Volts (microV)* divided by the excitation voltage in units of *Volts (V)*. This choice has two advantages. First, it makes the electrical outputs independent of the excitation voltage. In addition, outputs of a typical balance become more suitable for visual inspection as they will have numerical values between 0 and ± 3000 $microV/V$.

Electrical Output Threshold $\Longrightarrow$ Two electrical outputs of a balance bridge can be considered identical for all practical purposes if they differ by 1.0 $microV/V$ or less. Process improvements, hardware refinements, and laboratory staff training may lower this threshold to between 0.3 and 0.5 $microV/V$.

Natural Zeros $\Longrightarrow$ The natural zeros are the raw outputs of the balance bridges in an assumed weightless condition. In theory, they are physical constants of the balance. However, their exact measurement is influenced by small instrumentation–dependent bias errors. Therefore, it is suggested to measure the natural zeros each time an instrumentation change is made during use of the balance. Then, instrumentation–dependent bias errors can be removed from the output measurements if the difference between raw output and natural zero is used to process balance data.

Electrical Output Format $\Longrightarrow$ The difference between the raw output and the related natural zero of the bridge should be used as input for data analysis and load prediction. Then, zero output becomes the electrical representation of zero absolute load. In addition, absolute value terms can be included in the regression model of a load component if the *Non–Iterative Method* is used to process data of a balance with bi–directional outputs.

Maximum Output at Load Capacity $\Longrightarrow$ The maximum output at load capacity is a material constant of the balance. It indicates how well a balance bridge is matched to the capacity of the related load component. The metric is defined as the product of the primary sensitivity of a bridge with the capacity of the related load component. It is the electrical representation of the load capacity. The bridges of most force balances have maximum outputs that are between 1000 and 1500 $microV/V$. Some bridges of single–piece balances are known to have values between 2500 and 3000 $microV/V$. Values near or below 500 $microV/V$ are also sometimes observed. They indicate a bridge that does not get much output at capacity. This characteristic is often associated with an unwanted increase of the standard deviation of the load residuals of the related primary load component.

Flight Data Recorder $\Longrightarrow$ The raw electrical outputs of the balance bridges can be interpreted as information that is contained in a hypothetical flight data recorder of a strain–gage balance. They describe the true load state of the balance in a format that directly reflects the influence of tare loads and auxiliary loads on the balance. No corrections need to be applied to the raw outputs in order to evaluate them. Therefore, it is helpful for troubleshooting purposes if a balance engineer develops the ability to interpret the raw electrical outputs of the balance bridges. For example, a load component is probably not

applied if the raw output of the related bridge differs from its natural zero by less than 1 $microV/V$. Similarly, a load component may have been loaded way beyond its capacity if a raw output is greater than, say, 125 % of its maximum output at capacity.

Balance Loads

Load Format $\Longrightarrow$ Loads of a force or moment balance should be analyzed and predicted in their design format, i.e., in force balance or moment balance format. Afterwards, loads can be converted to direct–read format by applying simple transformations that are listed in App. 4. This approach has the advantage that a single load component will be responsible for more than 90 % of the electrical output of the related bridge if the load is given in the design format of the balance. Consequently, loads and outputs can more clearly be separated which simplifies both data interpretation and troubleshooting.

Tare Load Iteration $\Longrightarrow$ It is required to use tare corrected loads for the balance calibration data analysis if (i) the electrical outputs of the bridges are formatted as output differences relative to the natural zeros and (ii) global regression analysis is used to process the data. It is recommended to use a tare load iteration algorithm for the determination of tare loads. Then, the common center of gravity of the metric part and all attached calibration hardware does not have to be known in order to determine the tare loads.

Calibration Experiment

Load Schedule Design $\Longrightarrow$ The overall quality of global regression analysis results of balance calibration data and the reliability of the balance load predictions always benefits from a systematic load schedule design (see, e.g., Refs. [41] for a comparison of different load schedule designs). In particular, it is an advantage if either balance calibration hardware or a balance calibration machine allows for the application of load schedules that are based on the well known principles of *Designed Experiments* (see, e.g., Refs. [42] and [69] for more details). Unfortunately, the design of many manual calibration load schedules is dictated by (i) calibration hardware limitations and (ii) built–in characteristics of gravity weight sets that a calibration laboratory owns. Compromises have to be found in those situations so that useful single–component and combined loads are applied that allow for the development of reliable load prediction equations.

Load Schedule Symmetry $\Longrightarrow$ In general, a load schedule should be as symmetric as possible if global regression analysis is applied to balance calibration data. This approach makes sure that (i) the regression analysis does not favor data with a particular load sign, (ii) symmetric characteristics of the balance are captured, and (iii) bi–directional bridge output behavior can be quantified (if applicable).

Load Range $\Longrightarrow$ Single–component loads for each load component should be applied over the component's entire positive and negative load range (from -100 % capacity to $+100$ % capacity). Then, a data set is collected for the regression analysis that will result in the most accurate numerical estimates of the primary bridge sensitivities.

Single–component Loads $\Longrightarrow$ Global regression analysis implicitly assigns equal weight to all data points of a calibration load schedule. This characteristic can decrease the influence of single–component loads on the final regression analysis results because they are only a very small part of a typical calibration load schedule. This decrease could potentially lead to less accurate estimates of the primary sensitivities of the balance bridges (see Ref. [16] for a discussion of this issue). Therefore, it is recommended to repeat single–component loads in regular intervals in the calibration load schedule in order to increase the percentage of single–component loads in the data set. Alternatively, an analyst may use a weighted least squares approach to explicitly assign more weight to single–component loads during the global regression analysis (see App. 22 for more details).

Balance Axis System, Gravitational Acceleration, Alignment $\Longrightarrow$ In theory, the orientation of the forward face of the metric part of the balance in space defines the balance axis system during both balance calibration and use in the wind tunnel. Therefore, it is critical to precisely level the metric part during a balance calibration with gravity weights. Then, a known orientation of the balance axis system is established relative to the direction of the gravitational acceleration. This known orientation is needed so that gravity weights and distances on the calibration body can be interpreted as forces and moments that act on the balance. Alignment errors should be avoided at all cost as they cause unwanted bridge interactions that could negatively influence the calibration data analysis.

Application of Moments $\Longrightarrow$ It is more accurate to apply a moment during a balance calibration by using a small weight in combination with a long moment arm instead of using a large weight in combination with a short moment arm.

Data Analysis and Load Prediction

Non–Iterative versus Iterative Method $\Longrightarrow$ The load prediction accuracy of the *Non–Iterative Method* is as good as the load prediction accuracy of the *Iterative Method* as long as (i) tare corrected loads and output differences relative to the natural zeros are used to describe the balance calibration data and (ii) compatible function classes are used to build regression models of the loads and outputs. The *Non–Iterative Method*, however, does not require a load iteration to predict loads from outputs during a wind tunnel test. Therefore, it is less complex and more easily implemented in the data system of a tunnel.

Identification of Important Regression Model Terms $\Longrightarrow$ It is recommended to use the percent contribution of a regression model term for the assessment of the term's importance. A term is considered important if the absolute value of its percent contribution exceeds the empirical threshold of 0.5 % (threshold taken from App. 16, Table 16–3). Alternatively, the p–value of the regression model term could be used to assess a regression model term's importance. However, the percent contribution has the advantage that it is more easily implemented and understood.

Identification of Regression Model Terms of Minor Importance $\Longrightarrow$ The percent contribution may be used to identify regression model terms of minor importance. A term is considered a term of minor importance if the absolute value of its percent contribution

is between 0.1 % and 0.5 % (range taken from App. 16, Table 16–3). An analyst needs to use subject–matter knowledge and other information in order to decide if a term of minor importance needs to be used or can be omitted.

Identification of Insignificant Regression Model Terms $\Longrightarrow$ The percent contribution may be used to identify an insignificant term in the regression model of balance data. A term of the regression model is considered insignificant if the absolute value of its percent contribution is less than the empirical threshold of 0.1 % (threshold taken from App. 16, Table 16–3). It is acceptable to drop an insignificant regression model term as long as the final regression model remains hierarchical, i.e., has no missing lower order terms.

Hierarchical Regression Model $\Longrightarrow$ It is recommended to always use hierarchical regression models for the analysis of strain–gage balance data. These models do not have any missing lower order terms. Therefore, they can handle hidden offsets in the independent variables that are used to build the regression model (see Ref. [20], pp. 6–8).

Absolute Value Terms $\Longrightarrow$ An absolute value term should be included in the regression model of balance data if (i) it is supported by the calibration data and (ii) the absolute value of its percent contribution exceeds the threshold of 0.5 % (see App. 16, Table 16–3).

Linear and Massive Near–linear Dependencies $\Longrightarrow$ Hidden linear or massive near–linear dependencies in regression models of balance calibration data can greatly reduce the reliability of the balance load prediction process. Therefore, terms must be removed from the regression model that are responsible for these dependencies. For example, the *Variance Inflation Factor* (VIF) may be used to detect and remove linear and massive near–linear dependencies in regression models of balance calibration data. The following maximum values of the VIF of a regression model are acceptable $\Longrightarrow$ single–piece balance $\approx$ 10; force balance with bi–directional bridge outputs $\approx$ 20; semi–span balance $\approx$ 30 (thresholds taken from App. 18, Section 18.5). Unfortunately, many standard data analysis tools do not compute VIFs of a set of regression model terms. Therefore, a detailed description of the numerical calculation of the VIFs is given in App. 18 for reference.

Temperature Effects $\Longrightarrow$ The temperature difference relative to a reference temperature should be used as the independent variable for the description of balance temperature effects. Recommended correction methods for balance temperature effects are listed in App. 14 (see methods 2 and 3 in App. 14, Table 14–1). Experience has shown that single–component loads at three different temperatures should be applied during a temperature calibration of the balance if the expected temperature range of the balance during a wind tunnel test is between 294 $degK$ (70 $degF$) and 314 $degK$ (105 $degF$). This additional data will have the information needed to determine an explicit load correction that addresses an unwanted temperature–dependent bridge sensitivity shift.

Graphical Display of Calibration Load Residuals $\Longrightarrow$ Two types of plots should be used to display and assess balance calibration load residuals. First, load residuals should be plotted versus the tare corrected loads. This plot allows an analyst to understand (i) the load prediction accuracy over the given load range of the balance and (ii) the

level of interactions near zero load. Load residuals should also be plotted versus the data point index. This alternate plot allows an analyst to quickly identify individual data point numbers or point ranges that are responsible for larger–than–expected load residuals.

Assessment of the Standard Deviation of the Load Residuals $\Longrightarrow$ The standard deviation of calibration load residuals of a typical six–component strain–gage balance is expected to be less than or equal to the empirical threshold of 0.10 % of load capacity.

Assessment of the Load Residual of an Individual Data Point $\Longrightarrow$ The range of ± 0.25 % of load capacity should be used for the evaluation of the load residual of an individual calibration data point. It is ± 2.5 times the empirical threshold of 0.10 % that is traditionally used in aerospace testing for the evaluation of the standard deviation of load residuals. The threshold also means that 98.8 % of all residuals of a load component are expected to be within ± 0.25 % of the load capacity if the load residuals are normally distributed (percentages are taken from a table of two–tailed Gaussian probabilities).

Aerodynamic Loads $\Longrightarrow$ A goal of a wind tunnel test is the measurement of aerodynamic loads that act on a model. Both the *Non–Iterative Method* and the *Iterative Method* compute balance loads relative to the datum of zero absolute load whenever differences between raw outputs and natural zeros are used as input. Therefore, aerodynamic loads must be computed as the difference between a wind–on and a wind–off load set. The wind–on load set is caused by aerodynamic effects and the combined weight of the model and the metric part of the balance. It is obtained from outputs that are measured in wind–on condition during the test. The wind–off load set is caused by the combined weight of the model and the metric part of the balance. It can be computed if (i) weight, (ii) location of the center of gravity, and (iii) orientation of the model relative to the direction of the gravitational acceleration are known in the balance axis system. The weight and the location of the center of gravity of the model are typically obtained from a wind–off data set that is recorded for different model orientations (see Ref. [55]).

Balance Check Loads $\Longrightarrow$ Check loads need to be calculated by using two predicted load sets per data point whenever (i) gravity weights are used for their application and (ii) differences between raw outputs and natural zeros are the input for the load prediction. The first load set is predicted from the electrical outputs of the check load point. This load set is caused by the combined weight of the metric part of the balance, the calibration equipment, and the gravity weights. The second load set is predicted from the electrical outputs of the tare point of the check load series. This load set is caused by the combined weight of the metric part of the balance and the calibration equipment. The second load set must be subtracted from the first load set. Afterwards, the difference of the two predicted load sets is compared with the check load set that is directly obtained from the gravity weights and their distance to either the balance moment center or a balance bridge.

Interactions $\Longrightarrow$ Interactions are complex electro–mechanical phenomena that connect the loads to the outputs of a strain–gage balance. They are the result of the fact that bridges are attached to interconnected parts of the balance. These parts are deformed as

soon as the load state of the balance changes. Consequently, significant output changes may occur on more than one bridge even if only a single load component is applied.

Two types of interactions are always superimposed whenever calibration or check loads are applied to a balance. The first type is the result of small load misalignments. These interactions represent hidden errors in the data. They can be reduced or avoided by (i) refining the load application process, (ii) replacing worn–out hardware, and (iii) improving laboratory staff training. The second type is caused by physical characteristics of the balance. These interactions cannot be eliminated. However, they are repeatable and can be described with interaction terms in the regression models of balance calibration data.

Repeatable interactions are primarily characterized with linear interaction terms in regression models of balance calibration data that both the *Non–Iterative Method* and the *Iterative Method* use. The identification of these linear terms can be illustrated with two examples. First, it is assumed that interactions need to be quantified in a regression model that the *Non–Iterative Method* uses to describe the aft normal force $N2$ of a six–component force balance. In this case, the output difference D_2 of the aft normal force bridge is the primary output of the fitted load component. Consequently, the remaining five output differences, i.e., D_1, D_3, D_4, D_5 and D_6 are the linear interaction terms in the regression model of $N2$. Similarly, interactions may need to be quantified in a regression model that the *Iterative Method* uses to describe the output difference D_2 of the aft normal force bridge of a force balance. Now, the aft normal force $N2$ is the primary load component of the fitted output difference. Therefore, the remaining five load components, i.e., $N1$, $S1$, $S2$, AF and RM are the linear interaction terms in the regression model of D_2.

Different approaches may be used to visualize interactions. The author suggests to use balance data for the visualization that is recorded during the application of a single load component to the balance (see also App. 24 for more details). This approach makes the graphical description of interactions less complex. In addition, the description is completely independent of regression models that are needed for the balance load prediction.

The recommended approach can be demonstrated with real–world data from a six–component force balance. It was decided to plot interactions that result from the application of the aft normal force. Therefore, a data set of a load series was selected that fulfilled the following three requirements: (i) the aft normal force was applied during the load series while keeping all other load components close to zero absolute load; (ii) the first data point of the load series had outputs that were exclusively caused by tare loads; (iii) the tare loads of the load series were small. Then, loads and outputs of the first data point of the load series were subtracted from the loads and outputs of the remaining data points of the load series (see also the discussion of bridge output format *Difference Type 2* in App. 6). Finally, the interactions, i.e., the reformatted electrical outputs of all but the primary bridge of the aft normal force, were plotted versus the reformatted aft normal force. Figure 57 below shows the observed interactions of the aft normal force that were obtained for the chosen force balance. The output differences D_1,

D_3, D_4, D_5, and D_6 are the interactions that result from the application of the aft normal force as a single–component load. The output difference D_2 is intentionally omitted in the plot because it is the output difference of the aft normal force bridge itself. The in–

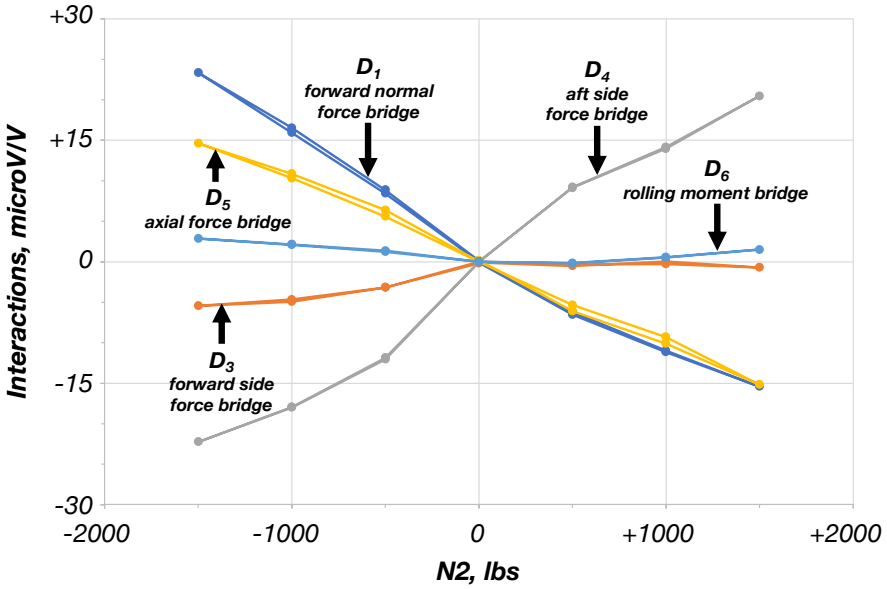

Fig. 57 Interactions plotted versus the aft normal force of a force balance.

teractions of the five bridges show a characteristic star pattern as, by design, all interactions must be zero when no load is applied.

Numerical estimates of the first derivatives of the interactions with respect to a load component, i.e., the slopes of the five lines that are shown in Fig. 57 above, can be obtained from the load prediction equations if interactions of single–component loads of balance calibration data are plotted. The first derivatives are the off–diagonal coefficients of the inverse matrix $\mathbf{L}^{-1}$ of the linear part of the regression coefficient matrix that the *Non–Iterative Method* needs for the load prediction (see App. 9, section 9.6). Alternatively, the first derivatives are the off–diagonal coefficients of the matrix $\mathbf{C_1}$ that the *Iterative Method* uses. This matrix equals the inverse of matrix $\mathbf{C_1}^{-1}$ that is part of the definition of the *Primary Load Iteration Equation* (see App. 10, section 10.12).

Interaction plots for the other five load components, i.e., $N1$, $S1$, $S2$, AF, and RM of the force balance can easily be generated by using the same approach that was used for the interaction plot of the aft normal force. It must be emphasized that the suggested interaction plot is the description of a built–in design characteristic of the balance. It is like a fingerprint of a single load component of the balance that is completely independent of both calibration process and load prediction method. Therefore, an analyst can use the suggested interaction plot to monitor the quality of a calibration or check load data set. Any significant change of the interaction plot may indicate a hidden misalignment of the load application hardware that should be investigated.

References

Concepts, Methods, Algorithms:

[1] Schlichting, H. and Truckenbrodt, E., *Aerodynamics of the Airplane*, translation of *Aerodynamik des Flugzeuges*, translated by Ramm, H. J., 1st edition, McGraw–Hill International Book Company, New York, 1979, pp. 12–15.

[2] Hufnagel, K., *Wind Tunnel Balances*, 1st edition, Book Series: Experimental Fluid Mechanics, Springer International Publishing, 2022.

[3] Hufnagel, K., and Schewe, G., "Force and Moment Measurement," in Tropea, C., Yarin, A. L., Foss, J. F. (eds.), *Springer Handbook of Experimental Fluid Mechanics,* Springer Handbooks, Springer, Berlin, Heidelberg, 2007, pp. 563–616.

[4] Staff Writers (Hewlett Packard), *Practical Strain Gage Measurements – Application Note 290–1,* Hewlett Packard Company, Palo Alto, California, September 1981.

[5] Cook, T. A., *A Note on the Calibration of Strain Gauge Balances for Wind Tunnel Models,* Royal Aircraft Establishment (Bedford), Technical Note No: AERO.2631, Ministry of Aviation, London, December 1959.

[6] Galway, R. D., *A Comparison of Methods for Calibration and Use of Multi–Component Strain Gauge Wind Tunnel Balances,* National Aeronautical Establishment, National Research Council Canada / Conseil National de Recherches Canada, NRC No. 18227, Aeronautical Report LR–600, Ottawa, March 1980, p. 13, pp. 21–23, p. 27.

[7] AIAA/GTTC Internal Balance Technology Working Group, *Recommended Practice: Calibration and Use of Internal Strain–Gage Balances with Application to Wind Tunnel Testing,* AIAA R–091A–2020, revised/expanded 2nd edition of AIAA R–091–2003, The American Institute of Aeronautics and Astronautics, Reston, Virginia, 2020.

[8] Ulbrich, N., "Application of the Concepts of Load State, Load Space, and Output Space to Strain-Gage Balances," AIAA 2021–0163, paper presented at the AIAA SciTech 2021 Forum, Virtual Event, 11–15 & 19–21 January 2021.

[9] Ulbrich, N., "Assessment of the Uniqueness of Strain–Gage Balance Load Predictions," AIAA 2016–4157, paper presented at the 32nd AIAA Aerodynamic Measurement Technology and Ground Testing Conference, Washington, D.C., June 2016.

[10] Ulbrich, N., "Comparison of Electrical Output Format Options for the Analysis of Strain-Gage Balance Calibration Data," AIAA 2019–3155, paper presented at the AIAA Aviation 2019 Forum, Dallas, Texas, June 2019.

[11] Ulbrich, N., "A Universal Tare Load Prediction Algorithm for Strain–Gage Balance Calibration Data Analysis," AIAA 2011–6090, paper presented at the 47th AIAA–ASME–SAE–ASEE Joint Propulsion Conf., San Diego, California, July/August 2011.

[12] Ulbrich, N., "Comparison of Iterative and Non–Iterative Strain–Gage Balance Load Calculation Methods," AIAA 2010–4202, paper presented at the 27th AIAA Aerodynamic Measurement Technology and Ground Testing Conference, Chicago, Illinois, June/July 2010.

[13] Ulbrich, N., "Iterative Strain–Gage Balance Calibration Data Analysis for Extended Independent Variable Sets," AIAA 2011–0949, paper presented at the 49th AIAA Aerospace Sciences Meeting, Orlando, Florida, January 2011.

[14] Ulbrich, N., "Influence of Primary Gage Sensitivities on the Convergence of Balance Load Iterations," AIAA 2012–0322, paper presented at the 50th AIAA Aerospace Sciences Meeting, Nashville, Tennessee, January 2012.

[15] Ulbrich, N., "Fundamental Improvement of a Convergence Test for Iterative Strain–Gage Balance Load Predictions," AIAA 2019–3152, paper presented at the AIAA Aviation 2019 Forum, Dallas, Texas, June 2019.

[16] Ulbrich, N., and Volden, T., "Wind Tunnel Strain–Gage Balance Calibration Data Analysis using a Weighted Least Squares Approach," AIAA 2017–4426, paper presented at the 33rd AIAA Aerodynamic Measurement Technology and Ground Testing Conference, Denver, Colorado, June 2017.

[17] Ulbrich, N., and Volden, T., "An Improved Weighted Least Squares Algorithm for the Analysis of Strain–Gage Balance Calibration Data," AIAA 2022–0138, paper presented at the AIAA SciTech 2022 Forum, San Diego, California, January 2022.

[18] Ulbrich, N., "Calibration Variable Selection and Natural Zero Determination for Semispan and Canard Balances," AIAA 2013–2998, paper presented at the AIAA Ground Testing Conference, San Diego, California, June 2013.

[19] Ulbrich, N., and Reed, M., "Calibration and Data Analysis Recommendations for Three–Component Moment Balances," AIAA 2019–3153, paper presented at the AIAA Aviation 2019 Forum, Dallas, Texas, June 2019.

Regression Analysis of Balance Calibration Data:

[20] Ulbrich, N., "Regression Model Optimization for the Analysis of Experimental Data," AIAA 2009–1344, paper presented at the 47th AIAA Aerospace Sciences Meeting, Orlando, Florida, January 2009.

[21] Ulbrich, N., "Analysis of Multivariate Experimental Data using a Simplified Regression Model Search Algorithm," AIAA 2013–2996, paper presented at the AIAA Ground Testing Conference, San Diego, California, June 2013.

[22] Ulbrich, N., and Volden, T., "Strain–Gage Balance Calibration Analysis using Automatically Selected Math Models," AIAA 2005–4084, paper presented at the 41st AIAA/ASME/SAE/ASEE Joint Propulsion Conference, Tucson, Arizona, July 2005.

[23] Ulbrich, N., and Volden, T., "Application of a New Calibration Analysis Process to the MK–III–C Balance," AIAA 2006–0517, paper presented at the 44th AIAA Aerospace Sciences Meeting, Reno, Nevada, January 2006.

[24] Ulbrich, N., and Volden, T., "Analysis of Floor Balance Calibration Data using Automatically Generated Math Models," AIAA 2006–3437, paper presented at the 24th AIAA Aerodynamic Measurement Technology and Ground Testing Conference, San Francisco, California, June 2006.

[25] Ulbrich, N., and Volden, T., "Analysis of Balance Calibration Machine Data using Automatically Generated Math Models," AIAA 2007–0145, paper presented at the 45th AIAA Aerospace Sciences Meeting, Reno, Nevada, January 2007.

[26] DeLoach, R., and Ulbrich, N., "A Comparison of Two Balance Calibration Model Building Methods," AIAA 2007–0147, paper presented at the 45th AIAA Aerospace Sciences Meeting, Reno, Nevada, January 2007.

[27] Ulbrich, N., and Volden, T., "Regression Analysis of Experimental Data using an Improved Math Model Search Algorithm," AIAA 2008–0833, paper presented at the 46th AIAA Aerospace Sciences Meeting, Reno, Nevada, January 2008.

[28] Ulbrich, N., and Bader, J., "Analysis of Sting Balance Calibration Data using Optimized Regression Models," AIAA 2009–5372, paper presented at the 45th AIAA–ASME–SAE–ASEE Joint Propulsion Conference, Denver, Colorado, August 2009.

[29] Ulbrich, N., "Optimization of Regression Models of Experimental Data using Confirmation Points," AIAA 2010–0930, paper presented at the 48th AIAA Aerospace Sciences Meeting, Orlando, Florida, January 2010.

[30] Ulbrich, N., and Volden, T., "Regression Model Term Selection for the Analysis of Strain–Gage Balance Calibration Data," AIAA 2010–4545, paper presented at the 27th AIAA Aerodynamic Measurement Technology and Ground Testing Conference, Chicago, Illinois, June/July 2010 (paper was also presented at the 7th International Symposium on Strain–Gauge Balances, Williamsburg, Virginia, May 2010).

[31] Ulbrich, N., and Kew, R., "Calibration of the NASA MC60 Five–Component Semi–span Balance," AIAA 2020–3100, paper presented at the AIAA AVIATION 2020 Forum, Virtual Event, June 15–19, 2020.

[32] Ulbrich, N., and Kew, R., "Comparison of two Calibrations of NASA's MC60 Five–component Semi–span Balance," AIAA 2021–0164, paper presented at the AIAA SciTech 2021 Forum, Virtual Event, 11–15 & 19–21 January 2021.

Bi–directional Bridge Outputs:

[33] Ulbrich, N., "A Universal Algorithm for the Detection of Bi–directional Gage Out–put Characteristics," AIAA 2021–2968, paper presented at the AIAA Aviation 2021 Forum, Virtual Event, August 2–6, 2021.

[34] Kammeyer, M. E., and Ulbrich, N., "The Use of Absolute–Value Terms in Regression Modeling of Multi–Piece Force Balances," AIAA 2015–3382, paper presented at the 31st AIAA Aerodynamic Measurement Technology and Ground Testing Conference, Dallas, Texas, June 2015.

[35] DeLoach, R., and Ulbrich, N., "A Statistical Theory of Bi–directionality," AIAA 2013–2995, paper presented at the AIAA Ground Testing Conference, San Diego, California, June 2013.

Temperature Effects:

[36] Ewald, B., Polanski, L., and Graewe, E., "The Cryogenic Balance Design and Balance Calibration Methods," AIAA–92–4001, paper presented at the 17th Aerospace Ground Testing Conference, Nashville, Tennessee, July 1992, p. 2, pp. 5–6.

[37] Ferris, A. T., *Cryogenic Strain Gage Techniques used in Force Balance Design for the National Transonic Facility*, NASA Technical Memorandum 87712, NASA–TM–87712, Langley Research Center, Hampton, Virginia, May 1986, p. 2, p. 9.

[38] Ulbrich, N., and Zimmermann, C., "Application of a Temperature–Dependent Load Prediction Method to a RUAG Six–Component Block–Type Balance," AIAA 2019–2294, paper presented at the 2019 AIAA SciTech Forum, San Diego, California, January 2019.

[39] Ulbrich, N., and Zimmermann, C., "Assessment of Temperature–Dependent Regression Model Terms of a RUAG Six–Component Block–Type Balance," AIAA 2020–0026, paper presented at the 2020 AIAA SciTech Forum, Orlando, Florida, January 2020.

Flow–Through Balances:

[40] Booth, D., and Ulbrich, N., "Calibration and Data Analysis of the MC–130 Air Balance," AIAA 2013–0545, paper presented at the 51st AIAA Aerospace Sciences Meeting, Grapevine, Texas, January 2013 (paper was also presented at the 8th International Symposium on Strain–Gauge Balances, Lucerne, Switzerland, May 2012).

Calibration Load Schedule Design:

[41] Rhew, D. R, and Parker, P. A., "Rigorous Design and Analysis of Wind Tunnel Balance Calibration Load Schedules," AIAA 2017–4427, paper presented at the AIAA Aviation Forum, Denver, Colorado, June 2017.

[42] Parker, P. A., Morton, M., Draper, N., and Line, W., "A Single–Vector Force Calibration Method Featuring the Modern Design of Experiments," AIAA 2001–0170, invited paper presented at the 39th AIAA Aerospace Sciences Meeting & Exhibit, Reno, Nevada, January 2001.

[43] Johnson, T. H., Parker, P. A., and Landman, D., *Calibration Modeling of Nonmonolithic Wind–Tunnel Force Balances,* Journal of Aircraft, Vol. 47, No. 6, November–December 2010, pp. 1860–1866.

[44] Lynn, K. C., Commo, S. A., Johnson, T. H., and Parker, P. A., "Thermal and Pressure Characterization of a Wind Tunnel Force Balance Using the Single Vector System," AIAA 2011–0950, paper presented at the 49th AIAA Aerospace Sciences Meeting, January 2011.

[45] Lynn, K. C., Commo, S. A., Ulbrich, N., Harris, C., "Experimental Design Consider–ations for Calibration of Semi–Span Force Measurement Systems," AIAA 2014–0276, paper presented at the 52nd AIAA Aerospace Sciences Meeting, National Harbor, Maryland, January 2014.

[46] Landman, D., and Yoder, D., *Wind-Tunnel Balance Calibration with Temperature Using Design of Experiments,* Journal of Aircraft, Vol. 51, No. 3, May–June 2014, pp. 841–848.

[47] Ulbrich, N., and Gisler, R., "A Baseline Load Schedule for the Manual Calibration of a Force Balance," AIAA 2013–1017, paper presented at the 51st AIAA Aerospace Sciences Meeting, Grapevine, Texas, January 2013.

[48] Ulbrich, N., Gisler, R., and Kew, R., "Assessment of New Load Schedules for the Machine Calibration of a Force Balance," AIAA 2015–2023, paper presented at the 53rd AIAA Aerospace Sciences Meeting, Kissimmee, Florida, January 2015.

[49] Ulbrich, N., "Pre-Test Assessment of the Use Envelope of the Normal Force of a Wind Tunnel Strain–Gage Balance," AIAA 2016–1632, paper presented at the 54th AIAA Aerospace Sciences Meeting, San Diego, California, January 2016.

[50] Ulbrich, N., "Combined Load Diagram for a Wind Tunnel Strain–Gage Balance," AIAA 2010–4203, paper presented at the 27th AIAA Aerodynamic Measurement Technology and Ground Testing Conference, Chicago, Illinois, June/July 2010.

Sequential Balance Data Analysis:

[51] Guarino, J. F., "Calibration and Evaluation of Multicomponent Strain–Gage Balances," paper presented at the NASA Interlaboratory Force Measurements Group Meeting, Jet Propulsion Laboratory (JPL), Pasadena, California, April 1964.

[52] Kammeyer, M. E., "Balance Calibration Analysis by Sequential Regression," AIAA 2021–0063, paper presented at the AIAA SciTech Forum, virtual event, January 2021.

Miscellaneous Topics:

[53] Ulbrich, N., and Volden, T., "A New Load Residual Threshold Definition for the Eval–uation of Wind Tunnel Strain–Gage Balance Data," AIAA 2016–1538, paper presented at the 54th AIAA Aerospace Sciences Meeting, San Diego, California, January 2016.

[54] Ulbrich, N., and Volden, T., "A Universal Threshold for the Assessment of Load and Output Residuals of Strain–Gage Balance Data," AIAA 2017–0483, paper presented at the 55th AIAA Aerospace Sciences Meeting, Grapevine, Texas, January 2017.

[55] Ulbrich, N., Bridge, T., and Amaya, M., "A New Global Regression Analysis Method for the Prediction of Wind Tunnel Model Weight Corrections," AIAA 2014–2797, paper presented at the 30th AIAA Aerodynamic Measurement Technology and Ground Testing Conference, Atlanta, Georgia, June 2014.

[56] Ulbrich, N., and L'Esperance, A., "Pre–Test Assessment of the Upper Bound of the Drag Coefficient Repeatability of a Wind Tunnel Model," AIAA 2017–0484, paper pre–sented at the 55th AIAA Aerospace Sciences Meeting, Grapevine, Texas, January 2017.

[57] Ulbrich, N., and L'Esperance, A., "Influence of Strain–Gage Balance Characteristics on the Precision Error of the Drag Coefficient," AIAA 2019–1826, paper presented at the 2019 AIAA SciTech Forum, San Diego, California, January 2019.

[58] Ulbrich, N., and Volden, T., "Load Envelope Analysis of Strain–Gage Balance Data," AIAA 2007–0354, paper presented at the 45th AIAA Aerospace Sciences Meeting, Reno, Nevada, January 2007.

[59] Ulbrich, N., Volden, T., and Booth, D., "Predictive Capabilities of Regression Models used for Strain–Gage Balance Calibration Analysis," AIAA 2008–4028, paper pre–sented at the 26th AIAA Aerodynamic Measurement Technology and Ground Testing Conference, Seattle, Washington, June 2008.

[60] Ulbrich, N., and Volden, T., "Evaluation Of Regression Models of Balance Calibration Data using an Empirical Criterion," AIAA 2012–3323, paper presented at the 28th AIAA Aerodynamic Measurement Technology, Ground Testing, and Flight Testing Conference, New Orleans, Louisiana, June 2012.

[61] Ulbrich, N., "Hidden Connections between Regression Models of Strain-Gage Balance Calibration Data," AIAA 2013–1018, paper presented at the 51st AIAA Aerospace Sciences Meeting, Grapevine, Texas, January 2013.

[62] Ulbrich, N., "Detection and Use of Load and Gage Output Repeats of Wind Tunnel Strain–Gage Balance Data," AIAA 2017–4428, paper presented at the 33rd AIAA Aerodynamic Measurement Technology and Ground Testing Conference, Denver, Colorado, June 2017.

[63] Smith, D. L., *An Efficient Algorithm Using Matrix Methods to Solve Wind–Tunnel Force–Balance Equations*, NASA Technical Note TN D–6860, Langley Research Center, Hampton, Virginia, August 1972.

Mathematics:

[64] Strang, G., *Introduction to Applied Mathematics,* Wellesley–Cambridge Press, Welles–ley, Massachusetts, 1986, pp. 35–39.

[65] Burden, R. L., and Faires, J. D., *Numerical Analysis,* 3rd edition, PWS–Kent Publishing Company, Boston, Massachusetts, 1985, p. 334.

[66] Press, W. H., Teukolsky, S. A., Vetterling, W. T., Flannery, B. P., *Numerical Recipes in Fortran 77,* 2nd edition, reprinted with corrections, Cambridge University Press, Cambridge, New York, Melbourne, 1996.

[67] Forsythe, G. E., Malcolm, M. A., Moler, C. B., "Computer Methods for Mathematical Computations," Prentice–Hall, Inc., Englewood Cliffs, New Jersey, 1977, pp. 13–14.

[68] Montgomery, D. C., Peck, E. A., and Vining, G. G., *Introduction to Linear Regression Analysis,* 4th ed., John Wiley & Sons, Inc., New York, 2006.

[69] Myers, R. H., and Montgomery, D. C., *Response Surface Methodology: Process and Product Optimization Using Designed Experiments,* 1st ed., John Wiley & Sons, Inc., New York, 1995.

[70] McClave, J. T., and Dietrich, F. H., *Statistics*, 2nd ed., Dellen Publishing Company, Santa Clara, California, 1982; pp. 273–275.

[71] Henrici, P., *Elements of Numerical Analysis*, 1st ed., John Wiley & Sons, Inc., New York, London, Sydney, 1964, pp. 97–105.

[72] Rosen, K. H., Michaels, J. G., Gross, J. L., Grossman, J. W., Shier, D. R., *Handbook of Discrete and Combinatorial Mathematics*, CRC Press LLC, 2000, Section 3.5.2 *(Elementary Transformation Rules for Sums)*, Fact 8 *(Interchanging dependent indices of a double sum).*

[73] Courant, R., and John, F., *Introduction to Calculus and Analysis*, Vol. 2, 1st. ed., Interscience Publishers, John Wiley & Sons, New York, 1974, pp. 261–277.

BALFIT Software:

[74] Ulbrich, N., and Volden, T., "Development of a New Software Tool for Balance Calibration Analysis," AIAA 2006–3434, paper presented at the 24th AIAA Aerodynamic Measurement Technology and Ground Testing Conference, San Francisco, California, June 2006.

[75] Ulbrich, N., and Volden, T., "Development of a User Interface for a Regression Analysis Software Tool," AIAA 2010–0932, paper presented at the 48th AIAA Aerospace Sciences Meeting, Orlando, Florida, January 2010.

[76] Ulbrich, N., and Volden, T., *BALFIT – Software Tool for the Regression Analysis of Multivariate Data, User Guide (revised and corrected 6th edition)*, Jacobs Technology, prepared for NASA Ames Research Center under contract NNA16BD26C, May 2019.

Additional References:

[77] Penrose, R., "On Best Approximate Solutions of Linear Matrix Equations," *Mathematical Proceedings of the Cambridge Philosophical Society*, Vol. 52, Issue 1, January 1956, pp. 17–19.

[78] Baksalary, O. M., Trenkler, G., "The Moore–Penrose inverse: a hundred years on a frontline of physics research," *The European Physical Journal H 46, Article 9 (2021)*, *Springer Nature Link*, Section 3, Section 4.

[79] Clark, H., Sink, J.–E., MacMaster, M., "The Enduring Role of TASK Balances in Wind Tunnel Testing at the National Research Council Canada," AIAA 2023–3894, paper presented at the AIAA Aviation 2023 Forum, San Diego, California, June 2023.

[80] Galway, R. D., "A Consideration of Tare Weight Effects in Calibration and Use of Wind Tunnel Strain–Gauge Balances," paper presented at the 2nd International Sym–posium on Strain–Gauge Balances, Bedford, England, 4–7 May, 1999.

[81] Wright, C. P., *Applied Measurement Engineering – How to Design Effective Mechan–ical Measurement Systems*, Prentice–Hall, Inc., Englewood Cliffs, New Jersey, 1995, pp. 131–151, p. 143, p. 150, Figure 5.9 .

[82] Cahill, D. M., " The AIAA/GTTC Internal Balance Technology Working Group," NASA/CP–1999–209101/PT1 (part 1), conference proceedings of the *First Interna–tional Symposium on Strain Gauge Balances*, NASA Langley Research Center, Hamp–ton, Virginia, October 22–25, 1996, p. 85, p. 88.

[83] Ulbrich, N., "New Approach for the Assessment of Interactions of a Strain–Gage Balance," AIAA 2025–0939, paper presented at the AIAA SciTech Forum, Orlando, Florida, January 2025.

Appendix 1

Balance Terminology

Absolute Load Datum ≡ It is the condition when (i) the balance is in a weightless state and (ii) all load components are perfectly zero. It is the origin of the **Load Space**. The **Natural Zeros** are its equivalent representation in the **Output Space** assuming that the electrical outputs of the balance are expressed as **Raw Outputs**.

Absolute Voltage Measurement ≡ Voltage measurement of a **Bridge Output** that uses zero volts as a datum. The output may have been corrected for small day–to–day temperature variations in a laboratory or wind tunnel. The output is often divided by the **Excitation Voltage** in order to make it dimensionless.

Aerodynamic Load ≡ **Wind–On Load** minus **Wind–Off Load**.

Aircraft–Fixed Axis System ≡ **Body Axis System**.

Alternate Load Iteration Equation ≡ One of two load iteration equations that are used in the aerospace testing community to predict balance loads from measured bridge outputs during a wind tunnel test. The method only converges if balance data is processed in its **Design Format**. A description of the equation is given in App. 10, Eq. (10.31a).

Applied Load ≡ Force or a moment that is applied to the balance during its calibration. It does not include the **Tare Load** that is caused by the weight of the **Metric Part** of the balance, the **Calibration Body**, and other **Calibration Fixtures**.

Auxiliary Load ≡ **Preload**.

Balance Assembly ≡ Assembly that consists of the balance plus all calibration hardware pieces that are temporarily attached to it.

Balance Axis System ≡ It is a Cartesian coordinate system that allows for a precise description of balance loads. It must be defined such that balance loads can easily be described in the body axis system of the wind tunnel model. Therefore, it is best to attach the coordinate system to the part of the balance that is rigidly connected to the test article. – Let us assume, for example, that the balance is a five–component semi–span balance or a six–component primary balance. In that case, the orientation of the **Metric Part** in space defines the coordinate system because it is the part of the balance that is rigidly connected to the test article. In addition, the orientation of the **Metric Part** in space always coincides with the orientation of the **Calibration Body** in space because both pieces of hardware are rigidly connected. Therefore, loads applied on the **Calibration Body** can easily be expressed in the coordinate system after the **Calibration Body** is leveled relative to the direction of the gravitational acceleration. – Alternatively, let us assume that the balance is an auxiliary three–component **Moment Balance**. In that case, the orientation of the **Non–Metric Part** in space must be used to define the coordinate system because it is the part of the balance that is rigidly connected to the test article. The orientation of the **Non–Metric Part** in space always coincides with the orientation of the **Balance Support System** in space because both pieces of hardware

are rigidly connected. Consequently, loads described relative to the **Balance Support System** during calibration can easily be expressed in the coordinate system after a known orientation of the **Balance Support System** relative to the direction of the gravitational acceleration is established.

Balance Load ≡ It is a positive or negative force or a moment that acts on the balance.

Balance Moment Center (BMC) ≡ Point on the balance that is used to define moments (pitching moment, yawing moment, rolling moment). It is often located halfway between the forward and aft bridges of the balance.

Balance Support System ≡ Piece of hardware that is connected to the **Non–Metric Part** of the balance during calibration. It applies the reaction loads to the balance. In addition, it has the capability to both roll and pitch the **Non–Metric Part** so that the balance can be leveled during calibration.

Bi–directional ≡ Characteristic of one widely used family of **Multi–Piece Balances** in which, e.g., the **Primary Bridge Sensitivity** of the two normal and the two side force bridges is dependent on the sign of the load. Absolute value terms are needed in the regression model of balance data to describe the characteristic.

Body Axis System ≡ It is a Cartesian coordinate system that is rigidly connected to the wind tunnel model or test article. It is also called **Aircraft–Fixed Axis System**.

Bridge ≡ Wheatstone Bridge

Bridge Output ≡ Electrical output of a **Bridge** in units of $milliV$, $microV$, $milliV/V$, or $microV/V$ (the recommended unit is $microV/V$). It is used for the prediction of balance loads during a wind tunnel test.

Bridge Output Datum ≡ It is a reference output for a load calculation. The **Raw Output** at the beginning of a **Load Series**, for example, may be used as the datum.

Bridge Output Residual ≡ Difference between the measured and fitted bridge output of a balance (or vice versa).

Buoyant Zero, Buoyant Component Offset ≡ Natural Zero

Calibration Body ≡ Piece of hardware that is rigidly connected to the **Metric Part** of the balance. It allows for the precise application of loads or load combinations that can easily be described in the **Balance Axis System**.

Calibration Fixture ≡ Piece of hardware (e.g., flexure, yoke, rod, moment arm) that is needed for the application of calibration loads to a balance.

Calibration Matrix ≡ Regression Coefficient Matrix

Capacity ≡ Largest permitted/observed value of either a load component or an electrical output of a balance bridge. It is often used to make a load or an output dimensionless.

Check Load ≡ Load or combination of loads that is used to check the wiring and installation of a balance prior to a wind tunnel test. Its alignment is often not as good as the alignment that was obtained during the balance calibration.

Combined Load Plot ≡ It is a plot of a pair of balance load components in a Cartesian coordinate system. A total of fifteen combined load plots can be defined for all possible load combinations of a six–component balance. A visual inspection of the combined load plot of a load pair may be used to decide if the given balance calibration data set supports the load pair's cross–product term in a regression model of the balance data.

Confirmation Load ≡ Load or combination of loads that is used to assess the predictive capability of the balance load prediction process. Ideally, it does not match any load or combination of loads that was used during the original calibration of the balance.

Confirmation Point ≡ Data point with a load combination that was not applied during the calibration of the balance.

Core ≡ Non–Metric Part

Count ≡ This term is often used in connection with the measurement of balance outputs. It comes from the digital world. It describes an increase/decrease in the least significant bit after an Analog–to–Digital (A/D) conversion takes place. The input change required is determined by the full–scale range of the digitizer that is used as a part of the balance output measurement system. For example, a measurement system with an A/D converter and an amplifier may have the following characteristics: full scale A/D converter input range = ±10.24 *Volts* (DC), A/D conversion = 16 bit, amplifier gain = 512. Then, the chosen output measurement system is capable of 2 to the 16th power (65536) unique values. One bit is reserved for the sign since the A/D converter input accepts both positive and negative values. This condition leaves 2 to the 15th power (32768) discrete values to describe the magnitude of the A/D converter input. Then, after dividing 10.24 *Volts* by 32768 and the gain of 512, it is concluded that one count equals an unamplified balance output change of 0.6104 *microVolts* for the given measurement system characteristics.

Curve–Fit Matrix ≡ Regression Coefficient Matrix

Data Reduction Matrix ≡ This matrix is the final result of using the **Iterative Method** for the analysis of balance calibration data. Its coefficients define the load iteration equation that the **Iterative Method** uses for the prediction of loads from the electrical outputs of the balance.

Dependent Variable ≡ It is a load component if the **Non–Iterative Method** is used to analyze balance calibration data. It is an electrical output of a balance bridge if the **Iterative Method** is used to analyze balance calibration data.

Design Format ≡ Description of the loads and outputs of a balance that satisfies the following requirement: each bridge is related to one single load component that, when applied, is responsible for on the order of 90 % or more of its output. The following three formats are traditionally used in the aerospace testing community: **Direct–Read Format**, **Force Balance Format**, and **Moment Balance Format**.

Direct–Compute Method ≡ Non–Iterative Method.

Direct–Read Balance ≡ Six–component balance whose load components are three forces and three moments. The bridges are wired such that their outputs are directly proportional to the corresponding force or moment (see also **Direct–Read Format**).

Direct–Read Format ≡ This format describes the loads of a balance by using three forces and three moments. They are defined as follows: normal force, axial force, side force, pitching moment, yawing moment, and rolling moment.

Excitation Voltage ≡ Voltage between 3.0 and 10.0 *Volts* that keeps the bridge circuits of a balance energized. It is also the reference voltage that is used to make bridge outputs dimensionless. The voltage is measured at a fixed reference point. The reference point is the end of the excitation wires if a **Four–Wire Balance** is energized. The reference point is either the end of the excitation wires or the end of the sense wires if a **Six–Wire Balance** is energized. Unwanted self–heating of a bridge may occur if the applied voltage is too high (for details see Ref. [7], p. 56, and, Ref. [81], p. 143). Sometimes, common excitation is applied to the bridges of a six–component balance. Then, a single voltage source is used to supply the excitation voltage in parallel to all balance bridges.

Fixed End ≡ **Non–Metric Part**

Flexure ≡ Part of a balance that elastically deforms under load. It is the interface between **Metric Part** and **Non–Metric Part**. Strain gages are often attached to its surface. – Spring–like calibration hardware that allows for an unrestrained alignment of a **Calibration Fixture** with the direction of the gravitational acceleration.

Force Balance ≡ Six–component balance whose load components are described with five forces and one moment. The forces at the forward & aft bridges are proportional to the corresponding bridge outputs (see also **Force Balance Format**).

Force Balance Format ≡ This format describes the loads of a balance by using five forces and one moment. They are defined as follows: forward/aft normal force, forward/aft side force, axial force, and rolling moment.

Four–Wire Balance ≡ Each bridge of this balance type is connected with two excitation wires and two signal wires to the signal conditioner (voltage source).

Gage ≡ Term describes a strain gage. It is also a synonym for **Wheatstone Bridge**.

Global Regression ≡ Single least squares fit is used to calculate the coefficients of a multivariate regression model of balance calibration data.

Independent Variable ≡ It is an electrical output of a balance bridge if the **Non–Iterative Method** is used to analyze balance calibration data. It is a load if the **Iterative Method** is used to analyze balance calibration data.

Inner Rod ≡ **Non–Metric Part** of a **Force Balance**.

Interactions ≡ Interactions are complex electro–mechanical phenomena that connect the acting loads to the observed outputs of a strain–gage balance. They result from the fact that bridges are attached to interconnected parts of the balance. These parts experience elastic deformations as soon as the **Load State** of the balance changes. Consequently, significant output changes may occur on more than one bridge even if only a single load

component is applied. – Two types of interactions are always superimposed in balance calibration or check load data. The first type is associated with small load misalignments. These interactions represent hidden errors in the given data set. They can be reduced or avoided by (i) refining the load application process, (ii) replacing worn–out hardware, and (iii) improving laboratory staff training. The second type is caused by physical characteristics of the balance. These interactions are repeatable. They are primarily described with **Linear Interaction Terms** in a regression model of balance calibration data.

Intercept ≡ Constant term in the math model of balance calibration data. It may have a physical interpretation. Let us assume, for example, that the **Iterative Method** is used to process the data. Then, the intercept is a least squares approximation of the **Natural Zero** of the bridge output whenever **Raw Outputs** are fitted as a function of loads.

Iterative Method ≡ Load prediction method that fits the electrical outputs of a balance bridge as a function of the calibration loads. Therefore, an iteration is required to predict loads from outputs during a wind tunnel test. More details can be found in App. 10.

Knife Edge ≡ Hardware that allows for an unrestrained alignment of a **Calibration Fixture** with the direction of the gravitational acceleration.

Leveling ≡ Term describes the fact that a **Calibration Body** must be aligned with the direction of the gravitational acceleration whenever gravity weights are used for the load application. Then, loads can easily be described in the **Balance Axis System**.

Linear Interaction Term ≡ Linear regression model term that describes interactions. For example, the difference between the output of the normal force bridge and its **Natural Zero** is a linear interaction term in the regression model of the axial force if the **Non–Iterative Method** is used for the balance data analysis. Similarly, the normal force is a linear interaction term in the regression model of the output of the axial force bridge if the **Iterative Method** is used for the balance data analysis.

Live End –or– **Live Side** ≡ **Metric Part**

Load ≡ Force or moment that acts on a strain–gage balance.

Load Envelope ≡ Closed boundary of a region in a **Combined Load Plot** that is defined by the **Tare Corrected Loads**.

Load Residual ≡ Difference between an applied and a predicted load (or vice versa).

Load Schedule ≡ Loads or load combinations that are used for the balance calibration.

Load Series ≡ Group of calibration or check load points. Groups differ by the load component and/or the load combination that is applied. The calibration hardware is also often changed from group to group. Each group should have at least one data point whose outputs are exclusively caused by the weight of the calibration equipment and the **Metric Part** of the balance. Then, it is possible to perform a **Tare Load Iteration** so that the combined weight of the **Metric Part** and the calibration hardware can be included in the final regression analysis of the balance data.

Load Space ≡ Multidimensional vector space. It contains all possible load combinations that may act on a balance. **Zero Absolute Load** is the origin of the vector space.

Load State ≡ Physical state or geometric shape of an elastically deformed strain–gage balance that results from the application of forces & moments.

Math Model ≡ Mathematical description of the balance behavior. Coefficients of math model terms are obtained after applying either **Global Regression** (p. 236f., p. 244ff.) or **Sequential Analysis** (App. 28, Refs. [51], [52]) to balance calibration data.

Metric Assembly ≡ **Metric Part** of a balance plus all calibration hardware pieces that are temporarily attached to it.

Metric Flange ≡ Part of a **Single–Piece Balance** that is used to attach the balance to either the test article or the **Calibration Body**.

Metric Part ≡ Let us assume, for example, that a balance is a primary five– or six–component balance. Then, it is the part of a balance that attaches either to the **Calibration Body** during calibration, or, to the model during a wind tunnel test. Calibration or wind tunnel model loads act on it. In addition, the **Balance Axis System** is assumed to be permanently attached to the **Metric Part**. Some analysts call the **Metric Part** the **Live End** or **Live Side** of a balance. - Alternatively, let us assume that a balance is an auxiliary three–component **Moment Balance**. Then, it is the unsupported part of a balance where either the calibration loads are applied or the wind tunnel loads act.

Model Support System ≡ Hardware that supports the model, the balance, the sting, and other hardware pieces during a wind tunnel test.

Moment Balance ≡ Six–component balance whose load components are described with five moments and one force. The moments at the forward and aft moment bridges are proportional to the corresponding bridge outputs (see also **Moment Balance Format**).

Moment Balance Format ≡ This format describes the loads of a balance by using five moments and one force. They are defined as follows: forward/aft pitching moment, forward/aft yawing moment, rolling moment, and axial force.

Multi–Piece Balance ≡ Balance type that is assembled from individual parts. Parts are machined separately and joined together using screws and pins. One widely used family of this balance type has **Bi–directional** normal and side force bridge outputs. In that case, absolute value terms are needed in regression models of its calibration data. Details about the connection between **Bi–directional** outputs and the use of absolute value terms in regression models of balance calibration data can be found in Refs. [33], [34], and [35].

Natural Zero ≡ **Raw Output** of a bridge if the balance is in a weightless state. It is the electrical description of **Zero Absolute Load**. It should be chosen as the **Bridge Output Datum** if **Raw Outputs** are used for the analysis of balance calibration data.

Non–Iterative Method ≡ Load prediction method that directly fits calibration loads as a function of the measured electrical outputs of the balance bridges. A detailed description of the method is given in App. 9.

Non–Metric Flange ≡ Part of a **Single–Piece Balance** that is used to attach the balance to either the **Balance Support System** or the **Model Support System**.

Non–Metric Part ≡ Let us assume that a balance is a five– or six–component balance. Then, it is the part of a balance that attaches to the **Balance Support System** during calibration, or, to the **Model Support System** during a wind tunnel test. Reaction loads act on it. Some analysts call the **Non–Metric Part** the **Fixed End** of a balance. Alternatively, let us assume that a given balance is an auxiliary three–component **Moment Balance**. Then, it is the part of a balance that is attached to the **Balance Support System** during calibration, or, to the test article during a wind tunnel test.

Orientation ≡ Position of the **Balance Axis System** in space relative to the direction of the gravitational acceleration. It is needed during the determination of the **Natural Zeros** of the balance. The balance, for example, may be rotated while keeping its roll axis perpendicular to the gravitational acceleration. In that case, four angles, i.e., 0 *deg*, 90 *deg*, 180 *deg*, and 270 *deg*, describe the position of the **Balance Axis System** in space. The balance may also be oriented such that its roll axis is parallel to the direction of the gravitational acceleration. Then, the terms up and down are used to describe the position of the **Balance Axis System** in space.

Outer Sleeve ≡ **Metric Part** of a **Force Balance**.

Output ≡ Electrical signal of a strain gage or balance bridge (see also **Bridge Output**).

Output Space ≡ Multidimensional vector space. It contains all possible bridge output combinations that could be measured on a strain–gage balance. The output vector defined by the **Natural Zeros** of the balance bridges is the representation of **Zero Absolute Load** whenever **Raw Outputs** are used to describe the outputs. Alternatively, the origin of the vector space is the representation of **Zero Absolute Load** whenever the difference between **Raw Outputs** and **Natural Zeros** is used to describe the outputs.

Preload ≡ Load component that is kept at a constant non–zero value while other load components of the balance are applied.

Primary Bridge Load ≡ Load component that is responsible for the greatest part of the **Bridge Output**. It can be defined for each bridge if a data set is analyzed in the **Design Format** of the balance (i.e., a **Force Balance** data set is analyzed in **Force Balance Format**, or, a **Moment Balance** data set is analyzed in **Moment Balance Format**, or, a **Direct–Read Balance** data set is analyzed in **Direct–Read Format**).

Primary Bridge Output ≡ Output that responds to a **Primary Bridge Load**.

Primary Bridge Sensitivity ≡ First derivative of a fitted **Primary Bridge Output** with respect to the related **Primary Bridge Load**. It should be described in units of *microV/V* per load unit. It can be defined for all balance bridges if a balance data set is analyzed in its **Design Format** (e.g., if a force balance data set is analyzed in **Force Balance Format**, or, if a **Moment Balance** data set is analyzed in **Moment Balance** format, or, if a **Direct–Read Balance** data set is analyzed in **Direct–Read Format**).

Primary Constant ≡ **Primary Bridge Sensitivity**

Primary Load Iteration Equation ≡ One of two load iteration equations that may be used to predict loads from measured bridge outputs during a wind tunnel test. It is the load iteration equation that is described in App. 10, Eq. (10.27a).

Raw Output ≡ Absolute Voltage Measurement

Regression Model ≡ Math Model that describes the balance behavior. It is obtained after applying **Global Regression** to balance calibration data (see p. 236f., p. 244ff.).

Regression Coefficient Matrix ≡ Matrix that describes the regression coefficients. The coefficients are the result of applying **Global Regression** to balance calibration data. The matrix has the coefficients of the regression model of a load component if the **Non–Iterative Method** is used to predict balance loads. Alternatively, it has the coefficients of the regression models of the bridge outputs if the **Iterative Method** is used to predict balance loads. Users of the **Iterative Method** also use the terms **Calibration Matrix** or **Curve–Fit Matrix** to describe the matrix.

Regular Data Points ≡ Loads and bridge outputs of these data points are recorded during the calibration of the balance. Information contained in these points is used to determine regression models that help predict the loads of the balance.

Resolved Balance Loads ≡ Loads of a **Force Balance** or **Moment Balance** that were transformed to **Direct–Read Format**.

Response ≡ Dependent variable of a balance calibration data set. It is a load if the **Non–Iterative Method** is used to predict balance loads. Alternatively, it is the electrical output of a balance bridge if the **Iterative Method** is used to predict balance loads.

Sensitivity ≡ Primary Bridge Sensitivity

Sequential Analysis ≡ Coefficients of the terms of a multivariate **Math Model** are obtained after superimposing analysis results of subsets of the balance calibration data.

Shell ≡ Metric Part of a **Force Balance**.

Shunt Resistor ≡ Resistor that simulates a load–induced **Bridge Output**.

Single Bridge Load ≡ Single–Component Load

Single–Component Load ≡ Non–zero load that is applied to a balance while keeping all other load components close to **Zero Absolute Load**.

Single–Component Load Series ≡ Group of calibration or check load data points that are obtained after applying a series of **Single–Component Loads** to a balance.

Single–Piece Balance ≡ Balance that is machined out of a single piece of metal. Loads are given in **Direct–Read Format**. Outputs are highly repeatable and may not have **Bi–directional** characteristics. Some outputs, however, may have large **Interactions**.

Six–Wire Balance ≡ Each bridge of this balance type is connected with two excitation wires, two signal wires, and two sense wires to the signal conditioner (voltage source).

Symmetric Load Schedule ≡ Type of **Load Schedule** that has both positive and negative loads or load combinations of similar magnitude.

Tare Corrected Load ≡ It is the sum of the **Applied Load** and the **Tare Load** of a **Regular Data Point**. It should be used as input for the final regression analysis of balance calibration data as it uses **Zero Absolute Load** as its load datum.

Tare Load ≡ Balance load that is caused by the combined weight of the **Metric Part**, the **Calibration Body**, **Calibration Fixtures**, and **Weight Pans**. It is added as a correction to the **Applied Load** so that all balance loads can be expressed relative to the universal load datum of **Zero Absolute Load**.

Tare Load Iteration Algorithm ≡ Numerical process that is used to determine the **Tare Loads**. It uses intermediate solutions of the regression models of the balance calibration data in order to obtain estimates of the **Tare Loads**.

Tare Output ≡ **Zero Load Output of Load Series**

Temperature Sensitivity ≡ Partial derivative of the electrical output of a bridge with respect to the temperature at the bridge location.

Weight Pan ≡ Hardware that supports gravity weights during the calibration of a balance. It is attached to the **Calibration Body**.

Wheatstone Bridge ≡ Electrical circuit that is the typical method of wiring four or more strain gages together in a measurement system (see also Ref. [81], pp. 131–151).

Wind–Off Load ≡ Force or moment that is caused by the combined weight of the wind tunnel model and the **Metric Part** of the balance. It is a function of the orientation of the model relative to the gravitational acceleration if a six–component balance is used with a full–span model. It is independent of the pitch angle of the model whenever a semi–span model is installed on either the floor or ceiling of a test section.

Wind–On Load ≡ Force or moment that is caused by (i) aerodynamic effects and (ii) the combined weight of the wind tunnel model and the **Metric Part** of the balance. It is a function of (i) the tunnel conditions, (ii) the orientation of the model relative to the free–stream direction of the flow in the test section, and (iii) the orientation of the model relative to the gravitational acceleration.

Zero Absolute Load ≡ Force or moment with zero magnitude that acts when the balance is in a weightless state. It is the origin of the **Load Space**. It should be used as the universal load datum for the description of all loads that a balance experiences during its calibration. The **Natural Zero** is its electrical representation in the **Output Space** whenever the outputs of the balance are described as **Raw Outputs**.

Zero Load Output ≡ **Natural Zero**.

Zero Load Output of Load Series ≡ Electrical output of a balance bridge at the beginning of a **Load Series**. It is caused by the combined weight of the (i) **Metric Part**, (ii) **Calibration Body**, (iii) **Calibration Fixtures**, and (iv) **Weight Pans**. A signal caused by a **Preload** may also be a part of the output if it is treated as a **Tare Load**.

Zero Load Point ≡ **Regular Data Point** of a **Load Series** that has the **Tare Outputs**.

Appendix 2

Statistical Terminology

Adjusted R–Square ≡ This statistic is related to the **R–Square** statistic that is also discussed in this appendix. Some analysts prefer to use it as it does not always increase as terms are added to the regression model. A description of the metric can be found in Ref. [68], p. 83, Eq. (3.27).

Degrees of Freedom (regression) ≡ Equals the number of regression coefficients not counting the intercept term. A description of the metric can be found in Ref. [68], p. 26/27, Table 2.4.

Degrees of Freedom (residual) ≡ Equals the number of observations minus the total number of regression coefficients. A description of the metric can be found in Ref. [68], p. 26/27, Table 2.4.

Degrees of Freedom (total) ≡ Equals the sum of the degrees of freedom of the regression and the degrees of freedom of the residual. A description of the metric can be found in Ref. [68], p. 26/27, Table 2.4.

F–Value of Regression ≡ Equals the ratio between the **Mean Square** of the regression and the **Mean Square** of the residual. It may be used to compare the predictive capability of different regression models. A description of the metric can be found in Ref. [69], p. 28, Eq. (2.21), pp. 649–651.

Mean Square (regression) ≡ Equals the **Sum of Squares** of the regression divided by the **Degrees of Freedom** of the regression. A description of the metric can be found in Ref. [69], p. 28, Eq. (2.21).

Mean Square (residual) ≡ Equals the **Sum of Squares** of the residual divided by the **Degrees of Freedom** of the residual. A description of the metric can be found in Ref. [69], p. 28, Eq. (2.21).

p–**Value of Coefficient** ≡ This metric is determined from a comparison of the *t*–Statistic with values in a Students T–Distribution. With a *p*–Value of, e.g., 10 % (or 0.1), an analyst can say with a 90 % probability of being correct that the coefficient is having some effect. More details on the *p*–Value can be found in Ref. [70], pp. 273–275.

p–**Value of Regression** ≡ This metric tells an analyst how confident he or she can be that the selected regression model has some correlation with the dependent variable. More details on the *p*–Value can be found in Ref. [70], pp. 273–275.

PRESS Statistic ≡ This statistic is computed by omitting one observation and fitting the regression model to the remaining observations. The fit is used (i) to predict the withheld observation and (ii) to compute the square of the difference between the observed and

fitted value. The process is repeated for all observations. Finally, the statistic is defined as the sum of all squared differences or residuals. – A large difference between the response residual and the PRESS residual indicates a point where the regression model fits the data well, but a regression model, built without that point, predicts poorly. A description of the metric can be found in Ref. [68], pp. 141–142.

PRESS R–Square ≡ This metric is an indicator of the predictive capability of the model. A description of the metric can be found in Ref. [69], p. 46–47.

R–Square ≡ This statistic of the regression is the fraction of the variation in the dependent variable that is accounted for by the independent variables. The statistic is a value between 0 and 1. However, a large value of the statistic does not necessarily indicate a good regression model. Adding a variable to the regression model will always increase the statistic, regardless of whether the additional variable is significant or not. Thus, it is possible for regression models that have large values of the statistic to yield poor predictions of new observations. A description of the metric can be found in Ref. [69], p. 30.

Standard Error ≡ This metric is an estimate of the standard deviation of the coefficient. It is a measure of the precision with which the coefficient is measured. A coefficient is probably different from zero if its magnitude is large compared to the value of the metric. A description of the metric can be found in Ref. [68], p. 23.

Sum of Squares (regression) ≡ This metric equals the difference between the sum of the product of the observed and fitted responses and the square of the sum of the observed responses divided by the number of observations. A description of the metric can be found in Ref. [69], p. 29, Eq. (2.22).

Sum Of Squares (residual) ≡ This metric equals the sum of the squared difference between the observed and fitted responses. A description of the metric can be found in Ref. [69], p. 26, Eq. (2.17).

Sum of Squares (total) ≡ This metric equals the difference between the sum of the squared observed responses and the square of the sum of the observed responses divided by the number of observations. It is also the sum of the regression sum of squares and the residual sum of squares. A description of the metric can be found in Ref. [69], p. 28/29, Eqs. (2.20), (2.24).

***t*–Statistic of Coefficient** ≡ This statistic equals the ratio between the coefficient value and its standard error. A coefficient is probably significant if the statistic is greater than the critical value of a Students T–Distribution. A description of the metric can be found in Ref. [69], p. 32, Eq. (2.29).

Variance Inflation Factor ≡ This metric is used to detect unwanted near–linear dependencies (also called collinearity or multicollinearity) that may exist between regression model terms. Near–linear dependencies are non–existent or weak if the metric is less than the literature recommended threshold of 10 (see, for example, the discussion in Ref. [68],

pp. 323–341; threshold of 10 is listed in Ref. [68], p. 334). – Different definitions of the metric exist in the literature. The author recommends to use the SAS compatible definition of the metric for strain–gage balance data applications. This definition can correctly handle balance data with bi–directional bridge output characteristics (see Method 2 in Ref. [20], p. 5, Table 1). – It is the author's experience that the threshold for the metric should be increased from 10 to 20 for the assessment of balance data with bi–directional bridge output characteristics (see also discussions in Ref. [34], p. 17).

Appendix 3

Balance Axis System and Load Sign Conventions

3.1 General Remarks

Forces and moments act on a strain–gage balance. They are described in a Cartesian coordinate system, i.e., the balance axis system, such that the predicted balance loads can easily be quantified in the body axis system of the wind tunnel model (see, e.g., the discussions of coordinate systems in Ref. [1], pp. 12–14, and Ref. [7], p. 3). In theory, the load transformation from the balance axis system to the body axis system of the wind tunnel model should be independent of the elastic deformation of the balance under load. Consequently, the balance axis system should be attached to the part of the balance that is rigidly connected to the wind tunnel model. This requirement means, for example, that the balance axis system should be attached to the metric part of a primary six–component balance as this part of the balance is rigidly connected to either the model or the calibration body. Similarly, the balance axis system should be attached to the non–metric part of a three–component moment balance as, in this case, the non–metric part of the balance is rigidly connected to the model (see also the discussions in App. 15).

3.2 Balance Axis System Conventions

It is best to express coordinates and load vectors of the balance in a right–handed coordinate system. This choice has the advantage that the rules of vector algebra and vector calculus can rigorously be used when mathematical operations are applied to the balance loads. The aircraft–fixed system described in Ref. [1], for example, is a right–handed coordinate system that is frequently used at wind tunnel facilities in Europe. Figure 3–1 below summarizes characteristics of this coordinate system and the resulting balance load sign definitions. Vectors with single arrows mark the positive direction of the

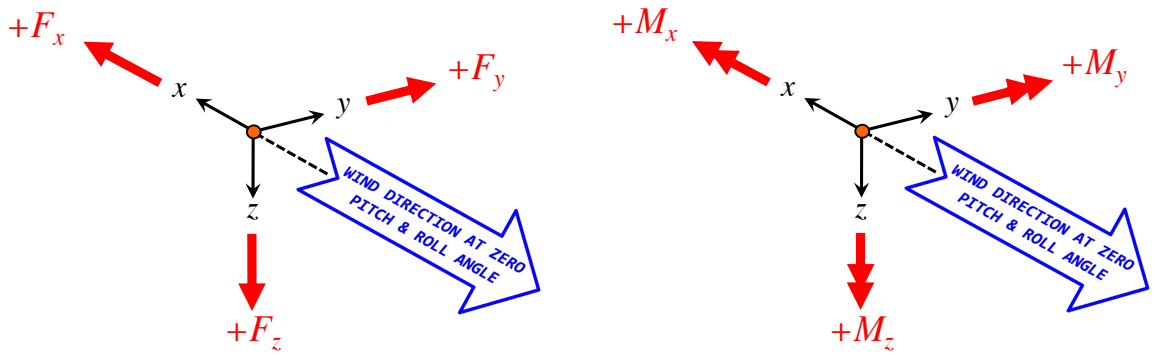

Fig. 3-1 Definition of the balance forces and moments in a right–handed balance axis system (taken from Ref. [1], p. 14, Figure 1–6).

three balance forces. Vectors with double arrows, on the other hand, are used to identify the positive direction of the three moments. It is also assumed that moment vectors are interpreted using the right–hand rule from classical mechanics.

Balance axis system and load sign conventions are also used in the aerospace testing community that are not right–handed. The North American balance axis system is one

such example. It is described in great detail in Ref. [7]. Axes and load sign definitions of the North American system are summarized in Fig. 3–2 below. Again, vectors with single and double arrows mark the positive direction of the forces and moments. It is observed

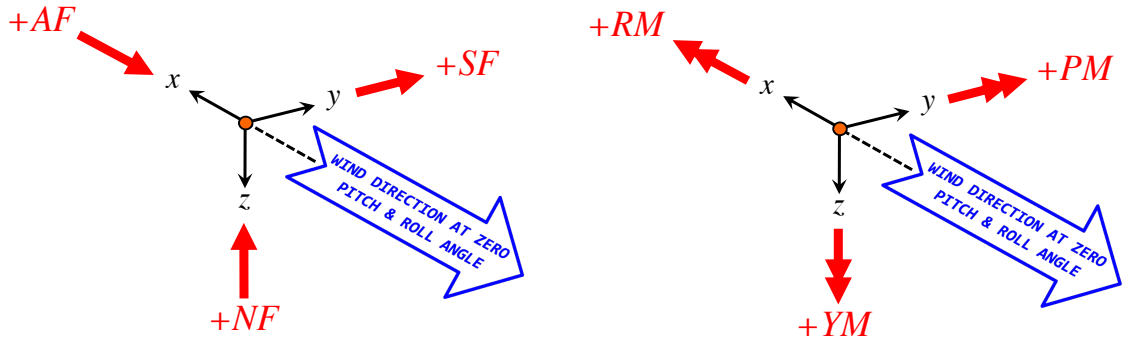

Fig. 3-2 Definition of the balance forces and moments in the North American balance axis system (taken from Ref. [7], p. 3, Fig. 1).

that the positive directions of the axial & normal force vectors are opposite to the positive directions of the related axes. Therefore, both vectors violate the requirement for a right–handed coordinate system. Consequently, the cross–product operator cannot be used with (i) the position vector and (ii) the resultant force vector for the calculation of the resultant moment vector in the North American balance axis system (see also Ref. [55], p. 14).

Load signs are critical pieces of information that describe the loads of a strain–gage balance. Therefore, *Tom Hegland* of the Wind Tunnel Division at NASA Ames Research Center came up with the following mnemonic to memorize the signs of balance loads that are described in the North American balance axis system:

Hegland's Mnemonic

The three forces and three moments of a six–component strain–gage balance are all positive in the North American balance axis system if an unpowered wind tunnel model of an airplane is envisioned to be in a climbing right turn.

By default, the North American balance axis system is used during tests at the NASA Ames Unitary Plan Wind Tunnel. Therefore, all forces and moments in the current document are described by using this balance axis system convention.

Appendix 4

Load Transformations

4.1 General Remarks

Force and moment balances are specifically designed such that the description of the balance loads can directly be linked to the physical location of the flexures and bridges on the balance. These two balance types have the built–in characteristic that only a single bridge shows a significant change of its electrical output if the related load component is applied at the bridge location. This design feature makes the connection between loads and outputs more transparent and easier to troubleshoot.

A force balance, for example, is designed such that five of its six bridges primarily respond to a single force that acts at a related bridge location. The load state of this balance type can be described in force balance format by using the forward & aft normal forces, the forward & aft side forces, the axial force, and the rolling moment. Then, the design format of a force balance can be summarized as follows:

$$force\ balance\ format \quad \Longrightarrow \quad \underbrace{N1,\ N2,\ S1,\ S2,\ AF}_{5\ forces} \quad and \quad \underbrace{RM}_{1\ moment}$$

Similarly, a moment balance is designed such that five of its six bridges primarily respond to a single moment that acts at a bridge location. In this case, the load state of the balance can be described in moment balance format by using the forward & aft pitching moments, the forward & aft yawing moments, the rolling moment, and the axial force. Then, the design format of a moment balance can be summarized as follows:

$$moment\ balance\ format \quad \Longrightarrow \quad \underbrace{PM1,\ PM2,\ YM1,\ YM2,\ RM}_{5\ moments} \quad and \quad \underbrace{AF}_{1\ force}$$

Many analysts recommend to predict loads of a force or moment balance in design format. Then, balance data can more easily be examined. However, it is required during a wind tunnel test to transform balance loads from design format to direct–read format so that aerodynamic loads in the body axis system of the test article can be computed from the predicted balance loads. Direct–read format uses three forces and three moments at the balance moment center (BMC) for the description of the load state of a balance. The forces are normal force, side force, and axial force. The moments are pitching moment, yawing moment, and rolling moment. Then, direct–read format can be defined as follows:

$$direct{-}read\ format \quad \Longrightarrow \quad \underbrace{NF,\ SF,\ AF}_{3\ forces} \quad and \quad \underbrace{PM,\ YM,\ RM}_{3\ moments}$$

No transformations are required for the axial force and the rolling moment. These two load components are common to all three load formats. However, transformations are needed from the normal and side force pairs to normal force, side force, pitching moment, and yawing moment if loads are predicted in force balance format. This first conclusion is summarized below.

$$\underbrace{N1,\ N2,\ S1,\ S2}_{force\ balance\ format} \quad \Longleftarrow transformations \Longrightarrow \quad \underbrace{NF,\ SF,\ PM,\ YM}_{direct{-}read\ format}$$

Similarly, transformations are needed from the pitching and yawing moment pairs to normal force, side force, pitching moment, and yawing moment if loads are predicted in moment balance format. This second conclusion is summarized below.

$$\underbrace{PM1,\ PM2,\ YM1,\ YM2}_{moment\ balance\ format} \quad \Longleftarrow \ transformations \ \Longrightarrow \quad \underbrace{NF,\ SF,\ PM,\ YM}_{direct-read\ format}$$

The description of the load state of a balance in force or moment balance format is equivalent to the description of the same load state in direct–read format. No information is lost. It is like describing something in two different languages.

4.2 Transformations for a Force Balance

The load transformations for a force balance can be defined if forces are introduced at the forward & aft bridge locations of the balance. They replace the force & moment that act at the BMC of the balance. Figure 4–1 below shows the relationship between the

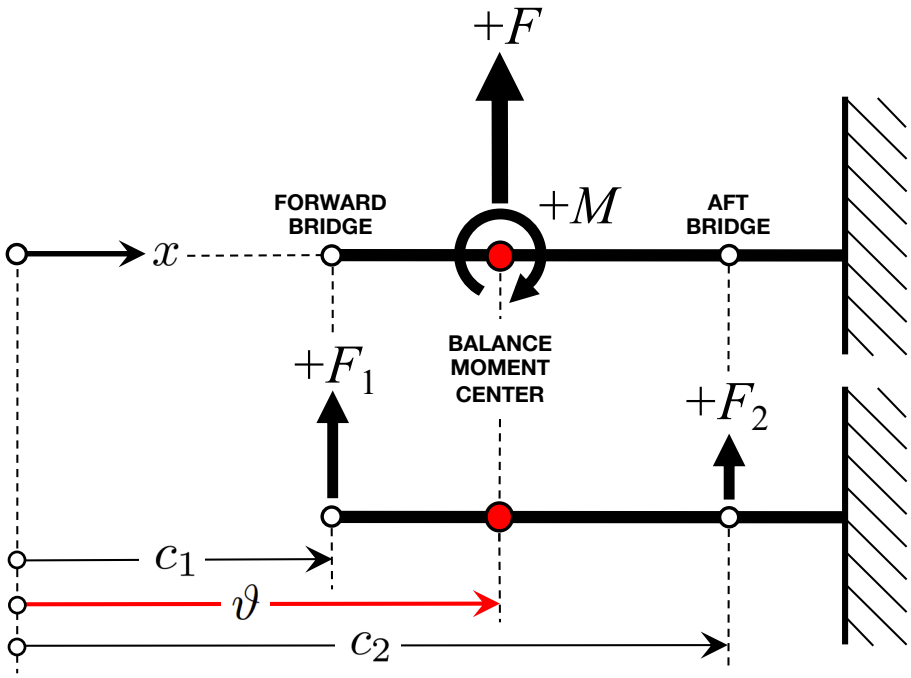

Fig. 4–1 Forces acting at the forward & aft bridges of a force balance.

force & moment at the BMC and the forces at the forward & aft bridge locations. The sum of the forces at the bridges must equal the total force at the BMC. Then, we get:

$$F \quad = \quad F_1 \ + \ F_2 \tag{4.1}$$

Similarly, it is known that the moment at the BMC equals the sum of the moment contributions from the two forces at the bridges. It is assumed that the location of the BMC and the bridge locations are described in a coordinate system that uses the balance centerline as the coordinate system axis (see Fig. 4–1). Then, the BMC has the coordinate ϑ, the forward bridge the coordinate c_1, and the aft bridge the coordinate c_2. Now, two auxiliary coordinate differences d_1 and d_2 may be introduced that describe the distance between the BMC and the forces F_1 and F_2 at the bridge locations. We get:

$$d_1 \quad = \quad \vartheta \; - \; c_1 \tag{4.2a}$$

$$d_2 \quad = \quad \vartheta \; - \; c_2 \tag{4.2b}$$

Then, using the sign definitions of (i) the balance loads and of (ii) the coordinates that are depicted in Fig. 4–1, the moment at the BMC can be expressed as follows:

$$M \quad = \quad F_1 \cdot d_1 \; - \; F_2 \cdot (-d_2) \tag{4.3}$$

Equations (4.1) and (4.3) are a linear system of equations that describes the relationship between the forces at the forward & aft bridge locations and the force & moment at the BMC. The linear system can be used to compute the forces F_1 and F_2 so that both forces are expressed as a function of the force and moment at the BMC. First, it is concluded from Eq. (4.1) that the following relationship is valid:

$$F_2 \quad = \quad F \; - \; F_1 \tag{4.4}$$

The right hand side of Eq. (4.4) may be used to replace the force F_2 in Eq. (4.3). We get:

$$M \quad = \quad F_1 \cdot d_1 \; - \; (F \; - \; F_1) \cdot (-d_2) \tag{4.5}$$

Then, after solving Eq. (4.5) for the force F_1 at the forward bridge location, we get:

$$F_1 \quad = \quad F \cdot \frac{-d_2}{d_1 \; - \; d_2} \quad + \quad M \cdot \frac{1}{d_1 \; - \; d_2} \tag{4.6}$$

Similarly, after using Eq. (4.6) to replace F_1 in Eq. (4.4) and simplifying the result, we get the corresponding relationship for the force F_2 at the aft bridge location:

$$F_2 \quad = \quad F \cdot \frac{d_1}{d_1 \; - \; d_2} \quad - \quad M \cdot \frac{1}{d_1 \; - \; d_2} \tag{4.7}$$

Finally, the set of universal load transformation equations for a force balance is obtained after using Eqs. (4.2a) and (4.2b) to replace the moment arms in Eqs. (4.3), (4.6), and (4.7), and summarizing the four transformations that were derived above:

Force Balance – Universal Load Transformations

$$F \quad = \quad F_1 \; + \; F_2 \tag{4.8a}$$

$$M \quad = \quad F_1 \cdot (\vartheta \; - \; c_1) \; - \; F_2 \cdot (c_2 \; - \; \vartheta) \tag{4.8b}$$

$$F_1 \quad = \quad F \cdot \frac{c_2 \; - \; \vartheta}{c_2 \; - \; c_1} \quad + \quad M \cdot \frac{1}{c_2 \; - \; c_1} \tag{4.8c}$$

$$F_2 \quad = \quad F \cdot \frac{\vartheta \; - \; c_1}{c_2 \; - \; c_1} \quad - \quad M \cdot \frac{1}{c_2 \; - \; c_1} \tag{4.8d}$$

Universal load transformations for the loads of a moment balance are derived in the next section of the appendix.

4.3 Transformations for a Moment Balance

The load transformations for a moment balance can be derived if moments are introduced at the forward & aft bridges of the balance. These moments replace the force & moment at the BMC of the balance. Figure 4–2 below shows the relationship between the force & moment at the BMC and the moments at the forward & aft bridges. It is known

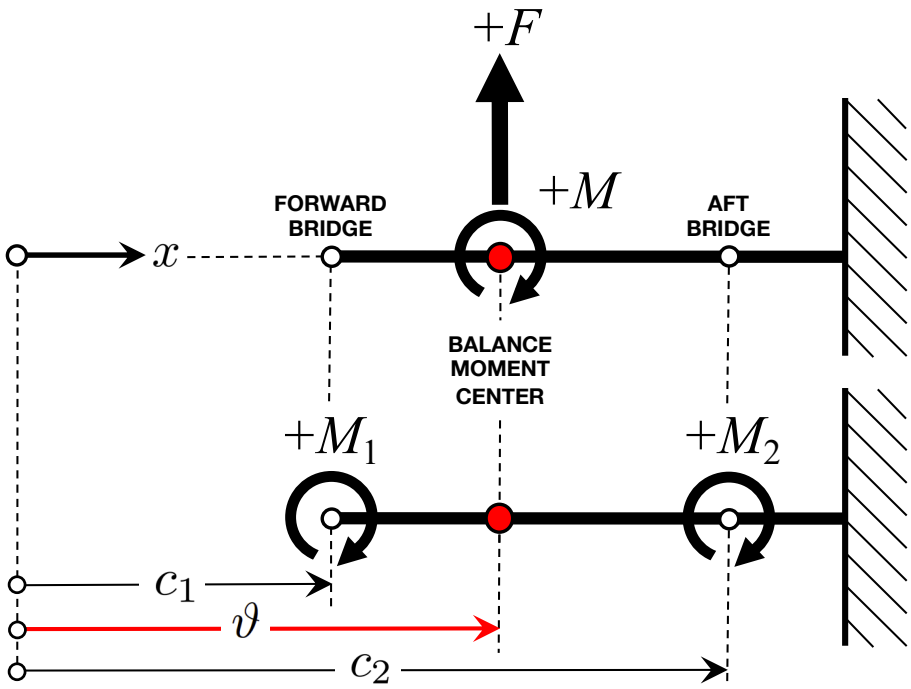

Fig. 4–2 Moments acting at the forward & aft bridges of a moment balance.

that the moment at the BMC of a strain–gage balance is a pure moment (force couple). In addition, basic principles of statics say that a pure moment can be moved to different locations on an object without changing anything. Therefore, after moving the pure moment from the BMC to the forward bridge location, the following relationship for the total moment at the forward bridge location is obtained:

$$M_1 \quad = \quad M \; - \; F \; \cdot \; (\vartheta \; - \; c_1) \tag{4.9}$$

Similarly, the moment at the BMC may be moved to the aft bridge location. Then, the corresponding relationship for the moment at the aft bridge location is obtained:

$$M_2 \quad = \quad M \; + \; F \; \cdot \; (c_2 \; - \; \vartheta) \tag{4.10}$$

Equations (4.9) and (4.10) are a linear system of equations that describes the relationship between the moments at the forward & aft bridge locations and the force & moment at the BMC. The linear system can used to compute the force & moment at the BMC so that both loads are expressed as functions of the moments at the forward & aft bridge locations. First, the left– and right–hand sides of Eq. (4.9) are subtracted from the left– and right–hand sides of Eq. (4.10). Then, after simplifying the result, we get:

$$M_2 \; - \; M_1 \quad = \quad F \; \cdot \; (c_2 \; - \; c_1) \tag{4.11}$$

Finally, after solving Eq. (4.11) above for the force at the BMC, we get:

$$F \quad = \quad \frac{M_2 \; - \; M_1}{c_2 \; - \; c_1} \tag{4.12}$$

In the next step, the left– and right–hand sides of Eq. (4.9) are added to the left– and right–hand sides of Eq. (4.10). Then, after simplifying the result, we get:

$$M_1 \; + \; M_2 \quad = \quad 2 \, M \; + \; F \; \cdot \; \left\{ \; c_1 \; + \; c_2 \; - \; 2 \, \vartheta \; \right\} \tag{4.13}$$

Now, after using the right–hand side of Eq. (4.12) to replace the force F on the right–hand side of Eq. (4.13), we get:

$$M_1 \; + \; M_2 \quad = \quad 2 \, M \; + \; \frac{M_2 \; - \; M_1}{c_2 \; - \; c_1} \; \cdot \; \left\{ \; c_1 \; + \; c_2 \; - \; 2 \, \vartheta \; \right\} \tag{4.14}$$

It is possible to solve Eq. (4.14) for the pure moment at the BMC. Then, the following relationship is obtained:

$$M \quad = \quad \frac{M_1 \; + \; M_2}{2} \quad - \quad \frac{M_2 \; - \; M_1}{2 \; (\; c_2 \; - \; c_1 \;)} \; \cdot \; \left\{ \; c_1 \; + \; c_2 \; - \; 2 \, \vartheta \; \right\} \tag{4.15}$$

It is an advantage to simplify the right–hand side of Eq. (4.15). Therefore, the multipliers of the moments at the bridge locations are assembled. Then, we get:

$$M \; = \; M_1 \cdot \left\{ \frac{1}{2} \; + \; \frac{c_1 \; + \; c_2 \; - \; 2 \, \vartheta}{2 \; (c_2 \; - \; c_1 \;)} \right\} \; + \; M_2 \cdot \left\{ \frac{1}{2} \; - \; \frac{c_1 \; + \; c_2 \; - \; 2 \, \vartheta}{2 \; (c_2 \; - \; c_1 \;)} \right\} \tag{4.16}$$

The multipliers of the moments at the forward and aft bridge locations can be simplified further because the following two relationships are valid:

$$\left\{ \frac{1}{2} \; + \; \frac{c_1 + c_2 - 2 \, \vartheta}{2 \; (c_2 \; - \; c_1 \;)} \right\} \quad = \quad \frac{(c_2 - c_1) + c_1 + c_2 - 2 \, \vartheta}{2 \; (c_2 \; - \; c_1 \;)} \quad = \quad \left\{ \frac{c_2 \; - \; \vartheta}{c_2 \; - \; c_1} \right\} \tag{4.17}$$

$$\left\{ \frac{1}{2} \; - \; \frac{c_1 + c_2 - 2 \, \vartheta}{2 \; (c_2 \; - \; c_1 \;)} \right\} \quad = \quad \frac{(c_2 - c_1) - c_1 - c_2 + 2 \, \vartheta}{2 \; (c_2 \; - \; c_1 \;)} \quad = \quad \left\{ \frac{\vartheta \; - \; c_1}{c_2 \; - \; c_1} \right\} \tag{4.18}$$

Now, after replacing the multipliers in Eq. (4.16) above with the right–hand sides of Eqs. (4.17) and (4.18), the following equation for the moment M at the BMC is obtained:

$$M \quad = \quad M_1 \; \cdot \; \left\{ \frac{c_2 \; - \; \vartheta}{c_2 \; - \; c_1} \right\} \; + \; M_2 \; \cdot \; \left\{ \frac{\vartheta \; - \; c_1}{c_2 \; - \; c_1} \right\} \tag{4.19}$$

Finally, the set of universal load transformation equations for a moment balance is obtained after assembling the four transformations that were derived above, i.e., Eqs. (4.9), (4.10), (4.12) and (4.19):

Moment Balance – Universal Load Transformations

$$F = \frac{M_2 - M_1}{c_2 - c_1} \tag{4.20a}$$

$$M = M_1 \cdot \left\{ \frac{c_2 - \vartheta}{c_2 - c_1} \right\} + M_2 \cdot \left\{ \frac{\vartheta - c_1}{c_2 - c_1} \right\} \tag{4.20b}$$

$$M_1 = M - F \cdot (\vartheta - c_1) \tag{4.20c}$$

$$M_2 = M + F \cdot (c_2 - \vartheta) \tag{4.20d}$$

Simplified versions of the universal load transformations for a force balance and a moment balance can be derived if the BMC is located halfway between the forward and aft bridges. These simplifications are discussed in the next section.

4.4 Simplified Transformations

The BMC of a balance is often located halfway between the forward and aft bridges. In that case, the universal load transformations can be simplified if the bridge distance d is introduced as a parameter. Consequently, after moving the coordinate system origin to the location of the forward bridge, we get:

$$c_1 = 0 \tag{4.21a}$$

$$c_2 = d \tag{4.21b}$$

$$\vartheta = d/2 \tag{4.21c}$$

Then, the following simplified transformations for a force balance are obtained after using Eqs. (4.21a) to (4.21c) in Eqs. (4.8a) to (4.8d):

Simplified Load Transformations – Force Balance

(only valid if the BMC is located halfway between the forward & aft force bridges)

$$F = F_1 + F_2 \tag{4.22a}$$

$$M = \left\{ F_1 - F_2 \right\} \cdot \frac{d}{2} \tag{4.22b}$$

$$F_1 = \frac{F}{2} + \frac{M}{d} \tag{4.22c}$$

$$F_2 = \frac{F}{2} - \frac{M}{d} \tag{4.22d}$$

The general relationships above can also be expressed by using the traditional nomenclature of the loads of a force balance. Then, the following simplified relationships between the normal forces and the pitching moment are obtained:

Transformations – Normal Forces & Pitching Moment

(only valid if the BMC is located halfway between the forward & aft normal force bridges)

$$NF = N1 + N2 \qquad (4.23a)$$

$$PM = \left\{ N1 - N2 \right\} \cdot \frac{a}{2} \qquad (4.23b)$$

$$N1 = \frac{NF}{2} + \frac{PM}{a} \qquad (4.23c)$$

$$N2 = \frac{NF}{2} - \frac{PM}{a} \qquad (4.23d)$$

where

$a \equiv$ *distance between normal force bridges*

Similarly, the following simplified relationships between the side forces and the yawing moment of a force balance are obtained:

Transformations – Side Forces & Yawing Moment

(only valid if the BMC is located halfway between the forward & aft side force bridges)

$$SF = S1 + S2 \qquad (4.24a)$$

$$YM = \left\{ S1 - S2 \right\} \cdot \frac{b}{2} \qquad (4.24b)$$

$$S1 = \frac{SF}{2} + \frac{YM}{b} \qquad (4.24c)$$

$$S2 = \frac{SF}{2} - \frac{YM}{b} \qquad (4.24d)$$

where

$b \equiv$ *distance between side force bridges*

In the next step, the following simplified transformations for a moment balance are obtained after using Eqs. (4.21a) to (4.21c) in Eqs. (4.20a) to (4.20d):

Simplified Load Transformations – Moment Balance

(only valid if the BMC is located halfway between the forward & aft moment bridges)

$$F = \frac{M_2 - M_1}{d} \qquad (4.25a)$$

$$M = \frac{M_1 + M_2}{2} \qquad (4.25b)$$

$$M_1 = M - F \cdot \frac{d}{2} \qquad (4.25c)$$

$$M_2 = M + F \cdot \frac{d}{2} \qquad (4.25d)$$

Again, the relationships above can be expressed by using the traditional nomenclature of the loads of a moment balance. Then, the following simplified relationships between the normal force and the pitching moments are obtained:

Transformations – Normal Force & Pitching Moments

(only valid if the BMC is located halfway between the forward & aft pitching moment bridges)

$$NF = \frac{PM2 - PM1}{g} \qquad (4.26a)$$

$$PM = \frac{PM1 + PM2}{2} \qquad (4.26b)$$

$$PM1 = PM - NF \cdot \frac{g}{2} \qquad (4.26c)$$

$$PM2 = PM + NF \cdot \frac{g}{2} \qquad (4.26d)$$

where

$g \equiv$ *distance between pitching moment bridges*

Finally, the following transformation equations are obtained after applying the simplified relationships given in Eqs. (4.25a) to (4.25d) to the side force and the yawing moments of a moment balance:

Transformations – Side Force & Yawing Moments

(only valid if the BMC is located halfway between the forward & aft yawing moment bridges)

$$SF = \frac{YM2 - YM1}{h} \qquad (4.27a)$$

$$YM = \frac{YM1 + YM2}{2} \qquad (4.27b)$$

$$YM1 = YM - SF \cdot \frac{h}{2} \qquad (4.27c)$$

$$YM2 = YM + SF \cdot \frac{h}{2} \qquad (4.27d)$$

where

$h \equiv$ *distance between yawing moment bridges*

Again, it must be emphasized that the simplified load transformations defined in Eqs. (4.22a) to (4.27d) are only valid if the BMC is located halfway between the forward and aft bridges of the balance. In all other cases, the universal load transformations defined in Eqs. (4.8a) to (4.8d) for a force balance and in Eqs. (4.20a) to (4.20d) for a moment balance must be applied.

Appendix 5
Combined Load Diagram

5.1 Introduction

Generic two–dimensional plots were developed at the NASA Ames Balance Calibration Laboratory for both visualization and interpretation of the relationship between magnitude & location of a calibration load in a combined load plot (see Ref. [50] for more details). These generic plots are called combined load diagrams. They were constructed by assuming that a calibration force is applied at a certain distance from the balance moment center. This calibration force is generated by using either gravity weights or a hydraulic actuator. It results in a force and moment pair at the balance moment center.

The interpretation of each combined load diagram depends on the format that is chosen to describe the loads (see also App. 4). Important lines and regions are highlighted in the diagram that help interpret calibration data. For example, lines of constant force and moment are marked. In addition, lines of pure force and pure moment may be highlighted. Lines for a fixed location of the applied calibration force may also be displayed. Finally, regions are marked in the diagram that help identify (i) the sign of a force or moment and (ii) the location of each load relative to the bridges and the balance moment center.

Combined load diagrams for typical balance load formats are discussed in the next three sections. Afterwards, a data set from the calibration of a force balance is used to illustrate the application of a combined load diagram to real–world data.

5.2 Direct–Read Format

It is assumed that balance loads are given in direct–read format at the balance moment center. Then, interpretation and use of the combined load diagram needs information describing the lines of (i) constant force, (ii) constant moment, and (iii) constant location of the force. The location of these lines is obtained after analyzing the basic relationship between the applied calibration force and the resulting load pair at the balance moment center in more detail.

Fundamental connections between (i) the applied calibration force and (ii) the resulting force & moment at the balance moment center are described in Fig. 5–1a below. Position 1 marks the location of the aft bridge, position 2 marks the location of the balance moment center, position 3 marks the location of the forward bridge, and position 4 is the location of the applied calibration force. The applied calibration force at position 4 can be moved to the balance moment center without changing the load state of the balance if a force couple is introduced. The force couple is defined by force $+F$ at position 4 and force $-F$ at position 2. The force couple can be substituted by a pure moment M at the balance moment center that is given in Eq. (5.1) below. Coordinate x describes the

$$M \;=\; F \cdot x \qquad \textit{where} \qquad |x| \;\equiv\; \textit{moment arm} \tag{5.1}$$

location of the applied calibration force relative to the balance moment center. The absolute value of the coordinate, i.e., $|x|$, is the moment arm. Coordinate values $x = \pm d/2$ identify the location of the forward & aft bridges of the balance if loads of either a force or a moment balance are given in direct–read format. The combined load diagram of the

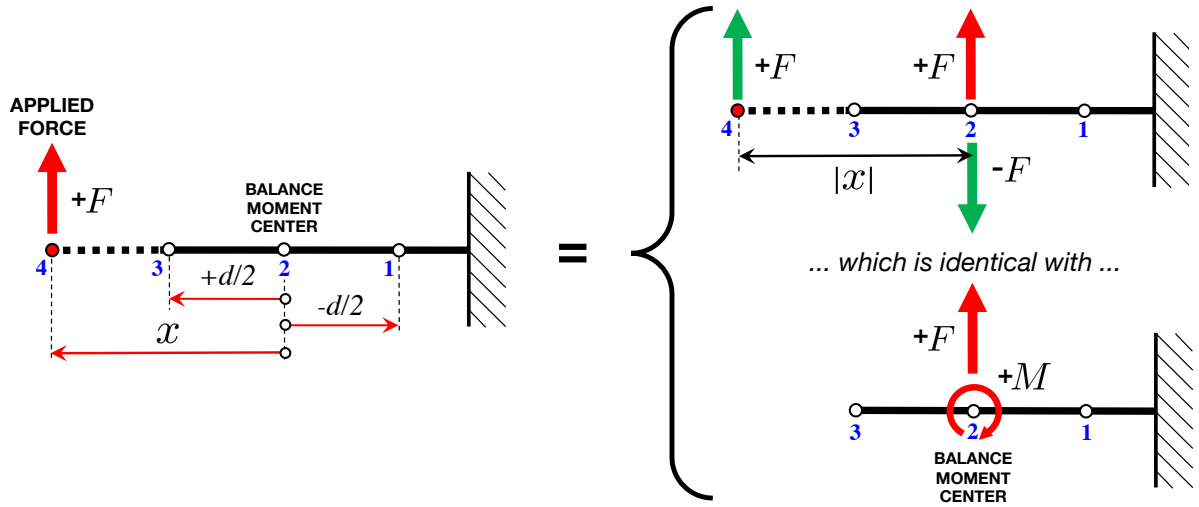

Fig. 5–1a Connection between applied force and load pair at balance moment center.

load pair at the balance moment center is simply defined as the generic plot of the moment M versus the applied force F. Figure 5–1b below shows the general layout of the diagram in this case. Lines of constant force are depicted as vertical lines in the diagram. They

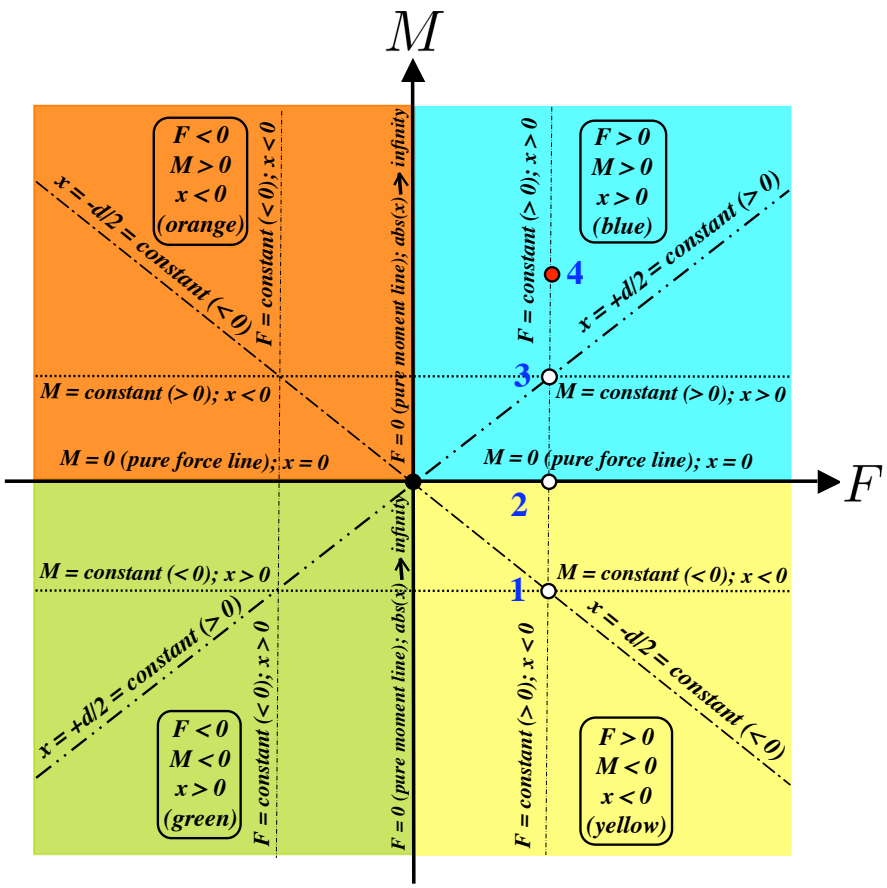

Fig. 5–1b Combined load diagram for load pair given in direct–read format.

can be described by using the relationship that is given in Eq. (5.2a) below.

$$line\ of\ constant\ force \implies F = const. \tag{5.2a}$$

The pure moment line, i.e., the line where the force is zero, is the vertical line that goes through the origin of the combined load diagram. It coincides with the ordinate of the coordinate system. Therefore, it can be described as follows:

$$line\ of\ pure\ moment \implies F = 0 \tag{5.2b}$$

The lines of constant moment are horizontal lines in the combined load diagram. They can be described by using the following equation:

$$line\ of\ constant\ moment \implies M = const. \tag{5.3a}$$

The pure force line, i.e., the line where the moment is zero, is the horizontal line that goes through the origin of the coordinate system. It coincides with the abscissa of the coordinate system. Therefore, it can be described by the following equation:

$$line\ of\ pure\ force \implies M = 0 \tag{5.3b}$$

It is also of interest to identify data points that are obtained by varying the magnitude of a force at a constant coordinate x relative to the balance moment center. These lines may be described by using the basic relationship between force F, moment M, and coordinate x. Then, assuming that coordinate x is fixed, it is concluded from Eq. (5.1) that all lines of constant moment arm (i.e., $|x| = const.$) must go through the origin of the coordinate system as the moment M is proportional to the force F. In addition, the partial derivative of the moment M with respect to the force F is given as:

$$\frac{\partial M}{\partial F} = x \tag{5.4}$$

The derivative equals the coordinate x of the applied force. A positive derivative, i.e., slope means that the coordinate of the applied force is positive. Likewise, a negative derivative means that the coordinate of the applied force is negative.

The line of constant x will coincide with the ordinate of the coordinate system if the absolute value of coordinate x approaches infinity. The force on the ordinate of the combined load diagram is zero as the ordinate is the pure moment line. This conclusion has an important practical implication. Often, it is difficult to apply a pure moment, i.e., a force couple, during the calibration of a balance as more complex calibration hardware setups are needed. These difficulties may be avoided if the influence of a pure moment on the measured balance bridge outputs is approximated by (i) combining a large moment arm with (ii) a force of small magnitude such that the design load limit of the balance is

not exceeded. Then, calibration data points can be obtained that are in the vicinity of the pure moment line.

Figure 5–1c below summarizes important characteristics of the combined load diagram for balance loads that are described in direct–read format. The color yellow marks regions

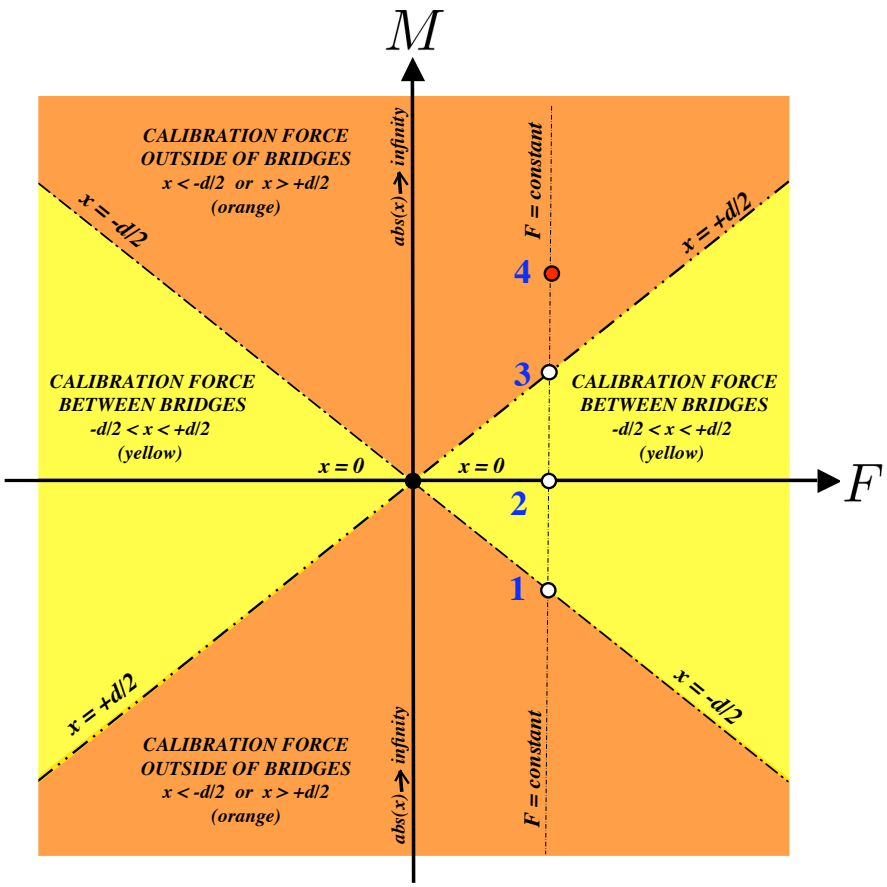

Fig. 5–1c Quadrant characteristics for load pair given in direct–read format.

where the force is applied at or between the forward and aft bridges of the balance assuming that loads of either a force or moment balance are described in direct–read format. The color orange marks regions where the force is applied outside of the location of the bridges. The dividing lines between the yellow and orange regions are the two diagonal lines. They represent the situation when the calibration force is exactly applied at the forward or aft bridge location of the balance ($x = \pm d/2$).

5.3 Force Balance Format

The interpretation of the combined load diagram for loads given in force balance format can be obtained by using the same approach that was used in the previous section. First, it is assumed that the balance moment center is located halfway between the forward & aft bridges of the force balance. Then, the loads described in direct–read format, i.e., F and M in Fig. 5–1a, are simply replaced by the resulting load pair F_1 and F_2 at the forward & aft bridges of the force balance. Figure 5–2a below shows corresponding load

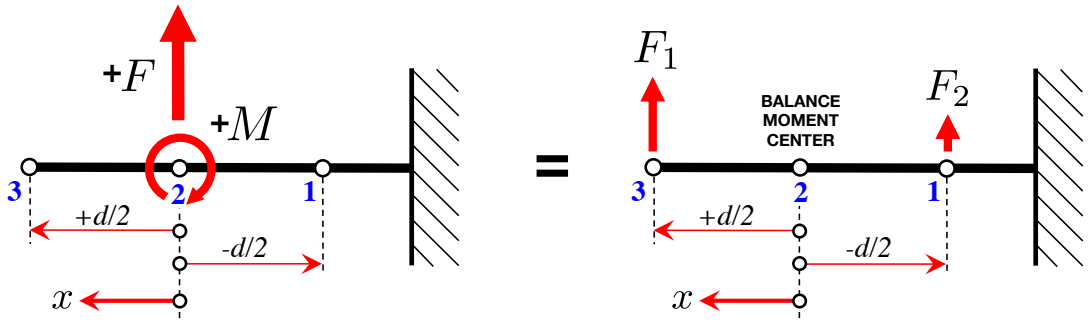

Fig. 5–2a Transformation from direct–read format to force balance format.

pairs in direct–read and force balance format that act on the balance assuming that positions 3 and 1 are the forward & aft bridge locations. Now, the combined load diagram of the load pair can be defined as the generic plot of the force F_2 at the aft bridge location plotted versus the force F_1 at the forward bridge location. Figure 5–2b below shows what

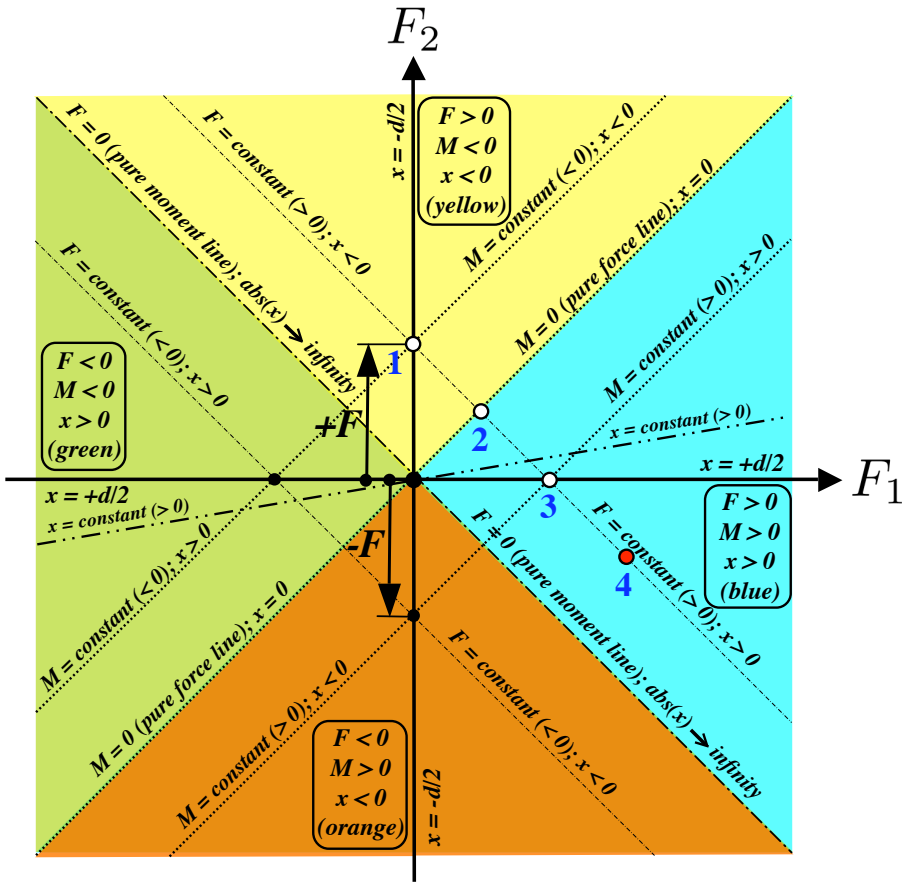

Fig. 5–2b Combined load diagram for load pair given in force balance format.

the diagram looks like in this case. The load transformation equations from direct–read to force balance format may be used to identify lines of constant force, constant moment, and constant moment arm in the combined load diagram above. We know, using

derivations presented in App. 4, that the relationship between the force and moment and the forces at the forward & aft bridges can be summarized by the following equations

$$F \;=\; F_1 \;+\; F_2 \tag{5.5a}$$

$$M \;=\; \Big[\; F_1 \;-\; F_2 \;\Big] \;\cdot\; d \;/\; 2 \tag{5.5b}$$

where d is the distance between the bridges. The lines of constant force F can be obtained from Eq. (5.5a). Solving, e.g., Eq. (5.5a) for F_2, we get:

$$\textit{line of constant force} \;\Longrightarrow\; F_2 \;=\; \underbrace{[\; F \;]}_{F \;\equiv\; const.} \;-\; F_1 \tag{5.6a}$$

The pure moment line is the line where the force F is zero. Therefore, after setting the force in Eq. (5.6a) to zero, we get the equation of the pure moment line:

$$\textit{line of pure moment} \;\Longrightarrow\; F_2 \;=\; -F_1 \tag{5.6b}$$

The line of constant moment still needs to be determined. It can be obtained after solving Eq. (5.5b) for F_2. Then, we get:

$$\textit{line of constant moment} \;\Longrightarrow\; F_2 \;=\; \underbrace{\left[\frac{-2 \cdot M}{d}\right]}_{M,d \;\equiv\; const.} + F_1 \tag{5.7a}$$

The pure force line is the line where the moment M is zero. Therefore, after setting the moment in Eq. (5.7a) to zero, we get the equation of the pure force line:

$$\textit{line of pure force} \;\Longrightarrow\; F_2 \;=\; F_1 \tag{5.7b}$$

Finally, lines of a constant coordinate x of the force are obtained in the combined load diagram after (i) replacing the moment on the left–hand side of Eq. (5.1) with the right–hand side of Eq. (5.5b) and (ii) the force on the right–hand side of Eq. (5.1) with the right–hand side of Eq. (5.5a). Then, we get the relationship below where x is the coordi–

$$\Big[\; F_1 \;-\; F_2 \;\Big] \;\cdot\; d \;/\; 2 \quad = \quad \Big[\; F_1 \;+\; F_2 \;\Big] \;\cdot\; x \tag{5.8}$$

nate of the applied force. Rearranging terms in Eq. (5.8) and solving for F_2, we get the relationship below for the line that corresponds to a constant value of coordinate x.

$$\textit{line of constant value of coordinate } x \textit{ (version 1)} \;\Longrightarrow\; F_2 \;=\; F_1 \cdot \left[\frac{d \;-\; 2 \cdot x}{d \;+\; 2 \cdot x}\right] \tag{5.9a}$$

The above equation can also be expressed in a different format if numerator and denominator of the fraction are divided by x. Then, we get:

$$\textit{line of constant value of coordinate } x \textit{ (version 2)} \implies F_2 \;=\; F_1 \cdot \left[\frac{d/x \;-\; 2}{d/x \;+\; 2} \right] \quad (5.9b)$$

Alternatively, Eq. (5.9a) may be solved for the force component F_1. Then, we get:

$$\textit{line of constant value of coordinate } x \textit{ (version 3)} \implies F_1 \;=\; F_2 \cdot \left[\frac{d \;+\; 2 \cdot x}{d \;-\; 2 \cdot x} \right] \quad (5.9c)$$

It is concluded from Eqs. (5.9a) and (5.9b) that the lines of constant moment arm are straight lines that must go through the origin of the combined load diagram as the fractions on the right hand side of the two equations satisfy the following conditions:

$$d \;\&\; x \equiv const. \implies \left[\frac{d \;-\; 2 \cdot x}{d \;+\; 2 \cdot x} \right] \equiv const. \implies (5.9a) \implies F_2 \;=\; F_1 \cdot const.$$

Similary, after taking a closer look at Eq. (5.9c), the following conclusions are made:

$$d \;\&\; x \equiv const. \implies \left[\frac{d \;+\; 2 \cdot x}{d \;-\; 2 \cdot x} \right] \equiv const. \implies (5.9c) \implies F_1 \;=\; F_2 \cdot const.$$

Now, four limiting cases are examined in order to complete the investigation of the equations of the constant coordinate x that describes the location of the total force relative to the balance moment center. Equations of the lines of the following four locations are of interest: $x = +d/2$ (forward bridge), $x = -d/2$ (aft bridge), $x = 0$ (balance moment center), and $x \to \pm\infty$ (approximation of pure moment). Equations (5.9a), (5.9b), and (5.9c) may be applied to find the corresponding lines in the combined load diagram. The first line is obtained after applying the condition $x = +d/2$ to Eq. (5.9a). Then, we get:

$$\textit{coordinate of forward bridge} \implies x \;=\; +d/2 \implies F_2 \;=\; 0 \quad (5.10a)$$

Then, after using $x = -d/2$ in Eq. (5.9c), we get the equation of the second line:

$$\textit{coordinate of aft bridge} \implies x \;=\; -d/2 \implies F_1 \;=\; 0 \quad (5.10b)$$

Similarly, after using $x = 0$ in Eq. (5.9a), we get the equation of the third line:

$$\textit{coordinate of balance moment center} \implies x \;=\; 0 \implies F_2 \;=\; F_1 \quad (5.10c)$$

It is observed that the equation of the line for $x = 0$, i.e., Eq. (5.10c), is identical with the equation of the pure force line that is given in Eq. (5.7b). This result is expected as the force is applied at the balance moment center (see also Fig. 5–2a).

Finally, after taking the limit $x \to \pm\infty$ of the fraction given on the right–hand side of Eq. (5.9b), we get the equation of the fourth line:

$$\textit{line of pure moment} \implies \lim_{x \to \pm\infty} \left[\frac{d/x \; - \; 2}{d/x \; + \; 2} \right] \; = \; -1 \implies F_2 \; = \; -F_1 \qquad (5.10d)$$

It is interesting to note that the fourth line, i.e., Eq. (5.10d), is identical with the pure moment line that is given in Eq. (5.6b). Therefore, outputs of the forward & aft bridges of a force balance will more and more resemble outputs resulting from the application of a pure moment whenever the absolute value of coordinate x, i.e., the moment arm, is significantly larger than the distance d between the forward & aft bridges of the balance. Figure 5–2c below summarizes quadrant characteristics of the combined load diagram for a load pair that is described in force balance format.

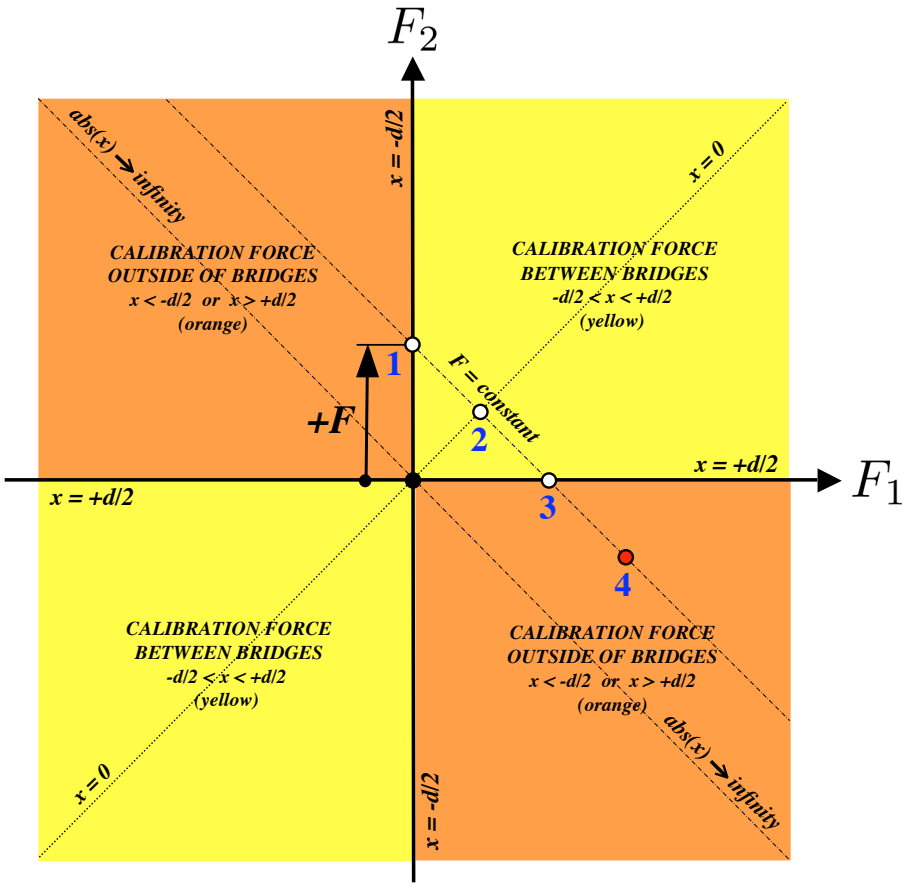

Fig. 5–2c Quadrant characteristics for load pair given in force balance format.

The first and third quadrants are identified by the yellow color. They have data points where the applied force is located between the forward & aft bridges. The second and fourth quadrants are marked using orange color. They have data points where the force is located outside of the bridges.

5.4 Moment Balance Format

Now, the interpretation of the combined load diagram for a load pair is discussed that is described in moment balance format. First, it is assumed that the balance moment center is located halfway between the forward & aft bridges of the moment balance. Then, the

loads described in direct–read format, i.e., F and M in Fig. 5–1a, are simply replaced by the resulting moment pair M_1 and M_2 at the forward & aft bridges of the moment balance. Figure 5–3a below shows the corresponding load pairs in direct–read and moment balance

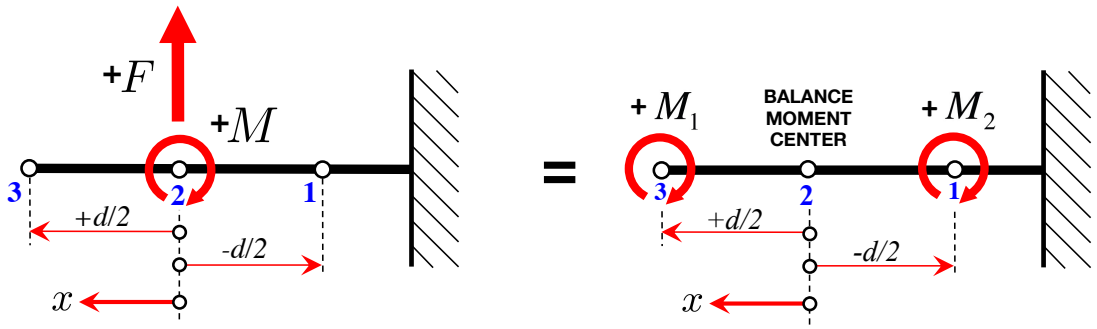

Fig. 5–3a Transformation from direct–read format to moment balance format.

format assuming that positions 3 and 1 are the forward & aft bridge locations identified using the coordinates $x = \pm d/2$. Now, the combined load diagram of the load pair can be defined as the generic plot of the moment M_2 at the aft bridge plotted versus the moment M_1 at the forward bridge. Figure 5–3b below shows what the diagram looks like in this case.

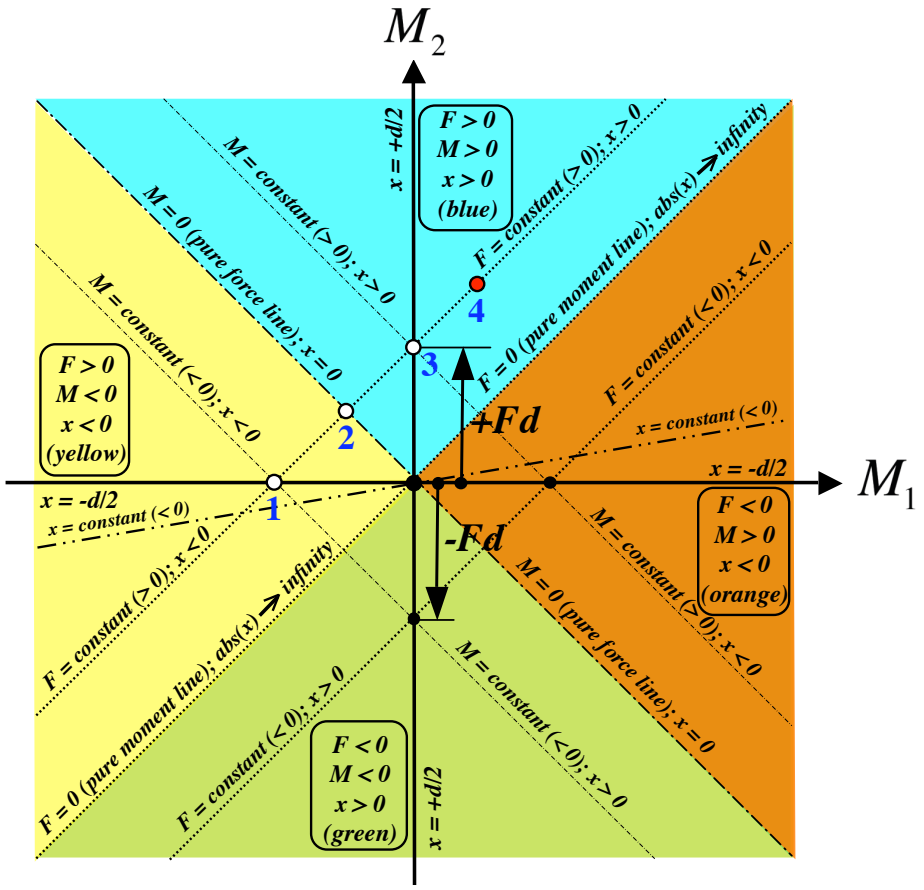

Fig. 5–3b Combined load diagram for load pair given in moment balance format.

Load transformation equations from direct–read to moment balance format may be used to identify lines of constant force, constant moment, and constant moment arm in the

combined load diagram above. We know, using derivations presented in App. 4, that the relationship between the force and moment and the moments at the forward & aft bridges can be summarized by the following equations:

$$F \;=\; \Big[\; M_2 \;-\; M_1 \;\Big] \;/\; d \tag{5.11a}$$

$$M \;=\; \Big[\; M_1 \;+\; M_2 \;\Big] \;/\; 2 \tag{5.11b}$$

Lines of constant force F in the combined load diagram can be obtained from Eq. (5.11a). Solving, e.g., Eq. (5.11a) for M_2, we get:

$$\textit{line of constant force} \;\Longrightarrow\; M_2 \;=\; \underbrace{[\; F \cdot d \;]}_{F,d \;\equiv\; const.} \;+\; M_1 \tag{5.12a}$$

The pure moment line is the line where the force F is zero. Then, after setting the force in Eq. (5.12a) to zero, we get the equation of the pure moment line:

$$\textit{line of pure moment} \;\Longrightarrow\; F \;=\; 0 \;\Longrightarrow\; M_2 \;=\; M_1 \tag{5.12b}$$

The line of constant moment still needs to be determined. Now, after solving Eq. (5.11b) for M_2, we get:

$$\textit{line of constant moment} \;\Longrightarrow\; M_2 \;=\; \underbrace{[\; 2 \cdot M \;]}_{M \;\equiv\; const.} \;-\; M_1 \tag{5.13a}$$

The pure force line is the line where the moment M is zero. Then, after setting the moment in Eq. (5.13a) to zero, we get the equation of the pure force line:

$$\textit{line of pure force} \;\Longrightarrow\; M \;=\; 0 \;\Longrightarrow\; M_2 \;=\; -M_1 \tag{5.13b}$$

Lines of coordinate x remain to be defined that describe a fixed location of force F. The required relationship is obtained after replacing the moment on the left–hand side of Eq. (5.1) with the right–hand side of Eq. (5.11b) and the force on the right–hand side of Eq. (5.1) with the right–hand side of Eq. (5.11a). Then, we get:

$$\Big[\; M_1 \;+\; M_2 \;\Big] \;/\; 2 \quad=\quad \Big[\; M_2 \;-\; M_1 \;\Big] \;\cdot\; x \;/\; d \tag{5.14}$$

Now, after rearranging terms in Eq. (5.14), solving for the moment component M_2, and simplifying the result, we get the following relationship:

$$\textit{line of constant value of coordinate } x \textit{ (version 1)} \Longrightarrow M_2 \;=\; M_1 \cdot \left[\; \frac{2\,x + d}{2\,x - d} \;\right] \tag{5.15a}$$

The relationship above may be expressed in a different format after dividing both the numerator and denominator of the fraction by the coordinate x. Then, we get:

$$\textit{line of constant value of coordinate } x \textit{ (version 2)} \Longrightarrow M_2 \;=\; M_1 \cdot \left[\; \frac{2 + d/x}{2 - d/x} \;\right] \tag{5.15b}$$

Alternatively, Eq. (5.15a) may be solved for the moment component M_1. Then, we get:

$$\textit{line of constant value of coordinate } x \textit{ (version 3)} \Longrightarrow M_1 \;=\; M_2 \cdot \left[\frac{2\,x - d}{2\,x + d} \right] \quad (5.15c)$$

It is concluded from Eqs. (5.15a) and (5.15b) that the lines of constant coordinate x are straight lines that go through the origin of the combined load diagram as the fractions on the right–hand side of the two equations satisfy the following conditions:

$$d \;\&\; x \equiv const. \;\Longrightarrow\; \left[\frac{2 \cdot x \;+\; d}{2 \cdot x \;-\; d} \right] \equiv const. \;\Longrightarrow\; (5.15a) \;\Longrightarrow\; M_2 \;=\; M_1 \cdot const.$$

Similarly, after taking a closer look at Eq. (5.15c), the following conclusions can be made:

$$d \;\&\; x \equiv const. \;\Longrightarrow\; \left[\frac{2 \cdot x \;-\; d}{2 \cdot x \;+\; d} \right] \equiv const. \;\Longrightarrow\; (5.15c) \;\Longrightarrow\; M_1 \;=\; M_2 \cdot const.$$

Now, four limiting cases need to be evaluated to complete the investigation of the equations of the constant coordinate x that describes the location of the applied force relative to the balance moment center. Equations of the lines for the following four coordinate values are of interest: $x = +d/2$ (forward bridge location), $x = -d/2$ (aft bridge location), $x = 0$ (balance moment center), and $x \to \pm\infty$ (approximation of pure moment). Equations (5.15a), (5.15b), and (5.15c) may be used to find the corresponding lines in the combined load diagram. The first line is obtained after applying the condition $x = -d/2$ to Eq. (5.15a). Then, we get:

$$\textit{coordinate of aft bridge} \;\Longrightarrow\; x \;=\; -d/2 \;\Longrightarrow\; M_2 \;=\; 0 \qquad (5.16a)$$

Now, after using $x = +d/2$ in Eq. (5.15c), we get the equation of the second line:

$$\textit{coordinate of forward bridge} \;\Longrightarrow\; x \;=\; +d/2 \;\Longrightarrow\; M_1 \;=\; 0 \qquad (5.16b)$$

Similarly, after using $x = 0$ in Eq. (5.15a), we get the equation of the third line:

$$\textit{coordinate of balance moment center} \;\Longrightarrow\; x \;=\; 0 \;\Longrightarrow\; M_2 \;=\; -M_1 \qquad (5.16c)$$

It is observed that the line for $x = 0$, i.e., Eq. (5.16c), is identical with the pure force line that was derived in Eq. (5.13b). This observation is expected as the force is applied in this case at the balance moment center (see also Fig. 5–3a).

Finally, after taking the limit $x \to \pm\infty$ of the fraction given on the right hand side of Eq. (5.15b), we get the equation of the fourth line:

$$\textit{line of pure moment} \;\Longrightarrow\; \lim_{x \to \pm\infty} \left[\frac{2 \;+\; d/x}{2 \;-\; d/x} \right] \;=\; 1 \;\Longrightarrow\; M_2 \;=\; M_1 \qquad (5.16d)$$

It is interesting to note that the fourth line, i.e., Eq. (5.16d), is identical with the pure moment line that is defined in Eq. (5.12b). Therefore, it is concluded that the outputs

of the forward & aft bridges of a moment balance will more and more resemble outputs resulting from the application of a pure moment whenever the absolute value of coordinate x, i.e., the moment arm, is significantly larger than the distance d between the forward & aft bridges of the balance.

Figure 5–3c below summarizes characteristics of each quadrant of the combined load diagram for a load pair that is described in moment balance format.

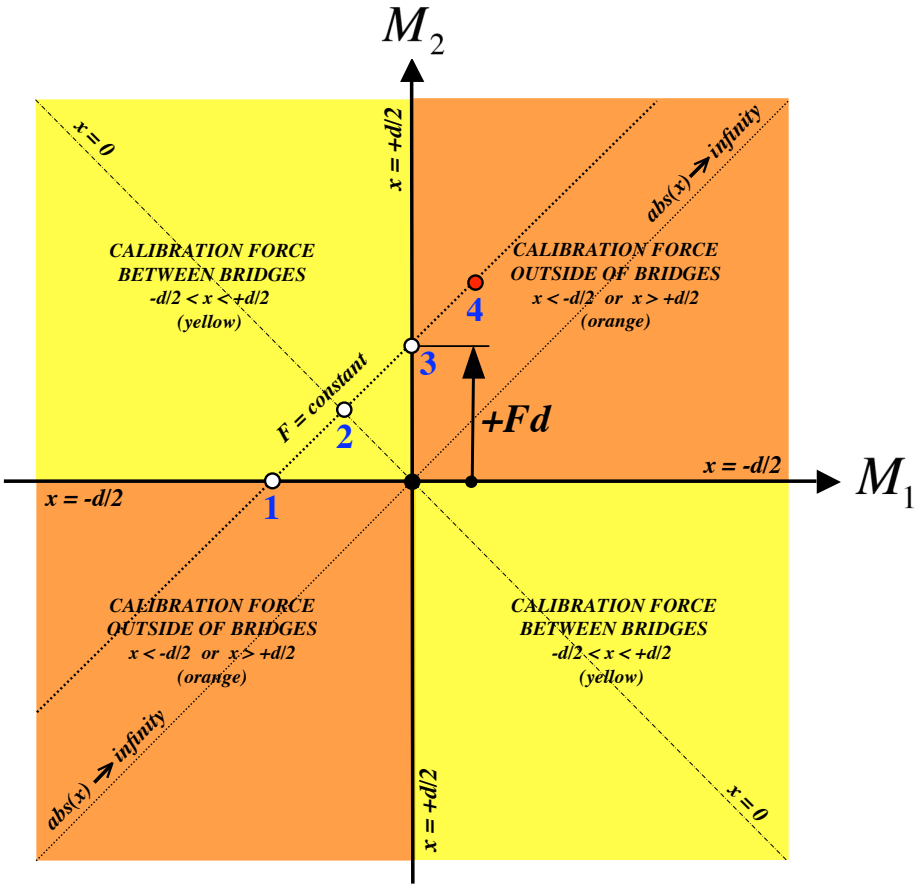

Fig. 5–3c Quadrant characteristics for load pair given in moment balance format.

The second and fourth quadrants (yellow color) have data points where the calibration force is located between the bridges. The first and third quadrants, on the other hand, have data points where the calibration force is located outside of the bridges.

We conclude, after comparing the diagram for a load pair given in moment balance format (Fig. 5–3b & Fig. 5–3c) with the diagram for a load pair given in force balance format (Fig. 5–2b & Fig. 5–2c), that lines of constant force, constant moment, and constant moment arm for a load pair given in moment balance format can be obtained from the corresponding lines of a load pair given in force balance format by using a $-90°$ rotation about the origin of the coordinate system.

5.5 Discussion of Example

A data set from a manual calibration of NASA's MK3C force balance may be used to illustrate the application of the combined load diagram to a realistic calibration data set.

The chosen balance is a six–component force balance of Task/Able design. It measures five forces and one moment ($N1$, $N2$, $S1$, $S2$, AF, RM). It has a diameter of 2.0 in and a length of 11.25 in. Table 5–1 below lists the capacity of each load component.

Table 5–1: Load capacities of NASA's MK3C balance ($lbs \equiv$ pounds of force).

$N1$, lbs	$N2$, lbs	$S1$, lbs	$S2$, lbs	AF, lbs	RM, $in-lbs$
900	900	450	450	500	1000

The balance calibration was performed using the hand load method. A total of 247 loads or load combinations were applied that were distributed across 13 load series. Combined loadings were only applied to the normal force components ($N1$, $N2$).

It was decided to focus the discussion in this section on loads that are visible in the combined load plot of the forward & aft normal force components (see Fig. 5–4 below). Five distinct lines can be seen in the plot. Figure 5–2b, i.e., the combined load diagram for a load pair given in force balance format, may be used to interpret them.

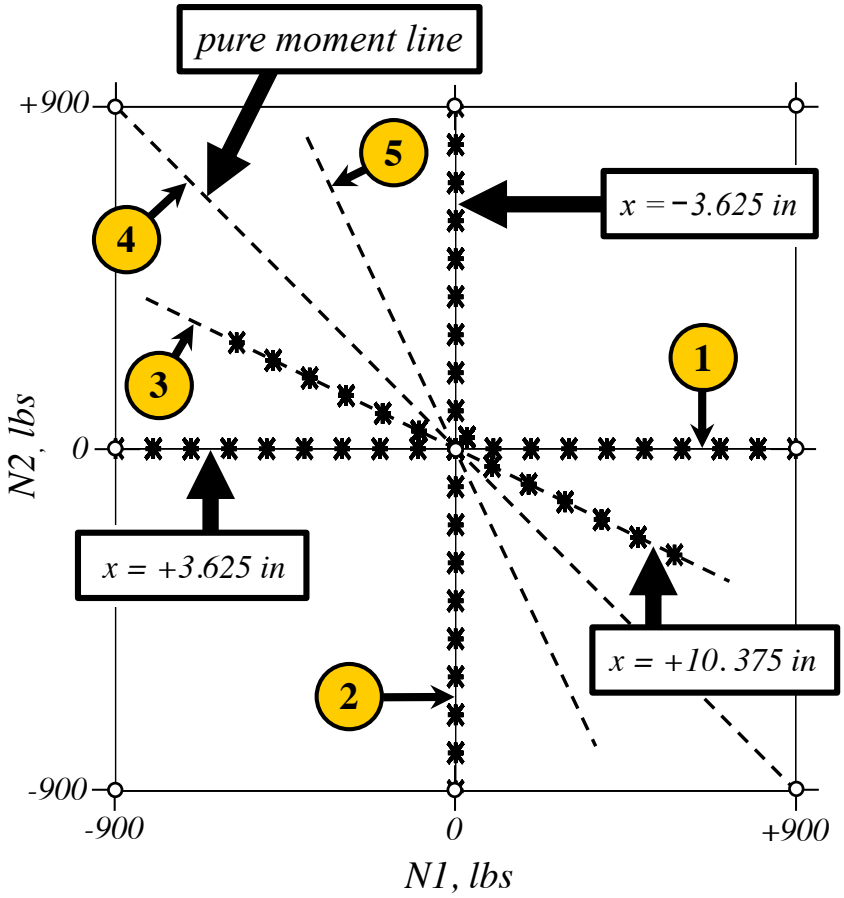

Fig. 5–4 Combined load plot for load pair $\{N1, N2\}$ of the MK3C balance.

Points on the abscissa (*Line 1*) have a $N2$ load value of zero. Therefore, these points represent loads that were applied at the forward bridge of the balance (coordinate $x = +3.625\,in$). Points on the ordinate (*Line 2*), on the other hand, have a $N1$ load value of

zero. Therefore, points located on the ordinate represent loadings that were applied at the aft bridge of the balance (coordinate $x = -3.625\,in$).

Comparing Fig. 5–2b with Fig. 5–4 we conclude that the calibration points located inside of the second and fourth quadrant (*Line 3*) must have been taken outside of the bridge locations. This observation can be confirmed if the load transformations given in App. 4 are applied to estimate the moment arm. The calculated coordinate of the applied calibration force is determined to be $x = +10.375\,in$. Therefore, the calibration force was located $6.75\,in$ forward of the forward normal force bridge of the balance.

The principal diagonal of the second and fourth quadrant (*Line 4*) is the pure moment line. In theory, calibration points can only be placed on this line if a force couple is applied during the calibration. It would have been possible to approximate the influence of a pure moment on the bridge outputs if calibration points would have also been obtained by applying the force at the coordinate $x = -10.375\,in$. In that case, calibration points would have appeared on *Line 5*. Consequently, points on both *Line 3* and *Line 5* could have been used for the regression analysis of the calibration data. Then, a very good approximation of the influence of a pure moment on the bridge outputs could have potentially been included in the regression model of the calibration data as the pure moment line (*Line 4*) is located halfway between *Line 3* and *Line 5*.

5.6 Summary and Conclusions

Combined load diagrams for balance load pairs were discussed in great detail that are given in direct–read, force balance, and moment balance format. The diagrams may be used to interpret the combined load plots of typical strain–gage balance calibration data. In particular, lines of constant force, pure force, constant moment, and pure moment were identified for each balance load format choice. Results of these investigations are summarized in Table 5–2 below.

Table 5–2: Description of constant and pure force & moment lines.

Load Line Description	Direct–Read Format (F, M)	Force Balance Format (F_1, F_2)	Moment Balance Format (M_1, M_2)
constant force	$F = const.$	$F_2 = F - F_1$	$M_2 = F \cdot d\ + M_1$
pure force	$M = 0$	$F_2 = F_1$	$M_2 = -M_1$
constant moment	$M = const.$	$F_2 = -2 \cdot M/d + F_1$	$M_2 = 2 \cdot M - M_1$
pure moment	$F = 0$	$F_2 = -F_1$	$M_2 = M_1$

Finally, a combined load plot from a basic calibration of a six–component force balance was used to illustrate benefits of the diagrams.

It was also illustrated during the investigation of the combined load diagrams how data points near the pure moment line may be obtained by combining a large moment arm with a force of small magnitude. This approach may help an analyst to approximate the influence of a pure moment on the bridge output measurements whenever the chosen calibration approach does not support the application of a pure moment to the balance.

Appendix 6

Bridge Output Format

6.1 Introduction

An analyst can describe bridge outputs of a strain–gage balance by using one of three formats. The bridge output format needs to be chosen carefully because it has an influence on the characteristics of the method that is selected for the balance load prediction. For example, outputs of balances with bi–directional characteristics must be formatted as output differences relative to the natural zeros of the bridges if the *Non–Iterative Method* in combination with absolute value terms of the outputs is used for the balance load prediction. Important characteristics of the three output format types are discussed in detail in the next section. Afterwards, a data set from a typical six–component strain–gage balance is used to illustrate application and interpretation of the three output formats. Finally, useful interpretations of the outputs of unloaded bridges are provided that are often observed during the manual calibration of a balance.

6.2 Bridge Output Format Types

Three bridge output format types exist that may be used to describe strain–gage balance data. The first type is the format *Raw Output*. It describes outputs as absolute voltage measurements. The output format is defined in Eq. (6.1) below where i is the bridge index,

$$\textit{Raw Output} \quad \Longrightarrow \quad rF_i(\eta) \qquad (6.1)$$

η is the data point index, and $rF_i(\eta)$ is the raw output of the bridge. The use of the format *Raw Output* makes the preparation of the input file for the regression analysis of balance calibration data trivial. First, outputs can be used as supplied by the calibration laboratory's instrumentation. In addition, the natural zeros of the bridges can directly be used for the regression analysis as they are the raw outputs of the balance in an assumed weightless condition. These non–zero values are the electrical representation of zero absolute load. They are needed for the tare load iteration process (see App. 12 and App. 13 for more details). Consequently, assuming that the *Iterative Method* is used for the calibration data analysis, the intercept term must always be included in the regression model of the outputs as it is a least squares approximation of the natural zeros.

The format *Raw Output* can be used to analyze balance calibration data of all balance types with all known output characteristics as long as an analyst applies the *Iterative Method*. However, *Raw Outputs* cannot be used to analyze calibration data of balances with bi–directional outputs if the *Non–Iterative Method* is chosen for the analysis. This limitation results from the fact that the traditionally used math term groups in the regression model of a load component do not allow for a constant output shift (this restriction is discussed in great detail in App. 7). Now, characteristics and application of the format *Raw Output* can be summarized in Table 6–1 below as follows:

Table 6–1: Output format ≡ *Raw Output* ; summary of characteristics.

- defined as an absolute voltage measurement that uses zero volts as a datum;
- data preparation is trivial as Raw Outputs are directly used as supplied;
- Raw Output can be used to analyze data of balances with all known bridge output characteristics as long as the Iterative Method is applied;
- Raw Output cannot be used to analyze data of balances with bi–directional bridge output characteristics whenever the Non–Iterative Method is applied;
- natural zeros are the Raw Outputs of a balance in a weightless condition;
- natural zeros could also be obtained from Raw Outputs of related load series;
- Iterative Method $\Longrightarrow$ intercepts are a least squares description of the natural zeros;
- Iterative Method $\Longrightarrow$ intercepts must be used in regression models of Raw Outputs;
- tare loads can be obtained from output data by using a tare load iteration;
- Raw Output can be used to analyze data of both primary & auxiliary balances;

The second output format type, i.e., *Difference Type 1*, uses the difference between the raw output and the natural zero of a balance bridge for the analysis. This alternate output format is defined in Eq. (6.2) below where i is the bridge index, η is the data point

$$\textit{Difference Type 1} \quad \Longrightarrow \quad D_i(\eta) \;=\; rF_i(\eta) \;-\; N_i \qquad (6.2)$$

index, $rF_i(\eta)$ is the raw output, and N_i is the natural zero of the balance bridge. The use of the format *Difference Type 1* requires a global subtraction of the natural zeros from all raw outputs of the balance bridges. In other words, it is a simple linear transformation (output shift) that is applied to the raw outputs. Consequently, the transformed values of the natural zeros are zeros. These zeros represent the updated electrical representation of zero absolute load of the balance. They are needed as data inputs if a tare load iteration is performed using the transformed bridge outputs as input. Therefore, assuming that the *Iterative Method* is used for the balance calibration data analysis, the intercept term is optional in the regression model of the outputs as it is a least squares approximation of zero, i.e., of the transformed original natural zeros.

Regression analysis results for the format *Difference Type 1* will exactly match corresponding analysis results obtained by directly using the format *Raw Output* if (i) an intercept term is included in the math models and (ii) the same math model is used for the analysis. *Difference Type 1* can be used to analyze balance calibration data of all balance types with all known output characteristics using either the *Iterative* or the *Non–Iterative Method*. In particular, *Difference Type 1* can be used in combination with the *Non–Iterative Method* to analyze data of balances with bi–directional outputs. Now, characteristics and use of the format *Difference Type 1* can be summarized in Table 6–2 below as follows:

Table 6–2: Output format ≡ *Difference Type 1* ; summary of characteristics.

- defined as difference between raw outputs and natural zeros of the balance;
- data preparation requires subtraction of natural zeros from all outputs;
- Difference Type 1 can be used to analyze data of balances with all known bridge output characteristics as long as the Iterative Method is applied;
- Difference Type 1 must be used to analyze data of balances with bi–directional bridge output characteristics whenever the Non–Iterative Method is applied;
- natural zeros equal zeros in transformed output space of the balance;
- Iterative Method $\Longrightarrow$ intercepts are a least squares description of zero output;
- Iterative Method $\Longrightarrow$ intercepts are optional in regression models of outputs;
- tare loads can be obtained from output data by using a tare load iteration;
- Difference Type 1 can be used to analyze primary & auxiliary balance data;
- analysis results match those for Raw Output if the same math terms are used;

The third output format type is called *Difference Type 2*. It uses the difference between the raw output of the data point and the output of the zero load point of the load series for the analysis. The zero load point is the data point of a load series whose outputs are exclusively caused by (i) the weight of the metric part of the balance, (ii) the weight of the calibration body, and (iii) the weight of all attached calibration hardware (flexures, yokes, threaded rods, weight pans, etc.). The third output format is defined in Eq. (6.3) below

$$\textit{Difference Type 2} \quad \Longrightarrow \quad D_i{}'(\eta) \;=\; rF_i(\eta) \;-\; Z_i\{\,\mu(\eta)\,\} \qquad (6.3)$$

where i is the bridge index, η is the data point index, μ is the load series index, $rF_i(\eta)$ is the raw output of the balance bridge, and $Z_i\{\,\mu(\eta)\,\}$ is the output of the zero load point of the load series that a data point belongs to.

Difference Type 2 requires a subtraction of the outputs of the zero load point of a load series from the raw outputs of the given data set. Therefore, the data input file preparation for the use of *Difference Type 2* is complex whenever a manual calibration data set consists of a large number of load series. *Difference Type 2*, similar to *Difference Type 1*, is a simple output transformation. However, *Difference Type 2* subtracts the electrical outputs of a local datum, i.e., the output of the zero load point of the load series, from the raw outputs. *Difference Type 1*, on the other hand, subtracts the electrical outputs of a global datum, i.e., the natural zeros, from the raw outputs. It is important to mention at this point that the transformed values of all natural zeros are zeros. These zeros are the updated electrical representation of zero absolute load. Again, assuming that the *Iterative Method* is used, the intercept term is optional in the regression model of the outputs.

Difference Type 2 can be used to analyze balance calibration data of all balance types with all known output characteristics as long as the maximum magnitude of the tare loads of all load series is less than the empirical threshold of $\approx 2\,\%$ of load capacity. In other words, the use of *Difference Type 2* implicitly assumes that the tare loads of each load series

are negligible. The output format does not support a tare load iteration as the subtraction of the outputs of a zero load point of a load series removes information in the data that quantifies the tare loads of a data point. Therefore, analysis results for *Difference Type 2* are not as accurate as results that can be obtained by using either *Difference Type 1* or *Raw Output* as those two alternate formats support a tare load iteration. Finally, characteristics of the format *Difference Type 2* are summarized in Table 6–3 below as follows:

Table 6–3: Output format ≡ *Difference Type 2* ; summary of characteristics.

- defined as difference between raw outputs and zero load outputs of load series
- data preparation is complex as output subtraction must be done series by series
- by design, tare loads are zero as transformed outputs imply negligible tare loads
- Difference Type 2 may be used if the magnitude of all tare loads is below 2 % of capacity
- transformed natural zeros equal zeros in transformed output space
- Iterative Method $\Longrightarrow$ intercepts are a least squares description of zero output
- Iterative Method $\Longrightarrow$ intercepts are optional in regression models of outputs

It is useful to summarize balance data processing characteristics that are associated with the output format choices. Table 6–4 below lists five processing options that are possible by using the three output formats that are described in this section.

Table 6–4: Balance data processing characteristics.

Option	Raw Output	Difference Type 1	Difference Type 2	Intercept	Comments
1	×	—	—	×	natural zeros $\neq 0$ tare loads $\neq 0$
2	—	×	—	×	natural zeros $= 0$ tare loads $\neq 0$
3	—	×	—	—	natural zeros $= 0$ tare loads $\neq 0$
4	—	—	×	×	natural zeros $= 0$ tare loads $= 0$
5	—	—	×	—	natural zeros $= 0$ tare loads $= 0$

A calibration data set of NASA's MK40A force balance is discussed in the next section to illustrate the three output format choices that an analyst may use for the analysis of strain–gage balance calibration data.

6.3 Discussion of Example

A data set from a basic manual calibration of the NASA's MK40A balance was selected to illustrate the application of the three bridge output formats to real–world data. The MK40A is a six–component force balance of Task/Able design that measures five forces and one moment ($N1$, $N2$, $S1$, $S2$, AF, RM). It has a diameter of 2.5 in (63.5 mm) and

a total length of 17.31 in (439.7 mm). Table 6–5 below lists the load capacity of each load component of the balance.

Table 6–5: Load capacities of NASA's MK40A balance ($lbs \equiv$ pounds of force).

$N1$, lbs	$N2$, lbs	$S1$, lbs	$S2$, lbs	AF, lbs	RM, $in-lbs$
3500	3500	2500	2500	400	8000

The calibration of the balance was performed by using gravity weights. A total of 164 data points were recorded that were distributed across 16 load series. Single component loadings of all load components were recorded. Limitations of the calibration hardware only allowed for the simultaneous application of the forward & aft normal & side forces. Calibration data input files were prepared in support of the five calibration data processing options that are listed in Table 6–4. Figure 6–1 below shows the natural zeros of the balance bridges and parts of the original calibration data input file of the balance when the measured outputs were described in the format *Raw Output*.

Natural Zeros of the MK40A Balance

$rN1$ $microV/V$	$rN2$ $microV/V$	$rS1$ $microV/V$	$rS2$ $microV/V$	rAF $microV/V$	rRM $microV/V$
-19.23	-1.99	-1.30	-56.85	-138.73	-19.71

		Applied Loads --->						Raw Outputs --->					
Point ID	Load Series	N1	N2	S1	S2	AF	RM	rN1	rN2	rS1	rS2	rAF	rRM
		lbs	lbs	lbs	lbs	lbs	in-lbs	microV/V	microV/V	microV/V	microV/V	microV/V	microV/V
P-0001	1	0	0	0	0	0	0	-3.87	1.17	-0.76	-56.9	-136.05	-19.48
P-0002	1	600	0	0	0	0	0	204.88	-22.86	2.22	-57.81	-130.4	-19.52
P-0003	1	1200	0	0	0	0	0	414.96	-45.95	4.11	-58.21	-127.75	-19.44
P-0004	1	1800	0	0	0	0	0	625.59	-68.89	5.47	-58.55	-126.11	-19.44
P-0005	1	2200	0	0	0	0	0	766.06	-84.17	6.71	-58.81	-125.21	-19.37
P-0006	1	1800	0	0	0	0	0	625.7	-68.76	5.62	-58.57	-125.49	-19.4
P-0007	1	1200	0	0	0	0	0	415.13	-45.87	4.02	-58.18	-126.8	-19.51
P-0008	1	600	0	0	0	0	0	205.59	-22.91	2.13	-57.83	-127.4	-19.43
P-0009	1	0	0	0	0	0	0	-3.95	1.11	-0.8	-56.98	-135.96	-19.55
P-0010	2	0	0	0	0	0	0	-33.45	-5.32	-1.22	-56.97	-136.28	-19.79
P-0011	2	-600	0	0	0	0	0	-239.1	20.47	-6.66	-57.51	-137.86	-19.61
P-0012	2	-1200	0	0	0	0	0	-445.78	45.18	-11.54	-57.53	-140.01	-19.26
P-0013	2	-1800	0	0	0	0	0	-652.28	69.81	-16.25	-57.55	-141.99	-19.03
P-0014	2	-2200	0	0	0	0	0	-789.84	86.24	-19.17	-57.42	-144.63	-18.86
...	...	...	...	...	...	...	...	...	...	...	...	...	...

Fig. 6–1 Natural zeros and as supplied calibration data of the MK40A balance if the format *Raw Output* is used to describe the outputs of each calibration data point.

The natural zeros of the bridges, data point identifications, load series numbers, applied loads, and measured raw outputs of the six balance bridges are listed in column format. In addition, the outputs of the first zero load point of each series quantify the influence of the tare loads on the electrical outputs of the bridges. The first zero load point of a series can easily be recognized in Fig. 6–1 above. It is the data point of a load series that has zero applied load for all load components. For example, outputs of point P-0001 of Series 1 and outputs of point P-0010 of Series 2 are outputs of zero load points.

Similarly, Fig. 6–2 below shows the transformed natural zeros and the revised calibration data input file of the balance when outputs are described in the format *Difference Type 1*. The last six data columns of Fig. 6–2 were obtained by simply subtracting the natural zeros given in the header of Fig. 6–1 from the last six data columns of Fig. 6–1.

Transformed Natural Zeros of the MK40A Balance

$rN1$ $microV/V$	$rN2$ $microV/V$	$rS1$ $microV/V$	$rS2$ $microV/V$	rAF $microV/V$	rRM $microV/V$
0.0	0.0	0.0	0.0	0.0	0.0

		Applied Loads --->						Difference Type 1 --->					
Point ID	Load Series	N1	N2	S1	S2	AF	RM	rN1	rN2	rS1	rS2	rAF	rRM
		lbs	lbs	lbs	lbs	lbs	in-lbs	microV/V	microV/V	microV/V	microV/V	microV/V	microV/V
P-0001	1	0	0	0	0	0	0	15.36	3.15	0.54	-0.05	2.69	0.23
P-0002	1	600	0	0	0	0	0	224.11	-20.87	3.53	-0.97	8.33	0.19
P-0003	1	1200	0	0	0	0	0	434.19	-43.96	5.41	-1.36	10.98	0.27
P-0004	1	1800	0	0	0	0	0	644.82	-66.9	6.77	-1.7	12.63	0.27
P-0005	1	2200	0	0	0	0	0	785.29	-82.18	8.01	-1.96	13.52	0.34
P-0006	1	1800	0	0	0	0	0	644.93	-66.77	6.92	-1.73	13.25	0.31
P-0007	1	1200	0	0	0	0	0	434.37	-43.88	5.32	-1.33	11.93	0.21
P-0008	1	600	0	0	0	0	0	224.83	-20.92	3.43	-0.99	11.34	0.28
P-0009	1	0	0	0	0	0	0	15.28	3.09	0.5	-0.13	2.77	0.16
P-0010	2	0	0	0	0	0	0	-14.22	-3.33	0.08	-0.12	2.45	-0.08
P-0011	2	-600	0	0	0	0	0	-219.87	22.46	-5.36	-0.66	0.87	0.1
P-0012	2	-1200	0	0	0	0	0	-426.55	47.17	-10.24	-0.69	-1.27	0.45
P-0013	2	-1800	0	0	0	0	0	-633.05	71.8	-14.95	-0.7	-3.26	0.68
P-0014	2	-2200	0	0	0	0	0	-770.61	88.23	-17.87	-0.57	-5.9	0.85
...	...	...	...	...	...	...	...	...	...	...	...	...	...

Fig. 6–2 Transformed natural zeros and calibration data of the MK40A balance if the format *Difference Type 1* is used to describe the outputs of each calibration data point.

Finally, Fig. 6–3 below shows the transformed natural zeros of the balance bridges and parts of the revised calibration data input file of the balance when outputs are described in the format *Difference Type 2*.

Transformed Natural Zeros of the MK40A Balance

$rN1$ $microV/V$	$rN2$ $microV/V$	$rS1$ $microV/V$	$rS2$ $microV/V$	rAF $microV/V$	rRM $microV/V$
0.0	0.0	0.0	0.0	0.0	0.0

		Applied Loads --->						Difference Type 2 --->					
Point ID	Load Series	N1	N2	S1	S2	AF	RM	rN1	rN2	rS1	rS2	rAF	rRM
		lbs	lbs	lbs	lbs	lbs	in-lbs	microV/V	microV/V	microV/V	microV/V	microV/V	microV/V
P-0001	1	0	0	0	0	0	0	0	0	0	0	0	0
P-0002	1	600	0	0	0	0	0	208.76	-24.03	2.98	-0.91	5.64	-0.04
P-0003	1	1200	0	0	0	0	0	418.84	-47.11	4.86	-1.31	8.29	0.04
P-0004	1	1800	0	0	0	0	0	629.46	-70.06	6.23	-1.65	9.94	0.04
P-0005	1	2200	0	0	0	0	0	769.93	-85.34	7.46	-1.91	10.84	0.12
P-0006	1	1800	0	0	0	0	0	629.57	-69.92	6.37	-1.67	10.56	0.09
P-0007	1	1200	0	0	0	0	0	419.01	-47.04	4.78	-1.28	9.24	-0.02
P-0008	1	600	0	0	0	0	0	209.47	-24.07	2.88	-0.93	8.65	0.05
P-0009	1	0	0	0	0	0	0	-0.08	-0.06	-0.04	-0.08	0.09	-0.07
P-0010	2	0	0	0	0	0	0	0	0	0	0	0	0
P-0011	2	-600	0	0	0	0	0	-205.65	25.79	-5.44	-0.54	-1.59	0.18
P-0012	2	-1200	0	0	0	0	0	-412.33	50.5	-10.32	-0.57	-3.73	0.53
P-0013	2	-1800	0	0	0	0	0	-618.83	75.13	-15.04	-0.58	-5.71	0.76
P-0014	2	-2200	0	0	0	0	0	-756.39	91.56	-17.95	-0.45	-8.36	0.93
...	...	...	...	...	...	...	...	...	...	...	...	...	...

Fig. 6–3 Transformed natural zeros and calibration data of the MK40A balance if the format *Difference Type 2* is used to describe the outputs of each calibration data point.

The last six data columns of Fig. 6–3 were obtained by subtracting the raw outputs of the zero load point of each load series from all other outputs of the corresponding load series. Therefore, for example, outputs of point P–0012 of Fig. 6–3 were obtained by

subtracting the outputs of point P–0010 of Fig. 6–1, i.e, the outputs of the zero load point of Series 2, from the outputs of point P–0012 of Fig. 6–1.

6.4 Interpretation of the Outputs of Unloaded Bridges

A good understanding of the electrical output format types of a balance bridge makes it possible to better understand hidden characteristics of individual data points that are contained in the calibration data set of a balance. In this section it is shown, for example, how the raw outputs of the calibration data set of a six–component force balance may directly be interpreted as the natural zeros of a bridge if an analyst is able to identify data points with unloaded bridges.

In theory, a data point with unloaded bridges can be identified if the following two conditions are fulfilled: (i) the data point is a zero load point of a load series; (ii) the orientation of the balance and/or the calibration body relative to the gravitational acceleration is known. Then, a subset of the bridges must be unloaded. In other words, the observed electrical outputs of a subset of the bridges must be close to the corresponding values of the natural zeros.

The previously discussed calibration data set of the MK40A balance may be used to illustrate the identification of unloaded bridges and the direct measurement of the natural zeros whenever outputs are given as raw outputs. Figure 6–4 below shows a typical setup that is used during the calibration of the MK40A balance just before gravity weights are placed on the weight pans (the calibration data itself is partially shown in Fig. 6–1).

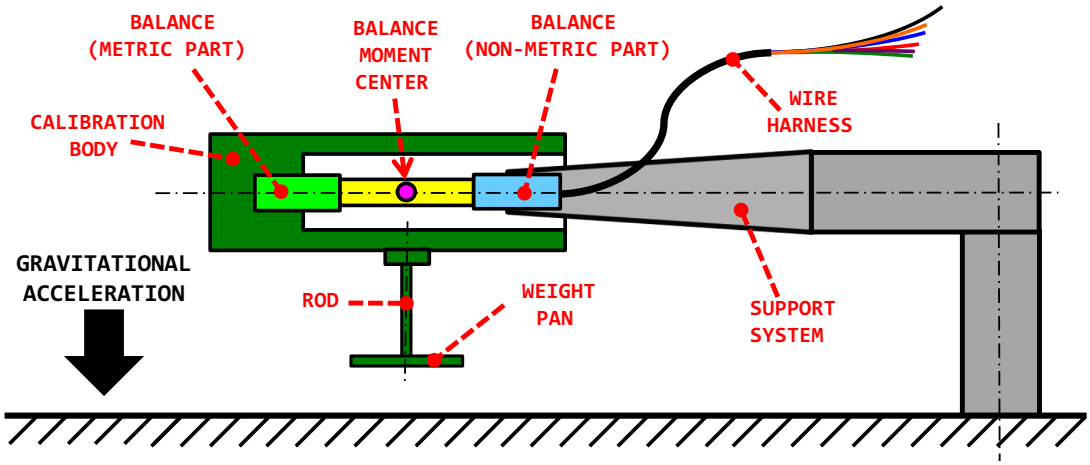

Fig. 6–4 Typical hardware setup for the manual calibration of a balance.

The setup shown in Fig. 6–4 above describes the load state of the balance that is responsible for the raw outputs of the zero load point of a load series. In this case, assuming that (i) the calibration body was leveled and (ii) the forward and aft normal forces of the balance are parallel to the direction of the gravitational acceleration, the two side force bridges, the rolling moment bridge, and the axial force bridge must be unloaded. Similar conclusions can be drawn for other orientations of the balance relative to the direction of the gravitational acceleration. Table 6–6 below lists the unloaded bridges for three different balance orientations relative to the direction of the gravitational acceleration.

The direction of a balance load component relative to the gravitational acceleration is used to describe the balance orientation.

Table 6–6: Force balance orientations relative to the direction of the gravitational acceleration that result in sets of unloaded bridges.

Load(s) acting in direction of the gravitational acceleration	List of unloaded bridges of a six–component force balance
$\pm N1$ *and* $\pm N2$	$rS1$, $rS2$, rAF, rRM
$\pm S1$ *and* $\pm S2$	$rN1$, $rN2$, rAF, rRM
$\pm AF$	$rN1$, $rN2$, $rS1$, $rS2$, rRM

For example, Fig. 6–5 below shows the zero load points (including repeats) of three of the 16 load series of the calibration data of the MK40A balance. The raw outputs of the

		Applied Loads --->						Raw Outputs --->					
Point ID	Load Series	N1	N2	S1	S2	AF	RM	rN1	rN2	rS1	rS2	rAF	rRM
		lbs	lbs	lbs	lbs	lbs	in-lbs	microV/V	microV/V	microV/V	microV/V	microV/V	microV/V
CASE 1 ---> (+N1) component parallel to gravitational acceleration; balance roll axis perpendicular to gravitational acceleration													
P-0001	1.00	0.00	0.00	0.00	0.00	0.00	0.00	-3.87	1.17	-0.76	-56.90	-136.05	-19.48
P-0009	1.00	0.00	0.00	0.00	0.00	0.00	0.00	-3.95	1.11	-0.80	-56.98	-135.96	-19.55
CASE 2 ---> (+S1) component parallel to gravitational acceleration; balance roll axis perpendicular to gravitational acceleration													
P-0037	5.00	0.00	0.00	0.00	0.00	0.00	0.00	-18.93	-1.17	20.04	-51.25	-136.00	-20.08
P-0045	5.00	0.00	0.00	0.00	0.00	0.00	0.00	-18.97	-1.24	18.27	-52.06	-135.61	-20.08
CASE 3 ---> (+AF) component parallel to gravitational acceleration; balance roll axis parallel to gravitational acceleration													
P-0073	9.00	0.00	0.00	0.00	0.00	0.00	0.00	-19.02	-1.57	-1.39	-56.81	89.01	-18.87
P-0081	9.00	0.00	0.00	0.00	0.00	0.00	0.00	-19.04	-1.58	-1.41	-56.85	89.63	-18.88

Fig. 6–5 Interpretation and use of the unloaded bridges for the measurement of the natural zeros of the MK40A balance.

bridges were simply copied from Fig. 6–1. Now, outputs of unloaded bridges need to be identified in Fig. 6–5 that are among the outputs of the zero load points of the calibration data. Load Series 1, for example, applied a positive forward normal force component ($+N1$). This situation is described by the first line in Table 6–6 above. Consequently, the two side force bridges, the rolling moment bridge, and the axial force bridge of the balance must be unloaded bridges. The electrical outputs of these four unloaded bridges of Series 1 are highlighted in blue color in Fig. 6–5. As expected, they are close to the natural zeros of the corresponding bridges that are reported in the header of Fig. 6–1 if experimental error associated with balance alignment imperfections is temporarily ignored.

Similarly, Load Series 5 applied a positive forward side force component ($+S1$). This situation is described by the second line in Table 6–6 above. Consequently, the two normal force bridges, the rolling moment bridge, and the axial force bridge of the balance must be unloaded bridges. The electrical outputs of these four unloaded bridges of Series 5 are highlighted in blue color in Fig. 6–5. Again, as expected, they are close to the natural zeros of corresponding bridges that are reported in the header of Fig. 6–1.

Finally, Load Series 9 applied a positive axial force component ($+AF$). In that case, the roll axis was parallel to the direction of the gravitational acceleration. This situation is described by the third line in Table 6–6 above. Consequently, the two normal force

bridges, the two side force bridges, and the rolling moment bridge of the balance must be unloaded bridges. The electrical outputs of these four unloaded bridges of Series 5 are highlighted in blue color in Fig. 6–5. Again, as it was the case for Series 1 and Series 5, they are close to the natural zeros of the corresponding bridges that are reported in the header of Fig. 6–1.

It is interesting to compare the blue values shown in Fig. 6–5 above with the natural zeros of the balance bridges that are listed in Fig. 6–1. The values shown in Fig. 6–1 were obtained by averaging output sets of the balance that were measured after rotating the balance four times on a leveling table. In all cases, differences between the averaged natural zeros given in Fig. 6–1 and corresponding direct measurements given in Fig. 6–5 are very small (within $\approx \pm 2$ $microV/V$).

6.5 Summary

Characteristics of three bridge output format choices were discussed. The first output format choice, i.e., *Raw Output*, works with balance data of all known output characteristics as long as (i) the *Iterative Method* is used for the load prediction and (ii) an intercept is included in the regression model of the outputs. However, the format *Raw Output* cannot be selected whenever (i) an analyst wants to use the *Non–Iterative Method* for the load prediction and (ii) the outputs of the balance have bi–directional characteristics (see also the related discussion in App. 7). It also must be mentioned that the use of the format *Raw Output* may make it possible to either determine or verify the natural zeros of a balance bridge if an analyst can identify unloaded balance bridges of a calibration data point.

The second output format choice, i.e., *Difference Type 1*, is universally applicable. It works with balance data of all known output characteristics if either the *Iterative Method* or the *Non–Iterative Method* is chosen for the load prediction. The data input file preparation is straight forward. The output differences are obtained by simply subtracting the natural zeros of the balance bridges from the raw outputs.

The third output format choice, i.e., *Difference Type 2*, also works with data of all known output characteristics if either the *Iterative Method* or the *Non–Iterative Method* is used for the load prediction. It is defined as the difference between the raw output of a bridge and the output of the zero load point of the load series of the given data point. It is important to mention that *Difference Type 2* only works correctly if the tare loads of each data point are very small. Therefore, load prediction results obtained by using the format *Difference Type 2* are often not as accurate as results for the two other format choices as those alternate formats support the tare load iteration process.

A good understanding of the bridge output format of a balance data set is not just beneficial during the preparation of a balance data input file. It may also help an analyst to correctly interpret calibration data that a wind tunnel customer used for the preparation of the load prediction equations. In that situation, it may be possible to perform an independent analysis of the customer's data for troubleshooting purposes if problems with the supplied load prediction equations surface during a wind tunnel test.

Appendix 7
Bi–directional Output Characteristics

7.1 Introduction

The bridge outputs of some balance designs are known to have bi–directional characteristics. In that case, it is observed that the primary bridge sensitivity, i.e., the first derivative of a bridge output with respect to the related primary bridge load, is a function of the sign of the load. In general, as *Galway* suggested in Ref. [6], absolute value terms† are needed in regression models of bi–directional balance data to mathematically describe this repeatable behavior (see Refs. [6], [7], [10], [33] to [35]).

Bi–directional output characteristics exist, for example, in data of Task/Able balances. The bi–directional behavior of a Task/Able balance can be illustrated with calibration data of NASA's MK40A balance. It is known that the outputs of the normal and side force bridges of this balance are bi–directional. Figure 7–1 below shows, for example, the out–put of the MK40A's forward side force bridge plotted versus the forward side force. It looks,

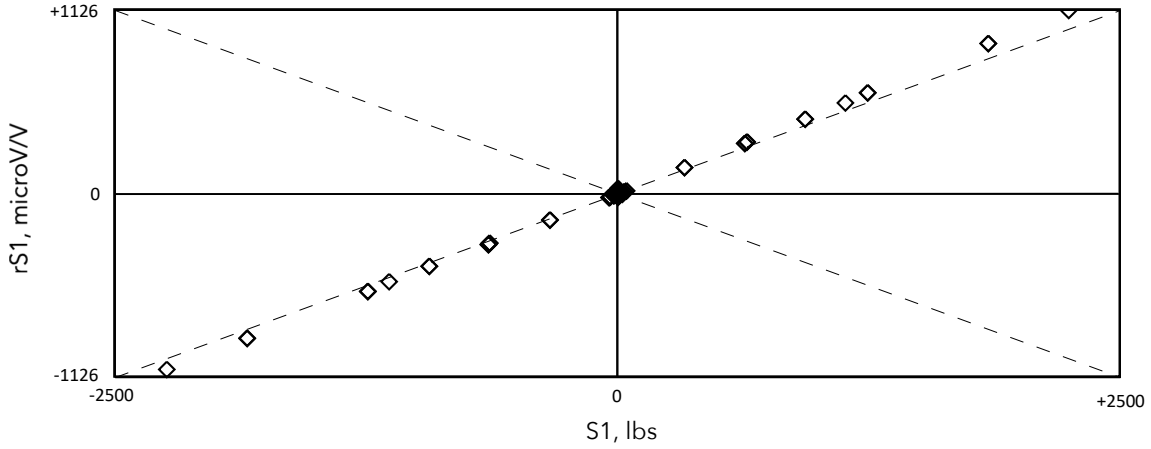

Fig. 7–1 Forward side force bridge output plotted versus the forward side force.

superficially viewed, as if the data plotted in Fig. 7–1 falls on a straight line. However, a closer examination reveals that the slope of the forward side force bridge output shifts by a small amount when the forward side force changes sign. This phenomenon accounts for about 22 *microV/V* at load capacity if the bi–directional part of the output at load capacity is extracted and plotted versus the forward side force (see Fig. 7–2 below).

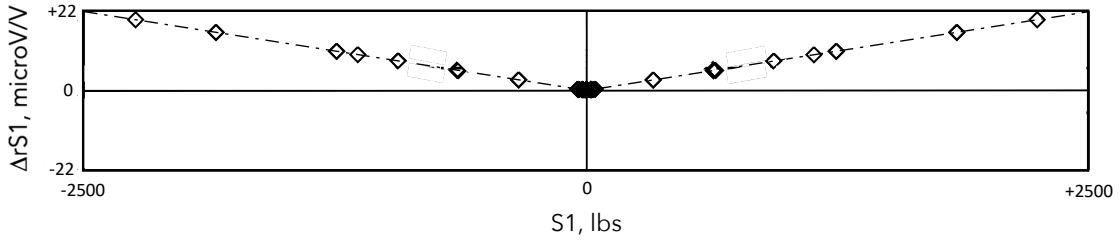

Fig. 7-2 Bi–directional part of the forward side force bridge output.

† The idea of using the absolute value function for the description of bi–directional output characteristics appears to have originated in Europe (Ref. [79], p. 5). *Galway* recognized benefits of this idea, extended it to higher–order terms, and combined it with the global regression analysis approach (Ref. [6], pp. 21–23).

The impact of bi–directional characteristics on the electrical outputs of a Task/Able balance is small but cannot be neglected. Therefore, absolute value terms of either the primary bridge outputs or the primary load components need to be included in regression models of balance calibration data if either the *Non–Iterative Method* or the *Iterative Method* is used for the data analysis and balance load prediction.

Important connections between (i) the chosen load prediction method, (ii) the bridge output format, and (iii) the use of absolute value terms in the regression models of balance data exist. They must be understood so that errors in the balance load prediction are kept to a minimum. The connections are discussed in detail in the next section.

7.2 Bridge Output Format Choices for Bi–directional Outputs

Connections between the bridge output format and the absolute value term can easily be understood if four different combinations of output format and data analysis method are examined. Table 7–1 below describes the four possible combinations.

Table 7–1: Possible combinations of load prediction method and bridge output format.

Combination	Load Prediction Method	Bridge Output Format
1†	Non–Iterative Method (App. 9)	Raw Output (App. 6)
2	Non–Iterative Method (App. 9)	Difference Type 1 (App. 6)
3	Iterative Method (App. 10)	Raw Output (App. 6)
4	Iterative Method (App. 10)	Difference Type 1 (App. 6)

†Non–Iterative Method cannot be used with format Raw Output if outputs are bi–directional.

Let us assume that the *Non–Iterative Method* is used for the load prediction. Then, loads are fitted as a function of the outputs by using the regression model that is defined in App. 9. Consequently, the loads are the dependent variables. They have to be plotted on the vertical axis of the Cartesian coordinate system that shows characteristics of a bridge with bi–directional outputs. Now, Combination 1 of Table 7–1 is examined. Then, a plot of the primary bridge load versus the primary bridge output could look like the graph that is shown in Fig. 7–3 below if the outputs are described using format *Raw Output*. The

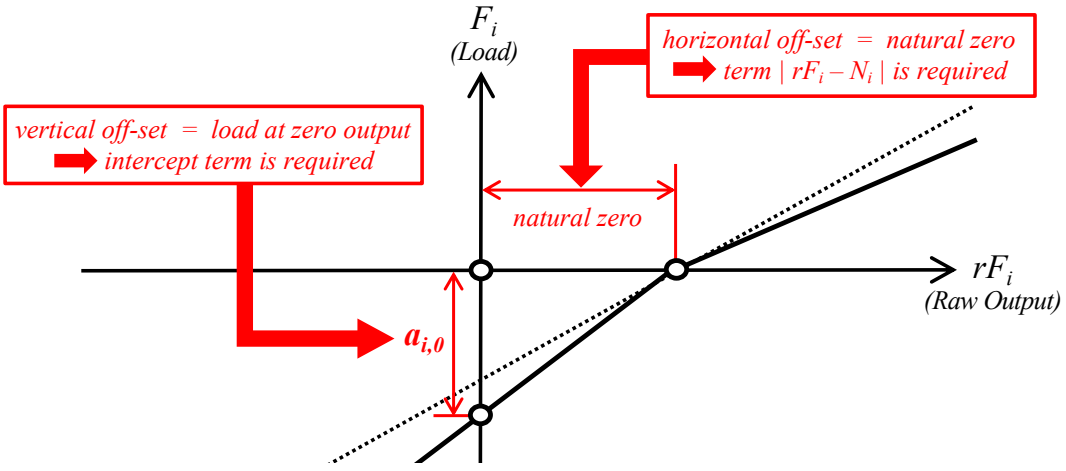

Fig. 7–3 Combination 1 ≡ Primary load plotted versus a bi–directional primary output that is formatted as *Raw Output*.

horizontal off–set of the solid line from the origin of Fig. 7–3 equals the natural zero of the bridge. Consequently, a term like $|rF_i - N_i|$ would be needed in the regression model of the load F_i in order to model the bi–directional characteristics of the bridge correctly. Unfortunately, this regression model term is not a part of the traditional list of terms that are given in App. 9. Therefore, the format *Raw Output* is not recommended for direct use with the *Non–Iterative Method* whenever a balance has bi–directional outputs. Numerical errors associated with the combined use of the terms rF_i and $|rF_i|$ instead of the terms rF_i and $|rF_i - N_i|$ in the regression model of the load are expected to be too large.

In the next step, it is assumed that Combination 2, i.e., the *Non–Iterative Method* and output format *Difference Type 1*, is used to analyze the data. Then, a plot of the primary bridge load versus the transformed output of a bi–directional balance bridge could look like the graph that is shown in Fig. 7–4 below. In that case, the horizontal off–set of the solid

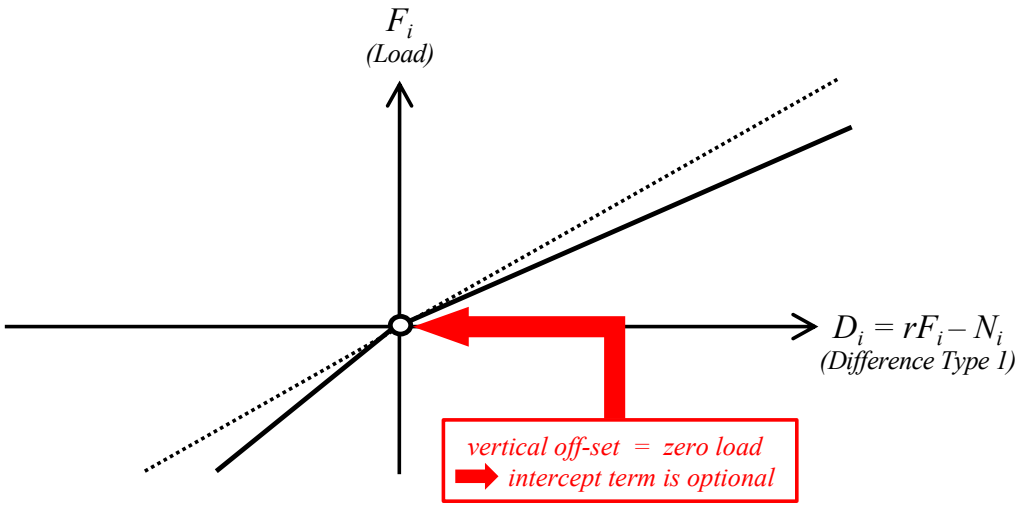

Fig. 7–4 Combination 2 ≡ Primary load plotted versus a bi–directional primary output that is formatted as *Difference Type 1*.

line from the origin has disappeared. Now, the intercept term of the regression model of the load becomes an approximation of zero absolute load. This case can be processed by using the *Non–Iterative Method* whenever (i) the linear term $D_i = rF_i - N_i$ and (ii) the absolute value term $|D_i| = |rF_i - N_i|$ are used in the regression model of the load.

Alternatively, the *Iterative Method* may be used instead of the *Non–Iterative Method* for the balance load prediction. Then, electrical outputs are fitted as a function of the balance loads by using the regression model that is defined in App. 10. Consequently, the electrical outputs are the dependent variables of the least squares fit of the balance calibration data. Now, Combination 3 can be examined that is described in Table 7–1. In this case, the electrical outputs are described as *Raw Outputs*. Then, the output of a bi–directional balance bridge plotted versus the related primary bridge load could look like the graph that is shown in Fig. 7–5 below. The solid black line in Fig. 7–5 represents the functional relationship between electrical output and load. The vertical off–set of the solid line from the coordinate system origin corresponds to the natural zero of the given bridge. This value can be described by the intercept term in the regression model of the output. Then, the bi–directional part of the output can be modeled in the regression model of the raw output by the absolute value $|F_i|$ of the related primary load component.

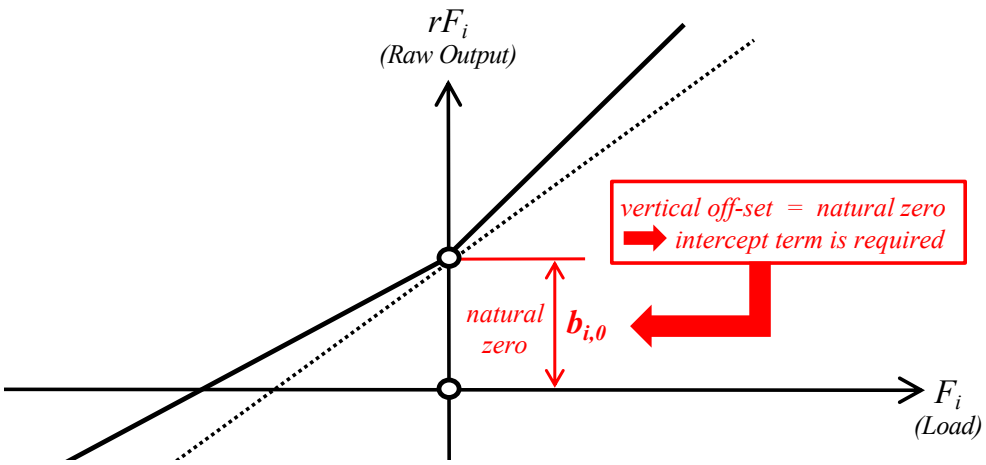

Fig. 7–5 Combination 3 ≡ *Raw Output* plotted versus the primary load of a bi–directional bridge.

Finally, Combination 4 is investigated. Now, all electrical outputs are shifted by the natural zero of the bridge. Consequently, output format *Difference Type 1* is used to analyze the balance data. Then, a plot of the shifted output versus the related primary bridge load could look like the graph that is shown in Fig. 7–6 below.

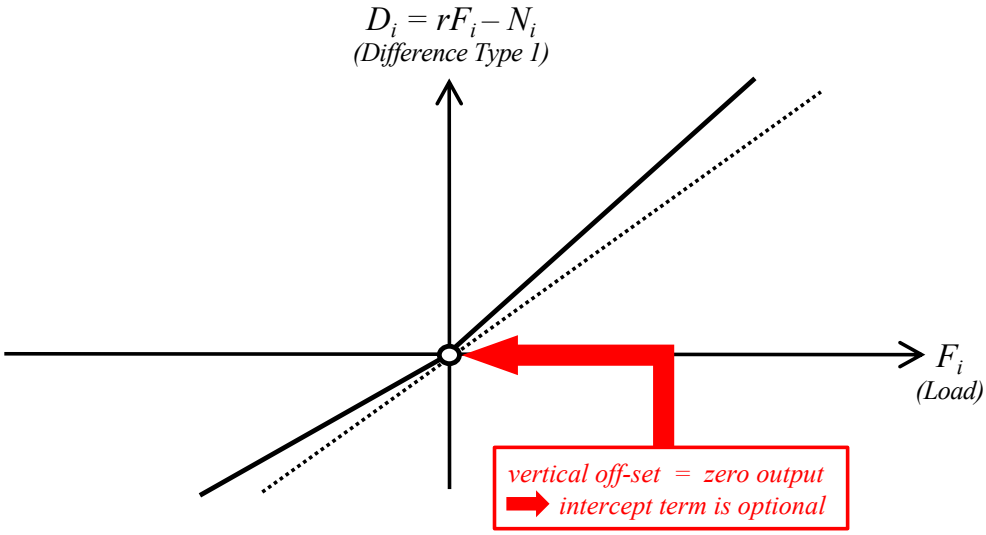

Fig. 7–6 Combination 4 ≡ *Difference Type 1* plotted versus the primary load of a bi–directional bridge.

The vertical off–set of the solid line from the origin has disappeared. Consequently, the intercept term in the regression model of the output difference becomes an approximation of zero output. In principle, the bi–directional characteristics of the two bridge output format options shown in Figs. 7–5 and 7–6 can successfully be processed by using the *Iterative Method* whenever at least (i) the intercept term, (ii) the linear term F_i, and (iii) the absolute value term $|F_i|$ are contained in the regression model of the output. Again, the use of the intercept term is optional whenever an analyst selects output format *Difference Type 1* for the description of balance data.

It is recommended to test if a bridge output has bi–directional characteristics. A semi–empirical test was developed for that purpose that is discussed in the next section.

7.3 Test of Bi–directional Characteristics

7.3.1 General Remarks

The following description of the bi–directional behavior of a bridge output is given in the literature (taken from Ref. [7], p. 12):

> . . . it is not uncommon for the load/output relationship of balances, especially those of multi–piece design, to exhibit some dependency on the sign of the strain in the measuring elements. . . .

The existence of bi–directional characteristics of the outputs is the justification for the use of absolute value terms in the regression models of balance data. Therefore, the following recommendation is made in the literature (taken from Ref. [7], p. 12):

> . . . this asymmetric load behavior can be modeled effectively by an extension of the basic math model to include terms combining the component loads with their absolute values. . . .

The authors of Ref. [7] only provided a qualitative description of the bi–directional behavior of the bridge outputs of a balance. They did not address three questions:

> Does every strain–gage balance of multi–piece design have bi–directional outputs ?
> Does every bridge of a multi–piece balance have bi–directional characteristics ?
> How large must the bi–directional part of an output be in order to be significant ?

Therefore, a semi–empirical test was developed for balance calibration data that systematically investigates the bi–directional characteristic of a balance bridge. The test makes it possible to quantify the characteristic for each balance type and bridge output combination. The original version of the test was intended for use with the *Iterative Method*. Key elements of the test were recently improved so that the test can also work with the *Non–Iterative Method* (see Ref. [33] for details).

7.3.2 Test Description

The improved semi–empirical test can be defined after making three assumptions: (i) the balance calibration data is described in the design format of the balance, i.e., each bridge output is primarily proportional to a single load component that, when applied, is responsible for $\approx 90\,\%$ or more of the output; (ii) the analyst chooses a temporary regression model for the test that includes linear and principal absolute value terms; (iii) the bi–directional part and the bridge output at load capacity are expressed in electrical units. Then, the test can be described as follows:

Semi–empirical Test of Bi–directional Output Characteristics

A bridge output is bi–directional if (i) the absolute value of the output's *bi–directional part at load capacity* exceeds the threshold[†] of $0.5\,\%$ of the absolute value of the *bridge output at load capacity*, and, (ii) the *p–value* of the *principal absolute value term* of the temporary regression model of the balance data is less than 0.001.

[†] A less conservative threshold of 0.3 % may be used for the test if (i) the given balance calibration data set has highly precise & repeatable output measurements near load capacity, and (ii) the largest positive and negative load values of each load component are of similar magnitude.

A temporary regression model is used for the test because absolute value terms may be omitted in the final model of the data if the bridge outputs are not bi–directional. The expressions *bi–directional part at load capacity*, *bridge output at load capacity*, *p–value*, and *principal absolute value term* are used in the definition of the test. They need to be explained in the context of (i) the given balance calibration data and (ii) the two data analysis methods. It is best to describe the expressions by using an example. Let us assume that the bi–directional characteristic of an axial force bridge output is examined. Then, the following statements can be made:

• The *bi–directional part at load capacity* is defined as the difference between (i) the output of the axial force bridge at axial force capacity and (ii) the linear part of the output at axial force capacity.

• The *bridge output at load capacity* equals the difference between the raw output of the axial force bridge at axial force capacity and the natural zero of the axial force bridge.

• The *principal absolute value term* of the temporary regression model equals the absolute value of the difference between the axial force bridge output and the natural zero if the *Non–Iterative Method* is used for the data analysis.

• The *principal absolute value term* of the temporary regression model equals the absolute value of the axial force if the *Iterative Method* is used for the data analysis.

• The *p–value* is used to assess if the *principal absolute value term* is statistically significant. A significant regression model term has a very small *p–value*. The threshold of 0.001 is often used to distinguish a significant from an insignificant term.

The *bi–directional part at load capacity* must be determined from the coefficients of the temporary regression model that the *Non–Iterative* and the *Iterative Method* use for the data analysis. These calculations are explained in the following two sections.

7.3.3 Bi–directional Part (Non–Iterative Method)

The *Non–Iterative Method* fits the tare corrected balance loads as a function of the output differences relative to the natural zeros. Then, the temporary regression model of a load component can be defined by the relationship that is given in Eq. (7.1) below.

Temporary Regression Model of a Load Component

$$F \;=\; a_0 \;+\; \ldots \;+\; a_\eta \;\cdot\; (\; rF{-}N \;) \;+\; \ldots \;+\; a_\psi \;\cdot\; |\; rF{-}N \;| \;+\; \ldots \qquad (7.1)$$

Symbol F represents the fitted primary load component. It is associated with the primary bridge output that symbol rF describes. The variable $rF{-}N$ equals the difference between the raw output and natural zero of the bridge. The coefficient a_0 describes the intercept term, a_η is the coefficient of the output difference of the primary bridge, and a_ψ is the coefficient of the absolute value of the output difference of the primary bridge.

It is helpful for the calculation of the bi–directional part of an output difference to identify the metric in a schematic. Figure 7–7 below shows the definition of the *bi–directional part at load capacity* from the viewpoint of the temporary regression model of a load component. Therefore, load F, i.e., the dependent variable, is shown on the vertical axis of the Cartesian coordinate system. It is plotted versus the output difference $rF{-}N$, i.e.,

the independent variable. The gray region contains the bi–directional parts of all output differences of the bridge. It is concluded from Fig. 7–7 that the *bi–directional part at load*

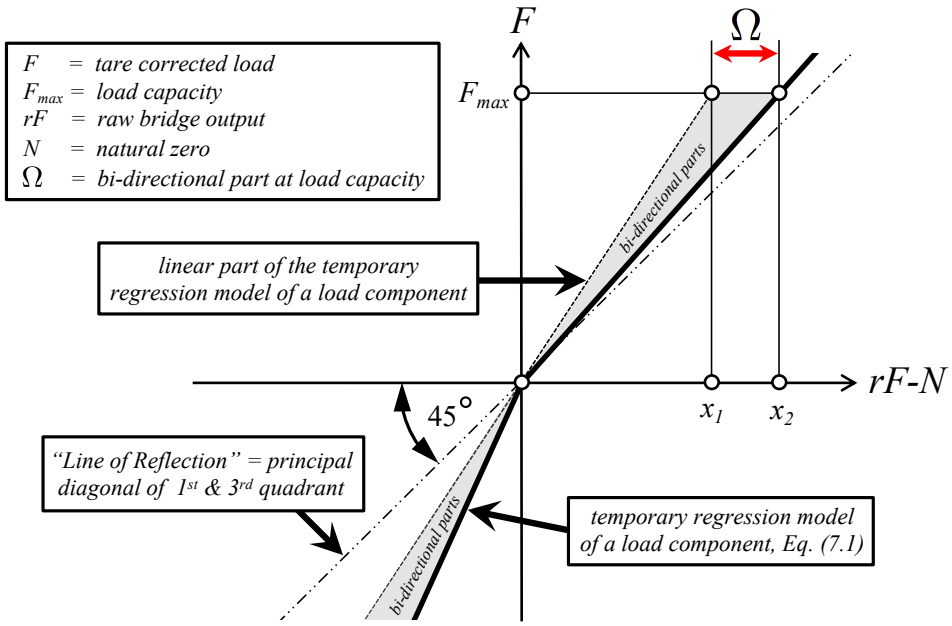

Fig. 7–7 Definition of the *bi–directional part at load capacity* when viewed from the perspective of the temporary regression model of a load component.

capacity is the difference of two coordinates. The first coordinate, i.e., x_1, can be obtained from a simplified version† of the temporary regression model of a load component that consists of (i) the intercept and (ii) the principal linear term. Then, we get the equation

$$Eq.\,(7.1) \quad \Longrightarrow \quad F_{max} \;=\; a_0 \;+\; a_\eta \;\cdot\; x_1 \tag{7.2a}$$

where F_{max} is the load capacity. Now, after solving Eq. (7.2a) for x_1, we get:

$$x_1 \;=\; \Big[\; F_{max} \;-\; a_0 \;\Big] \;/\; a_\eta \tag{7.2b}$$

Similarly, the second coordinate, i.e., x_2, can be obtained from a simplified version† of the temporary regression model of a load component that consists of (i) the intercept, (ii) the principal linear term, and (iii) the *principal absolute value term*. We get:

$$Eq.\,(7.1) \quad \Longrightarrow \quad F_{max} \;=\; a_0 \;+\; a_\eta \;\cdot\; x_2 \;+\; a_\psi \;\cdot\; |\, x_2 \,| \tag{7.3a}$$

It is also known that $|x_2|$ equals x_2 in the first quadrant of the coordinate system. Then, after replacing $|x_2|$ with x_2 in Eq. (7.3a) and solving the result for x_2, we get:

$$x_2 \;=\; \Big[\; F_{max} \;-\; a_0 \;\Big] \;/\; \Big[\; a_\eta \;+\; a_\psi \;\Big] \tag{7.3b}$$

†The simplified versions of the temporary regression model of a load component are sufficiently accurate for the determination of the two coordinates x_1 and x_2.

Finally, after subtracting the right–hand side of Eq. (7.2*b*) from the right–hand side of Eq. (7.3*b*) and simplifying the result, the *bi–directional part at load capacity* is obtained:

Bi–directional Part at Load Capacity

$$\Omega \;=\; x_2 \;-\; x_1 \;\;=\;\; \frac{(-a_\psi)\;\cdot\;(\;F_{max}\;-\;a_0\;)}{a_\eta\;\cdot\;(\;a_\eta\;+\;a_\psi\;)} \qquad (7.4a)$$

It is important to mention that the absolute value of the right–hand side of Eq. (7.4*a*) is compared with the threshold of 0.5 % of the absolute value of the *bridge output at load capacity* when the semi–empirical test is applied. It is also useful to define the bi–directional part for all load values (F) and not just for the load capacity (F_{max}). Then, by inspection, we get the following relationship from Eq. (7.4*a*) above:

$$\Omega' \;\;=\;\; \frac{(-a_\psi)\;\cdot\;(\;|F|\;-\;a_0\;)}{a_\eta\;\cdot\;(\;a_\eta\;+\;a_\psi\;)} \qquad (7.4b)$$

In the next section, the *bi–directional part at load capacity* is derived that results from the application of the *Iterative Method* to balance calibration data.

7.3.4 Bi–directional Part (Iterative Method)

Alternatively, the *Iterative Method* may be used to analyze balance calibration data. This approach first fits electrical outputs of the balance bridges as a function of the loads. Afterwards, an iteration equation is constructed from the regression coefficients of the outputs so that loads can be predicted from the outputs during a wind tunnel test.

The definition of the *bi–directional part at load capacity* has to start with the description of the temporary regression model of a bridge output that the *Iterative Method* uses. It is assumed that the difference between a raw output and the natural zero of a balance bridge is fitted as a function of the tare corrected balance loads. Then, the chosen temporary regression model of a bridge output difference can be described by Eq. (7.5) below. The

Temporary Regression Model of a Bridge Output Difference

$$rF{-}N \;\;=\;\; b_0 \;+\; \ldots \;+\; b_\eta \;\cdot\; F \;+\; \ldots \;+\; b_\psi \;\cdot\; |\;F\;| \;+\; \ldots \qquad (7.5)$$

expression $rF-N$ represents the output difference of the primary bridge relative to its natural zero. The symbol F is the primary load component associated with bridge output rF. The coefficient b_0 describes the intercept term, b_η is the coefficient of the primary load, and b_ψ is the coefficient of the absolute value of the primary load.

Again, it is helpful for the derivation of the *bi–directional part at load capacity* to describe the metric in a schematic. Figure 7–8 below shows the definition of the bi–directional part from the viewpoint of the temporary regression model of the bridge output difference. The output difference $rF-N$, i.e., the dependent variable, is shown on the vertical axis of the Cartesian coordinate system. It is plotted versus the primary load component F, i.e., the independent variable. The gray region contains the bi–directional parts of all output differences of the bridge. The graph shown in Fig. 7–8 can directly be

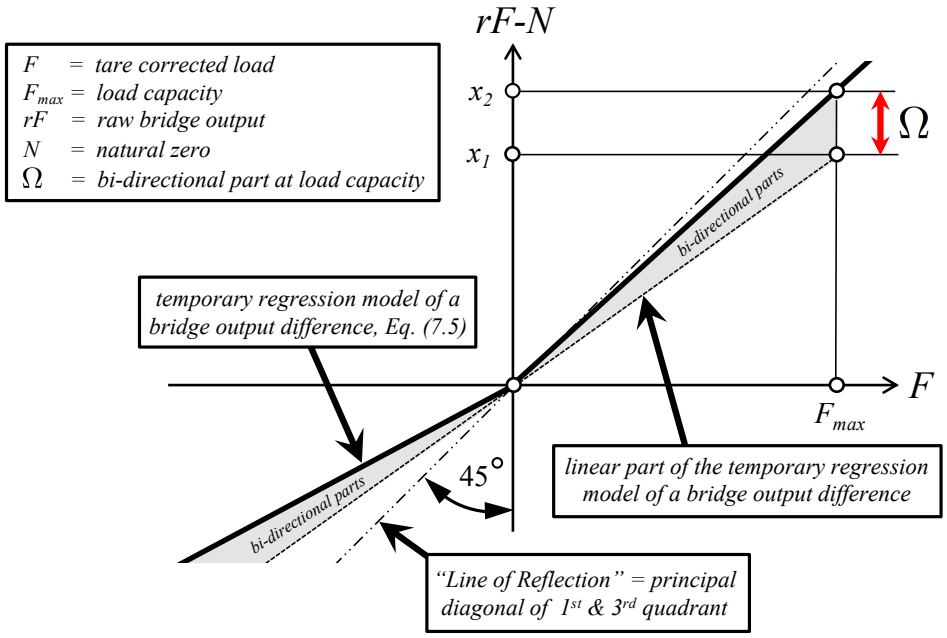

Fig. 7–8 Definition of the *bi–directional part at load capacity* when viewed from the perspective of the temporary regression model of a bridge output difference.

obtained from the graph shown in Fig. 7–7 (and vice versa). It is only required to reflect all data points about the straight line that is identified as the *Line of Reflection* in both graphs. This connection is valid as the relationship between the tare corrected load and the related bridge output difference must be reversible. In that case, the independent and dependent variables of a balance data set can be switched.

It is observed in Fig. 7–8 that the *bi–directional part at load capacity* is the difference of two coordinates. The first coordinate, i.e., x_1, can be derived from a simplified version[†] of the temporary regression model of an output difference that consists of (i) the intercept and (ii) the principal linear term. Then, assuming that F_{max} is the load capacity, we get:

$$Eq.\,(7.5) \quad \Longrightarrow \quad x_1 \quad = \quad b_0 \; + \; b_\eta \; \cdot \; F_{max} \tag{7.6a}$$

The second coordinate, i.e., x_2, can be obtained from a simplified version[†] of the temporary regression model of an output difference that consists of (i) the intercept, (ii) the principal linear term, and (iii) the *principal absolute value term*. Now, we get:

$$Eq.\,(7.5) \quad \Longrightarrow \quad x_2 \quad = \quad b_0 \; + \; b_\eta \; \cdot \; F_{max} \; + \; b_\psi \; \cdot \; |F_{max}| \tag{7.6b}$$

[†]The simplified versions of the temporary regression model of a bridge output difference are sufficiently accurate for the determination of the two coordinates x_1 and x_2.

It is also known that $|F_{max}|$ equals F_{max} in the first quadrant of the coordinate system. Then, after replacing $|F_{max}|$ with F_{max} in Eq. (7.6*b*), we get:

$$x_2 \;=\; b_0 \;+\; b_\eta \;\cdot\; F_{max} \;+\; b_\psi \;\cdot\; F_{max} \qquad (7.6c)$$

Finally, after subtracting the right–hand side of Eq. (7.6*a*) from the right–hand side of Eq. (7.6*c*), the *bi–directional part at load capacity* is obtained:

Bi–directional Part at Load Capacity

$$\Omega \;=\; x_2 \;-\; x_1 \;=\; b_\psi \;\cdot\; F_{max} \qquad (7.7a)$$

It is important to mention that the absolute value of the right–hand side of Eq. (7.7*a*) above is compared with the threshold of 0.5 % of the absolute value of the *bridge output at load capacity* when the semi–empirical test is applied. It is also useful to define the bi–directional part for all load values (F) and not just for the load capacity (F_{max}). Then, by inspection, we get the following relationship from Eq. (7.7*a*) above.

$$\Omega' \;=\; b_\psi \;\cdot\; |F| \qquad (7.7b)$$

The relationship defined in Eq. (7.7*b*) above, similar to Eq. (7.4*b*), may be used to plot the bi–directional part of a bridge output difference as a function of the tare corrected balance loads in order to visualize the connection between the bi–directional characteristic of a bridge output and the absolute value function.

The *bi–directional part at load capacity*, i.e., Ω, is a physical characteristic that does not depend on the method used for the regression analysis of the calibration data. Therefore, a relationship between the regression coefficient sets used in Eqs. (7.4*a*) and (7.7*a*) exists that is derived in the next section.

7.3.5 Relationship between Regression Coefficient Sets

A relationship between the regression coefficient sets used in Eqs. (7.4*a*) and (7.7*a*) exists that can be understood if the temporary regression model of a load component, i.e., Eq. (7.1), is examined in more detail. The temporary regression model of a load component was developed as a function of the output difference of the balance bridges relative to the corresponding natural zeros. The natural zeros themselves are the outputs of the bridges when the balance is at zero absolute load. Consequently, all terms on the right–hand side of Eq. (7.1) are zero with exception of the intercept if the left–hand side is zero. In other words, the intercept may be interpreted as a least squares approximation of zero absolute load if it is included in the temporary regression model of a load component. This conclusion also means that the use of the intercept is optional. Therefore, coefficient a_0 can be omitted whenever differences between a raw output of a bridge and its natural zero are used to fit a balance load. Then, the coefficient b_ψ on the right–hand side of Eq. (7.7*a*)

must equal the fraction $(-a_\psi)/\{a_\eta \cdot (a_\eta + a_\psi)\}$ on the right–hand side of Eq. (7.4a) as the *bi–directional part at load capacity* is a physical characteristic of the balance. This result can be summarized as follows:

Relationship between Regression Coefficient Sets

$$a_0 \approx 0 \quad \Longrightarrow \quad b_\psi = \frac{-\,a_\psi}{a_\eta \cdot (\,a_\eta + a_\psi\,)} \qquad (7.8)$$

The relationship above can be used to compare any regression model of a load component with the related regression model of a bridge output difference as long as the following two conditions are fulfilled: (i) the bridge output is known to be bi–directional; (ii) the use of the intercept is optional in the regression model of the load component.

7.4 Discussion of Examples

7.4.1 General Remarks

The semi–empirical test was applied to calibration data of two balance types to illustrate typical test results. Key elements of the verbal description of the semi–empirical test need to be revisited. Again, a bridge output is considered bi–directional if two conditions are fulfilled. First, the absolute value of the *bi–directional part at load capacity* must exceed the threshold of 0.5 % of the absolute value of the *bridge output at load capacity*. In addition, the *p–value* of the *principal absolute value term* of the regression model must be less than 0.001. The two conditions are summarized below. The term $|rF-N|$ is the

Bridge output is bi–directional if two conditions are fulfilled ...

$$\underbrace{\left|\begin{array}{c} bi-directional\ part \\ at\ load\ capacity \end{array}\right|}_{|\Omega|} > \underbrace{0.005 \times \left|\begin{array}{c} bridge\ output\ at \\ load\ capacity \end{array}\right|}_{\Theta\ \equiv\ output\ threshold}$$

$$\begin{array}{c} p-value\ of\ the\ principal\ absolute\ value \\ term\ of\ the\ temporary\ regression\ model \end{array} < 0.001$$

principal absolute value term if the given regression model fits a primary load component F of the balance. Similarly, the term $|F|$ is the *principal absolute value term* if the given regression model fits a primary bridge output difference $|rF-N|$ of the balance.

Test results for the two chosen balance types are presented in the next two sections. In addition, physical explanations for observed or detected bi–directional output characteristics are provided whenever possible.

7.4.2 MK40B Balance (Task/Able Design)

The first example uses data from a 2019 machine calibration of NASA's MK40B six–component multi–piece force balance to illustrate the application of the semi–empirical test. Figure 7–9 below shows the MK40B balance in its storage box. The MK40B is a

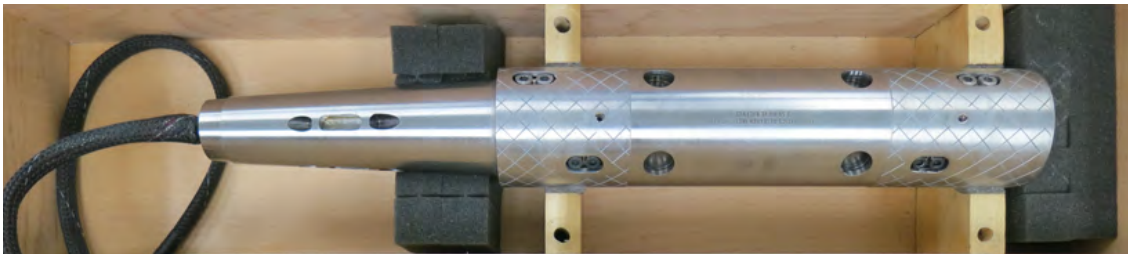

Fig. 7–9 NASA's 2.5 inch diameter MK40B six–component force balance.

balance of Task/Able design that was manufactured by Aerophysics Research Instruments of Corona, California. Table 7–2 below summarizes load capacities of the MK40B balance

Table 7–2: Load capacities of the MK40B Task/Able balance ($lbs \equiv$ pounds of force).

$N1$, lbs	$N2$, lbs	$S1$, lbs	$S2$, lbs	AF, lbs	RM, in–lbs
3500	3500	2500	2500	400	8000

in force balance format. The calibration of the balance was done in Calspan's Automatic Balance Calibration System (ABCS). The applied calibration load schedule consisted of a total of 1646 data points that were distributed across 17 load series. Up to three load components were applied simultaneously during the calibration. The data set was independently analyzed by using both the *Non–Iterative Method* and the *Iterative Method*.

Table 7–3 below shows test results for each bridge output that were obtained after applying the *Non–Iterative Method* to the machine calibration data. Absolute value terms of the output differences relative to the natural zeros were included in the temporary regression models of the balance loads so that the test could be performed. The first row

Table 7–3: Test results for the MK40B balance (Non–Iterative Method).

	$rN1$	$rN2$	$rS1$	$rS2$	rAF	rRM
Θ, microV/V	6.89	8.35	7.00	7.46	8.46	7.29
$\lvert\Omega\rvert$, microV/V	$4.57 < T$	$13.10 > T$	$16.90 > T$	$13.86 > T$	$5.21 < T$	$1.70 < T$
p–value, $\lvert rF - N\rvert$	< 0.001	< 0.001	< 0.001	< 0.001	< 0.001	< 0.001
Bi–directional ?	NO	**YES**	**YES**	**YES**	NO	NO

in Table 7–3 lists the output threshold (Θ) for each bridge output. It equals 0.5 % of the absolute value of the *bridge output at load capacity*. The second row has the absolute value of the *bi–directional part at load capacity* ($|\Omega|$) that was computed using Eq. (7.4*a*). The third row has the *p–values* of the *principal absolute value terms* of the regression model of each fitted load component. For example, the *principal absolute value term* of the forward normal force is the difference between the forward normal force bridge output and the related natural zero of the bridge. It is observed that three of the six bridge outputs of the MK40B balance simultaneously fulfill both conditions that are needed for an output to be bi–directional. Therefore, the use of absolute value terms of the related three bridge output differences in the final regression models of the loads of the MK40B balance can be justified if the *Non–Iterative Method* is applied.

It is useful to compare the predicted values of the *bi–directional part at load capacity* that are computed by using either the regression coefficients of the loads (*Non–Iterative Method*) or the regression coefficients of the output differences (*Iterative Method*). Table 7–4 below lists corresponding values for the MK40B balance. The agreement between

Table 7–4: Computed *bi–directional part at load capacity* for the MK40B balance.

	$rN1$ microV/V	$rN2$ microV/V	$rS1$ microV/V	$rS2$ microV/V	rAF microV/V	rRM microV/V
Non–Iterative Method, Eq. (7.4a)	+4.57	+13.10	+16.90	+13.86	+5.21	−1.70
Iterative Method, Eq. (7.7a)	+4.93	+11.25	+16.49	+13.35	+5.21	−1.71

the values is excellent as long as small numerical differences are ignored. This result is no surprise because the *bi–directional part at load capacity* is a physical property of the balance. Therefore, it is independent of the method that is used for the data analysis.

Figure 7–10 below shows a plot of the forward side force bridge output versus the tare corrected forward side force of the MK40B balance. The plot was obtained during the analysis of the data. The outputs range from approximately −1401 to +1401 *microV/V*.

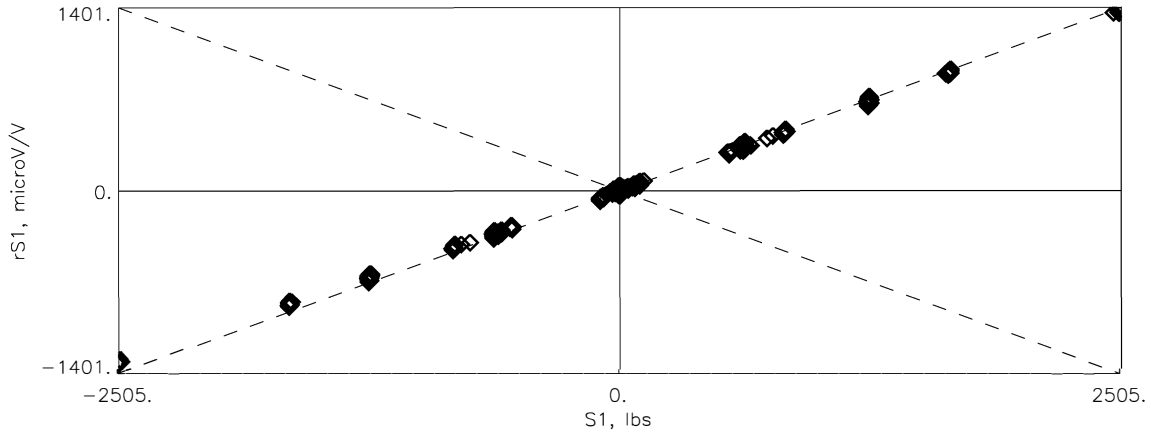

Fig. 7–10 Plot of the forward side force bridge output versus the forward side force of the MK40B balance.

Figure 7–11 below shows the *bi–directional part at load capacity* of the forward side force bridge output plotted versus the forward side force of MK40B balance. The absolute value of

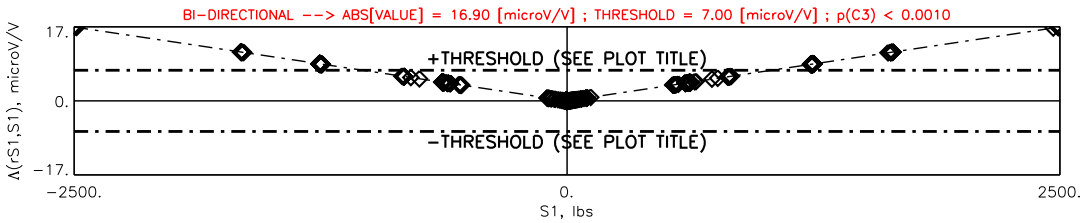

Fig. 7–11 The *bi–directional part at load capacity* of the forward side force bridge output plotted versus the forward side force (Eq. (7.4*b*), Non–Iterative Method).

the *bi–directional part at load capacity* was estimated to be 16.90 *microV/V* by using the coefficients of the regression model of the forward side force as input (see also second row & fourth column of Table 7–3). It is about 1.2 % of the output at load capacity. Consequently, bi–directional properties of the forward side force bridge output are significant and cannot be neglected. It must be mentioned that the bi–directional behavior is significant but still very small when compared with the overall range of the forward side force bridge output. Therefore, it cannot be detected by visual examination if an analyst plots the forward side force output versus the forward side force (compare Fig. 7–10 with Fig. 7–11).

It is important to identify the most likely cause of the bi–directional characteristic of a balance bridge in order to gain confidence in the chosen regression model's ability to model the physical behavior of the balance. The bi–directional characteristic can be interpreted as an asymmetry in the first derivative if a bridge output is plotted versus the related load component. This asymmetry may be associated with some kind of geometric asymmetry that is hidden in the design of the component parts of the balance. Figure 7–12 below shows, for example, parts of a typical Task/Able balance. The balance has a metric outer sleeve. It is the physical interface to the wind tunnel model. The balance also has a non–metric inner rod. It is the interface to the balance support system. Circumferential wall thickness variations of both the outer sleeve and inner rod can clearly be seen. They are a known design feature of Task/Able balances. The wall thick–

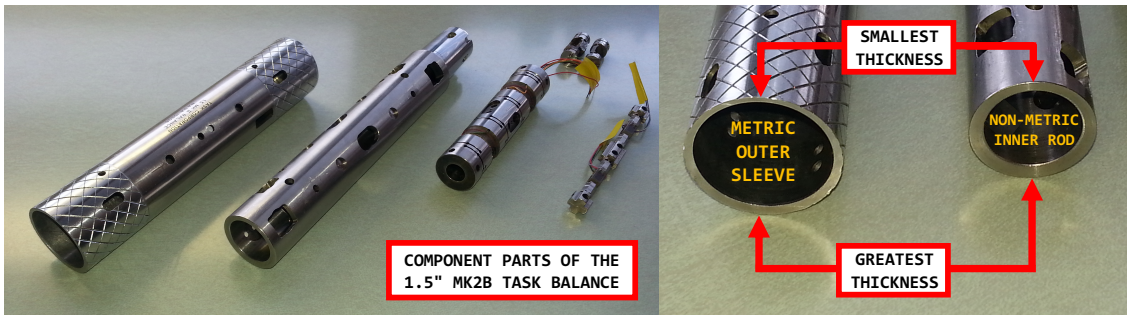

Fig. 7–12 Wall thickness variations of the metric outer sleeve and the non–metric inner rod of a Task/Able force balance.

ness variations are responsible for a change of the elastic behavior of the balance (see also related discussions in Ref. [2], p. 237). The change can be observed whenever (i) a load is applied perpendicular to the roll axis and (ii) the load changes sign. These loads are the forward & aft normal forces and the forward & aft side forces. The change in elastic behavior is observed as a change of the slope when an output is plotted versus the related

primary load component. The change is modeled during the analysis of balance calibration data by using both linear and absolute value terms in the chosen regression models.

Magnitudes of the circumferential wall thickness variations of a Task/Able balance are highly dependent on the design load capacities of the balance. The author observed over the years that the magnitudes of the bi–directional characteristic of the two normal force bridges and the two side force bridges of a Task/Able balance are often very close in magnitude. However, magnitudes of the bi–directional output at capacity of the side force bridge pair are often higher than corresponding values for the normal force bridge pair. These observations clearly point towards a direct connection between the bi–directional characteristics of the normal and side force bridges and the circumferential wall thickness variations of the metric and non–metric component parts of a Task/Able balance.

It is useful to compare the magnitude of the *bi–directional part at load capacity* for a family of Task/Able balances in order to better support the author's conclusions. Therefore, both the *Non–Iterative Method* and the *Iterative Method* were applied to calibration data of NASA's MK29B, MK40A, and MK4A balances so that an estimate of the *bi–directional part at load capacity* could be computed by using both Eq. (7.4a) and Eq. (7.7a). Table 7–5 below lists results for the three balances. The first value in each box

Table 7–5: *Bi–directional part at load capacity* for a family of Task/Able balances.

Balance (diameter)	$rN1$ microV/V	$rN2$ microV/V	$rS1$ microV/V	$rS2$ microV/V	rAF microV/V	rRM microV/V
MK29B	+7.65	+10.68	+12.45	+18.52	+0.14	–1.41
(2.0 in)	+7.30	+9.81	+10.89	+18.46	+0.17	+1.63
MK40A	+10.07	+13.49	+23.12	+24.70	+0.33	–1.33
(2.5 in)	+10.63	+12.71	+22.53	+23.76	+0.32	–1.26
MK4A	+4.78	+7.75	+7.53	+4.58	+0.02	–0.27
(4.0 in)	+4.82	+7.58	+7.38	+4.80	+0.00	–0.35

was obtained after applying Eq. (7.4a). This equation uses coefficients of the regression models of the tare corrected balance loads as input. The second value in each box was obtained after applying Eq. (7.7a). This alternate equation uses coefficients of the regression models of the bridge output differences as input. Several observations can be made after examining Table 7–5 in more detail. First, values for Eq. (7.4a) and Eq. (7.7a) show excellent agreement even though they were obtained by using coefficients of fundamentally different regression models as input. In most cases, the agreement between the values is on the order of 1.0 $microV/V$ or better. It can also be seen that the magnitude of the values for the normal and side force bridges of the balance are significantly larger than the magnitude of the values for the rolling moment and axial force bridges. This result confirms that bi–directional characteristics of the normal and side force bridges of a Task/Able balance are most likely caused by circumferential wall thickness variations.

7.4.3 MC60E Balance (HiCap Design)

The second example uses data from a machine calibration of NASA's MC60E six–component multi–piece force balance to illustrate the application of the semi–empirical test. Figure 7–13 below shows the MC60E balance in its storage box. The MC60E is a

Fig. 7–13 NASA's 2.0 inch diameter MC60E six–component force balance.

force balance of HiCap design that was manufactured by Calspan Force Measurement Systems of San Diego, California. Table 7–6 below summarizes load capacities of the balance in force balance format. The calibration of the balance was performed in 2016 in

Table 7–6: Load capacities of the MC60E HiCap balance (*lbs* ≡ pounds of force).

$N1$, lbs	$N2$, lbs	$S1$, lbs	$S2$, lbs	AF, lbs	RM, in–lbs
2500	2500	1250	1250	700	5000

Calspan's Automatic Balance Calibration System. The calibration load schedule consisted of a total of 2092 data points that were distributed across 16 load series. Up to five load components were applied simultaneously during the calibration. Again, similar to the MK40B balance data, the calibration data set was independently analyzed using both the *Non–Iterative Method* and the *Iterative Method*.

Table 7–7 below shows results of the semi–empirical test for each bridge output after applying the *Iterative Method* to the calibration data. Absolute value terms of the load components were included in the temporary regression model of the output differences so that the test could be performed. The first row of the table lists the output threshold (Θ)

Table 7–7: Test results for the MC60E balance (Iterative Method).

	$rN1$	$rN2$	$rS1$	$rS2$	rAF	rRM
Θ, microV/V	5.30	5.92	2.88	3.23	4.42	6.85
$\lvert\Omega\rvert$, microV/V	$0.86 < T$	$1.06 < T$	$0.25 < T$	$0.17 < T$	$1.10 < T$	$1.39 < T$
p–value, $\lvert F\rvert$	$<$ 0.001	$<$ 0.001	0.3471	0.5432	$<$ 0.001	$<$ 0.001
Bi–directional ?	NO	NO	NO	NO	NO	NO

for each bridge. It equals 0.5 % of the absolute value of the *bridge output at load capacity*. The second row has the absolute value of the *bi–directional part at load capacity* ($\lvert\Omega\rvert$) that was obtained by using Eq. (7.7a). The third row has the *p–values* of the *principal absolute value terms* of the regression model of each output that the *Iterative Method* uses. For example, the *principal absolute value term* of the forward normal force bridge output is the forward normal force. It is observed that none of the six bridge outputs of the MC60E balance simultaneously fulfills both conditions that are needed for bridge output to be

bi–directional. Therefore, the use of absolute value terms in the final regression models of the calibration data of the MC60E balance cannot be justified.

Again, it is interesting to compare estimates of the bi–directional part at load capacity that were computed by using either Eq. (7.4*a*) or Eq. (7.7*a*). Table 7–8 below lists corresponding values. The agreement between the predicted values is excellent. This result

Table 7–8: Computed *bi–directional part at load capacity* for the MC60E balance.

	$rN1$ microV/V	$rN2$ microV/V	$rS1$ microV/V	$rS2$ microV/V	rAF microV/V	rRM microV/V
Non-Iterative Method, Eq. (7.4a)	+0.78	−2.14	+0.16	+0.44	−1.12	−1.47
Iterative Method, Eq. (7.7a)	+0.86	−1.06	+0.25	+0.17	−1.10	−1.39

is expected as the *bi–directional part at load capacity* is a physical property of the balance. In other words, it must be independent of the method that is used for the regression analysis of the balance calibration data. Figure 7–14 below shows a plot of the aft normal force

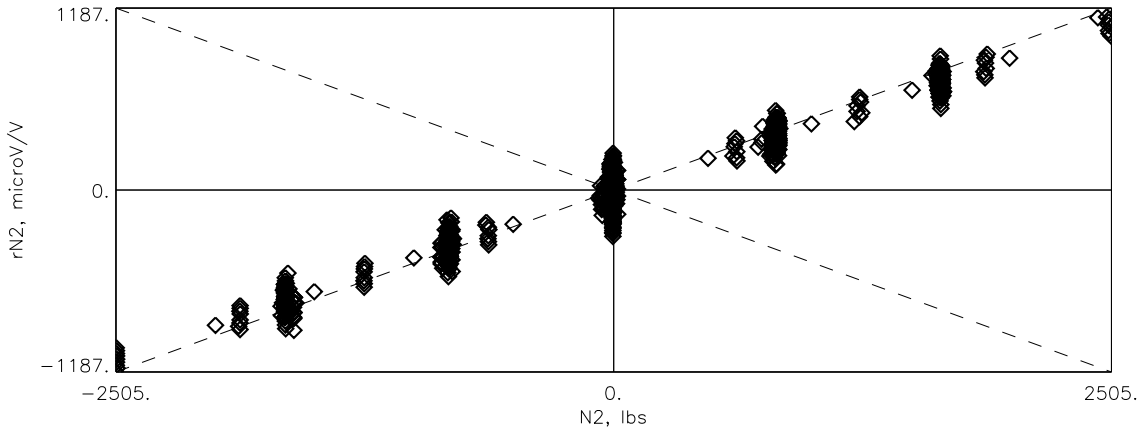

Fig. 7–14 Plot of the aft normal force bridge output versus the aft normal force of the MC60E balance.

bridge output versus the aft normal force of MC60E balance that was obtained during the regression analysis of the calibration data. The outputs ranged from approximately −1187 to +1187 *microV/V* during the calibration. Figure 7–15 below shows a plot of the *bi–directional part at load capacity* of the aft normal force bridge output versus the aft normal force of MC60E balance as an example. The absolute value of the *bi–directional*

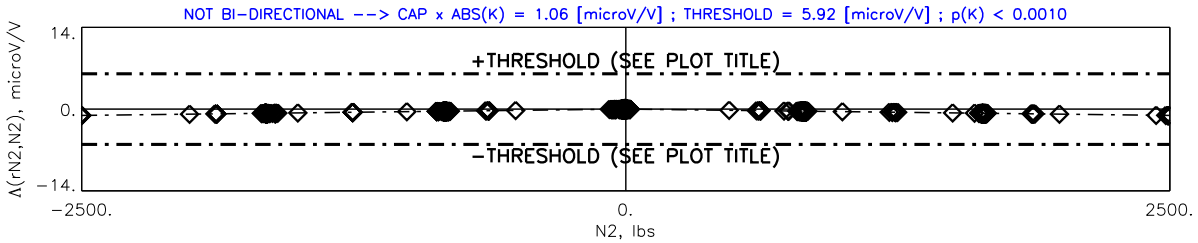

Fig. 7–15 The *bi–directional part at load capacity* of the aft normal force bridge output plotted versus the aft normal force (Eq. (7.7*b*), Iterative Method).

part at load capacity was estimated to be approximately 1.06 *microV/V* (see also second data row & second data column of Table 7–7). This value is less that 0.1 % of the output at load capacity. Consequently, bi–directional effects of the aft normal force bridge output of the MC60E balance are very small and can be neglected.

7.5 More Complex Bi–directional Characteristics

By design, the semi–empirical test defined in section 7.3.2 can only detect a bi–directional characteristic that may exist between a bridge output and the related primary balance load component. Consequently, the test cannot detect more complex bi–directional characteristics that may exist between a bridge output and a load component that is different from the primary load component of the bridge. In that case, it is suggested to investigate bi–directional characteristics by (i) temporarily including suitable groups of absolute value terms in the regression models of the balance calibration data, (ii) performing a preliminary regression analysis of the data, and (iii) assessing the importance of those absolute value terms by using the percent contribution of a regression model term as a test metric (see App. 16 for more details about the percent contribution). An analyst should use information about balance design and other subject matter knowledge as the basis for the selection of suitable absolute value term groups (available absolute value term groups are listed in App. 9, Table 9–1, and App. 10, Table 10–1). Theoretically, only very important absolute value terms should be included in the regression model of the calibration data in order to prevent over–fitting. Those absolute value terms should have a percent contribution with a magnitude that exceeds the empirical threshold of 0.5 % (percent contribution threshold is taken from App. 16, Table 16–3).

7.6 Summary and Conclusions

The use of absolute value terms in regression models of balance calibration data can only be justified if balance bridge outputs are bi–directional. Therefore, a semi–empirical test was developed that may be used to investigate the bi–directional characteristic of a bridge output. The test was defined such that it can be applied to balance calibration data that is processed by using either the *Non–Iterative* or the *Iterative Method*.

The test compares two metrics with thresholds in order to determine if a balance bridge has a bi–directional characteristic. First, the absolute value of the *bi–directional part at load capacity* has to exceed 0.5 % of the absolute value of the *bridge output at load capacity*. In addition, the *principal absolute value term* of the temporary regression model of the balance calibration data must be statistically significant. In other words, its *p–value* must be less than 0.001.

Calibration data examples of two six–component force balances were used to illustrate the application of the test. The first example discussed characteristics of a six–component balance of Task/Able design. In this case, three of the six bridge outputs have bi–directional characteristics. These bi–directional characteristics are most likely caused by circumferential wall thickness variations of the metric and non–metric component parts of the balance. The second balance is a six–component balance of HiCap design. No bi–directional characteristics of the bridge outputs were detected for this balance type. The test was also successfully applied to data of balances of single–piece design (these results are not reported in the appendix). These test results confirmed that bridge outputs of a typical single–piece balance are often not bi–directional.

The *bi–directional part at load capacity* is a very small quantity. Therefore, its reliable numerical determination highly depends on the calibration load schedule design and the overall quality of the given balance calibration data. The author observed over the years that a calibration load schedule design with positive and negative loads of similar magnitude for each load component in combination with excellent data quality will lead to the most accurate and repeatable estimates of the *bi–directional part at load capacity*.

The semi–empirical test has its limitations. It cannot be used to investigate the bi–directional characteristic between a bridge output and a load component that differs from the primary load component of the bridge. In that case, groups of absolute value terms have to be temporarily included in the regression models of the calibration data. Then, a preliminary regression analysis has to be performed. Afterwards, the percent contribution should be used as a test metric in order to determine if the use of the chosen absolute value terms in the regression models of the calibration data can be justified.

Appendix 8

Determination of Natural Zeros

8.1 General Remarks

The absolute load datum of a balance is an important reference during both balance data analysis and use. It is defined as the condition when the balance is in a weightless load state. Alternatively, as originally suggested by *Galway*, the weightless load state of a balance can be described by the raw electrical outputs of the bridges, i.e., the natural zeros that are observed when no load is acting on the balance (see Ref. [6], p. 27; *Galway's* term *buoyant component offset* is a synonym for the term *natural zero*).

The natural zeros have two important applications. First, natural zeros are measured as a part of the standard electrical checks of the balance. An unexpected large shift of the natural zeros may indicate possible damage to the balance since it was last used. In addition, it is best to describe all calibration loads of a balance relative to the datum of zero absolute load if global regression analysis is used to process the calibration data. This requirement can be fulfilled if estimates of the tare loads, i.e., estimates of loads associated with the weight of the calibration equipment are added to the applied loads. These estimates must be obtained numerically by using a tare load iteration algorithm that needs the natural zeros of the balance bridges as an input.

8.2 Six–Component Balance

Different methods may be used to determine the natural zeros of the bridges of a six–component strain–gage balance. Most of these methods are independent of the balance design. Consequently, they may be applied to single–piece, multi–piece, and other balance designs. Let us assume that an analyst needs to determine the natural zeros of the six bridges of a force balance. Figure 8–1 below shows NASA's MK34 Task/Able force balance

Fig. 8–1 NASA's 2.5 inch diameter MK34 six–component force balance.

as an example. Figure 8–2 below shows a cut through a force balance that has the MK34's general lay–out. The balance consists of a metric outer sleeve and a non–metric inner rod. The metric outer sleeve is the part that attaches the balance to the model. The non–metric inner rod, on the other hand, connects the balance to the balance support system. The metric part is marked using green color, the non–metric part is identified using blue, the flexures & bridges are marked using yellow, and the balance moment center (BMC) is highlighted as a magenta circle. The BMC is assumed to be located halfway between the forward and aft bridges of the balance.

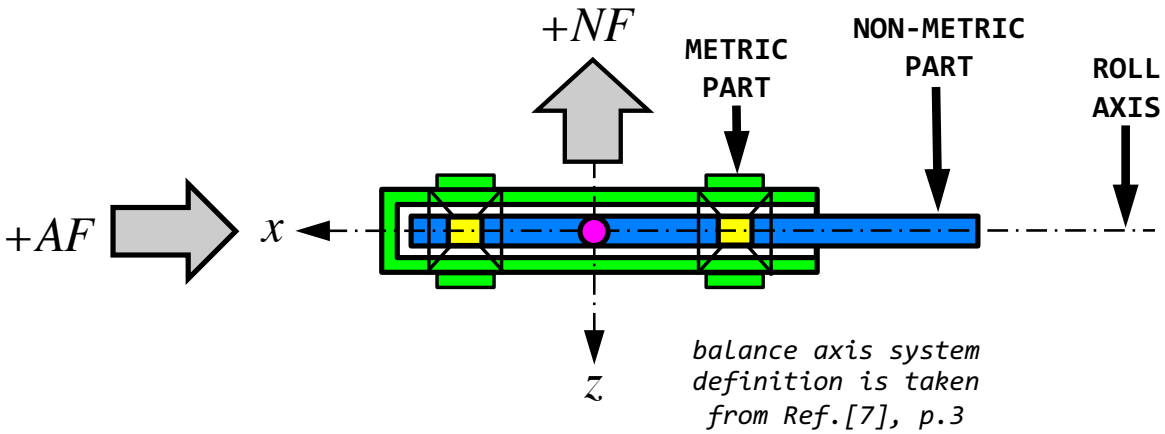

Fig. 8–2 Principal parts of a six–component force balance ; green ≡ metric part ; blue ≡ non–metric part ; yellow ≡ flexures ; magenta ≡ balance moment center.

Figure 8–3 below shows a force balance in a hypothetical weightless state. It is not possible to put a six–component balance into a weightless state in a calibration laboratory so that the natural zeros could directly be measured. Instead, the electrical outputs of a weightless balance have to be approximated by using mean values of sets of electrical

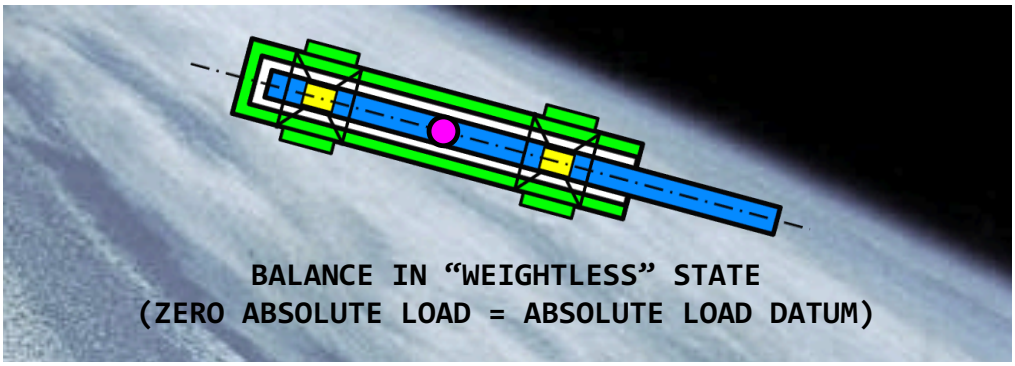

Fig. 8–3 Definition of the absolute load datum of a strain–gage balance.

outputs that are measured for a variety of balance orientations relative to the direction of the gravitational acceleration. These orientations are specifically selected such that, when combined, all balance loads cancel each other out.

Figure 8–4 below shows six orientations of a balance relative to the direction of the gravitational acceleration that are typically used for the determination of the natural zeros in a calibration laboratory. They can be split into two groups. The first group assumes that (i) the metric part of the balance is leveled and that (ii) its roll axis is perpendicular to the direction of the gravitational acceleration. Then, the balance is rotated through four angles that are identified by the values [0], [90], [180], and [270]. Only the normal force at the BMC or, alternatively, the normal forces at the forward and aft normal force bridges are acting when the balance is at [0] or [180]. Similarly, only the side force at the BMC or, alternatively, the side forces at the forward and aft side force bridges are acting when the balance is at [90] or [270]. Therefore, the balance loads cancel each other out if the loads

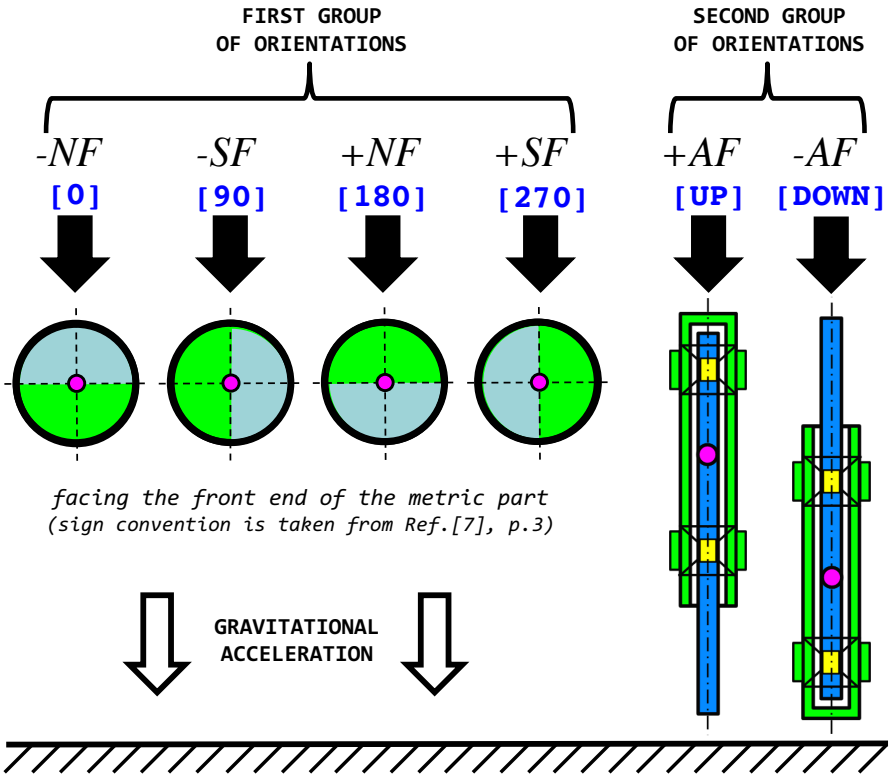

Fig. 8–4 Balance orientations relative to the gravitational acceleration.

of the four orientations are superimposed. Consequently, the averages of the raw electrical outputs of the balance bridges for these four orientations must be the outputs of the weightless balance. This result can be summarized by the following relationship where

$$N_i \;=\; \Big[\; rF_i\{[0]\} \;+\; rF_i\{[90]\} \;+\; rF_i\{[180]\} \;+\; rF_i\{[270]\} \;\Big] \;/\; 4 \quad ; \quad 1 \le i \le 6 \qquad (8.1)$$

N_i is the natural zero of the bridge, $rF_i\{[0]\}$ to $rF_i\{[270]\}$ are the raw electrical outputs of the bridge at the different balance orientations, and i is the bridge index.

The second group of orientations assumes that the balance is leveled such that its roll axis is parallel to the direction of the gravitational acceleration. Then, the balance may be rotated through two orientations that are identified as $[UP]$ and $[DOWN]$. Only the axial force at the BMC is acting when the balance is at each one of those two orientations. Again, loads cancel each other out when loads of the two orientations are superimposed. Therefore, the averages of the raw outputs of the two orientations for each one of the six balance bridges must be the outputs of the weightless balance. This result can be sum–marized by the relationship below where N_i is the natural zero of the bridge, $rF_i\{[UP]\}$

$$N_i \quad = \quad \Big[\; rF_i\{[UP]\} \;+\; rF_i\{[DOWN]\} \;\Big] \;/\; 2 \quad ; \quad 1 \le i \le 6 \qquad (8.2)$$

and $rF_i\{[DOWN]\}$ are the raw outputs at the two balance orientations, and i is the bridge index. The natural zeros are balance specific constants. Therefore, the values obtained by using either Eq. (8.1) or Eq. (8.2) are expected to not differ by more than 1.0 $microV/V$.

In principle, six specific methods can be defined for the determination of the natural zeros. They use the balance orientations shown in Fig. 8–4 above as input for the calculation of the natural zeros. First, Methods 1 and 2 are reviewed. These two methods use a leveling table and record outputs at orientations [0], [90], [180], and [270] so that Eq. (8.1) can be applied. Method 1 places the balance on a V–block that rests on the leveling table. This approach only works if either the balance has a metric outer sleeve, or, if the balance has metric and non–metric parts with matching diameters.

Figure 8–5 below shows the situation if Method 1 is applied to a typical force balance with a metric outer sleeve. In that case, the V–block supports the metric part of the

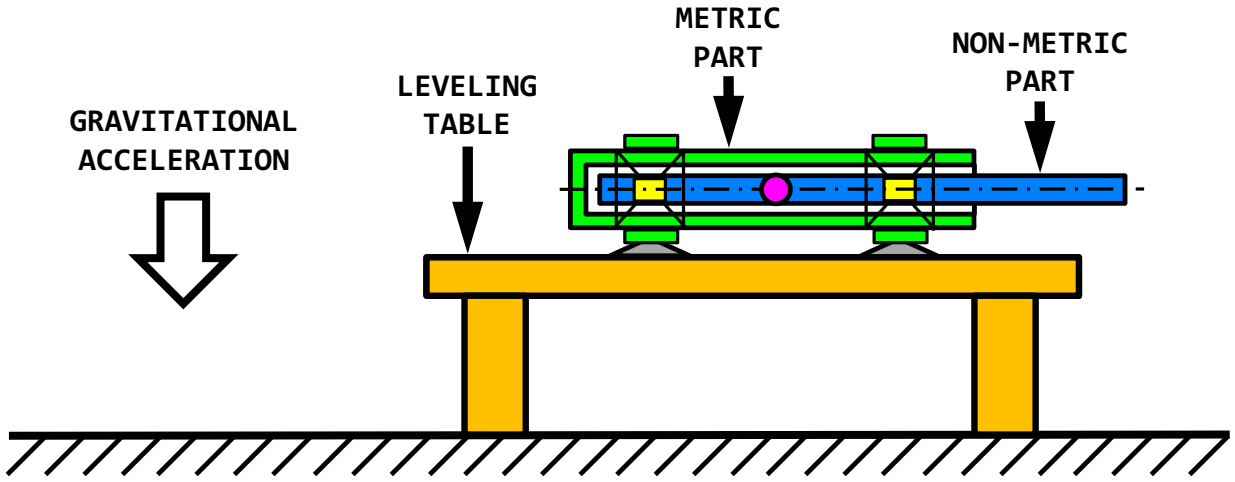

Fig. 8–5 Method 1 ≡ Force balance is supported by a V–block on a leveling table.

balance. Therefore, depending on the orientation of the balance in the V–block, either the normal or the side force bridges experience a physical load. This load is caused by the weight of the non–metric part of the balance.

Alternatively, Fig. 8–6 below shows the situation when Method 1 is applied to a single–piece balance. It is assumed that the balance has metric and non–metric parts with matching diameters. Then, the V–block supports both the metric and the non–metric part

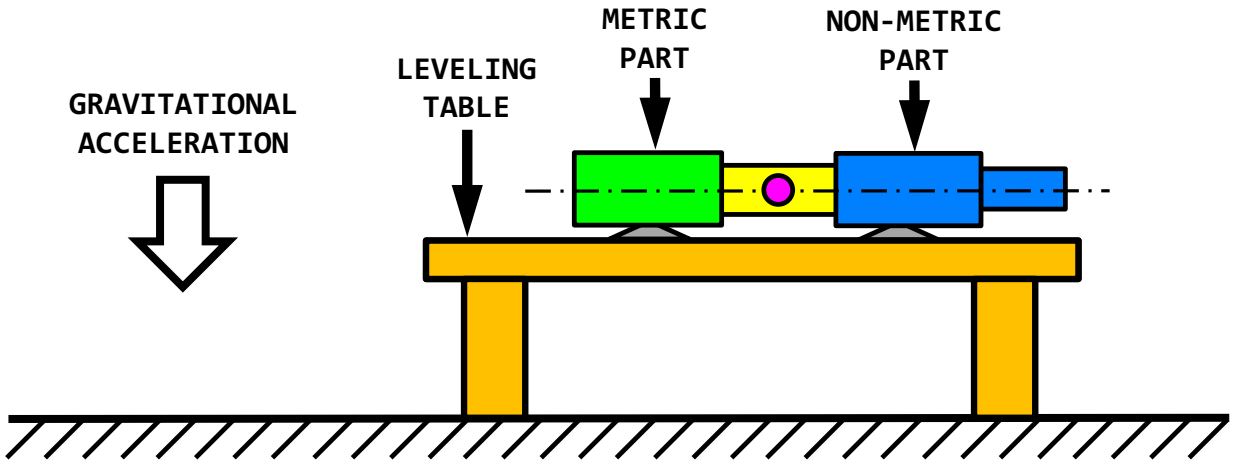

Fig. 8–6 Method 1 ≡ Single–piece balance is supported by a V–block on a leveling table.

of the balance while keeping its roll axis perpendicular to the direction of the gravitational acceleration. The balance may experience very small loads at each one of the four orientations that may be the result of balance design asymmetries.

Figure 8–7 below shows the situation when Method 2 is applied to a force balance. Now, the metric part of the balance is supported by the calibration body itself that is placed on a leveling table. Either the normal or the side force bridges experience a physical load depending on the orientation of the balance in the calibration body. Again, this load is exclusively caused by the weight of the non–metric part of the balance.

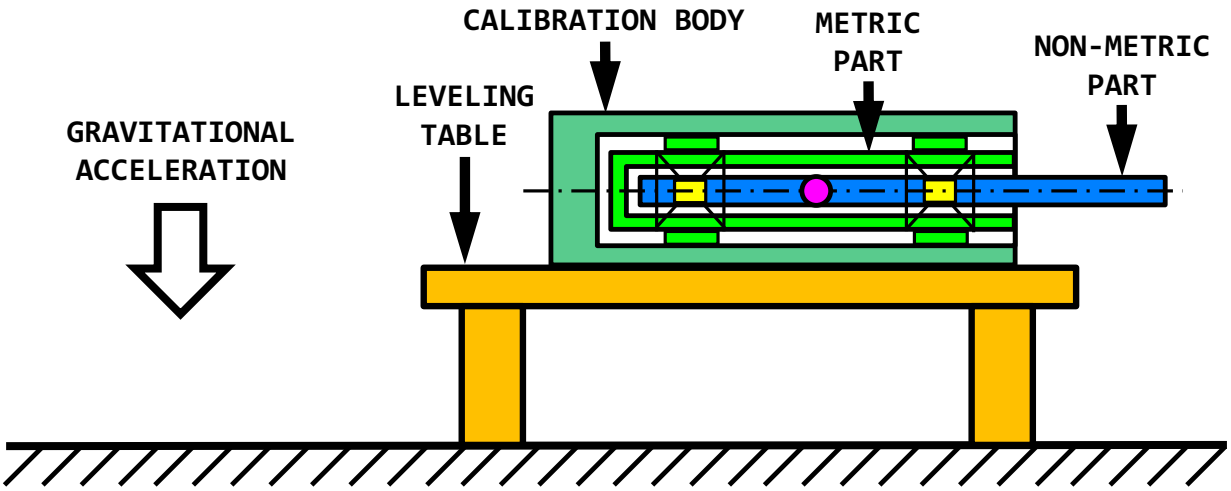

Fig. 8–7 Method 2 ≡ Balance is supported by a calibration body on a leveling table.

In the next step, Methods 3 and 4 are reviewed. They also use the four orientations [0], [90], [180], and [270] in combination with Eq. (8.1) for the determination of the natural zeros. The methods have two characteristics in common: (i) the non–metric part of the balance is mounted in a balance support system and (ii) the roll axis of the balance is perpendicular to the direction of the gravitational acceleration. Figure 8–8 below shows the situation for Method 3. This time, the weight of the metric part of the balance re–

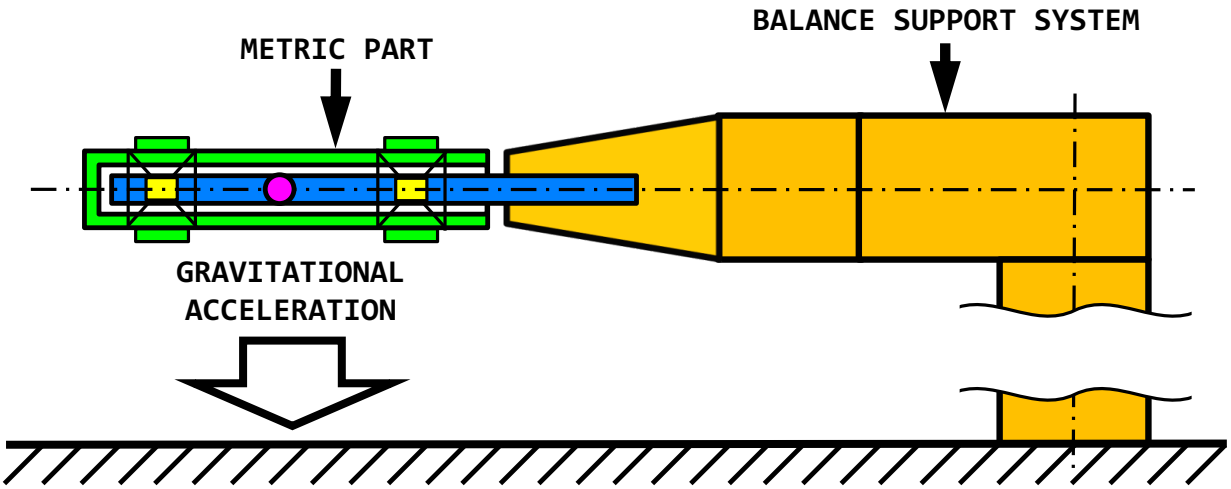

Fig. 8–8 Method 3 ≡ Balance is supported by the balance support system; the roll axis of the balance is perpendicular to the gravitational acceleration.

sults in a physical load on the normal or side force bridges of the balance depending on its orientation in space. Figure 8–9 below shows the situation for Method 4. Now, the weight of the metric assembly of the balance, i.e., the combined weight of the metric part and the calibration body results in a physical load on the normal or side force bridges.

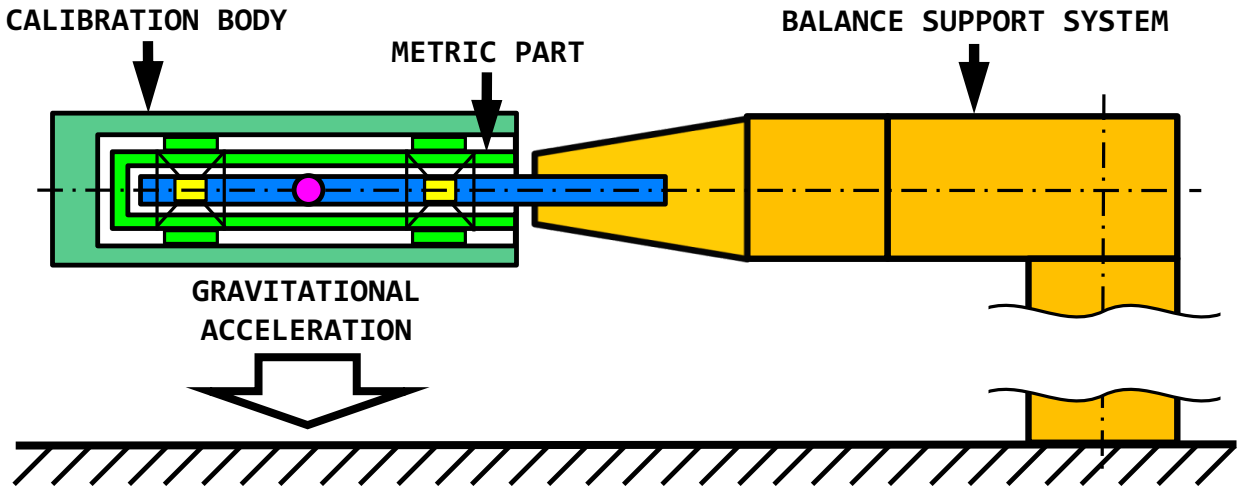

Fig. 8–9 Method 4 ≡ Balance assembly is supported by the balance support system; the roll axis of the balance is perpendicular to the gravitational acceleration.

Finally, Methods 5 and 6 are reviewed. They have the following common characteristics: (i) the non–metric part of the balance is mounted in a balance support system; (ii) the roll axis of the balance is parallel to the direction of the gravitational acceleration; (iii) orientations [*UP*] and [*DOWN*] of Fig. 8–4 are used. Figure 8–10 below shows the

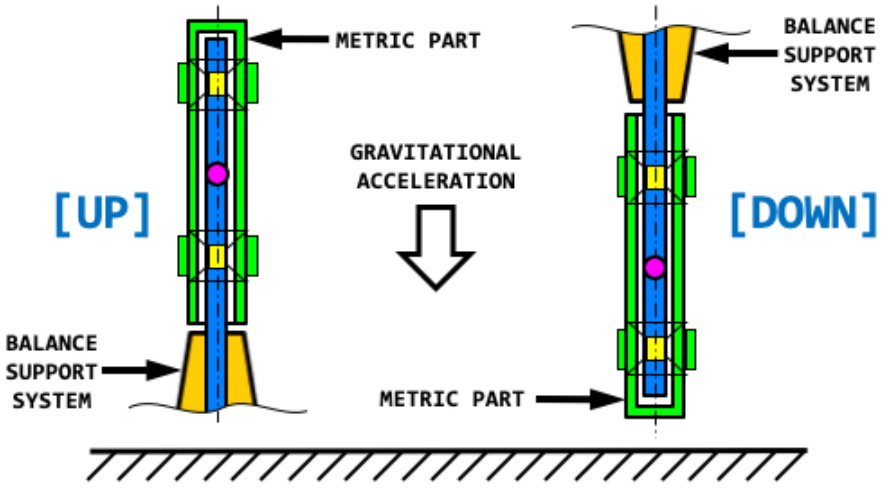

Fig. 8–10 Method 5 ≡ Balance is supported by the balance support system; the roll axis of the balance is parallel to the gravitational acceleration.

situation for Method 5. Again, similar to Method 3, the weight of the metric part is responsible for a physical load on the balance. This time, however, the load is detected by

the axial force bridge. Figure 8–11 below shows the corresponding situation for Method 6.

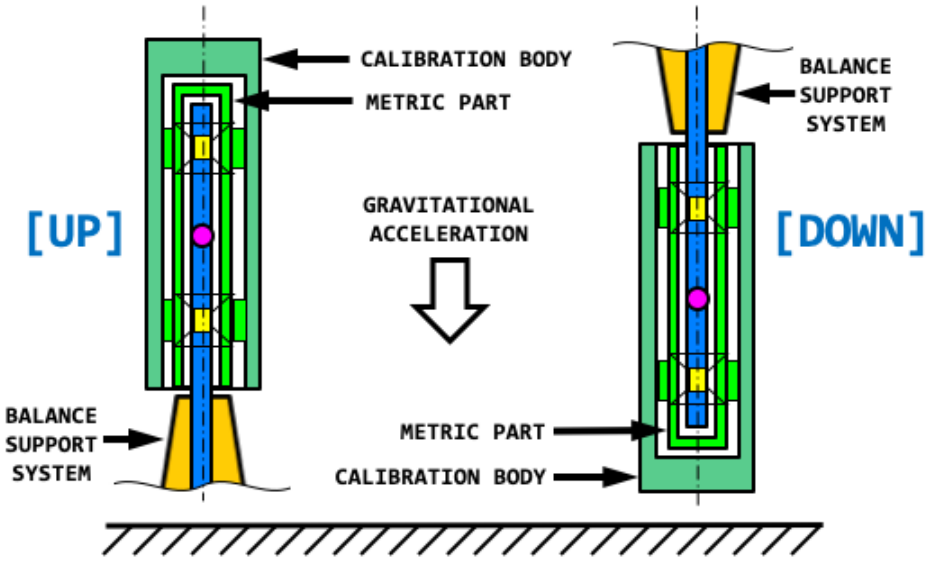

Fig. 8–11 Method 6 ≡ Balance assembly is supported by the balance support system; the roll axis of the balance is parallel to the gravitational acceleration.

Now, the weight of the metric assembly, i.e., the combined weight of the metric part and the calibration body results in a physical load that is detected by the axial force bridge of the balance. – Table 8–1 below summarizes key characteristics of the six methods that were discussed in this section. Method 2 to Method 6 may be applied to six–component balances of all current designs (single–piece, multi–piece, etc.). In addition, each method

Table 8–1: Determination of natural zeros of a six–component balance.

Method	Balance Orientations	Comments
1	[0], [90], [180], [270]	Balance† is supported by a V–block that is placed on a leveling table.
2	[0], [90], [180], [270]	Balance assembly, i.e., metric part plus calibration body, is placed on a leveling table.
3	[0], [90], [180], [270]	Balance is mounted on a support system; roll axis is perpendicular to the gravitational acceleration.
4	[0], [90], [180], [270]	Balance assembly is mounted on a support system; roll axis is perpendicular to the gravitational acceleration.
5	[*UP*], [*DOWN*]	Balance is mounted on a support system; roll axis is parallel to the gravitational acceleration
6	[*UP*], [*DOWN*]	Balance assembly is mounted on a support system; roll axis is parallel to gravitational acceleration

†Balance must have . . . a metric outer sleeve –or– metric & non–metric parts with matching diameters.

leads to an independent estimate of the natural zeros. Experience has shown that these independent estimates should not differ by more than 1.0 $microV/V$.

8.3 Five–Component Semi–span Balance

NASA owns a family of three five–component semi–span balances that are of single–piece design with common metric/non–metric flange geometries. They are called MC60, ARC30K, and MC400. These high–capacity balances are frequently used for tests in the NASA Ames 11–ft Transonic Wind Tunnel. Each balance weighs approximately 1300 *lbs*. Therefore, they must be handled with great care during both installation and check–out in order to avoid physical damage to the bridges.

NASA's five–component semi–span balances measure the following two forces and three moments on a wind tunnel model: normal force, axial force, pitching moment, rolling moment, and yawing moment. The omission of the side force measurement results in a unique characteristic of these balances: an orientation of the balance exists relative to the direction of the gravitational acceleration that allows an analyst to directly measure the natural zeros. Therefore, the determination of the natural zeros of NASA's five–component semi–span balances is treated separately in this section in order to better discuss this unique characteristic.

The determination of the natural zeros of a five–component semi–span balance can more easily be understood if the balance is described by using only its principal parts. Figure 8–12 below shows, for example, the general lay–out of the ARC30K five–component semi–span balance. The image was taken just before the balance flexures were gaged. The metric part, the non–metric part, and the balance flexures can clearly be identified.

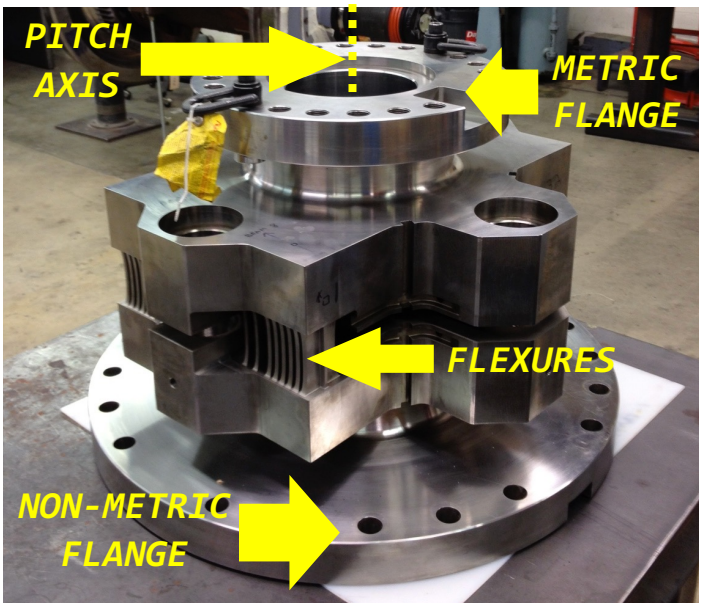

Fig. 8–12 NASA's ARC30K five–component semi–span balance.

Figure 8–13 below shows a cut through a balance that is similar to the ARC30K. The metric part is marked using green, the non–metric part is identified using blue, flexures

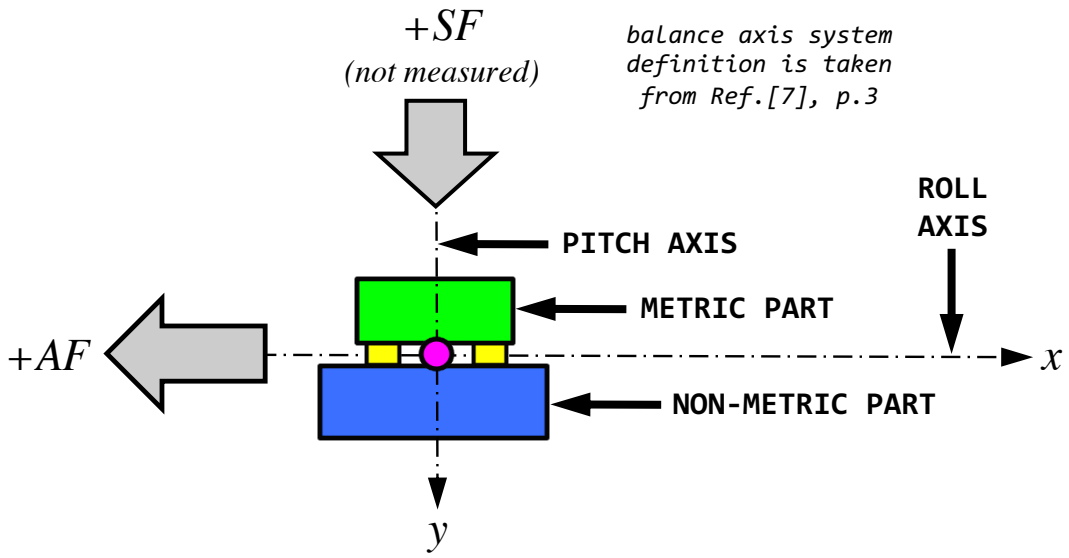

Fig. 8–13 Principal parts of a five–component semi–span balance; green ≡ metric part; blue ≡ non–metric part ; yellow ≡ flexures ; magenta ≡ balance moment center.

and bridges are marked using yellow, and the balance moment center is highlighted as a magenta circle. The pitch axis of the balance coincides with the y–axis of the balance axis system of the semi–span balance.

It was mentioned earlier that a five–component semi–span balance has an orientation relative to the direction of the gravitational acceleration that allows an analyst to directly measure the natural zeros. The balance simply has to be placed on a leveled surface in the $[UP]$ orientation such that its pitch axis is parallel to the direction of the gravitational acceleration. This approach, i.e., Method 7, is shown in Fig. 8–14 below. In this case, the

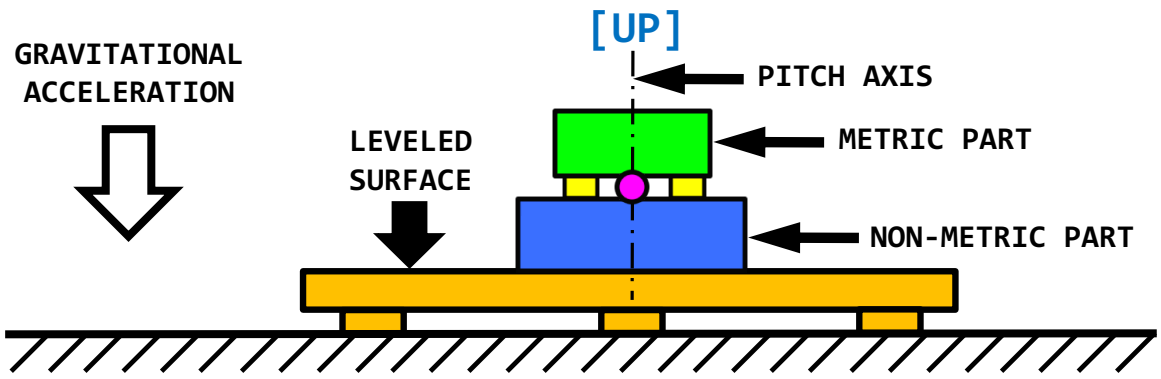

Fig. 8–14 Method 7 ≡ Non–metric flange of the semi–span balance is placed on a leveled surface; the pitch axis of the balance is parallel to the gravitational acceleration.

weight of the metric part acts in the direction of the side force. By design, the balance does not measure the side force. In addition, its bridge sets were installed such that they experience no load in this orientation. Then, their outputs match the natural zeros of the balance. This conclusion is summarized in Eq. (8.3) below where N_i is the natural zero of the bridge, $rF_i\{[UP]\}$ is the raw output in the $[UP]$ orientation, and i is the bridge index.

$$N_i \quad = \quad rF_i\{[UP]\} \quad ; \quad 1 \leq i \leq 5 \tag{8.3}$$

Basic ideas of Methods 3 & 4 of Table 8–1 may also be used for the determination of the natural zeros of a five–component semi–span balance if (i) the pitch axis instead of the roll axis of the balance is kept perpendicular to the gravitational acceleration and (ii) the balance is rotated through four angles. Figure 8–15 below shows the definition of the

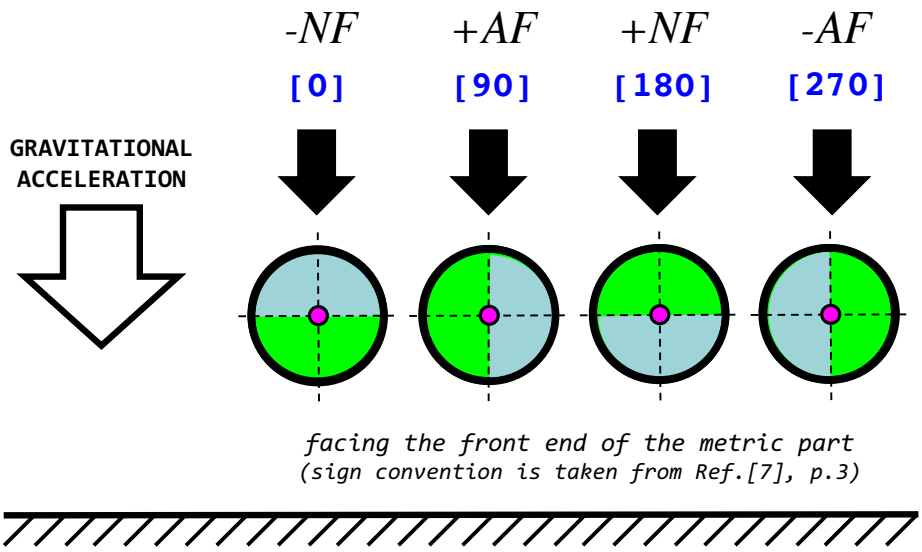

Fig. 8–15 Semi–span balance orientations relative to the gravitational acceleration.

required four balance orientations, i.e., [0], [90], [180], and [270], assuming that the balance is used for tests of a left wing model. Then, the natural zeros of the five bridges are obtained by averaging the raw electrical outputs that were obtained for the four balance orientations. This result can be described by the following relationship:

$$N_i \;=\; \Big[\; rF_i\{[0]\} \;+\; rF_i\{[90]\} \;+\; rF_i\{[180]\} \;+\; rF_i\{[270]\} \;\Big] \;/\; 4 \quad ; \quad 1 \le i \le 5 \qquad (8.4)$$

Now, Method 8 and Method 9 may be defined for a five–component semi–span balance. Figure 8–16 below shows the situation for Method 8. In this case, the weight of the metric

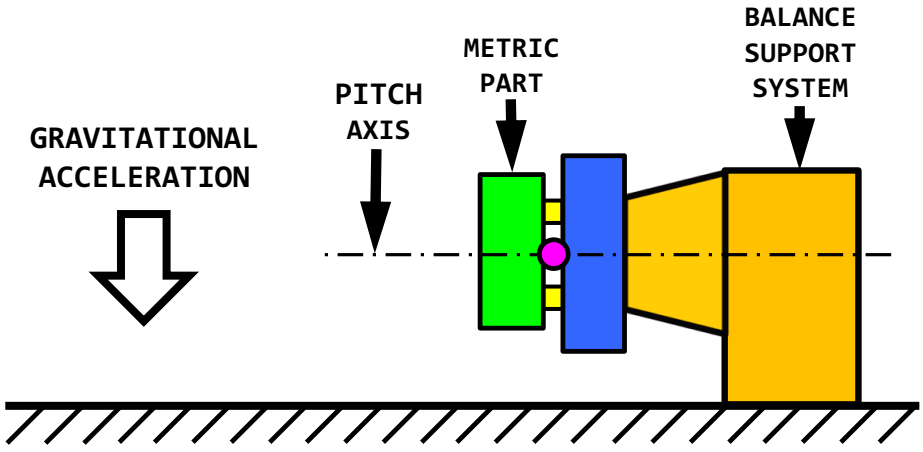

Fig. 8–16 Method 8 ≡ Semi–span balance is mounted on a balance support system; the pitch axis of the balance is perpendicular to the gravitational acceleration.

part of the balance results in a physical load on the normal or axial force bridges depending on the orientation of the balance. Figure 8–17 below shows the situation for Method 9.

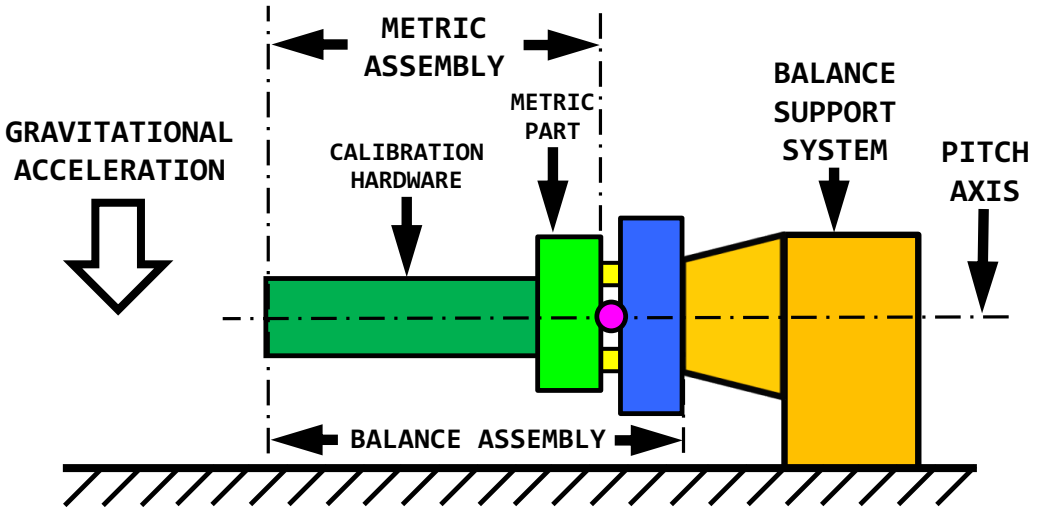

Fig. 8–17 Method 9 ≡ Semi–span balance assembly is mounted on a balance support system; the pitch axis of the balance is perpendicular to the gravitational acceleration.

Now, the weight of the metric assembly consisting of the metric part and the calibration hardware results in a physical load on the normal or axial force bridges.

Table 8–2 below summarizes characteristics of the three methods that were discussed in this section. Each method, if correctly applied, leads to an independent estimate of

Table 8–2: Determination of natural zeros of a five–component semi–span balance.

Method	Balance Orientations	Comments
7	$[UP]$	Non–metric flange is placed on a leveled surface; the natural zeros of the five bridges can directly be measured.
8	[0], [90], [180], [270]	Balance is mounted on a balance support system; pitch axis is perpendicular to the gravitational acceleration.
9	[0], [90], [180], [270]	Balance assembly is mounted on a balance support system; pitch axis is perpendicular to the gravitational acceleration.

the natural zeros. Ideally, these estimates should not differ by more than the empirical threshold of 1.0 $microV/V$. – It was mentioned earlier that a five–component semi–span balance is heavy and can easily get damaged during transport and/or installation. Therefore, the author recommends to use Method 7 for both determination & monitoring of the natural zeros of this balance type whenever the balance is moved between facilities. This approach will make sure that problems are detected and corrected well before the balance is installed in a wind tunnel facility.

8.4 Discussion of Examples

The determination of the natural zeros of two balances is discussed in this section to better illustrate the application of methods that were presented in the previous two

sections. The first balance is NASA's MK3C force balance. This Task/Able balance has a diameter of 2.0 *in*. It measures five forces and one moment (forward/aft normal force, forward/aft side force, axial force, rolling moment). Table 8–3 below lists its nominal load

Table 8–3: Load capacities of the MK3C balance ($lbs \equiv$ pounds of force).

$N1,\ lbs$	$N2,\ lbs$	$S1,\ lbs$	$S2,\ lbs$	$AF,\ lbs$	$RM,\ in-lbs$
900	900	450	450	500	1000

capacities. It was decided to determine the natural zeros of the MK3C by using Method 3 and Method 5 (see Table 8–1). First, Method 3 was applied (see Fig. 8–8). In that case, the non–metric part of the balance was attached to a balance support system such that the roll axis of the balance would be perpendicular to the direction of the gravitational acceleration. Then, the metric part of the balance, i.e., the metric outer sleeve, was leveled such that the positive normal force would point upward. This orientation is identified as [0] in Fig. 8–4. Afterwards, the electrical outputs of the six primary bridges were recorded. Then, the balance was rotated to the remaining three orientations, i.e., [90], [180], [270], and electrical outputs were recorded each time. The first four rows in Table 8–4 below list the measured electrical outputs that were obtained at the four orientations. Finally, Eq. (8.1) was applied and the mean of the outputs of the four orientations was computed for each bridge. These mean values are listed in the fifth data row of Table 8–4.

Table 8–4: Natural zeros $N_1,\ N_2,\ \ldots,\ N_6$ of the MK3C force balance.

	rF_1=$rN1$ $microV/V$	rF_2=$rN2$ $microV/V$	rF_3=$rS1$ $microV/V$	rF_4=$rS2$ $microV/V$	rF_5=rAF $microV/V$	rF_6=rRM $microV/V$
[0]	−321.0	+92.9	+55.8	−212.3	+169.1	−102.6
[90]	−318.1	+95.3	+51.0	−216.5	+169.1	−101.8
[180]	−315.4	+97.7	+55.9	−212.2	+169.2	−101.8
[270]	−318.3	+95.3	+60.8	−207.9	+169.2	−102.6
Method 3	−318.2	+95.3	+55.9	−212.2	+169.2	−102.2
[*UP*]	−319.3	+95.4	+55.8	−212.2	+177.7	−102.2
[*DOWN*]	−319.4	+95.1	+56.0	−212.7	+162.4	−102.3
Method 5	−319.4	+95.3	+55.9	−212.5	+170.1	−102.3
$N_i \implies$	−318.8	+95.3	+55.9	−212.4	+169.7	−102.3

In the next step, Method 5 was applied (see also Fig. 8–10). This time, the non–metric part of the balance was attached to a balance support system such that the roll axis of the balance would be parallel to the direction of the gravitational acceleration. Then, the metric part of the balance, i.e., the outer sleeve, was leveled such that the positive axial force would point upward. This orientation is identified as [*UP*] in Fig. 8–4. Afterwards, the electrical outputs of the six bridges were recorded. Then, the balance was rotated such

that the negative axial force would align with the direction of the gravitational acceleration and the six outputs were recorded again. This second orientation is described by the term [*DOWN*] in Fig. 8–4. Data rows six and seven in Table 8–4 above show the electrical outputs that were measured. Finally, Eq. (8.2) was applied and the mean of the outputs of the two orientations was computed for each bridge. These mean values are listed in the eighth data row of Table 8–4.

Now, after comparing results for Method 3 with results for Method 5, it is concluded that the two sets of independent estimates of the natural zeros do not differ by more than 1.2 $microV/V$. Finally, mean values of the two independent estimates of the natural zeros are computed and listed in the ninth data row of Table 8–4. Those values were used as input for the balance data analysis.

It was mentioned during the discussion of Methods 3 and 5 that the balance experiences a physical load in those two cases that is caused by the weight of the metric part. Therefore, it is possible to estimate the weight of the metric part if (i) the output changes for certain orientations are multiplied with (ii) the inverse of the sensitivities of related bridges. Table 8–5 below lists the sensitivities of the bridges of the MK3C balance.

Table 8–5: Bridge sensitivities of the MK3C force balance.

$\frac{\partial\ rN1}{\partial\ N1}$ $\frac{microV/V}{lbs}$	$\frac{\partial\ rN2}{\partial\ N2}$ $\frac{microV/V}{lbs}$	$\frac{\partial\ rS1}{\partial\ S1}$ $\frac{microV/V}{lbs}$	$\frac{\partial\ rS2}{\partial\ S2}$ $\frac{microV/V}{lbs}$	$\frac{\partial\ rAF}{\partial\ AF}$ $\frac{microV/V}{lbs}$	$\frac{\partial\ rRM}{\partial\ RM}$ $\frac{microV/V}{in-lbs}$
1.803	1.844	3.135	3.171	2.756	1.169

First, orientation [180] in Table 8–4 is selected. In that case, the weight of the metric part, i.e., the weight of the metric outer sleeve of the MK3C balance, acts in the normal force directions. Then, after combining the output changes of the normal force bridges relative to their natural zeros with related bridge sensitivities, we get the following result (natural zeros were taken from the last row of Table 8–4):

$$\begin{aligned} W &\approx \left[\frac{\partial\ rN1}{\partial\ N1}\right]^{-1} \cdot \Big[\ rF_1\{[180]\} \ - \ N_1\ \Big] \ + \ \left[\frac{\partial\ rN2}{\partial\ N2}\right]^{-1} \cdot \Big[\ rF_2\{[180]\} \ - \ N_2\Big] \\ &\approx \left[\frac{1}{1.803}\right] \cdot \Big[(-315.4) - (-318.8)\Big] \ + \ \left[\frac{1}{1.844}\right] \cdot \Big[(+97.7) - (+95.3)\Big] \qquad (8.5) \\ &\approx 3.19\ lbs \end{aligned}$$

Similarly, orientation [*UP*] in Table 8–4 is selected. In that case, the weight of the metric part acts in the axial force direction. Then, after combining the output changes of the axial force bridge relative to its natural zero with the related sensitivity, we get the following result (natural zero was taken from the last row of Table 8–4):

$$
\begin{aligned}
W &\approx \left[\frac{\partial\, rAF}{\partial\, AF}\right]^{-1} \cdot \Big[\, rF_5\{[UP]\} \;-\; N_5 \,\Big] \\
&\approx \left[\frac{1}{2.756}\right] \cdot \Big[\, (+177.7) \;-\; (+169.7) \,\Big] \\
&\approx 2.90\ lbs
\end{aligned}
\tag{8.6}
$$

The estimates of the weight of the metric part are 3.19 *lbs* and 2.90 *lbs*. These two values are within the expected range of values for the MK3C balance considering the facts that (i) the weight of the outer sleeve of a typical force balance is about half of the total weight of the balance and that (ii) the total weight of the MK3C balance is 6.79 *lbs*.

The second example uses data from NASA's MC400 five–component semi–span balance. The balance is a high–capacity single–piece balance that measures two forces and three moments (normal force, axial force, rolling moment, pitching moment, and yawing moment). Table 8–6 below lists capacities of its load components.

Table 8–6: Load capacities of the MC400 semi–span balance (*lbs* ≡ pounds of force).

NF, *lbs*	PM, *in−lbs*	YM, *in−lbs*	RM, *in−lbs*	AF, *lbs*
40000	240000	480000	2280000	8000

It was decided to use Method 7 (Fig. 8–14) and Method 8 (Fig. 8–16) for the determination of the natural zeros (see also Table 8–2 for a summary of the two methods). First, Method 7 was applied. In that case, the non–metric flange of the balance was placed on a leveled surface such that the side force would be parallel to the direction of the gravitational acceleration (this orientation is identified as $[UP]$ in Fig. 8–14). None of the five bridges of the balance experiences a load in this orientation as the balance does not measure the side force. Therefore, no averaging is needed and the natural zeros of the five bridges can directly be measured. Values of bridge set 1 are listed in the first data row of Table 8–7.

Table 8–7: Natural zeros $N_1,\ N_2,\ \ldots,\ N_5$ of bridge set 1 of the MC400 balance.

	$rF_1{=}rNF$ *microV/V*	$rF_2{=}rPM$ *microV/V*	$rF_3{=}rYM$ *microV/V*	$rF_4{=}rRM$ *microV/V*	$rF_5{=}rAF$ *microV/V*
Method 7	−78.3	+394.9	+35.2	−101.1	+17.0
[0]	−88.8	+397.2	+34.9	−102.1	+16.8
[90]	−79.2	+396.6	+32.8	−101.7	+53.9
[180]	−67.6	+397.5	+35.1	−101.5	+16.8
[270]	−77.2	+397.7	+37.1	−102.0	−20.3
Method 8	−78.2	+397.3	+35.0	−101.8	+16.8
$N_i \implies$	−78.3	+396.1	+35.1	−101.5	+16.9

In the next step, Method 8 was applied (see also Fig. 8–16). In that case, the non–metric part of the balance was attached to a balance support system such that the pitch axis of the balance would be perpendicular to the direction of the gravitational acceleration. Then, the metric part of the balance was leveled such that the positive normal force would point upward. This orientation is identified as [0] in Fig. 8–15. Afterwards, electrical outputs of the five bridges of bridge set 1 were recorded. Then, the balance was rotated to the remaining three orientations, i.e., [90], [180], [270], and the electrical outputs were recorded each time. Data rows two to five in Table 8–7 above list the measured electrical outputs that were obtained at the four orientations. Finally, Eq. (8.4) was applied and the mean of the outputs of the four orientations was computed for each bridge. These mean values are listed in the sixth data row of Table 8–7.

Now, after comparing results for Method 7 with results for Method 8, it is concluded that the two sets of independent estimates of the natural zeros do not differ by more than 2.4 $microV/V$. Finally, mean values of the two independent estimates of the natural zeros are computed and listed in the seventh data row of Table 8–7. The mean values were used for the balance data analysis.

It was mentioned during the discussion of Method 8 that the balance experiences a physical load that is caused by the weight of the metric part. Therefore, it is possible to estimate the weight of the metric part if (i) the output changes for certain orientations are multiplied with (ii) the inverse of the sensitivities of related bridges. Table 8–8 below lists sensitivities of the bridges of bridge set 1 of the MC400 balance.

Table 8–8: Bridge sensitivities of the MC400 semi–span balance (bridge set 1).

$\frac{\partial\, rNF}{\partial\, NF}$ $\frac{microV/V}{lbs}$	$\frac{\partial\, rPM}{\partial\, PM}$ $\frac{microV/V}{in-lbs}$	$\frac{\partial\, rYM}{\partial\, YM}$ $\frac{microV/V}{in-lbs}$	$\frac{\partial\, rRM}{\partial\, RM}$ $\frac{microV/V}{in-lbs}$	$\frac{\partial\, rAF}{\partial\, AF}$ $\frac{microV/V}{lbs}$
0.023278	0.004970	0.001651	0.000307	0.087830

First, orientation [180] in Table 8–7 is selected. In that case, the weight of the metric part acts in the positive normal force direction. Then, after combining the output changes of the normal force bridge relative to its natural zero with the related bridge sensitivity, we get the following result (natural zero was taken from the last row of Table 8–7):

$$\begin{aligned} W &\approx \left[\frac{\partial\, rNF}{\partial\, NF}\right]^{-1} \cdot \left[\, rF_1\{[180]\} \;-\; N_1 \,\right] \\ &\approx \left[\frac{1}{0.023278}\right] \cdot \left[\, (-67.6) \;-\; (-78.3) \,\right] \\ &\approx 459.7\ lbs \end{aligned} \tag{8.7}$$

Similarly, orientation [90] in Table 8–7 is selected. In that case, the weight of the metric part acts in the positive axial force direction. Then, after combining the output changes of the axial force bridge relative to its natural zero with related bridge sensitivity, we get the following result (natural zero was taken from the last row of Table 8–7):

$$\begin{aligned} W &\approx \left[\frac{\partial\, rAF}{\partial\, AF}\right]^{-1} \cdot \left[\, rF_5\{[90]\} \;-\; N_5 \,\right] \\ &\approx \left[\frac{1}{0.087830}\right] \cdot \left[\, (+53.9) \;-\; (+16.9) \,\right] \\ &\approx 421.4\ lbs \end{aligned} \tag{8.8}$$

The two independent estimates of the weight of the metric part of the balance are 459.7 *lbs* and 421.4 *lbs*. These values are close to the expected value of ≈ 420 *lbs* that was computed from estimates of the metric part's volume and density.

An empirical rule is often applied that describes the connection between the primary bridge sensitivity and the expected accuracy of the prediction of the related primary bridge load in engineering units. The rule can be summarized as follows (see also p. 17):

Empirical Evaluation of the Primary Bridge Sensitivity

The sensitivity of a primary bridge is a physical constant of the balance. The greater the sensitivity of a primary bridge is the more accurate the prediction of the related primary bridge load in engineering units will be.

Therefore, the estimate of 421.4 *lbs* is most likely the more accurate value because the sensitivity of the axial force bridge is almost four times as large as the sensitivity of the normal force bridge (see Table 8–8). In addition, it is observed that the weight estimate from the normal force bridge output change is 38.3 *lbs* larger than the estimate from the axial force bridge output change (459.7 *lbs* versus 421.4 *lbs*). This weight difference equals approximately 0.1 % of the normal force capacity of the MC400 balance. In other words, the weight difference is well within the threshold of ±0.25 % that is often used for the assessment of the difference between the applied and the predicted load of an individual calibration data point.

Appendix 9

Non–Iterative Method

9.1 General Remarks

The *Non–Iterative Method* is one of two balance load prediction approaches that are used in wind tunnel testing. First, it analyzes balance calibration data by fitting each load as a function of the measured outputs of all bridges. Then, loads are predicted during the wind tunnel test by directly combining output measurements of a data point with the regression models of the loads. These regression models are defined in the next section.

9.2 Regression Model of Single Load Component

In principle, the total number of load components of a balance must always match the total number of independent bridge output measurements (see Chapter II, p. 11 for more details). The loads can be described, for example, by using the symbols F_1, ..., F_n where n equals the total number of load components. Similarly, the independent output measurements can be described as raw outputs by using the symbols rF_1, ..., rF_n. Then, the load prediction equation of a single load component F_i can be defined as a regression model of the load that is constructed from the raw outputs rF_1, ..., rF_n of the bridges.

Bridge outputs may be used as independent variables of the regression model of a balance load component. They are typically reported as raw outputs (absolute voltages). This output format, however, makes the regression model difficult to use during a wind tunnel test as (i) raw output measurements frequently experience small instrumentation–induced shifts and (ii) significant instrumentation hardware differences may exist between the wind tunnel and the balance calibration laboratory. Alternatively, the difference between a raw output and the natural zero of a balance bridge may be used to construct the regression model of a load. Resulting output differences are defined in Eq. (9.1) below. The output difference is also called *Difference Type 1* in App. 6. The use of output differences for

$$Difference\ Type\ 1 \quad \Longrightarrow \quad D_i \ = \ rF_i \ - \ N_i \quad ; \quad 1 \leq i \leq n \tag{9.1}$$

the analysis of balance data has three benefits: (i) improved control of instrumentation–induced output shifts as the natural zeros are used as the output datum, (ii) better mathematical description of balance data characteristics near zero absolute load, and (iii) the use of the intercept term in the regression model is optional as it can be interpreted as a least squares approximation of zero absolute load. Then, the regression model of a load can be summarized as follows where λ equals the maximum number of terms (including

$$F_i \ = \ \underbrace{a_{i,0} \ + \ a_{i,1} \cdot D_1 \ + \ a_{i,2} \cdot D_2 \ + \ \ldots}_{\lambda \ = \ maximum\ number\ of\ model\ terms} \ = \ a_{i,0} \ + \ \sum_{\psi=1}^{9} S_\psi(a_{i,\omega}) \tag{9.2a}$$

where

$$intercept\ is\ optional\ as\ output\ differences\ are\ used \ \Longrightarrow \ a_{i,0} \ \approx \ 0 \tag{9.2b}$$

the optional intercept) and $a_{i,0},\ a_{i,1},\ \ldots$ are the regression coefficients. Table 9–1 below shows terms that are suitable for the definition of the regression model of a balance load

Table 9–1: Term group choices for the regression model of a load component.

ψ	$S_\psi(a_{i,\omega})$ *(summation definition)*	$\ldots \le \omega \le \ldots$ *(coefficient index range)*	σ_ψ *(number of terms)*
1	$\sum_{j=1}^{n} a_{i,\omega} \cdot D_j$	$1 \le \omega \le \sigma_1$	n
2	$\sum_{j=1}^{n} a_{i,\omega} \cdot \lvert D_j \rvert$	$1 + \sigma_1 \le \omega \le \sum_{\psi=1}^{2} \sigma_\psi$	n
3	$\sum_{j=1}^{n} a_{i,\omega} \cdot D_j^2$	$1 + \sum_{\psi=1}^{2} \sigma_\psi \le \omega \le \sum_{\psi=1}^{3} \sigma_\psi$	n
4	$\sum_{j=1}^{n} a_{i,\omega} \cdot D_j \cdot \lvert D_j \rvert$	$1 + \sum_{\psi=1}^{3} \sigma_\psi \le \omega \le \sum_{\psi=1}^{4} \sigma_\psi$	n
5	$\sum_{j=1}^{n-1} \sum_{k=j+1}^{n} a_{i,\omega} \cdot D_j \cdot D_k$	$1 + \sum_{\psi=1}^{4} \sigma_\psi \le \omega \le \sum_{\psi=1}^{5} \sigma_\psi$	$\frac{n \cdot (n-1)}{2}$
6†	$\sum_{j=1}^{n} \sum_{\substack{k=1 \\ k \ne j}}^{n} a_{i,\omega} \cdot D_j \cdot \lvert D_k \rvert$	$1 + \sum_{\psi=1}^{5} \sigma_\psi \le \omega \le \sum_{\psi=1}^{6} \sigma_\psi$	$n \cdot (n-1)$
7	$\sum_{j=1}^{n-1} \sum_{k=j+1}^{n} a_{i,\omega} \cdot \lvert D_j \cdot D_k \rvert$	$1 + \sum_{\psi=1}^{6} \sigma_\psi \le \omega \le \sum_{\psi=1}^{7} \sigma_\psi$	$\frac{n \cdot (n-1)}{2}$
8	$\sum_{j=1}^{n} a_{i,\omega} \cdot D_j^3$	$1 + \sum_{\psi=1}^{7} \sigma_\psi \le \omega \le \sum_{\psi=1}^{8} \sigma_\psi$	n
9	$\sum_{j=1}^{n} a_{i,\omega} \cdot \lvert D_j^3 \rvert$	$1 + \sum_{\psi=1}^{8} \sigma_\psi \le \omega \le \sum_{\psi=1}^{9} \sigma_\psi$	n
—	—	—	$\Sigma \equiv 2 \cdot n \cdot (n+2)$

†Alternate description of terms of groups 7 & 8 that are listed in App. 10, Table 10–1 (see also App. 20).

component. The term group order and choices given in Table 9–1 above for the regression model of a load component differ from those that are traditionally used to define the regression model of a bridge output (see App. 10, Table 10–1). The origin of these differences is discussed in great detail in App. 23.

By design, the order of the term groups of Table 9–1 is hierarchical (see also comments in App. 23). The table's last column has the maximum number of terms of each group.

Terms of groups 1, 3, 5, and 8 are derived from a multivariate *Taylor Series* expansion of the unknown relationship between the load and the outputs. Absolute value terms, i.e., terms of groups 2, 4, 6, 7, and 9, should only be used if the outputs of the given balance are known to have bi–directional behavior (see, e.g., Refs. [33] to [35] for a discussion of this phenomenon). The maximum number of regression model terms on the right–hand side of Eq. (9.2*a*) above can easily be expressed as a function of the total number of independent output measurements of the balance if (i) the sum of the values of the last column of Table 9–1 above is computed and (ii) one is added for the intercept term. Then, we get:

$$\lambda \quad = \quad 1 \; + \; \sum_{\psi=1}^{9} \sigma_{\psi} \quad = \quad 1 \; + \; \underbrace{6 \cdot n \; + \; 2 \cdot n \cdot (n-1)}_{contribution \; of \; S_1 \, , \ldots , \, S_9} \tag{9.3}$$

Let us assume, for example, that a calibration data set was obtained in order to characterize the behavior of a six–component balance. Then, the following maximum number of regression model terms of a load component is computed:

$$n \; = \; 6 \quad \Longrightarrow \quad Eq. \; (9.3) \quad \Longrightarrow \quad \lambda \; = \; 97 \tag{9.4}$$

Only a subset of the maximum number of terms is typically supported and/or chosen by an analyst whenever the regression model defined in Eq. (9.2*a*) is applied to real–world balance calibration data. This conclusion can be summarized by the following inequality:

$$\delta \; = \; number \; of \; supported/chosen \; terms \quad < \quad \lambda$$

The subset of terms may or may not include the optional intercept term depending on an analyst's preference.

Analysts have identified term group combinations that work with most balance designs. Table 9–2 below, for example, lists three group combinations that the author often uses for the definition of the upper bound of the regression model of a load component:

Table 9–2: Typical term group combinations (see also Table 9–1).

Balance Design Characteristic	Term Group Combination
single–piece balance	$D_j, \;\; D_j^2, \;\; D_j \cdot D_k$
balance with <u>known</u> bi–directional outputs (option 1)†	$D_j, \;\; \lvert D_j \rvert, \;\; D_j^2, \;\; D_j \cdot D_k$
balance with <u>known</u> bi–directional outputs (option 2)†	$D_j, \;\; \lvert D_j \rvert, \;\; D_j^2, \;\; D_j \cdot \lvert D_j \rvert, \;\; D_j \cdot D_k$

†For example, balances of Task/Able design have bi–directional normal & side force bridge outputs.

The author's group combination choices capture the most important physical characteristics of the corresponding balance design. In addition, they potentially prevent unwanted over–fitting of calibration data by keeping an analyst's term choices to a minimum.

Supported regression model terms (δ) must be used instead of the maximum number of terms (λ) for the definition of the regression model of a load. Then, the regression analysis problem of the calibration data will have a non–singular/unique solution. In that context, it is important to test the regression model term combination for linear or massive

near–linear dependencies by using the *Variance Inflation Factor* (VIF)†. The maximum VIF of the chosen regression model of a load should be less than an empirical threshold value. Then, the model is guaranteed to define a unique relationship between the fitted load and the outputs of the balance (see App. 18 for detailed discussions of the VIF and the selection of the empirical threshold for the dependency test).

9.3 Global Regression Analysis

The global regression analysis problem associated with the determination of the unknown coefficients of the supported/chosen regression model terms of a load component F_i can be expressed in matrix format if row and column vectors are used to describe Eq. (9.2a). It is assumed, for example, that an analyst chooses the intercept term and a supported subset of both linear & non–linear terms for the regression model of the load. In addition, it is assumed that tare corrections were added to the applied calibration loads (see App. 12 for more details). Then, three vectors can be defined:

$$\mathbf{A}_{1\times\delta} = \underbrace{\begin{bmatrix} 1 & D_1 & D_2 & \dots & D_1^2 & \dots \end{bmatrix}}_{\delta \,=\, number\ of\ supported\ terms} \tag{9.5a}$$

$$\mathbf{x}_{\delta\times 1} = \begin{bmatrix} a_{i,0} \\ a_{i,1} \\ a_{i,2} \\ \vdots \end{bmatrix} \tag{9.5b}$$

$$\mathbf{R}_{1\times 1} = F_i \tag{9.5c}$$

Now, the supported subset of Eq. (9.2a) can be described by the following matrix equation:

$$\mathbf{A}_{1\times\delta} \cdot \mathbf{x}_{\delta\times 1} = \mathbf{R}_{1\times 1} \tag{9.6}$$

In the next step, assuming that the balance calibration data set consists of a total number of p data points, i.e., of p individual load states, the row vector $\mathbf{A}$ on the left–hand side of Eq. (9.6) becomes a matrix with p rows. Similarly, the right–hand side of Eq. (9.6) becomes a column vector with p rows. We get the following extensions:

$$\mathbf{A}_{1\times\delta} \Longrightarrow \mathbf{A}_{p\times\delta} = \begin{bmatrix} 1 & D_1(1) & D_2(1) & \dots & D_1^2(1) & \dots \\ 1 & D_1(2) & D_2(2) & \dots & D_1^2(2) & \dots \\ \vdots & \vdots & \vdots & \vdots & \vdots & \vdots \\ 1 & D_1(p) & D_2(p) & \dots & D_1^2(p) & \dots \end{bmatrix} \tag{9.7a}$$

$$\mathbf{R}_{1\times 1} \Longrightarrow \mathbf{R}_{p\times 1} = \begin{bmatrix} F_i(1) \\ F_i(2) \\ \vdots \\ F_i(p) \end{bmatrix} \tag{9.7b}$$

† A connection between the reliability of multivariate regression models of balance data and the *Variance Inflation Factor* was first detected in 2007. At that time, an observed divergence of the load iterations of the *Iterative Method* was traced back to the presence of large *Variance Inflation Factors* (Ref. [27], p. 4).

Finally, after introducing the two extensions above in Eq. (9.6), the global regression analysis problem of the given balance calibration data can be summarized by the following equation where column vector $\mathbf{x}$ has the coefficients of the regression model of the load

Global Regression Analysis Problem

$$\underbrace{\mathbf{A}_{p\times\delta}}_{known} \cdot \underbrace{\mathbf{x}_{\delta\times 1}}_{unknown} = \underbrace{\mathbf{R}_{p\times 1}}_{known} \qquad (9.8)$$

component. The coefficients are obtained after solving the regression analysis problem that Eq. (9.8) describes. The solution is an application of the *Moore–Penrose Inverse* (see Ref. [64], pp. 35–39, and Refs. [77], [78]). It is described by the following matrix equation:

Regression Coefficients
(solution of global regression analysis problem)

$$\mathbf{x}_{\delta\times 1} = \left[\ \mathbf{A^T}\cdot\ \mathbf{A}\ \right]^{-1}_{\delta\times\delta} \cdot \left[\ \mathbf{A^T}\cdot\ \mathbf{R}\ \right]_{\delta\times 1} \qquad (9.9)$$

At this point, the analytical relationship between the load component of the balance and its electrical outputs is known as (i) the regression model of the load is defined in Eq. (9.2a) and (ii) the regression coefficients $a_{i,0},\ a_{i,1},\ \ldots$ of the supported/chosen terms are given by the right–hand side of Eq. (9.9). The current analysis implicitly assumes that all calibration loads contained in the right–hand side vector $\mathbf{R}$ are tare corrected. In other words, they include load contributions resulting from the weight of the metric part of the balance and all attached calibration hardware pieces. The analytic determination of these tare corrections is discussed in great detail in App. 12 of the current document.

9.4 Balance Load Calculation

Equation (9.9) above specifies coefficients of the regression model of a single load component of the balance. Coefficients of other load components have to be obtained by updating the contents of (i) matrix $\mathbf{A}$ that has the supported/chosen regression model terms and (ii) column vector $\mathbf{R}$ that has the calibration loads $F_i(1),\ \ldots,\ F_i(p)$ of the load component. Afterwards, computed coefficients of all load components can be stored in a rectangular matrix so that a single matrix multiplication may be used for the simultaneous calculation of all load components during a wind tunnel test.

The rectangular matrix needed for the calculation of all balance loads is obtained by first mapping the column vector $\mathbf{x}$ with the known coefficients of each load component from the supported/chosen δ terms to the maximum number of λ terms. The mapping is done without changing the result of the regression analysis of the loads as coefficients of unused terms of Eq. (9.2a) are explicitly set to 0. Then, the transformed solution vector

of the coefficients of the regression model of a single load component with index i can be expressed as follows:

$$\{\ \textit{supported terms}\ (\delta)\ \Longrightarrow\ \textit{all terms}\ (\lambda)\ \}\quad\Longrightarrow\quad\{\ \mathbf{x}_{\delta\times 1}\ \Longrightarrow\ \mathbf{y}_{\lambda\times 1}\ \}\qquad(9.10a)$$

The number and type of chosen terms of the individual load components of the balance may or may not be the same depending on an analyst's term selections. However, the transformed solution vectors $\mathbf{y}$ of the coefficients of each single load can be combined in a rectangular matrix with a total of λ rows and n columns after coefficients of each load were mapped one by one from the supported/chosen terms to the maximum number of terms. This conclusion can be summarized as follows:

$$\{\ \textit{single component}\ (1)\ \Longrightarrow\ \textit{all components}\ (n)\ \}\quad\Longrightarrow\quad\{\ \mathbf{y}_{\lambda\times 1}\ \Longrightarrow\ \mathbf{z}_{\lambda\times n}\ \}\qquad(9.10b)$$

Similarly, it is necessary to transform the columns of matrix $\mathbf{A}$ from the number of δ supported terms to the maximum number of λ terms. This time, however, matrix $\mathbf{A}$ consists of a single row as only information from a single data point is needed for the prediction of the balance loads for a given set of output differences $D_1,\ \ldots,\ D_n$ that is recorded during a wind tunnel test. Then, we get:

$$\{\ \textit{supported terms}\ (\delta)\ \Longrightarrow\ \textit{all terms}\ (\lambda)\ \}\quad\Longrightarrow\quad\{\ \mathbf{A}_{1\times\delta}\ \Longrightarrow\ \mathbf{B}_{1\times\lambda}\ \}\qquad(9.10c)$$

Now, the matrix multiplication describing the balance load prediction during a wind tunnel test can be expressed by the following equation where $\mathbf{F}_{bal}^{\mathbf{T}}$ is a row vector that has

$$\left\{\mathbf{F}_{bal}^{\mathbf{T}}\right\}_{1\times n}\quad=\quad[\ F_1\quad\ldots\quad F_i\quad\ldots\quad F_n\ ]\quad=\quad\{\mathbf{B}\}_{1\times\lambda}\ \cdot\ \{\mathbf{z}\}_{\lambda\times n}\qquad(9.11)$$

the predicted balance load components. Then, after taking the transpose of both sides of Eq. (9.11), knowing from matrix algebra that $(\mathbf{X}\,\mathbf{Y})^{\mathbf{T}}=\mathbf{Y}^{\mathbf{T}}\mathbf{X}^{\mathbf{T}}$ (see Ref. [65], p. 334), and dropping the subscripts that describe the vector or matrix size, we get the following exact relationship for the predicted absolute balance loads of a single data point if the *Non–Iterative Method* is applied:

Absolute Balance Loads *(exact relationship)*

(assumptions ≡ output differences are used as input ; regression models have intercepts)

$$\mathbf{F}_{bal}(rF_1,\ \ldots,\ rF_n) \quad = \quad \begin{bmatrix} F_1 \\ \vdots \\ F_i \\ \vdots \\ F_n \end{bmatrix} \quad = \quad \mathbf{z^T} \ \cdot \ \mathbf{B^T} \tag{9.12a}$$

$$\mathbf{z^T} \ = \ const. \ = \ \underbrace{\begin{bmatrix} & & & & |\leftarrow\cdots\cdots \textit{linear part} \cdots\cdots\rightarrow| & & & \\ a_{1,0} & a_{1,1} & a_{1,2} & \ldots & a_{1,n} & a_{1,n+1} & a_{1,n+2} & \ldots \\ a_{2,0} & a_{2,1} & a_{2,2} & \ldots & a_{2,n} & a_{2,n+1} & a_{2,n+2} & \ldots \\ \vdots & \vdots & \vdots & \vdots & \vdots & \vdots & \vdots & \vdots \\ a_{n,0} & a_{n,1} & a_{n,2} & \ldots & a_{n,n} & a_{n,n+1} & a_{n,n+2} & \ldots \end{bmatrix}}_{\textit{regression coefficient matrix}} \tag{9.12b}$$

$$\mathbf{B^T}(rF_1,\ \ldots,\ rF_n) \quad = \quad \begin{bmatrix} 1 \\ D_1 \\ D_2 \\ \vdots \\ D_1^2 \\ \vdots \end{bmatrix} \quad = \quad \underbrace{\begin{bmatrix} 1 \\ (rF_1 - N_1) \\ (rF_2 - N_2) \\ \vdots \\ (rF_1 - N_1)^2 \\ \vdots \end{bmatrix}}_{\textit{model terms}} \tag{9.12c}$$

The matrix multiplication defined by Eq. (9.12a) describes the load calculation for a single data point that is recorded during a wind tunnel test. It can easily be implemented in the data system of a wind tunnel. The coefficients of the regression coefficient matrix $\mathbf{z^T}$ remain constant for the balance that is used during a wind tunnel test. Only the coefficients of vector $\mathbf{B^T}$ need to be updated for every data point as they are a function of the electrical outputs of the data point and the natural zeros of the balance bridges.

9.5 Exclusion of Intercept Terms

It was mentioned earlier that the use of the intercept term in the regression model of a load is optional as long as regression model terms are generated from the difference between a raw output and the natural zero of a bridge. In this case, the predicted load values hardly change if the intercept is included in the regression model because it is, by choice, a least squares approximation of zero load. Therefore, the author recommends to always include the intercept term in the regression model of a load if the electrical outputs are described as output differences. Nevertheless, it is helpful to list equations of this appendix that can be simplified or need to be modified if an analyst chooses to exclude the intercept term. The following relationship is valid if the intercept term is omitted:

$$\textit{intercept is omitted} \quad \Longrightarrow \quad a_{i,0} \;=\; 0 \quad \textit{where} \quad 1 \;\leq\; i \;\leq\; n \tag{9.13}$$

Then, the following simplifications and modifications of a subset of equations can be made:

$$\textit{Eq. (9.5}a\textit{)} \quad \Longrightarrow \quad \mathbf{A}_{1\times\delta} \;=\; \underbrace{\begin{bmatrix} D_1 & D_2 & \ldots & D_1^2 & \ldots \end{bmatrix}}_{\delta \;=\; \textit{number of supported terms}} \tag{9.14a}$$

$$\textit{Eq. (9.5}b\textit{)} \quad \Longrightarrow \quad \mathbf{x}_{\delta\times 1} \;=\; \begin{bmatrix} a_{i,1} \\ a_{i,2} \\ \vdots \end{bmatrix} \tag{9.14b}$$

$$\textit{Eq. (9.7}a\textit{)} \quad \Longrightarrow \quad \mathbf{A}_{p\times\delta} \;=\; \begin{bmatrix} D_1(1) & D_2(1) & \ldots & D_1^2(1) & \ldots \\ \vdots & \vdots & \vdots & \vdots & \vdots \\ D_1(p) & D_2(p) & \ldots & D_1^2(p) & \ldots \end{bmatrix} \tag{9.14c}$$

$$\textit{Eq. (9.12}b\textit{)} \quad \Longrightarrow \quad \mathbf{z}^{\mathbf{T}} \;=\; \begin{bmatrix} 0 & a_{1,1} & a_{1,2} & a_{1,3} & \ldots \\ \vdots & \vdots & \vdots & \vdots & \vdots \\ 0 & a_{n,1} & a_{n,2} & a_{n,3} & \ldots \end{bmatrix} \tag{9.14d}$$

It must be pointed out that the number of rows or columns used in Eqs. (9.14a), (9.14b), and (9.14c) is reduced by one even though variable δ does not explicitly show that change. In addition, the first column of the matrix on the right–hand side of Eq. (9.14d) must explicitly be set to zero. This assignment is needed as the matrix is used in a fixed column format that, by design, always equals the maximum number of regression model terms of Eq. (9.2a). Finally, it has to be emphasized that the predicted absolute balance loads can still be considered exact values even if the intercept term is not used in the original regression model of the balance load. This conclusion results from the fact that the use of the intercept term is optional whenever output differences are used as input for the regression analysis of balance calibration data.

9.6 First Derivative of Interactions

The linear part of the regression coefficient matrix is explicitly identified in Eq. (9.12b). It is a square matrix that consists of the coefficients of the terms that the output differences $D_1,\ D_2,\ \ldots,\ D_n$ define. The matrix is summarized in Eq. (9.15) below.

$$\textit{Eq. (9.12}b\textit{)} \quad \Longrightarrow \quad \textit{linear part} \quad \Longrightarrow \quad \mathbf{L} \;=\; \begin{bmatrix} a_{1,1} & a_{1,2} & \ldots & a_{1,n} \\ a_{2,1} & a_{2,2} & \ldots & a_{2,n} \\ \vdots & \vdots & \vdots & \vdots \\ a_{n,1} & a_{n,2} & \ldots & a_{n,n} \end{bmatrix} \tag{9.15}$$

The inverse $\mathbf{L}^{-1}$ of square matrix $\mathbf{L}$ has an important practical interpretation. Its off–diagonal coefficients are the first derivatives of the interactions of the balance bridges with respect to the load components assuming that each load component is applied as a single–component load (see also related comments in Chapter 11, pp. 132–134).

Appendix 10
Iterative Method

10.1 General Remarks

The *Iterative Method* is one of two balance load prediction approaches that are used in wind tunnel testing. First, the method fits electrical outputs of balance calibration data as a function of the balance loads. Afterwards, a load iteration equation is constructed from the regression coefficients of the outputs so that loads can be predicted from outputs during a wind tunnel test (see also Ref. [7], pp. 22–24).

It is useful to develop a new derivation of the load iteration equation as often only one of two possible iteration equation types is discussed in the literature. The new derivation assumes that the *Iterative Method* is applied to a balance that measures n load components. In principle, the number of load components of a balance must always match the number of measured bridge outputs (a justification for this requirement is given in Chapter II, p. 11). Balance loads may be described by using the following symbols: $F_1,\ F_2,\ \ldots,\ F_n$. Similarly, the raw outputs of the balance bridges may be described by using the following symbols: $rF_1,\ rF_2,\ \ldots,\ rF_n$. Then, the regression model of a single raw output rF_i can be described by the following generic relationship where i is the bridge index:

$$rF_i \quad = \quad f_i(F_1,\ F_2,\ \ldots,\ F_n) \tag{10.1}$$

The coefficients of the regression model of each raw output rF_i may be computed by applying global regression analysis to balance calibration data. Then, the coefficients are used to define the load iteration equation. The regression model of a raw output is defined in detail in the next section. Afterwards, two load iteration equations are developed.

10.2 Regression Model of Single Raw Output

A balance calibration provides data for the development of the load iteration equation that the *Iterative Method* uses for the load prediction. In theory, a single raw output of a balance bridge may be a function of all loads that are applied to the balance. Then, assuming that a raw output, i.e., an absolute voltage measurement, with index i is expressed as a function of the traditional set of regression model terms for balance data (see Ref. [7], p. 12, Eq. (3.1.3)), the following regression model of the output can be defined:

Multivariate Regression Model *(Raw Output)*

$$rF_i \quad = \quad \underbrace{b_{i,0} \ + \ b_{i,1} \cdot F_1 \ + \ b_{i,2} \cdot F_2 \ + \ \cdots}_{\lambda \ = \ maximum\ number\ of\ model\ terms} \quad = \quad b_{i,0} \ + \ \sum_{\psi=1}^{10} T_\psi(b_{i,\omega}) \tag{10.2}$$

where

intercept is required as $b_{i,0} \approx N_i \equiv$ *natural zero of balance bridge*

The intercept term and various types of regression model terms are used on the right–hand side of Eq. (10.2) above. They may be described by using ten summation term groups T_1, T_2, …, T_{10} that are defined in Table 10–1 below.

Table 10–1: Term group choices for the regression model of an electrical output.

ψ	$T_\psi(b_{i,\omega})$ *(summation definition)*	$\ldots \le \omega \le \ldots$ *(coefficient index range)*	σ_ψ *(number of terms)*
1	$\sum_{j=1}^{n} b_{i,\omega} \cdot F_j$	$1 \le \omega \le \sigma_1$	n
2	$\sum_{j=1}^{n} b_{i,\omega} \cdot \lvert F_j \rvert$	$1 + \sigma_1 \le \omega \le \sum_{\psi=1}^{2} \sigma_\psi$	n
3	$\sum_{j=1}^{n} b_{i,\omega} \cdot F_j^2$	$1 + \sum_{\psi=1}^{2} \sigma_\psi \le \omega \le \sum_{\psi=1}^{3} \sigma_\psi$	n
4	$\sum_{j=1}^{n} b_{i,\omega} \cdot F_j \cdot \lvert F_j \rvert$	$1 + \sum_{\psi=1}^{3} \sigma_\psi \le \omega \le \sum_{\psi=1}^{4} \sigma_\psi$	n
5	$\sum_{j=1}^{n-1} \sum_{k=j+1}^{n} b_{i,\omega} \cdot F_j \cdot F_k$	$1 + \sum_{\psi=1}^{4} \sigma_\psi \le \omega \le \sum_{\psi=1}^{5} \sigma_\psi$	$\frac{n \cdot (n-1)}{2}$
6	$\sum_{j=1}^{n-1} \sum_{k=j+1}^{n} b_{i,\omega} \cdot \lvert F_j \cdot F_k \rvert$	$1 + \sum_{\psi=1}^{5} \sigma_\psi \le \omega \le \sum_{\psi=1}^{6} \sigma_\psi$	$\frac{n \cdot (n-1)}{2}$
7†	$\sum_{j=1}^{n-1} \sum_{k=j+1}^{n} b_{i,\omega} \cdot F_j \cdot \lvert F_k \rvert$	$1 + \sum_{\psi=1}^{6} \sigma_\psi \le \omega \le \sum_{\psi=1}^{7} \sigma_\psi$	$\frac{n \cdot (n-1)}{2}$
8†	$\sum_{j=1}^{n-1} \sum_{k=j+1}^{n} b_{i,\omega} \cdot \lvert F_j \rvert \cdot F_k$	$1 + \sum_{\psi=1}^{7} \sigma_\psi \le \omega \le \sum_{\psi=1}^{8} \sigma_\psi$	$\frac{n \cdot (n-1)}{2}$
9	$\sum_{j=1}^{n} b_{i,\omega} \cdot F_j^3$	$1 + \sum_{\psi=1}^{8} \sigma_\psi \le \omega \le \sum_{\psi=1}^{9} \sigma_\psi$	n
10	$\sum_{j=1}^{n} b_{i,\omega} \cdot \lvert F_j^3 \rvert$	$1 + \sum_{\psi=1}^{9} \sigma_\psi \le \omega \le \sum_{\psi=1}^{10} \sigma_\psi$	n
—	—	—	$\Sigma \equiv 2 \cdot n \cdot (n+2)$

†Terms of groups 7 & 8 are related; they must either be used together or not at all (see also App. 20).

The second column of Table 10–1 above lists the ten term groups that are traditionally used for the regression analysis of a bridge output. These term groups and their group

order have become the de–facto standard for all users of the *Iterative Method* ever since the first edition of Ref. [7] was published in 2003 (see also Ref. [7], p. 12, Eq. (3.1.3)).

The order of the ten term groups is non–hierarchical as the term group $|F_j \cdot F_k|$ comes before term groups $F_j \cdot |F_k|$ and $|F_j| \cdot F_k$ (see also the detailed discussion of term group hierarchy that is given in App. 23). Terms of groups 1, 3, 5, and 9 are derived from a multivariate Taylor series expansion of the unknown functional relationship between the outputs and the loads. Absolute value terms, i.e., terms of groups 2, 4, 6, 7, 8, and 10, should only be used if the outputs of the given balance are known to have bi–directional behavior (see, e.g., Refs. [33] to [35] for a discussion of this phenomenon). The maximum number of terms can be obtained by (i) computing the sum of the last column of Table 10–1 and (ii) adding one for the intercept. Then, we get the following formula:

$$\lambda \;=\; 1 \,+\, m \;=\; 1 \,+\, \sum_{\psi=1}^{10} \sigma_\psi \;=\; 1 \,+\, \underbrace{6 \cdot n \,+\, 2 \cdot n \cdot (n-1)}_{\textit{contribution of } T_1, \ldots, T_{10}} \tag{10.3}$$

Let us assume, for example, that a calibration data set from a six–component balance is analyzed. Then, the following maximum number of regression model terms is obtained:

$$n \;=\; 6 \quad \Longrightarrow \quad \textit{Eq. (10.3)} \quad \Longrightarrow \quad \lambda \;=\; 97 \tag{10.4}$$

Only a subset of the maximum number of possible regression model terms is typically supported/chosen by an analyst whenever the regression model of an output is derived from real–world balance calibration data. The total number of supported/chosen terms fulfills the following inequality:

$$\delta \;=\; \textit{number of supported/chosen terms} \;<\; \lambda$$

Analysts have identified term group combinations that work with most balance designs. Table 10–2 below, for example, lists three term group combinations that the author often uses for the definition of the upper bound of the regression model of an output:

Table 10–2: Typical term group combinations (see also Table 10–1).

Balance Design Characteristic	Term Group Combination
single–piece balance	$F_j,\;\; F_j^2,\;\; F_j \cdot F_k$
balance with <u>known</u> bi–directional outputs (option 1)†	$F_j,\;\; \lvert F_j \rvert,\;\; F_j^2,\;\; F_j \cdot F_k$
balance with <u>known</u> bi–directional outputs (option 2)†	$F_j,\;\; \lvert F_j \rvert,\;\; F_j^2,\;\; F_j \cdot \lvert F_j \rvert,\;\; F_j \cdot F_k$

†For example, balances of Task/Able design have bi–directional normal & side force bridge outputs.

The author's term group combination choices above have the advantage that they capture the most important physical behavior of the corresponding balance design. In addition, they help prevent unwanted over–fitting of calibration data by keeping an analyst's term choices to a minimum.

The number of supported/chosen terms must be used instead of the maximum number of possible terms for the definition of the global regression analysis problem so that a non–singular/unique solution of the analysis problem can exist. In that context, it is critical to

test the regression model term combination of an output for linear or massive near–linear dependencies by using the *Variance Inflation Factor* (VIF)†. The maximum VIF of the chosen regression model of an output should be less than an empirical threshold value. Then, the model is guaranteed to define a unique relationship between the fitted output and the loads of the balance (see App. 18 for detailed discussions of the VIF and the selection of the empirical threshold for the dependency test).

10.3 Global Regression Analysis for Single Raw Output

The global regression analysis problem associated with the determination of the unknown coefficients of the supported/chosen regression model terms of a raw output rF_i can be expressed in matrix format if Eq. (10.2) is described by using row and column vectors. It is assumed, for example, that an analyst chooses the intercept term and a supported subset of both linear and non–linear terms for the regression model of an output. In that case, the following three auxiliary vectors can be defined:

$$\mathbf{A}_{1\times\delta} = \underbrace{\begin{bmatrix} 1 & F_1 & F_2 & \dots & F_1^2 & \dots \end{bmatrix}}_{\delta \,=\, number\ of\ supported\ terms} \tag{10.5a}$$

$$\mathbf{x}_{\delta\times 1} = \begin{bmatrix} b_{i,0} \\ b_{i,1} \\ b_{i,2} \\ \vdots \end{bmatrix} \tag{10.5b}$$

$$\mathbf{R}_{1\times 1} = rF_i \tag{10.5c}$$

Then, the chosen subset of Eq. (10.2) can be described by the following matrix equation:

$$\mathbf{A}_{1\times\delta} \cdot \mathbf{x}_{\delta\times 1} = \mathbf{R}_{1\times 1} \tag{10.6}$$

Now, assuming that the balance calibration data set consists of a total number of p data points, i.e., of p individual load states, the two vectors $\mathbf{A}$ and $\mathbf{R}$ of Eq. (10.6) above must be extended from a single row to p rows. Then, we get:

$$\mathbf{A}_{1\times\delta} \Longrightarrow \mathbf{A}_{p\times\delta} = \begin{bmatrix} 1 & F_1(1) & F_2(1) & \dots & F_1^2(1) & \dots \\ 1 & F_1(2) & F_2(2) & \dots & F_1^2(2) & \dots \\ \vdots & \vdots & \vdots & \vdots & \vdots & \vdots \\ 1 & F_1(p) & F_2(p) & \dots & F_1^2(p) & \dots \end{bmatrix} \tag{10.7a}$$

$$\mathbf{R}_{1\times 1} \Longrightarrow \mathbf{R}_{p\times 1} = \begin{bmatrix} rF_i(1) \\ rF_i(2) \\ \vdots \\ rF_i(p) \end{bmatrix} \tag{10.7b}$$

† A connection between the reliability of multivariate regression models of balance data and the *Variance Inflation Factor* was first detected in 2007. At that time, an observed divergence of the load iterations of the *Iterative Method* was traced back to the presence of large *Variance Inflation Factors* (Ref. [27], p. 4).

Finally, after introducing the two extensions above in Eq. (10.6), the global regression analysis problem of the given balance calibration data for a single output can be summarized by the matrix equation below where vector $\mathbf{x}$ has the unknown coefficients of

Global Regression Analysis Problem

$$\underbrace{\mathbf{A}_{p\times\delta}}_{known} \cdot \underbrace{\mathbf{x}_{\delta\times 1}}_{unknown} = \underbrace{\mathbf{R}_{p\times 1}}_{known} \qquad (10.8)$$

the regression model of the output. The coefficients need to be determined by solving the global regression analysis problem. The solution of the regression analysis problem can directly be obtained from a well–known application of the *Moore–Penrose Inverse* that is described in the literature (see Ref. [64], pp. 35–39, and Refs. [77], [78]). Then, the solution of the global least squares problem, i.e., the regression coefficient set of a raw bridge output, is given by the following matrix equation:

Regression Coefficients
(solution of global regression analysis problem)

$$\mathbf{x}_{\delta\times 1} = \left[\ \mathbf{A^T}\cdot\ \mathbf{A}\ \right]^{-1}_{\delta\times\delta} \cdot \left[\ \mathbf{A^T}\cdot\ \mathbf{R}\ \right]_{\delta\times 1} \qquad (10.9)$$

It is possible to describe the regression coefficients of a single raw output above by using alternate nomenclature. Then, load iteration equations of the *Iterative Method* can be developed in a format that is compatible with relationships reported in Ref. [7]. The following four nomenclature substitutions are defined for that purpose:

$$\mathbf{x} = \mathbf{C'^T} \qquad (10.10a)$$

$$\mathbf{A^T} = \mathbf{G'} \qquad (10.10b)$$

$$\mathbf{A} = \mathbf{G'^T} \qquad (10.10c)$$

$$\mathbf{R} = \mathbf{rF^T} \qquad (10.10d)$$

Now, after applying the four substitutions above to Eq. (10.9), we get the following alternate format of the solution of the global least squares problem for a single output:

$$\mathbf{C'^T}_{\delta\times 1} = \left[\ \mathbf{G'}\cdot\ \mathbf{G'^T}\ \right]^{-1}_{\delta\times\delta} \cdot \left[\ \mathbf{G'}\cdot\ \mathbf{rF^T}\ \right]_{\delta\times 1} \qquad (10.11)$$

In the next step, after taking the transpose of both sides of Eq. (10.11) and using the two well–known relationships $(\mathbf{X^T})^\mathbf{T} = \mathbf{X}$ and $(\mathbf{X\,Y})^\mathbf{T} = \mathbf{Y^T X^T}$ to describe the result, we get (the relationships were taken from Ref. [65], p. 334):

$$\mathbf{C'}_{1\times\delta} \quad = \quad \mathbf{rF}_{1\times p} \cdot \mathbf{G'}^{\mathbf{T}}_{p\times\delta} \cdot \Big[\big[\mathbf{G'} \cdot \mathbf{G'}^{\mathbf{T}} \big]^{-\mathbf{1}} \Big]^{\mathbf{T}}_{\delta\times\delta} \tag{10.12a}$$

We also know that $(\mathbf{X^{-1}})^\mathbf{T} = (\mathbf{X^T})^{-\mathbf{1}}$ (see Ref. [65], p. 334). Then, we get

$$\mathbf{C'}_{1\times\delta} \quad = \quad \mathbf{rF}_{1\times p} \cdot \mathbf{G'}^{\mathbf{T}}_{p\times\delta} \cdot \Big[\big[\mathbf{G'} \cdot \mathbf{G'}^{\mathbf{T}} \big]^{\mathbf{T}} \Big]^{-\mathbf{1}}_{\delta\times\delta} \tag{10.12b}$$

In addition, using again the relationships $(\mathbf{X\,Y})^\mathbf{T} = \mathbf{Y^T X^T}$ and $(\mathbf{X^T})^\mathbf{T} = \mathbf{X}$, we get:

$$\big[\mathbf{G'} \cdot \mathbf{G'}^{\mathbf{T}} \big]^{\mathbf{T}} \quad = \quad \mathbf{G'} \cdot \mathbf{G'}^{\mathbf{T}} \tag{10.13}$$

Then, after using the right–hand side of Eq. (10.13) to simplify the contents of the outer square brackets on the right–hand side of Eq. (10.12*b*), we get the following alternate description of the fitted regression coefficients of a single output:

Regression Coefficients

(alternate description, compatible with nomenclature of Ref. [7])

$$\mathbf{C'}_{1\times\delta} \quad = \quad \mathbf{rF}_{1\times p} \cdot \mathbf{G'}^{\mathbf{T}}_{p\times\delta} \cdot \big[\mathbf{G'} \cdot \mathbf{G'}^{\mathbf{T}} \big]^{-\mathbf{1}}_{\delta\times\delta} \tag{10.14}$$

Both sides of Eq. (10.14) agree with both sides of Eq. (3.1.11) in Ref. [7] if remaining nomenclature differences are ignored and the subscript n in Eq. (3.1.11) of Ref. [7] is replaced by 1. The subscript n instead of 1 appears in Ref. [7] because the authors of Ref. [7] implicitly made the regression model term combination of all bridge outputs identical. The current derivation of the *Iterative Method*, on the other hand, is more general in nature. It allows an analyst to use regression models with different term combinations for each output of a balance bridge.

10.4 From Single Output to Multiple Outputs

It must be emphasized that Eq. (10.14) above only specifies coefficients of the regression model of a single raw output. Coefficients of other outputs of the balance have to be obtained by updating (i) row vector $\mathbf{rF} = \mathbf{R^T}$ that has the outputs $rF_i(1)$, ..., $rF_i(p)$ of the chosen bridge (see Eq. (10.7*b*) and (10.10*d*)) and (ii) matrix $\mathbf{G'} = \mathbf{A^T}$ that has the regression model terms derived from all load components of the n–component balance (see Eqs. (10.7*a*) and (10.10*b*)). Afterwards, it is possible to store the regression coefficients of all outputs in a rectangular matrix so that a single load iteration equation for all load components can be constructed. This rectangular matrix is obtained by first mapping the row vector $\mathbf{C'}$ with the coefficients of each output from the supported δ terms to the maximum number of λ terms. The mapping does not change the result of the regression

analysis of the output as coefficients of unused regression model terms of Eq. (10.2) are assigned to be zero. Then, the solution vector of the coefficients of the regression model of a single output with index i can be expressed as follows:

$$\{\ \textit{supported terms}\ (\delta)\ \Longrightarrow\ \textit{all terms}\ (\lambda)\ \}\quad\Longrightarrow\quad\{\ \mathbf{C'}_{1\times\delta}\ \Longrightarrow\ \mathbf{C'}_{1\times\lambda}\ \}\qquad(10.15a)$$

It is important to keep in mind that the analyst may choose to use different term combinations for the different balance outputs. However, the solution vectors $\mathbf{C'}$ of each single output can be combined in a rectangular matrix with a total of n rows and λ columns after coefficients of each output were mapped from the supported terms to the maximum number of terms. This conclusion can be summarized as follows:

$$\{\ \textit{single output}\ (1)\ \Longrightarrow\ \textit{all outputs}\ (n)\ \}\quad\Longrightarrow\quad\{\ \mathbf{C'}_{1\times\lambda}\ \Longrightarrow\ \mathbf{C'}_{n\times\lambda}\ \}\qquad(10.15b)$$

At this point, the analytical relationship between balance loads and electrical outputs is known for all outputs. It is described by the regression coefficient values that are stored in the extended matrix $\mathbf{C'}$ that has n rows and λ columns. It remains to construct a load iteration process from the extended matrix $\mathbf{C'}$ so that loads can be predicted from electrical outputs during a wind tunnel test. This load iteration process can be defined by using an output difference vector as a starting point. This vector is derived in the next section of the appendix.

10.5 Output Difference Vector

In principle, the load iteration equation of the balance can be developed from a modified version of Eq. (10.6) after subscript δ is replaced by λ. First, it is required to extend this relationship from a single output to all n outputs of the balance. Then, by inspection, Eq. (10.6) can be expressed as follows:

$$\underbrace{\mathbf{A}_{1\times\lambda}\cdot\mathbf{x}_{\lambda\times1}=\mathbf{R}_{1\times1}}_{\textit{single output ... from Eq. (10.6)}}\quad\Longrightarrow\quad\underbrace{\mathbf{A}_{1\times\lambda}\cdot\mathbf{x}_{\lambda\times n}=\mathbf{R}_{1\times n}}_{\textit{extension from 1 to n outputs}}\qquad(10.16a)$$

In addition, after applying the four nomenclature substitutions defined in Eqs. (10.10a) to (10.10d) to the second equation shown in Eq. (10.16a) above, we get:

$$\underbrace{\mathbf{A}_{1\times\lambda}\cdot\mathbf{x}_{\lambda\times n}=\mathbf{R}_{1\times n}}_{\textit{extension from 1 to n outputs}}\quad\Longrightarrow\quad\mathbf{G'^{T}}_{1\times\lambda}\cdot\mathbf{C'^{T}}_{\lambda\times n}=\mathbf{rF^{T}}_{1\times n}\qquad(10.16b)$$

Finally, after taking the transpose of the second equation of Eq. (10.16b) above, we get:

$$\mathbf{C'}_{n\times\lambda}\cdot\mathbf{G'}_{\lambda\times1}=\mathbf{rF}_{n\times1}\qquad(10.16c)$$

The load iteration equation can be derived from Eq. (10.16c) after the intercept term, i.e., $b_{i,0}$, of the regression model is subtracted from the raw output, i.e., rF_i, of the related bridge (see also Eq. (10.2)). Then, the load prediction becomes independent of any

instrumentation–induced output off–set that may be contained in the output measurements during a wind tunnel test. This approach has the added benefit that the intercept terms of the bridges themselves can practically be ignored during the load prediction as long as the differences between the measured raw output and the natural zero of the balance bridge, i.e., *Difference Type 1* of App. 6, is used as input for the balance load prediction during a wind tunnel test.

By design, intercept terms of the regression models of the outputs are stored in the first column of matrix $\mathbf{C}'$ that is used in Eq. (10.16c). Therefore, the subtraction of the intercepts can be accomplished if the matrix is split into a column vector and a matrix. Then, knowing from Eq. (10.3) that λ equals $1 + m$, we get the following relationship

$$\mathbf{C'}_{n\times\lambda} \quad = \quad \mathbf{C'}_{n\times(1+m)} \quad = \quad [\ \mathbf{b}_{n\times 1}\ \ \mathbf{C}_{n\times m}\ ] \tag{10.17a}$$

where vector $\mathbf{b}$ has the intercepts of the n balance bridges and matrix $\mathbf{C}$ has all remaining coefficients. The coefficients of vector $\mathbf{b}$ and matrix $\mathbf{C}$ are simply given as:

$$b(i) \quad = \quad C'(i,1) \qquad for \quad 1 \le i \le n \qquad where \qquad b(i) \ = \ b_{i,0} \tag{10.17b}$$

$$C(i,j) \quad = \quad C'(i,j+1) \qquad for \quad 1 \le i \le n \qquad and \qquad 1 \le j \le m \tag{10.17c}$$

Similarly, vector $\mathbf{G}'$ of Eq. (10.16c) may be split into two parts where $\mathbf{I}$ represents the

$$\mathbf{G'}_{(1+m)\times 1} \quad = \quad \begin{bmatrix} \mathbf{I}_{1\times 1} \\ \mathbf{G}_{m\times 1} \end{bmatrix} \tag{10.17d}$$

identity matrix described with the single scalar 1 and vector $\mathbf{G}$ is defined as follows:

$$G(i) \quad = \quad G'(i+1) \qquad for \qquad 1 \le i \le m \tag{10.17e}$$

Then, after using the right–hand sides of Eqs. (10.17a) and (10.17d) to replace $\mathbf{C}'$ and $\mathbf{G}'$ in Eq. (10.16c) and switching the left– and right–hand sides of the resulting equation, we get the following relationship for a total of n outputs:

$$\begin{aligned} \mathbf{rF}_{n\times 1} \quad &= \quad \mathbf{C'}_{n\times(1+m)} \ \cdot \ \mathbf{G'}_{(1+m)\times 1} \\ &= \quad [\ \mathbf{b}_{n\times 1}\ \mathbf{C}_{n\times m}\ ] \ \cdot \ \begin{bmatrix} \mathbf{I}_{1\times 1} \\ \mathbf{G}_{m\times 1} \end{bmatrix} \\ &= \quad \mathbf{b}_{n\times 1} \ \cdot \ \mathbf{I}_{1\times 1} \ + \ \mathbf{C}_{n\times m} \ \cdot \ \mathbf{G}_{m\times 1} \\ &= \quad \mathbf{b}_{n\times 1} \ + \ \mathbf{C}_{n\times m} \ \cdot \ \mathbf{G}_{m\times 1} \end{aligned} \tag{10.18}$$

It is necessary to rearrange Eq. (10.18) further so that the starting point for the derivation of the load iteration equations is obtained. Therefore, vector $\mathbf{b}$ is moved to the left–hand side of Eq. (10.18). Then, the following relationship is obtained:

$$\mathbf{rF}_{n\times 1} \ - \ \mathbf{b}_{n\times 1} \quad = \quad \mathbf{C}_{n\times m} \ \cdot \ \mathbf{G}_{m\times 1} \tag{10.19}$$

The left–hand side of Eq. (10.19) is a vector difference. It equals the difference between a vector consisting of raw outputs and a vector consisting of intercept terms. It can be abbreviated by introducing the output difference vector $\mathbf{\Delta rF}$. Then, we get:

Output Difference Vector

$$\mathbf{\Delta rF}_{n\times 1} = \underbrace{\mathbf{rF}_{n\times 1}}_{raw\ outputs} - \underbrace{\mathbf{b}_{n\times 1}}_{intercepts} \qquad (10.20)$$

The output difference vector $\mathbf{\Delta rF}$ defined in Eq. (10.20) above is the input for the load iteration equations that will be derived in the next section. The right–hand side of Eq. (10.19) has the regression models of the outputs that are left if intercept terms are ignored. Equation (10.19) can be written in more compressed form after replacing the left–hand side of Eq. (10.19) with the left–hand side of Eq. (10.20). Then, we get:

$$\mathbf{\Delta rF}_{n\times 1} = \mathbf{C}_{n\times m} \cdot \mathbf{G}_{m\times 1} \qquad (10.21)$$

Equation (10.21) above is the common starting point for the derivation of the two load iteration equations that may be used for the prediction of balance loads during a wind tunnel test. The load iteration equations are identified as *Primary Load Iteration Equation* and *Alternate Load Iteration Equation*. First, the *Primary Load Iteration Equation* is derived. Afterwards, the *Alternate Load Iteration Equation* is defined. Then, the calculation of balance loads during a wind tunnel test and differences between the two iteration equations are discussed.

10.6 Primary Load Iteration Equation

The coefficient matrix $\mathbf{C}$ used in Eq. (10.21) above has to be split into two parts in order to develop a load iteration process. The two parts are called matrix $\mathbf{C_1}$ and matrix $\mathbf{C_2}$. Then, we get:

$$\mathbf{C}_{n\times m} = \left[\begin{array}{cc} \mathbf{C_1}_{n\times n} & \mathbf{C_2}_{n\times(m-n)} \end{array} \right] \qquad (10.22a)$$

Regression coefficients of the n linear load terms are saved in square matrix $\mathbf{C_1}$. This matrix is defined as:

$$C_1(i,j) = C(i,j) \qquad for \quad 1 \le i \le n \quad and \quad 1 \le j \le n \qquad (10.22b)$$

Regression coefficients of all remaining load terms are saved in rectangular matrix $\mathbf{C_2}$. This matrix is defined as:

$$C_2(i,j) = C(i,j+n) \qquad for \quad 1 \le i \le n \quad and \quad 1 \le j \le m-n \qquad (10.22c)$$

Similarly, it is necessary to split the auxiliary column vector $\mathbf{G}$ into two corresponding parts. The two parts are called vector $\mathbf{F}$ and vector $\mathbf{H}$. Then, we get:

$$\mathbf{G}_{m\times 1} = \left[\begin{array}{c} \mathbf{F}_{n\times 1} \\ \mathbf{H}_{(m-n)\times 1} \end{array} \right] \qquad (10.23a)$$

where

$$F(i) \quad = \quad G(i) \qquad for \quad 1 \leq i \leq n \tag{10.23b}$$

$$H(i) \quad = \quad G(i+n) \qquad for \quad 1 \leq i \leq m-n \tag{10.23c}$$

Now, after using Eq. (10.22a) and Eq. (10.23a) to replace the matrix $\mathbf{C}$ and vector $\mathbf{G}$ in Eq. (10.21), we get:

$$\begin{aligned} \mathbf{\Delta rF}_{n\times 1} &= \mathbf{C}_{n\times m} \cdot \mathbf{G}_{m\times 1} \\ &= \left[\mathbf{C_1}_{n\times n} \; \mathbf{C_2}_{n\times(m-n)} \right] \cdot \begin{bmatrix} \mathbf{F}_{n\times 1} \\ \mathbf{H}_{(m-n)\times 1} \end{bmatrix} \\ &= \mathbf{C_1}_{n\times n} \cdot \mathbf{F}_{n\times 1} + \mathbf{C_2}_{n\times(m-n)} \cdot \mathbf{H}_{(m-n)\times 1} \end{aligned} \tag{10.24}$$

Then, after solving Eq. (10.24) above for load vector $\mathbf{F}$, we get:

$$\mathbf{F}_{n\times 1} \quad = \quad \left[\mathbf{C_1}^{-1}_{n\times n} \right] \cdot \mathbf{\Delta rF}_{n\times 1} \; - \; \left[\mathbf{C_1}^{-1}_{n\times n} \cdot \mathbf{C_2}_{n\times(m-n)} \right] \cdot \mathbf{H}_{(m-n)\times 1} \tag{10.25a}$$

Vector $\mathbf{H}$ is a function of $\mathbf{F}$ as (i) $\mathbf{H}$ is a subset of $\mathbf{G}$ and (ii) $\mathbf{G}$ is a subset of $\mathbf{G'}$ that is derived from matrix $\mathbf{A}$. This conclusion can be summarized as follows:

$$\mathbf{H} \quad = \quad \mathbf{H}(\mathbf{F}) \tag{10.25b}$$

Now, after (i) using the right–hand side of Eq. (10.25b) to replace vector $\mathbf{H}$ in Eq. (10.25a) and (ii) dropping auxiliary subscripts that describe the vector or matrix size, we get:

$$\mathbf{F} \quad = \quad \left[\mathbf{C_1}^{-1} \right] \cdot \mathbf{\Delta rF} \; - \; \left[\mathbf{C_1}^{-1} \; \mathbf{C_2} \right] \cdot \mathbf{H}(\mathbf{F}) \tag{10.26}$$

Load vector $\mathbf{F}$ appears on both sides of Eq. (10.26). Therefore, it can <u>only</u> be computed by using an iteration process. Finally, after introducing the iteration step index ξ in Eq. (10.26), we get the *Primary Load Iteration Equation*:

Primary Load Iteration Equation

$$\mathbf{F}_{\xi} \quad = \quad \left[\mathbf{C_1}^{-1} \right] \cdot \mathbf{\Delta rF} \; - \; \left[\mathbf{C_1}^{-1} \; \mathbf{C_2} \right] \cdot \mathbf{H}(\mathbf{F}_{\xi-\mathbf{1}}) \tag{10.27a}$$

... where the initial guess of the load vector equals ...

$$\mathbf{F}_{\xi=\mathbf{0}} \quad = \quad \begin{bmatrix} 0 \\ \vdots \\ 0 \end{bmatrix} \tag{10.27b}$$

The iteration equation defined in Eq. (10.27a) above computes the loads of a single data point by using the output difference vector $\mathbf{\Delta rF}$ as input that is used in Eq. (10.21). It

matches the iteration equation that is frequently recommended in the literature if nomenclature differences are temporarily ignored (see, e.g., Ref. [7], p. 23, Eq. (3.3.7)). – The derivation of a second alternate load iteration equation is described in the next section.

10.7 Alternate Load Iteration Equation

The rectangular coefficient matrix $\mathbf{C}$ used in Eq. (10.21) can also be decomposed into three parts that may be used to develop an alternate load iteration process. This task can be accomplished by splitting square matrix $\mathbf{C_1}$ of Eq. (10.22a) into two square matrices $\mathbf{B_1}$ and $\mathbf{B_2}$. Then, after modifying the right–hand side of Eq. (10.22a) accordingly, we get:

$$\mathbf{C}_{n\times m} \;=\; \Big[\; \underbrace{\big\{\mathbf{B_1}_{n\times n} + \mathbf{B_2}_{n\times n}\big\}}_{\mathbf{C_1}_{n\times n}} \;\Big\{\mathbf{C_2}_{n\times(m-n)}\Big\} \;\Big] \tag{10.28a}$$

The coefficients on the principal diagonal of the first $n \times n$ submatrix of matrix $\mathbf{C}$ are saved in matrix $\mathbf{B_1}$. This matrix is defined as:

$$B_1(i,j) \;=\; \begin{cases} C(i,j) & \text{for } \; i \;=\; j \;\; \textit{and} \;\; 1 \;\le\; i,j \;\le\; n \\ 0 & \text{for } \; i \;\neq\; j \;\; \textit{and} \;\; 1 \;\le\; i,j \;\le\; n \end{cases} \tag{10.28b}$$

Off–diagonal coefficients of the first $n \times n$ submatrix are saved in matrix $\mathbf{B_2}$. This matrix is defined as:

$$B_2(i,j) \;=\; \begin{cases} 0 & \text{for } \; i \;=\; j \;\; \textit{and} \;\; 1 \;\le\; i,j \;\le\; n \\ C(i,j) & \text{for } \; i \;\neq\; j \;\; \textit{and} \;\; 1 \;\le\; i,j \;\le\; n \end{cases} \tag{10.28c}$$

All remaining coefficients are saved in matrix $\mathbf{C_2}$. Its coefficients were already defined in Eq. (10.22c) above. Now, after using (i) the right–hand side of Eq. (10.28a) to replace matrix $\mathbf{C}$ and (ii) the right–hand side of Eq. (10.23a) to replace vector $\mathbf{G}$, Eq. (10.21) can be expressed as follows:

$$\begin{aligned} \mathbf{\Delta rF}_{n\times 1} \;&=\; \mathbf{C}_{n\times m} \cdot \mathbf{G}_{m\times 1} \\ &=\; \Big[\; \big\{\mathbf{B_1}_{n\times n} + \mathbf{B_2}_{n\times n}\big\} \;\Big\{\mathbf{C_2}_{n\times(m-n)}\Big\} \;\Big] \cdot \begin{bmatrix} \mathbf{F}_{n\times 1} \\ \mathbf{H}_{(m-n)\times 1} \end{bmatrix} \\ &=\; \big\{\; \mathbf{B_1}_{n\times n} + \mathbf{B_2}_{n\times n} \;\big\} \cdot \mathbf{F}_{n\times 1} \;+\; \mathbf{C_2}_{n\times(m-n)} \cdot \mathbf{H}_{(m-n)\times 1} \\ &=\; \mathbf{B_1}_{n\times n} \cdot \mathbf{F}_{n\times 1} \;+\; \mathbf{B_2}_{n\times n} \cdot \mathbf{F}_{n\times 1} \;+\; \mathbf{C_2}_{n\times(m-n)} \cdot \mathbf{H}_{(m-n)\times 1} \end{aligned} \tag{10.29}$$

Then, after multiplying both sides of Eq. (10.29) with the inverse of matrix $\mathbf{B_1}$, solving the result for load vector $\mathbf{F}$, dropping auxiliary subscripts that describe the vector or matrix size, and replacing vector $\mathbf{H}$ by the right–hand side of Eq. (10.25b), we get:

$$\mathbf{F} \;=\; \big[\; \mathbf{B_1}^{-1} \;\big] \cdot \mathbf{\Delta rF} \;-\; \big[\; \mathbf{B_1}^{-1} \cdot \mathbf{B_2} \;\big] \cdot \mathbf{F} \;-\; \big[\; \mathbf{B_1}^{-1} \cdot \mathbf{C_2} \;\big] \cdot \mathbf{H}(\mathbf{F}) \tag{10.30}$$

Again, as it was the case in Eq. (10.26), load vector $\mathbf{F}$ appears on both sides of Eq. (10.30). Therefore, it can only be computed by using an iteration process. Finally,

after introducing the iteration step index ξ in Eq. (10.30), we get the *Alternate Load Iteration Equation*:

Alternate Load Iteration Equation

$$\mathbf{F}_{\xi} \;=\; \left[\mathbf{B_1}^{-1}\right] \cdot \mathbf{\Delta rF} \;-\; \left[\mathbf{B_1}^{-1}\mathbf{B_2}\right] \cdot \mathbf{F}_{\xi-1} \;-\; \left[\mathbf{B_1}^{-1}\mathbf{C_2}\right] \cdot \mathbf{H}(\mathbf{F}_{\xi-1}) \qquad (10.31a)$$

... where the initial guess of the load vector equals ...

$$\mathbf{F}_{\xi=0} \;=\; \begin{bmatrix} 0 \\ \vdots \\ 0 \end{bmatrix} \qquad (10.31b)$$

The iteration equation defined in Eq. (10.31a) above computes the loads for a single data point by using the output difference vector $\mathbf{\Delta rF}$ as input. – Characteristics of the two load iteration equation choices are compared in the next section of the appendix.

10.8 Comparison of Load Iteration Equations

The author applied the *Primary* and the *Alternate Load Iteration Equation* to a wide variety of balance calibration data sets. He observed that both equations converge to identical load sets as long as (i) primary sensitivities of all bridges are defined, (ii) regression models of the outputs do not have hidden linear dependencies, and (iii) the influence of the higher order terms $[\mathbf{C_1}^{-1}\mathbf{C_2}] \cdot \mathbf{H}(\mathbf{F})$ and $[\mathbf{B_1}^{-1}\mathbf{C_2}] \cdot \mathbf{H}(\mathbf{F})$ is small. This observation is no surprise because the coefficients of both load iteration equations are derived from the same regression models of the outputs. Therefore, it possible to define a *Universal Load Iteration Equation* that simultaneously describes both equations (for details see App. 25).

It must not be overlooked that the *Primary Load Iteration Equation* is, by design, more widely applicable than the *Alternate Load Iteration Method*. It often converges even if not all primary bridge sensitivities are defined. On the other hand, the *Alternate Load Iteration Method* cannot converge in this situation (see Ref. [14] for a detailed discussion of this characteristic). These circumstances typically exist whenever (i) loads of a force or moment balance are given in direct–read format and (ii) electrical outputs of the bridges are described in their original design format.

The regression model of the difference between the raw output and the natural zero of a bridge, i.e., *Difference Type 1* of App. 6, may be used instead of the regression model of a raw output to analyze balance calibration data and construct a load iteration equation. This alternate approach is the author's recommended choice. It is discussed in detail in the next section.

10.9 Regression Model of Output Differences

Regression models of the difference between raw output and the natural zero of the related balance bridge may also be used to analyze balance calibration data and construct a load iteration equation for the balance load prediction. This output format choice has

the advantage that (i) instrumentation–induced shifts between output measurements in the calibration laboratory and the wind tunnel facility are better controlled and (ii) the use of the intercept term becomes optional. A good understanding of the alternate regression analysis approach starts with the definition of the natural zeros of the balance bridges. The set of natural zeros of the balance bridges are the electrical representation of zero absolute load (the determination of the natural zeros is described in great detail in App. 8). This definition of the natural zeros can be summarized as follows:

natural zeros of a balance $\equiv$ electrical description of zero absolute load

It is convenient to describe the natural zeros of an n–component balance in vector format. Then, we get:

$$natural\ zeros \implies \mathbf{N}_{n\times 1} = \begin{bmatrix} N_1 \\ \vdots \\ N_i \\ \vdots \\ N_n \end{bmatrix} \tag{10.32}$$

Raw outputs of balance bridges may also be described in vector format. We get:

$$raw\ outputs \implies \mathbf{rF}_{n\times 1} = \begin{bmatrix} rF_1 \\ \vdots \\ rF_i \\ \vdots \\ rF_n \end{bmatrix} \tag{10.33}$$

The difference between raw output and natural zero of a balance bridge, i.e., *Difference Type 1* of App. 6, is the new dependent variable of the regression analysis problem that the *Iterative Method* solves. The difference is defined by the following relationship:

$$D_i = rF_i - N_i \quad ; \quad 1 \leq i \leq n \tag{10.34a}$$

Again, it is convenient to describe the output differences in vector format. We get:

$$output\ differences \implies \mathbf{D}_{n\times 1} = \mathbf{rF}_{n\times 1} - \mathbf{N}_{n\times 1} = \begin{bmatrix} rF_1 - N_1 \\ \vdots \\ rF_i - N_i \\ \vdots \\ rF_n - N_n \end{bmatrix} \tag{10.34b}$$

Now, after replacing the raw outputs on the left–hand side of Eq. (10.2) with the corresponding output differences that are described above, the following multivariate regression model of an output difference *(Difference Type 1)* can be defined:

Multivariate Regression Model *(Difference Type 1)*

$$D_i = \underbrace{b_{i,0} + b_{i,1} \cdot F_1 + b_{i,2} \cdot F_2 + \cdots}_{\lambda \, = \, maximum \; number \; of \; model \; terms} = b_{i,0} + \sum_{\psi=1}^{10} T_\psi(b_{i,\omega}) \quad (10.35)$$

where

intercept is optional as $b_{i,0} \approx 0 \;\equiv\; approximation\ of\ zero\ output$

By design, the intercept term $b_{i,0}$ is a least squares approximation of zero output if tare corrected loads are used to fit output differences of a balance bridge. Therefore, the use of the intercept term becomes optional. The remaining regression model term groups used on the right–hand side of Eq. (10.35) match those that are used on the right–hand side of Eq. (10.2). In addition, all steps required for the definition of the two load iteration equations, i.e., Eqs. (10.27a) and (10.31a), remain valid if the regression model of an output difference instead of the regression model of a raw output is used.

It is mentioned above that the use of the intercept is optional if output differences of a balance bridge are fitted as a function of the balance loads. In this case, the predicted output values hardly change if the intercept is included in the regression model because it is, by choice, a least squares approximation of zero output. Therefore, the author recommends to always include the intercept term in the regression model of an output if the electrical outputs are described as either raw outputs or output differences. Nevertheless, it is helpful to list equations of this appendix that can be simplified or need to be modified if an analyst chooses to intentionally omit the intercept term. The following relationship is valid if the intercept term is omitted:

$$intercept\ is\ omitted \implies b_{i,0} = 0 \quad where \quad 1 \leq i \leq n \quad (10.36)$$

Then, the following simplifications and modifications of a subset of equations of this appendix can be made:

$$Eq.\ (10.5a) \implies \mathbf{A}_{1\times\delta} = \underbrace{\begin{bmatrix} F_1 & F_2 & \dots & F_1^2 & \dots \end{bmatrix}}_{\delta \, = \, number \; of \; supported \; terms} \quad (10.37a)$$

$$Eq.\ (10.5b) \implies \mathbf{x}_{\delta\times 1} = \begin{bmatrix} b_{i,1} \\ b_{i,2} \\ \vdots \end{bmatrix} \quad (10.37b)$$

$$Eq.\ (10.7a) \implies \mathbf{A}_{p\times\delta} = \begin{bmatrix} F_1(1) & F_2(1) & \dots & F_1^2(1) & \dots \\ F_1(2) & F_2(2) & \dots & F_1^2(2) & \dots \\ F_1(3) & F_2(3) & \dots & F_1^2(3) & \dots \\ \vdots & \vdots & \vdots & \vdots & \vdots \\ F_1(p) & F_2(p) & \dots & F_1^2(p) & \dots \end{bmatrix} \tag{10.37c}$$

$$Eq.\ (10.17b) \implies b(i) = C'(i,1) \quad for \quad 1 \le i \le n \quad where \quad b(i) = 0 \tag{10.37d}$$

It must be pointed out that the number of rows or columns used in Eqs. (10.37a), (10.37b), and (10.37c) and is reduced by one even though variable δ does not explicitly show that change. Differences exist between the two output formats when the resulting load iteration equations are used to compute the balance load during a wind tunnel test. These differences are discussed in the next two sections.

10.10 Balance Load Calculation (Raw Outputs)

It was demonstrated in the previous sections how load iteration equations for the prediction of balance loads can be developed from the regression models of raw outputs (see Eq. (10.2)). These load iteration equations predict balance loads, i.e., loads relative to the load datum of zero absolute load, using raw output measurements during a wind tunnel test as input. It is useful for the discussion of the balance load calculations to introduce the following abbreviation of the load iteration process where $\mathbf{F}$ is the final result of the load iterations, $\mathbf{F}_\xi$ is the load iteration equation, and $\mathbf{\Delta rF}$ is the output difference vector.

$$\mathbf{F} = \underset{|\delta\mathbf{F}| < TOL}{Iteration}\left\{ \mathbf{F}_\xi \right\} = \underset{|\delta\mathbf{F}| < TOL}{Iteration}\left\{ \mathbf{F}_\xi(\underbrace{\mathbf{\Delta rF}}_{input}) \right\} \tag{10.38}$$

The output measurements themselves are hidden in the components of vector $\mathbf{\Delta rF}$ that is an input for the load iteration equations (see Eqs. 10.20), (10.27a), and (10.31a)). It is assumed that the load iteration equations were generated from the regression models of the raw outputs. Then, intercepts terms are an essential part of the regression model of the output. They cannot be ignored. Consequently, using Eq. (10.20), the output difference vector for the load iteration equation is described by the following relationship:

$$raw\ outputs \implies \mathbf{\Delta rF}_{n\times 1} = \underbrace{\mathbf{rF}_{n\times 1}}_{raw\ outputs} - \underbrace{\mathbf{b}_{n\times 1}}_{intercepts} \tag{10.39}$$

The intercept terms of the regression models of the raw outputs are contained in vector $\mathbf{b}$ above. Their numerical values have a useful physical interpretation: they are the least squares approximation of the natural zeros of the bridges that were measured when the balance was calibrated in the laboratory. This conclusion can be summarized as follows:

$$\mathbf{b} \implies \left\{ \begin{matrix} vector\ with\ least\ squares\ approximations\ of\ natural \\ zeros\ that\ were\ recorded\ in\ the\ calibration\ laboratory \end{matrix} \right\}$$

The conclusion can also be described by using the following mathematical relationship:

$$\mathbf{b} \;=\; \begin{bmatrix} b_{1,0} \\ \vdots \\ b_{i,0} \\ \vdots \\ b_{n,0} \end{bmatrix} \;=\; \{\mathbf{b}\}_{lab.} \;\approx\; \{\mathbf{N}\}_{lab.} \;=\; \begin{bmatrix} N_1 \\ \vdots \\ N_i \\ \vdots \\ N_n \end{bmatrix}_{lab.} \tag{10.40}$$

Instrumentation used for the measurement of bridge outputs in the wind tunnel can substantially differ from the instrumentation that was used in the calibration laboratory. These differences can result in hidden output shifts that need to be taken into account when balance loads are computed. The output shifts are contained in both the raw outputs and the natural zeros that are measured in the wind tunnel. In addition, the intercept term is an essential part of the output difference vector $\mathbf{\Delta rF}$ that is the input for the load iteration equations. Consequently, absolute balance loads have to be computed in the wind tunnel by using the raw outputs and the natural zeros as input for two separate load iterations. The predicted absolute balance loads are simply the difference of the results of these two load iterations. Finally, the exact relationship for the calculation of absolute balance loads in the wind tunnel can be described by the following equations:

Absolute Balance Loads *(exact relationship)*

(assumptions ≡ raw outputs are used as input ; regression models have intercepts)

$$\mathbf{F}_{bal} \;=\; \underset{|\delta \mathbf{F}| \,<\, TOL}{Iteration}\Big\{\; \mathbf{F}_{\xi}(\mathbf{\Delta rF_1}) \;\Big\} \;-\; \underset{|\delta \mathbf{F}| \,<\, TOL}{Iteration}\Big\{\; \mathbf{F}_{\xi}(\mathbf{\Delta rF_2}) \;\Big\} \tag{10.41a}$$

where

$$\mathbf{\Delta rF_1} \;=\; \underbrace{\{\mathbf{rF}\}_{tunnel}}_{raw\ outputs} \;-\; \underbrace{\{\mathbf{b}\}_{lab.}}_{required} \tag{10.41b}$$

$$\mathbf{\Delta rF_2} \;=\; \underbrace{\{\mathbf{N}\}_{tunnel}}_{raw\ outputs} \;-\; \underbrace{\{\mathbf{b}\}_{lab.}}_{required} \tag{10.41c}$$

$$\mathbf{F}_{\xi} \;\equiv\; iteration\ equation\ obtained\ from\ fit\ of\ raw\ outputs$$

It is often observed that the intercepts of the regression models of the raw outputs, i.e., the components of vector $\{\mathbf{b}\}_{lab.}$ in Eqs. (10.41b) and (10.41c) above, are close to the natural zeros of the balance bridges, i.e., the components of vector $\{\mathbf{N}\}_{tunnel}$, that were measured using the tunnel's instrumentation. Then, the following approximation is valid:

$$approximation \quad \Longrightarrow \quad \{\mathbf{b}\}_{lab.} \approx \{\mathbf{N}\}_{tunnel} \tag{10.42}$$

Now, an approximation of Eq. (10.41a) can be developed after using the right–hand side of Eq. (10.42) to replace vector $\{\mathbf{b}\}_{lab.}$ in Eqs. (10.41b) and (10.41c). Then, the second

load iteration on the right–hand side of Eq. (10.41a) is no longer needed as $\mathbf{\Delta rF_2}$ equals zero. Consequently, the following approximation for the absolute balance loads is obtained:

Absolute Balance Loads *(approximation)*

(assumptions ≡ raw outputs are used as input ; regression models have intercepts)

$$\mathbf{F}_{bal} \approx \underset{|\delta \mathbf{F}| < TOL}{Iteration} \left\{ \mathbf{F}_{\xi}(\mathbf{\Delta rF_1}) \right\} \tag{10.43a}$$

where

$$\mathbf{\Delta rF_1} = \underbrace{\{\mathbf{rF}\}_{tunnel}}_{raw\ outputs} - \underbrace{\{\mathbf{N}\}_{tunnel}}_{raw\ outputs} \tag{10.43b}$$

$\mathbf{F}_{\xi} \equiv$ *iteration equation obtained from fit of raw outputs*

It must be mentioned for completeness that the vector $\mathbf{\Delta rF_1}$ defined in Eq. (10.43b) above is called delta bridge output vector in the literature (see Ref. [7], p. 22, Eq. (3.3.1)).

10.11 Balance Load Calculation (Difference Type 1)

A load iteration process for the prediction of balance loads during a wind tunnel test can also be developed from the regression models of output differences that are defined in Eq. (10.35). Resulting load iteration equations predict absolute balance loads, i.e., loads relative to the load datum of zero absolute load, using output difference measurements during a wind tunnel test as input. The output differences themselves are hidden in the components of vector $\mathbf{\Delta rF}$ that is an input for the load iteration equation (see Eqs. (10.20), (10.27a), and (10.31a) for more details).

Again, it is assumed that the load iteration equation was generated from the regression models of the output differences. Then, using Eq. (10.20), the output difference vector, i.e., the input for the load iteration process, is defined by the following relationship:

$$output\ differences \implies \mathbf{\Delta rF}_{n\times 1} = \underbrace{\mathbf{D}_{n\times 1}}_{differences} - \underbrace{\mathbf{b}_{n\times 1}}_{intercepts} \tag{10.44}$$

The intercept of the regression model of an output difference must be a least squares approximation of zero output. Therefore, vector $\mathbf{b}$ can be described as follows:

$$\mathbf{b} \implies \{\,\text{vector with least squares approximations of zero output}\,\}$$

The above description of vector $\mathbf{b}$ also means that the intercept of the regression model of an output difference may be omitted. Now, let us assume that no intercepts are used in the regression models of the output differences. Then, all components of vector $\mathbf{b}$ are perfectly zero. In that case, the output difference vector can be simplified as follows:

$$intercepts\ omitted \implies \mathbf{\Delta rF}_{n\times 1} = \mathbf{D}_{n\times 1} \tag{10.45}$$

It was mentioned in the previous section that instrumentation used for the measurement of bridge outputs in the wind tunnel can substantially differ from instrumentation that was used in the calibration laboratory. These differences can result in hidden output shifts that need to be taken into account when absolute balance loads are computed in the wind tunnel. The output shifts are present in both the raw outputs and the natural zeros that are measured using the tunnel's instrumentation. Consequently, they disappear if differences between the raw outputs and the natural zeros are computed using the tunnel's instrumentation (see Eq. (10.34a)). Therefore, the exact relationship for the calculation of the balance loads using the iteration equations from the regression analysis of the output differences can be described by the following equations:

Absolute Balance Loads *(exact relationship)*

(assumptions $\equiv$ output differences are used as input ; regression models have no intercepts)

$$\mathbf{F}_{bal} \quad = \quad \underset{|\delta \mathbf{F}| \, < \, TOL}{Iteration} \Big\{ \, \mathbf{F}_{\xi}(\mathbf{D}) \, \Big\} \qquad (10.46a)$$

where

$$\mathbf{D} \quad = \quad \underbrace{\{\mathbf{rF}\}_{tunnel} \; - \; \{\mathbf{N}\}_{tunnel}}_{Difference\ Type\ 1,\ Eq.\ (10.34b)} \qquad (10.46b)$$

$\mathbf{F}_{\xi} \quad \equiv \quad$ *iteration equation obtained from fit of output differences*

It is interesting to compare the exact relationship given by Eq. (10.46a) above with the corresponding exact relationship that is given in Eq. (10.41a). Both relationships correctly deal with hidden output shifts that may be introduced by instrumentation differences. However, the use of the iteration equation from the fitted output differences requires only one load iteration as intercepts can be omitted in corresponding regression models. Therefore, the iteration process described by Eq. (10.46a) is easier to implement than the iteration process described in Eq. (10.41a).

10.12 First Derivative of Interactions

It is explained in another part of the appendix how the regression coefficients of the fitted outputs can be used to construct the *Primary Load Iteration Equation*. A square matrix $\mathbf{C_1}$ is introduced for this purpose in Eq. (10.22a). It has the coefficients of the regression model terms that the load components F_1, F_2, ..., F_n themselves define. Matrix $\mathbf{C_1}$ has an important practical interpretation. Its off–diagonal coefficients are the first derivatives of the interactions of the balance bridges with respect to the load components assuming that each load component is applied as a single–component load (see also related comments in Chapter 11, pp. 132–134).

Appendix 11

Load Iteration Convergence Test

11.1 General Remarks

An iteration process is needed for the calculation of balance loads during a wind tunnel test whenever an analyst selects the *Iterative Method* for the balance load prediction (see App. 10 for more details). It is recommended to investigate convergence characteristics of the load iterations within the use envelope of the balance so that reliable load predictions can be guaranteed during the wind tunnel test. A new load iteration convergence test was derived in Ref. [15] for this task that is summarized in this appendix. The new test was developed in order to correct an analytical error in an alternate test that *Smith* describes in Ref. [63]. The analytical error was caused by the fact that the partial derivative $\partial f_i/\partial X_j$ of *Smith's* definition of the *Lipschitz Constant* is not always dimensionless (for details see Ref. [63], Eqs. (8), $(B6)$, $(B8)$). Consequently, *Smith's* definition is flawed because it computes the sum of quantities that are not all dimensionless.

The description of the new test starts with a discussion of the two load iteration equations that are used in the aerospace testing community. Table 11–1 below lists the iteration equations where $\mathbf{F}$ is a vector that has the predicted balance loads, $\mathbf{\Delta rF}$ is a vector that has the raw outputs or output differences of the balance bridges, $\mathbf{B_1}$, $\mathbf{B_2}$, $\mathbf{C_1}$, and $\mathbf{C_2}$ are coefficient matrices that uniquely define the load iteration characteristics of the chosen balance, and ξ is the iteration step index (see App. 10 for more details).

Table 11–1: Definition of balance load iteration equations.

Primary Load Iteration Equation ... App. 10, Eq. (10.27a) $\mathbf{F}_\xi = \left\{\mathbf{C_1}^{-1}\right\} \cdot \mathbf{\Delta rF} - \left\{\mathbf{C_1}^{-1}\mathbf{C_2}\right\} \cdot \mathbf{H}(\mathbf{F}_{\xi-1})$
Alternate Load Iteration Equation ... App. 10, Eq. (10.31a) $\mathbf{F}_\xi = \left\{\mathbf{B_1}^{-1}\right\} \cdot \mathbf{\Delta rF} - \left\{\mathbf{B_1}^{-1}\mathbf{B_2}\right\} \cdot \mathbf{F}_{\xi-1} - \left\{\mathbf{B_1}^{-1}\mathbf{C_2}\right\} \cdot \mathbf{H}(\mathbf{F}_{\xi-1})$

The new load iteration convergence test uses the *Lipschitz Condition* in combination with an estimate of the upper bound of the *Lipschitz Constant* for the assessment of convergence characteristics of the load iterations. The *Lipschitz Condition* and the related *Lipschitz Constant* are described in *Henrici's* textbook on numerical analysis (Ref. [71]). *Henrici* investigated convergence properties of the following vector sequence:

$$\mathbf{F}_0,\ \mathbf{F}_1,\ \mathbf{F}_2,\ \ldots,\ \mathbf{F}_\xi,\ \ldots \qquad \textit{where} \qquad \mathbf{F}_\xi = \mathbf{f}(\mathbf{F}_{\xi-1}) \tag{11.1a}$$

The column vector on the left–hand side of Eq. (11.1a) is defined by the equation below where ξ is the iteration step index (Ref. [71], p. 99, Eq. (95–6)). Vector $\mathbf{F}_\xi$ can be

$$\mathbf{F}_{\xi} \quad = \quad \begin{bmatrix} F_1 \\ \vdots \\ F_i \\ \vdots \\ F_n \end{bmatrix}_{n\times 1} \tag{11.1b}$$

interpreted as the load vector of an n–component balance. In addition, the right–hand side of Eq. (11.1a) above may be interpreted as the right–hand side of a load iteration equation that is defined in Table 11–1. Then, Eq. (11.1a) can be described as follows:

$$\mathbf{f}(\mathbf{F}_{\xi-\mathbf{1}}) = \begin{bmatrix} f_1(\mathbf{F}_{\xi-\mathbf{1}}) \\ \vdots \\ f_i(\mathbf{F}_{\xi-\mathbf{1}}) \\ \vdots \\ f_n(\mathbf{F}_{\xi-\mathbf{1}}) \end{bmatrix}_{n\times 1} = \begin{cases} \underbrace{\mathbf{C_1}^{-1}\mathbf{\Delta rF} \; - \; \mathbf{C_1}^{-1}\mathbf{C_2}\cdot\mathbf{H}(\mathbf{F}_{\xi-\mathbf{1}})}_{\textit{Primary Load Iteration Equation}} \\ \\ \underbrace{\mathbf{B_1}^{-1}\mathbf{\Delta rF} - \mathbf{B_1}^{-1}\mathbf{B_2}\cdot\mathbf{F}_{\xi-\mathbf{1}} - \mathbf{B_1}^{-1}\mathbf{C_2}\cdot\mathbf{H}(\mathbf{F}_{\xi-\mathbf{1}})}_{\textit{Alternate Load Iteration Equation}} \end{cases} \tag{11.1c}$$

Now, after replacing the left–hand side of Eq. (11.1a) with the right–hand side of Eq. (11.1b) and the right–hand side of Eq. (11.1a) with the term of Eq. (11.1c) that is between the equal signs, we get:

$$\mathbf{F}_0,\ \mathbf{F}_1,\ \mathbf{F}_2,\ \ldots,\ \mathbf{F}_{\xi},\ \ldots \qquad \textit{where} \qquad \underbrace{\begin{bmatrix} F_1 \\ \vdots \\ F_i \\ \vdots \\ F_n \end{bmatrix}}_{\mathbf{F}_{\xi}} \quad = \quad \underbrace{\begin{bmatrix} f_1(\mathbf{F}_{\xi-\mathbf{1}}) \\ \vdots \\ f_i(\mathbf{F}_{\xi-\mathbf{1}}) \\ \vdots \\ f_n(\mathbf{F}_{\xi-\mathbf{1}}) \end{bmatrix}}_{\mathbf{f}(\mathbf{F}_{\xi-1})} \tag{11.2}$$

The explicit description of the sequence above highlights two important facts: (i) the unit of component F_i on the left–hand–side of Eq. (11.2) must always match the unit of component f_i on the right–hand side of Eq. (11.2), and, (ii) units of load components F_1 to F_n are not necessarily all the same because the load component of a balance is either a force or a moment. These two facts have to be taken into account whenever *Henrici's* generic description of the *Lipschitz Condition* is applied to load iteration equations of a balance. This application is discussed in more detail in the next section.

11.2 Load Iteration Convergence Test

Henrici rigorously showed that the generic vector sequence $\mathbf{F}_0$, $\mathbf{F}_1$, $\mathbf{F}_2$, ... defined in Eq. (11.2) above will converge to a single value if the *Lipschitz Condition* is fulfilled, i.e., if the *Lipschitz Constant* of the iteration process is less than the threshold of one (see Ref. [71], p. 99–101). *Henrici's* description of the iteration convergence test can directly be applied to the load iteration process if a conservative upper bound L_{max} of the *Lipschitz Constant* is obtained using (i) a suitable upper bound $\mathbf{F}_{\psi}$ of the load vector and (ii) the

partial derivatives $\partial f_i(\mathbf{F}_\psi)/\partial F_j$ as input. Then, the *Lipschitz Condition* for the balance load iteration process can be summarized as follows:

Lipschitz Condition

$$L_{max}\left\{\frac{\partial\, f_1(\mathbf{F}_\psi)}{\partial\, F_1}\ ,\ \ldots\ ,\ \frac{\partial\, f_i(\mathbf{F}_\psi)}{\partial\, F_j}\ ,\ \ldots\ ,\ \frac{\partial\, f_n(\mathbf{F}_\psi)}{\partial\, F_n}\right\}\ <\ 1 \qquad (11.3)$$

It is critical to realize that *Henrici's* generic convergence test compares the *Lipschitz Constant* with the dimensionless threshold of one. Numerator and denominator of the partial derivatives $\partial f_i(\mathbf{F}_\psi)/\partial F_j$ describe balance loads in the current application of the test that do not necessarily have matching units. In addition, the derivatives are added during the calculation of the upper bound of the *Lipschitz Constant*. Therefore, all derivatives must be made dimensionless before use so that the resulting estimate of the upper bound of the *Lipschitz Constant*, i.e., L_{max}, is also dimensionless. Unfortunately, this important requirement was overlooked in Ref. [63]. Consequently, Eqs. (8), (B6), and (B8) of Ref. [63] are incorrect as some of the partial derivatives given in those equations could, for example, have a force in the numerator and a moment in the denominator (or vice versa).

The partial derivatives of the load components can be made dimensionless by simply multiplying each derivative with a scale factor. This scale factor equals the inverse of the ratio between the capacities of the related load pair. Then, the revised and improved definition of the upper bound of the *Lipschitz Constant* can be summarized as follows:

Upper Bound of the Lipschitz Constant

$$L_{max} \;=\; \sqrt{\sum_{i=1}^{n}\sum_{j=1}^{n}\underbrace{\left\{\frac{\partial\, f_i(\mathbf{F}_\psi)}{\partial\, F_j}\ \cdot\ \frac{\Gamma_j}{\Gamma_i}\right\}}_{dimensionless\ derivative}^{2}} \qquad (11.4)$$

where

$\mathbf{F}_\psi$ $\equiv$ *upper bound of the load vector*

$\dfrac{\partial\, f_i(\mathbf{F}_\psi)}{\partial\, F_j}$ $\equiv$ *coefficient of the Jacobian Matrix* $\mathcal{J}\{\mathbf{f}(\mathbf{F}_\psi)\}$

$\dfrac{\Gamma_j}{\Gamma_i}$ $\equiv$ *scale factor that makes* $\dfrac{\partial\, f_i(\mathbf{F}_\psi)}{\partial\, F_j}$ *dimensionless*

Γ_φ $\equiv$ *capacity of balance load component with index* φ

The upper bound of the *Lipschitz Constant* can be computed after (i) the upper bound of the load vector $\mathbf{F}_\psi$ and (ii) the partial derivatives $\partial f_i(\mathbf{F}_\psi)/\partial F_j$ are defined. First, the selection of the upper bound of the load vector is discussed.

Three choices for the upper bound of the load vector are suggested in the literature. Each choice is either a function of the load capacities of the balance or a function of the largest applied calibration load of each component (see, e.g., the discussion in Ref. [63], App. B). A fourth choice is also of interest. It is the load vector whose components equal the loads of the calibration data point with the greatest dimensionless length in n–dimensional space (length $\equiv$ *Euclidean Norm*). In theory, convergence characteristics of this fourth choice should be closest to the observed convergence characteristics of the balance calibration data set that generated the load iteration equation in the first place. All four choices for the upper bound of the load vector can be summarized as follows:

Upper Bound of Load Vector

$$\mathbf{F}_\psi = \begin{bmatrix} F_{\psi_1} \\ F_{\psi_2} \\ \vdots \\ F_{\psi_n} \end{bmatrix}_{n\times 1} = \begin{cases} \textit{Choice } 1 \implies 3/2 \cdot \mathbf{F}' \\ \textit{Choice } 2 \implies \mathbf{F}' \\ \textit{Choice } 3 \implies \mathbf{F}'' \\ \textit{Choice } 4 \implies \mathbf{F}''' \end{cases} \qquad (11.5)$$

where

$\mathbf{F}'$ $\equiv$ *vector of load capacities* $\Gamma_1,\ \Gamma_2,\ \ldots\ \Gamma_n$
$\mathbf{F}''$ $\equiv$ *vector of largest tare corrected loads*
$\mathbf{F}'''$ $\equiv$ *load vector of calibration point with greatest dimensionless length*

It is important to point out that *Choice 1*, *Choice 2*, and *Choice 3* above are very conservative in nature. They assume that all load components are simultaneously applied. This situation rarely exists during actual use of the balance. *Choice 4*, on the other hand, uses loads of the calibration data point with the greatest dimensionless length. Therefore, it is the least conservative choice.

In theory, partial derivatives used for the definition of the *Lipschitz Constant* above should be obtained from the *Jacobian Matrix* of the right–hand sides of the load iteration equations that are described in Table 11–1. This $n \times n$ matrix is defined as follows

$$\mathcal{J}\{\mathbf{f}(\mathbf{F}_\psi)\} = \left[\frac{\partial\, \mathbf{f}(\mathbf{F}_\psi)}{\partial\, F_1} \quad \cdots \quad \frac{\partial\, \mathbf{f}(\mathbf{F}_\psi)}{\partial\, F_j} \quad \cdots \quad \frac{\partial\, \mathbf{f}(\mathbf{F}_\psi)}{\partial\, F_n} \right]_{n\times n} \qquad (11.6a)$$

where vector $\mathbf{f}(\mathbf{F}_\psi)$ equals the right–hand side of Eq. (11.1c) after replacing $\mathbf{F}_{\xi-\mathbf{1}}$ with $\mathbf{F}_\psi$. Each column of the *Jacobian Matrix* can be described as a vector. Then, we get

$$j-th\ column\ of\ \mathcal{J}\{\mathbf{f}(\mathbf{F}_\psi)\} \quad \Longrightarrow \quad \frac{\partial\ \mathbf{f}(\mathbf{F}_\psi)}{\partial\ F_j} \quad = \quad \begin{bmatrix} \dfrac{\partial\ f_1(\mathbf{F}_\psi)}{\partial\ F_j} \\ \vdots \\ \dfrac{\partial\ f_i(\mathbf{F}_\psi)}{\partial\ F_j} \\ \vdots \\ \dfrac{\partial\ f_n(\mathbf{F}_\psi)}{\partial\ F_j} \end{bmatrix}_{n\times 1} \tag{11.6b}$$

which can also be expressed by explicitly using the load iteration equations. Then, we get:

$$\frac{\partial\ \mathbf{f}(\mathbf{F}_\psi)}{\partial\ F_j} \quad = \quad \begin{cases} \underbrace{\dfrac{\partial}{\partial\ F_j}\ \left\{\ \mathbf{C_1}^{-1}\mathbf{\Delta rF}\ -\ \mathbf{C_1}^{-1}\mathbf{C_2}\cdot\mathbf{H}(\mathbf{F}_\psi)\right\}}_{Primary\ Load\ Iteration\ Equation} \\ \underbrace{\dfrac{\partial}{\partial\ F_j}\left\{\mathbf{B_1}^{-1}\mathbf{\Delta rF}\ -\ \mathbf{B_1}^{-1}\mathbf{B_2}\cdot\mathbf{F}_\psi\ -\ \mathbf{B_1}^{-1}\mathbf{C_2}\cdot\mathbf{H}(\mathbf{F}_\psi)\right\}}_{Alternate\ Load\ Iteration\ Equation} \end{cases} \tag{11.6c}$$

The first term on the right–hand side of Eq. (11.6c) is independent of the balance load component F_j. Therefore, we get:

$$\frac{\partial}{\partial\ F_j}\ \left\{\ \mathbf{C_1}^{-1}\mathbf{\Delta rF}\ \right\} \quad = \quad \begin{bmatrix} 0 \\ \vdots \\ 0 \end{bmatrix}_{n\times 1} \tag{11.7a}$$

$$\frac{\partial}{\partial\ F_j}\ \left\{\ \mathbf{B_1}^{-1}\mathbf{\Delta rF}\ \right\} \quad = \quad \begin{bmatrix} 0 \\ \vdots \\ 0 \end{bmatrix}_{n\times 1} \tag{11.7b}$$

Then, after using Eqs. (11.7a) and (11.7b) to simplify the right–hand side of Eq. (11.6c), we get the following relationship for the columns of the *Jacobian Matrix*:

$$\frac{\partial\ \mathbf{f}(\mathbf{F}_\psi)}{\partial\ F_j} \quad = \quad \begin{cases} \underbrace{\dfrac{\partial}{\partial\ F_j}\ \left\{\ -\ \mathbf{C_1}^{-1}\mathbf{C_2}\cdot\mathbf{H}(\mathbf{F}_\psi)\ \ \right\}}_{Primary\ Load\ Iteration\ Equation} \\ \underbrace{\dfrac{\partial}{\partial\ F_j}\ \left\{\ -\ \mathbf{B_1}^{-1}\mathbf{B_2}\cdot\mathbf{F}_\psi\ -\ \ \mathbf{B_1}^{-1}\mathbf{C_2}\cdot\mathbf{H}(\mathbf{F}_\psi)\ \right\}}_{Alternate\ Load\ Iteration\ Equation} \end{cases} \tag{11.8}$$

The right–hand sides of Eqs. (11.6*b*) and (11.8) above define one of a total of n column vectors of partial derivatives $\partial f_i(\mathbf{F}_\psi)/\partial F_j$ that are needed for the calculation of the upper bound of the *Lipschitz Constant*. The author recommends to determine these partial derivatives numerically by using the *Central Difference Formula*. This approach is described in detail in the next section.

11.3 Numerical Calculation of Partial Derivatives

A numerical estimate of the partial derivatives $\partial f_i(\mathbf{F}_\psi)/\partial F_j$ can be computed by using the *Central Difference Formula* (see, e.g., Ref. [66], p. 181, Eq. (5.7.7), for more details). An auxiliary vector $\mathbf{g}(\mathbf{F}_\psi)$ is introduced to better describe the application of the *Central Difference Formula* in this context. It is defined as follows:

$$\mathbf{g}(\mathbf{F}_\psi) \quad = \quad \begin{bmatrix} g_1(\mathbf{F}_\psi) \\ \vdots \\ g_i(\mathbf{F}_\psi) \\ \vdots \\ g_n(\mathbf{F}_\psi) \end{bmatrix}_{n\times 1} \quad = \quad \begin{cases} \underbrace{\mathbf{C_1}^{-1}\mathbf{C_2}\cdot\mathbf{H}(\mathbf{F}_\psi)}_{Primary\ Load\ Iteration\ Equation} \\ \\ \underbrace{\mathbf{B_1}^{-1}\mathbf{B_2}\cdot\mathbf{F}_\psi \ + \ \mathbf{B_1}^{-1}\mathbf{C_2}\cdot\mathbf{H}(\mathbf{F}_\psi)}_{Alternate\ Load\ Iteration\ Equation} \end{cases} \tag{11.9}$$

Then, after taking the derivative $\partial/\partial F_j$ on both sides of Eq. (11.9) and comparing the result with the right–hand side of Eq. (11.8), we conclude:

$$\frac{\partial\ \mathbf{g}(\mathbf{F}_\psi)}{\partial\ F_j} \quad = \quad (-1)\ \cdot\ \frac{\partial\ \mathbf{f}(\mathbf{F}_\psi)}{\partial\ F_j} \tag{11.10}$$

In addition, it is concluded that the components $\partial g_i(\mathbf{F}_\psi)/\partial F_j$ and $\partial f_i(\mathbf{F}_\psi)/\partial F_j$ of vectors $\partial \mathbf{g}(\mathbf{F}_\psi)/\partial F_j$ and $\partial \mathbf{f}(\mathbf{F}_\psi)/\partial F_j$ satisfy the following relationship:

$$\left[\frac{\partial\ g_i(\mathbf{F}_\psi)}{\partial\ F_j}\right]^2 \quad = \quad \left[\frac{\partial\ f_i(\mathbf{F}_\psi)}{\partial\ F_j}\right]^2 \tag{11.11}$$

The right–hand side of Eq. (11.11) is used in the definition of the upper bound of the *Lipschitz Constant* that is given in Eq. (11.4). Therefore, $\partial g_i(\mathbf{F}_\psi)/\partial F_j$ can be used instead of $\partial f_i(\mathbf{F}_\psi)/\partial F_j$ in Eq. (11.4) without changing the result. This replacement has the advantage that all negative signs on the right–hand side of Eq. (11.8) can be avoided. Then, we get an alternate definition for the upper bound of the *Lipschitz Constant* that can be summarized by the following relationship:

Upper Bound of the Lipschitz Constant

$$L_{max} \quad = \quad \sqrt{\sum_{i=1}^{n}\sum_{j=1}^{n}\left\{\ \frac{\partial\ g_i(\mathbf{F}_\psi)}{\partial\ F_j}\ \cdot\ \frac{\Gamma_j}{\Gamma_i}\ \right\}^2} \tag{11.12}$$

Now, the *Central Difference Formula* may be applied to the i–th row of column vector $\mathbf{g}(\mathbf{F}_\psi)$ in Eq. (11.9) so that estimates of the partial derivatives $\partial g_i(\mathbf{F}_\psi)/\partial F_j$ are obtained. The application of the *Central Difference Formula* is described in Eq. (11.13a) below. The

Central Difference Formula

$$\frac{\partial\, g_i(\mathbf{F}_\psi)}{\partial\, F_j} \quad \approx \quad \frac{g_{i_{(+)}} \;-\; g_{i_{(-)}}}{2 \;\cdot\; \Delta F_j} \tag{11.13a}$$

where

$$g_{i_{(+)}} = \; g_i \left(\; F_{\psi_1} \;,\; \ldots \;,\; F_{\psi_j} + \Delta F_j \;,\; \ldots \;,\; F_{\psi_n} \; \right) \tag{11.13b}$$

$$g_{i_{(-)}} = \; g_i \left(\; F_{\psi_1} \;,\; \ldots \;,\; F_{\psi_j} - \Delta F_j \;,\; \ldots \;,\; F_{\psi_n} \; \right) \tag{11.13c}$$

$$\Delta F_j \quad \equiv \quad \textit{step size of load component } F_j$$

Central Difference Formula has to be applied a total of $n \times n$ times in order to compute all partial derivatives that are needed for the calculation of the upper bound of the *Lipschitz Constant* for an n–component balance.

It is known that the accuracy of the *Central Difference Formula* is influenced by the roundoff error in the chosen step size ΔF_j. Therefore, step size ΔF_j has to be selected such that F_{ψ_j} and $F_{\psi_j} \pm \Delta F_j$ differ by an exactly representable number. An optimal choice for the step size ΔF_j exists that is a function of a characteristic scale λ_j and the relative machine precision ε. The optimal choice of ΔF_j for the *Central Difference Formula* is given by the following formula where λ_j is the characteristic scale and ε is the relative

$$\Delta F_j \quad \approx \quad \lambda_j \;\cdot\; \varepsilon^{1/3} \tag{11.14a}$$

machine precision at runtime (the formula is taken from Ref. [66], p. 182, Eq. (5.7.8)). Estimates of the characteristic scale λ_j and the relative machine precision ε are needed in order to apply Eq. (11.14a). The scalar value of the perturbed variable itself, i.e., F_{ψ_j}, is a good choice for λ_j in our context because it is a positive number that is related to the load range of the j–th load component. Therefore, we can write:

$$\lambda_j \quad = \quad F_{\psi_j} \tag{11.14b}$$

In addition, the *Forsythe, Malcolm, and Moler* algorithm may be used to determine the relative machine precision ε at runtime (for more details see Ref. [67], pp. 13–14). This simple algorithm computes an approximate value for the smallest quantity such that $1 + \varepsilon$ is greater than 1 in floating point arithmetic. The implementation of the algorithm as a function call in a generic programming language could look as follows:

```
FUNCTION GetRelativeMachinePrecision
     Epsilon = 1.0D0
     Delta   = 1.0D0 + Epsilon
     WHILE ( Delta > 1.0D0 ) DO BEGIN
          Epsilon = Epsilon / 2.0D0
          Delta   = 1.0D0 + Epsilon
     ENDWHILE
     return, Epsilon
END
```

An estimate of the lower bound of the number of load iterations is derived in great detail in the next section.

11.4 Lower Bound of Number of Iterations

A theoretical estimate of the lower bound of the number of required load iterations can be computed as a function of (i) the upper bound of the *Lipschitz Constant*, (ii) the load vector, (iii) the load iteration equation type, and (iv) the chosen load iteration tolerance. The derivation of this estimate uses a generic inequality as a starting point that is given in the literature (Ref. [71], p. 99, Eq. (5–9)).

The generic inequality uses the *Euclidean Norm* of a vector as input. This scalar is defined by the following relationship assuming that $\mathbf{X}$ is a generic n–dimensional vector:

$$\underbrace{\mathbf{X}}_{vector} = \begin{bmatrix} X_1 \\ \vdots \\ X_n \end{bmatrix}_{n \times 1} \quad \Longrightarrow \quad \underbrace{\| \mathbf{X} \|}_{scalar} = \underbrace{\sqrt{ {X_1}^2 + {X_2}^2 + \ldots + {X_n}^2 }}_{Euclidean\ Norm} \tag{11.15}$$

In addition, a square matrix $\mathbf{S}$ needs to be defined so that balance loads or load differences can be made dimensionless. This $n \times n$ matrix has the inverse of the capacity of each load component on its principal diagonal. It is defined by the following relationship:

$$\mathbf{S} = \begin{bmatrix} 1/\Gamma_1 & 0 & \cdots & 0 \\ 0 & 1/\Gamma_2 & \cdots & 0 \\ \vdots & \vdots & \vdots & \vdots \\ 0 & 0 & \cdots & 1/\Gamma_n \end{bmatrix}_{n \times n} \tag{11.16}$$

Now, the generic inequality from the literature (Ref. [71], p. 99, Eq. (5–9)) can be written as follows after all balance loads were made dimensionless by using matrix $\mathbf{S}$

$$\| \mathbf{S} \cdot (\mathbf{F}_{\xi} - \mathbf{F}_{\infty}) \| \quad \leq \quad \frac{(L_{max})^{\xi}}{1 - L_{max}} \cdot \| \mathbf{S} \cdot (\mathbf{F}_{\eta} - \mathbf{F}_{\nu}) \| \qquad (11.17)$$

where ξ is the load iteration step, L_{max} is the upper bound of the *Lipschitz Constant* (see Eq. (11.12)), $\|\mathbf{F}_{\xi} - \mathbf{F}_{\infty}\|$ is the *Euclidean Norm* of a load vector difference that is associated with the lower bound of the load change, $\|\mathbf{F}_{\eta} - \mathbf{F}_{\nu}\|$ is the *Euclidean Norm* of a load vector difference that is associated with the upper bound of the load change, and $\mathbf{S}$ is the square matrix that is defined in Eq. (11.16) above. Finally, after solving Eq. (11.17) for the load iteration step ξ, we get the following inequality that defines the lower bound of the number of required load iterations:

Lower Bound of the Number of Required Load Iterations

$$\xi \quad \geq \quad \frac{ln \left\{ (1 - L_{max}) \cdot \dfrac{\| \mathbf{S} \cdot (\mathbf{F}_{\xi} - \mathbf{F}_{\infty}) \|}{\| \mathbf{S} \cdot (\mathbf{F}_{\eta} - \mathbf{F}_{\nu}) \|} \right\}}{ln \{ L_{max} \}} \qquad (11.18)$$

The upper bound L_{max} of the *Lipschitz Constant* was already defined in Eq. (11.12). It remains to estimate the lower and upper bounds of the load change.

The lower bound of the load change can be obtained from (i) the *Euclidean Norm* of the dimensionless upper bound $\mathbf{S} \cdot \mathbf{F}_{\psi}$ of load vector $\mathbf{F}_{\psi}$ and (ii) the chosen load iteration tolerance. The value of 0.0001 % of the upper bound of the loads is a suitable choice for the load iteration tolerance. Then, we get:

Lower Bound of Load Change

$$\| \mathbf{S} \cdot (\mathbf{F}_{\xi} - \mathbf{F}_{\infty}) \| \quad \approx \quad \frac{\Theta}{100} \cdot \| \mathbf{S} \cdot \mathbf{F}_{\psi} \| \qquad (11.19a)$$

where

$$\Theta \quad \equiv \quad \textit{tolerance in percent} \quad = \quad 0.0001\,\% \qquad (11.19b)$$

Similarly, the upper bound can be related to the *Euclidean Norm* of the load change that is obtained by using $\mathbf{F}_{\psi}$ as input on a modified right–hand side of Eq. (11.1*c*). The modified right–hand side of Eq. (11.1*c*) is obtained after temporarily removing the terms

$\mathbf{C_1^{-1}\Delta rF}$ and $\mathbf{B_1^{-1}\Delta rF}$ as those terms are independent of the load change. Then, after applying square matrix $\mathbf{S}$ such that the modified right–hand side of Eq. (11.1c) becomes dimensionless, we get the following estimate of the upper bound of the load change:

$$\| \mathbf{S} \cdot (\mathbf{F}_\eta - \mathbf{F}_\nu) \| \approx \begin{cases} \underbrace{\| \mathbf{S} \cdot \{ - \mathbf{C_1^{-1}C_2} \cdot \mathbf{H}(\mathbf{F}_\psi) \} \|}_{Primary\ Load\ Iteration\ Equation} \\ \\ \underbrace{\| \mathbf{S} \cdot \{ - \mathbf{B_1^{-1}B_2} \cdot \mathbf{F}_\psi - \mathbf{B_1^{-1}C_2} \cdot \mathbf{H}(\mathbf{F}_\psi) \} \|}_{Alternate\ Load\ Iteration\ Equation} \end{cases} \tag{11.20}$$

All negative signs on the right–hand side of Eq. (11.20) can be converged to positive signs without changing the result because the *Euclidean Norm* uses the square of each vector component as input. Then, we get the final relationship for the upper bound of the load change for the two load iteration equation types:

Upper Bound of Load Change

$$\| \mathbf{S} \cdot (\mathbf{F}_\eta - \mathbf{F}_\nu) \| \approx \begin{cases} \underbrace{\| \mathbf{S} \cdot \{ \mathbf{C_1^{-1}C_2} \cdot \mathbf{H}(\mathbf{F}_\psi) \} \|}_{Primary\ Load\ Iteration\ Equation} \\ \\ \underbrace{\| \mathbf{S} \cdot \{ \mathbf{B_1^{-1}B_2} \cdot \mathbf{F}_\psi + \mathbf{B_1^{-1}C_2} \cdot \mathbf{H}(\mathbf{F}_\psi) \} \|}_{Alternate\ Load\ Iteration\ Equation} \end{cases} \tag{11.21}$$

Detailed discussions of real–world balance data examples with estimates for both the *Lipschitz Constant* and the lower bound of the number of required load iterations can be found in Ref. [15].

Appendix 12

Tare Load Iteration for Non–Iterative Method

12.1 Introduction

Strain–gage balance calibration data should include loads in the description of the load state of the balance that are caused by the combined weight of (i) the metric part of the balance, (ii) the calibration body, (iii) calibration fixtures, and (iv) weight pans. These hidden loads are traditionally called tare loads. They make it possible to describe all loads relative to the common load datum of zero absolute load if they are added to the applied calibration loads. The tare loads can be defined as follows:

> **Tare Loads** $\equiv$ loads that are exclusively caused by the combined weight of the metric part of the balance and all attached calibration hardware pieces.

A balance calibration load schedule is often split into individual load series. Each load series consists of a set of loads or load combinations that were applied while keeping the calibration hardware itself unchanged. Therefore, tare loads must remain constant within a given load series. In addition, electrical outputs of the zero load points of the load series, i.e., outputs of the first and last point of the load series, are exclusively caused by the tare loads if no gravity weights are placed on a weight pan. Consequently, they are the electrical representation of the hidden tare loads of a load series.

In theory, it is possible to estimate the tare loads from the known weight and common center of gravity location of the metric part and the attached calibration hardware pieces. However, this approach is difficult to apply in a real–world situation as the determination of the common center of gravity of the metric part and the attached calibration hardware pieces can be become very complex. Therefore, many analysts use a tare load iteration algorithm for the assessment of the hidden tare loads. The basic idea behind this iteration process is summarized in the paragraph below:

> **Tare Load Iteration Algorithm**
>
> Electrical outputs of each zero load point of a load series may be used in combination with (i) the natural zeros of the balance bridges and (ii) interim regression models of the balance calibration data for an iterative determination of numerical estimates of the tare loads of all load series. This tare load iteration process is considered converged if the following conditions are met: (i) the maximum difference between two consecutive tare load estimates is below a specified tolerance; (ii) the tare load residuals decrease monotonically.

The first tare load iteration algorithm for balance calibration data was developed in the 1970s by *Robin Galway* of NRC Canada. His algorithm was finally published in the open literature in 1999 (Ref. [80]). Afterwards, AIAA's Internal Balance Technology Working Group adopted it for use with the *Iterative Method* (see 1st edition of Ref. [7]).

A new description of a tare load iteration algorithm was prepared for this appendix. It closely follows *Galway's* original algorithm as his basic ideas can also be used with the *Non–Iterative Method* (see Ref. [7], pp. 21–22, pp. 27–45). However, two differences between *Galway's* and the author's definition of a tare load iteration algorithm exist. First, *Galway's* algorithm exclusively uses output format *Difference Type 2* for the calculation of the coefficients of the linear matrix that the determination of a first estimate of the tare loads needs (see Ref. [7], p. 32; *Difference Type 2* is defined in App. 6, Eq. (6.3); see also the discussion in section 12.7 of the appendix). Furthermore, *Galway's* algorithm performs one load calculation for each iteration step. The author's algorithm, on the other hand, performs two load calculations for each iteration step. This modification was made in order to control an iteration convergence instability that results from the use of the intercept term in the regression model of a load component. The problem is illustrated with an example in section 12.6 of the appendix.

12.2 Natural Zeros, Zero Load Outputs

The development of an improved description of the tare load iteration algorithm for the *Non–Iterative Method* has to start with basic definitions. In principle, the *Non–Iterative Method* fits each balance load component of some given calibration data as a function of all electrical outputs that describe the load state of the balance. The required regression model is defined by using output differences as independent variables. The output differences equal the difference between the raw output and the natural zero of a bridge. This output format is identified as *Difference Type 1* in App. 6. The regression model is ultimately used for the load prediction during a wind tunnel test (see also App. 9 for more details).

It is assumed that a single load component F of an n–component balance is analyzed. The chosen balance measures a total of n raw outputs $rF_1, \ \ldots, \ rF_n$. In addition, the natural zeros of all bridges, i.e., $N_1, \ \ldots, \ N_n$, are known. Then, a generic regression model of the load component can be defined that uses the output differences as independent variables. This regression model can be described by the following relationship:

$$F \ = \ f(D_1, \ \ldots, \ D_i, \ \ldots, D_n) \qquad where \qquad D_i \ = \ rF_i \ - \ N_i \tag{12.1}$$

Equation (12.1) describes the final result of a multivariate least squares fit of the given balance calibration data. The balance load is assumed (i) to be a function of n independent output measurements and (ii) the loads include tare loads that were obtained after applying the tare load iteration algorithm to the balance calibration data.

It is helpful for the detailed description of the tare load iteration algorithm to express raw electrical outputs of the balance in vector format. Then, we get:

$$raw \ outputs \quad \Longrightarrow \quad \mathbf{rF} \ = \ \begin{bmatrix} rF_1 \\ \vdots \\ rF_i \\ \vdots \\ rF_n \end{bmatrix} \tag{12.2}$$

The components of the output vector are raw outputs, i.e., absolute voltage measurements. They cannot directly be used for the determination of the tare loads unless the

natural zeros of the balance bridges, i.e., the electrical descriptions of zero absolute load, are known (the determination of the natural zeros of the balance bridges is described in great detail in App. 8). The definition of the natural zeros can be summarized as follows:

Natural Zeros $\equiv$ electrical description of the load datum of zero absolute load.

Natural zeros of a balance can also be described in vector format. Then, we get:

$$\textit{natural zeros} \quad \Longrightarrow \quad \mathbf{N} \;=\; \begin{bmatrix} N_1 \\ \vdots \\ N_i \\ \vdots \\ N_n \end{bmatrix} \tag{12.3}$$

Tare loads of a load series, i.e., loads caused by the weight of the metric part and all attached calibration hardware pieces, are indirectly quantified by the raw electrical outputs that are measured at the beginning and end of each load series assuming no weights are attached to the calibration hardware. These raw voltage measurements are called zero load outputs of a load series. They can be defined as follows:

Zero Load Outputs of a Load Series $\equiv$ raw electrical outputs that are exclusively caused by the **Tare Loads** of a load series.

The zero load outputs of a load series with index k are assumed to be raw outputs. They can also be described by using an n–component vector that can be defined by the following equation ($q \equiv$ total number of load series of the given calibration data):

$$\textit{zero load outputs of a load series} \quad \Longrightarrow \quad \mathbf{Z}_k \;=\; \begin{bmatrix} Z_{1,k} \\ \vdots \\ Z_{i,k} \\ \vdots \\ Z_{n,k} \end{bmatrix} \quad ; \quad 1 \leq k \leq q \tag{12.4}$$

The difference between the zero load output of a load series and the natural zeros is the electrical description of the tare loads in the output space if it is assumed that output differences are used for the regression analysis of balance calibration data. This conclusion can be expressed as follows:

Electrical Description of Tare Loads
(output format ≡ *Difference Type 1*, App. 6)

$$\mathbf{\Delta Z}_k \;=\; \mathbf{Z}_k - \mathbf{N} \;=\; \begin{bmatrix} \Delta Z_{1,k} \\ \vdots \\ \Delta Z_{i,k} \\ \vdots \\ \Delta Z_{n,k} \end{bmatrix} \;=\; \begin{bmatrix} Z_{1,k} - N_1 \\ \vdots \\ Z_{i,k} - N_i \\ \vdots \\ Z_{n,k} - N_n \end{bmatrix} \quad ; \quad 1 \leq k \leq q \qquad (12.5a)$$

Similarly, the difference between the natural zeros of the bridges and themselves represents the electrical description of the load datum of zero absolute load if output differences are used for the regression analysis of balance calibration data. This conclusion can be expressed as follows:

Electrical Description of Zero Absolute Load
(output format ≡ *Difference Type 1*, App. 6)

$$\mathbf{\Delta Z}_0 \quad = \quad \mathbf{N} - \mathbf{N} \quad = \quad \begin{bmatrix} \Delta Z_{1,0} \\ \vdots \\ \Delta Z_{i,0} \\ \vdots \\ \Delta Z_{n,0} \end{bmatrix} \quad = \quad \begin{bmatrix} 0 \\ \vdots \\ 0 \\ \vdots \\ 0 \end{bmatrix} \qquad (12.5b)$$

Past experience has shown that the trivial electrical description of zero absolute load, i.e., Eq. (12.5*b*) above, is needed as input for the tare load iteration process in order to avoid iteration convergence stability problems whenever an analyst includes the intercept term in the regression model of a balance load.

The tare loads of each load series are a function of the output differences that are defined in Eqs. (12.5*a*) and (12.5*b*). This conclusion can also be described in vector format:

$$\textit{tare loads} \quad \Longrightarrow \quad \mathbf{\Delta F} \;=\; \begin{bmatrix} \Delta F_1(\mathbf{\Delta Z}_1, \mathbf{\Delta Z}_0) \\ \vdots \\ \Delta F_k(\mathbf{\Delta Z}_k, \mathbf{\Delta Z}_0) \\ \vdots \\ \Delta F_q(\mathbf{\Delta Z}_q, \mathbf{\Delta Z}_0) \end{bmatrix} \qquad (12.6)$$

At this point, all balance data inputs have been defined that make the numerical determination of the tare loads possible. Now, the tare load iteration algorithm itself

needs to be described. This description is split into two parts. First, the calculation of a first estimate, i.e., the initial guess of the tare loads is discussed. Afterwards, the tare load iteration process itself is summarized.

12.3 First Estimate of Tare Loads

The application of an iteration process requires the calculation of a first estimate of the tare loads that must be reasonably close to the final answer. The first estimate may be obtained from a simple linear regression model of the original balance calibration data. This regression model, i.e., *Regression Model A*, of a balance load F is defined in Eq. (12.7) below assuming that (i) the balance has n independent bridge outputs and (ii) the intercept term a_0 is included (see also related comments in App. 9). The symbols $D_1, \ \ldots, \ D_n$ are

Regression Model A

$$F = \underbrace{a_0}_{intercept} + \underbrace{a_1 \cdot D_1 + \cdots + a_n \cdot D_n}_{supported\ linear\ terms} \qquad (12.7)$$

the output differences of the bridges that are formatted as *Difference Type 1* (see also Eq. (12.1) or App. 6, Eq. (6.2)). The symbols $a_0, \ a_1, \ \ldots, \ a_n$ are regression coefficients.

The coefficients of *Regression Model A* above can be obtained by applying global regression analysis to the uncorrected balance calibration data (see, e.g., Ref. [64], pp. 35–39, for a description of the global regression analysis approach). The applied, i.e., uncorrected, calibration loads $F(1), \ldots, F(\nu), \ldots, F(p)$ of the calibration points are one input for the regression analysis ($\nu \equiv$ data point index; $p \equiv$ number of data points). They can be described by the following relationship:

Applied/Uncorrected Calibration Loads

$$\mathbf{F}_{unc} = \begin{bmatrix} F(1) \\ \vdots \\ F(\nu) \\ \vdots \\ F(p) \end{bmatrix}_{p \times 1} \qquad (12.8)$$

In addition, raw outputs $rF_1(1), \ \ldots, \ rF_i(\nu), \ \ldots, \ rF_n(p)$ of each data point were measured and the natural zeros $N_1, \ \ldots, \ N_n$ of the bridges are known. Then, the output difference used on the right–hand side of Eq. (12.7) above is defined by the following relationship if output format *Difference Type 1* of App. 6 is used:

Output Difference

$$D_i(\nu) \;=\; rF_i(\nu) \;-\; N_i \qquad (12.9)$$

where

$$1 \;\leq\; i \;\leq\; n \quad ; \quad 1 \;\leq\; \nu \;\leq\; p$$

Now, matrix $\mathbf{A}$ of the global regression analysis problem can be defined as a function of (i) the output differences and (ii) the chosen regression model terms. We get:

Regression Model Term Values for Regression Model A

$$\mathbf{A}_{p\times(n+1)} \;=\; \begin{bmatrix} 1 & D_1(1) & \dots & D_n(1) \\ \vdots & \vdots & \vdots & \vdots \\ 1 & D_1(p) & \dots & D_n(p) \end{bmatrix} \qquad (12.10)$$

The unknown coefficients of *Regression Model A* can be described by the following vector:

$$\mathbf{x} \;=\; \mathbf{x}_{(n+1)\times 1} \;=\; \begin{bmatrix} a_0 \\ a_1 \\ \vdots \\ a_n \end{bmatrix} \qquad (12.11)$$

Next, the tare load iteration step index needs to be initialized. Then, we get:

First Iteration Step

$$\mu \;=\; 1 \qquad (12.12)$$

At this point, the global regression analysis problem resulting from the application of *Regression Model A* to the balance calibration data can be defined. The dependent variable of the regression analysis is the balance load F. Its value is stored for each calibration point in vector $\mathbf{F}_{unc}$ that is defined in Eq. (12.8) above. Then, the load vector for the first iteration step is given by the following relationship:

$$\{\mathbf{F}_{cor}\}_{\mu=1} \;=\; \mathbf{F}_{unc} \qquad (12.13)$$

Now, the global regression analysis problem associated with the first iteration step can be described as a matrix equation. We get:

Global Regression Analysis Problem

$$\mathbf{A} \cdot \mathbf{x} \quad = \quad \{\mathbf{F}_{cor}\}_{\mu=1} \qquad (12.14a)$$

The solution of the global regression analysis problem above is the regression coefficient set of *Regression Model A*. The solution is an application of the *Moore–Penrose Inverse* that is given by the following matrix equation (taken from Ref. [64], pp. 35–39):

Solution of Global Regression Analysis Problem

$$\mathbf{x} \quad = \quad (\mathbf{A^T A})^{-1} \cdot \mathbf{A^T} \cdot \{\mathbf{F}_{cor}\}_{\mu=1} \qquad (12.14b)$$

Now, the first estimate of the tare loads of the load series can be computed as the coefficients $a_0,\ a_1,\ \ldots,\ a_n$ of *Regression Model A* are given by the right–hand side of Eq. (12.14*b*) above. It is only required to define a compatible auxiliary matrix $\mathbf{A'}$ that uses (i) the electrical description of the tare loads given in Eq. (12.5*a*) and (ii) the regression model definition itself as input. This $q \times (n+1)$ matrix can be expressed as follows where

$$\mathbf{A'}_{q\times(n+1)} \quad = \quad \begin{bmatrix} 1 & \Delta Z_{1,1} & \ldots & \Delta Z_{n,1} \\ \vdots & \vdots & \vdots & \vdots \\ 1 & \Delta Z_{1,k} & \ldots & \Delta Z_{n,k} \\ \vdots & \vdots & \vdots & \vdots \\ 1 & \Delta Z_{1,q} & \ldots & \Delta Z_{n,q} \end{bmatrix} \qquad (12.15)$$

index q is the total number of load series of the given calibration data set and index n is the total number of bridge outputs.

In the next step, the first estimate of the tare loads of all load series is obtained by simply multiplying matrix $\mathbf{A'}$ with vector $\mathbf{x}$ that has the regression coefficients. We get:

Tare Loads of Load Series *(first estimate)*

$$\{\mathbf{\Delta F'}\}_{\mu=1} \quad = \quad \begin{bmatrix} \Delta F_1 \\ \vdots \\ \Delta F_k \\ \vdots \\ \Delta F_q \end{bmatrix}_{q\times 1} \quad = \quad \mathbf{A'} \cdot \mathbf{x} \qquad (12.16)$$

The vector containing the first estimate of the tare loads has q rows, i.e., one row for each load series. The vector still needs to be mapped to a vector with p rows so that the tare load corrections can directly be added to all uncorrected calibration loads. It is assumed that a transformation $\sigma(\nu)$ exists that uniquely relates load series index k to data point index ν. This transformation could be expressed as follows:

$$\sigma(\nu) \;=\; k \quad \textit{where} \quad \sigma(1) = 1 \;,\; \sigma(2) = 1 \;,\; \ldots \;,\; \sigma(p-1) = q \;,\; \sigma(p) = q \qquad (12.17)$$

Then, after applying the transformation above to the first estimate of the tare loads, the first set of tare load corrections of the loads of the calibration data points can be defined as follows:

Tare Loads of Calibration Points *(first estimate)*

$$\{\mathbf{\Delta F}\}_{\mu=1} \;=\; \begin{bmatrix} \Delta F_{\sigma(1)} \\ \vdots \\ \Delta F_{\sigma(\nu)} \\ \vdots \\ \Delta F_{\sigma(p)} \end{bmatrix}_{p\times 1} \qquad (12.18)$$

The above estimate of the tare loads of the calibration loads will be used as the initial guess for the tare load iteration process that is described in the next section.

12.4 Tare Load Iteration Process

This section describes the tare load iteration process itself. Now, the analyst's chosen final regression model term combination is used instead of a simple linear term combination for the regression analysis of the calibration data. This regression model, i.e., *Regression Model B*, of load component F is defined by Eq. (12.19) below assuming that (i) the balance

Regression Model B

$$F \;=\; \underbrace{a_0}_{intercept} \;+\; \underbrace{a_1 \cdot D_1 \;+\; a_2 \cdot D_2 \;+\; \cdots \;+\; a_\omega \cdot D_1^2 \;+\; \cdots}_{supported\ linear,\ absolute\ value\ \&\ non-linear\ terms} \qquad (12.19)$$

has n independent bridge outputs, (ii) linear terms, non–linear terms, and the intercept are used, and (iii) a total of δ regression model terms are supported by the balance calibration data. At this point, matrix $\mathbf{B}$ of the global regression analysis problem can be defined as a function of (i) the output differences and (ii) the chosen regression model terms. We get:

Regression Model Term Values for Regression Model B

$$\mathbf{B}_{p\times\delta} = \begin{bmatrix} 1 & D_1(1) & D_2(1) & \dots & D_1^2(1) & \dots \\ \vdots & \vdots & \vdots & \vdots & \vdots & \vdots \\ 1 & D_1(\nu) & D_2(\nu) & \dots & D_1^2(\nu) & \dots \\ \vdots & \vdots & \vdots & \vdots & \vdots & \vdots \\ 1 & D_1(p) & D_2(p) & \dots & D_1^2(p) & \dots \end{bmatrix} \tag{12.20}$$

The unknown coefficients of *Regression Model B* can be described by the following vector:

$$\mathbf{y} = \mathbf{y}_{\delta\times 1} = \begin{bmatrix} a_0 \\ a_1 \\ a_2 \\ \vdots \end{bmatrix} \tag{12.21}$$

In the next step, the iteration step counter is increased by one. We get:

Iteration Step Increase

$$\mu \implies \mu + 1 \tag{12.22}$$

The tare corrected calibration loads need to be updated so that the coefficients of the new regression model of the calibration data can be obtained. Therefore, the previous estimate of the tare loads of the individual calibration points, i.e., $\{\mathbf{\Delta F}\}_{\mu-1}$, is added to the uncorrected calibration loads, i.e., $\mathbf{F}_{unc}$, that are defined in Eq. (12.8) above. Then, a new interim estimate of the tare corrected calibration loads is obtained. We get:

Tare Corrected Calibration Loads *(interim estimate)*

$$\{\mathbf{F}_{cor}\}_{\mu} = \mathbf{F}_{unc} + \{\mathbf{\Delta F}\}_{\mu-1} \tag{12.23}$$

Now, the global regression analysis problem associated with the interim tare load iteration step can be described as a matrix equation. We get:

Global Regression Analysis Problem

$$\mathbf{B} \cdot \mathbf{y} \quad = \quad \{\mathbf{F}_{cor}\}_{\mu} \qquad (12.24a)$$

The solution of the global regression analysis problem above describes the interim regression coefficients of *Regression Model B*. The solution is an application of the *Moore–Penrose Inverse*. It is given by the following equation (taken from Ref. [64], pp. 35–39):

Solution of Global Regression Analysis Problem

$$\mathbf{y} \quad = \quad (\mathbf{B^T B})^{-1} \cdot \mathbf{B^T} \cdot \{\mathbf{F}_{cor}\}_{\mu} \qquad (12.24b)$$

Finally, the new estimate of the tare loads of the load series can be computed as the interim coefficients $a_0,\ a_1,\ \ldots$ of *Regression Model B* are given by the right–hand side of Eq. (12.24*b*). It is only required to define a compatible auxiliary matrix $\mathbf{B}'$ that uses (i) the electrical description of the tare loads given in Eq. (12.5*a*) and (ii) the definition of the regression model itself as input. This $q \times \delta$ matrix can be expressed as follows:

$$\underbrace{\mathbf{\Delta Z}_1\ ,\ \ldots\ ,\ \mathbf{\Delta Z}_q}_{Eq.\ (12.5a)} \Longrightarrow \mathbf{B'}_{q\times\delta} = \begin{bmatrix} 1 & \Delta Z_{1,1} & \Delta Z_{2,1} & \ldots & \Delta Z_{1,1}^{2} & \ldots \\ \vdots & \vdots & \vdots & \vdots & \vdots & \vdots \\ 1 & \Delta Z_{1,k} & \Delta Z_{2,k} & \ldots & \Delta Z_{1,k}^{2} & \ldots \\ \vdots & \vdots & \vdots & \vdots & \vdots & \vdots \\ 1 & \Delta Z_{1,q} & \Delta Z_{2,q} & \ldots & \Delta Z_{1,q}^{2} & \ldots \end{bmatrix} \qquad (12.25a)$$

In addition, a second rectangular matrix $\mathbf{B}''$ needs to be defined that uses (i) the trivial electrical description of zero absolute load given in Eq. (12.5*b*) and (ii) the regression model definition itself as input. This $q \times \delta$ matrix can be expressed as follows:

$$\underbrace{\mathbf{\Delta Z}_0}_{Eq.\ (12.5b)} \Longrightarrow \mathbf{B''}_{q\times\delta} = \begin{bmatrix} 1 & 0 & 0 & \ldots & 0 & \ldots \\ \vdots & \vdots & \vdots & \vdots & \vdots & \vdots \\ 1 & 0 & 0 & \ldots & 0 & \ldots \\ \vdots & \vdots & \vdots & \vdots & \vdots & \vdots \\ 1 & 0 & 0 & \ldots & 0 & \ldots \end{bmatrix} \qquad (12.25b)$$

Now, the new estimate of the tare loads can be computed by (i) multiplying matrices $\mathbf{B}'$ and $\mathbf{B}''$ with vector $\mathbf{y}$ and (ii) taking the difference of the results. We get:

Tare Loads of Load Series *(interim estimate)*

$$\{\mathbf{\Delta F}'\}_{\mu} = \begin{bmatrix} \Delta F_1 \\ \vdots \\ \Delta F_k \\ \vdots \\ \Delta F_q \end{bmatrix}_{q \times 1} = \underbrace{\mathbf{B}' \cdot \mathbf{y}}_{tare\ loads} - \underbrace{\mathbf{B}'' \cdot \mathbf{y}}_{zero\ load} \qquad (12.26)$$

The second product $\mathbf{B}''\mathbf{y}$ is needed in Eq. (12.26) in order to avoid a known convergence instability. This instability prevents tare load residuals from decreasing monotonically whenever the intercept term a_0 is included in *Regression Model B*. Alternatively, the second product equals zero and can be dropped altogether if an analyst omits the intercept term in *Regression Model B*.

Again, the transformation defined in Eq. (12.17) needs to be applied so that the tare loads of each load series can be mapped to all calibration points. Then, the vector describing the new interim estimate of the tare loads of the calibration points can be described by the following equation:

Tare Loads of Calibration Points *(interim estimate)*

$$\{\mathbf{\Delta F}\}_{\mu} = \begin{bmatrix} \Delta F_{\sigma(1)} \\ \vdots \\ \Delta F_{\sigma(\nu)} \\ \vdots \\ \Delta F_{\sigma(p)} \end{bmatrix}_{p \times 1} \qquad (12.27)$$

A tare load iteration convergence test needs to be applied at this point. Therefore, the absolute values of the tare load changes δF, i.e., the absolute values of the difference between tare load estimates of the current and previous iteration step, are computed and made dimensionless by using the capacity Γ of the load component. Then, the maximum of the dimensionless tare load changes is expressed as a percentage. This test metric is compared with the empirical threshold of 0.0001 %. Two cases must be distinguished. First, the test metric could be greater or equal to the threshold. Then, the iteration process continues by going back to Eq. (12.22) and starting the calculation of a new set of tare loads. Alternatively, the test metric could be less than the threshold. In that case, the iteration converged and is terminated after the final set of tare corrected calibration loads is computed. The tare load iteration convergence test is summarized below.

Tare Load Iteration Convergence Test

$$\delta\mathbf{F} = \underbrace{\{\mathbf{\Delta F'}\}_{\mu} - \{\mathbf{\Delta F'}\}_{\mu-1}}_{tare\ load\ change} = \begin{bmatrix} \delta F_1 \\ \vdots \\ \delta F_k \\ \vdots \\ \delta F_q \end{bmatrix} \tag{12.28a}$$

$$\delta F_k = \{\Delta F_k\}_{\mu} - \{\Delta F_k\}_{\mu-1} \tag{12.28b}$$

$$V = MAX\left\{ \left|\frac{\delta F_1}{\Gamma}\right| , \ldots , \left|\frac{\delta F_q}{\Gamma}\right| \right\} \cdot 100\,\% \tag{12.28c}$$

$$V \geq 0.0001\,\% \implies \textit{go back to Eq. (12.22)} \implies \textit{continue} \ldots \tag{12.28d}$$

$$V < 0.0001\,\% \implies \textit{advance to Eq. (12.29)} \implies \textit{stop} \ldots \tag{12.28e}$$

The final set of tare corrected calibration loads is computed after the condition described in Eq. (12.28*e*) above is met. Then, the final tare loads of the calibration points are added to the uncorrected calibration load set. We get:

Final Set of Tare Corrected Calibration Loads

$$\mathbf{F}_{cor} = \underbrace{\mathbf{F}_{unc}}_{Eq.\,(12.8)} + \underbrace{\{\mathbf{\Delta F}\}_{\mu}}_{Eq.\,(12.27)} \tag{12.29}$$

The final set of regression coefficients of *Regression Model B* is computed by using (i) the output differences of the calibration data defined in Eq. (12.9) and (ii) the tare corrected calibration loads defined in Eq. (12.29) above as input.

The *Non–Iterative Method*, by design, performs a regression analysis for one load component at a time when it is applied to calibration data. Therefore, the tare load iteration process is only presented in this section for a single load component. Consequently, the process has to be independently applied to all load components of the balance by saving the applied/uncorrected load values of the load component in column vector $\mathbf{F}_{unc}$ and selecting a suitable regression model for the analysis.

12.5 Exclusion of Intercept Term

It was mentioned in App. 9 that the use of the intercept term in the regression model of a load is optional whenever output differences are used to define regression model terms. It is helpful to summarize simplifications of important equations whenever the intercept

term is not used. The following relationship is valid if the intercept term is omitted:

$$\textit{intercept is omitted} \quad \Longrightarrow \quad a_0 \;=\; 0 \tag{12.30}$$

Then, the following simplifications and modifications of a subset of equations of this appendix can be made:

$$\textit{Eq. (12.7)} \quad \Longrightarrow \quad F \;=\; \underbrace{a_1 \cdot D_1 \;+\; \cdots \;+\; a_n \cdot D_n}_{\textit{supported linear terms}} \tag{12.31a}$$

$$\textit{Eq. (12.10)} \quad \Longrightarrow \quad \mathbf{A}_{p\times n} \;=\; \begin{bmatrix} D_1(1) & \dots & D_n(1) \\ \vdots & \vdots & \vdots \\ D_1(p) & \dots & D_n(p) \end{bmatrix} \tag{12.31b}$$

$$\textit{Eq. (12.11)} \quad \Longrightarrow \quad \mathbf{x} \;=\; \mathbf{x}_{n\times 1} \;=\; \begin{bmatrix} a_1 \\ \vdots \\ a_n \end{bmatrix} \tag{12.31c}$$

$$\textit{Eq. (12.15)} \quad \Longrightarrow \quad \mathbf{A'}_{q\times n} \;=\; \begin{bmatrix} \Delta Z_{1,1} & \dots & \Delta Z_{n,1} \\ \vdots & \vdots & \vdots \\ \Delta Z_{1,k} & \dots & \Delta Z_{n,k} \\ \vdots & \vdots & \vdots \\ \Delta Z_{1,q} & \dots & \Delta Z_{n,q} \end{bmatrix} \tag{12.31d}$$

$$\textit{Eq. (12.19)} \quad \Longrightarrow \quad F \;=\; \underbrace{a_1 \cdot D_1 \;+\; a_2 \cdot D_2 \;+\; \cdots \;+\; a_\omega \cdot D_1^2 \;+\; \cdots}_{\textit{supported linear, absolute value \& non-linear terms}} \tag{12.31e}$$

$$\textit{Eq. (12.20)} \quad \Longrightarrow \quad \mathbf{B}_{p\times \delta} \;=\; \begin{bmatrix} D_1(1) & D_2(1) & \dots & D_1^2(1) & \dots \\ \vdots & \vdots & \vdots & \vdots & \vdots \\ D_1(\nu) & D_2(\nu) & \dots & D_1^2(\nu) & \dots \\ \vdots & \vdots & \vdots & \vdots & \vdots \\ D_1(p) & D_2(p) & \dots & D_1^2(p) & \dots \end{bmatrix} \tag{12.31f}$$

$$\textit{Eq. (12.21)} \quad \Longrightarrow \quad \mathbf{y} \;=\; \mathbf{y}_{\delta\times 1} \;=\; \begin{bmatrix} a_1 \\ a_2 \\ \vdots \end{bmatrix} \tag{12.31g}$$

$$\textit{Eq. (12.25a)} \quad \Longrightarrow \quad \mathbf{B'}_{q\times \delta} \;=\; \begin{bmatrix} \Delta Z_{1,1} & \Delta Z_{2,1} & \dots & \Delta Z_{1,1}^{\,2} & \dots \\ \vdots & \vdots & \vdots & \vdots & \vdots \\ \Delta Z_{1,k} & \Delta Z_{2,k} & \dots & \Delta Z_{1,k}^{\,2} & \dots \\ \vdots & \vdots & \vdots & \vdots & \vdots \\ \Delta Z_{1,q} & \Delta Z_{2,q} & \dots & \Delta Z_{1,q}^{\,2} & \dots \end{bmatrix} \tag{12.31h}$$

$$Eq.\ (12.25b) \implies \mathbf{B''}_{q\times\delta} = \begin{bmatrix} 0 & 0 & \dots & 0 & \dots \\ \vdots & \vdots & \vdots & \vdots & \vdots \\ 0 & 0 & \dots & 0 & \dots \\ \vdots & \vdots & \vdots & \vdots & \vdots \\ 0 & 0 & \dots & 0 & \dots \end{bmatrix} \tag{12.31i}$$

$$Eq.\ (12.26) \implies \{\mathbf{\Delta F'}\}_{\mu} = \begin{bmatrix} \Delta F_1 \\ \vdots \\ \Delta F_k \\ \vdots \\ \Delta F_q \end{bmatrix} = \underbrace{\mathbf{B'} \cdot \mathbf{y}}_{tare\ loads} \tag{12.31j}$$

It must be pointed out that the number of rows or columns used in Eqs. (12.31f), (12.31g), (12.31h), and (12.31i) is reduced by one even though the related variable δ does not explicitly show that change. The next section discusses typical tare load iteration results for data from the manual calibration of a force balance.

12.6 Discussion of Example

A data set from the manual calibration of a strain–gage balance is used in this section to illustrate the application of the tare load iteration algorithm for the *Non–Iterative Method*. The chosen balance is called the NASA MK3C. It was manufactured by the Task/Able Corporation. It is a six–component force balance that measures five forces and one moment ($N1$, $N2$, $S1$, $S2$, AF, RM). It has a diameter of 2.0 in and a total length of 11.25 in. Table 12–1 shows the capacity of each load component of balance.

Table 12–1: Load capacities of the MK3C force balance ($lbs \equiv$ pounds of force).

$N1,\ lbs$	$N2,\ lbs$	$S1,\ lbs$	$S2,\ lbs$	$AF,\ lbs$	$RM,\ in{-}lbs$
900	900	450	450	500	1000

It was decided to discuss the tare load iteration of the forward normal force component of the balance as an example. Absolute value terms of the output differences were included in *Regression Model B* of the forward normal force as the balance has bi–directional outputs. Three different approaches were applied to determine the tare loads. Table 12–2 below summarizes characteristics of the three approaches.

Approach 1 includes the intercept term in the regression model of the load and uses two load calculations for each tare load iteration step. This approach is described by Eq. (12.26) and matches *Method B* that is discussed in Ref. [11]. *Approach* 2 also includes the intercept term in the regression model of the load but uses one load calculation for each tare load iteration step (the second term on the right–hand side of Eq. (12.26), i.e., $\mathbf{B''y}$, is intentionally omitted). Finally, *Approach* 3 excludes the intercept term in the regression model of the load and uses one load calculation for each tare load iteration step. This approach is described in Eq. (12.31j) above.

Table 12–2: Description of investigated tare load iteration approaches.

Approach	Definition of interim estimate of tare loads	Is intercept included ?	Does the tare load iteration converge ?	Comments
1	$\mathbf{B}' \cdot \mathbf{y} - \mathbf{B}'' \cdot \mathbf{y}$	yes	yes	Eq. (12.26)
2	$\mathbf{B}' \cdot \mathbf{y} - \mathbf{0}$	yes	**no**	Eq. (12.26)
3	$\mathbf{B}' \cdot \mathbf{y}$	no	yes	Eq. (12.31j)

Table 12–3 below shows parts of the original calibration data of the MK3C balance. Only 21 of a total of 247 data points are shown. The natural zeros and the electrical outputs of all bridges are listed as raw outputs in units of $microV/V$. The applied, i.e., uncorrected forward normal force ($N1$) is also listed in the last column of the data table for each data point and load series.

Table 12–3: Description of the calibration data of the forward normal force using raw outputs (absolute voltage measurements) and applied/uncorrected loads.

NATURAL ZEROS (ABSOLUTE VOLTAGE MEASUREMENTS)

rN1	rN2	rS1	rS2	rAF	rRM
microV/V	microV/V	microV/V	microV/V	microV/V	microV/V
-318.58	95.28	55.89	-212.30	169.44	-102.23

PT. ID	SERIES	rN1	rN2	rS1	rS2	rAF	rRM	N1
-	-	microV/V	microV/V	microV/V	microV/V	microV/V	microV/V	lbs
P-1	1	-239.01	108.67	55.80	-211.46	170.56	-102.38	0
P-2	1	-59.90	105.07	56.21	-210.96	170.53	-102.37	100
P-3	1	120.30	101.70	56.67	-210.46	170.16	-102.56	200
P-4	1	301.18	98.20	56.92	-210.05	169.99	-102.47	300
P-5	1	482.15	94.78	56.83	-209.89	169.80	-102.61	400
P-6	1	663.20	91.43	57.28	-209.37	169.71	-102.40	500
P-7	1	843.98	87.96	57.31	-209.03	169.53	-102.57	600
P-8	1	1024.69	84.46	57.18	-208.81	169.53	-102.53	700
P-9	1	1204.81	80.95	57.27	-208.49	169.25	-102.57	800
P-10	1	1385.42	77.52	57.42	-208.20	169.28	-102.40	900
P-11	1	1207.31	80.99	57.23	-208.62	169.24	-102.54	800
P-12	1	1028.10	84.36	57.01	-208.80	169.43	-102.51	700
P-13	1	847.66	87.95	57.17	-209.02	169.44	-102.62	600
P-14	1	666.39	91.42	56.72	-209.31	169.40	-102.77	500
P-15	1	485.03	94.83	56.96	-209.89	169.60	-102.51	400
P-16	1	303.36	98.27	56.63	-210.23	169.78	-102.52	300
P-17	1	121.73	101.71	56.55	-210.57	169.89	-102.43	200
P-18	1	-59.20	105.21	56.39	-210.90	170.34	-102.41	100
P-19	1	-239.60	108.69	55.78	-211.44	170.66	-102.35	0
P-20	2	-297.66	166.53	55.96	-212.57	173.44	-102.40	0
P-21	2	-299.37	351.63	56.07	-213.30	177.60	-102.55	0
...	...	...	...	...	...	...	...	...

Table 12–4 below shows parts of the calibration data of the MK3C balance if output differences, i.e., *Difference Type 1* of App. 6, are used to describe the balance calibration data. Now, the natural zeros, i.e., the electrical representations of zero absolute load in output difference format equal zero $microV/V$. In addition, the electrical outputs of

the first point P–1 of load series 1 are the components of vector $\mathbf{\Delta Z_1}$ that is defined in Eq. (12.5a). They are the electrical description of the tare loads of load series 1. We get:

$$\textit{Table } 12\text{–}4 \implies \textit{Series } 1 \implies \mathbf{\Delta Z}_1 = \begin{bmatrix} +79.57 & \textit{microV/V} \\ +13.40 & \textit{microV/V} \\ -0.09 & \textit{microV/V} \\ +0.84 & \textit{microV/V} \\ +1.12 & \textit{microV/V} \\ -0.15 & \textit{microV/V} \end{bmatrix} \tag{12.32}$$

The data format shown in Table 12–4 below was used as input for the definition of the regression model of the forward normal force. Then, the three tare load iteration

Table 12–4: Description of the calibration data of the forward normal force using output differences *(Difference Type 1, App. 6)* and applied/uncorrected loads.

NATURAL ZEROS (OUTPUT DIFFERENCE RELATIVE TO NATURAL ZERO)								
		rN1	rN2	rS1	rS2	rAF	rRM	
		microV/V	microV/V	microV/V	microV/V	microV/V	microV/V	
		0.00	0.00	0.00	0.00	0.00	0.00	
PT. ID	SERIES	rN1	rN2	rS1	rS2	rAF	rRM	N1
-	-	microV/V	microV/V	microV/V	microV/V	microV/V	microV/V	lbs
P-1	1	79.57	13.40	-0.09	0.84	1.12	-0.15	0
P-2	1	258.68	9.79	0.31	1.34	1.08	-0.14	100
P-3	1	438.88	6.42	0.78	1.84	0.71	-0.33	200
P-4	1	619.77	2.93	1.03	2.25	0.55	-0.24	300
P-5	1	800.73	-0.50	0.93	2.41	0.36	-0.38	400
P-6	1	981.78	-3.85	1.39	2.93	0.27	-0.17	500
P-7	1	1162.56	-7.31	1.42	3.27	0.09	-0.34	600
P-8	1	1343.27	-10.81	1.28	3.49	0.09	-0.30	700
P-9	1	1523.39	-14.33	1.38	3.81	-0.19	-0.34	800
P-10	1	1704.01	-17.76	1.52	4.10	-0.16	-0.17	900
P-11	1	1525.89	-14.29	1.34	3.68	-0.20	-0.31	800
P-12	1	1346.68	-10.91	1.12	3.50	-0.01	-0.28	700
P-13	1	1166.24	-7.33	1.28	3.28	0.00	-0.39	600
P-14	1	984.97	-3.85	0.83	2.99	-0.04	-0.54	500
P-15	1	803.61	-0.45	1.07	2.41	0.16	-0.28	400
P-16	1	621.94	2.99	0.73	2.07	0.34	-0.29	300
P-17	1	440.31	6.43	0.66	1.73	0.45	-0.20	200
P-18	1	259.38	9.94	0.50	1.40	0.90	-0.18	100
P-19	1	78.98	13.42	-0.11	0.86	1.21	-0.12	0
P-20	2	20.92	71.25	0.06	-0.27	4.00	-0.17	0
P-21	2	19.21	256.35	0.18	-1.00	8.16	-0.32	0
...	...	...	...	...	...	...	...	...

approaches described in Table 12–2 above were applied and, whenever possible, tare loads of the 13 load series of the calibration data set were computed. Table 12–5 below shows the computed tare loads of each load series. In general, the predicted tare loads of *Approach 1* and *Approach 3* show excellent agreement because the maximum difference between the two tare load estimates is 0.006 % of the capacity of the forward normal force. No tare loads were obtained for *Approach 2* as the tare load iteration process did not converge. Further investigations confirmed the existence of an iteration convergence instability when *Approach 2* was applied to the balance calibration data. This instability prevented the tare load residuals from decreasing monotonically. The unwanted convergence instability

Table 12–5: Estimated tare loads of the forward normal force.

Load Series	$\Delta N1$, lbs *(Approach 1)*	$\Delta N1$, lbs *(Approach 3)*	| Tare Load Difference | (percent of load capacity)
1	+44.108	+44.137	0.003 %
2	+11.900	+11.928	0.003 %
3	+15.109	+15.125	0.002 %
4	–29.136	–29.117	0.002 %
5	–10.235	–10.214	0.002 %
6	+0.102	+0.157	0.006 %
7	+0.060	+0.115	0.006 %
8	–0.004	+0.052	0.006 %
9	+0.168	+0.224	0.006 %
10	–0.159	–0.106	0.006 %
11	–0.963	–0.929	0.004 %
12	–76.691	–76.640	0.006 %
13	+75.288	+75.339	0.006 %

can be avoided if either two load calculations for each tare load iteration step are performed *(Approach 1)*, or, alternatively, if the intercept term is omitted in the regression model of the forward normal force *(Approach 3)*. Observed tare load iteration convergence characteristics for the three approaches are summarized in the fourth column of Table 12–2.

12.7 Tare Load Iteration Algorithm Differences

It is mentioned in the introduction of the appendix that *Galway's* original tare load iteration algorithm uses output format *Difference Type 2* for the calculation of the linear matrix that is needed for the determination of a first estimate of the tare loads. In other words, *Galway's* algorithm replaces *Difference Type 1* with *Difference Type 2* in the definition of *Regression Model A* that is described in Eq. (12.7). This bridge output format choice difference is summarized in Table 12–6 below.

Table 12–6: Output format choices of tare load iteration algorithms.

	Regression Model A ... see Eq. (12.7)	Regression Model B ... see Eq. (12.19)
Galway's Algorithm	*Difference Type 2*	*Difference Type 1*
Author's Algorithm	*Difference Type 1*	*Difference Type 1*

It seems, superficially viewed, that this format change could influence the final result of the tare load iterations. However, the author observed that the final tare load estimates for both bridge output format choices are identical for all practical purposes. *Galway's* output format choice simply results in a more rapid convergence of the tare load iterations as his first estimate of the tare loads is closer to the final answer. The author's output

format choice, on the other hand, makes an implementation of the tare load iteration algorithm less complex as only one output format type, i.e., *Difference Type 1* is used in both *Regression Model A* and *Regression Model B* during the tare load iteration process.

Appendix 13

Tare Load Iteration for Iterative Method

13.1 Introduction

Strain–gage balance calibration data should include loads in the description of the load state of the balance that are caused by the combined weight of (i) the metric part of the balance, (ii) the calibration body, (iii) calibration fixtures, and (iv) weight pans. These hidden loads are traditionally called tare loads. They make it possible to describe all loads relative to the common load datum of zero absolute load if they are added to the applied calibration loads. The tare loads can be defined as follows:

> **Tare Loads** $\equiv$ balance loads that are exclusively caused by the combined weight of the metric part and all attached calibration hardware pieces.

A balance calibration load schedule is often split into individual load series. Each load series consists of calibration points, i.e., load states, that were applied while keeping the calibration hardware itself unchanged. Therefore, tare loads must remain constant within a given load series. In addition, electrical outputs of the zero load points of the load series, i.e., outputs of the first and last point of the load series, are exclusively caused by the tare loads if no gravity weights are placed on a weight pan. Consequently, they are the electrical representation of the hidden tare loads of a load series.

In theory, it would be possible to estimate the tare loads from the total weight and common center of gravity location of the metric part and all calibration hardware pieces. However, this approach is difficult to apply within the context of a real–world calibration. In particular, the determination of the common center of gravity of the metric part and all calibration hardware pieces can be challenging. Therefore, many analysts use a tare load iteration algorithm for the assessment of the hidden tare loads. The basic idea behind this iteration process is summarized in the paragraph below:

> **Tare Load Iteration Algorithm**
>
> The electrical outputs of each zero load point of a load series are used in combination with (i) the natural zeros of the balance bridges and (ii) interim regression models of the balance calibration data in order to successively compute numerical estimates of the tare loads for all load series. The iteration is considered converged if two conditions are met: (i) the maximum difference between two consecutive tare load estimates is below a specified iteration tolerance; (ii) the tare load residuals decrease monotonically.

The first tare load iteration algorithm for balance calibration data was developed in the 1970s by *Robin Galway* of NRC Canada. His algorithm was finally published in the open literature in 1999 (Ref. [80]). Afterwards, AIAA's Internal Balance Technology Working Group adopted it for use with the *Iterative Method* (see 1st edition of Ref. [7]).

A new description of a tare load iteration algorithm was prepared for this appendix. It closely follows *Galway's* original algorithm (see Ref. [7], pp. 21–22, pp. 27–45). However, two differences between *Galway's* and the author's definition of a tare load iteration algorithm exist. First, *Galway's* algorithm exclusively uses output format *Difference Type 2* for the calculation of the coefficients of the linear matrix that the determination of a first estimate of the tare loads needs (see Ref. [7], p. 32; *Difference Type 2* is defined in App. 6, Eq.(6.3); see also the discussion in section 13.7 of the appendix). Furthermore, *Galway's* algorithm performs one load calculation for each iteration step. The author's algorithm, on the other hand, performs two load calculations for each iteration step. This modification was made in order to control an iteration convergence instability that results from the use of the intercept term in the regression model of a load component if the tare load iteration algorithm is used in combination with the *Non–Iterative Method* (see example in App. 12). The modification is also used in the description of the algorithm for the *Iterative Method* even though it is not needed in this case. This choice was made so that a universal algorithm is defined that can reliably be used with either the *Non–Iterative Method* or the *Iterative Method*.

13.2 Balance Load and Output Descriptions

The development of the new description of the tare load iteration algorithm starts with basic definitions. In principle, the *Iterative Method* fits each bridge output as a function of all loads that describe the load state of the balance during its calibration. Afterwards, the regression models of the outputs are used to construct a load iteration process for the load prediction during a wind tunnel test (see also App. 10 for more details).

The balance bridge output is assumed to be a function of the loads of n load components. These loads are assumed to include tare loads that are obtained after applying the tare load iteration algorithm to the calibration data. It is helpful for the description of the tare load iteration algorithm to express loads of a balance in vector format. Then, we get:

$$loads\ (uncorrected) \quad \Longrightarrow \quad \mathbf{F} \quad = \quad \begin{bmatrix} F_1 \\ \vdots \\ F_i \\ \vdots \\ F_n \end{bmatrix} \tag{13.1}$$

Similarly, electrical outputs of the balance can be described in vector format. Then, assuming that the number of independent bridge output measurements matches the number of load components, the raw outputs of a balance can be described as follows:

$$raw\ outputs \quad \Longrightarrow \quad \mathbf{rF} \quad = \quad \begin{bmatrix} rF_1 \\ \vdots \\ rF_i \\ \vdots \\ rF_n \end{bmatrix} \tag{13.2}$$

The components of the output vector above are described as absolute voltage measurements (raw outputs). They cannot directly be used for the determination of the tare

loads unless the natural zeros of the balance bridges, i.e., the electrical descriptions of zero absolute load, are known (the determination of the natural zeros of the balance bridges is described in great detail in App. 8 of the current document). The definition of the natural zeros can be summarized as follows:

Natural Zeros $\equiv$ electrical description of the load datum of zero absolute load.

It is convenient to also express the natural zeros in vector format. Then, we get:

$$natural\ zeros \quad \Longrightarrow \quad \mathbf{N} \;=\; \begin{bmatrix} N_1 \\ \vdots \\ N_i \\ \vdots \\ N_n \end{bmatrix} \tag{13.3}$$

Now, it is possible to define an alternate bridge output format, i.e., *Difference Type 1* of App. 6, that may be used for the regression analysis of the balance data and the definition of a tare load iteration algorithm. This format uses the difference between the raw output of a bridge and its natural zero for the regression analysis of the balance calibration data and the load prediction. This output difference can be defined by the following relationship:

$$output\ differences \quad \Longrightarrow \quad \mathbf{D} \;=\; \begin{bmatrix} D_1 \\ \vdots \\ D_i \\ \vdots \\ D_n \end{bmatrix} \;=\; \begin{bmatrix} rF_1 - N_1 \\ \vdots \\ rF_i - N_i \\ \vdots \\ rF_n - N_n \end{bmatrix} \tag{13.4}$$

An analyst has the option to either fit raw outputs or output differences relative to the natural zeros during the regression analysis of balance calibration data whenever the *Iterative Method* is applied (see also comments in App. 10). Characteristics of the regression analysis of the outputs are briefly reviewed in the next section.

13.3 Regression Analysis of Calibration Data

The *Iterative Method* individually fits the outputs of the balance bridges as a function of all loads that describe the load state of the balance during its calibration. Afterwards, the resulting regression models are used to construct a load iteration process so that loads can be predicted from outputs during a wind tunnel test. It was mentioned in the previous section that an analyst can either fit raw outputs or output differences during the regression analysis of some given balance calibration data. It is useful for the discussion of the tare load iteration process to review basic characteristics of regression analysis that may be used to process the balance calibration data. Let us assume, for example, that an analyst decides to directly fit raw outputs. The resulting regression model of a single output may be defined by the following equation:

Regression Model of Outputs *(Raw Output)*

$$rF_i = \underbrace{b_{i,0}}_{intercept} + \underbrace{b_{i,1} \cdot F_1 + b_{i,2} \cdot F_2 + \cdots + b_{i,\omega} \cdot F_1^{\,2} + \cdots}_{supported\ linear,\ absolute\ value\ \&\ non-linear\ terms} \quad (13.5a)$$

where

$$b_{i,0} \approx N_i \equiv \textit{natural zero of balance bridge} \quad (13.5b)$$

In this case, the intercept must be used in the regression model of each output. This requirement results from the fact that all terms but the intercept disappear on the right–hand side of Eq. (13.5a) if the acting balance loads are zero. Then, the output of the balance bridge, i.e., the left–hand side of Eq. (13.5a) above, equals its natural zero. Consequently, the intercept term $b_{i,0}$ becomes a least squares approximation of the natural zero of the balance bridge after completion of the regression analysis of the calibration data.

Now, it is assumed that an analyst chooses to fit differences between the raw outputs and the natural zeros of the bridges. The resulting regression model is described by the relationship that is given in Eq. (13.6a) below. This time, the use of the intercept is

Regression Model of Outputs *(Difference Type 1)*

$$D_i = \underbrace{b_{i,0}}_{intercept} + \underbrace{b_{i,1} \cdot F_1 + b_{i,2} \cdot F_2 + \cdots + b_{i,\omega} \cdot F_1^{\,2} + \cdots}_{supported\ linear,\ absolute\ value\ \&\ non-linear\ terms} \quad (13.6a)$$

where

$$b_{i,0} \approx 0 \implies \textit{use of intercept is optional} \quad (13.6b)$$

optional as it is the least squares approximation of zero output. Again, all terms but the intercept term disappear on the right–hand side of Eq. (13.6a) when all loads of the balance are zero. Then, the output difference of the balance bridge, i.e., the left–hand side of Eq. (13.6a), must be zero. Consequently, the intercept term $b_{i,0}$ becomes the least squares approximation of zero output after completion of the regression analysis of the balance calibration data. In other words, it may be omitted as it will hardly influence the regression analysis result.

The coefficients of the regression models of all bridge outputs of an n–component balance can be obtained by combining global regression analysis of the balance calibration data with a tare load iteration process (see, e.g., Ref. [64], pp. 35–39, for a description of the global regression analysis approach). The applied, i.e., uncorrected, calibration loads $F_i(1)$, ..., $F_i(\nu)$, ..., $F_i(p)$ of the n load components and the p calibration points are one

input for the regression analysis and the tare load iteration. They can be described by the following rectangular matrix:

Applied Calibration Loads *(uncorrected)*

$$\mathbf{F}_{unc} = \begin{bmatrix} F_1(1) & \dots & F_1(\nu) & \dots & F_1(p) \\ \vdots & \vdots & \vdots & \vdots & \vdots \\ F_i(1) & \dots & F_i(\nu) & \dots & F_i(p) \\ \vdots & \vdots & \vdots & \vdots & \vdots \\ F_n(1) & \dots & F_n(\nu) & \dots & F_n(p) \end{bmatrix}_{n \times p} \tag{13.7}$$

In addition, electrical outputs are needed. In that case, an analyst has two options. First, an analyst can use the raw outputs $rF_i(1)$, ..., $rF_i(\nu)$, ..., $rF_i(p)$ of the n balance bridges and the p calibration points as input for the regression analysis and the tare load iteration. They can be described by the following rectangular matrix:

Measured Bridge Outputs *(Raw Output)*

$$\mathbf{rF}_{raw} = \begin{bmatrix} rF_1(1) & \dots & rF_1(\nu) & \dots & rF_1(p) \\ \vdots & \vdots & \vdots & \vdots & \vdots \\ rF_i(1) & \dots & rF_i(\nu) & \dots & rF_i(p) \\ \vdots & \vdots & \vdots & \vdots & \vdots \\ rF_n(1) & \dots & rF_n(\nu) & \dots & rF_n(p) \end{bmatrix}_{n \times p} \tag{13.8a}$$

Alternatively, an analyst may use output differences $D_i(1)$, ..., $D_i(\nu)$, ..., $D_i(p)$ of the n balance bridges and the p calibration points for the regression analysis and the tare load iteration. They can be described by the following rectangular matrix:

Measured Bridge Outputs *(Difference Type 1)*

$$\mathbf{rF}_{diff} = \begin{bmatrix} D_1(1) & \dots & D_1(\nu) & \dots & D_1(p) \\ \vdots & \vdots & \vdots & \vdots & \vdots \\ D_i(1) & \dots & D_i(\nu) & \dots & D_i(p) \\ \vdots & \vdots & \vdots & \vdots & \vdots \\ D_n(1) & \dots & D_n(\nu) & \dots & D_n(p) \end{bmatrix}_{n \times p} \tag{13.8b}$$

The coefficients of the regression models above have to be determined in an iterative process as tare load estimates need to be added to the originally applied calibration loads that are contained in matrix $\mathbf{F}_{unc}$. These tare loads are predicted from the zero load outputs of each load series. The definition of these subsets of outputs is discussed in more detail in the next section.

13.4 Electrical Description of Tare Loads and Zero Absolute Load

Tare loads of each load series of the balance calibration data set are indirectly quantified by electrical outputs that are measured at the beginning and end of each load series when no gravity weights are placed on a weight pan. These raw outputs are called the zero load outputs of a load series. They can be defined as follows:

> **Zero Load Outputs of a Load Series** $\equiv$ electrical outputs that are exclusively caused by the **Tare Loads** of a load series.

The zero load outputs of a load series with index k can be described by using an n–component vector. Then, we get:

$$\textit{zero load outputs of a load series (raw output format)} \implies \mathbf{Z}_k = \begin{bmatrix} Z_{1,k} \\ \vdots \\ Z_{i,k} \\ \vdots \\ Z_{n,k} \end{bmatrix} \quad (13.9)$$

The intercept terms of the regression models defined in Eq. (13.5a) and (13.6a) are least squares approximation of corresponding outputs at zero absolute load. They define an important output datum for the assessment of the zero load outputs of a load series. It is convenient to express the intercepts of the regression models of the outputs of an n–component balance in vector format. Then, we get:

$$\textit{intercepts} \implies \mathbf{b} = \begin{bmatrix} b_{1,0} \\ \vdots \\ b_{i,0} \\ \vdots \\ b_{n,0} \end{bmatrix} \quad (13.10)$$

By design, the output difference vector $\mathbf{\Delta rF}$ is the input for the load iteration. It is defined as the difference between (i) a raw output and (ii) the intercept if raw outputs are used as input for the load iteration (see App. 10, Eq. (10.39)). Similarly, it is defined as the difference between (i) the output difference and (ii) the intercept if output differences

are used as input for the load iteration (see App. 10, Eq. (10.44)). Therefore, the electrical description of the tare loads should be referenced to the intercept term so that the input for the load iteration of each tare load iteration step has the required format. This difference can be described by the following vector equation assuming that an analyst chose raw outputs for the regression analysis of the balance calibration data. In that case, the intercepts ($b_{i,0}$) are least squares approximations of the natural zeros (N_i).

Electrical Description of Tare Loads *(Raw Output)*

$$\underbrace{\mathbf{\Delta Z}_k}_{1\leq k\leq q} = \underbrace{\{\ \mathbf{Z}_k\ \}}_{raw} - \underbrace{\begin{bmatrix} b_{1,0} \\ \vdots \\ b_{i,0} \\ \vdots \\ b_{n,0} \end{bmatrix}}_{\substack{intercepts \\ b_{i,0}\ \approx\ N_i}} = \begin{bmatrix} Z_{1,k} - b_{1,0} \\ \vdots \\ Z_{i,k} - b_{i,0} \\ \vdots \\ Z_{n,k} - b_{n,0} \end{bmatrix} \qquad (13.11a)$$

Similarly, the difference between zero load outputs and intercepts of a load series with index k can be described by the following vector equation assuming differences between raw outputs and natural zeros are chosen for the regression analysis of the calibration data. Then, the intercepts ($b_{i,0}$) are least squares approximations of zero output.

Electrical Description of Tare Loads *(Difference Type 1)*

$$\underbrace{\mathbf{\Delta Z}_k}_{1\leq k\leq q} = \underbrace{\{\ \mathbf{Z}_k - \mathbf{N}\ \}}_{difference} - \underbrace{\begin{bmatrix} b_{1,0} \\ \vdots \\ b_{i,0} \\ \vdots \\ b_{n,0} \end{bmatrix}}_{\substack{intercepts \\ b_{i,0}\ \approx\ 0}} = \begin{bmatrix} (Z_{1,k} - N_1) - b_{1,0} \\ \vdots \\ (Z_{i,k} - N_i) - b_{i,0} \\ \vdots \\ (Z_{n,k} - N_n) - b_{n,0} \end{bmatrix} \qquad (13.11b)$$

An approximation the two electrical descriptions above can be introduced if the intercepts are substituted by related outputs. Then, after replacing either $b_{i,0}$ in Eq. (13.11a) with N_i or after replacing $b_{i,0}$ in Eq. (13.11b) with zero output, we get the following approximation of the two exact relationships that are defined in Eqs. (13.11a) and (13.11b):

Electrical Description of Tare Loads *(Approximation)*

$$\underbrace{\mathbf{\Delta Z}_k}_{1 \le k \le q} \approx \underbrace{\{\, \mathbf{Z}_k - \mathbf{N} \,\}}_{difference} = \begin{bmatrix} Z_{1,k} - N_1 \\ \vdots \\ Z_{i,k} - N_i \\ \vdots \\ Z_{n,k} - N_n \end{bmatrix} \qquad (13.11c)$$

An electrical description of zero absolute load can be developed that uses Eq. (13.11a) and Eq. (13.11b) as a starting point. In theory, vector $\mathbf{N}$ is the electrical description of zero absolute load. Therefore, it is only required to replace vector $\mathbf{Z}_k$ in Eqs. (13.11a) and (13.11b) by vector $\mathbf{N}$ and simplify the result. First, raw outputs are investigated. In that case, vector $\mathbf{Z}_k$ in Eq. (13.11a) is replaced by vector $\mathbf{N}$. Then, we get:

Electrical Description of Zero Absolute Load *(Raw Output)*

$$\mathbf{\Delta Z}_0 = \underbrace{\{\, \mathbf{N} \,\}}_{raw} - \underbrace{\begin{bmatrix} b_{1,0} \\ \vdots \\ b_{i,0} \\ \vdots \\ b_{n,0} \end{bmatrix}}_{\substack{intercepts \\ b_{i,0} \approx N_i}} = \begin{bmatrix} N_1 - b_{1,0} \\ \vdots \\ N_i - b_{i,0} \\ \vdots \\ N_n - b_{n,0} \end{bmatrix} \qquad (13.12a)$$

Now, output differences are investigated. In that case, vector $\mathbf{Z}_k$ in Eq. (13.11b) is replaced by vector $\mathbf{N}$. Then, we get:

Electrical Description of Zero Absolute Load *(Difference Type 1)*

$$\mathbf{\Delta Z}_0 = \underbrace{\{\, \mathbf{N} - \mathbf{N} \,\}}_{difference} - \underbrace{\begin{bmatrix} b_{1,0} \\ \vdots \\ b_{i,0} \\ \vdots \\ b_{n,0} \end{bmatrix}}_{\substack{intercepts \\ b_{i,0} \approx 0}} = \begin{bmatrix} -b_{1,0} \\ \vdots \\ -b_{i,0} \\ \vdots \\ -b_{n,0} \end{bmatrix} \qquad (13.12b)$$

Finally, similar to Eq. (13.11c), an approximation of the vectors defined in Eqs. (13.12a) and (13.12b) above can be introduced after either replacing $b_{i,0}$ in Eq. (13.12a) with N_i or after replacing $b_{i,0}$ in Eq. (13.12b) with zero. Then, we get:

Electrical Description of Zero Absolute Load *(Approximation)*

$$\mathbf{\Delta Z}_0 \approx \begin{bmatrix} 0 \\ \vdots \\ 0 \end{bmatrix} \qquad (13.12c)$$

The tare loads of each load series with series index k are a function of (i) the electrical description of the tare loads of the series and (ii) the electrical description of zero absolute load. This conclusion can also be described in vector format. We get:

$$\textit{tare loads} \implies \mathbf{\Delta F}_k = \begin{bmatrix} \Delta F_{1,k}(\mathbf{\Delta Z}_k, \mathbf{\Delta Z}_0) \\ \vdots \\ \Delta F_{i,k}(\mathbf{\Delta Z}_k, \mathbf{\Delta Z}_0) \\ \vdots \\ \Delta F_{n,k}(\mathbf{\Delta Z}_k, \mathbf{\Delta Z}_0) \end{bmatrix} \qquad (13.13)$$

Characteristics of different tare load iteration analysis options, i.e., possible combinations of the regression model of the outputs, the electrical description of the tare loads, and the electrical description of zero absolute load are summarized in Table 13–1 below.

Table 13–1: Characteristics of Tare Load Iteration Analysis Options.

Option	Output Format	Regression Model	$\mathbf{\Delta Z}_k$	$\mathbf{\Delta Z}_0$	Intercept	Comments
1	Raw Output	(13.5a)	(13.11a)	(13.12a)	used	exact input
2†	Raw Output	(13.5a)	(13.11c)	(13.12c)	used	approximation
3	Diff. Type 1	(13.6a)	(13.11b)	(13.12b)	used	exact input
4†	Diff. Type 1	(13.6a)	(13.11b)	(13.12b)	omitted	exact input
5†	Diff. Type 1	(13.6a)	(13.11c)	(13.12c)	used	approximation

†Option matches *Galway's* tare load iteration algorithm (see Ref. [7], pp. 21–22).

Options 1, 3, and 4 use the exact electrical description of (i) the tare loads and (ii) zero absolute load as input for the tare load iteration process. Options 2 and 5, on the other hand, use an approximate electrical description of (i) the tare loads and (ii) zero absolute load as input for the tare load iteration process.

At this point, all balance data inputs have been defined that make the numerical determination of the tare loads possible. Now, the tare load iteration algorithm itself

needs to be described. This description is split into two parts. First, the calculation of a first estimate (initial guess) of the tare loads is discussed. Afterwards, the tare load iteration process itself is summarized.

13.5 First Estimate of Tare Loads

The application of any iteration process requires the calculation of a first estimate of the solution that must be reasonably close to the final answer. It is possible to obtain the first estimate of the tare loads from a simple linear regression model of the original balance calibration data. First, let us assume that an analyst chooses to fit raw outputs of the given balance calibration data as a function of the balance loads. Then, the linear regression model of raw output rF_i, i.e., *Regression Model A–1*, can be defined in Eq. (13.14*a*) below

Regression Model A–1 *(Raw Output)*

$$rF_i \;=\; \underbrace{b_{i,0}}_{intercept} \;+\; \underbrace{b_{i,1}\cdot F_1 \;+\; \cdots \;+\; b_{i,n}\cdot F_n}_{supported\ linear\ terms} \qquad (13.14a)$$

where

$$b_{i,0} \;\approx\; N_i \;\equiv\; natural\ zero\ of\ balance\ bridge \qquad (13.14b)$$

assuming that (i) the balance has a total of n load components and that (ii) the intercept term is included. Alternatively, an analyst may choose to fit the output difference D_i of a balance bridge relative to the natural zeros as a function of the load components of the balance. The corresponding linear regression model, i.e., *Regression Model A–2*, can be defined by the equation below assuming that the intercept is included in the list of chosen

Regression Model A–2 *(Difference Type 1)*

$$D_i \;=\; \underbrace{b_{i,0}}_{intercept} \;+\; \underbrace{b_{i,1}\cdot F_1 \;+\; \cdots \;+\; b_{i,n}\cdot F_n}_{supported\ linear\ terms} \qquad (13.15a)$$

where

$$b_{i,0} \;\approx\; 0 \;\Longrightarrow\; use\ of\ intercept\ is\ optional \qquad (13.15b)$$

regression model terms. The coefficients of both *Regression Model A–1* and *Regression Model A–2* above can be obtained by applying global regression analysis to the uncorrected

balance calibration data (see, e.g., Ref. [64], pp. 35–39, for a description of the global regression analysis approach). The applied, i.e., uncorrected, calibration loads of the p calibration points are one input for the regression analysis. They are contained in the rectangular matrix $\mathbf{F}_{unc}$ that was defined in Eq. (13.7). In addition, the raw outputs of the p calibration points are needed if an analyst chooses *Regression Model A–1* for the data analysis. They are contained in the rectangular matrix $\mathbf{rF}_{raw}$ that was defined in Eq. (13.8*a*). Alternatively, the output differences of the p calibration points are needed if an analyst chooses *Regression Model A–2* for the data analysis. They are contained in the rectangular matrix $\mathbf{rF}_{diff}$ that was defined in Eq. (13.8*b*). Now, the tare load iteration step index needs to be initialized. Then, we get:

First Iteration Step

$$\mu \;=\; 1 \qquad (13.16)$$

At this point the global regression analysis problem can be defined that is posed by the balance calibration data and *Regression Model A–1* or *Regression Model A–2*. Individual steps of the global regression analysis process are described in great detail in App. 10. Therefore, it is sufficient for the discussion of the tare load iteration process to simply list inputs and outputs of the global regression analysis of the balance calibration data. The following inputs are needed for the global regression analysis:

$$inputs \implies \begin{cases} \underbrace{\{\mathbf{F}_{unc}\},\ \mathbf{rF}_{raw},\ \textbf{Regression Model A–1}}_{Applied\ Loads,\ Raw\ Output,\ Regression\ Model} \\ \\ \ldots\ or\ \ldots \\ \\ \underbrace{\{\mathbf{F}_{unc}\},\ \mathbf{rF}_{diff},\ \textbf{Regression Model A–2}}_{Applied\ Loads,\ Difference\ Type\ 1,\ Regression\ Model} \end{cases} \qquad (13.17)$$

The coefficient matrices $\mathbf{C_1}$ of the *Primary Load Iteration Equation* or $\mathbf{B_1}$ and $\mathbf{B_2}$ of the *Alternate Load Iteration Equation* are the results of the global regression analysis whenever regression models with only linear terms are used for the balance data analysis (the coefficient matrix $\mathbf{C_2}$ of the non–linear terms is zero in this case). These results can be summarized as follows:

$$regression\ analysis\ results \implies \mathbf{C_1} \quad or \quad \mathbf{B_1}, \mathbf{B_2} \quad where \quad \mathbf{C_2} = \{\mathbf{0}\} \qquad (13.18)$$

It is also known from App. 10 that the following relationship is valid for the matrices $\mathbf{C_1}$, $\mathbf{B_1}$, and $\mathbf{B_2}$:

$$App.\ 10,\ Eq.\,(10.28a) \implies \mathbf{C_1} \;=\; \mathbf{B_1} \;+\; \mathbf{B_2} \qquad (13.19)$$

Now, first estimates of the tare loads of the load series can be computed by using vectors $\mathbf{\Delta Z}_k$ and $\mathbf{\Delta Z}_0$ as input for the load prediction equation that can be constructed from the coefficient matrices $\mathbf{C_1}$, $\mathbf{B_1}$, and $\mathbf{B_2}$. It is sufficient to use approximations of the two vectors $\mathbf{\Delta Z}_k$ and $\mathbf{\Delta Z}_0$ for the load prediction as only an initial guess of the tare loads is computed. These approximations can be summarized by the following relationship where $\mathbf{\Delta Z}_k$ is the electrical description of the tare loads and $\mathbf{\Delta Z}_0$ is the electrical description of zero absolute load:

$$approximations \implies \begin{cases} \mathbf{\Delta Z}_k \approx \{ \mathbf{Z}_k - \mathbf{N} \} \ \ldots \ taken\ from\ Eq.\ (13.11c) \\ \mathbf{\Delta Z}_0 \approx \begin{bmatrix} 0 \\ \vdots \\ 0 \end{bmatrix} \ \ldots\ldots\ldots \ taken\ from\ Eq.\ (13.12c) \end{cases} \tag{13.20}$$

It was mentioned above that the coefficient matrix $\mathbf{C_2}$ of the non–linear terms is zero. Therefore, no load iteration is needed to compute the first estimate of the tare loads of each load series. In addition, the output difference vector $\mathbf{\Delta Z}_0$ is zero. Consequently, the tare loads of a single load series with index k are simply given by the following equations:

Tare Loads of Single Load Series *(first estimate, no load iteration)*

$$\{\mathbf{\Delta F}_k\}_{\mu=1} = \begin{cases} \mathbf{C_1}^{-1}\,\mathbf{\Delta Z}_k & \Longleftrightarrow Primary\ Load\ Iteration\ Equation \\ [\,\mathbf{B_1} + \mathbf{B_2}\,]^{-1}\mathbf{\Delta Z}_k & \Longleftrightarrow Alternate\ Load\ Iteration\ Equation \end{cases} \tag{13.21a}$$

where

$$\{\mathbf{\Delta F}_k\}_{\mu=1} = \begin{bmatrix} \Delta F_{1,k} \\ \vdots \\ \Delta F_{i,k} \\ \vdots \\ \Delta F_{n,k} \end{bmatrix}_{n\times 1} \tag{13.21b}$$

The above equations have to be applied using the output difference vectors $\mathbf{\Delta Z}_k$ of each load series as input. Afterwards, the tare loads of all load series can be assembled in a rectangular matrix that is defined as follows:

Tare Loads of <u>All</u> Load Series *(first estimate)*

$$\{\mathbf{\Delta F}'\}_{\mu=1} \;=\; [\mathbf{\Delta F}_1 \;\ldots\; \mathbf{\Delta F}_q] \;=\; \begin{bmatrix} \Delta F_{1,1} & \ldots & \Delta F_{1,k} & \ldots & \Delta F_{1,q} \\ \vdots & \vdots & \vdots & \vdots & \vdots \\ \Delta F_{i,1} & \ldots & \Delta F_{i,k} & \ldots & \Delta F_{i,q} \\ \vdots & \vdots & \vdots & \vdots & \vdots \\ \Delta F_{n,1} & \ldots & \Delta F_{n,k} & \ldots & \Delta F_{n,q} \end{bmatrix}_{n\times q} \qquad (13.22)$$

The tare load estimates contained in the rectangular matrix above still need to be mapped to a rectangular matrix with p columns so that the tare load corrections can directly be applied to all uncorrected calibration loads. It is assumed that a transformation $\sigma(\nu)$ exists that uniquely relates load series index k to data point index ν. This transformation could be expressed as follows:

$$\sigma(\nu) \;=\; k \quad \textit{where} \quad \sigma(1) = 1 \;,\; \sigma(2) = 1 \;,\; \ldots \;,\; \sigma(p-1) = q \;,\; \sigma(p) = q \qquad (13.23)$$

Then, after applying the above transformation to the first estimate of the tare loads that are contained in the rectangular matrix above, the first tare load corrections of the calibration loads can be defined in matrix format as follows:

Tare Loads of Calibration Points *(first estimate)*

$$\{\mathbf{\Delta F}\}_{\mu=1} \;=\; \begin{bmatrix} \Delta F_{1,\sigma(1)} & \ldots & \Delta F_{1,\sigma(\nu)} & \ldots & \Delta F_{1,\sigma(p)} \\ \vdots & \vdots & \vdots & \vdots & \vdots \\ \Delta F_{i,\sigma(1)} & \ldots & \Delta F_{i,\sigma(\nu)} & \ldots & \Delta F_{i,\sigma(p)} \\ \vdots & \vdots & \vdots & \vdots & \vdots \\ \Delta F_{n,\sigma(1)} & \ldots & \Delta F_{n,\sigma(\nu)} & \ldots & \Delta F_{n,\sigma(p)} \end{bmatrix}_{n\times p} \qquad (13.24)$$

The above estimates of the tare loads of the individual calibration data points are the initial guess of the tare loads that is needed for the tare load iteration process. The matrix of tare loads defined in Eq. (13.24) above is an $n \times p$ matrix. Therefore, it can be added to the matrix $\mathbf{F}_{unc}$ of applied/uncorrected calibration loads that is defined in Eq. (13.7). – The tare load iteration process itself is discussed in more detail in the next section.

13.6 Tare Load Iteration Process

This section describes the tare load iteration process. Now, the analyst's final regression model term combination choice with both linear and non–linear terms is used for the regression analysis of the balance calibration data.

Let us assume, for example, that an analyst chooses to fit raw outputs of the calibration data. Then, the final regression model of the raw output rF_i, i.e., *Regression Model B–1*, is defined as follows:

Regression Model B–1 *(Raw Output)*

$$rF_i \;=\; \underbrace{b_{i,0}}_{intercept} \;+\; \underbrace{b_{i,1}\cdot F_1 \;+\; b_{i,2}\cdot F_2 \;+\; \cdots \;+\; b_{i,\omega}\cdot F_1^{\,2} \;+\; \cdots}_{supported\ linear,\ absolute\ value\ \&\ non-linear\ terms} \qquad (13.25a)$$

where

$$b_{i,0} \;\approx\; N_i \;(natural\ zero\ of\ balance\ bridge) \qquad (13.25b)$$

Similarly, let us assume that an analyst chooses to fit output differences relative to the natural zeros instead of raw outputs. In that case, the final regression model of the output difference D_i, i.e., *Regression Model B–2*, can be defined as follows:

Regression Model B–2 *(Difference Type 1)*

$$D_i \;=\; \underbrace{b_{i,0}}_{intercept} \;+\; \underbrace{b_{i,1}\cdot F_1 \;+\; b_{i,2}\cdot F_2 \;+\; \cdots \;+\; b_{i,\omega}\cdot F_1^{\,2} \;+\; \cdots}_{supported\ linear,\ absolute\ value\ \&\ non-linear\ terms} \qquad (13.26a)$$

where

$$b_{i,0} \;\approx\; 0 \;\Longrightarrow\; use\ of\ intercept\ is\ optional \qquad (13.26b)$$

Now, the tare load iteration step is increased by one. We get:

Iteration Step Increase

$$\mu \;\Longrightarrow\; \mu \;+\; 1 \qquad (13.27)$$

In the next step, inputs for the global regression analysis of the calibration data need to be assembled. The electrical outputs of the calibration data points remain unchanged. Therefore, only the calibration loads need to be updated by simply adding the tare load estimates of the previous tare load iteration step to the uncorrected calibration loads. Then, an interim estimate of the tare corrected calibration loads of all calibration points is obtained that can be described by the following relationship assuming that the initial

guess $\{\mathbf{\Delta F}\}_{\mu=1}$ of the tare loads is given by Eq. (13.24):

Tare Corrected Calibration Loads *(interim estimate)*

$$\{\mathbf{F}_{cor}\}_{\mu} \quad = \quad \mathbf{F}_{unc} \; + \; \{\mathbf{\Delta F}\}_{\mu-1} \qquad (13.28)$$

Now, the inputs of the global regression analysis problem associated with the interim tare load iteration step can be summarized by the following equation:

$$inputs \implies \begin{cases} \underbrace{\{\mathbf{F}_{cor}\}_{\mu}, \; \mathbf{rF}_{raw}, \; \textbf{Regression Model B–1}}_{Corrected\ Loads,\ Raw\ Output,\ Regression\ Model} \\ \\ \ldots \; or \; \ldots \\ \\ \underbrace{\{\mathbf{F}_{cor}\}_{\mu}, \; \mathbf{rF}_{diff}, \; \textbf{Regression Model B–2}}_{Corrected\ Loads,\ Difference\ Type\ 1,\ Regression\ Model} \end{cases} \qquad (13.29)$$

Then, after solving the global regression analysis problem using the inputs specified in Eq. (13.29) above, the following coefficient matrices are obtained:

$$regression\ analysis\ results \implies \mathbf{C_1}, \mathbf{C_2} \; or \; \mathbf{B_1}, \mathbf{B_2}, \mathbf{C_2} \; where \; \mathbf{C_2} \neq \{\mathbf{0}\} \qquad (13.30)$$

Now, the load iteration equations resulting from the outputs of the global regression analysis can be defined by using the electrical descriptions of the tare loads of each load series with index k as input. We get:

$$\mathbf{F}_{\xi}(\mathbf{\Delta Z}_k) \quad = \quad \begin{cases} \underbrace{\mathbf{C_1}^{-1}\mathbf{\Delta Z}_k \; - \; \mathbf{C_1}^{-1}\mathbf{C_2} \cdot \mathbf{H}(\mathbf{F}_{\xi-1})}_{Primary\ Load\ Iteration\ Equation} \\ \\ \underbrace{\mathbf{B_1}^{-1}\mathbf{\Delta Z}_k \; - \; \mathbf{B_1}^{-1}\mathbf{B_2} \cdot \mathbf{F}_{\xi-1} \; - \; \mathbf{B_1}^{-1}\mathbf{C_2} \cdot \mathbf{H}(\mathbf{F}_{\xi-1})}_{Alternate\ Load\ Iteration\ Equation} \end{cases} \qquad (13.31a)$$

Similarly, the load iteration equations associated with the electrical description of zero absolute load are given by the following equations:

$$\mathbf{F}_{\xi}(\mathbf{\Delta Z}_0) \quad = \quad \begin{cases} \underbrace{\mathbf{C_1}^{-1}\mathbf{\Delta Z}_0 \; - \; \mathbf{C_1}^{-1}\mathbf{C_2} \cdot \mathbf{H}(\mathbf{F}_{\xi-1})}_{Primary\ Load\ Iteration\ Equation} \\ \\ \underbrace{\mathbf{B_1}^{-1}\mathbf{\Delta Z}_0 \; - \; \mathbf{B_1}^{-1}\mathbf{B_2} \cdot \mathbf{F}_{\xi-1} \; - \; \mathbf{B_1}^{-1}\mathbf{C_2} \cdot \mathbf{H}(\mathbf{F}_{\xi-1})}_{Alternate\ Load\ Iteration\ Equation} \end{cases} \qquad (13.31b)$$

Now, the interim estimate of the tare loads of each load series is obtained by performing the load iterations and taking the difference of the resulting two load vectors. We get:

Tare Loads of Single Load Series *(interim estimate)*

$$\{\mathbf{\Delta F}_k\}_\mu \;=\; \underset{|\delta\mathbf{F}|\,<\,TOL}{Iteration}\Big\{\,\mathbf{F}_\xi(\mathbf{\Delta Z}_k)\,\Big\} \;-\; \underset{|\delta\mathbf{F}|\,<\,TOL}{Iteration}\Big\{\,\mathbf{F}_\xi(\mathbf{\Delta Z}_0)\,\Big\} \qquad (13.32a)$$

where

$$\{\mathbf{\Delta F}_k\}_\mu \;=\; \begin{bmatrix} \Delta F_{1,k} \\ \vdots \\ \Delta F_{i,k} \\ \vdots \\ \Delta F_{n,k} \end{bmatrix} \qquad (13.32b)$$

The above load iterations have to be applied using the output difference vectors of all load series as input. Afterwards, similar to Eq. (13.22), the interim estimates of the tare loads of all load series can be stored in a rectangular matrix that is defined as follows:

Tare Loads of all Load Series *(interim estimate)*

$$\{\mathbf{\Delta F}'\}_\mu \;=\; [\mathbf{\Delta F}_1 \;\ldots\; \mathbf{\Delta F}_q] \;=\; \begin{bmatrix} \Delta F_{1,1} & \ldots & \Delta F_{1,k} & \ldots & \Delta F_{1,q} \\ \vdots & \vdots & \vdots & \vdots & \vdots \\ \Delta F_{i,1} & \ldots & \Delta F_{i,k} & \ldots & \Delta F_{i,q} \\ \vdots & \vdots & \vdots & \vdots & \vdots \\ \Delta F_{n,1} & \ldots & \Delta F_{n,k} & \ldots & \Delta F_{n,q} \end{bmatrix}_{n\times q} \qquad (13.33)$$

Then, after applying the transformations defined in Eq. (13.23) to the interim estimate of the tare loads that are contained in the rectangular matrix above, the interim tare load corrections of the calibration loads can be defined in matrix format as follows:

Tare Loads of Calibration Points *(interim estimate)*

$$\{\mathbf{\Delta F}\}_{\mu} = \begin{bmatrix} \Delta F_{1,\sigma(1)} & \dots & \Delta F_{1,\sigma(\nu)} & \dots & \Delta F_{1,\sigma(p)} \\ \vdots & \vdots & \vdots & \vdots & \vdots \\ \Delta F_{i,\sigma(1)} & \dots & \Delta F_{i,\sigma(\nu)} & \dots & \Delta F_{i,\sigma(p)} \\ \vdots & \vdots & \vdots & \vdots & \vdots \\ \Delta F_{n,\sigma(1)} & \dots & \Delta F_{n,\sigma(\nu)} & \dots & \Delta F_{n,\sigma(p)} \end{bmatrix}_{n \times p} \tag{13.34}$$

A tare load iteration convergence test is applied at this point. Therefore, tare load changes, i.e., differences between tare load estimates of the current and previous iteration step are computed. Then, the absolute value of the maximum difference is expressed as a percentage of the load capacity. This test metric is compared with the empirical threshold of 0.0001 % of load capacity. Two cases must be distinguished. First, the test metric could be greater than or equal to the threshold. Then, the iteration continues by going back to Eq. (13.27). Alternatively, the test metric could be less than the threshold. In that case, the iteration converged and is terminated after the final set of tare corrected calibration loads is computed. The iteration convergence test is summarized below.

Tare Load Iteration Convergence Test

$$\delta\mathbf{F}' = \underbrace{\{\mathbf{\Delta F}'\}_{\mu} - \{\mathbf{\Delta F}'\}_{\mu-1}}_{tare\ load\ change} = \begin{bmatrix} \delta F_{1,1} & \dots & \delta F_{1,k} & \dots & \delta F_{1,q} \\ \vdots & \vdots & \vdots & \vdots & \vdots \\ \delta F_{i,1} & \dots & \delta F_{i,k} & \dots & \delta F_{i,q} \\ \vdots & \vdots & \vdots & \vdots & \vdots \\ \delta F_{n,1} & \dots & \delta F_{n,k} & \dots & \delta F_{n,q} \end{bmatrix} \tag{13.35a}$$

$$\delta F_{i,k} = \{\Delta F_{i,k}\}_{\mu} - \{\Delta F_{i,k}\}_{\mu-1} \tag{13.35b}$$

$$V = MAX\left\{ \left|\frac{\delta F_{1,1}}{\Gamma_1}\right| , \dots , \left|\frac{\delta F_{i,k}}{\Gamma_i}\right| , \dots , \left|\frac{\delta F_{n,q}}{\Gamma_n}\right| \right\} \cdot 100\,\% \tag{13.35c}$$

$$V \geq 0.0001\,\% \implies \textit{go back to Eq. (13.27)} \implies \textit{continue} \dots \tag{13.35d}$$

$$V < 0.0001\,\% \implies \textit{advance to Eq. (13.36)} \implies \textit{stop} \dots \tag{13.35e}$$

The final set of tare corrected calibration loads is computed after the condition described in Eq. (13.35e) above is fulfilled. Then, the tare loads of the calibration points of the final iteration step are added to the applied/uncorrected loads in order to obtain the final set of tare corrected calibration loads. We get:

Final Set of Tare Corrected Calibration Loads

$$\mathbf{F}_{cor} = \underbrace{\mathbf{F}_{unc}}_{Eq.\,(13.7)} + \underbrace{\{\mathbf{\Delta F}\}_{\mu}}_{Eq.\,(13.34)} \qquad (13.36)$$

Now, the final set of regression coefficients of either *Regression Model B–1* or *Regression Model B–2* of the balance calibration data can be computed by using (i) the electrical outputs given in Eq. (13.8*a*) or Eq. (13.8*b*) and (ii) the tare corrected calibration loads given in Eq. (13.36) above as input.

13.7 Comparison of Tare Load Iteration Algorithms

It is mentioned in the introduction of the appendix that *Galway's* tare load iteration algorithm always uses output format *Difference Type 2* for the calculation of the linear matrix that is needed for the determination of the first estimate of the tare loads. In other words, *Galway's* algorithm replaces *Raw Output* with *Difference Type 2* in the definition of *Regression Model A–1* that is described in Eq. (13.14*a*). Similarly, *Galway's* algorithm replaces *Difference Type 1* with *Difference Type 2* in the definition of *Regression Model A–2* that is described in Eq. (13.15*a*). It seems, superficially viewed, that this change of the output format could influence the final result of the tare load iterations. However, the author observed that the final tare load estimates for both output format choices are identical for all practical purposes. *Galway's* output format choice simply results in a more rapid convergence of the tare load iterations as his first estimate of the tare loads is closer to the final answer. The author's output format choice, on the other hand, makes an implementation of the tare load iteration algorithm less complex as only one output format type, i.e., *Raw Output* in both *Regression Model A–1* and *Regression Model B–1* or *Difference Type 1* in both *Regression Model A–2* and *Regression Model B–2* is used during the entire tare load iteration process.

It is also mentioned in the introduction that the author's algorithm uses two load calculations for each tare load iteration step that are defined in Eq. (13.32*a*) above. The inputs for these two load calculations are (i) the electrical description $\mathbf{\Delta Z}_k$ of the tare loads of each load series and (ii) the electrical description $\mathbf{\Delta Z}_0$ of zero absolute load. Both load calculations lead to non–zero solutions whenever intercept terms are used in the regression models of the outputs. This situation exists if an analyst chooses either Option 1 or Option 3 for the tare load iteration process (Table 13–1).

Alternatively, an analyst may choose to use approximations of both $\mathbf{\Delta Z}_k$ and $\mathbf{\Delta Z}_0$ as input for the calculation of the interim tare loads of each iteration step. In that case, the predicted load for the electrical description of zero absolute load is zero. Consequently, only one load calculation is performed for each tare load iteration step. This situation exists whenever an analyst chooses either Option 2 or Option 5 of Table 13–1 for the tare load iteration process. Those two options match *Galway's* tare load iteration algorithm that is described in the literature. In other words, *Galway's* tare load iteration algorithm can be considered a special case of the author's tare load iteration algorithm if (i) approximations instead of the exact values for the electrical descriptions of the tare loads and zero absolute load are used and (ii) an intercept term is included in the regression models of the data.

Finally, an analyst (i) may use differences between raw outputs and natural zeros for the description of the outputs and (ii) decide to omit optional intercept terms in the regression models of the output differences. This case is identified as analysis Option 4 in Table 13–1. It uses exact electrical descriptions of the tare loads and zero absolute load. Only one load calculation for each tare load iteration step is performed as the second term on the right–hand side of Eq. (13.32a) is zero. Consequently, Option 4 also matches *Galway's* tare load iteration algorithm that is described in the literature.

A data set from the manual calibration of a six–component force balance is used in the next section in order to illustrate the application of the tare load iteration process.

13.8 Discussion of Example

A data set from the manual calibration of a strain–gage balance is used to illustrate the application of the tare load iteration algorithm for the *Iterative Method*. The chosen balance is called the NASA MK3C. It was manufactured by the Task/Able Corporation. It is a six–component force balance that measures five forces and one moment ($N1$, $N2$, $S1$, $S2$, AF, RM). It has a diameter of 2.0 in and a total length of 11.25 in. Table 13–2 shows the capacity of each load component of the balance.

Table 13–2: Load capacities of the MK3C force balance ($lbs \equiv$ pounds of force).

$N1,\ lbs$	$N2,\ lbs$	$S1,\ lbs$	$S2,\ lbs$	$AF,\ lbs$	$RM,\ in{-}lbs$
900	900	450	450	500	1000

It was decided to discuss the application of the tare load iteration algorithm for three of the five analysis options that are listed in Table 13–1. Absolute value terms of the loads were included in the regression models of the outputs for all options as the MK3C balance is known to have bi–directional outputs. Table 13–3 below describes basic assumptions associated with the three chosen analysis options.

Table 13–3: Description of investigated tare load iteration analysis options.

Option	Output Format	Regression Model of Outputs	Intercept
1	Raw Output (see App. 6, Eq. (6.1))	$rF_i = b_{i,0} + b_{i,1} \cdot N1 + \ldots$	$b_{i,0} \approx N_i$ (required)
3	Difference Type 1 (see App. 6, Eq. (6.2))	$D_i = b_{i,0} + b_{i,1} \cdot N1 + \ldots$	$b_{i,0} \approx 0$ (included)
4†	Difference Type 1 (see App. 6, Eq. (6.2))	$D_i = 0 + b_{i,1} \cdot N1 + \ldots$	$b_{i,0} = 0$ (omitted)

†Option matches *Galway's* tare load iteration algorithm (Ref. [7], pp. 21–22).

Options 1 and 3 use two load calculations for each tare load iteration step as the intercept term is included in both regression models (see also Eq. (13.32a) for the definition of the two load calculations). In addition, the author decided to use the same regression model term selection for the outputs of Options 1 and 3. Therefore, the regression coefficients of both options will be identical with the exception of the coefficient of the intercept term. Consequently, the tare loads estimates of those two approaches are identical even though the fitted outputs have different formats.

Option 4, on the other hand, uses one load calculation for each tare load iteration step. In that case, the optional intercept term is intentionally omitted in the regression model of the output differences. This analysis option matches *Galway's* tare load iteration algorithm that is described in the literature. It is are also identified as *Method A* in Ref. [11].

Table 13–4 below shows parts of the original calibration data of the MK3C balance. Only 21 of a total of 247 data points are shown. The natural zeros and the electrical outputs of all bridges are listed as raw outputs in units of $microV/V$. Both the applied/uncorrected loads and the raw outputs of each data point are shown for the first load series. The forward normal force component was applied during load series one.

Table 13–4: Calibration data of the MK3C balance described as (i) applied i.e., uncorrected loads and (ii) raw outputs (absolute voltage measurements).

								rN1	rN2	rS1	rS2	rAF	rRM
								microV/V	microV/V	microV/V	microV/V	microV/V	microV/V
							NATURAL ZEROS OF THE BALANCE BRIDGES ------>	-318.58	95.28	55.89	-212.30	169.44	-102.23
PT. ID	SERIES	N1	N2	S1	S2	AF	RM	rN1	rN2	rS1	rS2	rAF	rRM
-	-	lbs	lbs	lbs	lbs	lbs	in-lbs	microV/V	microV/V	microV/V	microV/V	microV/V	microV/V
P-1	1	0	0	0	0	0	0	-239.01	108.67	55.80	-211.46	170.56	-102.38
P-2	1	100	0	0	0	0	0	-59.90	105.07	56.21	-210.96	170.53	-102.37
P-3	1	200	0	0	0	0	0	120.30	101.70	56.67	-210.46	170.16	-102.56
P-4	1	300	0	0	0	0	0	301.18	98.20	56.92	-210.05	169.99	-102.47
P-5	1	400	0	0	0	0	0	482.15	94.78	56.83	-209.89	169.80	-102.61
P-6	1	500	0	0	0	0	0	663.20	91.43	57.28	-209.37	169.71	-102.40
P-7	1	600	0	0	0	0	0	843.98	87.96	57.31	-209.03	169.53	-102.57
P-8	1	700	0	0	0	0	0	1024.69	84.46	57.18	-208.81	169.53	-102.53
P-9	1	800	0	0	0	0	0	1204.81	80.95	57.27	-208.49	169.25	-102.57
P-10	1	900	0	0	0	0	0	1385.42	77.52	57.42	-208.20	169.28	-102.40
P-11	1	800	0	0	0	0	0	1207.31	80.99	57.23	-208.62	169.24	-102.54
P-12	1	700	0	0	0	0	0	1028.10	84.36	57.01	-208.80	169.43	-102.51
P-13	1	600	0	0	0	0	0	847.66	87.95	57.17	-209.02	169.44	-102.62
P-14	1	500	0	0	0	0	0	666.39	91.42	56.72	-209.31	169.40	-102.77
P-15	1	400	0	0	0	0	0	485.03	94.83	56.96	-209.89	169.60	-102.51
P-16	1	300	0	0	0	0	0	303.36	98.27	56.63	-210.23	169.78	-102.52
P-17	1	200	0	0	0	0	0	121.73	101.71	56.55	-210.57	169.89	-102.43
P-18	1	100	0	0	0	0	0	-59.20	105.21	56.39	-210.90	170.34	-102.41
P-19	1	0	0	0	0	0	0	-239.60	108.69	55.78	-211.44	170.66	-102.35
P-20	2	0	0	0	0	0	0	-297.66	166.53	55.96	-212.57	173.44	-102.40
P-21	2	0	100	0	0	0	0	-299.37	351.63	56.07	-213.30	177.60	-102.55
...	...	...	...	...	...	...	...	...	...	...	...	...	...

The electrical outputs of the first data point P–1 of load series 1 are the components of vector $\mathbf{Z}_1$ that is defined in Eq. (13.9). They are the electrical outputs of the zero load point of the load series 1. In addition, they are the electrical description of the tare loads of load series 1. We get:

$$\mathbf{Z}_1 = \begin{bmatrix} -239.01\ microV/V \\ +108.67\ microV/V \\ +55.80\ microV/V \\ -211.46\ microV/V \\ +170.56\ microV/V \\ -102.38\ microV/V \end{bmatrix} \tag{13.37}$$

Table 13–5 below shows parts of the calibration data of the MK3C balance after the differences between raw outputs and natural zeros of the balance bridges were computed. The output differences were simply obtained by subtracting the natural zeros from the raw outputs that are both listed in Table 13–4 above. We get:

Table 13–5: Calibration data of the MK3C balance described as (i) applied, i.e., uncorrected loads and (ii) output differences relative to the natural zeros.

PT. ID	SERIES	N1	N2	S1	S2	AF	RM	rN1	rN2	rS1	rS2	rAF	rRM
-	-	lbs	lbs	lbs	lbs	lbs	in-lbs	microV/V	microV/V	microV/V	microV/V	microV/V	microV/V
P-1	1	0	0	0	0	0	0	79.57	13.40	-0.09	0.84	1.12	-0.15
P-2	1	100	0	0	0	0	0	258.68	9.79	0.31	1.34	1.08	-0.14
P-3	1	200	0	0	0	0	0	438.88	6.42	0.78	1.84	0.71	-0.33
P-4	1	300	0	0	0	0	0	619.77	2.93	1.03	2.25	0.55	-0.24
P-5	1	400	0	0	0	0	0	800.73	-0.50	0.93	2.41	0.36	-0.38
P-6	1	500	0	0	0	0	0	981.78	-3.85	1.39	2.93	0.27	-0.17
P-7	1	600	0	0	0	0	0	1162.56	-7.31	1.42	3.27	0.09	-0.34
P-8	1	700	0	0	0	0	0	1343.27	-10.81	1.28	3.49	0.09	-0.30
P-9	1	800	0	0	0	0	0	1523.39	-14.33	1.38	3.81	-0.19	-0.34
P-10	1	900	0	0	0	0	0	1704.01	-17.76	1.52	4.10	-0.16	-0.17
P-11	1	800	0	0	0	0	0	1525.89	-14.29	1.34	3.68	-0.20	-0.31
P-12	1	700	0	0	0	0	0	1346.68	-10.91	1.12	3.50	-0.01	-0.28
P-13	1	600	0	0	0	0	0	1166.24	-7.33	1.28	3.28	0.00	-0.39
P-14	1	500	0	0	0	0	0	984.97	-3.85	0.83	2.99	-0.04	-0.54
P-15	1	400	0	0	0	0	0	803.61	-0.45	1.07	2.41	0.16	-0.28
P-16	1	300	0	0	0	0	0	621.94	2.99	0.73	2.07	0.34	-0.29
P-17	1	200	0	0	0	0	0	440.31	6.43	0.66	1.73	0.45	-0.20
P-18	1	100	0	0	0	0	0	259.38	9.94	0.50	1.40	0.90	-0.18
P-19	1	0	0	0	0	0	0	78.98	13.42	-0.11	0.86	1.21	-0.12
P-20	2	0	0	0	0	0	0	20.92	71.25	0.06	-0.27	4.00	-0.17
P-21	2	0	100	0	0	0	0	19.21	256.35	0.18	-1.00	8.16	-0.32
...	...	...	...	...	...	...	...	...	...	...	...	...	...

Now, tare load estimates for the 13 load series of the balance calibration data set were computed by using the three options that are listed in Table 13–3. Table 13–6 below shows the tare load estimates for Options 1 and 3.

Table 13–6: Estimated tare loads of the MK3C balance for Options 1 & 3.

Load Series	$\Delta N1$ lbs	$\Delta N2$ lbs	$\Delta S1$ lbs	$\Delta S2$ lbs	ΔAF lbs	ΔRM $in-lbs$
1	+43.914	+8.016	–0.112	+0.226	+0.518	–0.126
2	+11.901	+38.531	+0.018	–0.068	+1.059	–0.109
3	+15.098	+11.200	–0.167	+0.000	+0.555	–0.189
4	–29.003	–8.195	–0.428	+0.328	+0.143	–1.107
5	–10.207	–25.312	–0.378	+0.452	–2.083	–1.221
6	+0.061	+0.085	+42.537	+7.782	–0.728	–1.532
7	+0.037	+0.003	+10.698	+39.782	–0.821	–1.805
8	–0.001	–0.033	–43.063	–8.037	–0.461	–1.014
9	+0.167	–0.041	–11.387	–40.021	–0.427	+0.355
10	–0.146	–0.494	–0.251	+0.025	+55.037	–0.115
11	–1.006	+0.387	+0.295	–0.394	–36.575	–0.279
12	–76.599	+22.212	–0.272	–0.297	+1.345	–0.125
13	+75.177	–22.791	–0.043	+0.015	–0.041	+0.370

Similarly, tare load estimates for the 13 load series of the balance calibration data set were computed by using the Option 4 that is described in Table 13–3. Table 13–7 below shows the tare load estimates for Options 4.

Table 13–7: Estimated tare loads of the MK3C balance for Option 4.

Load Series	$\Delta N1$ *lbs*	$\Delta N2$ *lbs*	$\Delta S1$ *lbs*	$\Delta S2$ *lbs*	ΔAF *lbs*	ΔRM *in−lbs*
1	+43.942	+8.046	–0.116	+0.234	+0.501	–0.090
2	+11.928	+38.559	+0.014	–0.061	+1.043	–0.074
3	+15.113	+11.216	–0.170	+0.004	+0.546	–0.170
4	–28.985	–8.176	–0.430	+0.333	+0.132	–1.082
5	–10.189	–25.293	–0.380	+0.457	–2.094	–1.196
6	+0.114	+0.141	+42.531	+7.797	–0.759	–1.463
7	+0.090	+0.058	+10.691	+39.797	–0.851	–1.737
8	+0.052	+0.023	–43.069	–8.023	–0.492	–0.944
9	+0.219	–0.014	–11.393	–40.006	–0.458	+0.424
10	–0.096	–0.441	–0.257	+0.040	+55.008	–0.047
11	–0.973	+0.421	+0.291	–0.385	–36.594	–0.236
12	–76.553	+22.261	–0.278	–0.283	+1.318	–0.064
13	+75.223	–22.742	–0.048	+0.029	–0.069	+0.431

In general, the computed tare load estimates for Option 1 & 3 (Table 13–6) show excellent agreement with corresponding values for Option 4 (Table 13–7).

Computed tare load estimates for the forward normal force component ($\Delta N1$) can be compared with corresponding values that are reported for the *Non–Iterative Method* in Table 12–5 of App. 12. The agreement between the estimates reported in Table 12–5 *(Approach 3)* and Table 13–7 for the forward normal force component is very good. The maximum difference between the tare load estimates is less than 0.2 *lbs* or 0.02 % of the capacity of the forward normal force component.

Appendix 14

Balance Temperature Effects

14.1 Introduction

In general, the influence of temperature changes on the accuracy of the load prediction of a strain–gage balance is well understood. For example, *Ewald, Polanski,* and *Graewe* summarize related problems and challenges as follows (taken from Ref. [36], p. 2):

> ... Through the temperature range zero point shifts and sensitivity shifts occur. These effects must be minimized by careful matching of the gages and remaining errors must be calibrated and corrected by a numerical process for satisfying accuracy. ...

Similarly, *Ferris* writes (taken from Ref. [37], p. 2):

> ... To obtain accurate force data over the large temperature range experienced in the NTF, it is necessary to eliminate or correct for the effects of any thermally–induced output so that the remaining output is a function of the applied load only. These thermally–induced outputs may appear as changes in the zero load output (apparent strain), in the output for a given applied load (sensitivity shift), and in the output due to mechanical deformation caused by thermal transients. ...

Ferris emphasizes that thermal effects influence the measured electrical outputs of the balance bridges when a set of calibration loads is applied. Mechanical deformations associated with thermal transients are complex and very difficult to quantify. Therefore, it was decided to focus the discussions in this appendix on the first two temperature effects that *Ferris* mentions above. They can be summarized as follows:

- shifts of the zero load outputs, i.e., natural zeros of each bridge
- shifts of the sensitivities of each bridge.

Temperature–dependent shifts of the natural zeros can easily be addressed by applying a linear correction to the natural zeros. An analyst only needs to observe how the natural zero of each bridge changes whenever a temperature change occurs. Then, this experimental information is used to define the correction equations for the outputs.

The development of a correction for the temperature–dependent shift of the bridge sensitivity is more complicated. In that case, both balance temperature and primary load of the bridge need to be changed during a calibration to quantify the shift. An analyst has several options to address the influence of a sensitivity shift on the load prediction. For example, a correction for each balance load of a data point can be computed that is a function of (i) the observed bridge sensitivity shift, (ii) the temperature change, and (iii) the bridge output. Alternatively, it is possible to include temperature effects in the regression models of the calibration data that are used for the load prediction. Each option has advantages and disadvantages. The first option is simple to apply. However, it has the disadvantage that it separates the processing of calibration data recorded at a constant temperature from the processing of calibration data that describes temperature effects. The second option, on the other hand, generates regression models for the load prediction from a single temperature–dependent calibration data set.

Most derivations of this appendix are based on investigations and results that are presented in Ref. [38] and [39]. These references recommend to describe the temperature–dependent behavior of a balance by using the difference between the uniform balance temperature (T) and a suitable reference temperature ($T_\circ$) as input. This difference is a new independent variable for both balance calibration and load prediction. The balance itself must have a uniform temperature during both calibration and use. Otherwise, the associated increase in the number of independent variables makes the balance calibration task impractical. The importance of having a uniform temperature of the balance is also emphasized in the literature. For example, *Ewald, Polanski,* and *Graewe* summarize the requirement for uniform balance temperature distribution as follows (Ref. [36], p. 4):

> ... Even more important is the fact that copper beryllium has a heat conductivity five times higher than maraging steel. The advantage will be a more uniform temperature distribution in the balance or the same distribution in shorter times. ...

The use of the temperature difference as an independent variable for the description of temperature effects suggests itself because a Taylor series approximation of the multivariate behavior of a strain–gage balance can be considered the theoretical basis for the definition of the regression model terms of balance calibration data. Then, the extended independent variable set for calibration and use of the balance is given by the temperature difference in combination with either the output differences of the balance bridges (*Non–Iterative Method*) or the balance loads (*Iterative Method*). The new independent variable, i.e., the temperature difference, can be expressed as follows where T is the uniform

Temperature Difference

$$\Delta T = T - T_\circ \qquad (14.1)$$

balance temperature and $T_\circ$ is the chosen reference temperature for the balance calibration. Ideally, this reference temperature should be located within the range of all temperatures that the balance is expected to experience during the wind tunnel test. In most practical situations, however, the reference temperature equals the constant temperature that the balance had during its calibration.

At this point, the new variable needed for the characterization of temperature effects is defined. Now, correction methods can be discussed that address (i) the shift of the natural zeros of the bridges and (ii) the shift of the bridge sensitivities. First, a temperature–dependent correction for the shift of the natural zeros of the bridges is derived.

14.2 Natural Zero Shift

14.2.1 General Remarks

A temperature–dependent correction for the natural zero shift of a bridge can easily be obtained if the unknown output shift is approximated by a first order Taylor series. Alternatively, outputs may be compared in the model's wind–off home posi-

tion. Furthermore, it is an advantage for the derivation of the correction to describe the electrical outputs of a balance bridge as the difference between (i) the raw output and (ii) the natural zero of the bridge. Then, the output difference D_i of a balance bridge with index i can be described by the following equation where rF_i is the raw output of the bridge, N_i describes the natural zero of the bridge, and $T_\circ$ is the chosen reference

Bridge Output Difference *(temperature = constant)*

$$D_i(T_\circ) \quad = \quad rF_i(T_\circ) \; - \; N_i(T_\circ) \quad ; \quad 1 \leq i \leq n \qquad (14.2)$$

temperature of the balance. Now, it is assumed that (i) the temperature changes from the reference temperature $T_\circ$ to a new temperature T and (ii) all balance loads are close to zero load. In that case, the raw outputs of the balance bridge change by a small amount as no temperature compensation of a balance bridge is perfect. Then, the bridge output difference at the new temperature can be described by the following relationship as the

$$D_i(T) \quad = \quad rF_i(T) \; - \; N_i(T) \qquad (14.3)$$

natural zero, i.e., the raw output at zero absolute load, also changes. The exact relationship describing the temperature–dependent change of the natural zero is unknown. One of two options may be used to estimate the change. First, it is possible to record the natural zeros in a balance calibration laboratory at different temperatures and describe the bridge characteristics by using a first order Taylor series. Alternatively, output observations at the wind–off home position of the wind tunnel model can be used to determine the output change. First, the application of a Taylor series approximation for the description of the temperature–dependent output change is discussed. Afterwards, the use of data from the wind tunnel model's wind–off home position is explained.

14.2.2 Taylor Series Approximation of Output Change

In principle, it is possible to approximate the unknown relationship between the natural zero and the balance temperature by recording natural zeros in a balance calibration laboratory at difference temperatures. Afterwards, a first order Taylor series expansion is developed from the data in order to describe the temperature characteristics of the bridge near zero absolute load. Then, we get the following approximation of the temperature–

$$first\ order\ Taylor\ series \quad \Longrightarrow \quad N_i(T) \quad \approx \quad N_i(T_\circ) \; + \; \left[\frac{d\ rF_i}{d\ T} \right]_{T_\circ} \cdot \; \Delta T \qquad (14.4)$$

dependent natural zero of a bridge where $N_i(T_\circ)$ is the natural zero at the reference temperature $T_\circ$ and drF_i/dT is the first derivative of the bridge output with respect to the temperature. Finally, after replacing $N_i(T)$ in Eq. (14.3) with the right–hand side of Eq. (14.4), we get the following relationship for the output difference $D_i(T)$ where the

Bridge Output Difference *(temperature ≠ constant)*

$$D_i(T) \;\approx\; rF_i(T) \;-\; \underbrace{\{\, N_i(T_\circ) \;+\; \Delta N_i \,\}}_{corrected\ natural\ zero} \qquad (14.5a)$$

where

$$\Delta N_i \;\approx\; \left[\frac{d\, rF_i}{d\, T}\right]_{T_\circ} \cdot\; \Delta T \qquad (14.5b)$$

approximation ΔN_i of the temperature–dependent shift of the bridge output with index i is given by the right–hand side of Eq. (14.5b). The first derivative $dr F_i / dT$ must be obtained experimentally in the neighborhood of the reference temperature $T_\circ$ by recording the output of each bridge at different temperatures while keeping all balance loads near zero. For example, let us assume that only one additional temperature T_ξ is used to characterize the shift. Then, the following approximation is valid:

Temperature–dependent Output Change at Zero Load

$$F_1,\, \ldots,\, F_n \;\approx\; 0 \quad\Longrightarrow\quad \left[\frac{d\, rF_i}{d\, T}\right]_{T_\circ} \approx\; \frac{rF_i(T_\xi) \;-\; rF_i(T_\circ)}{T_\xi \;-\; T_\circ} \qquad (14.6)$$

It is important to mention that the correction of the natural zero, i.e., Eq. (14.5b) above, is a linear approximation of the output shift. It is only valid in the neighborhood of the reference temperature of the balance. Therefore, other correction approaches must be applied if the observed temperature change exceeds the empirical limit of 25 to 30 $Kelvin$.

14.2.3 Wind–Off Home Position

It is also possible to determine the shift of the natural zero of a bridge directly during a wind tunnel test. Then, the use of Eq. (14.5b) above can be avoided. An analyst only needs to frequently record the temperature–dependent change of the balance bridge outputs when the wind tunnel model is in its wind–off home position. Then, the output correction is given by the following relationship:

Temperature–dependent Bridge Output Change in Wind Tunnel Model's Wind–off Home Position

$$F_1,\, \ldots,\, F_n \;\approx\; 0 \quad\Longrightarrow\quad \Delta N_i \;\approx\; \underbrace{rF_i(T)}_{wind-off} \;-\; \underbrace{rF_i(T_\circ)}_{wind-off} \qquad (14.7)$$

Balance loads are a relatively small percentage of the load capacity of the balance when a wind tunnel model is in the wind–off home position. Therefore, the observed temperature–dependent shift of the outputs must be close to the expected temperature–dependent shift of the natural zeros even though the balance loads are not perfectly zero in that situation. – Correction methods for the temperature–dependent bridge sensitivity shift are discussed in the next section of the appendix.

14.3 Bridge Sensitivity Shift

14.3.1 General Remarks

The development of a correction for the temperature–dependent shift of the sensitivity of a bridge is complicated by the fact that both balance temperature and primary load of the bridge need to change during a calibration in order to quantify the shift. In addition, the bridge sensitivity value itself is hidden among the regression coefficients of the balance calibration data. This statement needs more explanation. Let us assume, for example, that the calibration data set of a balance is given in the design format of the balance (e.g., a force balance data set is described in force balance format). Now, an analyst decides to use the *Non–Iterative Method* for the balance load prediction (see App. 9). Then, the inverse of the sensitivity equals the coefficient $a_{i,i}$ of the primary bridge output difference D_i in the regression model of the primary load component F_i. Alternatively, an analyst may decide to use the *Iterative Method* for the balance load prediction (see App. 10). In that case, the sensitivity equals the coefficient $b_{i,i}$ of the primary load component F_i in the regression model of the primary bridge output difference D_i.

It is critical for the development of a correction for the temperature–dependent bridge sensitivity shift that the balance data set is given in the design format of the balance. Otherwise, balance calibration and the development of the correction approach for the sensitivity shift are complicated by the fact that the regression model of either a load (*Non–Iterative Method*) or a bridge output difference (*Iterative Method*) will need more than one temperature–dependent regression coefficient to quantify the shift. This important observation can be summarized as follows:

Balance Data Format Recommendation

Temperature–dependent balance calibration data should be given in the design format of the balance (e.g., force balance data should be described in force balance format, or, direct–read balance data should be described in direct–read format). Then, the development of a correction for the temperature–dependent shift of the bridge sensitivities is greatly simplified as the regression model of either a load component (Non–Iterative Method) or a bridge output difference (Iterative Method) will only need a single temperature–dependent regression coefficient to describe the shift.

An analyst has different options to develop a correction for an unwanted temperature–dependent shift of the bridge sensitivity. For example, a correction can be defined after (i) making the sensitivity itself a function of temperature and (ii) relating it to the uncorrected balance forces. Alternatively, temperature effects can directly be included in the regression models of the calibration data that are used for the balance load prediction. In

that case, new regression model terms are added to the regression model of the balance calibration data that quantify the temperature–dependent bridge sensitivity shift.

Each option has advantages and disadvantages. The first option is simple to apply. However, it has the disadvantage that it processes calibration data recorded at a constant temperature separately from calibration data that describes balance temperature effects. The second option, on the other hand, generates regression models for the load prediction from a single temperature–dependent balance calibration data set.

A variety of correction approaches for the *Non–Iterative Method* and the *Iterative Method* exist that are discussed in detail in the next four sections.

14.3.2 Temperature–dependent Load Correction

A direct load correction for the temperature–dependent shift of the bridge sensitivity can be developed that is applicable if either the *Non–Iterative Method* or the *Iterative Method* are used for the load prediction. The derivation of this correction can best be understood if it is developed from the viewpoint of the *Non–Iterative Method*. This approach directly fits tare corrected balance loads as a function of bridge output differences that are computed relative to the natural zeros of the bridges (for more details see App. 9). The regression model is typically obtained from a calibration data set that was recorded at a constant reference temperature $T_\circ$. The resulting regression model of a balance load is defined in Eq. (14.8) below where F_i is the balance load component, D_i is the output

Regression Model of Load Component

(inverse of the bridge sensitivity = constant coefficient)

$$F_i(T_\circ) \;=\; \underbrace{a_{i,0} \;+\; \ldots \;+\; a_{i,i}(T_\circ) \cdot D_i \;+\; \ldots}_{\textit{see also App. 9, Eq. (9.2a)}} \qquad (14.8)$$

difference of the related bridge, and $a_{i,i}$ is the inverse of the bridge sensitivity. The regression model above is, strictly speaking, only applicable if the balance temperature during the wind tunnel test matches the reference temperature $T_\circ$. Most regression coefficients in Eq. (14.8) can be considered constants as long as the temperature changes of the balance do not exceed the empirical limit of 30 $Kelvin$. The only exception is the coefficient $a_{i,i}$ that is associated with the inverse of the bridge sensitivity. It is the first derivative of a load F_i with respect to the output of the related primary balance bridge. This output is described as either the raw output rF_i or the output difference D_i of the bridge because the two output values only differ by a constant, i.e., the natural zero of the bridge. These conclusions can be summarized by the following equation:

Inverse of the Bridge Sensitivity

$$a_{i,i} \;=\; \frac{d\,F_i}{d\,D_i} \;=\; \frac{d\,F_i}{d\,rF_i} \;\equiv\; \frac{\textit{change of primary bridge load}}{\textit{change of primary bridge output}} \qquad (14.9)$$

A numerical estimate of the coefficient $a_{i,i}$, i.e., of the inverse of the bridge sensitivity is obtained during the regression analysis of the balance calibration that was recorded at a constant temperature. The coefficient is treated as a constant during the regression analysis. However, it is known that the bridge sensitivity and its inverse change whenever a temperature change occurs. Therefore, the coefficient $a_{i,i}$ can be interpreted as a temperature–dependent regression coefficient $a_{i,i}(T)$.

The impact of the sensitivity change on the balance load prediction must be considered if the regression model obtained from data at the reference temperature is used for the load prediction during the wind tunnel test. The sensitivity change is associated with an additional physical load. This load must be added to the load that is predicted from the regression model given in Eq. (14.7) above. Fortunately, it is possible to obtain an equation of the load correction for each load component if the temperature–dependent nature of the regression coefficient $a_{i,i}(T)$ is approximated by using a first order Taylor series. Then, assuming that the Taylor series is developed near the reference temperature $T_\circ$ of the balance, we get the following approximation of the temperature–dependent coefficient:

$$\textit{first order Taylor series} \implies a_{i,i}(T) \approx a_{i,i}(T_\circ) + \left[\frac{d\,a_{i,i}}{d\,T}\right]_{T_\circ} \cdot \Delta T \tag{14.10}$$

Now, the coefficient $a_{i,i}(T_\circ)$ in Eq. (14.8) must be replaced by the temperature–dependent coefficient $a_{i,i}(T)$ so that the temperature–dependent nature of the sensitivity is included during the load prediction. Then, Eq. (14.8) can be expressed as follows:

$$\begin{aligned} F_i(T) &= a_{i,0} + \ldots + \left\{ a_{i,i}(T) \right\} \cdot D_i + \ldots \\ &= a_{i,0} + \ldots + \left\{ a_{i,i}(T_\circ) + \left[\frac{d\,a_{i,i}}{d\,T}\right]_{T_\circ} \cdot \Delta T \right\} \cdot D_i + \ldots \\ &= \underbrace{\left\{ a_{i,0} + \ldots + a_{i,i}(T_\circ) \cdot D_i + \ldots \right\}}_{F_i(T_\circ)} + \underbrace{\left\{ \left[\frac{d\,a_{i,i}}{d\,T}\right]_{T_\circ} \cdot \Delta T \cdot D_i \right\}}_{\Delta F_i} \end{aligned} \tag{14.11}$$

It is assumed that the output difference D_i was corrected for any temperature–dependent natural zero shift using one of the methods that were described earlier. Therefore, output difference D_i is no longer a function of temperature. The right–hand side of Eq. (14.11) can be examined in more detail. The terms between the first pair of curly brackets equal the load $F_i(T_\circ)$ that the original regression model predicts if the *Non–Iterative Method* is applied (see Eq. (14.8)). These terms can also be interpreted as the load $F_i(T_\circ)$ that the *Iterative Method* would predict. This statement is true as long as the load iteration equation was obtained from the same calibration data set that was processed using the *Non–Iterative Method*. The terms between the second pair of curly brackets describe the load correction ΔF_i that is caused by the sensitivity shift. Then, we get:

Balance Load Prediction after Bridge Sensitivity Shift

$$F_i(T) \;=\; F_i(T_\circ) \;+\; \Delta F_i \qquad (14.12a)$$

where

$$F_i(T_\circ) \;\equiv\; \begin{Bmatrix} load\ obtained\ from\ regression\ model\ using \\ either\ Non-Iterative\ or\ Iterative\ Method \end{Bmatrix} \qquad (14.12b)$$

$$\Delta F_i \;\equiv\; \begin{Bmatrix} temperature-dependent \\ balance\ \ load\ \ correction \end{Bmatrix} \;=\; \left[\frac{d\,a_{i,i}}{d\,T}\right]_{T_\circ} \cdot\; \Delta T \cdot D_i \qquad (14.12c)$$

$$\left[\frac{d\,a_{i,i}}{d\,T}\right]_{T_\circ} \;=\; \left[\frac{d}{d\,T}\;\left(\frac{d\,F_i}{d\,rF_i}\right)\right]_{T_\circ} \qquad (14.12d)$$

Several important observations can be made after examining the equations above. First, the bridge sensitivity shift can be related to a load correction ΔF_i for each load component. It depends on (i) the temperature–dependent change of the inverse of the sensitivity of the primary bridge of the load, (ii) the temperature change, and (iii) the bridge output difference of the bridge. In addition, the equation for ΔF_i is independent of the method that is used for the load prediction. In other words, it can be applied if either the *Non–Iterative Method* or the *Iterative Method* is used for the balance load prediction as long as the change of the inverse of the bridge sensitivity is known. This change can be computed by using, for example, Eq. (14.13) below if it is assumed that (i) single–component loads

Change of the Inverse of the Bridge Sensitivity

$$\left[\frac{d\,a_{i,i}}{d\,T}\right]_{T_\circ} \;\approx\; \frac{\left[\dfrac{dF_i}{drF_i}\right]_{T_\xi} \;-\; \left[\dfrac{dF_i}{drF_i}\right]_{T_\circ}}{T_\xi \;-\; T_\circ} \qquad (14.13)$$

are applied at two different temperatures $T_\circ$ and T_ξ, (ii) the slope dF_i/drF_i is determined separately for each of the two temperatures, and (iii) the temperature–dependent change of the bi–directional characteristics of the bridge is negligible.

14.3.3 Extended Regression Model of a Load Component

It is also possible to develop a correction for the sensitivity shift after combining the original calibration data recorded at reference temperature $T_\circ$ with the additional single–component loads recorded at temperature T_ξ in a single temperature–dependent calibration data set. Then, a temperature–dependent regression model can directly be used to analyze

this data set if the cross–product term $D_i \cdot \Delta T$ is included in the regression model of the load that the *Non–Iterative Method* uses. The new term originates from the product of the Taylor series approximation of coefficient $a_{i,i}(T)$ with the bridge output difference D_i (see Eq. (14.11)). It describes the sensitivity shift of the primary bridge output of the load component. It is also suggested to include the term ΔT in the expanded regression model. Then, the temperature–dependent regression model will be hierarchical, i.e., the regression model will not have any missing lower order terms. Its coefficient will be close to zero if bridge output differences are already corrected for the temperature–dependent natural zero shift. In summary, the temperature–dependent regression model of a balance load component can be defined as follows:

Temperature–dependent Regression Model of Load Component

$$F_i \;=\; \ldots + a_{i,i} \cdot D_i + \ldots + a_{i,n+1} \cdot \Delta T + \ldots + a_{i,\mu} \cdot D_i \cdot \Delta T + \ldots \qquad (14.14)$$

The regression coefficients are obtained after applying a global regression analysis to the temperature–dependent balance calibration data set. Corresponding equations of App. 9 can directly be applied if the temperature difference ΔT is simply treated like another independent variable of the fit. Typical temperature–dependent global regression analysis results for fitted balance load components are discussed in detail in Ref. [38].

Correction approaches for the temperature–dependent bridge sensitivity shift are discussed in the next two sections that take the regression models and load prediction equations of the *Iterative Method* into account.

14.3.4 Temperature–dependent Load Iteration Equations

Key elements of the *Iterative Method* need to be reviewed so that a correction for the temperature–dependent shift of the bridge sensitivity can be developed. The *Iterative Method* processes balance calibration data by first fitting output differences of a bridge as a function of the tare corrected loads. Afterwards, a load iteration equation is constructed from the regression coefficients of the outputs so that loads can be predicted from outputs during a wind tunnel test (see App. 10 for more details). The regression model of an output difference is typically obtained from a data set that was recorded at a constant reference temperature $T_\circ$. The model is defined in Eq. (14.15) below where D_i is the output

Regression Model of Bridge Output Difference
(primary bridge sensitivity = constant coefficient value)

$$D_i \;=\; \underbrace{b_{i,0} \;+\; \ldots \;+\; b_{i,i}(T_\circ) \;\cdot\; F_i \;+\; \ldots}_{\textit{see also App. 10, Eq. (10.35)}} \qquad (14.15)$$

difference, F_i is the primary load of the bridge, and $b_{i,i}$ is the bridge sensitivity. The regression model above is, strictly speaking, only applicable if the balance temperature during the wind tunnel test matches the reference temperature $T_\circ$. Most regression coefficients in Eq. (14.15) above can be considered constants as long as the temperature changes of the balance do not exceed the empirical limit of 30 *Kelvin*. The only exception is the coefficient $b_{i,i}$ that is associated with the bridge sensitivity. It is the first derivative of an output difference D_i or raw output rF_i with respect to the primary load of the bridge. Either the output difference D_i or the raw output rF_i of the bridge can be used to define the bridge sensitivity because the two values only differ by a constant, i.e., the natural zero of the bridge. These conclusions can be summarized by the following equation:

Bridge Sensitivity

$$b_{i,i} \;=\; \frac{\partial\, D_i}{\partial\, F_i} \;=\; \frac{\partial\, rF_i}{\partial\, F_i} \;\equiv\; \frac{\textit{change of primary bridge output}}{\textit{change of primary bridge load}} \qquad (14.16)$$

Coefficient $b_{i,i}$ in Eq. (14.16) above, i.e., the bridge sensitivity, is obtained during the regression analysis of the balance calibration data set that was recorded at constant temperature. It is treated as a constant during the regression analysis. However, it is known that the bridge sensitivity changes whenever a temperature change occurs. Therefore, coefficient $b_{i,i}$ can be interpreted as a temperature–dependent coefficient $b_{i,i}(T)$. Then, the regression model of an output difference can be described by the following equation:

Regression Model of Bridge Output Difference
(primary bridge sensitivity = function of the balance temperature)

$$D_i \;=\; b_{i,0} \;+\; \ldots \;+\; b_{i,i}(T) \cdot F_i \;+\; \ldots \qquad (14.17)$$

The relationship describing the temperature–dependent value of the coefficient $b_{i,i}(T)$ can be found experimentally if single–component loads of all load components are applied to the balance at two or more temperatures. Afterwards, the temperature–dependent load values of the balance can be found by updating all parts of the load iteration equation that depend on the bridge sensitivities (i.e., on the coefficients $b_{1,1},\ b_{2,2},\ \ldots,\ b_{n,n}$).

Two types of load iteration equations are traditionally used in the aerospace testing community if the *Iterative Method* is used for the balance load prediction during a wind tunnel test. For example, it is known that the square matrix $\mathbf{C_1}^{-1}$ of the *Primary Load Iteration Equation* depends on the bridge sensitivities (see App. 10, Eq. (10.27a)). Therefore, two parts of the iteration equation, i.e., square matrix $\mathbf{C_1}^{-1}$ and rectangular matrix $\mathbf{C_1}^{-1}\mathbf{C_2}$, need to be updated each time the balance temperature changes so that bridge sensitivity shifts are included in the predicted loads. This result is summarized by the two relationships that are given in Eqs. (14.18a) and (14.18b) below.

Primary Load Iteration Equation

$$\mathbf{F}_{\xi}(T) \;=\; \left[\, \mathbf{C_1}^{-1}(T) \,\right] \cdot \mathbf{\Delta rF} \;-\; \left[\, \mathbf{C_1}^{-1}(T) \,\cdot\, \mathbf{C_2} \,\right] \,\cdot\, \mathbf{H}(\mathbf{F}_{\xi-\mathbf{1}}) \qquad (14.18a)$$

... where $\mathbf{C_1}^{-1}(T)$ *is the updated inverse of matrix ...*

$$\mathbf{C_1}(T) \;=\; \mathbf{C_1}\Big\{\, b_{1,1}(T),\; b_{2,2}(T),\; \ldots\;,\; b_{n,n}(T) \Big\} \qquad (14.18b)$$

Similarly, the square matrix $\mathbf{B_1}^{-1}$ of the *Alternate Load Iteration Equation* depends on the bridge sensitivities (see App. 10, Eq. (10.31a)). Therefore, three parts of the iteration equation, i.e., square matrix $\mathbf{B_1}^{-1}$, square matrix $\mathbf{B_1}^{-1}\mathbf{B_2}$, and rectangular matrix $\mathbf{B_1}^{-1}\mathbf{C_2}$, need to be updated each time the balance temperature changes so that bridge sensitivity shifts are included in the predicted loads. This result is summarized by the two relationships that are given in Eqs. (14.19a) and (14.19b) below.

Alternate Load Iteration Equation

$$\begin{aligned} \mathbf{F}_{\xi}(T) \;=\; & \left[\, \mathbf{B_1}^{-1}(T) \,\right] \cdot \mathbf{\Delta rF} \;-\; \left[\, \mathbf{B_1}^{-1}(T) \,\cdot\, \mathbf{B_2} \,\right] \,\cdot\, \mathbf{F}_{\xi-\mathbf{1}} \\ & -\; \left[\, \mathbf{B_1}^{-1}(T) \,\cdot\, \mathbf{C_2} \,\right] \,\cdot\, \mathbf{H}(\mathbf{F}_{\xi-\mathbf{1}}) \end{aligned} \qquad (14.19a)$$

... where $\mathbf{B_1}^{-1}(T)$ *is the updated inverse of matrix ...*

$$\mathbf{B_1}(T) \;=\; \mathbf{B_1}\Big\{\, b_{1,1}(T),\; b_{2,2}(T),\; \ldots\;,\; b_{n,n}(T) \Big\} \qquad (14.19b)$$

The explicit update of the load iteration equation is just one way of including the temperature–dependent nature of the bridge sensitivity in the balance load prediction. It is also possible to define temperature–dependent regression models of the bridge output differences and develop the corresponding load iteration equation from the fits of the outputs. This alternate approach is discussed in the next section of the appendix.

14.3.5 Extended Regression Model of Bridge Output Difference

Bridge sensitivity shifts can also be included in the iterative balance load prediction by defining a temperature–dependent regression model of the bridge output differences and using results of the fits of a temperature–dependent balance calibration data set for the definition of a load iteration equation. Again, temperature–dependent regression model terms can be obtained from a first order Taylor series approximation of the temperature–dependent coefficients $b_{1,1}(T),\; b_{2,2}(T),\; \ldots\;,\; b_{n,n}(T)$ that are used in Eq. (14.17). Then, assuming that the Taylor series is developed near the reference temperature $T_{\circ}$ of the balance, we get the following approximation of the temperature–dependent sensitivity:

$$first\ order\ Taylor\ series \implies b_{i,i}(T) \approx b_{i,i}(T_\circ) + \left[\frac{d\ b_{i,i}}{d\ T}\right]_{T_\circ} \cdot \Delta T \qquad (14.20)$$

Now, the coefficient $b_{i,i}(T)$ in Eq. (14.17) above must be replaced by the temperature–dependent coefficient $b_{i,i}(T)$ so that the temperature–dependent nature of the sensitivity is included in the regression model. Then, Eq. (14.17) can be expressed as follows:

$$\begin{aligned} D_i &= b_{i,0} + \ldots + \left\{ b_{i,i}(T) \right\} \cdot F_i + \ldots \\ &= b_{i,0} + \ldots + \left\{ b_{i,i}(T_\circ) + \left[\frac{d\ b_{i,i}}{d\ T}\right]_{T_\circ} \cdot \Delta T \right\} \cdot F_i + \ldots \\ &= b_{i,0} + \ldots + b_{i,i}(T_\circ) \cdot F_i + \underbrace{\left[\frac{d\ b_{i,i}}{d\ T}\right]_{T_\circ}}_{new\ coefficient} \cdot \underbrace{F_i \cdot \Delta T}_{new\ term} + \ldots \end{aligned} \qquad (14.21)$$

It is concluded from Eq. (14.21) above that the cross–product term $F_i \cdot \Delta T$ must be added to the regression model of each output difference in order to describe the temperature–dependent bridge sensitivity shift. In addition, similar to the temperature–dependent regression model of a load component, it is suggested to include the term ΔT itself in the expanded regression model of an output difference even though its coefficient will be close to zero if bridge output differences are already corrected for the temperature–dependent natural zero shift. Then, the temperature–dependent regression model will be hierarchical, i.e., the regression model will not have any missing lower order terms. In summary, the temperature–dependent regression model of a bridge output difference can be defined as follows:

Temperature–dependent Regression Model of Bridge Output Difference

$$D_i = \ldots + b_{i,i} \cdot F_i + \ldots + b_{i,n+1} \cdot \Delta T + \ldots + b_{i,\mu} \cdot F_i \cdot \Delta T + \ldots \qquad (14.22)$$

The regression coefficients are obtained after applying global regression analysis to the temperature–dependent balance calibration data set. Corresponding equations of App. 10 can directly be applied if the temperature difference ΔT is simply treated like another independent variable of the fit. Typical temperature–dependent global regression analysis results for fitted bridge outputs and resulting load predictions are discussed in great detail in Ref. [38]. It must be mentioned that the definition of the load iteration equation must be done carefully if the temperature is used as an independent variable for the load prediction. In that case, the temperature has to be introduced as both an independent and dependent variable so that a load iteration equation can be defined. This topic is discussed in more detail in App. 21 of the current document.

Important recommendations related to calibration and analysis of a temperature–dependent balance data set are summarized in the next section.

14.3.6 Calibration and Analysis Recommendations

The use of the previously discussed correction methods requires that a temperature–dependent balance calibration data set is obtained such that changes of the balance characteristics can be quantified and, if applicable, coefficients of the most important regression model terms can be computed with confidence. Therefore, the author recommends to perform the calibration by using the following steps.

Step 1: Calibration data sets should be collected at a minimum of three different temperatures. The data set at one of the temperatures, i.e., at the chosen reference temperature, should be obtained by applying all desired load and load combinations that are needed to describe the behavior of the balance. The data sets at the remaining temperatures, on the other hand, only need to be obtained by applying single–component loads. This simplification of the calibration load schedule can be justified by the fact that the suggested regression model of either a load component or a bridge output difference can only support the second order cross–product term $D_i \cdot \Delta T$ or $F_i \cdot \Delta T$ (no temperature–dependent third order cross–product terms are used).

Step 2: The natural zeros, i.e., the bridge outputs at zero absolute load, should be determined separately for each one of the chosen temperatures. The natural zeros are needed in order to obtain the tare corrected loads of the balance calibration data.

Step 3: The tare load iteration should be done for each one of the three temperature–dependent data sets separately by using the natural zeros of the given temperature as output datum. The result of this analysis step are the tare corrected loads of all three temperature–dependent calibration data sets.

Step 4: The final temperature–dependent balance calibration data input file should be assembled by combining the tare corrected load sets of Step 3 with bridge output differences that are computed relative to the natural zero of the chosen global reference temperature if the term ΔT is included in the regression models. Then, the temperature–dependent shift of the natural zero is quantified by the coefficient of the term ΔT. Alternatively, bridge output differences should be computed relative to the natural zero of the applicable balance temperature of the output set if the term ΔT is omitted and a separate correction process is used to account for the natural zero shift during the wind tunnel test.

Step 5: The regression analysis of the tare corrected calibration data should be performed by using the chosen analysis method. Regression model term reduction should be applied as needed.

14.4 Summary and Recommendations

Different methods were discussed that may be used to correct for the influence of temperature–dependent natural zero shifts and bridge sensitivity shifts during the prediction of balance loads. Two approaches were described that address the natural zero shift. Five approaches were presented that address the temperature–dependent bridge sensitivity shift. Table 14–1 below summarizes the application of the different correction approaches. Each correction approach has advantages and disadvantages.

Correction methods A and B address the natural zero shift that may occur if the balance experiences a temperature change. Both methods can be used with either the *Non–Iterative Method* or the *Iterative Method*. The author believes that correction method B

has an advantage over correction method A. It is the recommended approach because it can directly be applied during an ongoing wind tunnel test.

Table 14–1: Corrections Methods for Balance Temperature Effects.

Correction Method	Balance Temperature Effect	Correction Equation	*Non–Iterative Method*	*Iterative Method*
A	natural zero shift	(14.5*b*)	×	×
B†	natural zero shift	(14.7)	×	×
1†	sensitivity shift	(14.12*c*)	×	×
2	sensitivity shift	(14.14)	×	
3	sensitivity shift	(14.18*a*)		×
4	sensitivity shift	(14.19*a*)		×
5	sensitivity shift	(14.22)‡		×

†recommended correction approach ‡load iteration equation is described in App. 21

Correction methods 1 to 5 address the unwanted sensitivity shift that may occur if the balance experiences a temperature change. Method 1 defines a direct load correction for each balance load component. Method 2 uses an extended regression model of the load components in order to include the sensitivity shift in the load prediction. Methods 3 and 4 simply modify the load iteration equation if a bridge sensitivity shift occurs. Finally, Method 5 uses an extended regression model of the bridge output difference in order to include the sensitivity shift in the load prediction. The associated load iteration equation can only be constructed if the temperature is used as both an independent and dependent variable (see also discussion in App. 21). Method 1 is the recommended approach. It is simple to apply and also independent of the load prediction method.

It is important to point out that the total number of required temperature–dependent cross–product terms in a regression model of balance calibration data depends on the chosen load and output format of the balance. The author recommends to always describe balance loads and outputs in the design format of the balance (e.g., force balance data should be described in force balance format). Then, the number of required temperature–dependent regression model terms is at a minimum. Consequently, only a single cross–product term of the type $D_i \cdot \Delta T$ is needed in the regression model of a load component in order to describe the sensitivity shift if the *Non–Iterative Method* is applied (see correction method 2, Eq. (14.14)). Similarly, only a single cross–product term of the type $F_i \cdot \Delta T$ is needed in the regression model of a bridge output difference in order to describe the bridge sensitivity shift if the *Iterative Method* is applied (see correction method 5, Eq. (14.22)).

Appendix 15

Basics of Three–Component Moment Balances

15.1 Introduction

Three–component moment balances are used to measure aerodynamic loads on a subassembly that is attached to the fuselage or wing of a wind tunnel model. The subassembly could be, for example, a control surface, a fin, or a canard. A three–component moment balance can also be described as a gaged model part that allows for the measurement of loads that act at or near its attachment point to the wind tunnel model.

A wind tunnel customer is often interested in knowing the normal force, the bending moment, and the torsion moment that acts on the three–component moment balance so that the material stress acting on the model's subassembly can be monitored. These loads are indirectly measured by using electrical outputs of two bending moment bridges and a torsion moment bridge that are attached to the balance surface.

Fundamental differences between a three–component moment balance and a six–component primary balance exist that must be taken into consideration during design, calibration, and use of the balance. First, the metric part of a three–component moment balance is flexible. It goes from the outer edge of the balance to the first bending moment bridge, i.e., to the bridge that is closest to the outer edge of the balance. This definition of the metric part results from the fact that the output of the first bending moment bridge would remain constant and become unusable if (i) a hypothetical load is applied between its location and the balance moment center and (ii) no temporary load fixture is attached to the balance that allows for the application of loads between the first bending moment bridge and the model attachment point.

The non–metric part of a three–component moment balance, on the other hand, consists of (i) a flexible section with the bridges and (ii) a rigid section that is used to attach the balance to the wind tunnel model. The author recommends to use the rigid section of the non–metric part of the balance for the definition of the balance axis system. Then, loads are described in a coordinate system that can easily be related to the body axis system of the wind tunnel model. This choice also allows for a precise description of the calibration loads as only the orientation of the rigid section of the non–metric part relative to the gravitational acceleration must be quantified whenever dead weights are used for the load application. Table 15–1 below summarizes key differences between a three–component moment balance and a six–component primary balance.

Table 15–1: Differences between three– and six–component balances.

	Three–Component Moment Balance	Six–Component Primary Balance
Model Attachment	rigid section of the non–metric part attaches to the wind tunnel model	metric part attaches to the wind tunnel model
Elastic Characteristics of the Metric Part	flexible, i.e., elastically deforms when balance loads act	rigid, i.e., does not deform when balance loads act
Definition of the Balance Axis System	orientation of the rigid section of the non–metric part defines axis system	orientation of the metric part in space defines axis system

Dead weights are typically used in a calibration laboratory for the application of loads to a three–component moment balance. This approach limits the type of loads that can be applied unless a temporary fixture is attached to the metric part that makes it possible to apply loads between the first bending moment bridge and the balance moment center.

Figure 15–1 below shows a situation that may be observed during the application of a load to a three–component moment balance. The load is represented by a force that is parallel to the gravitational acceleration and perpendicular to the x–y plane of the balance. In addition, the y–axis is assumed to be the neutral axis for the definition of the torsion moment. Its location equals the halfchord line of the balance whenever all chordwise cross–sections of the balance and the model attachment are symmetric about the y–z plane. In all other cases, the location of the neutral axis must be determined experimentally. Then, three independent calibration variables, i.e., the applied force (F), the bending moment arm (a), and the torsion moment arm (b), can be varied during calibration. These variables are indirectly connected to the three loads, i.e., the normal force, the bending moment, and the torsion moment, that the balance experiences.

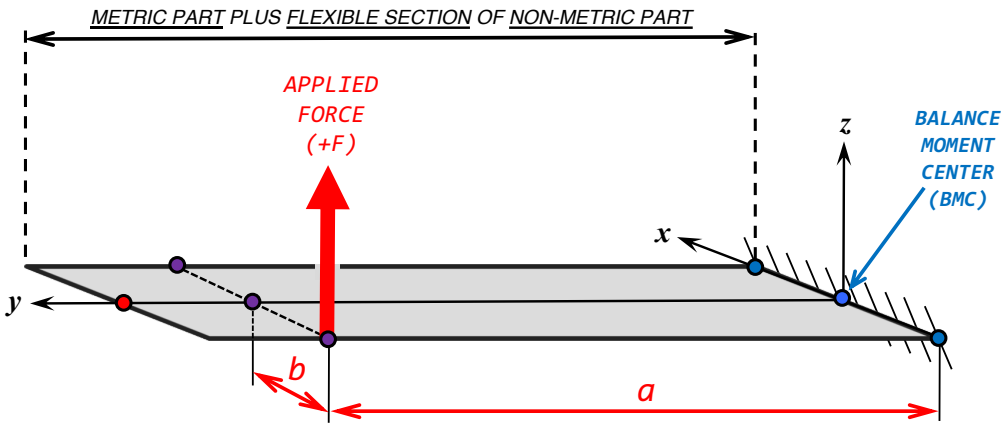

Fig. 15–1 Application of loads to a three–component moment balance; loads are described by the applied force, the bending moment arm, and the torsion moment arm.

Design, calibration data quality, and load prediction accuracy of three–component balances can vary substantially in a real–world test environment. These observations are not a surprise because three–component balances are highly customized and one–of–a–kind type sensors. Nevertheless, improvements to design, calibration, and use of three–component moment balances are possible that reduce load prediction errors and make it easier to apply them during a wind tunnel test.

A more detailed discussion of basic characteristics of a three–component moment balance is given in the next section. This discussion focuses primarily on the normal force and the bending moment. This choice was made because the prediction of these two load components is more complex than the prediction of the torsion moment.

15.2 Balance Characteristics

15.2.1 Load State Descriptions

An analyst has different variable choices in order to uniquely describe the load state of a three–component moment balance. For simplicity, it was decided to only focus on the

normal force and bending moment characteristics as the load prediction accuracy of this load pair is interrelated. Therefore, the torsion moment arm and, consequently, the torsion moment itself is assumed to be zero. Then, the load state of the balance can be described by using (i) the applied force and (ii) the bending moment arm. This situation is illustrated in Fig. 15–2a below. It describes the load state of the balance from the viewpoint of the technician who applies the loads. The balance moment center (BMC) was deliberately placed at the junction between flexible and rigid sections of the non–metric part of the balance. This choice makes the orientation of the three axes of the balance axis system in space independent of the deformation that the balance experiences under load.

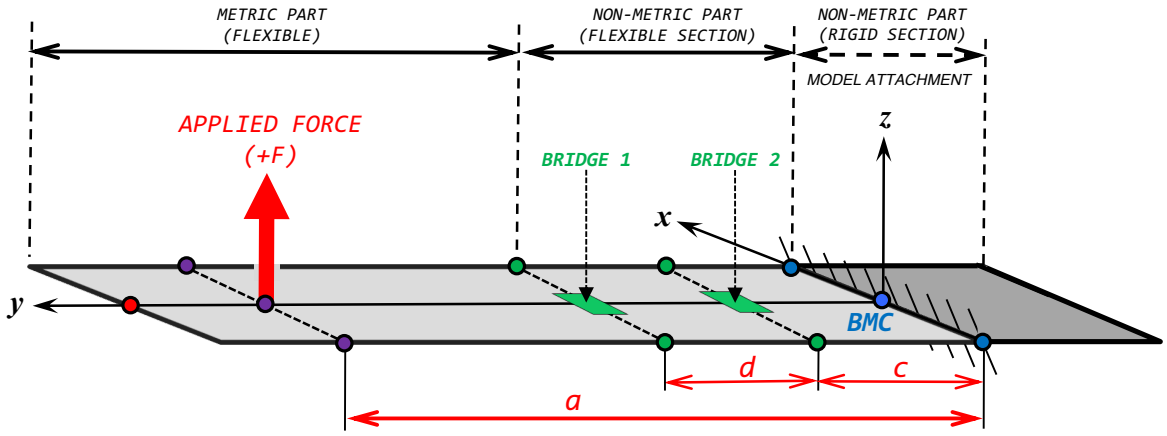

Fig. 15–2a Description of the load state of a three–component moment balance by using the applied force (F) and the bending moment arm (a).

Typical users of a three–component moment balance need a different variable set for the description of the load state of the balance. They prefer to express loads in direct–read format by using the normal force and the bending moment as independent variables. This alternate description of the load state is illustrated in Fig. 15–2b below.

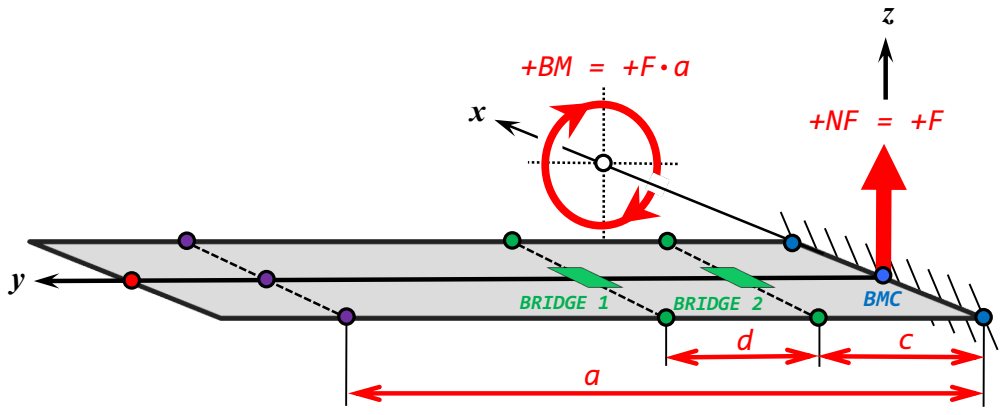

Fig. 15–2b Alternate description of the load state by using the normal force (NF) and the bending moment (BM) at the balance moment center.

A connection between the equivalent load state descriptions depicted in Fig. 15–2a and Fig. 15–2b exists that can be expressed by using the following equations:

$$NF = F \tag{15.1a}$$

$$BM = F \cdot a \tag{15.1b}$$

For completeness, the torsion moment must be included in the description even though it is not explicitly discussed in this section. It is defined as the product between the applied force (F) and, the torsion moment arm (b). Then, using the nomenclature defined in Fig. 15–1, we get the following relationship:

$$TM = F \cdot b \tag{15.1c}$$

Balance data analysts often prefer to describe the load state of a moment balance in moment balance format. Then, the first and second bending moment are used instead of the normal force and the bending moment for the description of two of the three load components. This approach has the advantage that (i) the sensitivities of all bridges can be defined and (ii) each load component is more or less proportional to the electrical output of the related bridge. This choice is illustrated in Fig. 15–2c below.

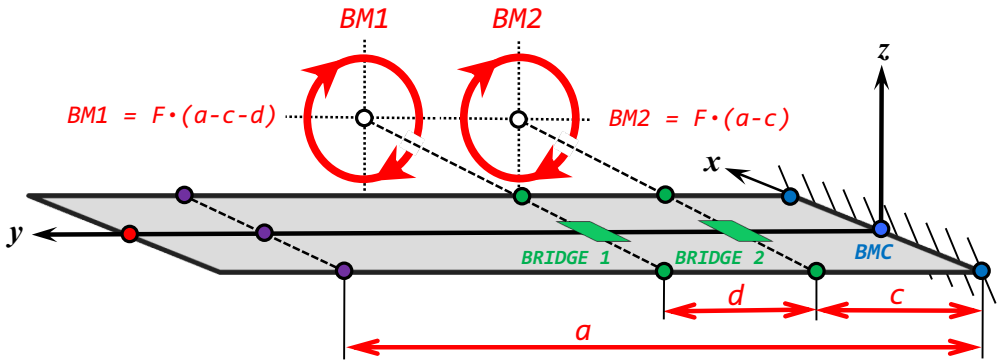

Fig. 15–2c Alternate description of the load state by using the bending moment at bridge 1 ($BM1$) and the bending moment at bridge 2 ($BM2$).

The first and second bending moments can be obtained by multiplying the applied force with the distances to the centers of the first and second bending moment bridges. Then, the two bending moments can be expressed by the following two relationships:

$$BM1 = F \cdot \left[a - c - d \right] \tag{15.2a}$$

$$BM2 = F \cdot \left[a - c \right] \tag{15.2b}$$

The torsion moment is not influenced by the new load format. It is still defined as the product between the applied force (F) and the torsion moment arm (b):

$$TM = F \cdot b \tag{15.2c}$$

Load transformations can easily be derived that relate the normal force and bending moment at the BMC to the bending moments at the two bending moment bridges. It is only required to substitute the applied load (F) and the bending moment arm (a) in Eqs. (15.2a) and (15.2b) by using the relationships $F = NF$ and $a = BM/NF$ that can be obtained from Eqs. (15.1a) and (15.1b). Then, after some algebra, we get transformation equations that relate the load pair NF & BM to the alternate load pair $BM1$ & $BM2$:

$$NF = [\, BM2 - BM1 \,] \,/\, d \tag{15.3a}$$

$$BM = BM2 + [\, BM2 - BM1 \,] \cdot (c/d) \tag{15.3b}$$

Improvements related to the calibration of a three–component moment balance are presented in a later section. These improvements can better be understood if the combined load diagrams of the normal force and the bending moments of the balance are discussed (see App. 5 or Ref. [50] for more details about combined load diagrams). These graphical representations of the balance load envelope are described in the next section.

15.2.2 Combined Load Diagrams

The combined load diagram of a pair of balance loads is a useful graphical aid. It provides a visual description of relationships between calibration loads. Therefore, it was decided to prepare the diagram for the load pairs that are related to the normal force and bending moment measurements of a three–component moment balance. First, the diagram is developed in direct–read format. In that case, the normal force and the bending moment at the balance moment center describe the load state of the balance. Figure 15–3a below depicts a typical load configuration in direct–read format. Loads can

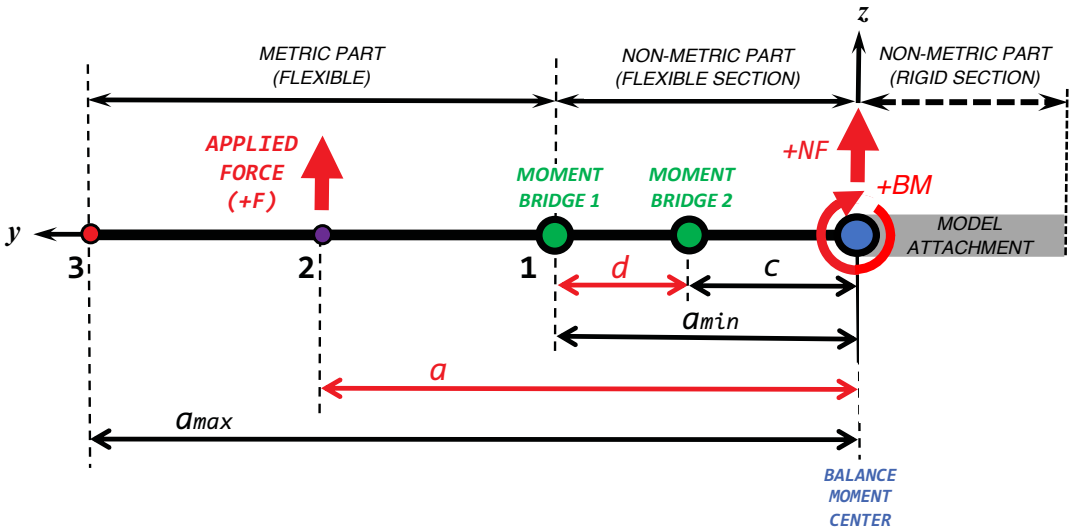

Fig. 15–3a Description of balance loads in direct–read format.

only be applied on the metric part of the balance between the outer edge of the balance and the first bending moment bridge if no temporary load fixtures are attached to the metric part of the balance. Related load points are located in Fig. 15–3a between point 1 and point 3. Then, after analyzing all possible load cases, the combined load diagram for the normal force and bending moment is obtained. It is shown in Fig. 15–3b below.

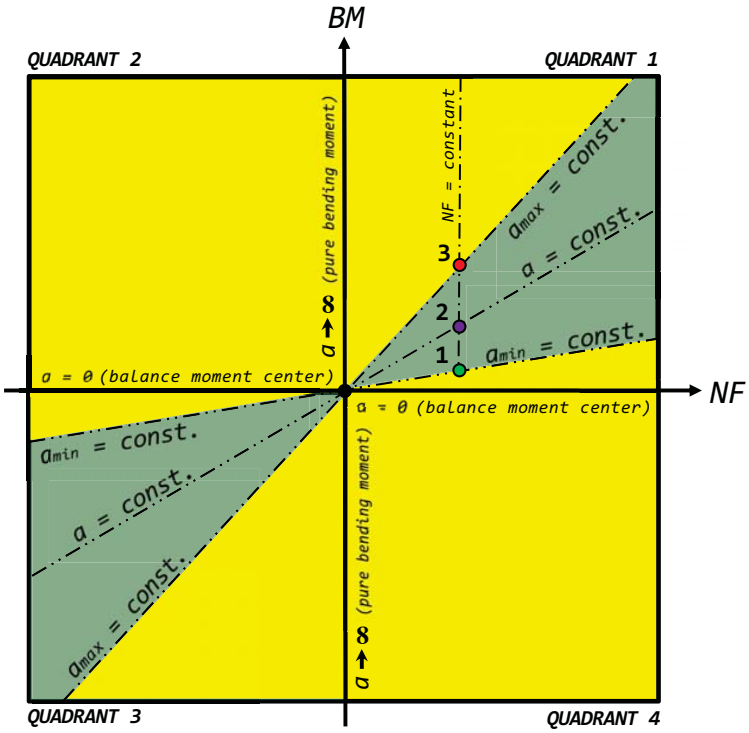

Fig. 15–3b Combined load diagram for loads given in direct–read format.

Loads can only appear in the dark green regions that are shown in Fig. 15–3b above assuming that (i) a single dead weight is applied at the load point and (ii) no fixtures are attached to the balance that allow for the application of loads between the first bending moment bridge and the BMC.

It is also possible to develop the combined load diagram in moment balance format. In that case, the first and second bending moment describe the load state of the balance. Figure 15–4a below shows a typical load configuration in moment balance format. Again,

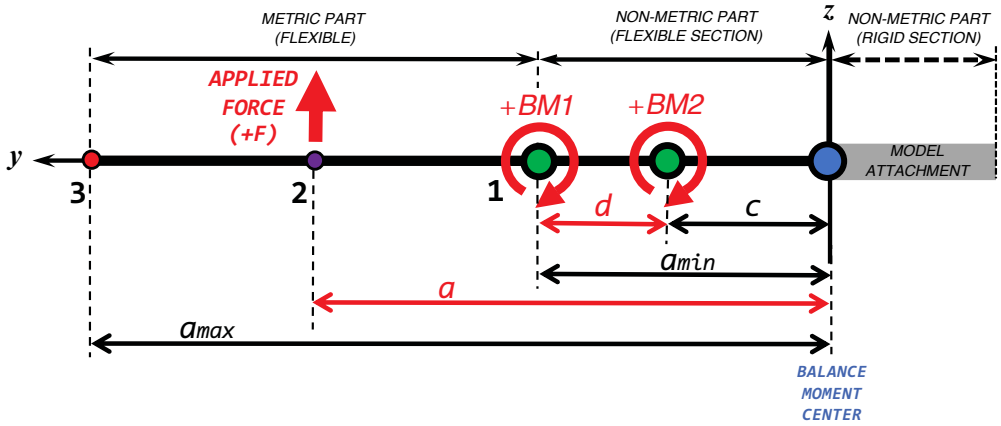

Fig. 15–4a Description of the balance loads in moment balance format.

the diagram is obtained after analyzing all possible load cases while assuming that no temporary fixtures are attached to the metric part of the balance. The resulting diagram for the bending moment pair is shown in Fig. 15–4b. It is assumed that (i) a single dead

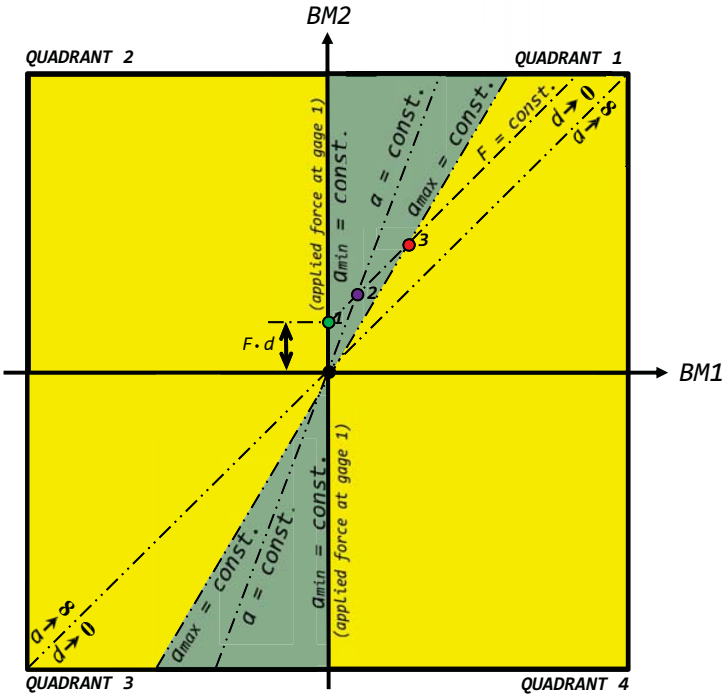

Fig. 15–4b Combined load diagram for loads given in moment balance format.

weight is applied at the load point and (ii) no fixtures are attached to the balance that allow for the application of loads between the first bending moment bridge and the BMC. Then, loads can only appear in the dark green regions that are shown in Fig. 15–4b.

The principal diagonal of the first and third quadrants of the diagram shown in Fig. 15–4b above has an important characteristic: it is the location of load points where the two bending moments are identical. This situation can be achieved by either making the distance between the two bending moment bridges zero or by using a bending moment arm of infinite length. Important consequences of these two conclusions will be discussed in more detail in the next section.

15.3 Design and Calibration Recommendations

15.3.1 Bridge Placement and Sensitivity Selection

It was mentioned in the previous section that the first and second bending moments are identical whenever the distance between the bridges approaches zero. Then, the outputs of the two bending moment bridges are no longer independent. Consequently, the balance would only have two instead of the required three independent electrical output measurements that are needed to predict the normal force, the bending moment, and the torsion moment.

An estimate of the upper bound of the error of the normal force as a function of the errors of the two bending moments can be used to illustrate this issue. A conservative upper bound of the error of the normal force may be obtained by taking the absolute values of both sides of Eq. (15.3a). Then, we get:

$$|\Delta NF| \quad \leq \quad \Big[\; |\Delta BM2| \; + \; |\Delta BM1| \; \Big] \; / \; d \tag{15.4}$$

In addition, it is known that the bridge sensitivity may be used to connect a load component to the related bending moment bridge output if balance loads are given in the design format of the balance. Then, assuming that the electrical outputs rBM_1 and rBM_2 of the two bending moment bridges are described as differences relative to their natural zeros N_1 and N_2, we get the following relationships between the two bending moments $BM1$ and $BM2$ and the two output differences D_1 and D_2 of the bending moment bridges:

$$BM1 \quad \approx \quad \frac{1}{\underbrace{\partial\, D_1 \;/\; \partial\, BM1}_{bridge\ sensitivity}} \;\cdot\; D_1 \tag{15.5a}$$

$$BM2 \quad \approx \quad \frac{1}{\underbrace{\partial\, D_2 \;/\; \partial\, BM2}_{bridge\ sensitivity}} \;\cdot\; D_2 \tag{15.5b}$$

where $D_1 = rBM_1 - N_1$ and $D_2 = rBM_2 - N_2$. Bending moment bridges of three–component moment balances are typically selected to have identical bridge sensitivities. Therefore, the following simplification is valid:

$$S_{BM} \quad \approx \quad \partial\, D_1 \;/\; \partial\, BM1 \quad \approx \quad \partial\, D_2 \;/\; \partial\, BM2 \tag{15.6}$$

Then, after using Eqs. (15.5a) and (15.5b) in combination with Eq. (15.6), we get the following approximations of the bending moment prediction errors assuming that the errors are observed as variations of the electrical outputs of the bending moment bridges:

$$\Delta BM1 \quad \approx \quad \frac{\Delta D_1}{S_{BM}} \tag{15.7a}$$

$$\Delta BM2 \quad \approx \quad \frac{\Delta D_2}{S_{BM}} \tag{15.7b}$$

Finally, after using the right–hand sides of Eqs. (15.7a) and (15.7b) to replace the bending moment errors in Eq. (15.4) above, we get the following conservative estimate of the error of the normal force:

$$|\Delta NF| \quad \leq \quad \frac{|\Delta D_1| \;+\; |\Delta D_2|}{d \;\cdot\; S_{BM}} \tag{15.8}$$

The product of (i) the distance between the bending moment bridges and (ii) the sensitivity of the bending moment bridges is in the denominator of the right–hand side of Eq. (15.8). Therefore, it is concluded that this product must be maximized within given geometric constraints of the three–component moment balance in order to minimize the error in the prediction of the normal force of the balance. This important conclusion can be summarized as follows:

Balance Design Recommendation

The product of (i) the distance between the two bending moment bridges and (ii) the sensitivity of the bending moment bridges must be maximized in order to minimize the overall error in the normal force prediction.

A connection between the sensitivities of the two bending moment bridges and the sensitivity of the torsion moment bridge exists that influences the load prediction accuracy. It is often observed that the range of the two bending moments is significantly larger than the range of the torsion moment. In that case, it is an advantage to increase the sensitivity of the torsion moment bridge within the design constraints of the balance so that the electrical outputs of all three bridges at maximum load are of similar magnitude.

The distance between the bending moment bridges also indirectly influences the reliability of the regression models of the loads. Small distances may create bending moment bridge output sets with hidden linear or near–linear dependencies unless a significant number of calibration loadings is applied in the vicinity of the first bending moment bridge. This calibration load schedule design issue is discussed in more detail in the next section.

15.3.2 Calibration Load Schedule Improvement

It was indicated in Fig. 15–4b that either an excessively large bending moment arm or a very small distance between the bending moment bridges makes the two bending moments and related bridge outputs almost identical. This characteristic can become a serious data analysis problem if either a very large bending moment arm is used during the calibration or a balance with a very small distance between the bending moment bridges is calibrated. The ratio between the two bending moments can be used to illustrate this problem. Then, after dividing both sides of Eq. (15.2a) by both sides of Eq. (15.2b), we get the following equation for the ratio of the bending moments:

$$\frac{BM1}{BM2} \quad = \quad \frac{a \ - \ c \ - \ d}{a \ - \ c} \quad = \quad 1 \ - \ \frac{1}{(\ a \ - \ c\ )\ /\ d} \tag{15.9}$$

It is also reasonable to assume that the bending moment arm (a) is significantly larger than the distance between the second bending moment bridge and the BMC (c). Then, using the assumption $a \gg c$ in Eq. (15.9) above, we get the following approximation of the ratio of the bending moments:

$$\frac{BM1}{BM2} \quad \approx \quad 1 \ - \ \frac{1}{a\ /\ d} \tag{15.10}$$

Consequently, the ratio $BM1/BM2$ between the two bending moments will be close to the unwanted value of one whenever the ratio a/d between bending moment arm and bending moment bridge distance is large. The same situation will be observed for the

ratio D_1/D_2 of the electrical output differences of the bending moment bridges as D_1 is proportional to $BM1$ and D_2 is proportional to $BM2$. This conclusion can be summarized as follows:

$$a \,/\, d \gg 1 \implies \frac{BM1}{BM2} \approx 1 \implies BM1 \approx BM2 \implies D_1 \approx D_2 \qquad (15.11)$$

The smallest value of ratio a/d is between four and six for many calibration load schedules of real–world three–component moment balances. These data sets make it difficult during an analysis to define robust regression models of the loads as the two bending moment bridge outputs appear to be almost linearly related. This issue can also be illustrated by assuming that bending moments are only applied over a narrow bending moment arm range. This hypothetical case is illustrated in Fig. 15–5a below.

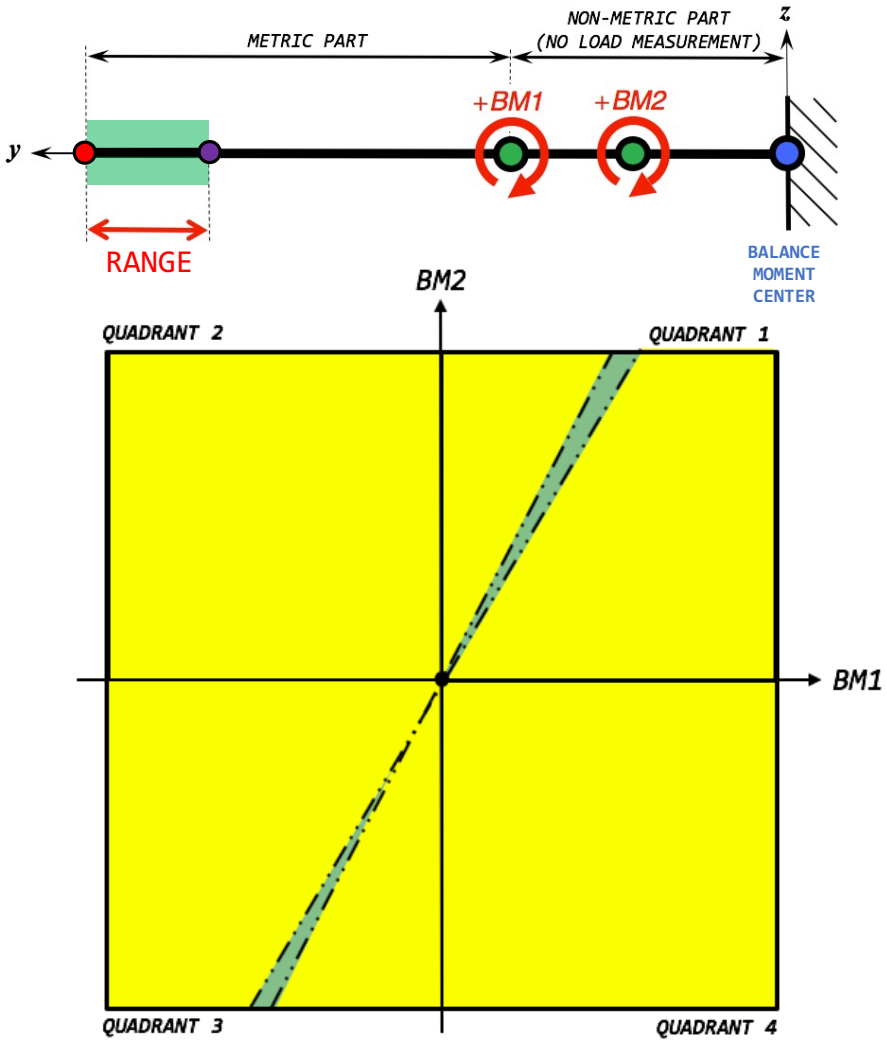

Fig. 15–5a Unwanted bending moment arm range.

It can be seen in the combined load diagram above that data points only appear in a very narrow green region for the unwanted moment arm range. Consequently, it looks as

if the second bending moment equals a constant times the first bending moment. In other words, the applied bending moment combinations appear to be dependent.

The load schedule design issue depicted in Fig. 15–5a above can be corrected if the bending moment arm range extends from the outer tip of the balance to the vicinity of the first bending moment bridge. The resulting recommended bending moment arm range is depicted in Fig. 15–5b below.

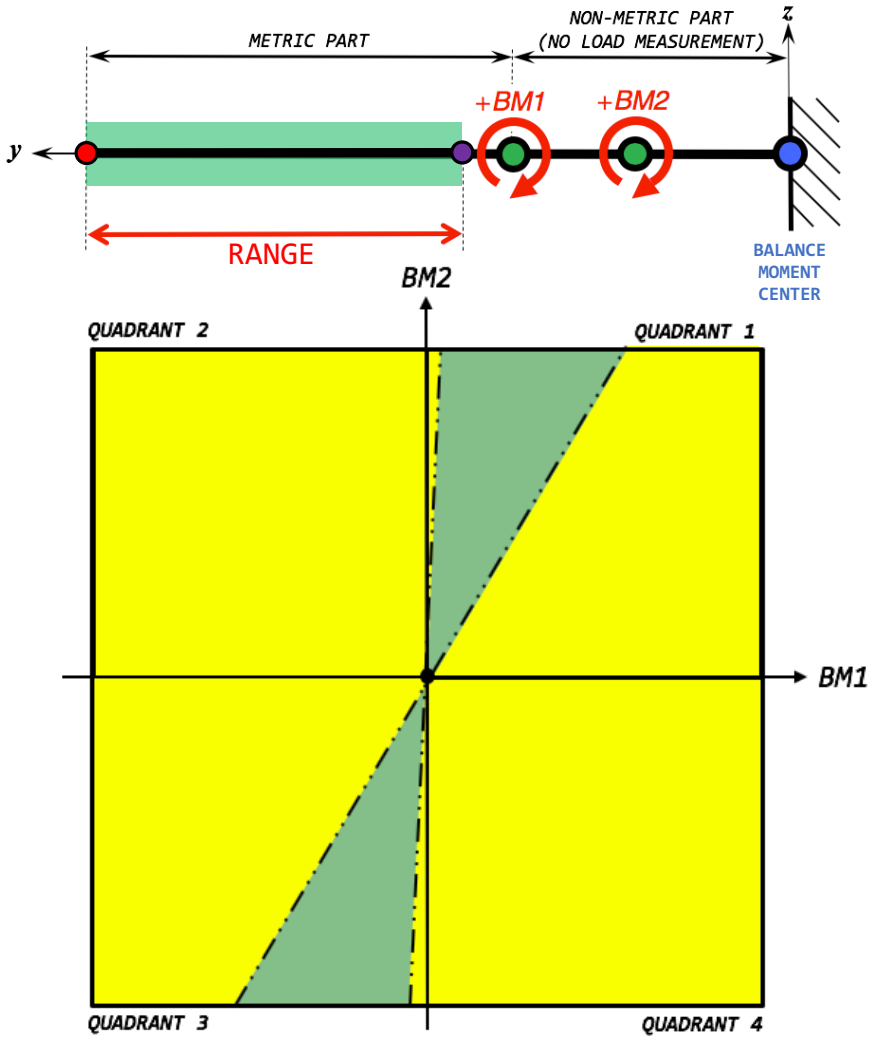

Fig. 15–5b Recommended bending moment arm range.

Now, calibration data points will appear in the enlarged green region that is shown in the combined load diagram above. Consequently, the applied bending moment pairs and related bending moment bridge outputs no longer appear to be dependent variables during the development of a regression model of the balance data.

It is concluded that calibration load schedule design issues related to the ratio between bending moment arm and bending moment bridge distance can easily be addressed by taking a significant number of calibration points near the first bending moment bridge. This load schedule design recommendation can be summarized as follows:

Calibration Load Schedule Design Recommendation

Large ratios between bending moment arm and bending moment bridge distance generate outputs of the bending moment bridges that are almost identical. Therefore, it is important to include a significant number of calibration points in the load schedule that are close to the first bending moment bridge so that the electrical outputs of the calibration data do not appear linearly related.

It was mentioned in Table 15–1 above that both the metric and the bridged part of the non–metric part of a three–component moment balance are subject to elastic deformation. Therefore, depending on the degree of deformation, it may be necessary to apply a moment arm correction when the bending moments are computed. This correction is discussed in the next section of the appendix.

15.3.3 Bending Moment Arm Correction

The metric part and parts of the non–metric part of a three–component moment balance elastically deform when the balance experiences a load. Then, the moment arm of an applied force at a fixed load point is not constant. Consequently, a moment arm correction was developed that takes the elastic deflection of the balance under load into account. The deflection of the balance in a loaded state is shown in Fig. 15–6a below.

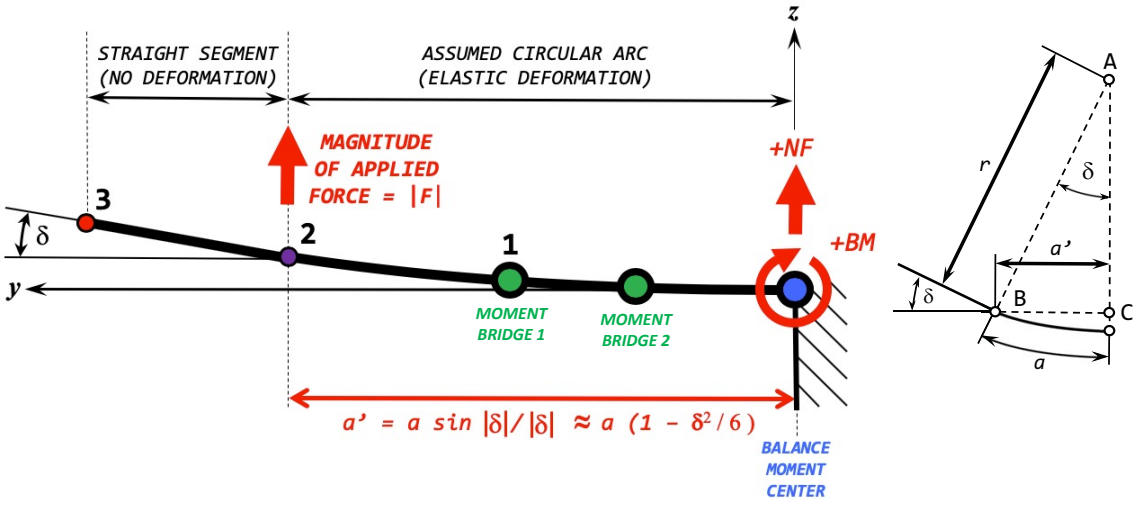

Fig. 15–6a Moment arm correction for a three–component moment balance.

The moment arm correction can be computed if the deflection angle δ is measured at the location where a calibration load is applied. In addition, the assumption is made that the shape of the deflection curve between the balance moment center and the load point is a circular arc. Figure 15–6a above shows the connection between basic geometric parameters that results from this assumption. Now, knowing that the ratio between the

arc (a) and the circumference of the circle ($2\pi r$) equals the ratio between the deflection angle (δ) and 2π, and, solving the resulting equation for the radius of the circle, we get:

$$\frac{a}{2\ \pi\ r} \quad = \quad \frac{|\delta|}{2\ \pi} \qquad \Longrightarrow \qquad r \quad = \quad \frac{a}{|\delta|} \tag{15.12a}$$

The absolute value of the deflection angle in radians is used in Eq. (15.12a) above as the radius of the circular arc must be a positive quantity. In addition, triangle ABC in Fig. 15–6a is a right triangle. Then, the sine of the deflection angle can be computed as a function of the corrected moment arm (a') and the radius (r). Now, after solving the resulting equation again for the radius, we get:

$$\sin|\delta| \quad = \quad \frac{a'}{r} \qquad \Longrightarrow \qquad r \quad = \quad \frac{a'}{\sin|\delta|} \tag{15.12b}$$

Then, after using the right–hand side of Eq. (15.12a) to replace the radius (r) in Eq. (15.12b) and solving the result for the corrected moment arm (a'), we get:

$$a' \quad = \quad a\ \cdot\ \frac{\sin|\delta|}{|\delta|} \tag{15.13}$$

The scale factor $sin|\delta|/|\delta|$ may cause numerical problems during evaluation because the deflection angle is a small measured quantity that appears in the denominator of a fraction. Therefore, it is better to replace the scale factor by a related second order Taylor series approximation that is developed in the neighborhood of $\delta = 0$. The development of this approximation requires successive applications of L'Hôspital's rule as the fraction $0/0$ appears multiple times during the calculation of terms of the Taylor series. Finally, the following second order Taylor series approximation is obtained:

$$\frac{\sin|\delta|}{|\delta|} \quad \approx \quad 1 \ - \ \frac{\delta^{\,2}}{6} \tag{15.14}$$

The second order Taylor series approximation $1 - \delta^{\,2}/6$ can easily be compared with the exact value $\sin|\delta|/|\delta|$ in order to demonstrate that the approximation is sufficiently accurate. For example, the following family of deflection angles may be chosen for the comparison between exact value and approximation: $2\,deg$, $5\,deg$, and $10\,deg$. Results of the comparison for these deflection angles are summarized in Table 15–2 below:

Table 15–2: Accuracy of scale factor approximation.

$\delta \ \equiv \ deflection\ angle$	$\sin\|\delta\|/\|\delta\|$	$1 - \ \delta^{\,2}/\,6$	$\frac{exact\ value}{approximation}$
$0.03491\ rad \ \equiv \ \ 2\ deg$	0.999797	0.999797	1.0
$0.08727\ rad \ \equiv \ \ 5\ deg$	0.998731	0.998731	1.0
$0.17453\ rad \ \equiv \ 10\ deg$	0.994931	0.994923	1.000008

As expected, differences between exact value and approximation are very small within the chosen deflection angle range as their ratios are very close to one. Finally, after replacing the scale factor used in Eq. (15.13) with its second order Taylor series approximation, the corrected moment arm can be expressed as follows:

$$a' \quad \approx \quad a \cdot \left[1 - \frac{\delta^2}{6} \right] \tag{15.15}$$

Now, the corrected applied loads in direct–read format can be described by the following equations assuming that (i) the sign convention introduced in Fig. 15–6a above is used and (ii) the magnitude of the applied force at position 2 is represented by symbol $|F|$ (see also Eqs. (15.1a), (15.1b)). Then, the following two relationships are obtained:

Corrected Balance Loads (Version 1)

$$NF' \quad = \quad |F| \tag{15.16a}$$

$$BM' \quad = \quad |F| \cdot a \cdot \left[1 - \frac{\delta^2}{6} \right] \tag{15.16b}$$

The error of the computed bending moment can be obtained by taking the difference of the bending moments for the two bending moment arm choices where BM is the uncorrected bending moment and BM' is the corrected bending moment. Then, using the bending moment definition given in Eq. (15.1b), we get:

$$\Delta BM \quad = \quad BM - BM' \quad = \quad \underbrace{|F| \cdot a}_{uncorrected} - \underbrace{|F| \cdot a \cdot (\, 1 - \delta^2/\, 6\,)}_{corrected} \tag{15.17a}$$

The right–hand side of Eq. (15.17a) can be simplified for improved clarity. Then, we get:

$$\Delta BM \quad = \quad |F| \cdot a \cdot (\delta^2/\, 6\,) \quad = \quad BM \cdot (\delta^2/\, 6\,) \tag{15.17b}$$

Consequently, after rearranging Eq. (15.17b) and multiplying the result by 100 %, the relative error of the bending moment can be computed in units of percent as follows:

$$\left\{ \frac{\Delta BM}{BM} \right\}_{\%} \quad = \quad (\delta^2/\, 6\,) \cdot 100\,\% \tag{15.18}$$

It is useful to evaluate the error estimate given in Eq. (15.18) for the three small deflection angles that are listed in Table 15–2. Table 15–3 below lists the result of the error estimate of the bending moment for the three chosen deflection angles.

Table 15–3: Estimates of the relative bending moment error.

$\delta \equiv$ deflection angle	$\{\Delta BM/BM\}_{\%}$
0.03491 *rad* ≡ 2 *deg*	0.02 %
0.08727 *rad* ≡ 5 *deg*	0.13 %
0.17453 *rad* ≡ 10 *deg*	0.51 %

It is observed that the bending moment correction may not have to be applied if the deflection angle is less equal 5 *deg* because the difference between uncorrected and corrected bending moments is on the order of 0.1 % or less. The larger deflection angle of 10 *deg*, on the other hand, is causing differences that are on the order of 0.5 %. Therefore, it is concluded that the bending moment correction may have to be applied if (i) the deflection angle exceeds the threshold of 5 *deg* and (ii) the user of a three–component moment balance has very high accuracy requirements.

Gravity weights are typically used to apply a load to a three–component moment balance. In addition, the load point instead of the attachment of the balance to a load stand is often leveled so that the calibration hardware cannot accidentally move or slip relative to the balance surface. Unfortunately, this calibration strategy means that the z–coordinate of the balance axis system is no longer parallel to the direction of the gravitational acceleration when a load is applied to the balance. Consequently, it becomes necessary to apply deflection corrections to both the normal force and the bending moment. Figure 15–6b below shows the connection between applied load, balance deflection, normal force, and bending moment at the balance moment center in that situation.

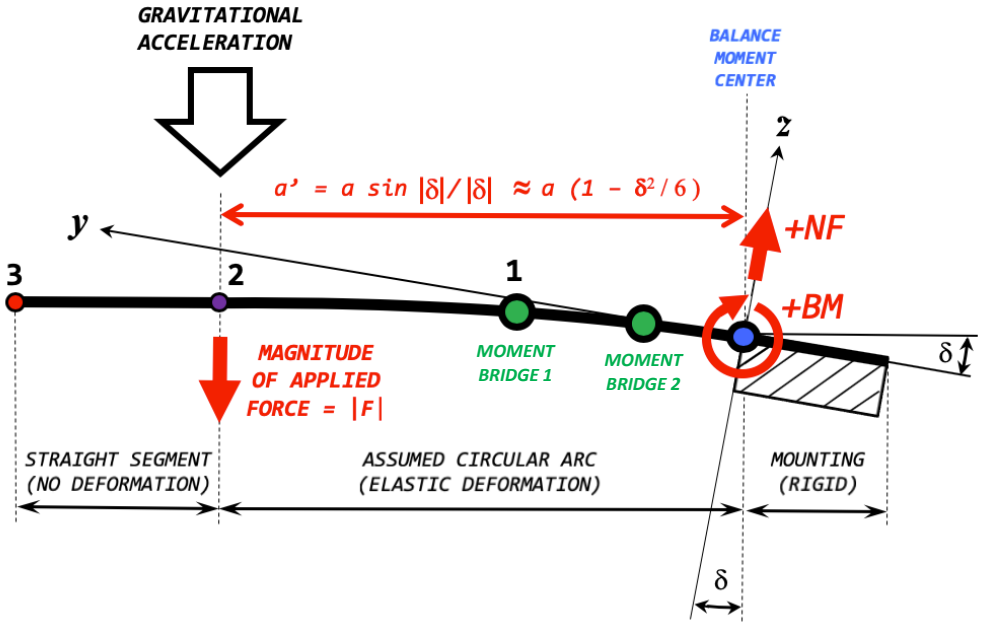

Fig. 15–6b Alternate application of balance loads using gravity weights.

Now, the corrected load pair in direct–read format can be described by the following equations assuming that (i) the sign convention introduced in Fig. 15–6b above is used and (ii) the magnitude of the applied force at load point 2 is represented by symbol $|F|$:

Corrected Balance Loads (Version 2)

$$NF' = (-1) \cdot |F| \cdot \cos|\delta| \qquad (15.19a)$$

$$BM' = (-1) \cdot |F| \cdot a \cdot \left[1 - \frac{\delta^2}{6} \right] \qquad (15.19b)$$

A temporary load fixture may be attached to a three–component moment balance in order to obtain load pairs that are located inside the second and fourth quadrants of the combined load diagram. This option is discussed in the next section of the appendix.

15.4 Temporary Load Fixture

Some three–component moment balances allow for the attachment of a temporary fixture between the metric outer edge of the balance and the first bending moment bridge (moment bridge 1). Then, a force can be applied between the two bending moment bridges. This situation is shown in Fig. 15–7a below. It is assumed that the attachment of the

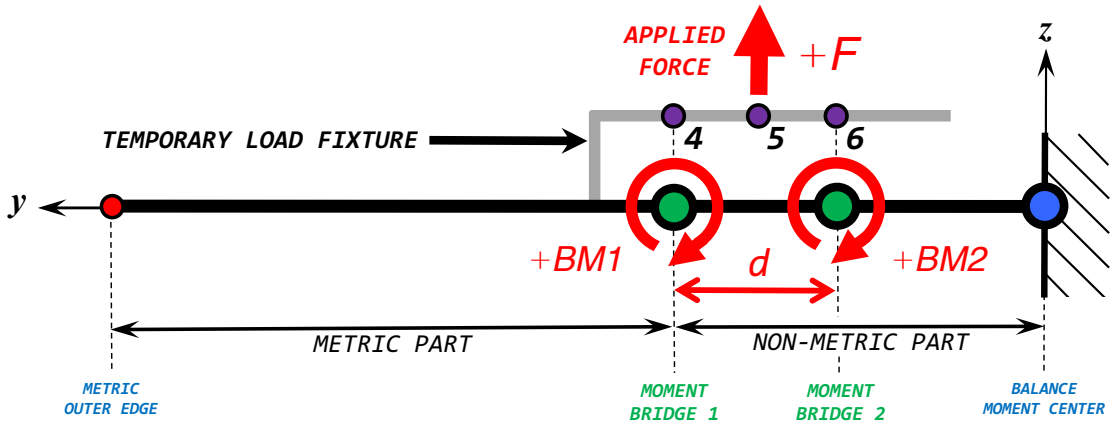

Fig. 15–7a Application of a bending moment pair using a temporary load fixture.

temporary fixture does not significantly change the elastic behavior of the balance. Then, bending moment pairs can be obtained that are located inside the second and fourth quadrant of the combined load diagram if a force is applied to the temporary load fixture. This conclusion can be illustrated with load points 4, 5, and 6 that are shown in Fig. 15–7a above. First, load point 5 is discussed. It allows for the application of a force that is located halfway between the two bending moment bridges. Resulting bending moments at the two bridges will be equal in magnitude but opposite in sign. Consequently, all bending moment pairs associated with the application of a force at load point 5 must be located on the principal diagonal of the second and fourth quadrant of the combined load diagram. On the other hand, load points 4 and 6 allow for the application of a force directly over a bending moment bridge. The first bending moment is zero if a force is applied at load point 4. Similarly, the second bending moment is zero if a force is applied at load point 6. Therefore, bending moment pairs associated with the application of a force at either load point 4 or load point 6 must be located on a coordinate system axis of the combined load

diagram. Locations of bending moment pairs are summarized in Fig. 15–7b below that may result from the application of a force at load point 4, 5, or 6. Two important conclusions can be drawn from the combined load diagram that is shown in Fig. 15–7b. A positive force

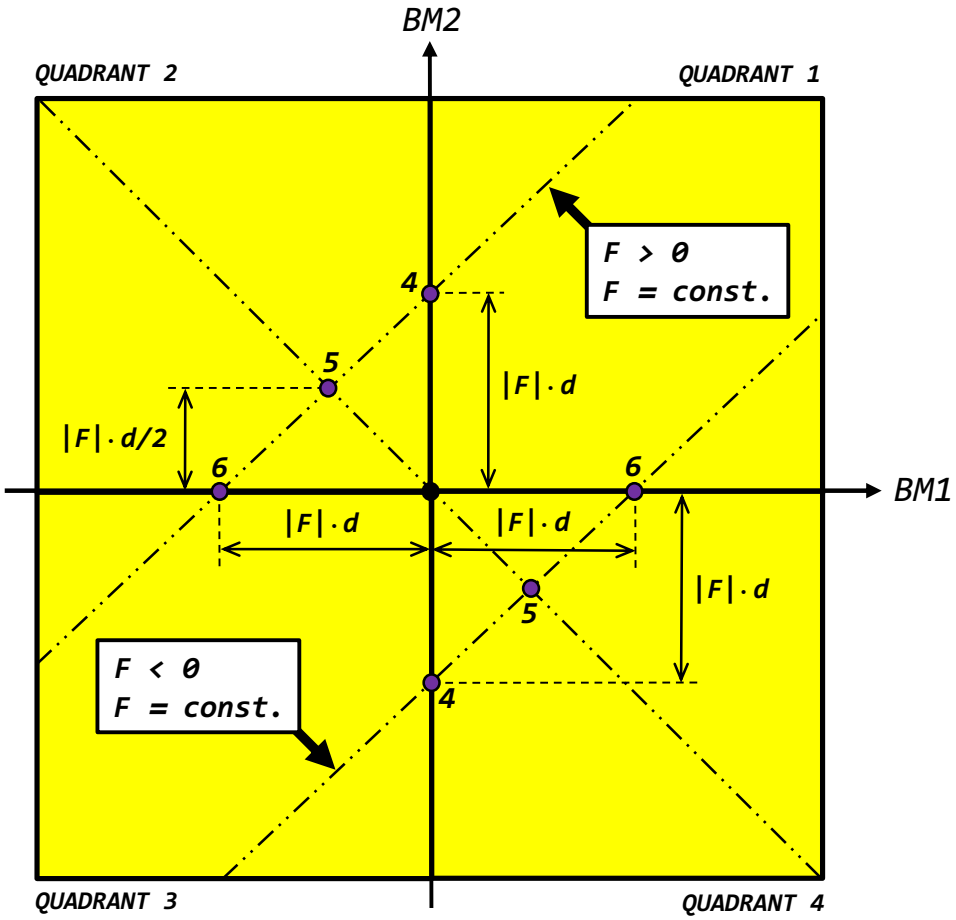

Fig. 15–7b Location of the bending moment pairs that result from the application of a positive or negative force at load point 4, 5, or 6.

generates bending moment pairs inside the second quadrant of the combined load diagram whenever it is applied between load points 4 and 6. Similarly, a negative force generates bending moment pairs inside the fourth quadrant of the combined load diagram whenever it is applied between load points 4 and 6. – Analysis of calibration data of a three–component moment balance and the load prediction are discussed in the next section.

15.5 Data Analysis and Load Prediction

Two different methods are used in the aerospace testing community for the prediction of strain–gage balance loads. Their load prediction equations are obtained from balance calibration data. Some analysts prefer the *Iterative Method* (see App. 10). This approach first fits the measured outputs as a function of the applied calibration loads. Afterwards, a load iteration scheme is constructed from the regression coefficients of the outputs so that loads can be predicted from outputs during a wind tunnel test. Alternatively, the *Non–Iterative Method* may be used for the load prediction (see App. 9). This approach directly fits the applied calibration loads as a function of the measured outputs. The

overall accuracy of the two methods is the same for all practical purposes as long as linear or near–linear dependencies between regression model terms of the calibration data are avoided. Therefore, it was decided to recommend the less complex *Non–Iterative Method* for the prediction of the loads of a three–component moment balance.

The application of the *Non–Iterative Method* to a three–component moment balance needs to be explained in more detail. The method directly fits calibration loads as a function of output differences that are computed using either the natural zeros of the bridges or the raw outputs of the zero load point of a load series as a datum (see App. 9). It is useful to introduce the concepts of output space and load space during the discussion of the *Non–Iterative Method*. In principle, the *Non–Iterative Method* generates a mapping function between these two vector spaces that is used for the load prediction. The mapping is justified by the fact that one output combination can only correspond to one load combination and vice versa. This idea is summarized in Fig. 15–8 below. Each point of the output

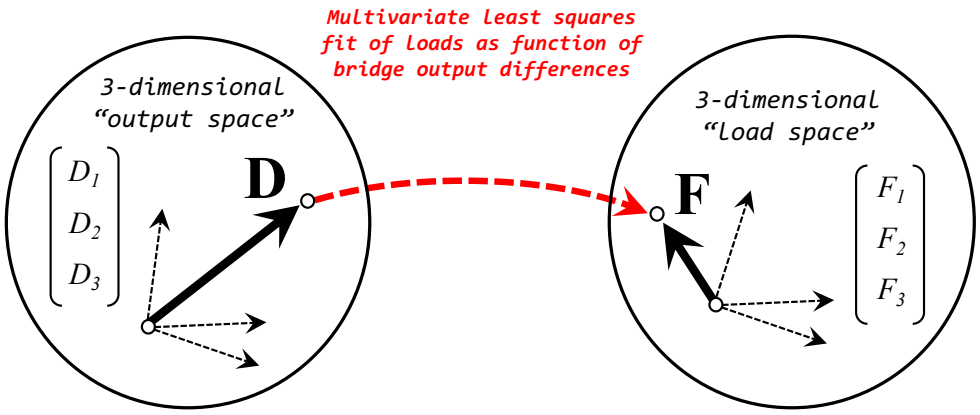

Fig. 15–8 Load and output space definition for a three–component balance.

space represents a specific load state of the balance. This load state is also described by a point in the load space. Points in the output space are identified as three–dimensional vectors. The components of each vector are the output differences D_1 and D_2 of the two bending moment bridges and the output difference D_3 of the torsion moment bridge. The output vector is defined in Eq. (15.20) below. The output differences can be formatted

$$outputs \quad \Longrightarrow \quad \mathbf{D} \;=\; \begin{bmatrix} D_1 \\ D_2 \\ D_3 \end{bmatrix} \tag{15.20}$$

as either *Difference Type 1* or *Difference Type 2* (see App. 6). *Difference Type 1* is defined as the difference between a raw output and the natural zero of the bridge. Alternatively, *Difference Type 2* is defined as the difference between a raw output and the raw output of the first data point of the related load series.

The definition of a point in the load space depends on the chosen load format. For example, the load vector has the following components if direct–read format is used:

$$direct-read\ format \quad \Longrightarrow \quad \mathbf{F} \;=\; \begin{bmatrix} F_1 \\ F_2 \\ F_3 \end{bmatrix} \;=\; \begin{bmatrix} NF \\ BM \\ TM \end{bmatrix} \tag{15.21a}$$

It is also possible to define the load vector in moment balance format. Then, the load vector is described by the following equation:

$$\textit{moment balance format} \quad \Longrightarrow \quad \mathbf{F} \;=\; \begin{bmatrix} F_1 \\ F_2 \\ F_3 \end{bmatrix} \;=\; \begin{bmatrix} BM1 \\ BM2 \\ TM \end{bmatrix} \tag{15.21b}$$

The final load format choice depends on an analyst's preferences or other constraints. Now, regression models need to be developed so that the measured outputs of the three bridges can be used to predict the balance loads. The selection of the terms for the regression models of the three load components depends on characteristics of the calibration load schedule. A typical load schedule for a three–component moment balance may support a total of ten terms as the torsion moment and the bending moments are often applied simultaneously. These terms are listed in Table 15–4 below.

Table 15–4: Term choices for the regression model of a load component.

Type	List of Regression Model Terms
constant	$Intercept$
linear	$(D_1)\ ,\ (D_2)\ ,\ (D_3)$
quadratic†	$(D_1)^2\ ,\ (D_2)^2\ ,\ (D_3)^2$
cross–product	$(D_1)\cdot(D_2)\ ,\ (D_1)\cdot(D_3)\ ,\ (D_2)\cdot(D_3)$

†The square of D_3 is typically not supported as torsion moment arms are often too small.

First, it is assumed that loads are given in direct–read format. Then, the regression models of normal force and bending moment can be defined by the following equations:

$$\begin{aligned} NF \;=\; \eta_0 \;+\; & \underbrace{\eta_1\cdot(D_1) \;+\; \eta_2\cdot(D_2) \;+\; \eta_3\cdot(D_3)}_{linear\ terms} \\ & +\; \underbrace{\eta_4\cdot(D_1)^2 \;+\; \eta_5\cdot(D_2)^2 \;+\; \eta_6\cdot(D_3)^2}_{quadratic\ terms} \\ & +\; \underbrace{\eta_7\cdot(D_1)\cdot(D_2) \;+\; \eta_8\cdot(D_1)\cdot(D_3) \;+\; \eta_9\cdot(D_2)\cdot(D_3)}_{cross-product\ terms} \end{aligned} \tag{15.22a}$$

$$\begin{aligned} BM \;=\; \lambda_0 \;+\; & \underbrace{\lambda_1\cdot(D_1) \;+\; \lambda_2\cdot(D_2) \;+\; \lambda_3\cdot(D_3)}_{linear\ terms} \\ & +\; \underbrace{\lambda_4\cdot(D_1)^2 \;+\; \lambda_5\cdot(D_2)^2 \;+\; \lambda_6\cdot(D_3)^2}_{quadratic\ terms} \\ & +\; \underbrace{\lambda_7\cdot(D_1)\cdot(D_2) \;+\; \lambda_8\cdot(D_1)\cdot(D_3) \;+\; \lambda_9\cdot(D_2)\cdot(D_3)}_{cross-product\ terms} \end{aligned} \tag{15.22b}$$

Alternatively, loads may be expressed in moment balance format. This approach has the advantage that the sensitivities of all balance bridges are defined. In addition, troubleshooting is simplified because the bending moment bridge output differences are directly proportional to the applied first and second bending moment. Then, the regression models of the first and second bending moment can be defined as follows:

$$\begin{aligned} BM1 \;=\; \nu_0 \;+\; & \underbrace{\nu_1 \cdot (D_1) \;+\; \nu_2 \cdot (D_2) \;+\; \nu_3 \cdot (D_3)}_{linear\ terms} \\ & +\; \underbrace{\nu_4 \cdot (D_1)^2 \;+\; \nu_5 \cdot (D_2)^2 \;+\; \nu_6 \cdot (D_3)^2}_{quadratic\ terms} \\ & +\; \underbrace{\nu_7 \cdot (D_1) \cdot (D_2) \;+\; \nu_8 \cdot (D_1) \cdot (D_3) \;+\; \nu_9 \cdot (D_2) \cdot (D_3)}_{cross-product\ terms} \end{aligned} \tag{15.23a}$$

$$\begin{aligned} BM2 \;=\; \xi_0 \;+\; & \underbrace{\xi_1 \cdot (D_1) \;+\; \xi_2 \cdot (D_2) \;+\; \xi_3 \cdot (D_3)}_{linear\ terms} \\ & +\; \underbrace{\xi_4 \cdot (D_1)^2 \;+\; \xi_5 \cdot (D_2)^2 \;+\; \xi_6 \cdot (D_3)^2}_{quadratic\ terms} \\ & +\; \underbrace{\xi_7 \cdot (D_1) \cdot (D_2) \;+\; \xi_8 \cdot (D_1) \cdot (D_3) \;+\; \xi_9 \cdot (D_2) \cdot (D_3)}_{cross-product\ terms} \end{aligned} \tag{15.23b}$$

Finally, the regression model of the torsion moment is defined by the following equation:

$$\begin{aligned} TM \;=\; \mu_0 \;+\; & \underbrace{\mu_1 \cdot (D_1) \;+\; \mu_2 \cdot (D_2) \;+\; \mu_3 \cdot (D_3)}_{linear\ terms} \\ & +\; \underbrace{\mu_4 \cdot (D_1)^2 \;+\; \mu_5 \cdot (D_2)^2 \;+\; \mu_6 \cdot (D_3)^2}_{quadratic\ terms} \\ & +\; \underbrace{\mu_7 \cdot (D_1) \cdot (D_2) \;+\; \mu_8 \cdot (D_1) \cdot (D_3) \;+\; \mu_9 \cdot (D_2) \cdot (D_3)}_{cross-product\ terms} \end{aligned} \tag{15.24}$$

The given balance calibration data set may only support a subset of the regression model terms of the load components that are defined in Eqs. (15.22a) to (15.24). Therefore, it is critical to screen the chosen set of regression model terms for hidden linear or massive near-linear dependencies by using the *Variance Inflation Factor* (see App. 18 for more details). In particular, the outputs of the two bending moment bridges can easily appear linearly dependent if none or too few calibration loads are applied near the first bending moment bridge. In addition, a calibration data set may not support the square of D_3 as often only three closely spaced moment arm positions are available for the application of the torsion moment.

The accuracy of the load prediction may improve if (i) all bridge outputs are formatted as *Difference Type 1* and (ii) a tare load iteration is performed during the application of

the *Non–Iterative Method*. Then, all loads can be described relative to the load datum of zero absolute load (see App. 12 for more details).

The regression coefficients are obtained after performing the least squares fit of the calibration data. Afterwards, three explicit equations for the prediction of the balance loads are known that can easily be implemented in the data system of a wind tunnel.

15.6 Summary and Recommendations

Fundamental characteristics of design, calibration, and use of a three–component moment balance were presented. First, basic features of this balance type were reviewed. Then, different load format choices and the definition of the combined load diagram were discussed. Afterwards, balance design and calibration recommendations were made. Whenever possible, the sensitivities of the three balance bridges should be selected such that their electrical outputs at maximum load are of similar magnitude. In addition, it is suggested to maximize the product between (i) the bending moment bridge distance and (ii) the bending moment bridge sensitivity in order to minimize the load prediction error for the normal force. A balance user needs to work closely with the balance manufacturer in order to achieve these goals if the load prediction accuracies are critical for a given test objective. It is also recommended to apply a significant number of calibration loads in the vicinity of the first bending moment bridge. Then, it is less likely that the electrical outputs of the two bending moment bridges appear to be linearly related. A correction formula for the bending moment arm was also developed that takes the elastic deformation of the metric part of the balance under load into account. Finally, basic elements of the use of the *Non–Iterative Method* for the prediction of the loads of a three–component moment balance were discussed.

Appendix 16

Percent Contribution of a Regression Model Term

16.1 Introduction

The *Percent Contribution* is a useful metric that can be computed for each regression model term that either the *Non–Iterative Method* or the *Iterative Method* use for the analysis of balance calibration data. In principle, the *Percent Contribution* assesses a regression model term's importance during the prediction of balance data whenever its magnitude is compared with a set of recommended empirical thresholds.

The *Percent Contribution* has the advantage that it is easily understood and applied. It is defined as a fraction that is multiplied by 100 %. The numerator of the fraction equals the product of (i) the regression coefficient of the term and (ii) the term's value after being computed for the related capacities of the balance. Similarly, the denominator of the fraction equals the product of (i) the regression coefficient of the most important term and (ii) the term's value after being computed for the related capacity of the balance. Then, the absolute value of the *Percent Contribution* is compared with a family of empirical thresholds in order to determine the regression model term's importance.

It is helpful for a better understanding of the definition of the *Percent Contribution* if the expressions *primary load*, *primary output*, and *primary output difference* are explained in more detail. Therefore, a brief description of them is given in the box below.

Primary Load / Primary Output / Primary Output Difference

A primary load of a strain–gage balance is defined as a load component that is responsible for more or less 90 % of the electrical signal of the related primary output or primary output difference whenever the load is exclusively applied to the balance. The axial force, for example, is a primary load of a six–component balance. The axial bridge output is the related primary output because more or less 90 % of its signal is caused by the axial force whenever this load component is exclusively applied to the balance. Similarly, the difference between the electrical output of the axial bridge and its natural zero is the related primary output difference because more or less 90 % of this difference is caused by the axial force whenever this load component is exclusively applied to the balance.

The definition of the *Percent Contribution* for regression model terms of a load component is discussed in the next section. This definition is needed whenever a balance calibration data set is analyzed by using the *Non–Iterative Method* (see also App. 9 for a detailed description of this analysis method).

16.2 Percent Contribution for Non–Iterative Method

The definition of the *Percent Contribution* for regression model terms is derived in this section assuming that the *Non–Iterative Method* is applied during the balance load prediction. In principle, the *Percent Contribution* of a term is obtained from the regression model of a load component that is defined in Eq. (16.1a) below where F_μ is the fitted

$$F_\mu \;=\; a_0 \;+\; a_1 \cdot D_1 \;+ \ldots + \; a_\mu \cdot D_\mu \;+ \ldots + \; a_n \cdot D_n \;+ \ldots + \; a_\xi \cdot \mathcal{S}_\xi \;+ \ldots \qquad (16.1a)$$

load component (see also App. 9). For simplicity, it is assumed that the regression model is only defined by using differences between the raw outputs and natural zeros of the balance bridges as independent variables. Then, the output differences for an n–component balance are defined as follows in Eq. (16.1b) below where rF_i equals the raw output of a bridge, the

$$D_i \;=\; rF_i \;-\; N_i \quad ; \quad 1 \;\leq\; i \;\leq\; n \tag{16.1b}$$

symbol N_i describes the natural zero of a bridge, and i is the bridge index. The symbols $a_0,\ a_1,\ \ldots$ in Eq. (16.1a) are the regression coefficients. Consequently, each regression model term $\mathcal{S}_\xi$ must be a function of the output differences $D_1, \ldots, D_n$ that are used as independent variables. This conclusion can be summarized by the following relationship:

$$\mathcal{S}_\xi \;\;=\;\; \mathcal{S}_\xi(D_1,\ D_2,\ \ldots\ ,\ D_n) \tag{16.1c}$$

Now, the *Percent Contribution* of a regression model term of a balance load component can verbally be described. The following definition is suggested:

Definition of Percent Contribution *(Non–Iterative Method)*

The *Percent Contribution* $P\{\mathcal{S}_\xi\}$ of term $\mathcal{S}_\xi$ of the regression model of load component F_μ is a fraction that is multiplied by 100 %. The numerator of this fraction equals the product of the term's coefficient, i.e., a_ξ, with the capacities of all variables, i.e., outputs and other independent variables, that define the term. The denominator of the fraction equals the product of the coefficient a_μ of the primary output difference of load component F_μ and the related capacity. The output capacity may be defined, for example, as the output at load capacity.

It is helpful to summarize the verbal description of the *Percent Contribution* above by using the following simple mathematical relationship:

$$P\{\mathcal{S}_\xi\} \;\;=\;\; \frac{a_\xi \;\times\; Capacity\left\{\mathcal{S}_\xi\right\}}{a_\mu \;\times\; Capacity\left\{D_\mu\right\}} \;\times\; 100\,\% \tag{16.2}$$

where

$$\begin{aligned}
\mathcal{S}_\xi &\equiv \textit{term of the regression model of load component } F_\mu \\
D_\mu &\equiv \textit{primary output difference of load component } F_\mu \\
a_\xi &\equiv \textit{regression coefficient of model term } \mathcal{S}_\xi \\
a_\mu &\equiv \textit{regression coefficient of primary output difference } D_\mu
\end{aligned}$$

Analysis results from a balance calibration data set may be used to illustrate the application of the *Percent Contribution*. A data set from a machine calibration of NASA's MK34B six–component force balance was chosen for that purpose. The data consisted of 2082 data points that were distributed across 16 load series. The data set allowed for the definition of six independent output differences of the balance. They are the independent variables for the least squares fit of the balance loads. The output differences are defined in Eqs. (16.3a) to (16.3f) below. Symbols $rN1$, $rN2$, ..., rRM represent the

$$D_1 = rN1 - N_1 \tag{16.3a}$$

$$D_2 = rN2 - N_2 \tag{16.3b}$$

$$D_3 = rS1 - N_3 \tag{16.3c}$$

$$D_4 = rS2 - N_4 \tag{16.3d}$$

$$D_5 = rAF - N_5 \tag{16.3e}$$

$$D_6 = rRM - N_6 \tag{16.3f}$$

raw outputs of the bridges. Symbols N_1, N_2, ..., N_6 are the corresponding natural zeros, i.e., the raw outputs of the bridges at zero absolute load. Table 16–1 below lists the capacities of the six output differences in electrical units.

Table 16–1: Output capacities of the MK34A balance.

D_1 *microV/V*	D_2 *microV/V*	D_3 *microV/V*	D_4 *microV/V*	D_5 *microV/V*	D_6 *microV/V*
1200	1200	1200	1200	1500	1200

A regression model for the prediction of the axial force as a function of the six independent output differences of the balance was developed. The regression model of the axial force had the following general form ...

$$AF = \underbrace{\ldots + a_\xi \cdot \overbrace{D_1}^{\mathcal{S}_\xi} + \ldots + a_\mu \cdot D_\mu + \ldots}_{\textit{regression model of the axial force}} \tag{16.4a}$$

where

$$D_\mu \equiv \underbrace{\textit{primary output difference associated with the axial force}}_{\textit{see also the definition of the difference that is given in Eq. (16.3e)}} \tag{16.4b}$$

The regression model consisted of a total of 39 terms that were chosen using a regression model search algorithm (see, e.g., App. 19 of the current document for a detailed description of the search algorithm). Now, the primary output difference D_μ of the axial force needs to be identified as it will be used as a reference during the calculation of the *Percent Contribution* of the terms of the regression model of the axial force. This difference

must include the raw output rAF of the axial force bridge of the balance. Therefore, the output difference D_5 defined in Eq. (16.3e) above must equal D_μ. Then, we get:

$$D_\mu \quad = \quad D_5 \tag{16.5a}$$

It was decided to compute the *Percent Contribution* of the term D_1 that is used in Eq. (16.4a). Consequently, we get the following equality:

$$\mathcal{S}_\xi \quad = \quad D_1 \tag{16.5b}$$

Now, all inputs for the calculation of the *Percent Contribution* of term $\mathcal{S}_\xi$ can be identified. First, capacities of the reference term (D_μ) and the chosen term ($\mathcal{S}_\xi$) of the regression model need to be obtained. Then, after using the contents of Table 16–1 as input, we get the following relationships:

$$Capacity \left\{ D_\mu = D_5 \right\} \quad = \quad 1500 \ microV/V \tag{16.6a}$$

$$Capacity \left\{ \mathcal{S}_\xi = D_1 \right\} \quad = \quad 1200 \ microV/V \tag{16.6b}$$

In addition, the two required regression coefficients need to be obtained from the least squares fit of the axial force. The following coefficients of the reference term (D_μ) and the chosen term ($\mathcal{S}_\xi$) were computed:

$$a_\mu \quad = \quad +2.688057\,\mathrm{E}{-1} \ \ lbs\,/\,(microV/V) \tag{16.6c}$$

$$a_\xi \quad = \quad +3.694008\,\mathrm{E}{-3} \ \ lbs\,/\,(microV/V) \tag{16.6d}$$

Finally, the *Percent Contribution* of the term $\mathcal{S}_\xi = D_1$ can be computed by using the values on the right–hand sides of Eqs. (16.6a) to (16.6d) as input on the right–hand side of Eq. (16.2). Then, the following result is obtained:

$$P\left\{\mathcal{S}_\xi = D_1\right\} \quad = \quad +1.10\,\% \tag{16.7}$$

In the next section, the regression model of a raw electrical output or an output difference and the resulting definition of the *Percent Contribution* of a regression model term are discussed. This type of regression model is used whenever an analyst chooses to apply the *Iterative Method* to strain–gage balance calibration data.

16.3 Percent Contribution for Iterative Method

The definition of the *Percent Contribution* for the *Iterative Method* is discussed in this section (see App. 10 for a description of this method). In this case, the *Percent Contribution* is derived from the regression model of an output. First, it is assumed that the raw output of a bridge is fitted as a function of the calibration loads. Then, the regression model of the output may be defined by Eq. (16.8) below where rF_μ represents the raw output of a

$$rF_\mu \quad = \quad \underbrace{b_0 \ + \ b_1 \cdot F_1 \ + \ldots + \ b_\mu \cdot F_\mu \ + \ldots + \ b_n \cdot F_n \ + \ldots + \ b_\xi \cdot \mathcal{T}_\xi \ + \ldots}_{Option\ 1 \ \Longrightarrow \ regression\ model\ of\ the\ raw\ output} \tag{16.8}$$

balance bridge, $F_1, \ldots, F_n$ are the tare corrected balance loads, F_μ is the primary load of output rF_μ, $\mathcal{T}_\xi$ represents a regression model term, and $b_0, b_1, \ldots$ are the regression coefficients. Each individual regression model term is a function of the set of tare corrected load components. This conclusion is summarized in Eq. (16.9) below.

$$\mathcal{T}_\xi \quad = \quad \mathcal{T}_\xi(F_1,\ F_2,\ \ldots\ ,\ F_n) \tag{16.9}$$

It is also possible to develop a regression model of the difference between the raw output and the natural zero of a balance bridge. This output difference of a bridge may simply be defined by Eq. (16.10) below where D_μ equals the output difference, rF_μ is the

$$D_\mu \quad = \quad rF_\mu \ - \ N_\mu \tag{16.10}$$

raw output, and N_μ is the natural zero. Then, the regression model of the output difference can be defined by Eq. (16.11) below. It must be mentioned at this point that the fitted

$$D_\mu \quad = \quad \underbrace{b_0 \ + \ b_1 \cdot F_1 \ + \ldots + \ b_\mu \cdot F_\mu \ + \ldots + \ b_n \cdot F_n \ + \ldots + \ b_\xi \cdot \mathcal{T}_\xi \ + \ldots}_{\textit{Option 2} \implies \textit{regression model of the output difference}} \tag{16.11}$$

coefficients of the two regression model options for an electrical output, i.e., the coefficients listed in Eq. (16.8) and Eq. (16.11), are directly related if the same set of regression model terms is used for the analysis. In that case, all coefficients of the two regression model options will be identical with the exception of the intercept terms. This statement can be understood if a physical interpretation is attached to the two intercept terms. For example, the fitted intercept term b_0 of the regression model of the raw output rF_μ must be a least squares approximation of the natural zero as the left–hand side of Eq. (16.8) equals the natural zero whenever all tare corrected loads on the right–hand side of Eq. (16.8) are zero. This first conclusion is summarized in Eq. (16.12a) below.

$$\textit{Option 1} \implies \textit{interpretation of intercept term} \implies b_0(rF_\mu) \ \approx \ N_\mu \tag{16.12a}$$

Similarly, the fitted intercept term b_0 of the regression model of the output difference D_μ must be a least squares approximation of zero output as the left–hand side of Eq. (16.11) equals zero output whenever all loads on the right–hand side of Eq. (16.11) are zero. This second conclusion is summarized in Eq. (16.12b) below:

$$\textit{Option 2} \implies \textit{interpretation of intercept term} \implies b_0(D_\mu) \ \approx \ 0 \tag{16.12b}$$

Now, the *Percent Contribution* of a regression model term of an output or an output difference can verbally be described. The following definition is suggested:

Definition of Percent Contribution *(Iterative Method)*

The *Percent Contribution* $Q\{\mathcal{T}_\xi\}$ of a term $\mathcal{T}_\xi$ of the regression model of either an output rF_μ or an output difference D_μ is a fraction that is multiplied by 100 %. The numerator of this fraction equals the product of the term's coef–ficient b_ξ and the capacities of all variables, i.e., loads and other variables, that define the term. The denominator of the fraction equals the product of the coefficient b_μ of the primary load F_μ of the output or output difference with the load capacity (capacity definition depends on the chosen load format).

For clarity, the verbal description of the *Percent Contribution* of a regression model term for the *Iterative Method* is summarized in Eq. (16.13) below.

$$Q\{\mathcal{T}_\xi\} \quad = \quad \frac{b_\xi \ \times \ Capacity\left\{\ \mathcal{T}_\xi\ \right\}}{b_\mu \ \times \ Capacity\left\{F_\mu\right\}} \ \times \ 100\,\% \qquad (16.13)$$

where

$$\begin{array}{rcl} \mathcal{T}_\xi & \equiv & \textit{term of the regression model of output } rF_\mu \textit{ or } D_\mu \\ F_\mu & \equiv & \textit{primary load related to outputs } rF_\mu \textit{ and } D_\mu \\ b_\xi & \equiv & \textit{regression coefficient of model term } \mathcal{T}_\xi \\ b_\mu & \equiv & \textit{regression coefficient of the primary load } F_\mu \end{array}$$

Again, a data set from a machine calibration of NASA's MK34B six–component force balance may be used to illustrate the application of the *Percent Contribution* whenever the *Iterative Method* is used for the balance calibration data analysis. Now, the load capacities of the balance load components are needed for the calculation of the *Percent Contribution*. Table 16–2 below lists the load capacities of the balance.

Table 16–2: Load capacities of the MK34A balance ($lbs \equiv$ pounds of force).

$N1,\ lbs$	$N2,\ lbs$	$S1,\ lbs$	$S2,\ lbs$	$AF,\ lbs$	$RM,\ in{-}lbs$
3500	3500	1800	1800	400	5000

It was decided to compute the *Percent Contribution* of a term of the regression model of the output difference of the forward side force bridge. This regression model is described in Eq. (16.14) below assuming that Eq. (16.3*c*) is used to define the output difference. The

$$D_3 \ = \ rS1{-}N_3 \ = \ \underbrace{\ldots \ + \ b_\mu \cdot S1 \ + \ \ldots \ + \ b_\xi \ \cdot \ \overbrace{(N1 \cdot S1)}^{\mathcal{T}_\xi} \ + \ \ldots}_{regression\ model\ of\ the\ forward\ side\ force\ bridge\ output\ difference} \qquad (16.14)$$

cross–product term $N1 \cdot S1$ was chosen for the calculation of the *Percent Contribution*. In the next step, the inputs for the calculation of the *Percent Contribution* need to be identified. The primary load of the forward side force bridge output of a force balance is the forward side force itself. This conclusion is summarized in Eq. (16.15*a*) below.

$$F_\mu \quad = \quad S1 \qquad (16.15a)$$

Similarly, the chosen regression model term needs to be related to the terminology that is used in Eq. (16.13) above. Equation (16.15*b*) may be used to describe the term.

$$\mathcal{T}_\xi \quad = \quad N1 \cdot S1 \qquad (16.15b)$$

Now, capacities used on the right–hand side of Eq. (16.13) can be assigned. The following values are obtained:

$$Capacity\left\{F_\mu = S1\right\} \quad = \quad 1800\ lbs \tag{16.16a}$$

$$Capacity\left\{\mathcal{T}_\xi = N1 \cdot S1\right\} \quad = \quad 3500\ lbs\ \cdot\ 1800\ lbs \tag{16.16b}$$

In addition, the coefficients of (i) the primary load and of (ii) the cross–product term were obtained from the fitted calibration data. The following values were computed:

$$b_\mu \quad = \quad +6.024261\,\mathrm{E}{-1}\ \ (microV/V)\,/\,lbs \tag{16.16c}$$

$$b_\xi \quad = \quad -2.785648\,\mathrm{E}{-6}\ \ (microV/V)\,/\,lbs^{\,2} \tag{16.16d}$$

Finally, the *Percent Contribution* of the term $\mathcal{T}_\xi = N1 \cdot S1$ can be computed by using the values on the right–hand sides of Eqs. (16.16*a*) to (16.16*d*) as input on the right–hand side of Eq. (16.13). Then, the following result is obtained:

$$Q\,\{\mathcal{T}_\xi = N1 \cdot S1\} \quad = \quad -1.62\,\% \tag{16.17}$$

The *Percent Contribution* can only be used for an objective assessment of the importance of a regression model term if its magnitude is compared with empirical thresholds. These thresholds are discussed in detail in the next section.

16.4 Interpretation of Percent Contribution Values

The magnitude of the *Percent Contribution* of a regression model term needs to be compared with thresholds in order to decide if the term's use is critical, important, or insignificant as far as the description of the physical characteristics of the balance is concerned. The thresholds themselves may vary from analyst to analyst as these values are typically the result of empirical observations. Nevertheless, a table of threshold values can be assembled that may be acceptable to most analysts. These suggested thresholds and associated interpretations are listed in Table 16–3 below.

Table 16–3: Empirical interpretation of *Percent Contribution* values.

Percent Contribution	Interpretation
$\{P\ or\ Q\}\ =\ 100\,\%$	reference term $\Longrightarrow$ most important term
$0.5\,\% \leq \{\lvert P\rvert\ or\ \lvert Q\rvert\} < 100\,\%$	very important term $\Longrightarrow$ term is <u>required</u>
$0.1\,\% \leq \{\lvert P\rvert\ or\ \lvert Q\rvert\} < 0.5\,\%$	term of minor importance $\Longrightarrow$ term is <u>optional</u>
$\{\lvert P\rvert\ or\ \lvert Q\rvert\}\ <\ 0.1\,\%$	term of no importance $\Longrightarrow$ term can be <u>omitted</u>
$\{\lvert P\rvert\ or\ \lvert Q\rvert\}\ \approx\ 100\,\%$	value is observed for second linear term if data set is <u>not</u> analyzed in the design format† of the balance

†design format $\Longleftrightarrow$ direct–read balance data set is analyzed in direct–read format, or, force balance data set is analyzed in force balance format, or, moment balance data set is analyzed in moment balance format.

The thresholds were chosen based on the assumptions that (i) the standard deviation of the fitted dependent variable is on the order of 0.1 % and (ii) the balance data set is analyzed in the design format of the balance (see also the footnote at the bottom of Table 16–3). Then, the primary load, primary output, or primary output difference of the regression model becomes, by design, the single most important term. By design, it has a *Percent Contribution* of 100 %. *Percent Contribution* magnitudes above 0.5 % belong to a term that makes a very important contribution. A term with a *Percent Contribution* magnitude between 0.1 % and 0.5 % is located in a gray zone. It may or may not be important. Then, engineering judgement must be used to decide if the term makes an important contribution. Finally, a term with a *Percent Contribution* magnitude below 0.1 % is considered insignificant. It can be omitted without negatively influencing the balance load prediction accuracy.

It must be mentioned for completeness that pairs of *Percent Contribution* magnitudes in the neighborhood of 100 % may be observed among terms of the regression models of the outputs or output differences whenever a balance data set is not analyzed in the design format of the balance. This situation exists, for example, if an analyst uses the *Iterative Method* for the balance data analysis and processes force balance data in direct–read format.

16.5 Relationship between Percent Contributions

It was observed after applying the *Non–Iterative* and *Iterative Method* to identical balance calibration data sets that *Percent Contribution* values $P\{\mathcal{S}_\xi\}$ and $Q\{\mathcal{T}_\xi\}$ of related regression model terms $\mathcal{S}_\xi$ and $\mathcal{T}_\xi$ are similar in magnitude but opposite in sign. This characteristic can rigorously be proven for a subset of terms if the following five assumptions are made: (a) the balance data set is analyzed in its design format (i.e., direct–read balance data set is analyzed in direct–read format, or, force balance data set is analyzed in force balance format, or, moment balance data set is analyzed in moment balance format); (b) the electrical outputs of the balance are supplied as differences between the raw output and the natural zero of a bridge; (c) the type and number of terms of the regression model of a primary load matches the type and number of terms of the regression model of the related primary output; (d) the capacity of an output is assigned to be the maximum output at load capacity; (e) the absolute value of the percent contribution of a term is less/equal 10 % if the term is not a primary output, output difference, or load.

The proof starts by comparing an approximation of the regression model of an output difference with the corresponding regression model of a load. First, the regression model of the output difference, i.e., Eq. (16.11), is simplified after taking assumptions (a) and (b) into account. Then, it is reasonable to assume that the intercept term is negligible and only the primary load and one additional regression model term make significant contributions on the right–hand side of Eq. (16.11). Consequently, the following approximation of the regression model of an output difference can be made:

$$D_\mu \quad \approx \quad b_\mu \cdot F_\mu \quad + \quad b_\xi \cdot \mathcal{T}_\xi \tag{16.18a}$$

Now, after dividing both sides of Eq. (16.18a) by the product $b_\mu \cdot F_\mu$, we get:

$$\frac{D_\mu}{b_\mu \cdot F_\mu} \quad \approx \quad 1 \quad + \quad \frac{b_\xi \cdot \mathcal{T}_\xi}{b_\mu \cdot F_\mu} \tag{16.18b}$$

We also know that the regression model term b_μ is the prime sensitivity, i.e., the partial derivative of the primary output difference D_μ with respect to the primary load F_μ. Then, we can write:

$$b_\mu \quad = \quad \frac{\partial\ D_\mu}{\partial\ F_\mu} \tag{16.18c}$$

Then, after using (i) the right–hand side of Eq. (16.18c) to replace the coefficient b_μ on the left–hand side of Eq. (16.18b) and (ii) multiplying both sides of the resulting equation with 100 %, we get:

$$\frac{D_\mu}{(\partial D_\mu / \partial F_\mu)\ \cdot\ F_\mu}\ \cdot\ 100\,\% \quad \approx \quad 100\,\% \quad + \quad \frac{b_\xi\ \cdot\ \mathcal{T}_\xi}{b_\mu\ \cdot\ F_\mu}\ \cdot\ 100\,\% \tag{16.18d}$$

The fraction on the right–hand side of Eq. (16.18d) becomes the *Percent Contribution* $Q\{\mathcal{T}_\xi\}$ of the term $\mathcal{T}_\xi(F_1, F_2, \ldots, F_n)$ of the regression model of the output D_μ if the capacities of all variables, i.e., ${F_1}^\star, {F_2}^\star, \ldots, {D_\mu}^\star$, are used on both sides of the equation (see also Eq. (16.13)). Therefore, Eq. (16.18d) can be written as follows:

$$\frac{{D_\mu}^\star}{(\partial D_\mu / \partial F_\mu)\ \cdot\ {F_\mu}^\star}\ \cdot\ 100\,\% \quad \approx \quad 100\,\% \quad + \quad Q\{\mathcal{T}_\xi\} \tag{16.18e}$$

Numerator and denominator of the fraction on the left–hand side of Eq. (16.18e) are identical because the numerator can be replaced by the product of the prime sensitivity $\partial D_\mu / \partial F_\mu$ with the capacity ${F_\mu}^\star$ of the primary load. Therefore, the fraction on the left–hand side of Eq. (16.18e) equals one. Then, Eq. (16.18e) can be simplified. We get:

$$100\,\% \quad \approx \quad 100\,\% \quad + \quad Q\{\mathcal{T}_\xi\} \tag{16.18f}$$

Similarly, the regression model of a load, i.e., Eq. (16.1a), can be simplified. Again, it is reasonable to assume that (i) the intercept term is negligible and (ii) only the primary output and one additional regression model term make significant contributions on the right–hand side of Eq. (16.1a) if assumptions (a) and (e) are taken into account. Then, the following approximation of the regression model of a load is obtained:

$$F_\mu \quad \approx \quad a_\mu \cdot D_\mu \quad + \quad a_\xi\ \cdot\ \mathcal{S}_\xi \tag{16.19a}$$

Now, after dividing both sides of Eq. (16.19a) by the product $a_\mu \cdot D_\mu$, we get:

$$\frac{F_\mu}{a_\mu\ \cdot\ D_\mu} \quad \approx \quad 1 \quad + \quad \frac{a_\xi\ \cdot\ \mathcal{S}_\xi}{a_\mu\ \cdot\ D_\mu} \tag{16.19b}$$

We also know that the regression model term a_μ is the partial derivative of the primary load F_μ with respect to the primary output D_μ. Then, we can write:

$$a_\mu \quad = \quad \frac{\partial\ F_\mu}{\partial\ D_\mu} \tag{16.19c}$$

Now, after using (i) the right–hand side of Eq. (16.19c) to replace the coefficient a_μ on the left–hand side of Eq. (16.19b) and (ii) multiplying both sides of the resulting equation with 100 %, we get:

$$\frac{F_\mu}{(\partial F_\mu / \partial D_\mu) \ \cdot \ D_\mu} \ \cdot \ 100\,\% \quad \approx \quad 100\,\% \quad + \quad \frac{a_\xi \ \cdot \ \mathcal{S}_\xi}{a_\mu \cdot D_\mu} \ \cdot \ 100\,\% \qquad (16.19d)$$

The last term on the right–hand side of Eq. (16.19d) becomes the percent contribution $P\{\mathcal{S}_\xi\}$ of the term $\mathcal{S}_\xi(D_1, D_2, \ldots, D_n)$ of the regression model of F_μ if the capacities of all variables, i.e., ${D_1}^\star, {D_2}^\star, \ldots, {F_\mu}^\star$, are used on both sides of the equation (see also Eq. (16.2)). Then, Eq. (16.19d) can be written as follows:

$$\frac{{F_\mu}^\star}{(\partial F_\mu / \partial D_\mu) \ \cdot \ {D_\mu}^\star} \ \cdot \ 100\,\% \quad \approx \quad 100\,\% \quad + \quad P\{\mathcal{S}_\xi\} \qquad (16.19e)$$

We also know that

$$(\partial F_\mu / \partial D_\mu) \quad = \quad 1 \ / \ (\partial D_\mu / \partial F_\mu) \qquad (16.19f)$$

Then, after replacing the partial derivative on the left–hand side of Eq. (16.19e) with the right–hand side of Eq. (16.19f), we get the following result for Eq. (16.19e):

$$\frac{(\partial D_\mu / \partial F_\mu) \ \cdot \ {F_\mu}^\star}{{D_\mu}^\star} \ \cdot \ 100\,\% \quad \approx \quad 100\,\% \quad + \quad P\{\mathcal{S}_\xi\} \qquad (16.19g)$$

Numerator and denominator of the fraction on the left–hand side of Eq. (16.19g) are identical because the denominator can be replaced by the product of the prime sensitivity $\partial D_\mu / \partial F_\mu$ with the capacity ${F_\mu}^\star$ of the primary load. Therefore, the fraction on the left–hand side of Eq. (16.19g) equals one. Then, Eq. (16.19g) can be simplified. We get:

$$100\,\% \quad \approx \quad 100\,\% \quad + \quad P\{\mathcal{S}_\xi\} \qquad (16.19h)$$

In the next step, after multiplying the left– and right–hand sides of Eq. (16.18f) with the left– and right–hand sides of Eq. (16.19h), we get:

$$(100\,\%)^2 \quad \approx \quad \Big[\ 100\,\% \ + \ Q\{\mathcal{T}_\xi\} \ \Big] \ \cdot \ \Big[\ 100\,\% \ + \ P\{\mathcal{S}_\xi\} \ \Big] \qquad (16.20)$$

In addition, after expanding the brackets on the right–hand side of Eq. (16.20), we get:

$$(100\,\%)^2 \ \approx \ (100\,\%)^2 \ + \ 100\,\% \cdot Q\{\mathcal{T}_\xi\} \ + \ 100\,\% \cdot P\{\mathcal{S}_\xi\} \ + \ Q\{\mathcal{T}_\xi\} \cdot P\{\mathcal{S}_\xi\} \qquad (16.21)$$

Equation (16.21) can be simplified further after (i) the square of 100 % is subtracted from both sides of the equation and (ii) the result is divided by 100 %. Then, we get

$$0 \quad \approx \quad Q\{\mathcal{T}_\xi\} \quad + \quad P\{\mathcal{S}_\xi\} \quad + \quad \frac{Q\{\mathcal{T}_\xi\} \ \cdot \ P\{\mathcal{S}_\xi\}}{100\,\%} \qquad (16.22)$$

Now, after subtracting $Q\{\mathcal{T}_\xi\}$ from both sides of Eq. (16.22) and observing that $P\{\mathcal{S}_\xi\}$ is a common multiplier of the last two terms on the right–hand side of Eq. (16.22), we get:

$$-Q\{\mathcal{T}_\xi\} \quad \approx \quad P\{\mathcal{S}_\xi\} \cdot \left[\, 1 \, + \, \frac{Q\{\mathcal{T}_\xi\}}{100\,\%} \, \right] \tag{16.23}$$

It is known from experience that the magnitude of the *Percent Contribution* for the majority of regression model terms of real–world balance data is $\leq 10\,\%$ if a balance has highly linear behavior and the metric is not computed for the term that is defined by the primary output or the primary load itself (see also assumption (e) that is listed in the first paragraph of this section). This observation can be described by the following inequality:

$$\mid Q\{\mathcal{T}_\xi\} \mid \quad \leq \quad 10\,\% \tag{16.24}$$

The absolute value of the *Percent Contribution* must be used on the left–hand side of the inequality above because the *Percent Contribution* is either a positive or negative quantity. Then, after using the above inequality to simplify the contents of the bracket on the right–hand side of Eq. (16.23), we get:

$$\left[\, 1 \, + \, \frac{Q\{\mathcal{T}_\xi\}}{100\,\%} \, \right] \quad \approx \quad 1 \, \pm \, \frac{10\,\%}{100\,\%} \quad \approx \quad 1 \, \pm \, 0.1 \quad \approx \quad 1 \tag{16.25}$$

Finally, after substituting the bracket on the right–hand side of Eq. (16.23) with the value of 1, i.e., with the approximation derived in Eq. (16.25), we get a direct relationship between the *Percent Contribution* of a term of the primary output difference and the *Percent Contribution* of the related term of the primary load:

$$\boxed{-Q\{\mathcal{T}_\xi\} \quad \approx \quad P\{\mathcal{S}_\xi\} \qquad (16.26)}$$

The final result given in Eq. (16.26) above confirms that the *Percent Contribution*s $Q\{\mathcal{T}_\xi\}$ and $P\{\mathcal{S}_\xi\}$ of related terms of the regression models of the output differences and loads are similar in magnitude but opposite in sign. This result is valid for the *Percent Contribution*s of most regression model terms of balance data as long as the absolute value of the *Percent Contribution* of a term is on the order of $10\,\%$ or less.

Appendix 17

Detection of Linear Dependencies

17.1 Introduction

It is critical that a multivariate regression model of strain–gage balance calibration data does not have linear dependencies between the chosen set of regression model terms. Only this characteristic guarantees the existence of a unique mapping between the given loads and electrical outputs of the balance that is needed for a reliable load prediction during a wind tunnel test.

A numerical technique called *Singular Value Decomposition* (SVD) may be used for the detection of linear dependencies in a multivariate regression model of balance calibration data (see also Ref. [66], pp. 51–63, Ref. [22], p. 5, and Ref. [23], p. 3). This technique examines characteristics of the vector space that is defined by the chosen terms of the regression model of the given balance calibration data. SVD determines a set of singular values for the chosen regression model terms. The minimum of this set has to be greater than a machine–precision–dependent threshold in order to guarantee that the chosen regression model does not have linear dependencies. Results of the *Singular Value Decomposition* of a regression model may also be used during a regression model search process to identify the *Permitted Math Model*. It is the largest regression model for the given balance calibration data set that will not lead to a singular solution of the related global regression analysis problem. Therefore, it is often used as an upper bound of the regression models that are tested during a regression model search process.

It is helpful for a better understanding of the benefits of the application of SVD if general characteristics of a regression model of balance calibration data are first reviewed. Afterwards, the calculation of the regression coefficients using global regression analysis is summarized. Then, the specific application of SVD to balance calibration data is discussed and the linear dependency test is defined. Finally, steps associated with the application of SVD during the identification of the *Permitted Math Model* are summarized.

17.2 Regression Model of Balance Calibration Data

Both the *Non–Iterative* and the *Iterative Method* use multivariate regression models of balance calibration data for the balance load prediction during a wind tunnel test. The author recommends to use SVD to test these regression models for the existence of unwanted linear dependencies before the global regression analysis itself is performed.

It is useful for both the discussion of SVD and the recommended linear dependency test to clearly identify dependent and independent variables of the regression models of the balance calibration data that the *Non–Iterative Method* and the *Iterative Method* apply. For example, the *Non–Iterative Method* directly fits load components of the balance as a function of the bridge outputs (App. 9). Consequently, the bridge outputs are the independent variables $X_1,\ X_2,\ \ldots$ of the regression model and the fitted load component is the dependent variable Y. The *Iterative Method*, on the other hand, fits the bridge outputs of the balance as a function of the load components and constructs a load iteration scheme from the results (App. 10). In that case, the load components are the independent variables $X_1,\ X_2,\ \ldots$ of the regression model and the bridge output is the dependent variable Y.

General characteristics of the regression model of balance calibration data are summarized in Eq. (17.1) below where symbols $c_0,\ c_1,\ c_2,\ \ldots$ are the coefficients of the regression model

Regression Model of Balance Calibration Data

$$Y = \underbrace{c_0 + c_1 \cdot X_1 + c_2 \cdot X_2 + \ldots + c_\omega \cdot X_1^2 + \ldots}_{\delta = \text{number of chosen regression model terms}} \tag{17.1}$$

$$Non-Iterative\ Method \implies X_1,\ X_2,\ \ldots \equiv \text{bridge outputs}\ ;\ Y \equiv \text{load}$$

$$Iterative\ Method \implies X_1,\ X_2,\ \ldots \equiv \text{loads}\ ;\ Y \equiv \text{bridge output}$$

and parameter δ describes the total number of chosen terms for the regression model of balance calibration data. The regression coefficients are obtained by applying global regression analysis to the balance calibration data. They describe the physical behavior of the balance within the limitations of the applied calibration load schedule.

It is helpful for the discussion of SVD and the linear dependency test to briefly review steps that are associated with the application of global regression analysis to balance calibration data. Therefore, a generic solution of the regression coefficients $c_0,\ c_1,\ c_2,\ \ldots$ of the dependent variable is developed in the next section.

17.3 Global Regression Analysis

The global regression analysis problem associated with the determination of the unknown coefficients of the chosen regression model terms of a dependent variable Y can be expressed in matrix format if row and column vectors are used to describe Eq. (17.1). An analyst may choose the intercept term and a subset of both linear and non–linear terms for the regression model of the dependent variable. Then, three vectors can be defined in Eqs. (17.2a), (17.2b), and (17.2c) below that may be used to describe the regression model of the dependent variable in matrix format.

$$\mathbf{A}_{1\times\delta} = \underbrace{\begin{bmatrix} 1 & X_1 & X_2 & \ldots & X_1^2 & \ldots \end{bmatrix}}_{\delta = \text{number of chosen regression model terms}} \tag{17.2a}$$

$$\mathbf{x}_{\delta\times 1} = \begin{bmatrix} c_0 \\ c_1 \\ c_2 \\ \vdots \\ c_\omega \\ \vdots \end{bmatrix} \tag{17.2b}$$

$$\mathbf{R}_{1\times 1} = Y \tag{17.2c}$$

Now, after interpreting the dependent variable Y as a vector with a single component, the regression model given in Eq. (17.1) above can be described by the following equivalent matrix equation where column vector $\mathbf{x}$ has the coefficients of the regression model of the

$$\mathbf{A}_{1\times\delta} \cdot \mathbf{x}_{\delta\times 1} = \mathbf{R}_{1\times 1} \tag{17.3}$$

dependent variable. Furthermore, it is assumed that the given balance calibration data set consists of a total of p data points. The information contained in each data point has to be modeled in the least squares sense by using the chosen regression model that is defined in Eq. (17.3) above. Consequently, matrix $\mathbf{A}$ and vector $\mathbf{R}$ have to be extended from a single data point to all data points. Then, the following relationships are obtained that describe the entire balance calibration data set in matrix format:

$$\mathbf{A}_{1\times\delta} \Longrightarrow \mathbf{A}_{p\times\delta} = \begin{bmatrix} 1 & X_1(1) & X_2(1) & \dots & X_1^2(1) & \dots \\ \vdots & \vdots & \vdots & \vdots & \vdots & \vdots \\ 1 & X_1(\nu) & X_2(\nu) & \dots & X_1^2(\nu) & \dots \\ \vdots & \vdots & \vdots & \vdots & \vdots & \vdots \\ 1 & X_1(p) & X_2(p) & \dots & X_1^2(p) & \dots \end{bmatrix} \tag{17.4a}$$

$$\mathbf{R}_{1\times 1} \Longrightarrow \mathbf{R}_{p\times 1} = \begin{bmatrix} Y(1) \\ \vdots \\ Y(\nu) \\ \vdots \\ Y(p) \end{bmatrix} \tag{17.4b}$$

The global regression analysis problem of the given balance calibration data can be expressed in matrix format after introducing the two equations above as extensions of the corresponding vectors in Eq. (17.3). Then, the following description of the global regression analysis problem is obtained:

Global Regression Analysis Problem

$$\mathbf{A}_{p\times\delta} \cdot \mathbf{x}_{\delta\times 1} = \mathbf{R}_{p\times 1} \tag{17.5}$$

The regression coefficient set contained in vector $\mathbf{x}$ above is determined by solving the global regression analysis problem that Eq. (17.5) describes. This relationship can only have a unique, i.e., non–singular solution if the column vectors of matrix $\mathbf{A}$ are linearly independent. It will be shown in the next section how SVD is used to test if matrix $\mathbf{A}$ fulfills the necessary condition that its column vectors are linearly independent. Only in that case will it be possible to successfully compute the inverse of square matrix $\mathbf{A^T A}$ that is needed for the calculation of the regression coefficients.

17.4 Singular Value Decomposition

The application of SVD to a regression model of balance calibration data can more easily be understood if matrix $\mathbf{A}$ of Eq. (17.4a) is described with a set $\mathbf{A}_0$, $\mathbf{A}_1$, ... of column vectors. The resulting alternate description of matrix $\mathbf{A}$ is given in Eq. (17.6a) below

$$\mathbf{A}_{p\times\delta} \;=\; \mathbf{A}\Big\{X_1(1)\;,\;\ldots\;,\;X_n(p)\Big\} \;=\; \Big[\;\mathbf{A}_0\quad\mathbf{A}_1\quad\ldots\quad\mathbf{A}_k\quad\ldots\quad\mathbf{A}_{\delta-1}\;\Big] \tag{17.6a}$$

where δ equals the number of chosen regression model terms and $\mathbf{A}_k$ is defined as follows:

$$\mathbf{A}_k \;=\; \begin{bmatrix} A_k(1) \\ \vdots \\ A_k(\nu) \\ \vdots \\ A_k(p) \end{bmatrix} \quad ; \quad 0 \;\le\; k \;\le\; \delta - 1 \tag{17.6b}$$

Then, the four column vectors shown in Eq. (17.4a) can be described as follows:

$$\mathbf{A}_0 \;=\; \begin{bmatrix} 1 \\ \vdots \\ 1 \\ \vdots \\ 1 \end{bmatrix} \;;\; \mathbf{A}_1 \;=\; \begin{bmatrix} X_1(1) \\ \vdots \\ X_1(\nu) \\ \vdots \\ X_1(p) \end{bmatrix} \;;\; \mathbf{A}_2 \;=\; \begin{bmatrix} X_2(1) \\ \vdots \\ X_2(\nu) \\ \vdots \\ X_2(p) \end{bmatrix} \;;\; \mathbf{A}_\omega \;=\; \begin{bmatrix} X_1^2(1) \\ \vdots \\ X_1^2(\nu) \\ \vdots \\ X_1^2(p) \end{bmatrix} \tag{17.7}$$

In theory, linear dependencies between the regression model terms can be identified if SVD is applied to matrix $\mathbf{A}$ (Ref. [66], p. 59–63). However, more reliable results can be obtained with real–world data if SVD is applied to an auxiliary matrix $\mathbf{A}^\star$. It is obtained after transforming the independent variables that define matrix $\mathbf{A}$. The transformation is specified in Eq. (17.8a) below. It sets an independent variable X_i temporarily to zero if its magnitude is below the threshold Υ_i.[†] Two threshold choices are listed in Eq. (17.8b). Each threshold is the product of an empirical constant[‡] with the capacity Γ_i of the independent variable. The more conservative threshold is the recommended default choice.

Transformation of Independent Variables

$$X_i^\star(\nu) \;=\; \begin{cases} X_i(\nu) & \text{if} \quad |X_i(\nu)| \;>\; \Upsilon_i \\ 0 & \text{if} \quad |X_i(\nu)| \;\le\; \Upsilon_i \end{cases} \quad ; \quad \begin{matrix} 1 \le i \le n \\ 1 \le \nu \le p \end{matrix} \tag{17.8a}$$

where

$$\Upsilon_i \;=\; \begin{cases} 0.1 \times \Gamma_i \implies \textit{less conservative} \\ 0.2 \times \Gamma_i \implies \textit{more conservative (recommended choice)} \end{cases} \tag{17.8b}$$

[†] Threshold Υ_i is also called Math Model Selection Threshold. It is the first threshold that a regression model search process needs. The second threshold is defined in Eq. (17.11e).

[‡] Empirical constants 0.1 and 0.2 were chosen so that supported cross–product terms are reliably identified during the application of SVD.

The transformed matrix $\mathbf{A}^\star$ is obtained by simply using the transformed variable values $X_1^\star(1)$, ..., $X_n^\star(p)$ instead of the original variable values $X_1(1)$, ..., $X_n(p)$ for the calculation of matrix $\mathbf{A}$. Then, the transformation can be summarized as follows:

$$\mathbf{A}^\star \quad = \quad \mathbf{A}\Big\{X_1^\star(1)\ ,\ \ldots\ ,\ X_n^\star(p)\Big\} \tag{17.9}$$

Finally, singular values of the transformed matrix $\mathbf{A}^\star$ may be computed by using any standard SVD algorithm that is described in the literature (see, e.g., Ref. [66], pp. 51–63). The resulting singular values $s_1\ \ldots\ s_\delta$ are summarized in Eq. (17.10) below.

$$\mathbf{A}^\star \implies \begin{array}{c}\textit{Singular Value}\\ \textit{Decomposition}\end{array} \implies \underbrace{s_1\ ,\ s_2\ ,\ \ldots\ ,\ s_k\ ,\ \ldots\ ,\ s_\delta}_{\textit{singular values of regression model}} \tag{17.10}$$

The minimum of the set of singular values of the transformed matrix $\mathbf{A}^\star$ above may be used as input for a test that assesses linear dependencies. This test is described in detail in the next section.

17.5 Linear Dependency Test

The temporary use of transformed instead of original independent variable values was recommended in the previous section in order to make results of the application of SVD to the chosen regression model term combination more reliable. The minimum of the resulting singular value set may be used as a test metric for the definition of a linear dependency test. The test itself is summarized in Eqs. (17.11a) to (17.11e) below.

Linear Dependency Test ($\Phi \equiv$ Test Metric)

$$\Phi \ = \ MIN\left[\underbrace{s_1\ ,\ s_2\ ,\ \ldots\ ,\ s_k\ ,\ \ldots\ ,\ s_\delta}_{\textit{singular values of regression model}}\right] \tag{17.11a}$$

$$\Phi \ \geq \ \Lambda \implies \textit{negligible linear dependencies exist} \tag{17.11b}$$

$$\Phi \ < \ \Lambda \implies \textit{unwanted linear dependencies exist} \tag{17.11c}$$

$$\Phi \ = \ 0 \implies \textit{column vectors are linear dependent} \tag{17.11d}$$

where

$$\Lambda \ = \ 100 \cdot \varepsilon \quad \textit{and} \quad \varepsilon \ \equiv \ \textit{relative machine precision}^\dagger \tag{17.11e}$$

†Upper bound on the relative error due to rounding in floating point arithmetic (see also p. 265 f.).

The test compares the minimum of the singular values with a threshold Λ that is machine–precision–dependent (see Eq. (17.11e)). It is two orders of magnitude above the

relative machine precision. The relative machine precision may be determined by using the *Forsythe, Malcolm, Moler* algorithm (see App. 11, p. 265f.). Three different results of the linear dependency test are possible. They need to be discussed in more detail.

First, the test metric could exceed the threshold (see Eq. (17.11*b*)). This result indicates that the chosen regression model has negligible linear dependencies. Consequently, the solution of the global regression analysis problem is expected to be non–singular. It is still possible that the regression model has unwanted near–linear dependencies. Therefore, the regression model must also be screened for near–linear dependencies before it is applied to balance calibration data (see App. 18 for the description of a near–linear dependency test that may be applied to the chosen regression model).

It is also possible that the test metric is less than the threshold (see Eq. (17.11*c*)). This result indicates that the chosen regression model has linear dependencies. It must not be used for the analysis of the balance calibration data unless terms responsible for the linear dependencies are removed.

Finally, the test metric could equal zero (see Eq. (17.11*d*)). This case is observed whenever (i) independent variable values are explicitly set to zero after applying Eq. (17.8*a*) and (ii) linear dependencies exist. Again, this result indicates that the regression model has linear dependencies. It must not be used for the analysis of the balance calibration data unless terms responsible for the linear dependencies are removed.

17.6 Regression Model Search Process

A regression model search process can be defined that uses the result of the linear dependency test as the term selection criterion. The search process identifies the largest regression model term combination that a given balance calibration data set supports (see also App. 19). This regression model is called *Permitted Math Model*. The step–by–step identification of terms of the *Permitted Math Model* requires the application of the linear dependency test each time a new term is added to an existing linearly independent term combination. This new term is only permanently included in the existing term combination if the test metric, i.e., the minimum of the singular values, is above the machine–precision–dependent threshold that is defined in Eq. (17.11*e*). Experience showed that the search process should start from lower to higher order terms during the step–by–step determination of terms of the *Permitted Math Model*. It may also be an advantage to exclusively assess hierarchical term combinations during the regression model search process (see related comments in Ref. [20]).

Appendix 18

Detection of Near–Linear Dependencies

18.1 Introduction

It is important that a multivariate regression model of strain–gage balance calibration data does not have unwanted near–linear dependencies between the chosen regression model terms. This characteristic guarantees the existence of a unique mapping between loads and electrical outputs of the balance that results in a reliable load prediction during a wind tunnel test.

Objective test metrics may be used to identify and avoid unwanted near–linear dependencies in a multivariate regression model of balance calibration data. The author recommends to use the maximum of the *Variance Inflation Factor* set of the regression model as a test metric for the detection of near–linear dependencies (see, e.g., the description of *Method 2* in Ref. [20]; *Method 2* is identical with the approach that is recommended in this appendix). This maximum is compared with empirical thresholds in order to assess the level of near–linear dependencies. The application of the *Variance Inflation Factor (VIF)* as a test metric has two major advantages: (i) the metric can easily be computed for a regression model of balance calibration data; (ii) the metric may be used as input for a regression model search process that needs to avoid regression models with unwanted near–linear dependencies during the search.

Basic characteristics of a multivariate regression model of balance calibration data are reviewed in the next section. Then, the application of global regression analysis to balance calibration data is summarized. These explanations are needed for a better understanding of the determination of the *Variance Inflation Factor* set of a regression model and the proposed near–linear dependency test. Finally, it is indicated how the test could be implemented in a regression model search process.

18.2 Regression Model of Balance Calibration Data

Both the *Non–Iterative* and the *Iterative Method* use multivariate regression models of balance calibration data for the balance load prediction during a wind tunnel test. These regression models should be tested for the existence of unwanted near–linear dependencies so that a reliable balance load prediction can be guaranteed.

It is useful for the discussion of both the near–linear dependency test and the *Variance Inflation Factor* to identify independent and dependent variable sets of the balance calibration data that the *Non–Iterative Method* and the *Iterative Method* use for the data analysis. The *Non–Iterative Method*, for example, directly fits load components of the balance as a function of the electrical outputs of the balance bridges (see App. 9). Consequently, the load component is the dependent variable Y and the electrical outputs of the bridges are the independent variables $X_1,\ X_2,\ X_3,\ \ldots$ of the regression model. The *Iterative Method*, on the other hand, first fits electrical outputs of the balance bridges as a function of the load components. Afterwards, a load iteration equation is constructed from the regression coefficients of the outputs so that balance loads can be predicted from the outputs during a wind tunnel test (see App. 10). Therefore, the *Iterative Method* uses the electrical output as the dependent variable Y and the load components as the independent

variables $X_1,\ X_2,\ X_3,\ \ldots$ of the regression model. These universal characteristics of the regression models of balance calibration data are summarized in Eq. (18.1) below where

Regression Model of Balance Calibration Data

$$Y = \underbrace{c_0 + c_1 \cdot X_1 + c_2 \cdot X_2 + \ldots + c_\omega \cdot X_1^2 + \ldots}_{\delta = number\ of\ chosen\ terms} \qquad (18.1)$$

$$Non-Iterative\ Method \implies X_1,\ X_2,\ \ldots \equiv bridge\ outputs\ ;\ Y \equiv load$$

$$Iterative\ Method \implies X_1,\ X_2,\ \ldots \equiv loads\ ;\ Y \equiv bridge\ output$$

symbols $c_0,\ c_1,\ c_2,\ \ldots$ are the coefficients of the regression model and parameter δ describes the total number of regression model terms. The regression coefficients are obtained after applying global regression analysis to a balance calibration data set that is assumed to describe the physical behavior of the balance.

It is useful for both the discussion of the calculation of the *Variance Inflation Factor* and the definition of the near–linear dependency test to briefly review steps that are associated with the application of global regression analysis to balance calibration data. Therefore, a generic solution of the regression coefficient set $c_0,\ c_1,\ c_2,\ \ldots$ is developed in the next section.

18.3 Global Regression Analysis

The global regression analysis problem associated with the determination of the coefficients of the regression model terms of a dependent variable can be expressed in matrix format if row and column vectors are used to describe Eq. (18.1) above. It is assumed, for example, that an analyst chooses the intercept term and a subset of both linear and non–linear terms for the regression model of the dependent variable. Then, the following three vectors can be defined that may be used to obtain a description of the regression model of the dependent variable in matrix format:

$$\mathbf{A}_{1\times\delta} = \underbrace{\begin{bmatrix} 1 & X_1 & X_2 & \ldots & X_1^2 & \ldots \end{bmatrix}}_{\delta = number\ of\ chosen\ regression\ model\ terms} \qquad (18.2a)$$

$$\mathbf{x}_{\delta\times 1} = \begin{bmatrix} c_0 \\ c_1 \\ c_2 \\ \vdots \\ c_\omega \\ \vdots \end{bmatrix} \qquad (18.2b)$$

$$\mathbf{R}_{1\times 1} = Y \qquad (18.2c)$$

Now, after interpreting the dependent variable itself as a vector with a single component, the regression model defined in Eq. (18.1) can be described by the following equivalent matrix equation where column vector $\mathbf{x}$ has the coefficients of the regression model of the

$$\mathbf{A}_{1\times\delta} \cdot \mathbf{x}_{\delta\times 1} = \mathbf{R}_{1\times 1} \tag{18.3}$$

dependent variable. Furthermore, it is assumed that the given balance calibration data set consists of a total of p data points. The information contained in each data point is modeled in the least squares sense by using the chosen regression model that is defined in Eq. (18.3). Consequently, matrix $\mathbf{A}$ and vector $\mathbf{R}$ have to be extended from a single data point to all data points in order to describe the entire balance calibration data set. Then, we get the following relationships between the independent and dependent variables:

$$\mathbf{A}_{1\times\delta} \Longrightarrow \mathbf{A}_{p\times\delta} = \begin{bmatrix} 1 & X_1(1) & X_2(1) & \dots & X_1^2(1) & \dots \\ \vdots & \vdots & \vdots & \vdots & \vdots & \vdots \\ 1 & X_1(\nu) & X_2(\nu) & \dots & X_1^2(\nu) & \dots \\ \vdots & \vdots & \vdots & \vdots & \vdots & \vdots \\ 1 & X_1(p) & X_2(p) & \dots & X_1^2(p) & \dots \end{bmatrix} \tag{18.4a}$$

$$\mathbf{R}_{1\times 1} \Longrightarrow \mathbf{R}_{p\times 1} = \begin{bmatrix} Y(1) \\ \vdots \\ Y(\nu) \\ \vdots \\ Y(p) \end{bmatrix} \tag{18.4b}$$

Finally, after introducing the two equations above as extensions in Eq. (18.3), the global regression analysis problem of the given balance calibration data can be summarized by the matrix equation that is defined Eq. (18.5) below. Column vector $\mathbf{x}$ has the regression

Global Regression Analysis Problem

$$\mathbf{A}_{p\times\delta} \cdot \mathbf{x}_{\delta\times 1} = \mathbf{R}_{p\times 1} \tag{18.5}$$

coefficients. They are obtained after solving the regression analysis problem that Eq. (18.5) defines. The solution is an application of the *Moore–Penrose Inverse* (see Ref. [64], pp. 35–39, and Refs. [77], [78]). It is described by the following matrix equation:

Solution of Global Regression Analysis Problem

$$\mathbf{x}_{\delta\times 1} \;=\; \left[\; \mathbf{A^T}\cdot\mathbf{A}\;\right]^{-1}_{\delta\times\delta}\cdot\left[\;\mathbf{A^T}\cdot\mathbf{R}\;\right]_{\delta\times 1} \qquad (18.6)$$

Now, the analytical relationship between the independent and dependent variables of the given balance calibration data set is known as (i) the regression model of the dependent variable is defined in Eq. (18.1) and (ii) the coefficients $c_0,\ c_1,\ c_2,\ \ldots$ of the chosen terms are given by the right–hand side of Eq. (18.6). However, it is still possible that the chosen regression model has hidden near–linear dependencies that will negatively influence the reliability of the load prediction during a wind tunnel test. They can be detected by using the *Variance Inflation Factor* set of the chosen regression model. The determination of the *Variance Inflation Factor* set is closely related to the description of the global regression analysis problem of the balance calibration data. This connection is described in more detail in the next section.

18.4 Variance Inflation Factor Set

The description of the calculation of the *Variance Inflation Factor* set closely follows steps that are described in the literature (see, e.g., Ref. [68], pp. 331–335). In principle, the *Variance Inflation Factor* set is derived from the original global regression analysis problem. First, matrix $\mathbf{A}$ of the global regression analysis problem is expressed by using a set of column vectors. Then, Eq. (18.4a) can be described by Eq. (18.7a) below

$$\mathbf{A}_{p\times\delta} \;=\; \underbrace{\left[\;\mathbf{A}_0\quad\mathbf{A}_1\quad\mathbf{A}_2\quad\ldots\quad\mathbf{A}_k\quad\ldots\quad\mathbf{A}_{\delta-1}\;\right]}_{\textit{intercept is assumed to be a chosen term}} \qquad (18.7a)$$

where the individual column vectors are defined by the following relationship:

$$\mathbf{A}_k \;=\; \begin{bmatrix} A_{k,1} \\ \vdots \\ A_{k,\nu} \\ \vdots \\ A_{k,p} \end{bmatrix} \quad ; \quad 0 \;\le\; k \;\le\; \delta-1 \quad ; \quad 1 \;\le\; \nu \;\le\; p \qquad (18.7b)$$

The intercept term is a constant. It is <u>not</u> a function of the independent variable set $X_1,\ X_2,\ X_3,\ \ldots$ that is used to construct the regression model of the data. Therefore, the intercept term is excluded from the determination of the *Variance Inflation Factors*. Then, an alternate matrix $\mathbf{J}$ can be defined that omits the column vector $\mathbf{A}_0$ of the intercept terms. This alternate matrix is used for the determination of the *Variance Inflation Factors* of the chosen regression model. Matrix $\mathbf{J}$ can be described by the following relationship

$$\mathbf{J}_{p\times\eta} \;=\; \underbrace{\left[\;\mathbf{J}_1\quad\mathbf{J}_2\quad\ldots\quad\mathbf{J}_k\quad\ldots\quad\mathbf{J}_\eta\;\right]}_{\textit{intercept is omitted (even if chosen)}} \qquad (18.8a)$$

where the number η of column vectors of $\mathbf{J}$ is defined in Eq. (18.8b) below. By design,

$$\eta \;=\; \begin{cases} \delta - 1 & \ldots \text{ if intercept term is included in the regression model} \\ \delta & \ldots \text{ if intercept term is not used in the regression model} \end{cases} \tag{18.8b}$$

vector $\mathbf{J}_k$ equals column vector $\mathbf{A}_k$. Then, vector $\mathbf{J}_k$ can be described by Eq. (18.8c) below.

$$\mathbf{J}_k \;=\; \mathbf{A}_k \;=\; \begin{bmatrix} A_{k,1} \\ \vdots \\ A_{k,\nu} \\ \vdots \\ A_{k,p} \end{bmatrix} \quad ; \quad 1 \;\leq\; k \;\leq\; \eta \quad ; \quad 1 \;\leq\; \nu \;\leq\; p \tag{18.8c}$$

In the next step, the numerical values of the column vectors $\mathbf{J}_k$ need to be centered and scaled before the *Variance Inflation Factor* set can be computed. The centering of the values is done by subtracting the arithmetic mean of each column vector from the associated column vector values. Then, the centered column vectors $\mathbf{J}'_k$ can be defined by Eqs. (18.9a) & (18.9b) below. Now, unit scaling needs to be applied to the centered

Centered Column Vector

$$\mathbf{J}'_k \;=\; \begin{bmatrix} J'_{k,1} \\ \vdots \\ J'_{k,\nu} \\ \vdots \\ J'_{k,p} \end{bmatrix} \quad ; \quad 1 \;\leq\; k \;\leq\; \eta \tag{18.9a}$$

where

$$J'_{k,\nu} \;=\; A_{k,\nu} \;-\; \frac{1}{p} \sum_{\xi=1}^{p} A_{k,\xi} \quad ; \quad 1 \;\leq\; \nu \;\leq\; p \tag{18.9b}$$

column vector values that are described in Eq. (18.9a). Therefore, each centered value is divided by the square root of the sum of squares of the centered values of each column vector. The resulting centered & scaled vectors are given in Eqs. (18.10a) & (18.10b) below.

Centered & Scaled Column Vector

$$\mathbf{J}''_k \;=\; \begin{bmatrix} J''_{k,1} \\ \vdots \\ J''_{k,\nu} \\ \vdots \\ J''_{k,p} \end{bmatrix} \quad ; \quad 1 \;\leq\; k \;\leq\; \eta \qquad (18.10a)$$

where

$$J''_{k,\nu} \;=\; \frac{J'_{k,\nu}}{\sqrt{\sum_{\xi=1}^{p} \left\{ J'_{k,\xi} \right\}^2}} \quad ; \quad 1 \;\leq\; \nu \;\leq\; p \qquad (18.10b)$$

All centered & scaled column vectors $\mathbf{J}''_k$ are known at this point. These column vectors can be assembled in an auxiliary rectangular matrix $\mathbf{J}''$ that is defined in Eq. (18.11) below.

$$\mathbf{J''}_{p\times\eta} \;=\; \underbrace{\left[\;\; \mathbf{J}''_1 \quad \ldots \quad \mathbf{J}''_k \quad \ldots \quad \mathbf{J}''_\eta \;\; \right]}_{centered\ \&\ scaled\ column\ vectors} \qquad (18.11)$$

Now, the correlation matrix Ψ of the regression model terms of the dependent variable can be computed. It is a square matrix that is defined as the product of the transpose of rectangular matrix $\mathbf{J}''$ with itself. The resulting matrix is shown in Eq. (18.12) below.

Correlation Matrix of Regression Model Terms

$$\Psi_{\,\eta\times\eta} \;=\; \mathbf{J''}^{\,\mathbf{T}} \;\cdot\; \mathbf{J}'' \qquad (18.12)$$

In the next step, the inverse of the correlation matrix Ψ needs to be computed in order to obtain the *Variance Inflation Factor* set of the chosen regression model. This inverse matrix and its coefficients are described in Eq. (18.13) below.

Inverse of Correlation Matrix

$$\mathbf{E}_{\eta\times\eta} \;=\; \{\,\Psi\,\}^{-1} \;=\; \begin{bmatrix} E_{1,1} & E_{1,2} & \dots & E_{1,\eta} \\ \vdots & \vdots & \vdots & \vdots \\ E_{k,1} & E_{k,2} & \dots & E_{k,\eta} \\ \vdots & \vdots & \vdots & \vdots \\ E_{\eta,1} & E_{\eta,2} & \dots & E_{\eta,\eta} \end{bmatrix} \qquad (18.13)$$

Finally, the *Variance Inflation Factors* of the chosen regression model terms can be identified. They are the coefficients $E_{1,1}\,,\; E_{2,2}\,,\; \ldots,\; E_{\eta,\eta}$ on the principal diagonal of the inverse of the correlation matrix. This conclusion is summarized in Eq. (18.14) below.

Variance Inflation Factor Set

$$\{VIF\}_k \;\equiv\; E_{k,k} \quad ; \quad 1 \;\leq\; k \;\leq\; \eta \qquad (18.14)$$

The maximum of the *Variance Inflation Factor* set of the chosen regression model may be used as a test metric for the assessment of near–linear dependencies between regression model terms. This metric is simply compared with either a literature recommended or an empirical threshold. Details of the proposed test are described in the next section.

18.5 Near-Linear Dependency Test

The determination of the *Variance Inflation Factor* set of the regression model terms was discussed in the previous section. The set's maximum may be used to test if unwanted near–linear dependencies exist in the regression model. The test is defined as follows:

Near–Linear Dependency Test ($\Phi \equiv$ Test Metric)

$$\Phi \;=\; MAX\left[\; \{VIF\}_1 \;,\; \ldots \;,\; \{VIF\}_\eta \;\right] \qquad (18.15a)$$

$$\Phi \;<\; 10 \;\Longrightarrow\; \textit{negligible dependencies} \qquad (18.15b)$$

$$10 \;\leq\; \Phi \;\leq\; 20 \;\Longrightarrow\; \textit{moderate dependencies} \qquad (18.15c)$$

$$20 \;<\; \Phi \;\leq\; 50 \;\Longrightarrow\; \textit{moderate to severe dependencies} \qquad (18.15d)$$

$$\Phi \;>\; 50 \;\Longrightarrow\; \textit{severe to massive dependencies} \qquad (18.15e)$$

In principle, the suggested near–linear dependency test compares the maximum of the *Variance Inflation Factor* set with an empirical threshold. Four different cases are distinguished in the test's definition above.

The first case assumes that the observed test metric is below the threshold of 10 (threshold is taken from Ref. [68], p. 334). This test result means that near–linear dependencies are negligible or nonexistent.

The second case assumes that the test metric is between the values of 10 and 20. This situation is often observed for regression models of data sets that come from balances with bi–directional output characteristics (see the discussion of this issue in App. 7). In this case, near–linear dependencies can be described as moderate. They are not expected to negatively influence the load prediction reliability during a wind tunnel test.

The third case assumes that the test metric is between the values of 20 and 50. This result means that the regression model of the balance calibration data may have moderate to severe near–linear dependencies. Now, an analyst's subject–matter knowledge must be applied in order to decide if the detected level of near–linear dependency can be tolerated or if regression model terms need to be removed.

The fourth case assumes that the test metric exceeds the value of 50. In that case, the regression model of the given balance calibration data has severe to massive near–linear dependencies. The regression model must not be used for the load prediction. Instead, regression model terms need to be removed in order to lower the test metric to a value that is below the threshold of 50. Alternatively, it may be necessary to modify or extend the original calibration load schedule of the balance until acceptable values of the test metric can be obtained.

18.6 Regression Model Search Process

An analyst may be forced to remove terms from a regression model if the maximum of its *Variance Inflation Factor* set exceeds the threshold of 50. Then, it is often observed that several *Variance Inflation Factors* are above the threshold. Unfortunately, it is not always obvious which term causes the unwanted near–linear dependencies. Consequently, an analyst's subject–matter knowledge in combination with a trial–and–error approach may have to be used in order to identify the term that will lower the maximum of the *Variance Inflation Factor* set after its removal from the regression model.

In theory, the near–linear dependency test defined in the previous section can be integrated in an automated regression model search process that uses either forward addition or backward elimination for the selection of regression model terms of balance calibration data. Then, unwanted near–linear dependencies can directly be avoided during the model building process if only models with negligible or moderate near–linear dependencies are examined during the term selection. This approach was implemented in the two regression model search algorithms that NASA's BALFIT software tool supports (see, e.g., App. 19 and Refs. [20] and [21] for more details).

Appendix 19

Regression Model Search Algorithm

19.1 Introduction

The author concluded during the development of a software tool for the analysis of strain–gage balance calibration data that it is an advantage to use an analyst's subject–matter knowledge in combination with objective metrics from linear algebra & statistics for the selection of the regression model of balance calibration data. This approach makes sure that the final regression model captures important hidden characteristics of the data that result from both the design of the balance and the chosen calibration load schedule. In addition, unwanted overfitting of calibration data is prevented. Consequently, highly reliable balance load predictions can be obtained from the regression models that work well within limitations of the given balance design and calibration load schedule.

In principle, an analyst's subject–matter knowledge is needed for the selection of types of regression model terms, i.e., function classes, that best model known characteristics of the chosen balance. Linear terms, quadratic terms, and cross–product terms are typically selected to model data of single–piece balances. Absolute value terms may have to be included if a data set of a Task/Able balance is analyzed. This specific balance design is known to have bi–directional outputs as the prime sensitivity of four of its six bridges depends on the sign of the corresponding primary load component (see also App. 7).

An analyst's knowledge may also be used to select individual regression model terms that support known characteristics of the calibration load schedule itself. However, this process can be very time consuming. In addition, its successful application highly depends on an analyst's ability to interpret loads and load combinations that were applied during the calibration. Alternatively, it is possible to construct a regression model search algorithm that uses metrics from linear algebra and statistics for the selection of individual regression model terms. This approach has the advantage that the selection of individual terms no longer depends on an analyst's ability to interpret a given calibration load schedule.

The author developed two regression model search algorithms over the years that are sometimes applied to multivariate strain–gage balance calibration data sets at the NASA Ames Balance Calibration Laboratory. Key elements of the first search algorithm are described in great detail in the literature (see, e.g., Ref. [20]). The second search algorithm is less complex. It can more easily be implemented in a data analysis tool (see Ref. [21]). Therefore, it was decided to include a description of the second search algorithm in the current document. Then, the reader gets a better understanding of basic ideas that make a term selection algorithm possible.

The second search algorithm was obtained after simplifying some parts of the first search algorithm. Important elements of the second search algorithm are reviewed in the next section.

19.2 Description of Second Search Algorithm

The second search algorithm was derived from the more complex first algorithm that was originally developed for the NASA Ames Balance Calibration Laboratory (see Refs. [20], [22], [23], [27] for details about the original algorithm). The second algorithm,

like the first algorithm, can be used to assemble either a regression model of a load component (*Non–Iterative Method*) or a regression model of an electrical output (*Iterative Method*). The second algorithm also uses many of the statistical metrics and constraints that the first algorithm applies (see Ref. [30] for a general discussion of metrics that may be used to evaluate a regression model of experimental data). However, these metrics and constraints are applied differently in order to reduce the total number of numerical operations that have to be performed during the regression model search. In addition, the second algorithm omits the search metric minimization that the first algorithm performs (see Ref. [27] for a discussion of a search metric minimization).

The flowchart in Fig. 19–1 on p. 374 of the current document summarizes basic elements of the second search algorithm. The search starts by first selecting a combination of math term groups (function classes) that help define a hypothetical upper limit of the so–called *Permitted Math Model* (see *Part 1* in Fig. 19–1). This math model is defined as the largest regression model that leads to a non–singular solution of the least squares fit of the data. In general, an analyst should select the math term group combination by taking design characteristics of the given balance into account. The chosen combination may consist, for example, of linear terms, cross–product terms, quadratic terms, and absolute value terms if (i) a data set of a balance with bi–directional outputs is processed and (ii) pairs of load components were loaded simultaneously during the balance calibration. Math term group choices are listed in App. 9 (Table 9–1) for the *Non–Iterative Method* and App. 10 (Table 10–1) for the *Iterative Method* that are suitable for the analysis of strain–gage balance calibration data.

Not every term of the chosen term group combination may be supported by the given balance calibration data set. Consequently, an upper bound of the *Permitted Math Model* needs to be determined so that only non–singular least squares solutions of the tested regression models are examined during the search (see *Part 2* in Fig. 19–1). This requirement means that the chosen regression model terms must not result in linearly dependent regressors. Therefore, a numerical technique called *Singular Value Decomposition* (SVD) is applied whenever a new term is added to the *Permitted Math Model* (see App. 17 for more details). Lower order terms should be added to the regression model before higher order terms. In addition, a tested term should only be retained in the *Permitted Math Model* if it is not resulting in linearly dependent regressors. The final *Permitted Math Model* is known after the successful completion of the SVD process. It defines the upper bound of all math models that the algorithm can evaluate during the regression model search.

In the next step, a search constraint is applied in order to avoid near–linear dependencies in the final regression model (see *Part 3* in Fig. 19–1). The constraint uses the *Variance Inflation Factor* (VIF) as a test metric. The constraint expects the largest VIF of the regression model terms to be less than an empirical threshold (see also the related discussion in App. 18). A threshold value of 10 is recommended in the literature for the test (see, e.g., Ref. [68], p. 111). In addition, experience showed that a threshold value of 20 is acceptable for the evaluation of regression models of data from a balance with bi–directional bridge outputs. Threshold values between 20 and 50 are in a gray zone and should only be used with extreme caution. A threshold value beyond 50 must be avoided because it would make the dependency test unreliable.

The search constraint is iteratively enforced. At first, VIFs of all terms of the *Permitted Math Model* are computed (Step 1). Then, the term with the largest VIF is removed if

its VIF exceeds the chosen empirical threshold (Step 2). Now, the VIFs of all terms of the updated regression model are computed (Step 3). Step 2 and Step 3 are repeated until the largest VIF of the remaining model is below the chosen threshold (Step 4). The remaining model is the first estimate of the final regression model (Step 5). The author recommends to make the first estimate hierarchical by adding missing lower order terms (see *Part 4* in Fig. 19–1). The enforcement of the *Hierarchy Rule* guarantees that the final regression model will correctly describe hidden offsets in the independent variables (see Ref. [20] for a detailed discussion of the *Hierarchy Rule*).

Finally, the p–values of the t–statistic of all regression coefficients of the hierarchical first estimate of the final regression model are computed (see *Part 5* in Fig. 19–1). The calculation of the p–values of the coefficients helps identify and remove statistically insignificant terms. A term is removed from the first estimate of the final regression model if its p–value exceeds the literature recommended threshold of 0.001 (taken from Ref. [68], p. 85, first paragraph; some analysts prefer the more conservative threshold of 0.0001). The p–values are processed by examining higher order terms before lower order terms. In addition, a term is only removed if the remaining regression model remains hierarchical. The resulting regression model is the final model that the second search algorithm suggests to use for the regression analysis of the given balance calibration data.

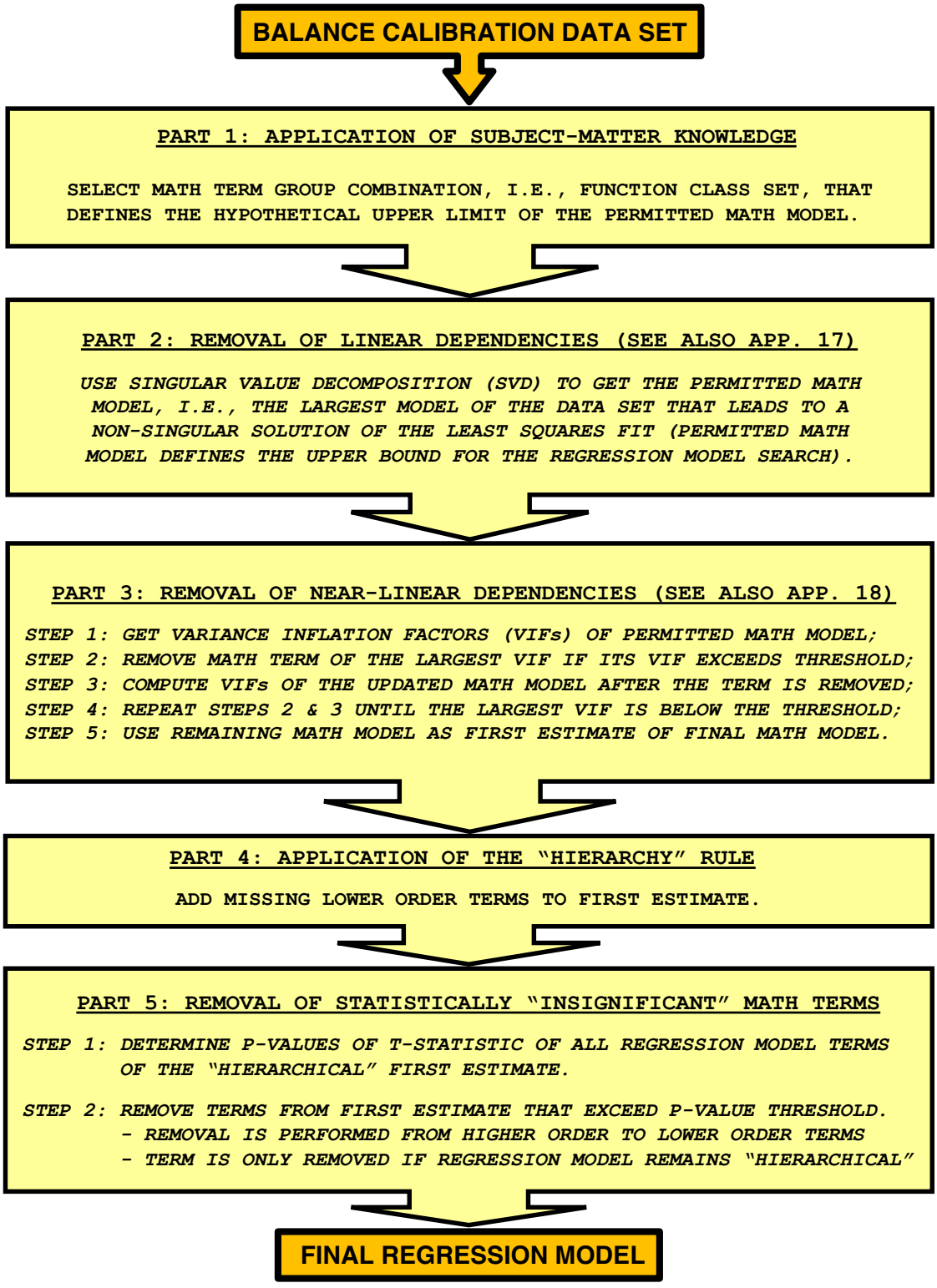

Fig. 19–1 Description of second regression model search algorithm.

Appendix 20

Regression Model Term Group Simplification

20.1 Introduction

Different term groups may be used to construct a regression model of strain–gage balance calibration data so that balance loads may be predicted from the electrical outputs of the bridges during a wind tunnel test. For example, a user of the *Non–Iterative Method* constructs term groups from the bridge outputs as this approach uses regression models of the loads for the load prediction. Similarly, a user of the *Iterative Method* constructs term groups from the balance loads as this alternate approach uses regression models of the bridge outputs for the definition of a load iteration equation.

AIAA's Internal Balance Technology Working Group (IBTWG) recommends a regression model term group combination for the *Iterative Method* that consists, superficially viewed, of ten term groups (see Ref. [7], Eq. (3.1.3), or, App. 10, Table 10–1). However, it can be proven that two of the ten groups, i.e., $F_j \cdot |F_k|$ and $|F_j| \cdot F_k$, are related to each other. They can be combined in a single group whose terms are defined as $F_j \cdot |F_k|$. This simplification is possible because the following equality is valid where $F_j \cdot |F_k|$ and $|F_j| \cdot F_k$ are regression model terms and $\alpha_{j,k}$, $\beta_{j,k}$, and $\gamma_{j,k}$ are regression coefficients:

$$\sum_{j=1}^{n} \sum_{\substack{k=1 \\ k \neq j}}^{n} \alpha_{j,k} \cdot F_j \, |F_k| \; = \sum_{j=1}^{n-1} \sum_{k=j+1}^{n} \beta_{j,k} \cdot F_j \, |F_k| \; + \sum_{j=1}^{n-1} \sum_{k=j+1}^{n} \gamma_{j,k} \cdot |F_j| \, F_k \qquad (20.1)$$

The relationship above simply describes the fact that the sum of all products of a variable with the absolute value of another variable match on both sides of the equation. In other words, it is always possible to identify a term $\alpha_{j,k} \cdot F_j \cdot |F_k|$ on the left–hand side of Eq. (20.1) that matches either a term $\beta_{j,k} \cdot F_j \cdot |F_k|$ or a term $\gamma_{j,k} \cdot |F_j| \cdot F_k$ on the right–hand side. The validity of Eq. (20.1) above means that IBTWG's regression model of an electrical output of a balance has two groups, i.e., $F_j \cdot |F_k|$ and $|F_j| \cdot F_k$, that are related to each other. They must either be used together or not at all if a regression model of an output is constructed.

20.2 Mathematical Proof

A proof of Eq. (20.1) can be developed after omitting the regression coefficients. The coefficients can be dropped because it only needs to be shown that all combinations of a variable with the absolute value of another variable on both sides of Eq. (20.1) match. Consequently, we get the following alternate relationship that needs to be proven:

$$\sum_{j=1}^{n} \sum_{\substack{k=1 \\ k \neq j}}^{n} F_j \cdot |F_k| \; = \sum_{j=1}^{n-1} \sum_{k=j+1}^{n} F_j \cdot |F_k| \; + \sum_{j=1}^{n-1} \sum_{k=j+1}^{n} |F_j| \cdot F_k \qquad (20.2)$$

The rigorous proof of Eq. (20.2) above is possible with the help of simple algebraic operations if the *Kronecker delta* is used to describe its left–hand side in a format that avoids the summation constraint $k \neq j$. By inspection, the alternate format of the left–hand side of Eq. (20.2) can be described by using the following relationship ...

$$\sum_{j=1}^{n} \sum_{\substack{k=1 \\ k \neq j}}^{n} F_j \cdot |F_k| \quad = \quad \sum_{j=1}^{n} \sum_{k=1}^{n} \left(1 \; - \; \delta_{jk} \right) \cdot F_j \cdot |F_k| \tag{20.3a}$$

where

$$Kronecker\ delta \quad \Longrightarrow \quad \delta_{jk} \; = \; \begin{cases} 0 & \text{if} \quad j \neq k \\ 1 & \text{if} \quad j = k \end{cases} \tag{20.3b}$$

Then, after replacing the left–hand side of Eq. (20.2) with the right–hand side of Eq. (20.3a), we get the following modified version of Eq. (20.2):

$$\overbrace{\sum_{j=1}^{n} \sum_{k=1}^{n} (1 - \delta_{jk}) \cdot F_j \cdot |F_k|}^{left-hand\ side} \; = \overbrace{\sum_{j=1}^{n-1} \sum_{k=j+1}^{n} F_j \cdot |F_k| \; + \; \sum_{j=1}^{n-1} \sum_{k=j+1}^{n} |F_j| \cdot F_k}^{right-hand\ side} \tag{20.4}$$

The proof of Eq. (20.4) applies the following basic strategy: the left–hand side of Eq. (20.4) is exclusively modified until all terms on the right–hand side of Eq. (20.4) are obtained. The proof starts by first expanding the round brackets on the left–hand side of Eq. (20.4). Then, we get the relationship shown in Eq. (20.5) below where symbol L is

$$\overbrace{\sum_{j=1}^{n} \sum_{k=1}^{n} (1 - \delta_{jk}) \cdot F_j \cdot |F_k|}^{left-hand\ side} \; = \overbrace{\underbrace{\sum_{j=1}^{n} \sum_{k=1}^{n} F_j \cdot |F_k|}_{Summation\ 1} \; - \; \underbrace{\sum_{j=1}^{n} \sum_{k=1}^{n} \delta_{jk} \cdot F_j \cdot |F_k|}_{Summation\ 2}}^{left-hand\ side} \; = \; L \tag{20.5}$$

used to abbreviate the left–hand side of Eq. (20.4) for later use. Now, terms shown between the two equal signs of Eq. (20.5) above need to be modified until the right–hand side of Eq. (20.4) is obtained. Then, the proof will be completed.

Summation 1 of Eq. (20.5) above can be split into a double sum and a single sum after treating terms associated with the condition $j = n$ separately. Then, we get the following alternate version of *Summation 1* of Eq. (20.5):

$$\underbrace{\sum_{j=1}^{n} \sum_{k=1}^{n} F_j \cdot |F_k|}_{Summation\ 1} \quad = \quad \sum_{j=1}^{n-1} \underbrace{\sum_{k=1}^{n} F_j \cdot |F_k|}_{Summation\ 3} \; + \; \sum_{k=1}^{n} F_n \cdot |F_k| \tag{20.6a}$$

Summation 3 on the right–hand side of Eq. (20.6a) can be split into two parts. Then, we get the following alternate version of Eq. (20.6a):

$$\underbrace{\sum_{j=1}^{n}\sum_{k=1}^{n} F_j\cdot|F_k|}_{Summation\ 1} = \sum_{j=1}^{n-1}\underbrace{\left[\sum_{k=1}^{j} F_j\cdot|F_k| + \sum_{k=j+1}^{n} F_j\cdot|F_k|\right]}_{Summation\ 3} + \sum_{k=1}^{n} F_n\cdot|F_k| \quad (20.6b)$$

Now, after expanding the brackets on the right–hand side of Eq. (20.6b), we get:

$$\underbrace{\sum_{j=1}^{n}\sum_{k=1}^{n} F_j\cdot|F_k|}_{Summation\ 1} = \sum_{j=1}^{n-1}\sum_{k=1}^{j} F_j\cdot|F_k| + \sum_{j=1}^{n-1}\sum_{k=j+1}^{n} F_j\cdot|F_k| + \underbrace{\sum_{k=1}^{n} F_n\cdot|F_k|}_{Summation\ 4} \quad (20.6c)$$

The index of *Summation 4* on the right–hand side of Eq. (20.6c) can be switched from k to j without changing the result. Then, we get:

$$\underbrace{\sum_{j=1}^{n}\sum_{k=1}^{n} F_j\cdot|F_k|}_{Summation\ 1} = \sum_{j=1}^{n-1}\sum_{k=1}^{j} F_j\cdot|F_k| + \sum_{j=1}^{n-1}\sum_{k=j+1}^{n} F_j\cdot|F_k| + \sum_{j=1}^{n} F_n\cdot|F_j| \quad (20.6d)$$

We also know from the *Commutative Law* that $F_n\cdot|F_j|$ equals $|F_j|\cdot F_n$. Then, we get:

$$\underbrace{\sum_{j=1}^{n}\sum_{k=1}^{n} F_j\cdot|F_k|}_{Summation\ 1} = \underbrace{\sum_{j=1}^{n-1}\sum_{k=1}^{j} F_j\cdot|F_k|}_{Summation\ 5} + \underbrace{\sum_{j=1}^{n-1}\sum_{k=j+1}^{n} F_j\cdot|F_k|}_{Summation\ 6} + \sum_{j=1}^{n}|F_j|\cdot F_n \quad (20.6e)$$

The order of the addition of the *Summation 5* and *Summation 6* on the right–hand side of Eq. (20.6e) can be switched without changing the result. Then, we get:

$$\underbrace{\sum_{j=1}^{n}\sum_{k=1}^{n} F_j\cdot|F_k|}_{Summation\ 1} = \underbrace{\sum_{j=1}^{n-1}\sum_{k=j+1}^{n} F_j\cdot|F_k|}_{Summation\ 6} + \underbrace{\sum_{j=1}^{n-1}\sum_{k=1}^{j} F_j\cdot|F_k|}_{Summation\ 5} + \sum_{j=1}^{n}|F_j|\cdot F_n \quad (20.6f)$$

It remains to simplify *Summation 2* on the right–hand side of Eq. (20.5). This summation can be substituted by a single sum after realizing that the summation term of the double sum only has a non–zero value if index j equals index k. Then, we get:

$$\underbrace{\sum_{j=1}^{n}\sum_{k=1}^{n}\delta_{jk}\cdot F_j\cdot|F_k|}_{Summation\ 2} = \sum_{j=1}^{n} F_j\cdot|F_j| \quad (20.7a)$$

The *Commutative Law* states that $F_j \cdot |F_j|$ equals $|F_j| \cdot F_j$. Then, we get for Eq. (20.7a):

$$\underbrace{\sum_{j=1}^{n} \sum_{k=1}^{n} \delta_{jk} \cdot F_j \cdot |F_k|}_{Summation\ 2} \quad = \quad \sum_{j=1}^{n} |F_j| \cdot F_j \tag{20.7b}$$

In the next step, after replacing the difference between *Summation 1* and *Summation 2* of Eq. (20.5) by the difference between the right–hand side of Eq. (20.6f) and the right–hand side of Eq. (20.7b), we get the following alternate version of Eq. (20.5):

$$L \quad = \quad \underbrace{\sum_{j=1}^{n-1} \sum_{k=j+1}^{n} F_j \cdot |F_k| \; + \; \sum_{j=1}^{n-1} \sum_{k=1}^{j} F_j \cdot |F_k| \; + \; \overbrace{\sum_{j=1}^{n} |F_j| \cdot F_n}^{Summation\ 7}}_{Summation\ 1} \; - \; \underbrace{\sum_{j=1}^{n} |F_j| \cdot F_j}_{Summation\ 2} \tag{20.8}$$

The difference between *Summation 7* and *Summation 2* on the right–hand side of Eq. (20.8) can be written in an alternate form without changing the result if the last term of each sum is treated separately. Then, we get:

$$\begin{aligned} \underbrace{\sum_{j=1}^{n} |F_j| \cdot F_n \; - \; \sum_{j=1}^{n} |F_j| \cdot F_j}_{Summation\ 7 \; - \; Summation\ 2} \quad = \quad & \left\{ \sum_{j=1}^{n-1} |F_j| \cdot F_n \; + \; |F_n| \cdot F_n \right\} \\ & - \; \left\{ \sum_{j=1}^{n-1} |F_j| \cdot F_j \; + \; |F_n| \cdot F_n \right\} \end{aligned} \tag{20.9a}$$

The right–hand side of Eq. (20.9a) can be simplified. Then, we get the following equation:

$$\underbrace{\sum_{j=1}^{n} |F_j| \cdot F_n \; - \; \sum_{j=1}^{n} |F_j| \cdot F_j}_{Summation\ 7 \; - \; Summation\ 2} \quad = \quad \sum_{j=1}^{n-1} |F_j| \cdot F_n \; - \; \sum_{j=1}^{n-1} |F_j| \cdot F_j \tag{20.9b}$$

In the next step, after replacing the difference between *Summation 7* and *Summation 2* on the right–hand side of Eq. (20.8) with the right–hand side of Eq. (20.9b), we get the following alternate version of Eq. (20.8):

$$L \quad = \quad \sum_{j=1}^{n-1} \sum_{k=j+1}^{n} F_j \cdot |F_k| \; + \underbrace{\sum_{j=1}^{n-1} \sum_{k=1}^{j} F_j \cdot |F_k|}_{Summation\ 8} \; + \; \underbrace{\sum_{j=1}^{n-1} |F_j| \cdot F_n \; - \sum_{j=1}^{n-1} |F_j| \cdot F_j}_{Summation\ 7 \; - \; Summation\ 2} \tag{20.10}$$

Summation 8 on the right–hand side of Eq. (20.10) above can be rewritten by using a universally applicable relationship that describes how dependent indices of a double sum

are to be interchanged (see Ref. [72], Section 3.5.2, Fact 8). This relationship can be expressed as follows after (i) both the sides of the original equation given in Ref. [72] are switched, (ii) index i is replaced by index k, and (iii) the symbol of the upper limit n is replaced by the alternate generic symbol ψ:

$$\textit{Ref. [72], Section 3.5.2, Fact 8} \implies \sum_{j=1}^{\psi} \sum_{k=1}^{j} \varphi(j,k) = \sum_{k=1}^{\psi} \sum_{j=k}^{\psi} \varphi(j,k) \quad (20.11a)$$

The symbol $\varphi(j,k)$ above represents a summation term that depends on two indices. Then, after (i) applying the generic relationship defined in Eq. (20.11a) to *Summation 8* on the right–hand side of Eq. (20.10) and (ii) replacing the generic upper bound ψ of the summations with $n-1$, we get:

$$\underbrace{\sum_{j=1}^{n-1} \sum_{k=1}^{j} F_j \cdot |F_k|}_{Summation\ 8} = \sum_{k=1}^{n-1} \sum_{j=k}^{n-1} F_j \cdot |F_k| \quad (20.11b)$$

Indices used on the right–hand side of Eq. (20.11b) can be switched without changing the result. Then, we get:

$$\underbrace{\sum_{j=1}^{n-1} \sum_{k=1}^{j} F_j \cdot |F_k|}_{Summation\ 8} = \sum_{j=1}^{n-1} \sum_{k=j}^{n-1} F_k \cdot |F_j| \quad (20.11c)$$

It is known from the *Commutative Law* that $F_k \cdot |F_j|$ equals $|F_j| \cdot F_k$ on the right–hand side of Eq. (20.11c). Then, we get the following alternate form of Eq. (20.11c):

$$\underbrace{\sum_{j=1}^{n-1} \sum_{k=1}^{j} F_j \cdot |F_k|}_{Summation\ 8} = \sum_{j=1}^{n-1} \sum_{k=j}^{n-1} |F_j| \cdot F_k \quad (20.11d)$$

Now, the right–hand side of Eq. (20.11d) can be used to replace *Summation 8* on the right–hand side of Eq. (20.10). Then, we get the following alternate form of Eq. (20.10):

$$L = \sum_{j=1}^{n-1} \sum_{k=j+1}^{n} F_j \cdot |F_k| + \underbrace{\sum_{j=1}^{n-1} \sum_{k=j}^{n-1} |F_j| \cdot F_k}_{Summation\ 8} + \sum_{j=1}^{n-1} |F_j| \cdot F_n - \sum_{j=1}^{n-1} |F_j| \cdot F_j \quad (20.12)$$

The outer summation of the last three sums on the right–hand side of Eq. (20.12) is identical. Therefore, the last three sums can be combined. Then, we get the following alternate form of Eq. (20.12):

$$L = \sum_{j=1}^{n-1} \sum_{k=j+1}^{n} F_j \cdot |F_k| + \sum_{j=1}^{n-1} \left[\underbrace{\sum_{k=j}^{n-1} |F_j| \cdot F_k}_{Summation\ 9} + |F_j| \cdot F_n - |F_j| \cdot F_j \right] \quad (20.13)$$

Summation 9 on the right–hand side of Eq. (20.13) above can be expressed in a different form after both the lower and upper bounds of the summation are shifted by one. Then, by inspection, the following relationship applies:

$$\underbrace{\sum_{k=j}^{n-1} |F_j| \cdot F_k}_{Summation\ 9} = \underbrace{\sum_{k=j+1}^{n} |F_j| \cdot F_k}_{Summation\ 10} - |F_j| \cdot F_n + |F_j| \cdot F_j \tag{20.14}$$

Now, after solving the above equation for *Summation 10*, we get:

$$\underbrace{\sum_{k=j+1}^{n} |F_j| \cdot F_k}_{Summation\ 10} = \underbrace{\sum_{k=j}^{n-1} |F_j| \cdot F_k}_{Summation\ 9} + |F_j| \cdot F_n - |F_j| \cdot F_j \tag{20.15}$$

It is observed that the right–hand side of Eq. (20.15) matches all terms that are given inside the square brackets on the right–hand side of Eq. (20.13). Therefore, *Summation 10* can be used to replace the contents of the square brackets on the right–hand side of Eq. (20.13). Then, Eq. (20.13) takes on the following form:

$$L = \sum_{j=1}^{n-1} \sum_{k=j+1}^{n} F_j \cdot |F_k| + \sum_{j=1}^{n-1} \sum_{k=j+1}^{n} |F_j| \cdot F_k \tag{20.16}$$

It can be seen that the right–hand side of Eq. (20.16) matches the right–hand side of Eq. (20.4). Therefore, the proof of Eq. (20.4) is completed. In addition, we know that Eq. (20.4) equals Eq. (20.2). Therefore, the validity of Eq. (20.1) was proven as Eq. (20.1) and Eq. (20.2) only differ by the fact that each summation term is multiplied by a constant.

It should be mentioned that individual terms on the left– and right–hand sides of Eq. (20.1) match. However, the summation order differs. Therefore, users of the *Iterative Method* must continue to use the two term groups $F_j \cdot |F_k|$ and $|F_j| \cdot F_k$ on the right–hand side of Eq. (20.1) for the regression model definition of an electrical output. This approach guarantees that the chosen term order is compatible with the standard term order that AIAA's IBTWG first established in 2003 (Ref. [7], p. 12, Eq. (3.1.3)). However, any new implementation of the *Non–Iterative Method* in the data system of a wind tunnel can take advantage of the simplification that the left–hand side of Eq. (20.1) describes as no industry–wide standard for implementation & use of the *Non–Iterative Method* exists.

Appendix 21

Load Iteration Equation for Extended Variable Sets

21.1 Introduction

It is demonstrated in the literature that the *Iterative Method* can be used in combination with an extended set of independent variables for the balance load prediction (see the discussions in Ref. [13] and Ref. [38]). The extended variable set consists of (i) the balance loads and (ii) additional independent variables that influence the electrical outputs of the balance bridges. The balance temperature or the bellows pressure of an air balance may be interpreted as an additional independent variable. The additional independent variables have to be introduced as both independent and dependent variables in order to make the load iteration equation work. Then, it is possible to fulfill the fundamental requirement that the number of independent and dependent variables of a strain–gage balance data set must match.

It is helpful to demonstrate the use of an extended variable set with the *Iterative Method* by using an example. Therefore, the balance temperature is chosen as the additional independent variable for the load prediction. It is best to quantify the temperature as the difference between the uniform balance temperature and a suitable reference temperature. The new independent variable, i.e., the temperature difference, can be described by Eq. (21.1) below where T is the balance temperature and $T_\circ$ is the chosen reference

$$\Delta T \quad = \quad T \; - \; T_\circ \tag{21.1}$$

temperature. The reference temperature often equals the calibration temperature of the balance. Ideally, the reference temperature should be located within the range of all temperatures that the balance is expected to experience during the wind tunnel test.

In principle, the extended variable set of the balance can be used with both load iteration equation types that support the application of the *Iterative Method*. Definitions of the two load iteration equation choices are given in App. 10 (see Eqs. (10.27a) and (10.31a)). The use of the extended variable set with the *Iterative Method* becomes possible after making a few changes to the data analysis software that (i) analyzes balance calibration data and (ii) computes balance loads during a wind tunnel test. These changes are briefly summarized in the following three paragraphs. More detailed explanations are provided in a later section.

• The analysis software must be able to process a regression model of a bridge output that is constructed from an extended set of independent variables. Existing software often only supports a six–component balance. In that case, the software must be modified to generate a data reduction matrix that uses 7 independent and dependent variables because the temperature difference must be added to both the load and bridge output set.

• The analysis software must be able to automatically assign coefficients of the regression model of the additional dependent variable. All numerical values of the additional dependent variable must exactly match all numerical values of the additional independent variable. The regression coefficient of this matching independent variable must be set to one. The coefficients of all other terms of the regression model of the additional dependent variable must be set to zero.

• The analysis software must be able to read and interpret an extended data reduction matrix format so that balance loads can be predicted during a wind tunnel test from (i) the measured strain–gage outputs and (ii) the measured values of the additional independent variable, i.e., of the temperature difference.

At this point, the extended variable set is defined. It remains to describe the implementation of some of the data analysis requirements in more detail.

21.2 Extended Variable Sets and Regression Models

The use of the temperature difference as both an independent and dependent variable for the definition of the load iteration equation is supported by the interpretation of the balance temperature as a state variable. This interpretation can be better understood if the balance is placed inside of the control volume that is shown in Fig. 21–1 below (see also pp. 10–14, Ref. [8], and Ref. [9] for more details). The inputs into the control volume

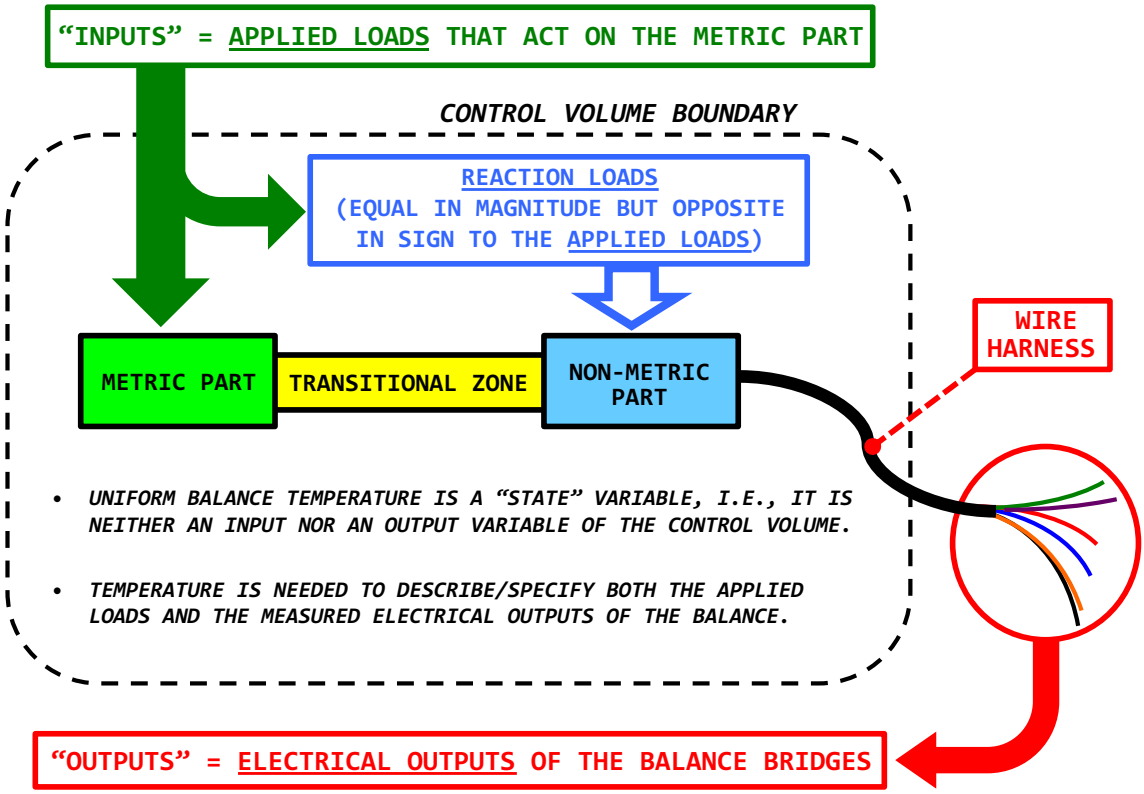

Fig. 21–1 Input, output, and state variables of the control volume of a balance.

are the applied loads that act on the metric part of the balance. The outputs are the measured electrical outputs at the balance bridges. The balance itself remains at a constant uniform temperature as long as no temperature gradient exists across the control volume boundary. Then, the temperature can be interpreted as a variable that describes the state of the balance while (i) loads are applied to the metric part and (ii) electrical outputs are measured at the balance bridges. In other words, the temperature, or, more precisely, the temperature difference is a state variable that accompanies both the description of the

applied loads and measured electrical outputs of the balance. The resulting extended set of independent variables of an n–component balance can be defined as follows:

$$\underline{\textit{extended}}\ \textit{set of}\ \underline{\textit{independent}}\ \textit{variables}: \underbrace{F_1,\ F_2,\ \ldots,\ F_n,\ F_{n+1}}_{n+1\ \textit{independent variables}}$$

$$F_1,\ F_2,\ \ldots,\ F_n \implies \textit{load components of } n-\textit{component balance}$$

$$F_{n+1} = \Delta T \implies \textit{temperature difference, defined in Eq. (21.1)}$$

The extended variable set consists of (i) the total number of loads of the balance and (ii) the temperature difference. It is possible to describe the extended set of <u>independent</u> variables of the balance by using the following equation:

$$\textit{independent variable set} \implies F_i = \begin{cases} F_i & \ldots \textit{ for } \ldots\ i \leq n \\ \Delta T & \ldots \textit{ for } \ldots\ i = n+1 \end{cases} \tag{21.2}$$

Similarly, the extended set of dependent variables of an n–component balance can be defined. It consists of (i) the electrical outputs of the balance bridges and (ii) the temperature difference. This conclusion can be summarized as follows:

$$\underline{\textit{extended}}\ \textit{set of}\ \underline{\textit{dependent}}\ \textit{variables}: \underbrace{D_1,\ D_2,\ \ldots,\ D_n,\ D_{n+1}}_{n+1\ \textit{dependent variables}}$$

$$D_1,\ D_2,\ \ldots,\ D_n \implies \textit{bridge output differences of } n-\textit{component balance}$$

$$D_{n+1} = \Delta T \implies \textit{temperature difference, defined in Eq. (21.1)}$$

It is possible to describe the extended set of <u>dependent</u> variables of the balance by using the following equation:

$$\textit{dependent variable set} \implies D_i = \begin{cases} rF_i - N_i & \ldots \textit{ for } \ldots\ i \leq n \\ \Delta T & \ldots \textit{ for } \ldots\ i = n+1 \end{cases} \tag{21.3}$$

The extended dependent variable set consists of the total number of bridge outputs and the temperature difference. Each dependent variable is a function of the extended independent variable set that consists of the balance loads and the temperature difference. Then, the extended regression model of a bridge output difference with index i can be defined by the following equation:

Extended Regression Model of Bridge Output Difference

$$D_i \;=\; b_{i,0} \;+\; \ldots \;+\; b_{i,n} \cdot F_n \;+\; b_{i,n+1} \cdot \Delta T \;+\; \ldots \;+\; b_{i,m} \cdot |\Delta T^{\,3}| \qquad (21.4a)$$

where

$$1 \;\leq\; i \;\leq\; n' \;=\; n \;+\; 1 \qquad (21.4b)$$

$$m \;=\; \underbrace{2 \;\cdot\; n' \;\cdot\; (\; n' \;+\; 2\;)}_{\textit{taken from App. 10}} \qquad (21.4c)$$

The coefficients of the regression model of the bridge output difference are obtained after applying global regression analysis to the temperature–dependent balance calibration data set. It is important to mention that the regression model described in Eq. (21.4*a*) above uses the same ten term groups that are defined in Table 10–1 of App. 10. The temperature difference ΔT is simply treated as if it would be an additional load component F_{n+1} of the balance. Consequently, the maximum number of possible coefficients of the regression model of a bridge output difference of a six–component balance is given by the following equation (not counting the intercept term):

$$n' \;=\; 6+1 \;=\; 7 \;\;\Longrightarrow\;\; \textit{Eq.}\;(21.4c) \;\;\Longrightarrow\;\; m \;=\; 2 \cdot n' \cdot (n'+2) \;=\; 126 \qquad (21.5)$$

The number of regression model terms of a temperature–dependent six–component balance data set is substantially smaller than 126. Many terms are simply not supported or, if used, may cause massive near–linear dependencies between regression model terms. The square or the cube of the temperature difference can probably not be used because calibration data may only exist at two or three different temperatures. In addition, it makes no sense to use terms that have the absolute value of the temperature difference as these terms model the bi–directional behavior of an output. Then, only two temperature–dependent terms for each output difference remain. They are (i) the term defined by the temperature difference ΔT itself and (ii) the cross–product term $F_i\,\Delta T$ that is constructed from the primary load component F_i of the bridge and the temperature difference ΔT. The first term models the output shift of the balance bridge near zero load. The second term describes the bridge sensitivity shift. All these observations and conclusions result in significant regression model simplifications that can be summarized as follows:

Regression Model Simplification

Coefficients of all but two temperature–dependent terms are explicitly set to zero. Only the coefficient of ΔT and the coefficient of $F_i \cdot \Delta T$ are fitted during the regression analysis of bridge output difference D_i. They model the output shift near zero load and the sensitivity shift that influence the load prediction (see App. 14).

Equation (21.4a) describes a set of $n+1$ least squares problems of the temperature–dependent balance calibration data set. Each problem needs to be solved individually by using, for example, the global regression analysis approach (see also App. 10). One of the least squares problems has a trivial–but–correct solution. It is the regression model with index $n+1$ that uses the temperature difference ΔT as the dependent variable. All coefficients of this regression model are explicitly known as the temperature difference ΔT also appears on the right–hand side of Eq. (21.4a). In this case, all but one coefficient on the right–hand side of Eq. (21.4a) equals zero. Only the coefficient of the regression model term ΔT equals one. This important result can be summarized as follows:

Regression Model of Temperature Difference *(trivial–but–correct)*

$$\underbrace{\Delta T}_{D_{n+1}} = 0 + 0 \cdot F_1 + 0 \cdot F_2 + \ldots + 0 \cdot F_n + 1 \cdot \underbrace{\Delta T}_{F_{n+1}} + 0 \cdot |F_1| + 0 \cdot |F_2| + \ldots + 0 \cdot F_1 \cdot \Delta T + \ldots \quad (21.6a)$$

or

$$b_{n+1,\vartheta} = \begin{cases} 1 & \ldots \textit{ for } \ldots \ \vartheta = n+1 \\ 0 & \ldots \textit{ for } \ldots \ \vartheta \neq n+1 \end{cases} \quad (21.6b)$$

The simple addition of the trivial–but–correct relationship defined in Eq. (21.6a) above to the set of least squares problems given by Eq. (21.4a) makes it ultimately possible to construct a load iteration scheme that (i) uses temperature–dependent bridge outputs as input and (ii) does not require a modification of the load iteration equations that support the use of the *Iterative Method*.

21.3 Load Iteration Equations

The load iteration equations can be constructed as outlined in App. 10 after the regression analysis of each output difference is completed. Then, the *Primary Load Iteration Equation* of the extended variable set can be described by using Eq. (21.7a) below if it is assumed that bridge output differences and the temperature difference are used as input for the load prediction (nomenclature was copied from App. 10, Eq. (10.27a) and Eq. (10.34b)). The size of a vector or a matrix of the load iteration equation is specified

$$\textit{Primary Load Iteration Equation} \implies \underbrace{\mathbf{F}_{\xi}}_{n' \times 1} = \underbrace{\left[\ \mathbf{C_1}^{-1}\ \right]}_{n' \times n'} \cdot \underbrace{\mathbf{D}}_{n' \times 1} - \underbrace{\left[\ \mathbf{C_1}^{-1}\mathbf{C_2}\ \right]}_{n' \times (m-n')} \cdot \underbrace{\mathbf{H}\{\mathbf{F}_{\xi-1}\}}_{(m-n') \times 1} \quad (21.7a)$$

below its symbol for reference. Similarly, the *Alternate Load Iteration Equation* of the extended variable set can be described by using Eq. (21.7b) below (nomenclature was copied from App. 10, Eq. (10.31a) and Eq. (10.34b)). Vector $\mathbf{F}$ of the two iteration equations has

$$\textit{Alternate Load Iteration Equation} \implies \underbrace{\mathbf{F}_{\xi}}_{n'\times 1} = \underbrace{\left[\ \mathbf{B_1}^{-1}\ \right]}_{n'\times n'} \cdot \underbrace{\mathbf{D}}_{n'\times 1} - \underbrace{\left[\ \mathbf{B_1}^{-1}\mathbf{B_2}\ \right]}_{n'\times n'} \cdot \underbrace{\mathbf{F}_{\xi-1}}_{n'\times 1} - \underbrace{\left[\ \mathbf{B_1}^{-1}\mathbf{C_2}\ \right]}_{n'\times(m-n')} \cdot \underbrace{\mathbf{H}\{\mathbf{F}_{\xi-1}\}}_{(m-n')\times 1} \tag{21.7b}$$

the load values and the temperature difference. It is defined in Eq. (21.8*a*) below. Its values are the result of the load iteration process that the *Iterative Method* performs. On the

$$\underbrace{\mathbf{F}}_{n'\times 1} = \begin{bmatrix} F_1 \\ F_2 \\ \vdots \\ F_n \\ \Delta T \end{bmatrix} \tag{21.8a}$$

other hand, vector $\mathbf{D}$ of the two iteration equations has the output differences of the balance bridges and the temperature difference. It is defined in Eq. (21.8*b*) below. Its

$$\underbrace{\mathbf{D}}_{n'\times 1} = \begin{bmatrix} D_1 \\ D_2 \\ \vdots \\ D_n \\ D_{n'} \end{bmatrix} = \begin{bmatrix} rF_1 - N_1 \\ rF_2 - N_2 \\ \vdots \\ rF_n - N_n \\ \Delta T \end{bmatrix} \tag{21.8b}$$

values are the input of the load iteration process that the *Iterative Method* performs. Again, it must be pointed out that the temperature difference ΔT appears as a state variable in <u>both</u> the independent and dependent variable sets that vectors $\mathbf{F}$ and $\mathbf{D}$ describe. This variable format makes it possible to use the temperature difference as an input variable for the load iteration equations.

Appendix 22

Weighted Least Squares Fit of Balance Calibration Data

22.1 Introduction

Equations of a weighted least squares fit of balance calibration data are developed in this appendix. This analysis approach is sometimes needed in order to increase the weight of data points whose bridge outputs describe a single–component load.† These data points have a significant influence on the numerical estimates of the primary bridge sensitivities. First, basic characteristics of regression models of balance calibration data are reviewed. Afterwards, the application of a weighted least squares fit to the data is discussed.

22.2 Regression Models of Balance Calibration Data

The regression analysis of balance calibration data of an n–component balance needs to describe both loads and electrical outputs of the balance in a suitable format. In addition, the balance loads $F_1, F_2, \ldots, F_n$ should be corrected for the combined weight of the metric part of the balance and the calibration equipment so that all loads are described relative to the absolute load datum of zero load. It is also best to describe the electrical outputs of an n–component balance as differences $D_1, D_2, \ldots, D_n$ between a raw output of a bridge and the corresponding natural zero. This recommended bridge output format is summarized by Eq. (22.1) below where D_i is the output difference, rF_i is the raw output

$$D_i \;=\; rF_i \;-\; N_i \quad ; \quad 1 \;\leq\; i \;\leq\; n \tag{22.1}$$

of the bridge, and N_i is the natural zero. A balance experiences a series of finite load states during its calibration. They can be described by using either the tare corrected loads or the measured bridge output differences. These loads and output differences define the input data set for the regression analysis that results in the load prediction equations. Then, assuming that the given calibration data set has a total of p data points, i.e., individual load states, the input data set for the regression analysis of an n–component balance can be summarized by the following relationship ($\varphi \equiv$ data point index):

$$\textit{calibration data} \quad \Longrightarrow \quad D_i(\varphi),\; F_i(\varphi) \quad \textit{where} \quad 1 \;\leq\; i \;\leq\; n \quad \textit{and} \quad 1 \;\leq\; \varphi \;\leq\; p$$

Now, regression models have to be chosen that are used to process the balance calibration data set. They also define the load prediction equations. An analyst can use either the *Non–Iterative Method* or the *Iterative Method* for the regression analysis of the balance calibration data (see App. 9 and App. 10 for more details). First, let us assume that an analyst uses the *Non–Iterative Method* for the balance load prediction. Then, balance loads are directly fitted as a function of bridge output differences. The corresponding regression model of a balance load component is described by Eq. (22.2) below where the symbol

Non-Iterative Method $\Longrightarrow$ Regression Model of Balance Load

$$F_i \;=\; a_{i,0} \;+\; a_{i,1} \cdot D_1 \;+\; a_{i,2} \cdot D_2 \;+\; \ldots \tag{22.2}$$

† A data point has the electrical outputs of a single–component load whenever one load component is applied to the balance while keeping all other load components close to zero absolute load.

F_i represents the fitted balance load component, symbols D_1, D_2, ... are the bridge output differences, and $a_{i,0}$, $a_{i,1}$, $a_{i,2}$, ... are the regression coefficients. Alternatively, an analyst may choose the *Iterative Method* for the analysis of balance calibration data. This approach fits the bridge output differences as a function of the balance loads. The resulting regression model of the output difference of a balance bridge is summarized by Eq. (22.3) below where

Iterative Method $\Longrightarrow$ Regression Model of Output Difference

$$D_i \quad = \quad b_{i,0} \; + \; b_{i,1} \; \cdot \; F_1 \; + \; b_{i,2} \; \cdot \; F_2 \; + \; \ldots \qquad (22.3)$$

the symbol D_i represents the fitted output difference of the bridge, symbols F_1, F_2, ... are the balance load components, and $b_{i,0}$, $b_{i,1}$, $b_{i,2}$, ... are the regression coefficients.

At this point, the balance calibration data and possible regression model choices have been specified. It remains to translate this information into equations of a multivariate least squares fit. First, the least squares problem and the solution of an ordinary least squares fit need to be reviewed. They are a special case of a weighted least squares fit as a weight of one is assigned to all data points during an ordinary least squares fit.

22.3 Ordinary Least Squares Fit

It is convenient to describe an ordinary least squares fit in matrix format. This approach assembles regression model term values in a rectangular matrix **A**. In our application, the number of rows of matrix **A** equals the total number p of calibration data points. The number of columns of matrix **A**, on the other hand, equals the total number m of regression model terms. These terms depend on the independent variables of the fit. Values of the dependent variable are also needed for the description of an ordinary least squares problem of the calibration data. They are assembled in a column vector **R**. The number of rows of vector **R** equals the total number p of calibration data points. Then, the ordinary least squares problem of the calibration data can be described by the relationship that is given in Eq. (22.4) below. Vector **x** describes a column vector with m rows. It has

Ordinary Least Squares Problem

$$\mathbf{A}_{p\times m} \; \cdot \; \mathbf{x}_{m\times 1} \quad = \quad \mathbf{R}_{p\times 1} \qquad (22.4)$$

the coefficients of the regression model of the balance calibration data.

Now, the coefficients of matrix **A** and the components of vector **R** and vector **x** need to be related to the two regression model choices that are defined by Eqs. (22.2) and (22.3) above. First, matrices and vectors are described for the regression model of a balance load component that is defined in Eq. (22.2). In that case, the tare corrected load is interpreted as the dependent variable and the bridge output differences are interpreted as the independent variables. Consequently, the matrices and vectors of the resulting ordinary

least squares problem can be summarized by Eqs. (22.5a) to (22.5c) below.

$$Non-Iterative\ Method \implies outputs \implies \mathbf{A}_{p\times m} = \underbrace{\begin{bmatrix} 1 & D_1(1) & D_2(1) & \cdots \\ 1 & D_1(2) & D_2(2) & \cdots \\ \vdots & \vdots & \vdots & \vdots \\ 1 & D_1(p) & D_2(p) & \cdots \end{bmatrix}}_{coefficient\ columns\ \equiv\ m} \tag{22.5a}$$

$$Non-Iterative\ Method \implies loads \implies \mathbf{R}_{p\times 1} = \begin{bmatrix} F_i(1) \\ F_i(2) \\ \vdots \\ F_i(p) \end{bmatrix} \tag{22.5b}$$

$$Non-Iterative\ Method \implies coefficients \implies \mathbf{x}_{m\times 1} = \begin{bmatrix} a_{i,0} \\ a_{i,1} \\ a_{i,2} \\ \vdots \end{bmatrix} \tag{22.5c}$$

Similarly, matrix $\mathbf{A}$, vector $\mathbf{R}$, and vector $\mathbf{x}$ can be described for the regression model of a bridge output difference that is defined in Eq. (22.3) above. In this case, the tare corrected loads are interpreted as the independent variables and the bridge output difference is interpreted as the dependent variable. Consequently, matrices and vectors of the resulting ordinary least squares problem can be summarized as follows:

$$Iterative\ Method \implies loads \implies \mathbf{A}_{p\times m} = \underbrace{\begin{bmatrix} 1 & F_1(1) & F_2(1) & \cdots \\ 1 & F_1(2) & F_2(2) & \cdots \\ \vdots & \vdots & \vdots & \vdots \\ 1 & F_1(p) & F_2(p) & \cdots \end{bmatrix}}_{coefficient\ columns\ \equiv\ m} \tag{22.6a}$$

$$Iterative\ Method \implies outputs \implies \mathbf{R}_{p\times 1} = \begin{bmatrix} D_i(1) \\ D_i(2) \\ \vdots \\ D_i(p) \end{bmatrix} \tag{22.6b}$$

$$Iterative\ Method \implies coefficients \implies \mathbf{x}_{m\times 1} = \begin{bmatrix} b_{i,0} \\ b_{i,1} \\ b_{i,2} \\ \vdots \end{bmatrix} \tag{22.6c}$$

The solution of the ordinary least squares problem, i.e., vector $\mathbf{x}$ of Eq. (22.4) above, is a well–known application of the *Moore–Penrose Inverse* (see Ref. [64], pp. 35–39, and Refs. [77], [78]). It is defined by the following matrix equation:

Solution of Ordinary Least Squares Problem

$$\mathbf{x}_{m\times 1} \;=\; \Big[\,\mathbf{A}^{\mathbf{T}}\cdot\mathbf{A}\,\Big]^{-1}_{m\times m}\cdot\Big[\,\mathbf{A}^{\mathbf{T}}\cdot\mathbf{R}\,\Big]_{m\times 1} \qquad (22.7)$$

The solution above implicitly assumes that the weighting factor w_φ of each data point equals one. This assumption can be expressed as follows:

$$\textit{ordinary least squares} \implies w_1 = w_2 = \ldots = w_\varphi = \ldots = w_p = 1.0 \qquad (22.8)$$

Now, it needs to be explained how equations of an ordinary least squares problem can be converted to corresponding equations of a weighted least squares problem.

22.4 Weighted Least Squares Fit

An analyst may want to use subject–matter knowledge in order to increase the influence of certain groups of balance calibration data points during the regression analysis. Then, a weighted least squares fit has to be applied that assigns an individual weighting factor to each data point (basic elements of a weighted least squares fit are described in Ref. [68], pp. 179–183). The matrix equation of a weighted least squares problem can easily be obtained from the equation of an ordinary least squares problem if the auxiliary matrix $\mathbf{W}$ is introduced. This matrix stores the chosen weighting factors of the individual data points on its principal diagonal. The matrix $\mathbf{W}$ is defined as follows:

$$\mathbf{W}_{p\times p} \;=\; \begin{bmatrix} w_1 & 0 & \cdots & 0 & 0 \\ 0 & w_2 & \cdots & 0 & 0 \\ \vdots & \vdots & \vdots & \vdots & \vdots \\ 0 & 0 & \cdots & w_{p-1} & 0 \\ 0 & 0 & \cdots & 0 & w_p \end{bmatrix} \qquad (22.9)$$

Now, weighting factors are introduced into the equations of an ordinary least squares fit by simply multiplying both sides of Eq. (22.4) with matrix $\mathbf{W}$. Then, the matrix equation of a weighted least squares problem can be expressed by Eq. (22.10) below where vector $\mathbf{x}$ has the regression coefficients that result from the weighted least squares fit.

Weighted Least Squares Problem

$$\mathbf{W}_{p\times p}\cdot\mathbf{A}_{p\times m}\cdot\mathbf{x}_{m\times 1} \;=\; \mathbf{W}_{p\times p}\cdot\mathbf{R}_{p\times 1} \qquad (22.10)$$

The normal equations of the weighted least squares problem are obtained by simply multiplying both sides of Eq. (22.10) with the transpose of matrix $\mathbf{A}$ (see Ref. [68] for more details and explanations). Then, we get:

$$\textit{normal equations} \implies \mathbf{A}^{\mathbf{T}}_{m\times p}\cdot\mathbf{W}_{p\times p}\cdot\mathbf{A}_{p\times m}\cdot\mathbf{x}_{m\times 1} = \mathbf{A}^{\mathbf{T}}_{m\times p}\cdot\mathbf{W}_{p\times p}\cdot\mathbf{R}_{p\times 1} \qquad (22.11)$$

It is useful to transform the normal equations of the weighted least squares problem to the normal equations of an ordinary least squares problem. Then, existing computer code can be used to solve the weighted least squares problem as long as the code was originally developed for an ordinary least squares problem. The transformation can be done with the help of an auxiliary matrix $\mathcal{W}$ that is defined in Eq. (22.12a) below:

$$\mathcal{W}_{p\times p} \;=\; \begin{bmatrix} \sqrt{w_1} & 0 & \cdots & 0 & 0 \\ 0 & \sqrt{w_2} & \cdots & 0 & 0 \\ \vdots & \vdots & \vdots & \vdots & \vdots \\ 0 & 0 & \cdots & \sqrt{w_{p-1}} & 0 \\ 0 & 0 & \cdots & 0 & \sqrt{w_p} \end{bmatrix} \tag{22.12a}$$

The following simple relationship between matrices $\mathbf{W}$ and $\mathcal{W}$ is also valid:

$$\mathbf{W}_{p\times p} \;=\; \mathcal{W}_{p\times p} \cdot \mathcal{W}_{p\times p} \tag{22.12b}$$

Then, after matrix $\mathbf{W}$ in Eq. (22.11) is replaced by the right–hand side of Eq. (22.12b), we get the following transformed normal equations of the weighted least squares problem:

$$\mathbf{A}^{\mathbf{T}}_{m\times p} \cdot \mathcal{W}_{p\times p} \cdot \mathcal{W}_{p\times p} \cdot \mathbf{A}_{p\times m} \cdot \mathbf{x}_{m\times 1} \;=\; \mathbf{A}^{\mathbf{T}}_{m\times p} \cdot \mathcal{W}_{p\times p} \cdot \mathcal{W}_{p\times p} \cdot \mathbf{R}_{p\times 1} \tag{22.13}$$

It is known from operator rules of matrix algebra that $\mathcal{W}^{\mathbf{T}} = \mathcal{W}$ because square matrix $\mathcal{W}$ only has non–zero values on its principal diagonal. In addition, we know that $\mathbf{A}^{\mathbf{T}}\mathcal{W} = [\mathcal{W}\mathbf{A}]^{\mathbf{T}}$. Consequently, Eq. (22.13) can be expressed as follows:

$$[\mathcal{W}_{p\times p} \cdot \mathbf{A}_{p\times m}]^{\mathbf{T}} \cdot [\mathcal{W}_{p\times p} \cdot \mathbf{A}_{p\times m}] \cdot \mathbf{x}_{m\times 1} \;=\; [\mathcal{W}_{p\times p} \cdot \mathbf{A}_{p\times m}]^{\mathbf{T}} \cdot [\mathcal{W}_{p\times p} \cdot \mathbf{R}_{p\times 1}] \tag{22.14}$$

Now, auxiliary matrix $\mathbf{U}$ and auxiliary vector $\mathbf{V}$ are introduced so that Eq. (22.14) can be expressed in the format of an ordinary least squares problem. We get:

$$\mathbf{U}_{p\times m} \;=\; \mathcal{W}_{p\times p} \cdot \mathbf{A}_{p\times m} \tag{22.15a}$$

$$\mathbf{V}_{p\times 1} \;=\; \mathcal{W}_{p\times p} \cdot \mathbf{R}_{p\times 1} \tag{22.15b}$$

Then, after using the left–hand sides of Eqs. (22.15a) & (22.15b) to replace the brackets in Eq. (22.14), we get the normal equations of the weighted least squares fit:

$$\mathbf{U}^{\mathbf{T}}_{m\times p} \cdot \mathbf{U}_{p\times m} \cdot \mathbf{x}_{m\times 1} \;=\; \mathbf{U}^{\mathbf{T}}_{m\times p} \cdot \mathbf{V}_{p\times 1} \tag{22.16}$$

Finally, the solution of the weighted least squares problem, i.e., the regression coefficients of either the fitted load component defined in Eq. (22.2) or the fitted output difference defined in Eq. (22.3) can be described by the following equation:

Solution of Weighted Least Squares Problem

$$\mathbf{x}_{m\times 1} \;=\; \Big[\, \mathbf{U}^{\mathbf{T}}\, \mathbf{U} \,\Big]^{-1}_{m\times m} \cdot \Big[\, \mathbf{U}^{\mathbf{T}}\, \mathbf{V} \,\Big]_{m\times 1} \tag{22.17}$$

The weighting factor of each individual data point of a balance calibration data set needs to be specified so that the weighted least squares fit can be performed. Two weighting factor definitions were developed for that purpose that are described in the next sections.

22.5 First Weighting Factor Definition

A weighting factor definition was developed that can easily be used with data points of a balance calibration data set if the subset of single–component load series[†] is known. The weighting factor definition assigns the constants 1.0 and 0.2 as weights. The value of 1.0 is assigned to data points that belong to the subset of single–component load series. This value is also used for the zero load points, i.e., the tare points of each single–component load series. All other data points use 0.2 as weighting factor. Equations (22.18a) and (22.18b) below summarize the first weighting factor definition ($\varphi \equiv$ data point index).

First Weighting Factor Definition

$$w_\varphi = 1.0 \iff \left\{\begin{array}{l}\text{assign 1.0 to all data points that belong to a single–}\\ \text{component load series (including zero load points)}\end{array}\right\} \qquad (22.18a)$$

$$w_\varphi = 0.2 \iff \left\{\begin{array}{l}\text{assign 0.2 to data points that do not}\\ \text{belong to a single–component load series}\end{array}\right\} \qquad (22.18b)$$

In theory, an increase of the percentage of single–component loads in a calibration data set improves the accuracy of the primary sensitivities that are derived from the regression coefficients of a global fit. Therefore, the first weighting factor definition can lead to better numerical estimates of the primary sensitivities because data points of single–component load series have a five times greater weighting factor than all other points.

The first weighting factor definition works well with data from calibration load schedules that have characteristics of NASA Langley's 9–point design (the design is described, e.g., in Ref. [41], Fig. 16). The definition is also suited for the processing of data sets that support the application of *Cook's* sequential analysis approach (see App. 28, section 28.3). It is important during the application of the first weighting factor definition to these data set types that the weighted least squares fit is performed in combination with a tare load iteration. The tare load iteration must use the mean zero load outputs of each load series as the electrical description of the tare loads (see also App. 12 and App. 13).

22.6 Second Weighting Factor Definition

A weighting factor definition can be based on a count of the number of intentionally loaded bridges of a data point. The weighting factor is constructed such that an increase of the number of intentionally loaded bridges decreases the influence of the data point on the regression coefficient estimates. Consequently, the influence of data points with single–component loads increases during the regression analysis of the data.

An individual balance bridge is considered intentionally loaded if the absolute value of the difference between raw bridge output and natural zero of a data point exceeds the empirical threshold of 20 % of the output capacity (see also section 22.7). This conservative

[†] A data point of a single–component load series is obtained by applying one load component to the balance while keeping all other load components close to zero absolute load.

threshold guarantees that data points with small to moderate load levels always get the highest weighting factor if the weighting factor definition is applied.

It is convenient to map weighting factor values to the fixed interval between zero and one. Then, the second weighting factor definition can be summarized by Eqs. (22.19a) to (22.19d) below where w_φ is the weighting factor of the data point with index φ and n_φ is the number of intentionally loaded bridges of the data point. The definition below uses an exponent to control the strength of the weighting. Three choices are listed in Eq. (22.19d). The exponent $\psi = 0$ describes *Equal Weighting*. It results in the constant weighting

Second Weighting Factor Definition

$$n_\varphi > 0 \implies w_\varphi = \left[\frac{\lambda_\varphi}{MAX\ \{\ \lambda_1\ ,\ \ldots\ ,\ \lambda_p\ \}} \right]^\psi \qquad (22.19a)$$

or

$$n_\varphi = 0 \implies w_\varphi = 1.0 \quad \ldots \quad \textit{special case} \qquad (22.19b)$$

where

$$\lambda_\varphi = MAX\ \{\ n_1\ ,\ \ldots\ ,\ n_p\ \}\ /\ n_\varphi \qquad (22.19c)$$

$$\psi = \begin{cases} 0 \implies w_\varphi = 1.0 & \ldots\ \textit{Equal Weighting} \\ 2 \implies w_\varphi \leq 1.0 & \ldots\ \textit{Weighting Method A} \\ 3 \implies w_\varphi \leq 1.0 & \ldots\ \textit{Weighting Method B} \end{cases} \qquad (22.19d)$$

factor of 1.0 for all data points. The exponent $\psi = 2$ suggested itself because the square root of the weighting factors is needed to describe the weighted least squares problem in terms of the normal equations of an ordinary least squares problem (see Eq. (22.12a)). This choice is called *Weighting Method A*. By design, an increase of the number n_φ of loaded balance bridges decreases a data point's weight during the regression analysis if *Weighting Method A* is chosen. The exponent $\psi = 3$ is the third choice. This choice is called *Weighting Method B*. It is similar to *Weighting Method A* but stronger. The special case must be considered when the number of loaded bridges of a data point is zero. Then, the weighting factor of the data point is set to the default value of 1.0 (see Eq. (22.19b)).

It is useful to illustrate the calculation of the weighting factors that are defined in Eqs. (22.19a) and (22.19b). It is assumed, for example, that a six–component balance is calibrated in force balance format. It is also assumed that the final calibration data set consists of 500 data points and that the maximum number of intentionally loaded bridges equals four. These calibration load schedule characteristics can be summarized as follows:

$$\textit{total number of data points} \implies p = 500$$
$$\textit{maximum number of intentionally loaded bridges} \implies MAX\{n_1, \ldots, n_\varphi, \ldots, n_{500}\} = 4$$
$$\textit{possible number of intentionally loaded bridges} \implies 0 \leq n_\varphi \leq 4$$

Now, all possible weighting factors of the balance calibration data set can be computed by applying the definitions given in Eqs. (22.19a) and (22.19b) and using the exponents $\psi = 2$ and $\psi = 3$ as input. Table 22–1 below shows corresponding weights for each possible

Table 22–1: Possible weighting factors w_φ of the balance calibration data example.

n_φ	λ_φ	$\lambda_\varphi / MAX\{\lambda_\varphi\}$	$w_\varphi(\psi = 2)$	$w_\varphi(\psi = 3)$
0	–	–	(22.19b) $\Longrightarrow 1.0$	(22.19b) $\Longrightarrow 1.0$
1	$4/1 = 4.00$	$4.00/4.00 = 1.00$	$(1.00)^2 = 1.0$	$(1.00)^3 = 1.0$
2	$4/2 = 2.00$	$2.00/4.00 = 0.50$	$(0.50)^2 = 0.25$	$(0.50)^3 = 0.125$
3	$4/3 = 1.3\overline{3}$	$1.3\overline{3}/4.00 = 0.3\overline{3}$	$(0.3\overline{3})^2 = 0.\overline{1}$	$(0.3\overline{3})^3 = 0.0\overline{370}$
4	$4/4 = 1.00$	$1.00/4.00 = 0.25$	$(0.25)^2 = 0.0625$	$(0.25)^3 = 0.015625$

number of intentionally loaded bridges of a data point. The successful application of the two weighting factor definitions to calibration data depends on an analyst's ability to objectively count the number of intentionally loaded bridges of each data point. This task and its relationship to the weighting factor definitions is discussed in the next section.

22.7 Determination of Intentionally Loaded Balance Bridges

Weighting factors could be read from the calibration data input file. In that case, the analyst must first determine the number of intentionally loaded bridges of each data point because this information is needed for the application of either the first or second weighting factor definition. The determination of the load status of a bridge can become complex if a calibration data set is large. Then, it is better to include an analytical test in the analysis software that determines if a bridge is intentionally loaded. Afterwards, test results for all bridges could be supplied to an algorithm that determines if the data points of a load series belong to a single–component load series. This information is needed for the application of the first weighting factor definition. Alternatively, test results could be supplied to an algorithm that determines the number of loaded bridges n_φ of the data point. This information is needed for the application of the second weighting factor definition.

The analytical test of the load status of a bridge can be defined if two conditions are fulfilled: (i) each bridge output of a data point is described as the difference between raw bridge output and natural zero; (ii) the analyst specifies an output capacity for each bridge. The output capacity could be, for example, the product of a preliminary estimate of the bridge sensitivity with the capacity of the related primary load component of the bridge. Then, the following condition may be used to test if a bridge is intentionally loaded: *A balance bridge is considered "intentionally loaded" if the absolute value of the output difference of the bridge exceeds the threshold of* 20 % *of output capacity.* The test is summarized in Eq. (22.20) below where rF_i is the raw output of the bridge, N_i is the natural zero of the bridge, and rC_i is the output capacity of the bridge. The test uses the

$$|D_i(\varphi)| = | rF_i(\varphi) - N_i | \geq 0.2 \times rC_i \Longrightarrow \textit{bridge is intentionally loaded} \quad (22.20)$$

empirical threshold of 20 % of the output capacity for the assessment of the load status of the bridge. This choice leads to meaningful test results for most data points.

Appendix 23
Regression Model Definition Differences

23.1 Introduction

A comparison of the term groups for the regression model of a balance load component (App. 9, Table 9–1) with the terms groups for the regression model of a bridge output difference (App. 10, Table 10–1) shows that the total number of all possible terms is the same for a given balance design. However, the total number and the order of the term groups is different. Origins of these differences need to be understood in order to justify the use of the alternate term group order that is described in Table 9–1.

23.2 Number of Term Groups

First, the difference in the total number of term groups is examined. Table 9–1 lists nine term groups. Table 10–1, on the other hand, lists ten term groups. The difference of one term group comes from the fact that Table 9–1 only has a single double summation for the product of an independent variable with the absolute value of another independent variable ($D_j \cdot |D_k|$). On the other hand, Table 10–1 has two double summations for the same type of regression model term ($F_j \cdot |F_k|$ and $|F_j| \cdot F_k$). The simplification of the cross–product term groups in Table 9–1, i.e., the use of a single group $D_j \cdot |D_k|$ instead of two groups $D_j \cdot |D_k|$ and $|D_j| \cdot D_k$, is possible because (i) the commutative law can be applied to the second group and (ii) the result can algebraically be described by a single double summation (see also App. 20).

23.3 Term Group Hierarchy

It is also observed that group $|D_j \cdot D_k|$ comes <u>after</u> group $D_j \cdot |D_k|$ if the term group order of Table 9–1 is compared with the term group order of Table 10–1. This group arrangement results in a hierarchical term group order in Table 9–1 that is better suited for use with a regression model term selection algorithm.

The importance of using a hierarchical term group order as input for a term selection algorithm can be illustrated by using the hypothetical calibration data set of a two–component balance as an example. It is assumed that the chosen balance has two independent load components (F_1 and F_2) and two independent bridge output difference measurements (D_1 and D_2). An analyst decided to use the *Iterative Method* for the load prediction of the two–component balance. Therefore, regression models of the two independent bridge output differences are needed so that the required load iteration equation can be constructed (see App. 10 for more details).

An initial examination of the balance calibration data led the analyst to the conclusion that the given data set only supports terms from groups 1, 2, 5, 6, 7, and 8 of Table 10–1. Therefore, the upper bound of all possible regression models of a bridge output difference of the two–component balance can be constructed by using the eight regression model terms that are listed below. The terms are <u>not</u> in hierarchical order as the term

$$\underbrace{\overbrace{F_1\ ;\ F_2}^{group\ 1}\quad \overbrace{|F_1|\ ;\ |F_2|}^{group\ 2}\quad \overbrace{F_1 \cdot F_2}^{group\ 5}\quad \overbrace{|F_1 \cdot F_2|}^{\textbf{GROUP 6}}\quad \overbrace{F_1 \cdot |F_2|}^{group\ 7}\quad \overbrace{|F_1| \cdot F_2}^{group\ 8}}_{non-hierarchical\ group\ order}$$

of group 6 comes before the terms of groups 7 and 8. Now, a term selection algorithm is applied to the calibration data of the two–component balance. The algorithm is assumed to use *Singular Value Decomposition* (SVD) in combination with the hierarchy rule in order to obtain a regression model that satisfies the following two requirements: (i) the regression model is free of linear dependencies; (ii) the regression model is hierarchical, i.e, the model has no missing lower order terms (see, e.g., App. 19 for the description of key elements of a typical term selection algorithm). The algorithm applies SVD during the model building process by sequentially adding and testing terms for linear dependencies. Terms are added in exactly the original non–hierarchical term group order, i.e., $F_1,\ F_2,\ |F_1|,\ \ldots,\ |F_1| \cdot F_2$, that is given above.

The SVD analysis determined that the terms F_1, F_2, and $|F_1|$ are supported because (i) the load component F_1 has both positive and negative values and (ii) the load component F_2 only has positive values. The SVD analysis also led to the conclusion that the first cross–product term, i.e., $F_1 \cdot F_2$, is supported.

In the next step, the SVD analysis was used to test if the three remaining cross–product terms, i.e., $|F_1 \cdot F_2|$ (group 6), $F_1 \cdot |F_2|$ (group 7), and $|F_1| \cdot F_2$ (group 8) can be added to the regression model. Now, as a result of the non–hierarchical term group order used in Table 10–1, $|F_1 \cdot F_2|$ was examined first and temporarily added to the regression model because it is linearly independent of the cross–product term $F_1 \cdot F_2$. However, the alternate correct term $|F_1| \cdot F_2$ could have been used instead of $|F_1 \cdot F_2|$. This term exchange is possible because $|F_1 \cdot F_2| = |F_1| \cdot |F_2|$ and $|F_2| = F_2$, i.e., the calibration data set only has positive values of F_2. Unfortunately, SVD rejected the correct term $|F_1| \cdot F_2$ because (i) it was examined after term $|F_1 \cdot F_2|$ and (ii) its numerical values are identical with $|F_1 \cdot F_2|$. Consequently, in order to satisfy the hierarchy rule, the incorrect term $|F_1 \cdot F_2| = |F_1| \cdot |F_2|$ is also removed because $|F_2|$ is not in the list of supported lower order terms. In addition, the earlier rejection of the correct term $|F_1| \cdot F_2$ means that it will no longer be considered as the term selection algorithm progresses.

The removal of the incorrect term $|F_1 \cdot F_2|$ and the omission of the correct term $|F_1| \cdot F_2$ may cause data analysis problems if the term is statistically significant. The SVD analysis would have retained the correct term, i.e., $|F_1| \cdot F_2$ if a hierarchical term group order would have been used to define the regression model of the bridge output difference. This hierarchical term group order would look as follows:

$$\underbrace{\overbrace{F_1\ ;\ F_2}^{group\ 1}\quad \overbrace{|F_1|\ ;\ |F_2|}^{group\ 2}\quad \overbrace{F_1 \cdot F_2}^{group\ 5}\quad \overbrace{F_1 \cdot |F_2|}^{group\ 7}\quad \overbrace{|F_1| \cdot F_2}^{group\ 8}\quad \overbrace{|F_1 \cdot F_2|}^{\textbf{GROUP 6}}}_{hierarchical\ group\ order}$$

In that case, the term $|F_1| \cdot F_2$ would not have been removed as (i) the SVD analysis would examine the term $|F_1| \cdot F_2$ before the term $|F_1 \cdot F_2|$ and (ii) the two associated lower order terms, i.e., $|F_1|$ and F_2 are supported by the given calibration data.

23.4 Term Group Order Requirement

It is important for the reader to realize that a hierarchical term group order must be enforced at all times whenever a regression model term selection algorithm uses SVD to test for linear dependencies and the hierarchy rule is applied. Table 9–1 uses a hierarchical term group order to define all possible terms of the regression model of a balance load

component. Unfortunately, Table 10–1 uses a non–hierarchical term group order to define all possible terms of the regression model of a bridge output difference.

The non–hierarchical term group order of Table 10–1 is traditionally used for the definition of the regression model of a bridge output difference that the *Iterative Method* needs for the preparation of the load iteration equation. It was originally defined by AIAA's Internal Balance Technology Working Group. It is the de–facto standard of the group order for anyone who wants to use the *Iterative Method* for the load prediction (see Ref. [7], p. 12, Eq. (3.1.3)). Therefore, a term index mapping procedure must be added to an algorithm that builds the regression model of an output difference. This procedure must make sure that the terms of groups 7 and 8 of Table 10–1 are examined before the terms of group 6 whenever the regression model of an output difference is built.

It must be mentioned for completeness that an earlier hierarchical version of the term group order for the *Iterative Method* is described in the literature. In that case, term groups $F_j \cdot |F_k|$ and $|F_j| \cdot F_k$ of Table 10–1 come before term group $|F_j \cdot F_k|$ (see Ref. [6], p. 22, Eq. (50), cross–product vectors FCP2, FCP3, and FCP4). It is unknown why the hierarchical term group order of Ref. [6] was not adopted when AIAA's Internal Balance Technology Working Group defined the regression model of an electrical output that the *Iterative Method* needs.

Appendix 24
Balance Interactions

24.1 Introduction

Interactions are complex electro–mechanical phenomena that connect the acting balance loads with the observed bridge outputs. They are caused by the fact that bridges are attached to interconnected parts of the balance. These parts are elastically deformed as soon as the load state of the balance changes. Consequently, significant output changes may occur on more than one bridge even if only a single load component is applied.

Two types of interactions are always superimposed whenever calibration or check loads are applied to a balance. The first type is caused by unwanted small load misalignments (see also App. 26). These interactions can be reduced or avoided by (i) refining the load application process, (ii) replacing worn–out load application hardware, and (iii) improving laboratory staff training. The second type, on the other hand, is caused by physical characteristics of the balance. These interactions are repeatable and cannot be eliminated. They must be quantified with interaction terms in a regression model of balance calibration data if the highest load prediction accuracy is to be achieved.

24.2 Linear Interaction Terms

The relationship between a balance load and its interactions is primarily described with linear interaction terms in the regression models of balance calibration data. A linear interaction term is either an electrical output difference or a load. For example, a subset of the output differences $D_1,\ D_2,\ D_3,\ \ldots$ of the balance bridges defines the linear interaction terms that regression models of the *Non–Iterative Method* need (see App. 9, Table 9–1, term group 1). Similarly, a subset of the load components $F_1,\ F_2,\ F_3,\ \ldots$ represents the linear interaction terms that regression models of the *Iterative Method* use (see App. 10, Table 10–1, term group 1).

The identification of linear interaction terms can be demonstrated with two examples. First, it is assumed that interactions have to be described in the regression model of the aft normal force $N2$ of a balance. This regression model is needed whenever the *Non–Iterative Method* is applied to force balance data. It is also assumed that all outputs are formatted as *Difference Type 1*, i.e., as differences relative to the natural zeros of the bridges (see App. 6 for a discussion of output formats). Then, output difference D_2 of the aft normal force bridge is the primary bridge output of $N2$. The remaining five output differences, i.e., D_1, D_3, D_4, D_5 and D_6 are the linear interaction terms in the regression model of $N2$. Similarly, interactions may need to be quantified in a regression model that the *Iterative Method* uses for the prediction of the output difference D_2 of the aft normal force bridge of a force balance. Now, the aft normal force $N2$ is the primary load component of the output difference. Therefore, the remaining five load components, i.e., $N1$, $S1$, $S2$, AF and RM are the linear interaction terms in the regression model of D_2.

24.3 Description of Interactions

It is suggested to use data from a single–component load series for the graphical description of balance interactions. This choice has the advantage that single–component loads can easily be repeated at different sites. In addition, the description is independent of the regression models of the balance data if manual loads are processed. It works with force, moment, and single–piece balance designs as long as (i) single–component loads exist

in the balance data and (ii) the primary sensitivities of all balance bridges are defined.

The suggested approach can be illustrated with data from a force balance. A data set was chosen that fulfilled three requirements: (i) the aft normal force was applied during a load series while keeping all other load components near zero load; (ii) the first data point of the series had outputs that were exclusively caused by tare loads; (iii) tare loads of the series were small. With these conditions met, loads & outputs of the first data point of the series were subtracted from the loads & outputs of the remaining data points. Consequently, the loads were transformed to load differences. Similarly, the outputs were transformed to output format *Difference Type 2* (see also the discussion in App. 6). Finally, the interactions, i.e., the transformed outputs of all but the aft normal force bridge can be plotted versus the transformed aft normal force. The plot on the left–hand side of Fig. 24–1 below shows the interactions that result from the application of the aft normal force as a single–component load. Output difference symbols D_1', D_3', D_4', D_5' and D_6' identify the

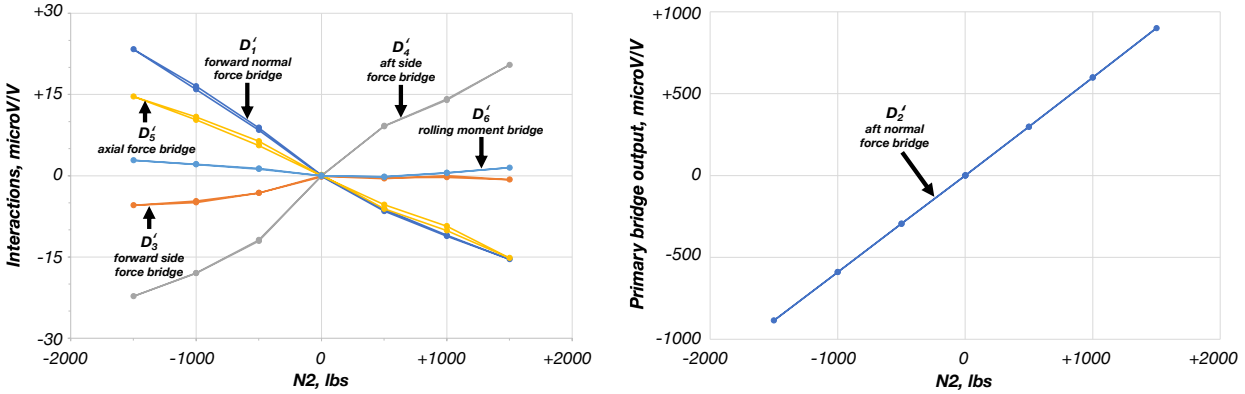

Fig. 24–1 Interactions & primary bridge output differences of the aft normal force.

five interactions. The plot has a characteristic "star" pattern because interactions are, by design, zero if no load is applied. The five interactions have values between −22 and +23 *microV/V*. The omitted primary bridge output difference, i.e., output difference D_2' of the aft normal force bridge is also shown in a separate plot on the right–hand side of Fig. 24–1. Its values vary between −885 and +900 *microV/V*. Therefore, it is concluded that the interactions of the aft normal force of the chosen force balance are small when compared with the range of the corresponding primary bridge output.

Numerical estimates of the first derivatives of the interactions with respect to a primary load component, i.e., the slopes of the five lines shown in Fig. 24–1 above can be obtained from the balance load prediction equations. The first derivatives are the off–diagonal coefficients of inverse matrix $\mathbf{L}^{-1}$ of the linear part of the regression coefficient matrix that the *Non–Iterative Method* needs for the load prediction ($\mathbf{L}^{-1}$ is defined in App. 9, Section 9.6). Similarly, the first derivatives are the off–diagonal coefficients of matrix $\mathbf{C_1}$ that the *Iterative Method* uses ($\mathbf{C_1}$ is defined in App. 10, Section 10.6). Matrix $\mathbf{C_1}$ is the inverse of matrix $\mathbf{C_1}^{-1}$ that is part of the definition of the *Primary Load Iteration Equation* (see App. 10, Section 10.6, Eq. (10.27a)). A more detailed discussion of the use of matrices $\mathbf{L}^{-1}$ and $\mathbf{C_1}$ is given in a later part of this appendix.

Interaction plots of the other five load components, i.e., for $N1$, $S1$, $S2$, AF and RM can be generated by using the same approach that is described above for the aft normal

force. It must be emphasized that the suggested interaction plot becomes the description of a repeatable physical characteristic if the alignment of the balance during the application of a load is perfect. It is like a "fingerprint" of the balance that is independent of both calibration process and load prediction method. Therefore, an analyst can use previously obtained interaction plots for the assessment of the quality of new calibration or check load data sets. Any significant change of the interaction plot may indicate a misalignment of the applied load or a hidden load path change that should be investigated.

24.4 Discussion of Examples

24.4.1 Balance Description

Two calibration data sets of NASA's MK40A balance were selected to illustrate both the graphical and numerical description of balance interactions. The MK40A is a six–component force balance of Task/Able design. It measures five forces and one moment ($N1$, $N2$, $S1$, $S2$, AF, RM). Figure 24–2 below shows the balance in its storage

Fig. 24–2 NASA's MK40A six–component force balance.

box. The MK40A has a diameter of 2.5 inches (63 mm) and a length of 17.3 inches (439 mm). Table 24–1 below lists load capacities of the balance. A basic calibration of the

Table 24–1: Load capacities of the MK40A force balance ($lbs \equiv$ pounds of force).

$N1$, lbs	$N2$, lbs	$S1$, lbs	$S2$, lbs	AF, lbs	RM, $in-lbs$
3500	3500	2500	2500	400	8000

balance was completed in 2006 at the NASA Ames Balance Calibration Laboratory. In addition, a machine calibration was performed at Calspan in 2015 using Calspan's Automatic Balance Calibration System. Results from the two calibrations are discussed in the following sections to illustrate benefits of the suggested description of interactions.

24.4.2 Manual Calibration Data Set of 2006

Gravity weights and a pair of rolling moment arms were used for the load application during the manual calibration at NASA Ames. Loads and outputs of 164 data points were recorded. They were distributed across 16 load series. Single–component loads were applied to all load components. In addition, weights were applied at the balance moment center so that either a normal or side force pair could be applied to the balance.

The calibration data input file was formatted such that a tare load iteration could be performed during the analysis. Bridge output format *Difference Type 1* was used during the calibration data analysis for the description of the electrical outputs. Therefore, the natural zeros of the balance bridges were subtracted from the raw output measurements that were recorded for each data point during the calibration.

Figure 24–3 below shows calibration data from load series 5 and 6 as an example. In this case, the forward side force was applied as a single–component load directly over the

forward side force bridge. The loads are described as differences relative to the loads of the first data point of each load series. The outputs are formatted as *Difference Type 1*. Blue color identifies the applied forward side force and the related output differences of the forward side force bridge. Red color is used to highlight outputs of all other bridges.

		Load Format = Applied Loads = Load Differences --->						Output Format = Difference Type 1 --->					
Point ID	Load Series	N1	N2	S1	S2	AF	RM	D_1	D_2	D_3	D_4	D_5	D_6
		lbs	lbs	lbs	lbs	lbs	in-lbs	microV/V	microV/V	microV/V	microV/V	microV/V	microV/V
...	...	...	...	...	...	...	...	...	...	...	...	...	...
P-0037	5	0	0	0	0	0	0	0.30	0.82	21.34	5.60	2.73	-0.37
P-0038	5	0	0	600	0	0	0	-1.38	2.03	321.67	-6.43	0.67	-0.16
P-0039	5	0	0	1200	0	0	0	-2.44	3.33	623.26	-18.93	-1.10	0.17
P-0040	5	0	0	1800	0	0	0	-3.56	4.58	925.58	-31.33	-3.51	0.36
P-0041	5	0	0	2200	0	0	0	-4.03	5.37	1127.79	-39.51	-4.64	0.57
P-0042	5	0	0	1800	0	0	0	-3.51	4.54	924.73	-31.60	-2.37	0.31
P-0043	5	0	0	1200	0	0	0	-2.44	3.24	621.45	-19.64	-0.34	0.14
P-0044	5	0	0	600	0	0	0	-1.33	2.01	319.53	-7.45	1.76	-0.15
P-0045	5	0	0	0	0	0	0	0.26	0.75	19.57	4.78	3.13	-0.37
P-0046	6	0	0	0	0	0	0	-0.29	-0.09	-20.73	-4.51	2.36	-0.03
P-0047	6	0	0	-600	0	0	0	-1.03	-2.36	-310.27	9.17	4.83	-0.47
P-0048	6	0	0	-1200	0	0	0	-1.43	-4.38	-598.13	22.76	6.46	-0.84
P-0049	6	0	0	-1800	0	0	0	-1.52	-6.18	-885.32	36.52	7.91	-1.13
P-0050	6	0	0	-2200	0	0	0	-1.23	-7.47	-1075.38	45.92	8.97	-1.30
P-0051	6	0	0	-1800	0	0	0	-1.46	-6.35	-882.97	36.90	8.30	-1.14
P-0052	6	0	0	-1200	0	0	0	-1.51	-4.58	-595.17	23.18	6.44	-0.87
P-0053	6	0	0	-600	0	0	0	-1.14	-2.69	-307.33	9.46	4.46	-0.47
P-0054	6	0	0	0	0	0	0	-0.26	-0.20	-19.84	-4.47	2.32	-0.03
...	...	...	...	...	...	...	...	...	...	...	...	...	...

Fig. 24–3 Load & output differences of load series 5 and 6 of the manual calibration data of 2006 if electrical outputs are formatted as *Difference Type 1* (blue ≡ primary load & output; black ≡ residual load; red ≡ output difference).

The format shown in Fig. 24–3 above was used during the analysis of the calibration data. Afterwards, all outputs of the balance bridges were transformed from output format *Difference Type 1* to output format *Difference Type 2* so that interactions could be plotted as described in the previous chapter. Figure 24–4 below shows data of load series 5 and 6 after the outputs were transformed to *Difference Type 2*. The last six columns of Fig. 24–4 were obtained from the outputs of Fig. 24–3 by subtracting the outputs of

		Load Format = Applied Loads = Load Differences --->						Output Format = Difference Type 2 --->					
Point ID	Load Series	N1	N2	S1	S2	AF	RM	D_1'	D_2'	D_3'	D_4'	D_5'	D_6'
		lbs	lbs	lbs	lbs	lbs	in-lbs	microV/V	microV/V	microV/V	microV/V	microV/V	microV/V
...	...	...	...	...	...	...	...	...	...	...	...	...	...
P-0037	5	0	0	0	0	0	0	0.00	0.00	0.00	0.00	0.00	0.00
P-0038	5	0	0	600	0	0	0	-1.68	1.21	300.33	-12.03	-2.06	0.21
P-0039	5	0	0	1200	0	0	0	-2.74	2.51	601.91	-24.54	-3.83	0.54
P-0040	5	0	0	1800	0	0	0	-3.86	3.77	904.24	-36.93	-6.24	0.73
P-0041	5	0	0	2200	0	0	0	-4.33	4.55	1106.45	-45.11	-7.37	0.94
P-0042	5	0	0	1800	0	0	0	-3.80	3.72	903.39	-37.20	-5.10	0.68
P-0043	5	0	0	1200	0	0	0	-2.74	2.42	600.10	-25.24	-3.07	0.51
P-0044	5	0	0	600	0	0	0	-1.63	1.19	298.18	-13.05	-0.97	0.22
P-0045	5	0	0	0	0	0	0	-0.03	-0.07	-1.77	-0.82	0.40	0.00
P-0046	6	0	0	0	0	0	0	0.00	0.00	0.00	0.00	0.00	0.00
P-0047	6	0	0	-600	0	0	0	-0.74	-2.28	-289.53	13.68	2.47	-0.44
P-0048	6	0	0	-1200	0	0	0	-1.14	-4.30	-577.40	27.27	4.10	-0.80
P-0049	6	0	0	-1800	0	0	0	-1.23	-6.10	-864.59	41.03	5.55	-1.10
P-0050	6	0	0	-2200	0	0	0	-0.94	-7.38	-1054.65	50.43	6.61	-1.27
P-0051	6	0	0	-1800	0	0	0	-1.17	-6.27	-862.24	41.41	5.94	-1.10
P-0052	6	0	0	-1200	0	0	0	-1.22	-4.49	-574.43	27.70	4.08	-0.84
P-0053	6	0	0	-600	0	0	0	-0.85	-2.61	-286.60	13.98	2.10	-0.43
P-0054	6	0	0	0	0	0	0	0.03	-0.12	0.89	0.04	-0.04	0.00
...	...	...	...	...	...	...	...	...	...	...	...	...	...

Fig. 24–4 Load & output differences of load series 5 and 6 of the manual calibration data of 2006 if electrical outputs are formatted as *Difference Type 2* (blue ≡ primary load & output; black ≡ residual load; red ≡ interaction).

the zero load point of the load series from all other outputs of the series. Therefore, for example, the outputs of point P–0050 of Fig. 24–4 were obtained by subtracting the outputs

of point P–0046 of Fig. 24–3, i.e., the outputs of the zero load point of series 6, from the outputs of point P–0050 of Fig. 24–3. Again, color is used in Fig. 24–4 to identify loads and outputs. Blue color marks the applied single–component loads and related output differences of the primary bridge. Red color identifies interactions.

Finally, interactions of the forward side force can be plotted as described in the previous chapter. Figure 24–5 below shows the graphical representation of the interactions that are given in Fig. 24–4. The plot has the expected star pattern. The aft side force bridge shows the largest interactions of the five bridges. This result is no surprise because the

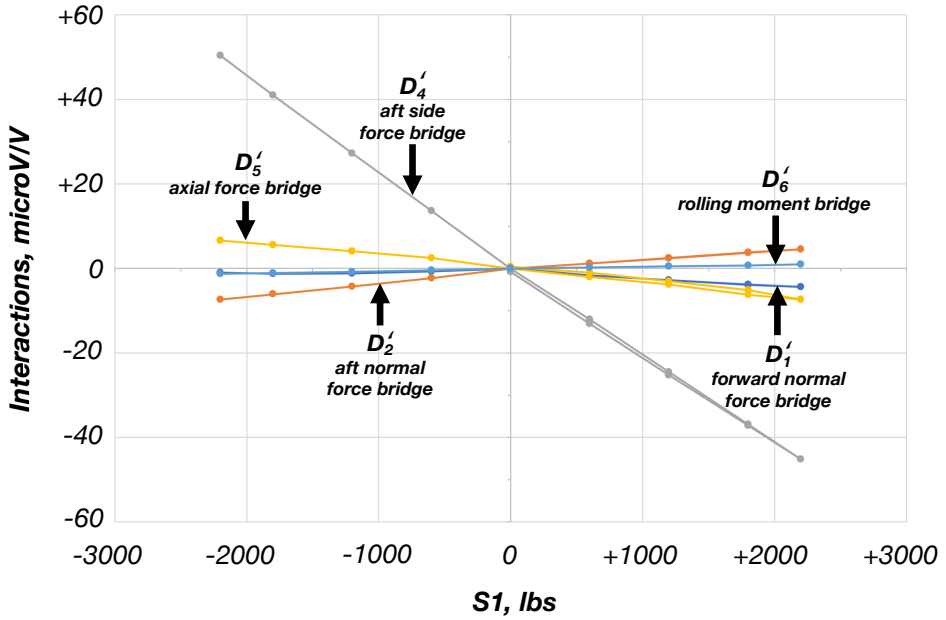

Fig. 24–5 Interactions of the forward side force of the MK40A force balance that were observed during the manual calibration of 2006.

forward & aft side force bridges are located in planes that are almost parallel to each other. The remaining four bridges show much smaller interactions.

It is possible to quantify the slopes of the lines that are shown in Fig. 24–5 above. The slopes are obtained after processing a subset of the coefficients of the load prediction equations that the *Non–Iterative* and *Iterative Method* obtained from the calibration data. First, the load prediction equations of the *Non–Iterative Method* are examined. In this case, slopes can be reverse–engineered from the coefficients of the linear terms of the regression models of the six load components. This subset of thirty–six coefficients is assembled in an auxiliary matrix **L** that is shown in Fig. 24–6 below. By design, matrix **L** uses the six

	D1	D2	D3	D4	D5	D6
N1	2.918350E+00	8.005132E-02	-1.366696E-03	-4.574781E-03	1.107305E-03	-1.857555E-02
N2	3.356263E-01	2.693939E+00	-1.980768E-02	-1.254993E-02	2.544596E-03	1.872111E-03
S1	-4.603911E-02	-9.689182E-03	2.042009E+00	2.943083E-02	6.549501E-06	-5.959835E-02
S2	-4.640791E-03	-2.131397E-02	8.825172E-02	1.990231E+00	6.384245E-04	-6.636981E-02
AF	-5.719457E-03	3.638223E-03	1.258844E-03	-3.409930E-03	2.802507E-01	-4.757801E-03
RM	2.147850E-04	1.485202E-03	-5.926800E-03	6.005366E-03	-2.189307E-02	6.102772E+00

Fig. 24–6 Coefficients of matrix **L** ; they are the coefficients of the linear terms of the regression models of the loads that the *Non–Iterative Method* uses.

loads as dependent variables. However, the slopes shown in Fig. 24–5 above interpret the bridge outputs as dependent variables. Therefore, numerical estimates of the slopes are obtained by simply computing the inverse of matrix **L**. The coefficients of this inverse matrix are listed in Fig. 24–7 below. The estimates of the slopes of the five lines shown

	N1	N2	S1	S2	AF	RM
D1	3.438340E-01	-1.021006E-02	1.038034E-04	7.192045E-04	-1.184847E-03	1.057602E-03
D2	-4.278840E-02	3.725095E-01	3.491363E-03	2.194006E-03	-3.233067E-03	-1.890754E-04
D3	7.549872E-03	1.477942E-03	4.900594E-01	-7.233855E-03	3.312766E-04	4.729928E-03
D4	7.405044E-06	3.897886E-03	-2.167574E-02	5.027822E-01	-7.697984E-04	5.254481E-03
D5	7.539300E-03	-5.005390E-03	-2.499942E-03	6.128099E-03	3.568458E+00	2.848731E-03
D6	3.268344E-05	-1.106532E-04	4.874368E-04	-4.803579E-04	1.280339E-02	1.638696E-01

Fig. 24–7 Coefficients of matrix $\mathbf{L}^{-1}$; the off–diagonal values shown in "black" color are the numerical estimates of the slopes of the interactions.

in Fig. 24–5 can be found inside the red boxes that are visible in Fig. 24–7 above.

A similar approach may be used to obtain the slopes from the load prediction equation of the *Iterative Method*. In this case, slopes must be reverse–engineered from the coefficients of the square matrix that is the "non–iterative" part of the *Primary Load Iteration Equation*. This matrix is traditionally called matrix $\mathbf{C_1}^{-1}$ (see App. 10). Its thirty–six coefficients are listed in Fig. 24–8 below. By design, matrix $\mathbf{C_1}^{-1}$ uses the six loads as de–

	D1	D2	D3	D4	D5	D6
N1	2.920622E+00	8.035905E-02	-1.454707E-03	-4.509540E-03	1.182913E-03	-1.818541E-02
N2	3.378920E-01	2.694380E+00	-1.997439E-02	-1.247347E-02	2.580479E-03	2.102796E-03
S1	-4.629670E-02	-9.757370E-03	2.041806E+00	2.911605E-02	-1.243538E-04	-6.037029E-02
S2	-5.405324E-03	-2.152418E-02	8.837550E-02	1.989473E+00	4.965192E-04	-6.683237E-02
AF	-5.710808E-03	3.736958E-03	1.216919E-03	-3.478078E-03	2.803089E-01	-4.763753E-03
RM	-6.120413E-04	2.112007E-03	-5.772905E-03	6.177156E-03	-2.216850E-02	6.102964E+00

Fig. 24–8 Coefficients of matrix $\mathbf{C_1}^{-1}$; they describe the "non–iterative" part of the load iteration equation that the *Iterative Method* uses.

pendent variables. However, the slopes shown in Fig. 24–5 above interpret the bridge outputs as dependent variables. Therefore, numerical estimates of the slopes can be obtained by computing the inverse $\mathbf{C_1}$ of matrix $\mathbf{C_1}^{-1}$. The resulting coefficients of matrix $\mathbf{C_1}$ are listed in Fig. 24–9 below. Again, estimates of the slopes of the five lines shown in Fig. 24–5

	N1	N2	S1	S2	AF	RM
D1	3.435784E-01	-1.024009E-02	1.176780E-04	7.074213E-04	-1.274973E-03	1.035228E-03
D2	-4.303731E-02	3.724613E-01	3.519993E-03	2.181080E-03	-3.265353E-03	-2.004185E-04
D3	7.585821E-03	1.486876E-03	4.901056E-01	-7.160100E-03	5.634067E-04	4.792228E-03
D4	1.318257E-04	3.932005E-03	-2.171627E-02	5.029711E-01	-5.188113E-04	5.291755E-03
D5	7.543697E-03	-5.134354E-03	-2.433624E-03	6.248902E-03	3.567722E+00	2.853439E-03
D6	8.379365E-05	-1.511453E-04	4.755338E-04	-4.938437E-04	1.296151E-02	1.638645E-01

Fig. 24–9 Coefficients of matrix $\mathbf{C_1}$; the off–diagonal values shown in "black" color are the numerical estimates of the slopes of the interactions.

can be found inside the red boxes that are visible in Fig. 24–9 above.

It is interesting to compare the slope estimates for the forward side force interactions that were obtained from the coefficients of the two load prediction methods. Estimates are

summarized in Table 24–2 below. Overall, the agreement between the estimates is very good considering the fact that the slopes were reverse–engineered from subsets of the coef–

Table 24–2: Interaction slopes of the forward side force in units of $(microV/V)/lbs$.

Method	$\partial D_1' \ / \ \partial S1$	$\partial D_2' \ / \ \partial S1$	$\partial D_4' \ / \ \partial S1$	$\partial D_5' \ / \ \partial S1$	$\partial D_6' \ / \ \partial S1$
$Non-Iterative$ †	+1.0380 E−4	+3.4914 E−3	−2.1676 E−2	−2.4999 E−3	+4.8744 E−4
$Iterative$ ‡	+1.1768 E−4	+3.5200 E−3	−2.1716 E−2	−2.4336 E−3	+4.7553 E−4

†numerical values were copied from Fig. 24–7 ; ‡numerical values were copied from Fig. 24–9.

ficients of the load prediction equations. The connection between the estimated slopes shown in Table 24–2 and the observed interactions listed in Fig. 24–4 can be illustrated by directly computing the slope of the aft side force bridge output from the calibration data subset that is shown in Fig. 24–4. This new slope estimate is obtained from the load and output differences of data points P–0041 and P–0050. The corresponding result is given in Eq. (24.1) below. The new slope estimate agrees almost to the third significant

$$\frac{\partial\, D_4'}{\partial\, S1} \;\approx\; \Big\{(-45.11) \;-\; (+50.43)\Big\} \,/\, \Big\{2 \;\times\; 2200\Big\} \;=\; -2.171\overline{36}\ \text{E}{-2} \qquad (24.1)$$

digit with the two original estimates that are listed in the fourth column of Table 24–2.

24.4.3 Machine Calibration Data Set of 2015

A machine calibration of the MK40A balance was also performed in 2015 in Calspan's Automatic Balance Calibration System. The calibration data set consisted of both single– and multi–component loads. Therefore, it can be used for an alternate assessment of the interactions of the forward side force of the MK40A balance.

A total of 2287 data points were recorded during the calibration that were distributed across 23 load series. Single–component loads of the forward side force were applied during load series 3. Figure 24–10 below shows data of load series 3 after the outputs were formatted as *Difference Type 2*. The output differences were obtained by subtracting the

		Applied Machine Loads of Single-Component Load Series --->						Output Format = Difference Type 2 --->					
Point ID	Load Series	N1	N2	S1	S2	AF	RM	D_1'	D_2'	D_3'	D_4'	D_5'	D_6'
		lbs	lbs	lbs	lbs	lbs	in-lbs	microV/V	microV/V	microV/V	microV/V	microV/V	microV/V
...	...	...	...	...	...	...	...	...	...	...	...	...	...
P-0130	3	0	0	0	0	0	0	0.00	0.00	0.00	0.00	0.00	0.00
P-0131	3	-0.07	-0.15	-813.36	55.57	0.11	1.62	-1.66	-3.89	-392.58	44.79	4.86	-0.14
P-0132	3	0.83	-1.16	-1638.03	54.24	0.56	4.93	-2.48	-7.49	-787.21	62.21	9.37	-0.05
P-0133	3	-0.58	-0.82	-2487.36	53.76	0.52	10.23	-3.12	-10.20	-1190.29	80.99	12.17	0.35
P-0134	3	0.82	-0.63	-1987.29	52.59	1.21	4.81	-2.79	-8.71	-951.91	70.58	11.18	-0.28
P-0135	3	-0.27	-1.33	-1488.65	52.94	0.97	4.51	-2.96	-7.08	-714.03	60.22	7.75	-0.14
P-0136	3	-0.77	-1.94	-988.93	52.96	0.83	2.24	-2.46	-5.32	-474.96	48.88	5.99	-0.10
P-0137	3	0.95	-0.86	-489.76	53.64	0.09	0.01	-0.85	-2.69	-235.45	38.03	1.77	-0.20
P-0138	3	-0.52	-0.96	9.47	53.43	-0.11	-1.95	-0.27	-0.03	4.17	26.47	-0.29	-0.26
P-0139	3	2.10	0.03	501.90	51.69	-0.10	-8.26	1.08	2.18	245.71	14.68	-2.18	-1.31
P-0140	3	1.25	0.50	1004.22	53.19	-1.28	-8.85	-0.63	3.50	498.41	5.27	-9.15	-1.45
P-0141	3	2.03	1.38	1504.69	53.90	-2.69	-13.38	-1.35	4.83	750.94	-4.31	-16.51	-2.23
P-0142	3	1.89	1.51	2006.07	54.36	-2.48	-17.27	-2.38	6.06	1004.26	-14.15	-17.79	-2.89
P-0143	3	2.02	2.18	2506.06	53.61	-2.99	-20.80	-3.31	7.35	1257.00	-24.48	-21.28	-3.45
P-0144	3	1.69	0.36	1658.81	54.48	0.03	-14.89	-1.93	4.70	828.18	-7.98	-6.37	-2.72
P-0145	3	1.27	0.32	835.97	54.48	1.12	-8.58	-0.61	2.64	412.34	8.17	1.00	-1.53
P-0146	3	-0.46	-0.90	-3.92	56.94	0.45	-3.50	-0.18	-0.14	-5.51	27.12	2.13	-0.65
...	...	...	...	...	...	...	...	...	...	...	...	...	...

Fig. 24–10 Applied load & output differences of load series 3 of the machine calibration data set of 2015 if the outputs are formatted as *Difference Type 2* (blue ≡ primary load & output; black ≡ residual load; red ≡ uncor. interaction).

raw outputs of data point P–0130 from the raw outputs of all other data points of the load series. Figure 24–11 below shows the uncorrected interactions, i.e., the red values of Fig. 24–10 plotted versus the forward side force. It can be seen that the plot of the un–

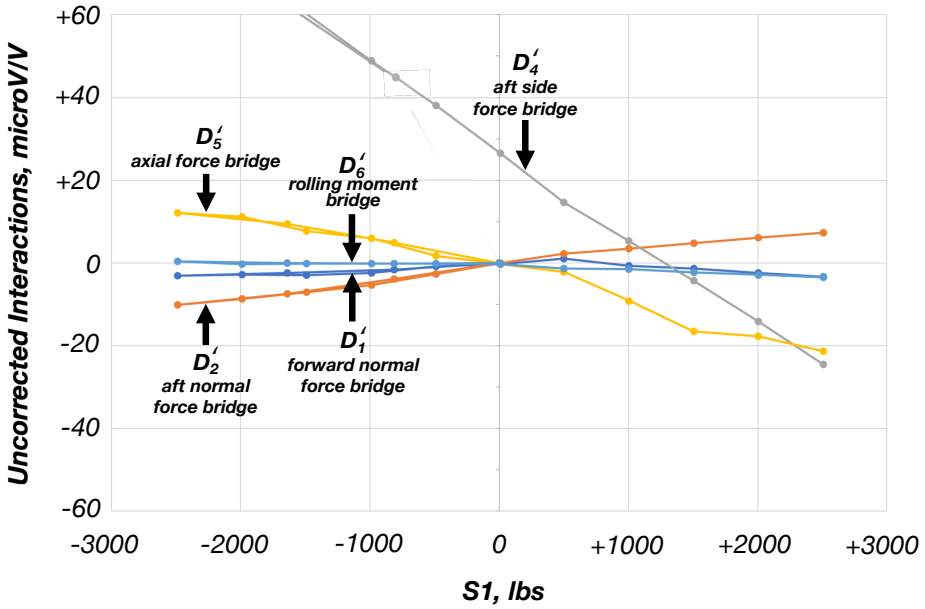

Fig. 24–11 Uncorrected interactions of the forward side force of the MK40A force balance that were observed during the machine calibration of 2015.

corrected interactions does not show the expected star pattern. It is also observed in Fig. 24–10 that the calibration machine's control logic applied small residual machine loads to the balance. These residual loads are true physical loads. Black color is used in the load columns of Fig. 24–10 for the identification of the residual loads. It is possible to remove the effects of the small residual machine loads from the uncorrected interactions. The resulting corrected values are the true interactions that are associated with the application of the forward side force as a single–component load.

In theory, the true interactions, i.e., the corrected output differences of a data point of a single–component load series are obtained after subtracting outputs associated with the residual machine loads from the original output differences of a data point. Linear approximations of these output corrections can be computed by using (i) the coefficients of the linear terms of the regression models of the outputs and (ii) the residual machine loads as input. The coefficients are contained in inverse matrix $\mathbf{L}^{-1}$ of the linear part of the regression coefficient matrix that the *Non–Iterative Method* needs for the load prediction (see App. 9, Eq. (9.15)). Similarly, the coefficients can be found in matrix $\mathbf{C_1}$ that the *Iterative Method* uses. This matrix equals the inverse of matrix $\mathbf{C_1}^{-1}$ that is part of the *Primary Load Iteration Equation* (see App. 10, Eq. (10.22a)). It is also known that matrices $\mathbf{L}^{-1}$ and $\mathbf{C_1}$ are approximately equal to each other if (i) the same calibration data set is processed, (ii) the same regression model term classes are used for the analysis, and (iii) a tare load iteration is performed. Therefore, symbol $\mathbf{P}$ may be introduced to describe both matrices. Coefficients of the linear terms of the regression models of the outputs are listed in Eq. (24.2) below. Symbol D_i represents an output difference of a bridge with index i that is formatted as *Difference Type 1*. Symbol F_j is a load component with index j.

$$\mathbf{P} \;=\; \begin{bmatrix} \dfrac{\partial\, D_1}{\partial\, F_1} & \cdots & \dfrac{\partial\, D_1}{\partial\, F_j} & \cdots & \dfrac{\partial\, D_1}{\partial\, F_6} \\ \vdots & \vdots & \vdots & \vdots & \vdots \\ \dfrac{\partial\, D_i}{\partial\, F_1} & \cdots & \dfrac{\partial\, D_i}{\partial\, F_j} & \cdots & \dfrac{\partial\, D_i}{\partial\, F_6} \\ \vdots & \vdots & \vdots & \vdots & \vdots \\ \dfrac{\partial\, D_6}{\partial\, F_1} & \cdots & \dfrac{\partial\, D_6}{\partial\, F_j} & \cdots & \dfrac{\partial\, D_6}{\partial\, F_6} \end{bmatrix} \;\approx\; \mathbf{L}^{-1} \;\approx\; \mathbf{C_1} \tag{24.2}$$

It is also helpful to describe the residual machine loads of a single–component load series as the product of an auxiliary square matrix with a column vector that has the acting machine loads of each data point. The column vector with the acting machine loads is defined in Eq. (24.3) below. Symbol ν identifies the data point. Symbol ξ is the subscript of the load component that is applied during the given load series.

$$\mathbf{F}(\nu) \;=\; \begin{bmatrix} F_1(\nu) \\ \vdots \\ F_\xi(\nu) \\ \vdots \\ F_6(\nu) \end{bmatrix} \tag{24.3}$$

Auxiliary square matrix $\mathbf{Q}_\xi$ is defined in Eq. (24.4) below. Its coefficients equal the coefficients of the identity matrix with the exception of the coefficient on the principal

$$\mathbf{Q}_\xi \;=\; \begin{bmatrix} q_{1,1} & \cdots & q_{1,j} & \cdots & q_{1,6} \\ \vdots & \vdots & \vdots & \vdots & \vdots \\ q_{i,1} & \cdots & q_{i,j} & \cdots & q_{i,6} \\ \vdots & \vdots & \vdots & \vdots & \vdots \\ q_{6,1} & \cdots & q_{6,j} & \cdots & q_{6,6} \end{bmatrix} \quad where \quad q_{i,j} \;=\; \begin{cases} 0 & \text{if } \; i \neq j \\ 0 & \text{if } \; i = j \;\; \& \;\; i = \xi \\ 1 & \text{if } \; i = j \;\; \& \;\; i \neq \xi \end{cases} \tag{24.4}$$

diagonal that has the subscript ξ of the applied load component of the series. This coefficient is set to zero. Now, the column vector $\mathbf{F}_{res}$ with the residual machine loads of the data point can be described as the product of square matrix $\mathbf{Q}_\xi$ with column vector $\mathbf{F}$. Then, the following relationship is obtained:

$$\mathbf{F}_{res}(\nu) \;=\; \mathbf{Q}_\xi \;\cdot\; \mathbf{F}(\nu) \tag{24.5}$$

Finally, the corrected output differences of a data point are obtained after (i) multiplying matrix $\mathbf{P}$ with column vector $\mathbf{F}_{res}$ and (ii) subtracting the result from the uncorrected output differences. The following relationship is obtained:

$$\mathbf{D}''(\nu) \;=\; \mathbf{D}'(\nu) \;-\; \overbrace{\mathbf{P}\cdot\underbrace{\mathbf{Q}_{\xi}\cdot\mathbf{F}(\nu)}_{\mathbf{F}_{res}(\nu)}}^{linear\ corrections} \qquad (24.6a)$$

where

$$\underbrace{\mathbf{D}''(\nu) \;=\; \begin{bmatrix} D_1''(\nu) \\ \vdots \\ D_6''(\nu) \end{bmatrix}}_{corrected\ outputs} \;;\quad \underbrace{\mathbf{D}'(\nu) \;=\; \begin{bmatrix} D_1'(\nu) \\ \vdots \\ D_6'(\nu) \end{bmatrix}}_{uncorrected\ outputs} \qquad (24.6b)$$

In theory, better estimates of the corrected output differences can be obtained if more complex regression models of the outputs are used for the calculation of the corrections. These types of regression models are generated, for example, if the *Iterative Method* is applied to balance calibration data and outputs are formatted as *Difference Type 1* (see App. 10, Eq. (10.35)). However, experience showed that the linear corrections used in Eq. (24.6*a*) above are sufficiently accurate for most machine calibration data sets.

The relationships described in Eqs. (24.2) to (24.6*b*) can easily be applied to the given machine calibration data set. First, matrix **P** has to be determined from Calspan's machine calibration data of 2015. It was decided to apply the *Non–Iterative Method* to the data. Therefore, matrix **P** equals the inverse of matrix **L** that is obtained during the analysis. The coefficients of this matrix are listed in Fig. 24–12 below. It is observed that the most

	N1	N2	S1	S2	AF	RM
D1	3.445460E-01	-8.727058E-03	7.374985E-04	1.293747E-04	-2.592163E-04	5.809138E-04
D2	-4.320775E-02	3.746786E-01	3.935917E-03	1.298728E-03	-1.849461E-03	-6.768421E-04
D3	9.917392E-03	1.068966E-03	4.881267E-01	-7.094531E-03	4.020643E-04	4.212135E-03
D4	2.711497E-04	6.316608E-03	-2.074025E-02	5.000594E-01	8.206360E-04	5.147821E-03
D5	3.665357E-03	-4.130385E-03	-5.503902E-03	2.940954E-03	3.574673E+00	2.208708E-03
D6	5.913257E-04	1.035551E-03	-2.798090E-04	-1.387067E-03	1.436095E-02	1.636654E-01

Fig. 24–12 Coefficients of matrix **P**, i.e., of matrix $\mathbf{L}^{-1}$ that were obtained after processing Calspan's machine calibration data with the *Non–Iterative Method*.

important coefficients of matrix **P** are close to corresponding values that are given in Fig. 24–7 for the matrix from the 2006 calibration data. Larger differences exist for the off–diagonal values. They are expected as the calibration load schedule of 2015 had a large number of combined loadings that were not applied during the calibration of 2006.

The forward side force is the acting single–component load of load series 3. It is the third component of the load vector. Therefore, subscript ξ equals 3. Now, the residual machine load vector of each data point of the load series can be assigned. The corrected output differences are obtained after (i) multiplying matrix **P** with the residual machine load vector of each data point and (ii) subtracting the resulting corrections from the uncorrected outputs that are listed in Fig. 24–10. Figure 24–13 below shows final results of these calculations. All residual loads of the series were set to zero because their influence

		Adjusted Machine Loads of Single-Component Load Series --->						Adjusted Outputs of Difference Type 2 --->					
Point ID	Load Series	N1	N2	S1	S2	AF	RM	D_1''	D_2''	D_3''	D_4''	D_5''	D_6''
		lbs	lbs	lbs	lbs	lbs	in-lbs	microV/V	microV/V	microV/V	microV/V	microV/V	microV/V
...	...	...	...	...	...	...	...	...	...	...	...	...	...
P-0130	3	0	0	0	0	0	0	0.00	0.00	0.00	0.00	0.00	0.00
P-0131	3	0	0	-813.36	0	0	0	-1.65	-3.91	-392.19	16.99	4.32	-0.33
P-0132	3	0	0	-1638.03	0	0	0	-2.79	-7.09	-786.86	35.06	7.18	-0.79
P-0133	3	0	0	-2487.36	0	0	0	-2.94	-9.98	-1189.94	54.06	10.14	-1.26
P-0134	3	0	0	-1987.29	0	0	0	-3.08	-8.50	-951.56	44.26	6.69	-1.01
P-0135	3	0	0	-1488.65	0	0	0	-2.89	-6.66	-713.67	33.73	4.10	-0.81
P-0136	3	0	0	-988.93	0	0	0	-2.22	-4.69	-474.58	22.40	2.86	-0.40
P-0137	3	0	0	-489.76	0	0	0	-1.19	-2.40	-235.08	11.21	1.29	-0.13
P-0138	3	0	0	9.47	0	0	0	-0.11	0.24	4.56	-0.24	-0.04	0.14
P-0139	3	0	0	501.90	0	0	0	0.36	2.18	246.09	-11.12	-1.96	0.11
P-0140	3	0	0	1004.22	0	0	0	-1.06	3.29	498.82	-21.29	-4.70	0.09
P-0141	3	0	0	1504.69	0	0	0	-2.04	4.32	751.36	-31.21	-7.01	0.07
P-0142	3	0	0	2006.07	0	0	0	-3.01	5.50	1004.69	-41.26	-9.04	0.05
P-0143	3	0	0	2506.06	0	0	0	-3.98	6.53	1257.45	-51.19	-10.71	0.07
P-0144	3	0	0	1658.81	0	0	0	-2.51	4.56	828.62	-35.15	-6.62	-0.21
P-0145	3	0	0	835.97	0	0	0	-1.05	2.50	412.75	-19.04	-3.14	-0.06
P-0146	3	0	0	-3.92	0	0	0	-0.04	0.10	-5.08	-1.32	0.38	-0.01
...	...	...	...	...	...	...	...	...	...	...	...	...	...

Fig. 24–13 Corrected load & output differences of load series 3 of the machine calibration data set of 2015 if the outputs are formatted as *Difference Type 2* (blue ≡ primary load & output; black ≡ residual load; red ≡ interaction).

on the outputs was removed. The corrected output differences, i.e., the values listed in red color in Fig. 24–13 describe the true interactions. The output differences D_3'' of the forward side force bridge itself are listed in blue color. Their values also changed by a small amount after effects of residual machine loads were removed from the original output differences. These changes can be seen if the uncorrected outputs listed in column D_3' of Fig. 24–10 are compared with the corrected outputs that are listed in column D_3'' of Fig. 24–13.

Figure 24–14 below shows the true interactions of the forward side force, i.e., the red values given in Fig. 24–13 plotted versus the forward side force. Now, the expected star

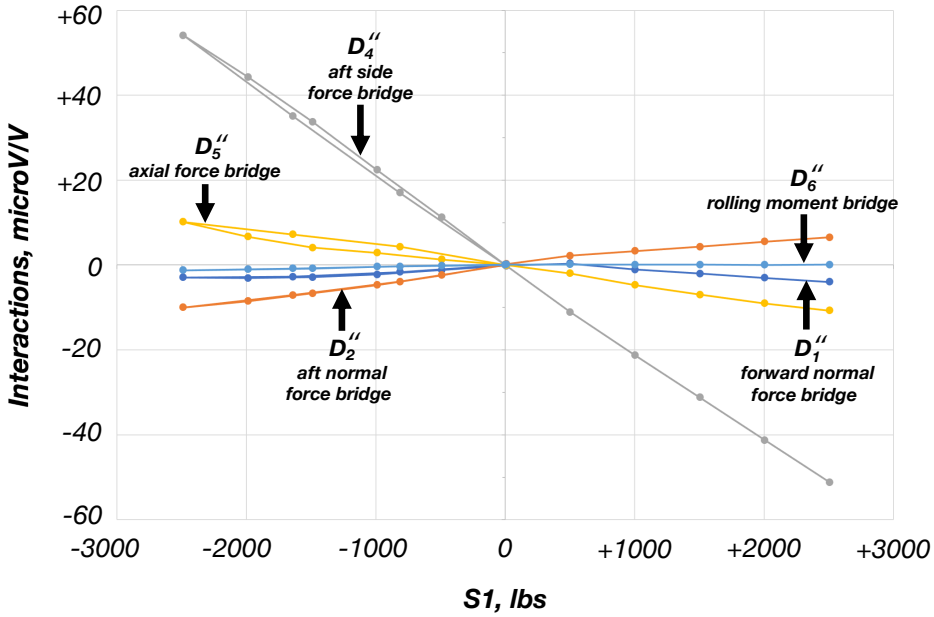

Fig. 24–14 Interactions of the forward side force of the MK40A force balance that were observed during the machine calibration of 2015.

pattern is observed. In addition, the interactions show excellent quantitative agreement with interactions that are plotted in Fig. 24–5 for the manual calibration data of 2006.

Several conclusions can be drawn. First, the interactions of the forward side force are physical characteristics of the MK40A balance that can be repeated at different laboratories as long as load alignment errors are negligible and effects of residual machine loads are removed (if applicable). Furthermore, the excellent agreement between the two independent sets of observed interactions confirms that the machine calibration data of load series 3 is an accurate description of the physical behavior of the balance.

24.5 Quantification and Assessment of Interaction Differences

Differences between the interactions of the single–component loads of calibration and check load data can be quantified and assessed if alignment errors of the calibration loads are negligible. Then, the interactions of the calibration data become the point of reference for the interaction assessment after they are fitted with simple second order polynomials (for additional details see Ref. [83]). An absolute value term may be included in the simple regression model if both positive and negative values of the load were applied. The simple regression model of an interaction of a single–component load is defined in Eq. (24.7) below. Each load component of a six–component balance has five interactions. Therefore,

$$Interaction \;\equiv\; b_1 \times Load + b_2 \times \{Load\}^2 + b_3 \times |Load| \qquad (24.7)$$

a total number of thirty regression models are needed for the complete assessment of the interactions of the single–component loads of the check load data.

The assessment of the interactions of check load data is done in several steps. First, the single–component load values of the check load data are used as inputs for the simple regression models of the interactions of the calibration data. The resulting values are the "predicted" interactions of the check load data. Then, absolute values of the differences between "predicted" and "observed" interactions of the check load data are computed. Finally, the largest difference for each load component is compared with empirical thresholds to decide if the interactions meet data quality expectations. Experience showed that the agreement between the interactions of the calibration and check load data sets is "excellent" if the largest difference is less than 2.0 *microV/V*. The agreement is still considered "acceptable" if the largest difference is less than 4.0 *microV/V*. In all other cases, a data quality problem may exist in the check load data set that should be investigated.

The coefficients of the multivariate regression model of a bridge output are obtained as intermediate results when the *Iterative Method* is used to analyze balance calibration data. A subset of these coefficients can directly be compared with the coefficients b_1, b_2, and b_3 of the simple regression model of an interaction that is defined in Eq. (24.7). For example, coefficient $\partial D_4 / \partial S1$ of the multivariate regression model of the aft side force bridge output difference D_4 of a machine calibration data set should be close to coefficient b_1 of the simple regression model of the interaction D_4'' of the forward side force $S1$. Similarly, coefficient $\partial D_4 / \partial (S1^2)$ of the multivariate regression model should be close to coefficient b_2 of the simple regression model of D_4'' of the forward side force $S1$. The agreement between corresponding coefficients of the two regression models is expected to be good whenever the term from the multivariate regression model of the calibration data is considered a "very important" term. This characteristic is fulfilled if the absolute value of the term's *Percent Contribution* exceeds 0.5 % (see also App. 16, Table 16–3, p. 351).

Appendix 25

Universal Load Iteration Equation

25.1 Load Iteration Equation Types

The *Iterative Method* may be used to predict loads of an n–component strain–gage balance during a wind tunnel test (see App. 10 for more details). This approach first fits the electrical outputs of balance calibration data using regression models that are constructed from the calibration loads. Afterwards, a load iteration equation is generated from the regression models of the fitted outputs so that loads can be predicted from the measured outputs of the balance bridges during a wind tunnel test.

Two types of load iteration equations are traditionally used in the aerospace testing community whenever the *Iterative Method* is chosen for the balance load prediction. The first type is called *Primary Load Iteration Equation* (see App. 10, Eq. (10.27a)). It is defined in Eq. (25.1) below where $\mathbf{F}_\xi$ is the load vector, $\mathbf{\Delta rF}$ is the output difference vector,

$$\mathbf{F}_\xi \;=\; \left[\ \mathbf{C_1}^{-1}\ \right] \cdot \mathbf{\Delta rF} \;-\; \left[\ \mathbf{C_1}^{-1}\,\mathbf{C_2}\ \right] \;\cdot\; \mathbf{H}(\mathbf{F}_{\xi-\mathbf{1}}) \tag{25.1}$$

$\mathbf{H}(\mathbf{F}_{\xi-\mathbf{1}})$ is a matrix that depends on the load vector $\mathbf{F}_{\xi-\mathbf{1}}$ of the previous iteration step, $\mathbf{C_1}^{-1}$ and $\mathbf{C_1}^{-1}\mathbf{C_2}$ are two auxiliary matrices that are obtained from the regression models of the outputs, and ξ is the iteration step index. The second iteration equation type is called *Alternate Load Iteration Equation* (see App. 10, Eq. (10.31a)). It is defined in Eq. (25.2) below where $\mathbf{F}_\xi$ is the load vector, $\mathbf{\Delta rF}$ is the output difference vector, $\mathbf{H}(\mathbf{F}_{\xi-\mathbf{1}})$

$$\mathbf{F}_\xi \;=\; \left[\ \mathbf{B_1}^{-1}\ \right] \cdot \mathbf{\Delta rF} \;-\; \left[\ \mathbf{B_1}^{-1}\mathbf{B_2}\ \right] \cdot \mathbf{F}_{\xi-\mathbf{1}} \;-\; \left[\ \mathbf{B_1}^{-1}\mathbf{C_2}\ \right] \cdot \mathbf{H}(\mathbf{F}_{\xi-\mathbf{1}}) \tag{25.2}$$

is a matrix that depends on the load vector $\mathbf{F}_{\xi-\mathbf{1}}$ of the previous iteration step, $\mathbf{B_1}^{-1}$, $\mathbf{B_1}^{-1}\mathbf{B_2}$, and $\mathbf{B_1}^{-1}\mathbf{C_2}$ are three auxiliary matrices that are derived from the regression models of the outputs, and ξ is the iteration step index.

It is observed that the right–hand sides of Eq. (25.1) and Eq. (25.2) have many similarities. In addition, it is known that the two equations converge to identical load vectors as long as (i) the equations are obtained from the same regression coefficient set, (ii) the primary sensitivities of all bridges are defined, (iii) the regression models of the outputs do not have linear dependencies, and (iv) the influence of the higher order contributions $[\ \mathbf{C_1}^{-1}\mathbf{C_2}\ ] \cdot \mathbf{H}(\mathbf{F}_{\xi-\mathbf{1}})$ and $[\ \mathbf{B_1}^{-1}\mathbf{C_2}\ ] \cdot \mathbf{H}(\mathbf{F}_{\xi-\mathbf{1}})$ is small. Therefore, it is possible to describe the two equations with a single relationship that is derived in the next section.

25.2 Definition of a Universal Load Iteration Equation

The two load iteration equations of the *Iterative Method* may be combined in a single iteration equation after the *Primary Load Iteration Equation* is described in a format that is compatible with the format of the *Alternate Load Iteration Equation*. This goal can be accomplished if an $n \times n$ square matrix $\mathbf{K}$ is introduced that is populated with zeros. Matrix $\mathbf{K}$ may be described by the following equation:

$$\mathbf{K} \;=\; \begin{bmatrix} 0 & \cdots & 0 \\ \vdots & \vdots & \vdots \\ 0 & \cdots & 0 \end{bmatrix}_{n\times n} \tag{25.3}$$

Load vector $\mathbf{F_{\xi-1}}$ has n components. Therefore, matrix $\mathbf{K}$ may be multiplied with vector $\mathbf{F_{\xi-1}}$. The product equals a vector with n components that are zeros. This result is summarized in Eq. (25.4) below. Consequently, the left–hand side of Eq. (25.4) may be

$$[\ \mathbf{K}\ ]_{n\times n}\ \cdot\ [\ \mathbf{F_{\xi-1}}\ ]_{n\times 1}\ =\ \begin{bmatrix} 0 \\ \vdots \\ 0 \end{bmatrix}_{n\times 1} \tag{25.4}$$

subtracted from the right–hand side of Eq. (25.1) without changing the result. Then, the *Primary Load Iteration Equation* can be expressed in the following format:

$$\mathbf{F_\xi}\ =\ \left[\ \mathbf{C_1}^{-1}\ \right]\cdot\mathbf{\Delta rF}\ -\ [\ \mathbf{K}\ ]\cdot\mathbf{F_{\xi-1}}\ -\ \left[\ \mathbf{C_1}^{-1}\mathbf{C_2}\ \right]\cdot\mathbf{H}(\mathbf{F_{\xi-1}}) \tag{25.5}$$

It is concluded after comparing Eq. (25.2) with Eq. (25.5) that the two load iteration equations have three common multipliers: $\mathbf{\Delta rF}$, $\mathbf{F_{\xi-1}}$, and $\mathbf{H}(\mathbf{F_{\xi-1}})$. Therefore, a single relationship can be used to describe the two load iteration equations. The resulting *Universal Load Iteration Equation* is defined in Eq. (25.6*a*) below. This equation was first

Universal Load Iteration Equation

$$\mathbf{F_\xi}\ =\ [\ \mathbf{D_0}\ ]\ \cdot\ \mathbf{\Delta rF}\ -\ [\ \mathbf{D_1}\ ]\ \cdot\ \mathbf{F_{\xi-1}}\ -\ [\ \mathbf{D_2}\ ]\ \cdot\ \mathbf{H}(\mathbf{F_{\xi-1}}) \tag{25.6a}$$

where

$$\mathbf{D_0}\ =\ \begin{cases} \mathbf{C_1}^{-1} & \Longrightarrow \text{ Primary Load Iteration Equation} \\ \mathbf{B_1}^{-1} & \Longrightarrow \text{ Alternate Load Iteration Equation} \end{cases} \tag{25.6b}$$

$$\mathbf{D_1}\ =\ \begin{cases} \mathbf{K} & \Longrightarrow \text{ Primary Load Iteration Equation} \\ \mathbf{B_1}^{-1}\,\mathbf{B_2} & \Longrightarrow \text{ Alternate Load Iteration Equation} \end{cases} \tag{25.6c}$$

$$\mathbf{D_2}\ =\ \begin{cases} \mathbf{C_1}^{-1}\,\mathbf{C_2} & \Longrightarrow \text{ Primary Load Iteration Equation} \\ \mathbf{B_1}^{-1}\,\mathbf{C_2} & \Longrightarrow \text{ Alternate Load Iteration Equation} \end{cases} \tag{25.6d}$$

suggested by *Thomas Bridge* of Jacobs Technology. It simplifies the implementation of the *Iterative Method* in the data system of a wind tunnel whenever a facility operator needs to support both types of load iteration equations.

Appendix 26

Assessment of an Axial Force Error

26.1 General Remarks

A misalignment of the normal or side force of a six–component strain–gage balance during either calibration or check loading results in an unwanted force that acts in the axial force direction. This hidden axial force changes the electrical output of the axial force bridge. The output change could be interpreted as an interaction that is associated with the application of the normal or side force to the balance (see also discussions in App. 24). This type of interaction is avoidable or can be controlled as long as load alignment errors are minimized during the application of a normal or side force.

No alignment of an applied balance force is perfect. Therefore, it is useful to estimate the upper bound of the axial force error that results from a misaligned normal or side force. This estimate may help an analyst to understand if an observed interaction of an axial force bridge is a physical characteristic of the balance or if it is caused by an alignment error. The axial force error resulting from the misalignment of the normal force of a direct–read balance is derived in the next section as an example. Corresponding equations of the axial force error for the side force of a direct–read balance, the two normal forces of a force balance, or the two side forces of a force balance can be obtained by simply replacing the normal force with the corresponding applied side or normal force component.

26.2 Axial Force Error

It is assumed that the normal force NF is applied to a balance using gravity weights. A small misalignment occurred during the load application that is shown in Fig. 26–1 below. This misalignment is described by angle ξ that is measured relative to the z–axis of the balance axis system. The alignment error resulted in a small axial force component δAF

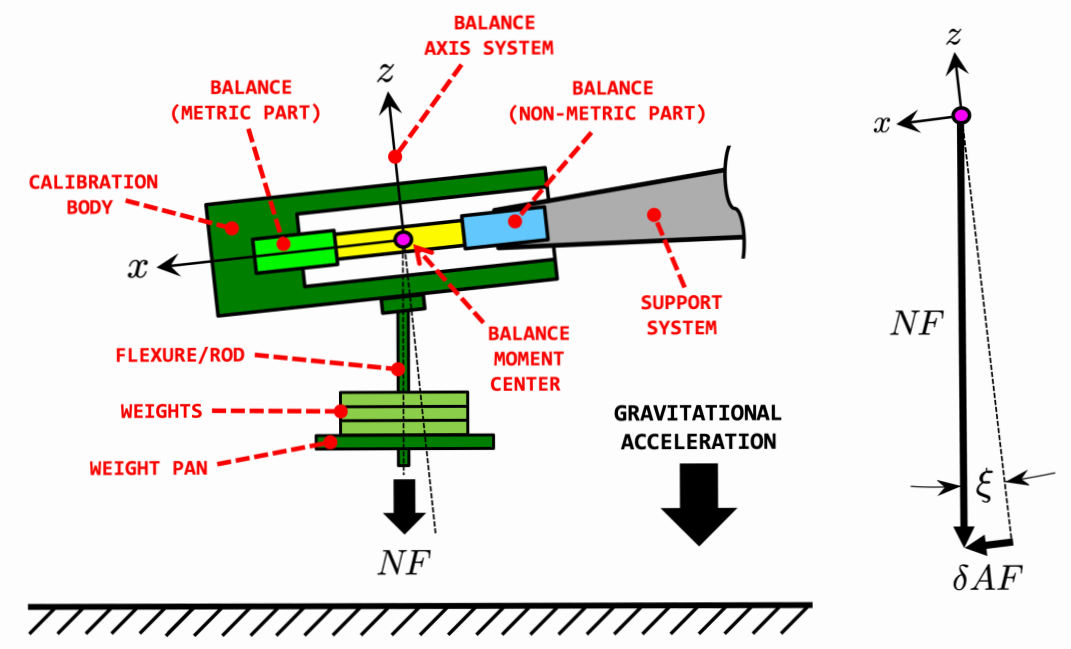

Fig. 26–1 Connection between a misaligned normal force and the axial force error.

that acted in the direction of the x–axis of the balance axis system. The absolute value of the unwanted axial force can be described by the following relationship:

$$|\delta AF| \quad = \quad |NF| \cdot sin(\xi) \qquad where \qquad \xi \geq 0 \tag{26.1}$$

A small angle approximation of $sin(\xi)$ may be applied that simplifies the analysis without significantly changing the error estimate. This simplification is defined as follows:

$$|\xi| \ll 1 \quad \Longrightarrow \quad sin(\xi) \approx \xi_{rad} \approx \frac{\pi}{180} \cdot \xi_{deg} \tag{26.2}$$

Now, after using the right–hand side of Eq. (26.2) to replace $sin(\xi)$ in Eq. (26.1), we get:

$$|\delta AF| \approx |NF| \cdot \frac{\pi}{180} \cdot \xi_{deg} \tag{26.3}$$

Finally, the axial force error in dimensionless form is obtained after (i) dividing both sides of Eq. (26.3) by the capacity AF_{max} of the axial force and (ii) multiplying the result by 100 %. Then, the following relationship is obtained:

Axial Force Error

$$\frac{|\delta AF|}{AF_{max}} \cdot 100\ \% \approx \left\{ 100\ \% \cdot \frac{\pi}{180} \cdot \xi_{deg} \right\} \cdot \frac{|NF|}{AF_{max}} \tag{26.4}$$

Equation (26.4) above can be interpreted as a straight line with a slope that is proportional to the misalignment angle. Therefore, it is possible to develop a nomograph that may be used to quickly estimate the axial force error. The inputs of the nomograph are the force ratio $|NF|/AF_{max}$ and the alignment angle error ξ_{deg}. The output of the nomograph is the axial force error that is described as a percentage of the axial force capacity.

26.3 Nomograph

A nomograph for the assessment of the axial force error can be developed from Eq. (26.4). It is only required to interpret the angle ξ_{deg} as a constant and plot the dimensionless axial force error versus the ratio between the absolute value of the normal force and the axial force capacity. The resulting nomograph is shown in Fig. 26–2 below. The nomograph illustrates the fact that the axial force error increases as the ratio between the absolute value of an applied normal force and the axial force capacity increases. Therefore, it is often a challenge to keep the axial force error below the accepted limit of *0.1* % if (i) the "built–in" ratio between the normal and axial force capacities of a given balance exceeds *10* and (ii) the normal force is applied to capacity.

An example is shown in Fig. 26–2 that demonstrates the use of the nomograph. The example assumes that the absolute value of an applied normal force is *3680 lbs*, the axial force capacity of the balance equals *400 lbs*, and the alignment angle error equals *0.014°* . Then, the ratio $|NF|/AF_{max}$ between the absolute value of the applied normal force and

the axial force capacity equals *9.2*. Now, the estimated axial force error of the example can be obtained from the nomograph. It is *0.225* % of the axial force capacity.

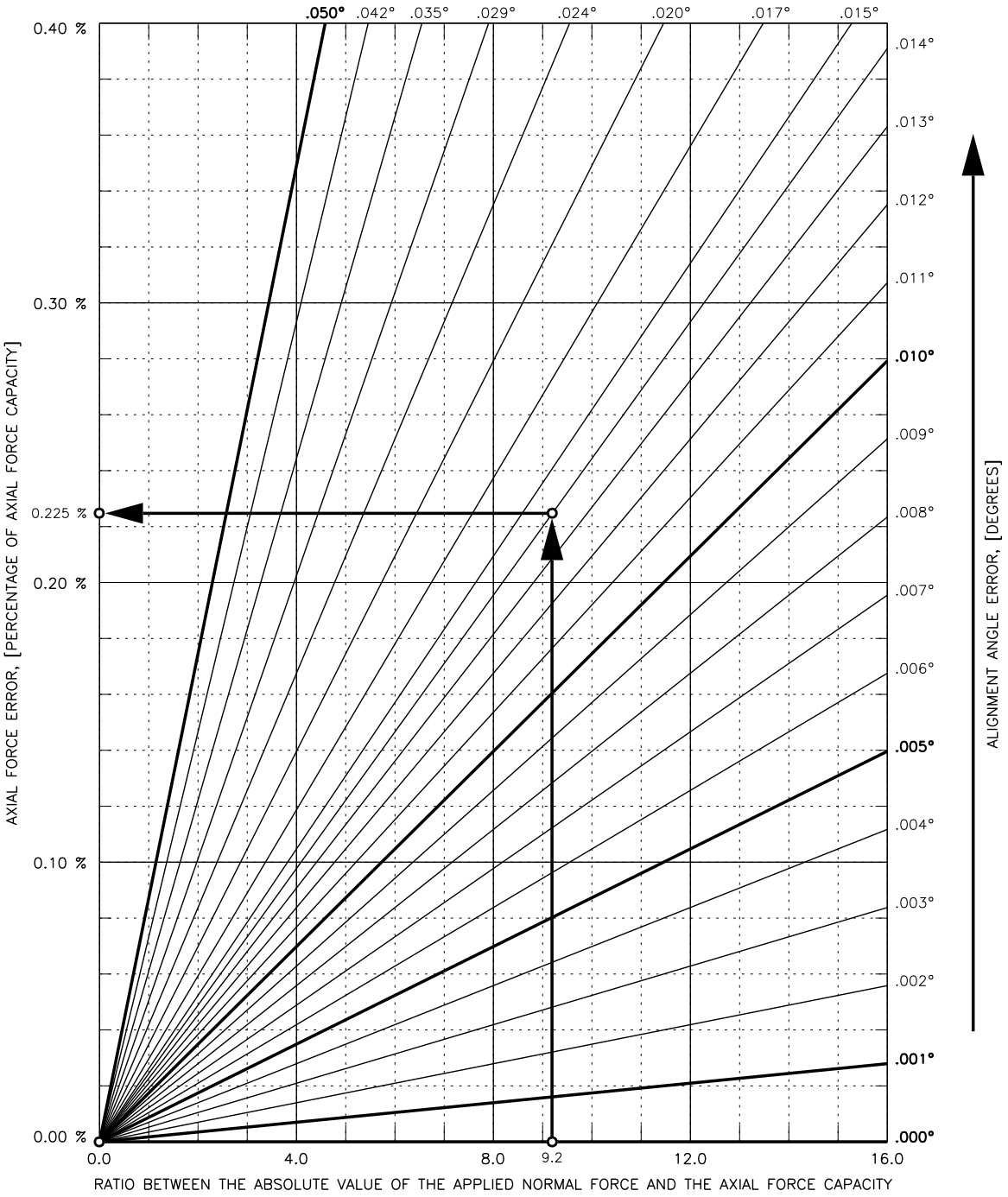

Fig. 26–2 Nomograph for the assessment of the axial force error that is caused by the misalignment of an applied normal force.

It has to be mentioned for completeness that the nomograph can also be used for the assessment of the axial force error if the applied force is a side force of a direct–read

balance, a forward/aft normal force component of a force balance, or a forward/aft side force component of a force balance. It is only required to interpret the force ratio on the abscissa of the nomograph as the ratio between the chosen force component and the axial force capacity.

Appendix 27
Load Cell Example

27.1 General Remarks

A new analysis of a simple balance calibration data example from the open literature can be used to demonstrate connections between the load prediction equations that the *Iterative Method* and *Non–Iterative Method* use. The example describes calibration data of a one–component load cell (load & output values are listed in Ref. [81], p. 150). First, analysis results are discussed that were obtained after applying the *Iterative Method* to the load cell data. Afterwards, alternate results for the *Non–Iterative Method* are presented so that they can be compared with corresponding results for the *Iterative Method*.

27.2 Iterative Method

The *Iterative Method* is an approach that can be used to generate the load prediction equation of a load cell. The method first fits the electrical outputs of the load cell as a function of the applied force. Then, a load iteration equation is constructed from the regression model of the output so that the load cell's force can be predicted from the measured outputs. Equation (27.1) below defines the second order regression model of the

Regression Model of the Electrical Output

$$rF = c_0 + c_1 \cdot F + c_2 \cdot F^2 \qquad (27.1)$$

electrical output of the load cell that was chosen for the application of the *Iterative Method* to the calibration data example. Symbol rF describes the measured electrical output of the load cell given in units of $[mV]$, symbol F describes the load cell's force given in units of $[lbf]$, and $c_0,\ c_1,\ c_2$ are the regression coefficients.

Only the first eleven data points of the example were used for the new analysis of the load cell data because this subset was chosen when the data was originally processed in 1992. The eleven data points were recorded while the load cell was in tension. In addition, loads and outputs were increasing from one data point to the next (see Ref. [81], p. 150). Therefore, the resulting regression model is, to some degree, load–direction–dependent.† It works best if the force is increasing while the load cell is in tension. Equations (27.2a) to (27.2c) below list coefficients that were computed during the regression analysis of the

$$intercept \implies c_0 = -1.1888\text{E}{-}04\ [mV] \qquad (27.2a)$$

$$sensitivity \implies c_1 = +3.8715\text{E}{-}01\ [mV/lbf] \qquad (27.2b)$$

$$coefficient\ of\ higher\ order\ term \implies c_2 = +1.8648\text{E}{-}06\ [mV/lbf^2] \qquad (27.2c)$$

eleven–point data subset. As expected, the computed coefficients show excellent agreement with values that are listed in the literature (see Ref. [81], p. 150). In theory, a load iteration

† An alternate load–direction–independent description of the physical behavior of the load cell can be obtained if all twenty–one calibration points of the data example are used for the analysis.

equation can be constructed from Eq. (27.1) if the influence of the higher order term F^2 is small. This requirement can be tested if the term's *Percent Contribution* is computed using an equation that is given in App. 16. The load cell's capacity F_{max} is $50\,[lbf]$. Then, after applying Eq. (16.13), the *Percent Contribution* of term F^2 is obtained. We get:

$$Q(F^2) \;=\; \frac{c_2 \cdot \{F_{max}\}^2}{c_1 \cdot F_{max}} \times 100\,\% \;=\; \frac{1.8648\,\mathrm{E}{-}06 \cdot 50^2}{3.8715\,\mathrm{E}{-}01 \cdot 50} \times 100\,\% \;\approx\; 0.024\,\% \qquad (27.3)$$

The *Percent Contribution* is very small. It is well below the threshold of $0.1\,\%$ that identifies terms of no importance (threshold is taken from Table 16–3 on p. 351). A load iteration equation can still be derived from Eq. (27.1) even though term F^2 is not needed for an accurate load prediction. This iteration equation may be used to illustrate basic characteristics of the *Iterative Method* with simple scalar relationships.

The iteration equation of the load cell data is defined in Eq. (27.4) below. It is obtained after subtracting $c_2 \cdot F^2$ from both sides of Eq. (27.1), solving the right–hand side of the resulting equation for F, and adding iteration step indices ξ and $\xi + 1$ as subscripts to the

Load Iteration Equation

$$F_{\xi+1} \;=\; (1/c_1) \;\cdot\; [\; rF - c_0 \;] \;-\; (c_2/c_1) \;\cdot\; {F_\xi}^2 \qquad (27.4)$$

two force symbols. Equation (27.4) has an interesting interpretation if it is compared with the multivariate load iteration equation that Eq. (10.27a) in App. 10 defines. First, multiplier $1/c_1$ of Eq. (27.4) is the scalar equivalent of inverse matrix $\mathbf{C_1}^{-1}$ of Eq. (10.27a). Similarly, multiplier c_2/c_1 of Eq. (27.4) is the scalar equivalent of matrix $\mathbf{C_1}^{-1}\mathbf{C_2}$ of Eq. (10.27a). Therefore, Eq. (27.4) becomes the scalar representation of Eq. (10.27a) if a second order polynomial is used for the analysis of the bridge outputs of a one–component balance. Equations (27.5a) and (27.5b) below list coefficients of the load iteration equation that were obtained from the right–hand sides of Eqs. (27.2b) & (27.2c). Tests showed that

$$(1\,/\,c_1) \;=\; +2.5830\,\mathrm{E}{+}00\;[lbf\,/\,mV] \;\ldots\ldots\ldots\ldots\; \textit{inverse of the sensitivity} \qquad (27.5a)$$

$$(c_2\,/\,c_1) \;=\; +4.8167\,\mathrm{E}-06\;[1/lbf] \;\ldots\; \textit{scaled coefficient of higher order term} \qquad (27.5b)$$

the convergence tolerance of $0.0001\,\%$ of load capacity is met after two iterations. The rapid convergence is expected because the term F^2 has a very small *Percent Contribution*. The initial guess F_0 of the force is zero. This choice can be expressed as follows:

$$\textit{initial guess} \;\;\Longrightarrow\;\; F_0 \;=\; 0 \qquad (27.6)$$

Now, the first two force estimates are obtained after using Eq. (27.4) twice. Then, we get:

$$\textit{first estimate} \;\;\Longrightarrow\;\; F_1 \;=\; (1/c_1) \cdot [\; rF - c_0 \;] \qquad (27.7a)$$

$$\textit{second estimate} \;\;\Longrightarrow\;\; F_2 \;=\; (1/c_1) \cdot [\; rF - c_0 \;] \;-\; (c_2/c_1) \cdot {F_1}^2 \qquad (27.7b)$$

An alternate description of the second estimate can be derived from Eq. (27.7b) after replacing ${F_1}^2$ on the right–hand side of Eq. (27.7b) with the square of the right–hand side of Eq. (27.7a) and simplifying the result. Then, the following relationship is obtained:

Second Estimate of the Force

$$F_2 \;=\; (1/c_1) \cdot [\, rF - c_0 \,] \;-\; (c_2/c_1^3) \cdot [\, rF - c_0 \,]^2 \qquad (27.8)$$

By inspection, it is concluded that the second estimate of the force is a second order polynomial of the electrical output rF of the load cell.

27.3 Non–Iterative Method

The load cell data example was also processed with the *Non–Iterative Method* to demonstrate hidden connections between its load prediction equation and the iteration equation that the *Iterative Method* uses for the load prediction. The application of the *Non–Iterative Method* to the example was possible because the load cell's electrical outputs are given as differences relative to an output datum that describes zero load (see also App. 9). Equation (27.9) below shows the second order regression model of the force that was chosen

Regression Model of the Force

$$F \;=\; a_0 \;+\; a_1 \cdot rF \;+\; a_2 \cdot rF^{\,2} \qquad (27.9)$$

for the application of the *Non–Iterative Method* to the load cell data. Equations (27.10a) to (27.10c) below list coefficients that were computed during the regression analysis. Again,

$$\textit{intercept} \implies a_0 \;=\; +3.0772\,\mathrm{E}{-}04\;[lbf] \qquad (27.10a)$$

$$\textit{inverse of the sensitivity} \implies a_1 \;=\; +2.5830\,\mathrm{E}{+}00\;[lbf\,/\,mV] \qquad (27.10b)$$

$$\textit{coefficient of higher order term} \implies a_2 \;=\; -3.2120\,\mathrm{E}{-}05\;[lbf\,/\,mV^{\,2}] \qquad (27.10c)$$

only the first eleven data points were used for the analysis so that the coefficients can be compared with the coefficients of the load iteration equation.

27.4 Regression Coefficient Comparison

It is observed that the second estimate of the force from the load iterations, i.e., Eq. (27.8) and the regression model of the force, i.e., Eq. (27.9) are second order polynomials of the electrical output rF of the load cell. Therefore, a connection must exist between their coefficients. The intercept c_0 is given in Eq. (27.2a) as $-1.1888\,\mathrm{E}{-}04\,[mV]$. It is $-0.00059\,\%$ of the load cell's output range of $20\,[mV]$ (range estimate was taken from Ref. [81], p. 150). Similarly, intercept a_0 is listed in Eq. (27.10a) as $+3.0772\,\mathrm{E}{-}04\,[lbf]$. It

is 0.00062% of the load cell's capacity of 50$[lbf]$. It is concluded that both intercepts are very small. Therefore, they can be omitted. Then, after replacing c_0 in Eq. (27.8) with zero and dropping the iteration step index, we get:

$$Eq.\ (27.8) \implies F \approx (1/c_1) \cdot rF - (c_2/c_1^3) \cdot rF^2 \tag{27.11}$$

Similarly, after replacing a_0 in Eq. (27.9) with zero, we get:

$$Eq.\ (27.9) \implies F \approx a_1 \cdot rF + a_2 \cdot rF^2 \tag{27.12}$$

Finally, after comparing the coefficients on the right–hand side of Eq. (27.11) with corresponding coefficients on the right–hand side of Eq. (27.12), we get:

$$a_1 \equiv (1/c_1) = +2.5830\text{E+00}\ [lbf/mV] \tag{27.13}$$

$$a_2 \equiv -(c_2/c_1^3) = -3.2136\text{E-05}\ [lbf/mV^2] \tag{27.14}$$

Numerical values shown on the right–hand sides of Eqs. (27.13) and (27.14) were computed with the values of the coefficients c_1 and c_2 that are listed on the right–hand sides of Eqs. (27.2*b*) and (27.2*c*). The inverse $(1/c_1)$ of the sensitivity agrees within five digits with coefficient a_1 that is shown in Eq. (27.10*b*). Similarly, the coefficient $-(c_2/c_1^3)$ of the higher order term agrees within three digits with coefficient a_2 that is shown in Eq. (27.10*c*). These observations indicate that the load iteration equation, i.e., Eq. (27.4) and the alternate regression model of the force, i.e., Eq. (27.9) will lead to load values of compatible accuracy. It is important to remind the reader that Eq. (27.8) describes the intermediate second estimate of the force from the load iteration process that the *Iterative Method* uses. On the other hand, the force defined in Eq. (27.9) is the final value that the *Non–Iterative Method* computes.

Appendix 28
Cook's Sequential Analysis Method

28.1 Introduction

Cook's sequential analysis method was often used in the 1960s and 1970s for the development of the load iteration equation of a six–component balance (Ref. [5]). Basic elements of *Cook's* method can still be found in modern balance calibration designs that support a sequential analysis approach (see, e.g., Ref. [52]). *Cook's* method is an early version of the *Iterative Method* (see also App. 10). It uses sequential graphical analysis instead of global regression for the determination of the coefficients of the math models of the bridge outputs (Ref. [5], pp. 4–5). This approach was possible because *Cook's* calibration design consists of twenty–one carefully selected data subsets. Table 28–1 below describes the data subsets that *Cook's* method uses as input for the analysis. A maximum number of two

Table 28–1: Twenty–one data subsets of *Cook's* sequential analysis method.

DATA SET NUMBER (SINGLE-COMPONENT LOAD) ➡	SET 1 *AF*	SET 2 *SF*	SET 3 *NF*	SET 4 *RM*	SET 5 *PM*	SET 6 *YM*
DATA SET NUMBER (TWO-COMPONENT LOAD PAIR) ➡	SET 7 *AF, SF*	SET 8 *SF, NF*	SET 9 *NF, RM*	SET 10 *RM, PM*	SET 11 *PM, YM*	
DATA SET NUMBER (TWO-COMPONENT LOAD PAIR) ➡	SET 12 *AF, NF*	SET 13 *SF, RM*	SET 14 *NF, PM*	SET 15 *RM, YM*		
DATA SET NUMBER (TWO-COMPONENT LOAD PAIR) ➡	SET 16 *AF, RM*	SET 17 *SF, PM*	SET 18 *NF, YM*			
DATA SET NUMBER (TWO-COMPONENT LOAD PAIR) ➡	SET 19 *AF, PM*	SET 20 *SF, YM*				
DATA SET NUMBER (TWO-COMPONENT LOAD PAIR) ➡	SET 21 *AF, YM*					

load components are simultaneously applied within a data subset. The twenty–one subsets were intentionally designed to support a multivariate 27–term math model. This math model was the default choice for the analysis of six–component balance data before absolute value terms were introduced in the 1970s. *Cook's* math model consists of six linear terms, six quadratic terms, and fifteen cross–product terms. He implicitly assumed that bridge outputs are formatted as differences relative to the outputs at the beginning of each load series (see also bridge output format *Difference Type 2* in App. 6). Therefore, no intercept is needed. *Cook's* bridge output format choice also means that the impact of the weight of the calibration equipment on the bridge outputs is neglected. Equation (28.1) below shows, for example, the 27–term math model of the axial force bridge output of a six–component balance that *Cook's* twenty–one data subsets support.

$$\begin{aligned} rAF \;=\; & b_1 \cdot AF \;+\; b_2 \cdot SF \;+\; b_3 \cdot NF \;+\; \ldots \;+\; b_6 \cdot YM \\ & + b_7 \cdot AF^2 \;+\; b_8 \cdot SF^2 \;+\; b_9 \cdot NF^2 \;+\; \ldots \;+\; b_{12} \cdot YM^2 \\ & + b_{13} \cdot \{AF \cdot SF\} \;+\; b_{14} \cdot \{AF \cdot NF\} \;+\; \ldots \;+\; b_{27} \cdot \{PM \cdot YM\} \end{aligned} \tag{28.1}$$

The same term combination is used for the definition of the math models of the outputs of the remaining five bridges. Therefore, a total of 6×27 coefficients need to be

obtained from the twenty–one data subsets that *Cook's* sequential analysis method uses for the development of the load iteration equation of a six–component balance.

The coefficients $b_1,\ b_2,\ \ldots,\ b_{27}$ of the math model of the axial force bridge output example are the unknowns in Eq. (28.1). In theory, they could be obtained by applying *global regression* in combination with a *weighted least squares fit* to *Cook's* twenty–one data subsets (see also section 28.3). However, numerical methods and computer resources were limited when *Cook* defined his method in 1959. Therefore, he developed an analysis approach that uses combinations of data subsets for the coefficient determination.

28.2 Discussion of Example

Cook's method can be illustrated by reviewing the determination of the five coefficients b_1, b_3, b_7, b_9, and b_{14} of the axial force bridge output that are defined in Eq. (28.1). First, data of Set 1 is used to obtain the coefficients b_1 and b_7. The axial force is applied as a single–component load during Set 1. Therefore, data of Set 1 only supports a simplified version of Eq. (28.1) that is defined in Eq. (28.2) below.

$$Set\ 1 \quad \Longrightarrow \quad rAF \;=\; b_1 \cdot AF \;+\; b_7 \cdot AF^2 \tag{28.2}$$

Now, the axial force bridge output is plotted versus the axial force (see Fig. 28–1 below).

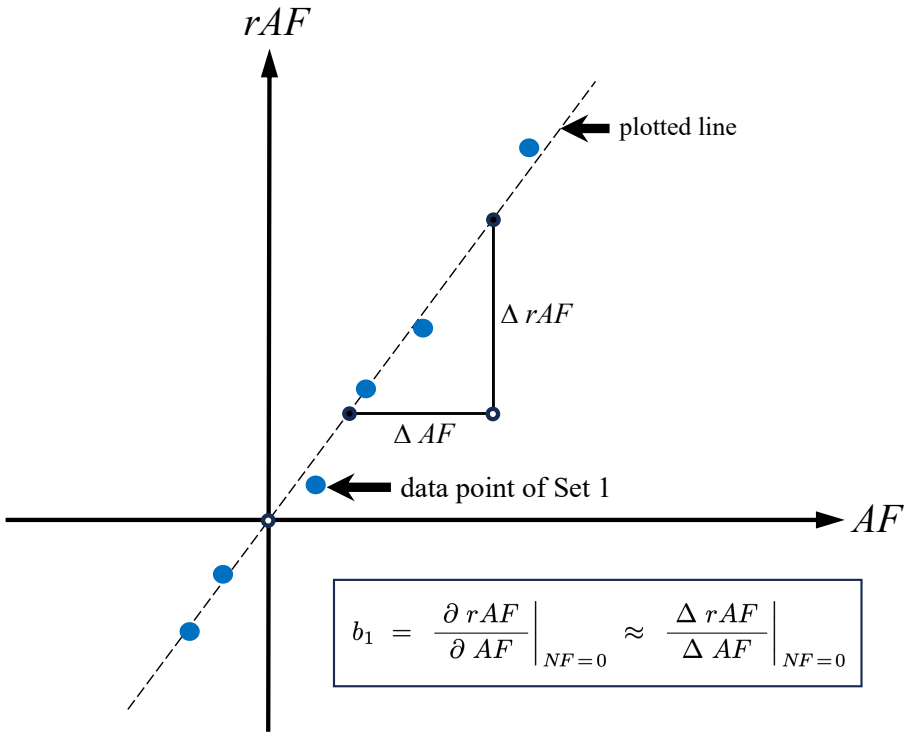

Fig. 28–1 Graphical determination of coefficient b_1 of term AF (blue dot = data point of Set 1).

Coefficient b_1 describes the slope of the plotted line. It remains to determine coefficient b_7 of the quadratic term from the data of Set 1. Therefore, both sides of Eq. (28.2) are

divided by the axial force. Equation (28.3) below shows the resulting equation. It can be interpreted as a straight line. Coefficient b_1 is the intercept. Coefficient b_7 is the slope. It

$$Set\ 1 \quad \Longrightarrow \quad rAF\,/\,AF \quad = \quad b_1 \ + \ b_7 \ \cdot \ AF \tag{28.3}$$

can be computed using a graphical approach after the left–hand side of Eq. (28.3), i.e., rAF/AF, is plotted versus the axial force (see Fig. 28–2 below).

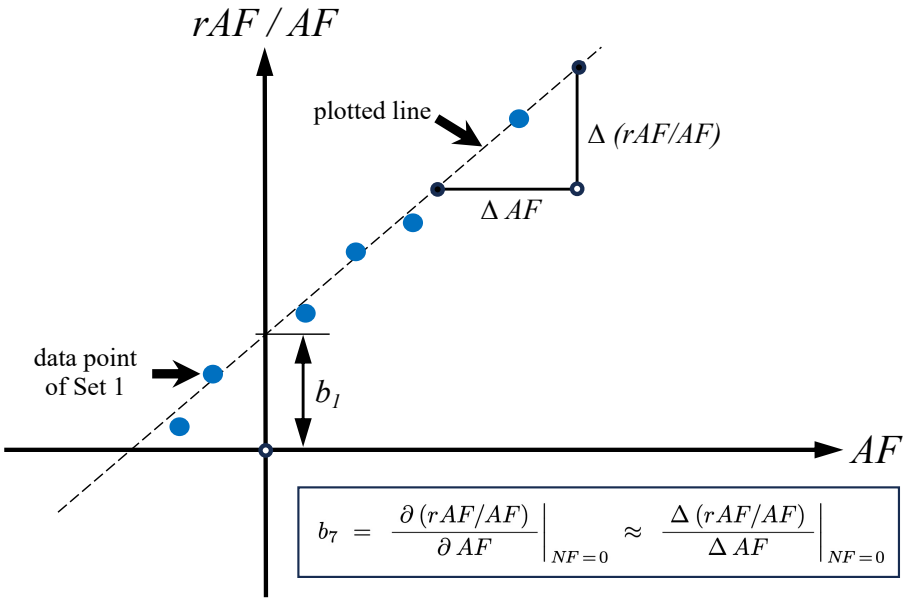

Fig. 28–2 Graphical determination of coefficient b_7 of term AF^2 (blue dot = data point of Set 1).

It is also known that the normal force is applied as a single–component load in Set 3. Therefore, data of Set 3 supports a simplified version of Eq. (28.1) that is defined in Eq. (28.4) below. Coefficient b_3 can directly be obtained using graphical analysis after

$$Set\ 3 \quad \Longrightarrow \quad rAF \quad = \quad b_3 \ \cdot \ NF \ + \ b_9 \ \cdot \ NF^2 \tag{28.4}$$

plotting the axial force bridge output versus the normal force. In addition, similar to the determination of coefficient b_7, coefficient b_9 can be obtained after dividing both sides of Eq. (28.4) by the normal force. The result is shown in Eq. (28.5) below. It can be inter–

$$Set\ 3 \quad \Longrightarrow \quad rAF\,/\,NF \quad = \quad b_3 \ + \ b_9 \ \cdot \ NF \tag{28.5}$$

preted as a straight line where coefficient b_9 represents the slope. Again, the slope is obtained using graphical analysis after plotting rAF/NF versus the normal force.

Coefficient b_{14} of cross–product term $AF \cdot NF$ still needs to be determined. It is obtained after applying *Cook's* method to data of Set 12. This data subset supports terms that both AF and NF define. Therefore, a five–term math model subset of Eq. (28.1) can be used to process the data (coefficients $b_1, b_3, b_7, b_9 \equiv$ known; coefficient $b_{14} \equiv$ unknown):

$$Set\ 12 \ \Longrightarrow \ rAF \ = \ b_1 \cdot AF \ + \ b_3 \cdot NF \ + \ b_7 \cdot AF^2 \ + \ b_9 \cdot NF^2 \ + \ b_{14} \cdot \{AF \cdot NF\} \tag{28.6}$$

Set 12 has data that was recorded by varying the axial force while keeping the normal force at a constant non–zero value. Outputs of the axial force bridge of Set 12 can be plotted versus the axial force for constant normal force. In addition, the partial derivative of the axial force bridge output with respect to the axial force can be obtained by treating the normal force as a constant. Then, the following value is obtained:

$$\{\, NF \;=\; const. \,\} \;\;\Longrightarrow\;\; \partial\, rAF\,/\,\partial AF \;=\; b_1 \;+\; 2 \;\cdot b_7 \cdot\, AF \;+\; b_{14} \cdot\, NF \qquad (28.7)$$

Consequently, the partial derivative at zero axial force is given by the following relationship:

$$\left\{ \begin{array}{rcc} NF & = & const. \\ AF & = & 0 \end{array} \right\} \;\;\Longrightarrow\;\; \partial\, rAF\,/\,\partial AF \;=\; b_1 \;+\; b_{14} \cdot\, NF \qquad (28.8)$$

Furthermore, it is assumed that data of Set 12 is recorded for the required minimum of two constant values NF' and NF'' of the normal force. The first normal force is positive ($NF' > 0$). The second normal force is negative ($NF'' < 0$). Now, the axial force bridge output observed for NF' and NF'' can separately be plotted versus the axial force so that the slope $\partial\, rAF\,/\,\partial\, AF$ for each of the two lines can be obtained. The data points of Set 12 are plotted as red dots in Fig. 28–3 below. It is also known from the earlier analysis

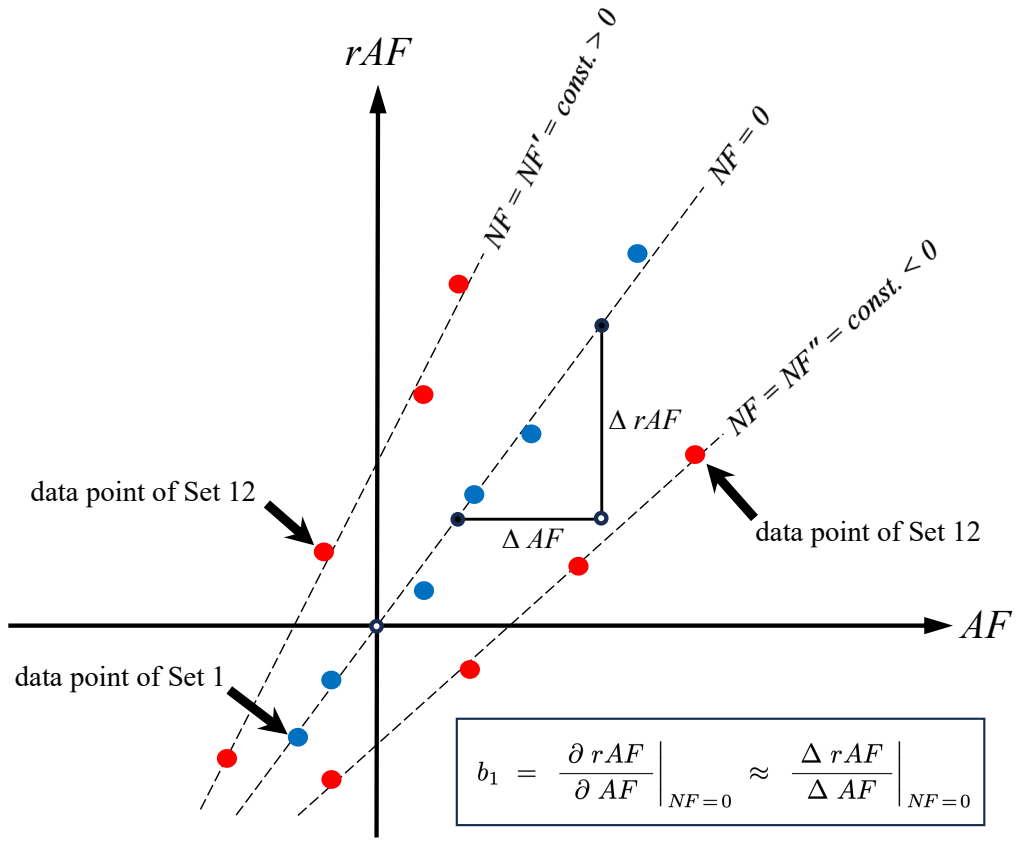

Fig. 28–3 Graphical determination of the slope $\partial\, rAF\,/\,\partial\, AF$ for a constant normal force (red dot = data point of Set 12; blue dot = data point of Set 1).

of Set 1 that the slope $\partial\, rAF / \partial\, AF$ equals coefficient b_1 if the normal force is zero (see blue dots in Fig. 28–3). Finally, the three slopes $\partial\, rAF / \partial\, AF$ can be plotted versus the related three normal force values $NF = 0$, $NF = NF'$, and $NF = NF''$. The slope of the resulting straight line is shown in Fig. 28–4 below. It is the graphical estimate of coef–

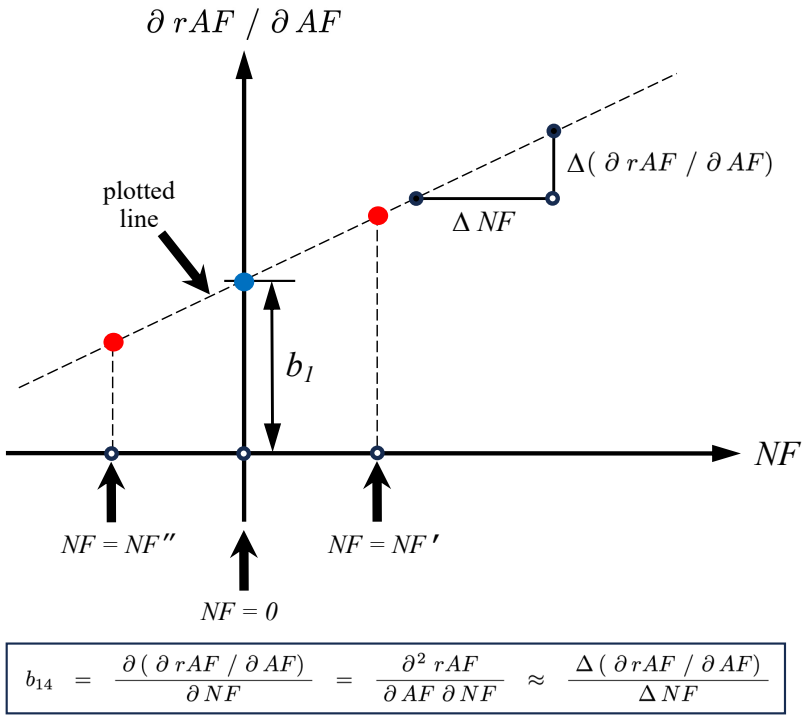

Fig. 28–4 Graphical determination of coefficient b_{14} of term $\{AF \cdot NF\}$.

ficient b_{14} of the cross–product term $\{AF \cdot NF\}$. – The determination of (i) the remaining 22 coefficients of the math model of the axial force bridge output and (ii) the 5×27 coefficients of the 27–term math models of the other five bridge outputs follows *Cook's* process steps that are described in this example.

The discussion of the example illustrates both complexity and bookkeeping challenges of *Cook's* method. It also reminds the reader why *Galway's* introduction of *global regression* to balance calibration data analysis represents a significant milestone in the development of load prediction methods (see Ref. [6]). First, *global regression* simplifies the analysis task because the given calibration data is processed with a single least squares fit for each dependent variable. *Global regression* also allows for the assessment of the regression models of the balance data with metrics like the p–value, the t–statistic, the standard error, and the *Variance Inflation Factor*. Therefore, the models can more easily be justified from a statistical viewpoint. Finally, *global regression* makes it possible to systematically include absolute value terms in regression models of calibration data from balances with bi–directional bridge outputs.

28.3 Application of Global Regression

Sometimes, *Cook's* twenty–one data subsets cannot be processed successfully with *global regression* unless a *weighted least squares fit* is performed during the analysis. The

weighted fit must assign greater weight to the data points of the first six data subsets that are defined in Table 28–1. A detailed description of the application of a *weighted least squares fit* to balance calibration data can be found in App. 22. Two weighting factor definitions are listed in App. 22. Experience showed that the first definition works best with data from *Cook's* calibration design (see also App. 22, Section 22.5). Finally, assuming that the natural zeros and the raw bridge outputs of the calibration data points are known, a tare load iteration should be performed during the *global regression* analysis of data from *Cook's* design. This tare load iteration must use the mean zero load outputs of each load series as the electrical description of the tare loads.

Appendix 29
History of Load Prediction Methods

The development of balance load prediction methods started in the 1950s when internal strain–gage balances became widely available for aerospace testing applications (Fig. 29–1). Mathematical relationships between loads and bridge outputs had to be found so that loads could be predicted from measured bridge outputs during a wind tunnel test.

Strain–gage balances are unique sensors. They are used to simultaneously predict up to six loads from the measured bridge outputs. This characteristic has greatly influenced the development of balance load prediction methods. It is also not a good fit for a traditional metrology organization whose mission may be the calibration of sensors that predict a single physical quantity. Therefore, highly specialized laboratories have been established at many aerospace testing centers that exclusively calibrate strain–gage balances.

The geometric complexity of a strain–gage balance also had a significant impact on the development of load prediction methods. Balance bridges of most multicomponent balance designs are attached to interconnected structures that are located inside a small cylindrical volume. This space constraint is responsible for interactions between the loads and the bridge outputs. They are repeatable if alignment errors during the application of loads are kept to a minimum. Interactions cannot be neglected if typical load prediction accuracies for aerospace testing applications are to be met. Therefore, multivariate regression models must be used for the description of balance characteristics that correctly represent the influence of interactions on the predicted loads.

Different justifications for the assignment of the independent & dependent variables of balance calibration data exist. They are directly linked to the evolution of balance load prediction methods. In theory, a reversible mapping between loads and bridge outputs must exist. Then, an analyst can interpret the loads as either the dependent or independent variables during the calibration data analysis (see also comments on p. 12 and p. 19). On the other hand, the *Iterative Method* uses loads as independent variables and bridge outputs as dependent variables. This choice can be traced back to *Cook's* Technical Note of 1959 where he makes the following statement (taken from Ref. [1], p. 3): *"Each bridge indicator reading, as a consequence of interactions, is a function of all six load components."* Many users of the *Iterative Method* also believe that it is logical to use bridge outputs as dependent variables because bridge outputs are "measured" while loads are "applied" during the calibration. This belief and *Cook's* statement come from the *traditional approach*[†] that many metrology organizations use for the reporting of a sensor's calibration data. The primary mission of a metrology organization is the calibration of sensors that measure a single physical quantity. In addition, a sensor's electrical output may have highly linear characteristics. Then, the following information is provided in a metrology organization's calibration report: (i) raw calibration data, (ii) the sensitivity, i.e., the first derivative of the sensor's electrical output with respect to the physical quantity, and (iii) a regression model of the electrical output. Consequently, the end user needs to figure out how this information should be used so that the predicted quantity meets given accuracy requirements.

Cook's technical note of 1959 defines both the math model of the bridge outputs and the load iteration scheme that was initially used for the prediction of balance loads (see

[†] *Wright* illustrates the *traditional approach* with the calibration report of a load cell (Ref. [81], p. 150).

Ref. [5]). *Cook's Method* is an early version of the *Iterative Method* that is still in use today (see Fig. 29–1). In some sense, *Cook's Method* is a multivariate extension of processes that were originally developed for sensors that predict a single physical quantity. The primary difference between *Cook's Method* and the *Iterative Method* is the fact that the *Iterative Method* uses *global regression*[†] for the determination of the math model coefficients of the bridge outputs. *Cook's Method*, on the other hand, determines coefficients by performing a sequential graphical analysis of balance calibration data (Ref. [5], pp. 4–5). This approach was possible because *Cook's* calibration data consisted of twenty–one data subsets that were designed to support specific math model terms (see App. 28 for details). Finally, *Cook's Method* constructs a load iteration scheme from the math models of the outputs so that loads can be predicted from outputs during a wind tunnel test (Ref. [5], pp. 5–7). *Global regression* was not considered for the processing of balance data in the late 1950s and 1960s because (i) the *matrix solution*[‡] of a multivariate least squares problem was not yet widely known and (ii) computer resources were limited.

Researchers also started using the *Non–Iterative Method* for the load prediction in the 1960s. This alternate approach directly fits the loads as a function of the measured bridge outputs. Therefore, no load iterations are required. However, hidden dependencies between math model terms were not rigorously investigated before the 2000s. Therefore, incorrect load predictions were occasionally obtained when the regression model of a load was applied. These observations are one of the reasons why the *Iterative Method* became the preferred balance load prediction method in North American wind tunnels.

Significant advances were made in the 1970s that greatly benefited the generation of the load prediction equations (see Fig. 29–1). First, *Galway* recognized the advantage of applying *global regression*, i.e., the *matrix solution* of the least squares problem to balance calibration data (Ref. [6], p. 13, Eq. (36)). He also understood benefits of the use of the *absolute value function*[⋆] in regression models of data from balances with bi–directional outputs and extended the idea to higher–order terms (Ref. [6], pp. 21–23; Ref. [79], p. 5). Furthermore, he recommended the use of the natural zero as the global datum for the electrical output of a balance bridge (Ref. [6], p. 27; *Galway* uses the synonym *buoyant component offset* in that context). Finally, *Galway* developed a tare load iteration process. His algorithm was first published in 1999 (Ref. [80]). *AIAA's Internal Balance Technology Working Group* (IBTWG) adopted *Galway's* algorithm for use with the *Iterative Method* (see Ref. [7]). *Galway's* four ideas were first implemented with the *Iterative Method* because (i) the *Iterative Method* was *Galway's* preferred load prediction method and (ii) the reliability problem of the load prediction equations of the *Non–Iterative Method* had not yet been resolved. Finally, the development of minicomputers (PDP, VAX) in the 1970s made computational resources more accessible. Consequently, *global regression* could more easily be used to derive the load prediction equations from balance calibration data.

No significant improvements of balance load prediction methods appear to have been made in the 1980s. However, the personal computer and FORTRAN & BASIC compilers

[†] The term *global regression* indicates that a single least squares fit is used to calculate the coefficients of a multivariate regression model of balance calibration data.

[‡] The *matrix solution* of the least squares problem is an application of the *Moore-Penrose* pseudo inverse that British physicist and Nobel Prize laureate *R. Penrose* first proposed in 1956 (Ref. [77]).

[⋆] The idea of using the *absolute value function* for the description of bi–directional bridge output characteristics appears to have originated in Europe (Ref. [79], p. 5).

became widely available. Now, analysts could more easily implement the more complex data analysis algorithms that emerged in the 1970s.

It became obvious in the 1990s that the application of the *Iterative Method* had to be standardized so that a given set of balance load prediction equations could be used at multiple wind tunnel facilities. This conclusion was one of the reasons why *AIAA's* IBTWG was established (see Ref. [82], p. 85, p. 88). A major accomplishment of this working group was the development of a standard description of the *Iterative Method*. This description was published in 2003 in the first edition of *AIAA's* Recommended Practice document that discusses the calibration and use of internal strain–gage balances (Ref. [7]).

Again, advances were made during the 2000s after many analysts adopted IBTWG's description of the *Iterative Method* and more powerful programming languages & software tools became available. For example, *Parker et al.* started to use the principles of *Design of Experiments* during both preparation and execution of balance calibration experiments (Ref. [42]). The primary goal of these efforts was the reduction of the total number of data points needed for a manual calibration of a balance. In addition, *Ulbrich* applied *Singular Value Decomposition (SVD)* during the analysis to analytically determine regression model terms that a given balance calibration data set supports (Ref. [23]). He recognized that *SVD* needs to be applied to a transformed set of independent variables of the calibration data to be effective (App. 17, p. 360). Furthermore, it was discovered that unsupported regression model terms associated with the use of the *Iterative Method* can be identified by using the *Variance Inflation Factor (VIF)* as a test metric (Ref. [27], p. 4). This discovery also meant that *VIFs* could be used to assess the reliability of regression models of the loads that the *Non–Iterative Method* uses (see App. 18). Then, load predictions resulting from the application of the *Non–Iterative Method* could be made as reliable as load predictions resulting from the application of the *Iterative Method*.

It was observed in 2010 that a convergence instability sometimes appeared when *Galway's* tare load iteration algorithm was used in combination with the *Non–Iterative Method*. Therefore, an improved version of *Galway's* algorithm was developed that avoids the instability. It was first published in 2011 (see Ref. [11] and App. 12).

The second edition of *AIAA's* Recommended Practice document on calibration and use of strain–gage balances was published in 2020 (Ref. [7]). In addition, a new implementation of the *Non–Iterative Method* was completed in the same year at NASA Ames Research Center. This new implementation made it possible to systematically compare load prediction accuracies of the *Non–Iterative* and *Iterative Method*. Since 2020, accuracy comparisons were performed for many types of balances and calibration load schedule designs. They showed beyond doubt that the load prediction accuracies of both methods are the same if four conditions are met: (i) bridge outputs are formatted as differences relative to the natural zeros, (ii) loads are tare corrected, i.e., described as differences relative to the datum of zero absolute load, (iii) the same function classes are used to define regression models of the dependent variables, and (iv) the selected regression models are free of unwanted linear or near–linear dependencies. A NASA contractor report was published in 2022 (NASA/CR–20210026455). It is the first publication that presents highly detailed side–by–side descriptions of the *Non–Iterative* and *Iterative Method* in a single document. The current document is the revised and enlarged third edition of the report.

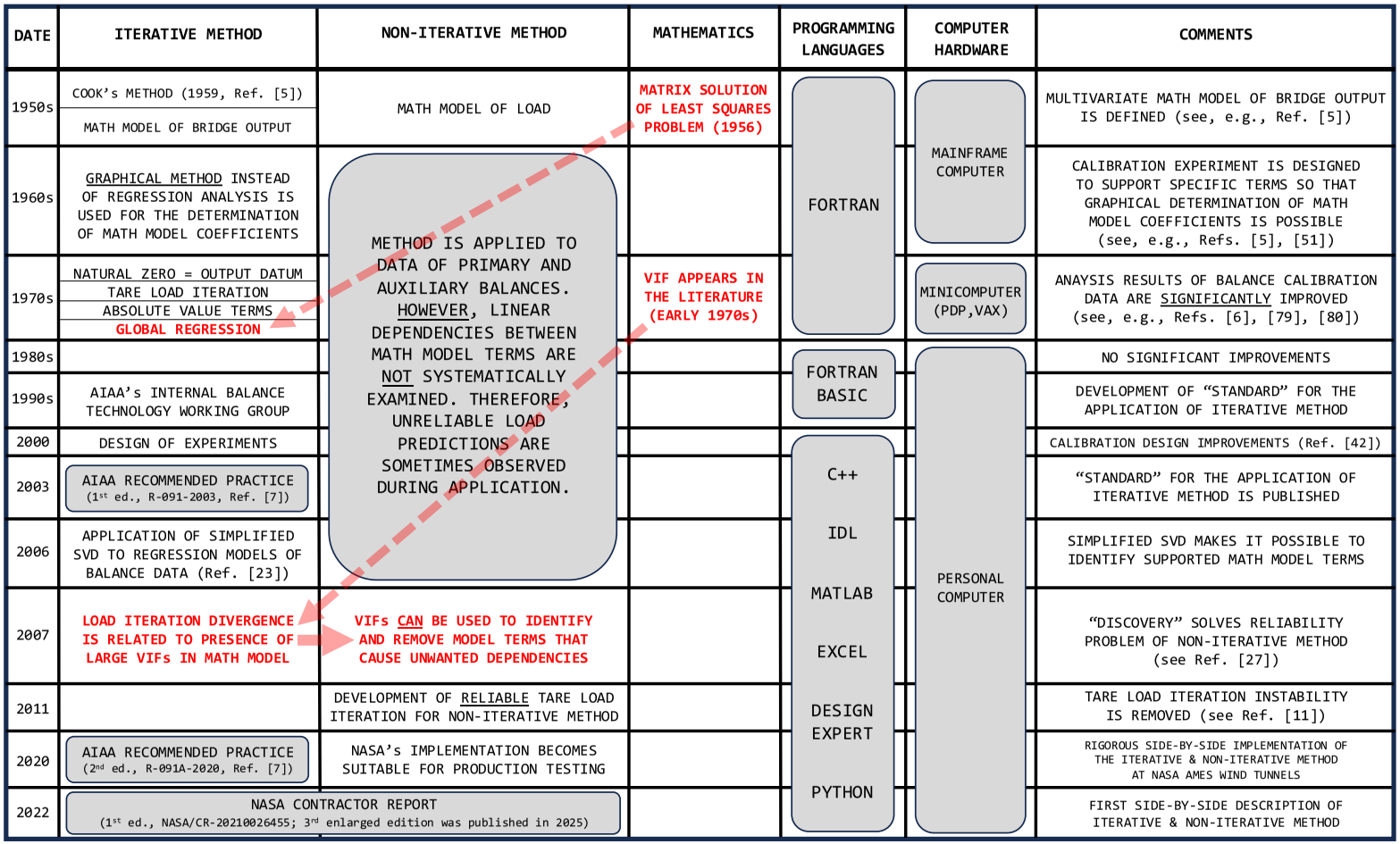

Fig. 29-1 The historical evolution of strain-gage balance load prediction methods.

Subject Index